UNIVERSITÉ SORBONNE PARIS NORD
ÉCOLE DOCTORALE GALILÉE – ED 146

# DOCTORAT

Discipline : Sciences de la vie et de la santé

**Traitement ciblé des maladies thrombotiques grâce à des particules de polysaccharides submicroniques fonctionnalisées**

Présenté et soutenu publiquement par

**Alina ZENYCH**
le 29 janvier 2021

Thèse dirigée par le Docteur Cédric CHAUVIERRE

Devant le jury composé de :

| | |
|---|---|
| Dr. Christine VAUTHIER, Ph.D. | Rapporteur |
| Pr. Aymeric ROUCHAUD, Ph.D., M.D. | Rapporteur |
| Pr. Laurence MOTTE, Ph.D. | Examinateur |
| Pr. Frédéric CHAUBET, Ph.D. | Examinateur |
| Dr. Mathieu CHARVERIAT, Ph.D. | Examinateur |
| Dr. Cédric CHAUVIERRE, Ph.D., HDR | Directeur de thèse |

Laboratory for Vascular Translational Science (LVTS) – INSERM U1148
Hôpital Bichat – Claude Bernard, Paris, France

# ACKNOWLEDGEMENT

First, I would like to thank Dr. Christine Vauthier and Pr. Aymeric Rouchaud for agreeing to be the rapporteurs and their evaluation of my PhD manuscript, as well as jury members Pr. Laurence Motte, Pr. Frédéric Chaubet, and Dr. Mathieu Charveriat who reviewed my work.

I express my sincere gratitude to my PhD supervisor Dr. Cedric Chauvierre for his visionary leadership during my PhD project, his kindness, patience, continuous support, and vast scientific expertise while providing me with the independence to progress as a researcher. His encouragement, energy, and professionalism, along with a good sense of humor and extensive knowledge of French culture, made me enjoy our cooperation.

My deepest thanks go to Dr. Didier Letourneur, the head of the LVTS laboratory and of the Team 3 “Cardiovascular Bioengineering”, who provided me an opportunity to join the LVTS laboratory and Team 3, for sharing his expertise on biomaterials, valuable guidance, positive outlook, and constant encouragement. I am grateful for the vast opportunities I had as a PhD student at the LVTS for scientific growth, participation and presenting my work at the French and international conferences.

I wish to sincerely thank Team 1 of Pr. Denis Vivien in the Laboratory PhIND - INSERM U1237 at Centre CYCERON in Caen, particularly Dr. Thomas Bonnard and PhD student Charlène Jacqmarcq, for their warm welcome, insightful comments, and precious experiences in their laboratory during the *in vivo* tests.

I cannot express enough thanks to all the members of the LVTS, and especially Team 3, for the stimulating discussions, extensive technical assistance, and for all the unique traditions and the wonderful time we had during these three years. My pleasure to warmly thank Rachida Aid, who was teaching me most of the methods and assisted in the *in vivo* studies. Many thanks to Dr. Laura M. Forero Ramirez and Fernanda Moraes for the

collaborative work on the development of the nanocarrier. I want to thank Albane Carré, Ibrahim Wane, and Louise Fournier (current PhD student), who helped me advance my project during their internships in the laboratory. I kindly thank Pr. Antonino Nicoletti for his expertise with designing an rtPA release study and Dr. Kevin Guedj for assistance with flow cytometry. I also thank Dr. Yoann Lalatonne for the technical support with the TXRF technique, Dr. Samira Benadda with confocal microscopy, and Christine Choqueux for performing SEM images. Big thanks to Dr. Véronique Ollivier, who introduced me to the microfluidic technique, and Dr. Stephane Loyau for the help with a blood collection and sharing his knowledge on coagulation processes. I sincerely thank Pr. Frédéric Chaubet and Murielle Maire for their kind assistance and expertise in polymer chemistry. Many thanks to Katia Yahiaoui and Raphael Martos for providing the animals for the experiments, sometimes at short notice. I would also like to thank my other current and previous colleagues from LVTS: Dr. Bo Li, Dr. Joana Antunes, Dr. Soraya Lanouar, Dr. Graciela Pavon-Djavid, Dr. Teresa Simon-Yarza, Dr. Jerome Grenier, Dr. Marie-Noelle Labour, Xavier Ferraretto, Elnaz Gholizadeh, Lucie Gernez, Abbas Asoudehfard, Dr. Camille Le Guilcher, Dr. Paola Aprile, Chau Le, Alessandra Dellaquila, Rodolphe Migneret for their kindness, willingness to help, and diverse scientific background. It has been a privilege and pleasure to work in the open-minded, friendly, and supportive international research environment.

I am also immensely grateful to the INSPIRE Project of the European Union's Horizon 2020 Marie Sklodowska-Curie program, which funded my PhD project and gave me a chance to conduct my research. Moreover, their multiple social and professional events allowed me to build friendships with other INSPIRE fellows.

I thank my parents for the continuous encouragement and unconditional love, and my close friends who supported me through this time. Finally, my gratitude goes to my boyfriend

João Pedro for his love, support, and patience during these three years that we spent together following our own INSPIRE PhD journeys.

# TABLE OF CONTENTS

*ACKNOWLEDGEMENT* ..... *iii*

*ABBREVIATIONS* ..... *2*

*LIST OF FIGURES* ..... *3*

*LIST OF TABLES* ..... *5*

*GENERAL INTRODUCTION & PROJECT* ..... *6*

*Chapter 1. INTRODUCTION* ..... *12*

**PART 1. NANOMEDICINE PROGRESS IN THROMBOLYTIC THERAPY** ..... **14**

1 CARDIOVASCULAR DISEASES AS A GLOBAL THREAT ..... 14
2 NANOMEDICINE FOR TARGETED DRUG DELIVERY ..... 24
3 LIPID DRUG DELIVERY ..... 29
4 POLYMERIC DRUG DELIVERY ..... 34
5 INORGANIC NANOPARTICLES ..... 43
6 BIO-INSPIRED NANOCARRIERS ..... 52
7 NANOPARTICLE OPTIMAL DESIGN FOR THROMBOLYTIC THERAPY ..... 58
8 DISCUSSION & PERSPECTIVES ..... 64

**PART 2. POLYSACCHARIDE HYDROGEL NANOCARRIERS FOR CARDIOVASCULAR DISEASES** ..... **69**

1 HYDROGELS & HYDROGEL-BASED NANO- & MICROPARTICLES ..... 69
2 POLYSACCHARIDES AS A STRUCTURAL BIOMATERIAL ..... 71
3 FABRICATION METHODS OF MICROGELS FROM BIOPOLYMERS ..... 74
4 FUNCTIONALISATION OF THE NANOPARTICLES TO TARGET THROMBI ..... 78

*Chapter 2. EXPERIMENTAL PART* ..... *84*

**FUCOIDAN-FUNCTIONALIZED POLYSACCHARIDE SUBMICROPARTICLES WITH ALTEPLASE FOR TARGETED THROMBOLYTIC THERAPY** ..... **86**

1 INTRODUCTION ..... 87
2 MATERIALS AND METHODS ..... 91
3 RESULTS AND DISCUSSION ..... 103
4 CONCLUSIONS ..... 123

*Chapter 3. GENERAL DISCUSSION & PERSPECTIVES* ..... *126*

*GENERAL CONCLUSION* ..... *138*

*REFERENCES* ..... *142*

*ANNEXES* ..... *182*

# ABBREVIATIONS

| | | | |
|---|---|---|---|
| WHO | World Health Organisation | CT | Computed Tomography |
| CVD | Cardiovascular diseases | SPECT | Single-Photon Emission Computed Tomography |
| MMP | Matrix metallo-proteinases | PET | Positron Emission Tomography |
| HDL | High-Density Lipoproteins | MRI | Magnetic Resonance Imaging |
| LDL | Low-Density Lipoproteins | US | Ultrasound |
| VCAM-1 | Vascular Cell Adhesion Molecule-1 | NIR | Near-infrared |
| NOS | Nitric Oxide Synthase | MI | Myocardial Infarction |
| HIF-1 | Hypoxia-Inducible Factor-1 | IS | Ischemic Stroke |
| EGR-1 | Early Growth Response 1 | DVT | Deep Vein Thrombosis |
| MCP-1 | Monocyte Chemoattractant Protein-1 | VT | Venous Thrombosis |
| PA | Plasminogen Activators | NPs | Nanoparticles |
| rtPA | Recombinant-tissue plasminogen activator | SPs | Submicronic particles |
| SK | Streptokinase | MPs | Microparticles |
| MT | Mechanical thrombectomy | MNP | Magnetic nanoparticles |
| mAb | Monoclonal antibodies | SPIONs | Superparamagnetic iron oxide nanoparticles |
| scFv | Single-chain antibody | SLNs | Solid Lipid Nanoparticles |
| ROS | Reactive Oxygen Species | RBC | Red blood cell |
| BBB | Blood-brain barrier | VNPs | Viral nanoparticles |
| vWF | von Willebrand factor | PAM | Polyacrylic acid-co-maleic acid |
| FXIIIa | Activated factor XIII | Cs | Chitosan |
| FDA | U.S. Food and Drug Administration | PLA | Polylactic acid |
| EMA | European Medicine Agency | PCL | Polycaprolactone |
| GMP | Good Manufacturing Practice | POx | Poly(2-oxazoline) |
| PSGL-1 | P-selectin glycoprotein ligand-1 | PAA | Poly (acrylic acid) |
| MPS | Mononuclear Phagocyte System | PLGA | Poly(lactic-co-glycolic acid) |
| W/O | Water-in-oil | PEG | Polyethylene glycol |
| STMP | Sodium trimetaphosphate | PVP | Polyvinyl pyrrolidone |
| PGPR | Polyglycerol polyricinoleate | PVA | Poly(vinyl alcohol) |
| HUVEC | Human umbilical vein endothelial cells | PAMAM | Poly(amidoamine) |
| MCA | Middle cerebral artery | PACA | Poly (alkyl cyanoacrylate) |
| BSA | Bovine serum albumin | IP | Isoelectric point |
| HSA | Human serum albumin | MW | Molecular weight |

# LIST OF FIGURES

Figure 1. Schematic of thrombotic diseases. ..... 16

Figure 2. Tackling thrombosis with nanomedicine. ..... 20

Figure 3. The timeline of evolution and milestones in the progress of nanomedicine for fibrinolytic therapy: history and current trends. ..... 26

Figure 4. Nanomedicine-based platforms with Plasminogen Activators. ..... 28

Figure 5. Platelet-derived liposomal microparticles for thrombosis. ..... 32

Figure 6. Polymer NPs with fucoidan for venous thrombosis. ..... 39

Figure 7. Polymer micelle NPs with rtPA and antioxidant. ..... 42

Figure 8. Example of heparin-coated MNPs in thrombosis. ..... 48

Figure 9. Enhancement of thrombosis via hyperthermia. ..... 51

Figure 10. Nanoplatelets as an efficient carrier of rtPA in multiple thrombosis models ..... 54

Figure 11. Synergic effect of neuroprotection and thrombolysis using nanoplatelets. ..... 56

Figure 12. Schematic illustration of the main strategies in the development of thrombolytic drug delivery nanocarriers. ..... 67

Figure 13. Schematic image of hydrogels. ..... 70

Figure 14. Chemical structure and origin of different polysaccharides. ..... 72

Figure 15. P-selectin links inflammation and thrombotic pathophysiology pathways at the arterial vessel wall. ..... 79

Figure 16. Quantification of fucoidan content in hydrogel Fuco-SPs by a colorimetric assay. ..... 96

Figure 17. Synthesis and the *in vivo* proposed mechanism of action of the Fuco-SPs. ..... 104

Figure 18. FTIR spectra of the polysaccharides and SPs. ..... 105

Figure 19. Physico-chemical characterization of the SPs. ..... 107

Figure 20. Formulation and cytocompatibility of polysaccharide submicronic particles from other polymers or their mixtures. ..... 108
Figure 21. Biocompatibility of the SPs. ..... 110
Figure 22. Schematic illustration of the *in vitro* microfluidic targeting assay. ..... 111
Figure 23. Evaluation of the SPs interactions with selectins..... 112
Figure 24. Loading rtPA & its release from the SPs as well as thrombolytic efficacy *in vitro*. ..... 115
Figure 25. Adhesion of the Fuco-SPs over activated platelet aggregates. ..... 117
Figure 26. Histological analysis of Fuco-SPs in four organs of excretion. ..... 118
Figure 27. Thrombolytic efficacy *in vivo* as the analysis of blood reperfusion in the murine ischemic stroke model. ..... 120
Figure 28. Thrombolytic efficacy *in vivo* with an assessment of brain injury in the murine ischemic stroke model. ..... 122
Figure 29. *In vivo* targeting in the $FeCl_3$ murine model of thrombosis. ..... 123

# LIST OF TABLES

Table 1. Thrombolytic agents approved by the FDA ..... 22

Table 2. Different nanocarriers for thrombolytic therapy. ..... 65

Table 3. The synthesis parameters for the polysaccharide SPs. ..... 92

# GENERAL INTRODUCTION & PROJECT

Thrombotic occlusions of blood vessels are responsible for life-threatening arterial or venous cardiovascular disorders such as myocardial infarction, ischemic stroke, and venous thromboembolism.

Thrombolytic therapy is performed to lyse the blood clot and restore the blood flow, minimizing the tissue ischemic damage. Thrombolysis is currently achieved by injection of Plasminogen Activators (PA); however, it exhibits limited clinical efficacy due to a narrow therapeutic window and rapid drug elimination; thus, high quantities of the drug need to be administrated. The consequent risks of hemorrhagic complications explain why less than 10% of the patients benefit from the treatment.

Nanomedicine and nano-delivery systems are a relatively new but rapidly growing science area where nanomaterial tools are employed for molecular diagnostics or delivery of therapeutic agents specifically to targeted sites in a controlled manner. Nanomedicine vectorization of macromolecules protects the drug from enzymatic degradation, improves the therapeutic outcomes, and diminishes adverse effects in preclinical models. Henceforth, nanomedicine is a hot research subject nowadays that has made tremendous growth and extension beyond its primary oncological applications. Despite lesser attention to cardiovascular pathologies research, there is a dire need for nanomedicine-based innovative solutions for thrombotic diseases. The challenge is to design a non-toxic, biocompatible, and biodegradable nanocarrier from natural compounds, and capable to target thrombi. Polysaccharides are a clever choice of materials to form nanocarriers as these polymers are relatively cheap, nontoxic, biodegradable, and abundant in nature.

A key biological marker, P-selectin, which is expressed on the activated platelets and activated endothelium, serves as a hallmark of acute thrombotic events. Fucoidan, a sulfated polysaccharide found in brown seaweed, has shown a strong binding ability to P-selectin and an excellent safety profile in previous preclinical and clinical research, coordinated by our

laboratory. Thus, it is considered a favorable targeting ligand for molecular imaging and targeted treatment of thrombotic pathologies.

The objective of my PhD project is a safer and more efficient targeted thrombolysis due to the application of nanomedicine, the use of natural resources, and green chemistry processes. To specify, the first aim of my project was to design a 100% polysaccharide nano-/microcarrier using biocompatible and FDA-approved compounds. A clinically approved thrombolytics, alteplase, was to be loaded on the particles beforehand functionalized with a thrombus targeted agent (fucoidan). The safety and efficacy of the developed system had to be assessed in the *in vitro* and *in vivo* animal models of thrombosis.

This PhD manuscript consists of three major chapters: Introduction (Literature review), Experimental part, and General Discussion & Perspective.

The introduction chapter is divided into two parts. In the first part, current challenges and perspectives of nanomedicine are outlined as a valued approach for the personalized treatment of acute thrombotic pathologies. We briefly review the pathophysiology of arterial and venous thrombosis. Clinically approved plasminogen activators that are currently applied for the treatment of acute thrombotic diseases are summarized. We analyze recent key research on various (lipid, polymeric, inorganic, biological) targeted nanocarriers intended for the local delivery of PA. In the second part of the chapter, we introduce hydrogels & hydrogel-based nano/microparticles. We focus more specifically on the advantages of polysaccharides as a biomaterial of the preference for the synthesis of the nano- & microsystems, particularly in the management of cardiovascular diseases. Thereafter, an overview of synthesis methods of nanoparticles from the biopolymers is provided. Finally, we explicate the choice of the molecular target P-selectin and its high-affinity binding ligand, fucoidan, that fulfills a targeting strategy in my project.

In the experimental part, the obtained results are presented in the form of publication. It contains all major accomplishments and is submitted to the scientific journal for peer-reviewed research publication. It deals with the potential of hydrogel-like polysaccharide submicronic particles (SPs) for the personalized treatment of acute thrombotic events. These highly biocompatible SPs were elaborated and functionalized with a fucoidan for targeting P-selectin on the thrombi. The complex of the SPs with loaded onto them alteplase showed an enhanced thrombolytic efficacy and higher brain protection in a murine model of acute ischemic stroke.

In Chapter 3, we interpret and analyze the findings of fucoidan-functionalized polysaccharide SPs in terms of academic achievement, clinical significance, and regulatory potential as a novel treatment of thrombotic diseases. The perspectives and current limitations of the study are further discussed.

# Chapter 1. INTRODUCTION

# PART 1. NANOMEDICINE PROGRESS IN THROMBOLYTIC THERAPY

Part 1 of the Introduction is an adapted version of the Review article published in *Biomaterials* in August 2020 (doi.org/10.1016/j.biomaterials.2020.120297) that is presented in **Annex 1**. We start by reviewing the pathophysiology of arterial and venous thrombosis and summarizing clinically approved PA to treat acute thrombotic diseases. We examine historical evolution and milestones, current challenges, as well as future perspectives in the recent key research on various (lipid, polymeric, inorganic, biological) targeted nanocarriers intended for the local delivery of PA. Moreover, this section features strategies for the rational design of nanocarriers for targeted thrombolysis and effective PA encapsulation in view of interactions between nanomaterials and biological systems. Remarkable preclinical research suggests that nanomedicine represents a valued approach for the precise treatment of acute thrombotic pathologies.

## 1 CARDIOVASCULAR DISEASES AS A GLOBAL THREAT

Cardiovascular diseases (CVD), the major global health threat, are associated with high morbidity and mortality that account for an estimated 17.9 million lives each year (31% of all deaths worldwide) [1], and this figure is expected to rise to >23.6 million annual deaths by 2030 [2]. CVD are a group of disorders of the heart (e.g., heart failure, rheumatic heart disease, abnormal heart rhythms, inflammatory heart diseases, cardiomyopathy) and blood vessels (coronary artery disease, cerebrovascular disease, aortic aneurysms, peripheral artery disease, *etc*.). CVD affect almost equally men as women; however, the disease develops about seven to ten years later in women as compared to men [3]. Furthermore, CVD are associated with substantial healthcare costs estimated at $329.7 billion annually in the United States [2] and nearly €200 billion in the European Union [4].

A large number of CVD may be prevented by addressing major risk factors through lifestyle interventions and pharmaceutical treatment where necessary [1]. Nevertheless, hypertension, the leading cardiovascular risk factor, is attributed to ~13% of global deaths (7.5 million deaths), followed by tobacco use 9%, diabetes 6%, physical inactivity 6%, obesity 5%, and high cholesterol level 4.5% [3].

Three major cardiovascular disorders – myocardial infarction (heart attack), ischemic stroke, and venous thromboembolism defined as deep vein thrombosis and/or pulmonary embolism – are severe complications of thrombosis, the formation of a blood clot in the vessels **(Figure 1)**. Among all deaths from CVD, 85% are caused by heart attacks and strokes, one-third of them in people under the age of 70 years [1]. To improve human survival and quality of life, early detections and effective treatments are principal.

Thrombolytic drugs are administered to dissolve a thrombus and restore the blood flow in acute thrombotic events; however, they are rapidly inactivated in the blood and trigger hemorrhagic complications, as we explain below. Paradoxically, while rapid reperfusion is the standard of care to minimize the infarct size, the restoration of blood flow itself may provoke irreversible tissue damage in a process called reperfusion injury [5]. Therefore, the pursuit of innovative solutions for the management of thrombotic diseases remains an open field of

research, where nanomedicine is emerging to be a promising strategy to improve both the efficacy and safety of thrombolytic therapy.

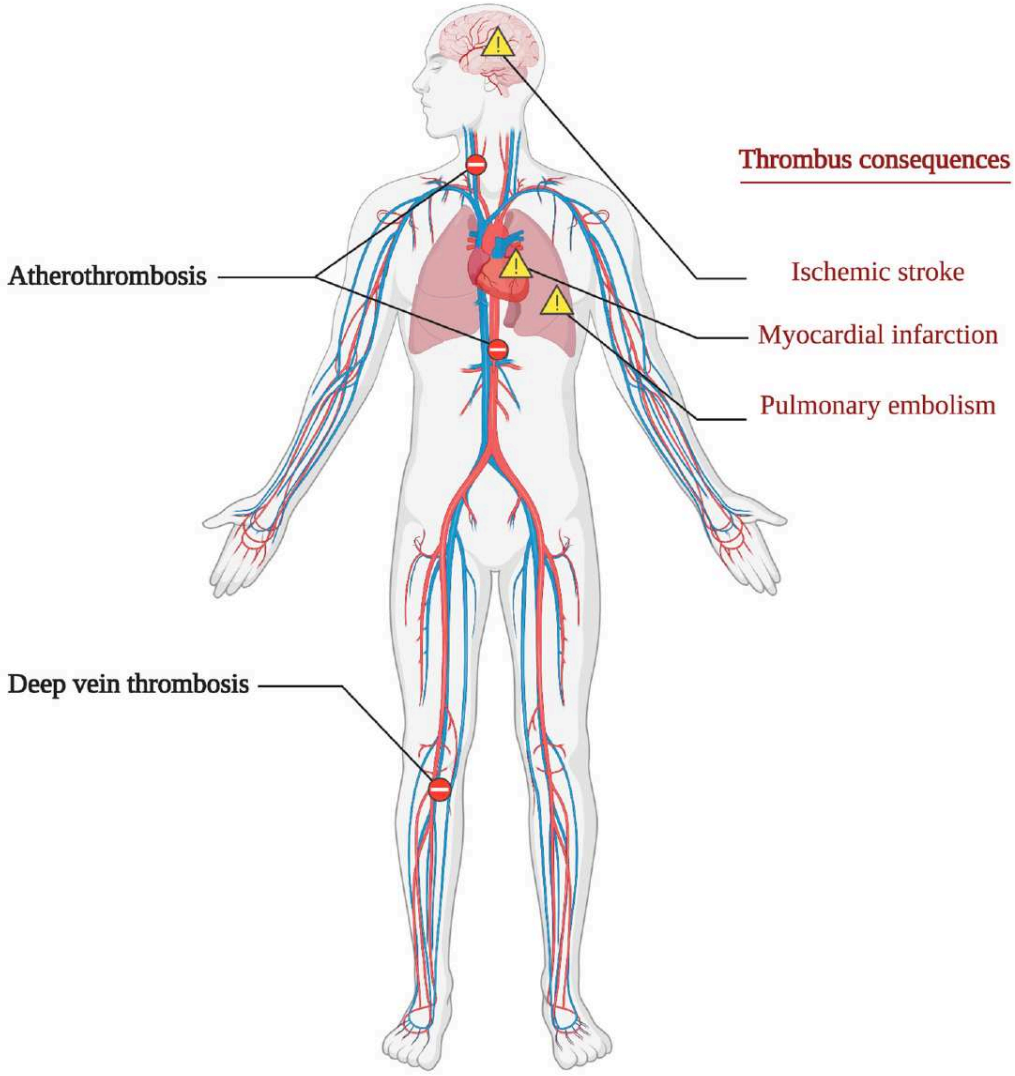


**Figure 1. Schematic of thrombotic diseases.** Congenital diseases and environmental factors influence blot clot formation in arteries (atherothrombosis) and veins (deep vein thrombosis). When the clot obstructs blood vessels in the brain, lungs, or heart, it may induce life-threatening consequences such as ischemic stroke, pulmonary embolism, or myocardial infarction.

# Chapter 1. INTRODUCTION

## 1.1 PATHOPHYSIOLOGY OF ARTERIAL AND VENOUS THROMBOSIS

Atherosclerosis is the key precursor of cardiovascular pathologies and it starts in adolescence. Atherosclerosis is a complex immune-inflammatory disorder whose progression involves multiple biological pathways influenced by genetic and environmental factors. Elevated plasma cholesterol level, hypertension, diabetes, tobacco smoking, male gender, and some inflammatory markers are among the proatherogenic risk factors of atherosclerosis, while physical exercise, a healthy diet, and high High-Density Lipoproteins (HDL) counts have an atheroprotective role [6].

Atherosclerotic lesions are initiated when the endothelium is activated by atherogenic and pro-inflammatory stimuli, such as primarily Vascular Cell Adhesion Molecule-1 (VCAM-1), intercellular adhesion molecule-1, E-selectin, and P-selectin [7]. It has been demonstrated a direct hemodynamic role in atherogenesis, notably by endothelial cells as their numerous signaling pathways are dependent on the hemodynamic patterns [8,9]. Low shear stress and turbulent flow at arterial curvature and branch points are major drivers of plaque development and instability. Plasma molecules and Low-Density Lipoproteins (LDL) penetrate dysfunctional endothelium into the subendothelial space where atherogenic lipoproteins are oxidized, mediated by myeloperoxidase, 15-lipoxygenase, and/or Nitric Oxide Synthase (NOS) [7]. Low-grade inflammation contributes to the disease progression due to the focal recruitment of circulating monocytes and T-lymphocytes [10]. Modulated by chemotactic cytokines, such as oxidized LDL and Monocyte Chemoattractant Protein-1 (MCP-1) [11], monocytes infiltrate arterial intima through transendothelial migration and differentiate into macrophages by internalizing the atherogenic lipoproteins via scavenger receptors. The incidence of the foam cells (lipid-laden macrophages) and their death by apoptosis and necrosis contribute to the formation of destabilizing atheromatous lipid-rich core within the plaque. Moreover, the foam cells express an array of inflammatory factors and produce proteolytic enzymes, such as Matrix

MetalloProteinases (MMPs) [11], which are implicated in matrix degradation and plaque disruption [12]. To insulate the thrombogenic lipid-rich core of the atheroma from the bloodstream, the fibrous cap develops at the lesion site as a fibroproliferative response mediated by intimal smooth muscle cells. The recruitment of the smooth muscle cells and the production of the collagen-rich matrix are considered as beneficial since they protect the plaques against rupture and subsequent thrombosis. Conversely, the disintegration of foam cells and loss of smooth muscle cells may have detrimental consequences, leading to the formation of a destabilizing lipid-rich core and a fragile and rupture-prone fibrous cap. Atherosclerotic plaque calcification is an inflammation-driven process that manifests in all stages of the disease and should be defined as a two-phase process: microcalcification, the early stage of intimal calcium formation, and the end-stage of macrocalcification. While coronary Computed Tomography (CT)-detected macroscopic calcification in artery plaque acts as a biomarker of the overall disease progression, it is believed to stabilize the plaque and prevent acute events [13]. On the contrary, microcalcification, which can be identified by Positron Emission Tomography (PET)/CT imaging with $^{18}$F-sodium fluoride, is associated with plaque vulnerability and an increased risk of rupture since it aggravates plaque inflammation and augments mechanical stress in the fibrous cap [14].

Injury of the fibrous cap of atherosclerotic plaque is a primary trigger for arterial thrombosis, promoting hemorrhage and luminal pro-thrombotic response [15]. For initial flow obstruction, the blood coagulation cascade activates the platelets that are rapidly recruited to the site and aggregate, resulting in rapid thrombus growth [16] **(Figure 2A)**. The fibrin network then develops for the stabilization of platelet-rich thrombosis. Although most ruptured fibrous cap episodes occur silently without clinical symptoms, plague rupture with subsequent thrombosis often culminates in devastating clinical events such as myocardial infarction (MI) or ischemic stroke [15].

Contrary to atherothrombosis, the pathogenesis of Venous Thrombosis (VT) is only partially understood. The venous thrombi's main components are fibrin and erythrocytes and less activated platelets [17] **(Figure 2B)**. VT is initiated at the venous valves where stasis may occur under low shear blood flow [18]. Valvular sinus stasis aggravates hypoxia, promoting activation of the endothelium and leukocytes via mainly Hypoxia-Inducible Factor-1 (HIF-1) and Early Growth Response 1 (EGR-1) pathways. Besides, hypoxia condition modulates hypercoagulability. HIF-1 and EGR-1 pathways up-regulate P-selectin expression on endothelium, prompting monocytes to release microvesicles bearing tissue factor, which initiates thrombin production and fibrin deposition around the intact endothelial wall [19]. Both inherited and environmental factors raise the likelihood of venous thrombotic diseases such as an imbalance of pro- vs. anti-coagulation proteins, as well as cancer, obesity, and major surgery [16].

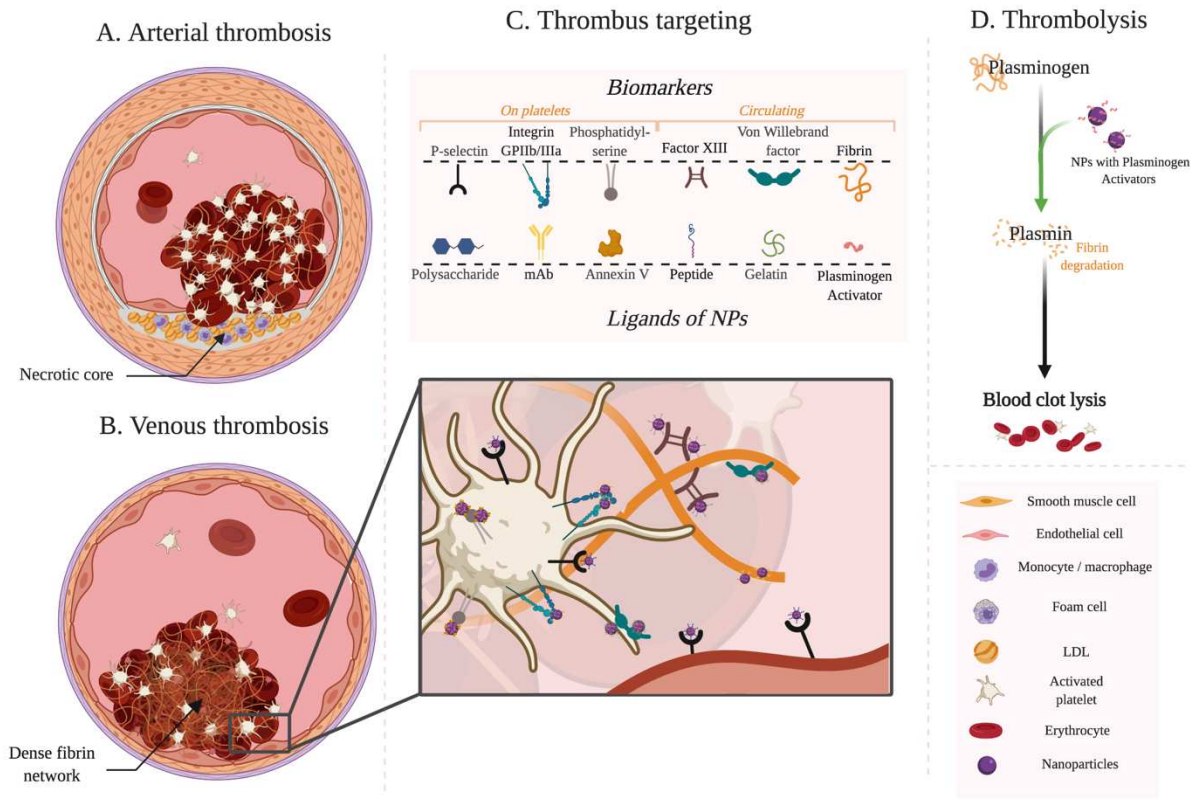


**Figure 2. Tackling thrombosis with nanomedicine.** Comparison of the arterial **(A)** and venous **(B)** thrombosis. Arterial clots (A) are composed of a high platelet ratio and are so-called "white thrombi". They are mostly the result of atherosclerosis. Multiple cellular pathways that initiate the activation of the endothelial cells are involved in thrombus formation. LDL penetrate the tissue, causing local inflammation and recruitment of circulating inflammatory cells. The disruption of the atherosclerotic plaque triggers the recruitment of smooth muscle cells to prevent wall rupture. Eventually, platelets aggregate on the impaired vessel wall with a consecutive formation of a fibrin network. On the other hand, venous clots (B), "red thrombi", contain erythrocytes and a denser fibrin network with fewer platelets. The thrombus formation is responsive to the following triggers: a vessel wall injury, a stasis of the blood flow, and the blood's hypercoagulability. **C.** Thrombus targeting with functionalized nano-/microparticles. Thrombi express a variety of cellular and molecular components – the surface of activated platelets (P-selectin, integrin GPIIb/IIIa, phosphatidylserine) or circulating proteins (Factor XIII, vWF, or fibrin) – that can be employed for specific targeting. NPs are designed with different ligands to these biomarkers: polysaccharide fucoidan, peptides, monoclonal antibodies, *etc*. **D.** Thrombolysis with PA-bearing and targeted to the thrombi NPs. The PA convert plasminogen into plasmin that breaks down the fibrin network and releases the components of the blood clot. **Abbreviations**: *LDL*, low-density lipoproteins; *mAb*, monoclonal antibodies; *NPs*, nanoparticles.

## 1.2 CLINICAL TREATMENT OF ACUTE THROMBOTIC DISEASES

For the treatment of acute arterial or venous thrombotic events, fibrinolytic drugs can be administered in order to proteolytically disrupt blood clots and restore blood flow. Fibrinolytic, or thrombolytic, agents are Plasminogen Activators (PA) that activate the proenzyme plasminogen to plasmin that then cleaves fibrin network into soluble degradation products. This activation of the fibrinolytic system destabilizes the structure of a thrombus [20]. Thrombolytic therapy is thereby used in patients with such pathologies as acute MI, acute ischemic stroke, peripheral arterial disease, deep vein thrombosis, and massive pulmonary embolism [21].

U.S. Food and Drug Administration (FDA)-approved "clot busters" drugs for use in thrombotic diseases are recombinant-based plasminogen activators (e.g., alteplase – rtPA, reteplase – rPA, and tenecteplase – TNK), streptokinase (SK), and urokinase (uPA). The main differences between them relate to their antigenicity, half-life, lytic potential, fibrin specificity, and hemorrhagic risks [22]. First-generation thrombolytic drugs (urokinase, streptokinase) are non-fibrin specific when second and third-generation (alteplase and its variants) overcome this issue. Generally, human protein-derived PA (urokinase, alteplase, reteplase, tenecteplase) are nonantigenic, contrary to those derived from a bacterial species (streptokinase) [23]. The half-life of each PA determines their mode of administration (a bolus injection, short infusion, or continuous intravenous infusion). A comparison of different FDA-approved PA with their clinical indications is summarized in **Table 1**.

**Table 1.** Thrombolytic agents approved by the FDA.

| Agent | Abbreviation | Source | Safety [immunogenicity, fibrin specificity] | Half-life, min | Regimen | Total Dose | Metabolism | Indication |
|---|---|---|---|---|---|---|---|---|
| | | | ***First-generation*** | | | | | |
| Streptokinase | SK | β-hemolytic streptococcus | Immunogenic Non-fibrin specific | 20 | Infusion | 1.5 x $10^6$ IU | Renal | PE Acute MI PAO, DVT |
| Urokinase | uPA | Human urine & kidney cell culture | Non-fibrin specific | 15 | Infusion | 2.25-6.25 x $10^6$ IU | Renal | PE Acute MI PAO, DVT |
| | | | ***Second-generation*** | | | | | |
| Alteplase | rtPA | Recombinant DNA technology | Fibrin specific (++) | 4-8 | Infusion | MI: 50-100 mg IS: 0.9 mg/kg PE: 100 mg | Hepatic | Acute MI Acute IS PE |
| | | | ***Third-generation*** | | | | | |
| Reteplase | rPA | Recombinant DNA technology | Fibrin specific (+) | 14-18 | Double bolus | 20 IU | Renal | Acute MI PAO |
| Tenecteplase | TNK | | Fibrin specific (+++) | 11-20 | Bolus | 30-50 mg | Renal | Acute MI |

**Abbreviations**: *DVT*, Deep Vein Thrombosis; *MI*, Myocardial Infarction, *PAO*, Peripheral Arterial Occlusion; *PE*, Pulmonary Embolism; *IS*, Ischemic Stroke; *IU*, International Units.

The leading drawbacks of fibrinolytic therapy include treatment failures such as ineffectiveness, re-thrombosis resulting from a persistent vascular lesion and plasma hypercoagulability, and a high risk of bleeding complications, with intracerebral hemorrhages occurring in 1 to 7% of treated patients [21]. Moreover, PA are physiologically inhibited by Plasminogen Activator Inhibitors (PAI) such as PAI-1 and PAI-2 while alpha 2-antiplasmin and alpha 2-macroglobulin inactivate plasmin, thereby reducing the treatment efficacy [24]. In view of these limitations, the constant development of novel molecules aims to address the problems associated with available thrombolytics. The novel candidates that are mutants of available PA or might be produced from the microbial, plant, and animal origin are discussed in the review [25].

The association of thrombolytic drugs with endovascular methods significantly improved interventional management of acute thrombotic events. The percutaneous coronary intervention has become more common for reperfusion, improving survival rates in patients with MI [26,27]. When available, this catheter-based procedure, which an interventional cardiologist performs, has to be offered promptly after / or in place of initial thrombolytic therapy. Since 2015, mechanical thrombectomy (MT) using a stent retriever is recommended as a complementary treatment to fibrinolytic therapy for ischemic stroke related to large vessel occlusions in the anterior circulation such as in the internal carotid artery and proximal middle cerebral artery [28,29] after multiple positive randomized control trials [30,31]. Yet, since MT needs to be performed by a qualified neurointerventionist at comprehensive stroke centers, access to them often remains difficult. In France, in particular, out of 135 nationwide neurovascular centers, only 40 can perform thrombectomy to date [32]. Therefore, there is still a dire need for a safe and non-invasive solution.

With the advent of nanotechnology, there has been considerable interest in integrating nanomedicine and thrombolytic therapy for the treatment of acute thrombotic events. Nanomedical approaches for targeted fibrinolysis could advance clinical outcomes by improving current pharmaceutical methods when interventional catheter-based strategies are not available or not recommended (as, for example, in ischemic stroke due to occlusions in smaller vessels or posterior circulation). By acting locally at the thrombus site, there is a promise that nanomedicine-delivered “clot-busting” agents deliver superior recanalization rates and attenuate life-threatening bleeding complications associated with their intravenous administration. One may also expect the chance to replace intravenous infusion with a bolus injection of the first- and second-generation PA due to the extended drug half-life. In the ideal treatment settings, the synergic combination of endovascular and nanotherapeutic methods would represent a more precise approach to manage thrombotic pathologies.

## 2 NANOMEDICINE FOR TARGETED DRUG DELIVERY

Nanomedicine, a medical application of nanotechnology, combines a powerful set of nano-engineered devices for diagnostic and/or therapeutic applications. Nanoparticle (NP)-based drug delivery can increase drug circulation time, improve therapeutic efficacy, and reduce unwanted off-target effects by delivering an active molecule to the injury site [33]. The liposomal formulation of doxorubicin – Doxil® – was the first clinically approved nanomedicine therapy by the FDA in 1995 for Kaposi's sarcoma and other cancers that reduced cardiotoxicity compared with a conventional formulation [34]. Other NP formulations are approved for the treatment of distinct pathologies, such as cancers, fungal infections, iron-deficient anemia, macular degeneration, as well as vaccines for hepatitis A and influenza [35,36].

Different nano- or microcarriers (e.g., liposomes, polymeric, magnetic nano- & microparticles, quantum dots, nanotubes, dendrimers) are similarly researched in the therapeutic area of CVD [37]. Nanotechnology plays a role for wide-ranging cardiovascular applications, such as hypertension [38], atherosclerosis [39], prevention of restenosis following interventional cardiology [40], ablation for atrial fibrillation [41], cardiac tissue engineering [42], but also in the management of aneurysms [43] as well as CVD prevention [44].

### 2.1 EVOLUTION AND MILESTONES IN THE PROGRESS OF NANOMEDICINE FOR FIBRINOLYTIC THERAPY

The field of nanomedicine in fibrinolytic therapy is evolving vibrantly, as evidenced by the expanding list of preclinical concepts of nanomaterial complexation with PA. An ideal vehicle for thrombolytic drug delivery should be biocompatible, non-toxic, non-immunogenic, biodegradable, and avoids rapid clearance by the immune system [45]. The benefits of utilization of the nanoparticles (NPs) are attributed to their high surface-volume ratio,

multifunctionality, high bioavailability, and possible control of therapeutic agent release. Control drug release facilitates the release of the payload from the NPs at the thrombus site upon internal or external stimuli such as temperature [46,47], pH [48], US [49], or magnetic field [46], *etc*. Specific thrombus targeting can be achieved by modifying the surface of nanocarriers with targeting moieties (antibodies, aptamers, polysaccharides, peptides, and small molecules) and/or application of magnetic energy, enhancing the therapeutic effect due to accumulation of thrombolytic drug at the clot surface [50] **(Figure 2C & D)**. Furthermore, encapsulation of the fibrinolytic drug onto the NPs can protect it from inactivation by PAI-1 in the bloodstream [51] and prolong its blood circulation time [48,52,53], thus achieving safe and effective thrombolysis at a lower dose [54,55]. Nanocarrier protection may further limit drug leakage during circulation, reducing the risk of hemorrhagic complications [56,57] such as cerebral hemorrhages that often accompany the injection of free plasminogen activators.

The timeline shown in **Figure 3** depicts evolution and milestones in the conceptual advances of nanomedicine-facilitated thrombolysis.

The story begins in the late '80s when dextran-coated iron oxide microparticles loaded with SK were utilized for magnetically driven thrombolysis of the carotid arteries in dogs [58]. Around the same time, SK-bearing liposomes entered the field by accelerating reperfusion in acute MI [59]. The first reported microbubbles for sonothrombolysis in 1996 were initially composed of denatured albumin shells; however, this formulation is no longer used due to stability/immunogenicity issues [60]. Polymeric platforms in thrombolytic therapy started to emerge a decade later in order to improve the stability profile of the liposomes in biological fluids. In 2004, first-reported polymer microparticles were designed from Polyethylene Glycol (PEG) and loaded with SK to tackle coronary thrombosis in a canine model [61]. The early success of the rtPA-conjugated erythrocytes in thromboprophylaxis in 2003 led to the further investigation and development of diverse bio-inspired nano solutions [62].

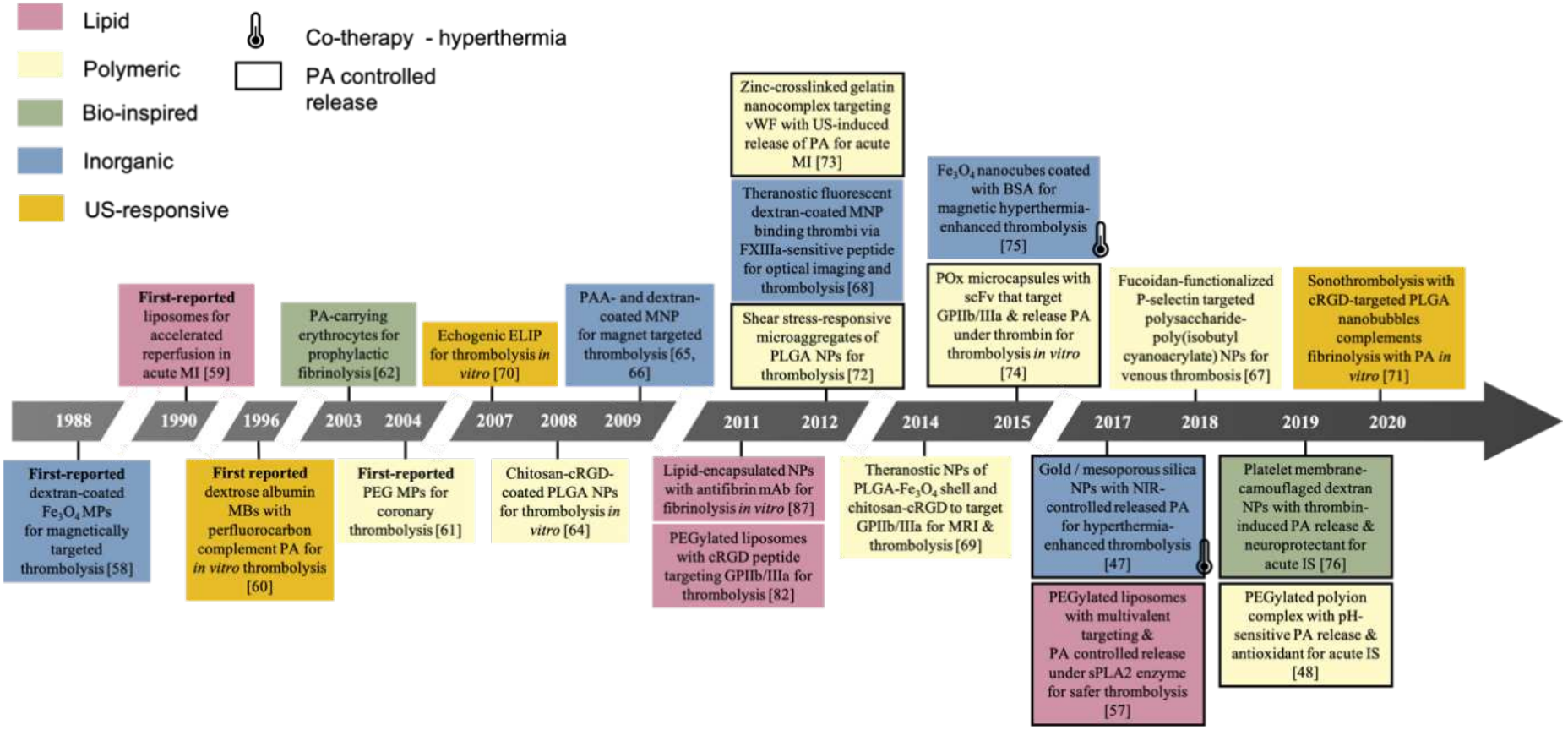


**Figure 3. The timeline of evolution and milestones in the progress of nanomedicine for fibrinolytic therapy: history and current trends.** This Figure mostly comprises the PA-loaded platforms tested with *in vivo* experiments; however, we also included several remarkable *in vitro* concepts. **Abbreviations**: *PA*, plasminogen activator; *MI*, myocardial infarction; *IS*, ischemic stroke; *PEG*, polyethylene glycol; *PLGA*, poly(lactic-co-glycolic acid); *PAA*, poly (acrylic acid); *BSA*, bovine serum albumin; *POx*, poly(2-oxazoline); *vWF*, von Willebrand Factor; *FXIIIa*, activated factor XIII; *$sPLA_2$*, secreted phospholipase A2 enzyme; *MNP*, magnetic nanoparticles; *MPs*, microparticles; *NPs*, nanoparticles; *MBs*, microbubbles; *ELIP*, echogenic liposomes; *mAb*, monoclonal antibodies; *scFv*, single-chain antibody; *MRI*, magnetic resonance imaging; *US*, ultrasound; *NIR*, near-infrared.

These initial studies evidenced undoubtedly the potential of nanomedicine to boost thrombolytic therapy in animal models; however, they often lacked a complete analysis in terms of particle physico-chemistry and safety, drug loading efficiency/release, targeting and thrombolytic efficacy in appropriate *in vitro* and subsequently *in vivo* models that is currently recognized and adopted [63].The evolution of nanomedicine-based fibrinolysis continued with the development of surface-coated, mostly nanosized particles that exhibit longer circulation half-life *in vivo* and superior safety profiles than uncoated microparticles. Notable examples from late 00' are the PA-bearing polymer NPs that were coated with chitosan and cRGD peptide, a prototype of the utilization of a popular targeting ligand of GPIIb/IIIa [64], as well as magnetic NPs coated with dextran [65] and polyacrylic acid [66] for magnetically guided thrombolysis.

The last decade, which we review in this Section, was fruitful for progress in nanomedicine-assisted thrombolysis. During these years, researchers commonly used active targeting strategies. Apart from the magnetic targeting of iron oxide NPs, the utilization of monoclonal antibodies (mAb) and peptides that recognize biomarkers associated with thrombotic pathologies have allowed the development of more selective nanosystems that advanced into the multivalent design in 2017 [57]. In 2018, polymeric NPs were functionalized with fucoidan, an affordable high-quality P-selectin ligand for site-specific fibrinolytic activity [67] as an alternative to costly mAb and peptides. From 2012, theranostic hybrid approaches emerge: inorganic nanocarriers that serve for thrombolysis and optical imaging [68] or Magnetic Resonance Imaging (MRI) [69]. Echogenic liposomes are widely studied with the *in vitro* clot model for sonothrombolysis due to tunable designs like targeting and/or rtPA loading [70]. Recently, targeting nanobubbles were published that complemented PA with sonothrombolysis, as they penetrate deeper into the clots comparing to microbubbles [71]. The nanoformulations with a controlled release start appearing more frequently: via hemodynamic

phenomena – increased shear stress in the stenotic arteries [72] and US-induced [73] in 2012, upon enzyme exposure since 2015 [74], and elevated temperature since 2017 [47] and low pH in 2019 [48]. To enhance thrombolysis, adjuvant therapy in the form of local hyperthermia by a magnetic field [75] or near-infrared (NIR) light [47] was used in the late 10's.

Nowadays, the trend is to create complex multifunctional but, at the same time, biocompatible and biodegradable nanocarriers. The application of novel biomaterials, hybrid nanoparticles with biomimetic surfaces, incorporating active targeting molecules, and the ability to modulate the release spatially and temporally is being widely researched. The researchers also commenced investigating the solution to complement nanomedicine-based fibrinolysis and to counteract the pathological processes related to ischemia with an antioxidant [48] and neuroprotection [76] approach for ischemic stroke in 2019.

In the next sections, we will describe in detail the complexation of PA with different types of nanocarriers summarized in **Figure 4** and their corresponding therapeutic effects in preclinical studies.

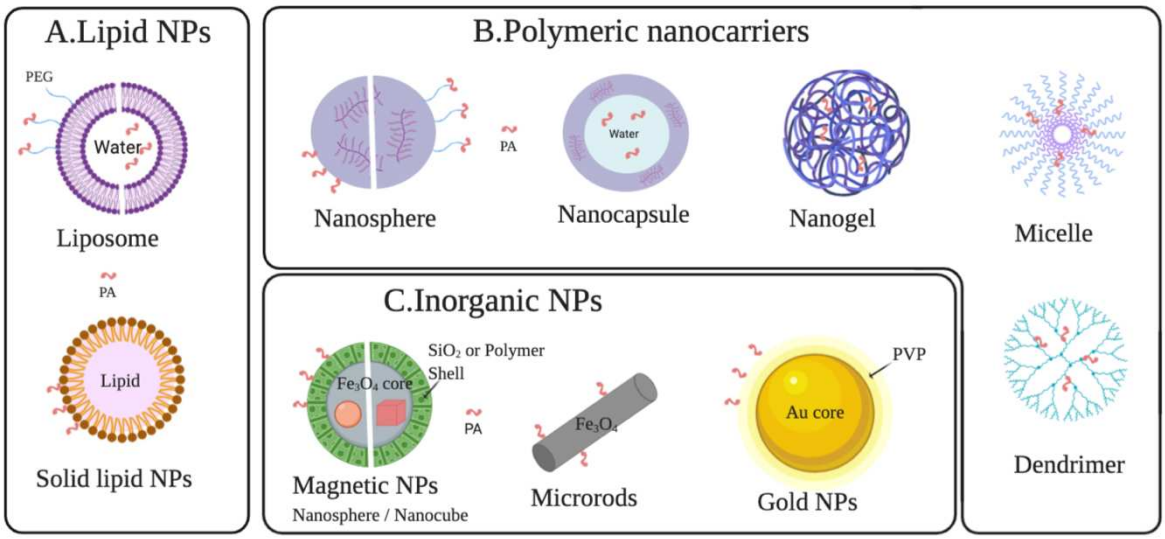


**Figure 4. Nanomedicine-based platforms with Plasminogen Activators. A.** Lipid nanocarriers. In liposomes, PA may be embodied into the aqueous core or adsorbed / covalently conjugated onto the PEGylated phospholipid shell. In solid lipid NPs, PA is covalently grafted

to their surface. **B.** Polymer-based nanoplatforms. PA are typically entrapped inside amphiphilic micelles and self-assembled gelatin or chitosan nanogels due to electrostatic interactions, incorporated into the aqueous core of nanocapsules, or covalently attached to the surface of the nanospheres and dendrimers via EDC/NHS chemistry. Surface decoration with PEGylation or polysaccharides is common for better stealth effects, particularly crucial for the NPs from hydrophobic synthetic polymers. **C.** Inorganic nanoparticles. In magnetic NPs, the inner core – in the shape of nanospheres or nanocubes – is mostly iron oxide ($Fe_3O_4$), and the surface is decorated with organic (e.g., dextran, chitosan, polyacrylic acid) or inorganic ($SiO_2$) shell. PA is conjugated to the surface via EDC/NHS or simple adsorption. Uncoated iron oxide microrods may load PA via glutaraldehyde. Gold NPs immobilized PA via bio-affinity ligation. **Abbreviations**: *PEG*, Polyethylene glycol; *PA*, plasminogen activator; *NPs*, nanoparticles; *PVP*, polyvinyl pyrrolidone.

# 3 LIPID DRUG DELIVERY

## *3.1 LIPOSOMAL DRUG DELIVERY*

Liposomes, first described in the mid-'60s, are defined as spherical vehicles made of an aqueous core surrounded by phospholipid bilayers. Since then, because of their excellent biocompatibility, low toxicity, and easy preparation methods, liposomes are considered as one of the most promising tools for drug delivery in medical fields of principally small molecules (e.g., chemotherapeutics), with some being clinically approved [77], but also proteins, DNA, RNA, and imaging probes [78].

Liposomes are generally fabricated by thin-film hydration, which consists of dissolving lipid components in an organic solvent, drying down by rotary evaporation, and rehydrating in water, as well as by freeze-drying, reverse-phase evaporation, or injection of ethanol with phospholipids into an aqueous phase. Membrane extrusion, sonication, and/or freeze-thawing are further employed to modulate the particle size [79]. In terms of the size and number of bilayers, different types of liposomes can be produced, such as small unilamellar vesicles (single phospholipid bilayer sphere), large unilamellar vesicles, and multilamellar vesicles (an

onion structure of bilayers) [78]. The amphiphilic properties of liposomes allow them to internalize both hydrophilic and hydrophobic compounds.

Liposomal encapsulation of plasminogen activators for thrombus-specific drug delivery is frequently exploited to improve the drug half-life and reduce hemorrhagic side effects. Given that the conventional liposomes aggregate *in vivo* and undergo rapid systemic clearance via Mononuclear Phagocyte System (MPS) after contact with plasma proteins, decoration with FDA-approved PEG has been adopted to provide steric stabilization and reduce liposomal opsonization, and, therefore, to improve the pharmacokinetics of PA in blood [79].

The liposomal surface modification strategies by site-directed target ligands, such as antibodies, peptides, or stimuli-responsive drug release (thermo- or pH-sensitive liposomes), have been tested in the preclinical development. Most targeting approaches are directed towards GlycoProtein IIb/IIIa (GPIIb/IIIa). GPIIb/IIIa is an integrin complex on the platelet membrane, which mediates platelet adhesion and aggregation during hemostasis. Normally present in its inactive state on resting platelets, it undergoes conformational changes to allow the platelets to bind to fibrin upon platelet stimulation by physiologic ligands such as thrombin or collagen [80]. Thrombolytics are generally incorporated into the inner aqueous core of the liposomes during the synthesis process; however, they can also be adsorbed onto the surface or covalently grafted to the PEGylated liposomes [81].

In the study of Vaidya *et al.,* long circulatory PEGylated liposomes were coupled with a cyclic Arg-Gly-Asp (cRGD) [CNPRGDY(OEt)RC] and targeted GPIIb/IIIa receptor both *in vitro* and *in vivo* [82]. Despite a low level of streptokinase release (12.20 ± 0.94%) throughout 35 h, the study reported the improved thrombolysis rate of cRGD-targeting liposomal SK compared with free SK after 1 h in rats (34% vs. 22%). When rtPA was loaded onto both non-PEGylated and PEGylated GPIIb/IIIa- targeting liposomes, a favorable rtPA release profile from PEGylated ones was demonstrated in the work [52], with a substantial amount of drug

released within 30 min after administration followed by a slow continuous release over 24 h. This strategy intends to achieve reperfusion and prevent re-thrombosis. The half-life of rtPA in plasma was prolonged from 7 min for native rtPA to 103 and 141 min for non-PEGylated and PEGylated liposomes. Besides, rtPA-loaded liposomes were 35% more potent than native rtPA for vessel recanalization but produced a 4.3-fold less depletion of circulating fibrinogen, potentially reducing hemorrhagic risks, in the $FeCl_3$-rat venous thrombosis model.

Huang *et al.* exploited the targeted delivery and controlled release of rtPA incorporated into PEGylated liposomes coated with cRGD peptide [83]. Membrane fusion attributed to interactions between cRGD peptides on liposomes and GPIIb/IIIa integrins on activated platelets caused liposomal membrane destabilization and rtPA release. Due to this, over 90% of the entrapped rtPA was released within 1 h in targeted liposomes compared to <10% after 6 h in untargeted ones, and this release profile could be adjusted by altering the concentration of activated platelets. Zhang *et al.* [56] combined the active thrombus targeting with cRGD and gradual release of the drug from the liposomes without burst effect over 5 h. They improved the *in vivo* thrombolytic efficacy by ~4-fold over free uPA, at the same time, shortening the bleeding time of the tail bleeding assay of hemostasis, thereby potentially reducing the side effects of uPA.

In the elegant study [57], Pawlowski *et al.* took inspiration from platelet-derived microparticles, which are plasma membrane vehicles shed from platelets that are undergoing activation, stress, or apoptosis **(Figure 5A)** [84]. They designed a liposomal system with a multivalent targeting strategy towards both GPIIb/IIIa and P-selectin on activated platelets using the peptides CGSSSG***RGD***SPA and CDA***EWVDV***S, respectively **(Figure 5B & C)**. As the constructs could be degraded under secreted phospholipase A2 ($sPLA_2$) enzyme, secreted from leukocytes and active platelets in the thrombus, it could so release encapsulated SK **(Figure 5D & E)**. While the thrombolytic efficacy of the targeted liposomes was comparable

to free SK in the $FeCl_3$-induced carotid artery thrombosis model, hemostatic capability for liposome-encapsulated SK was improved as measured by mouse tail bleeding time.

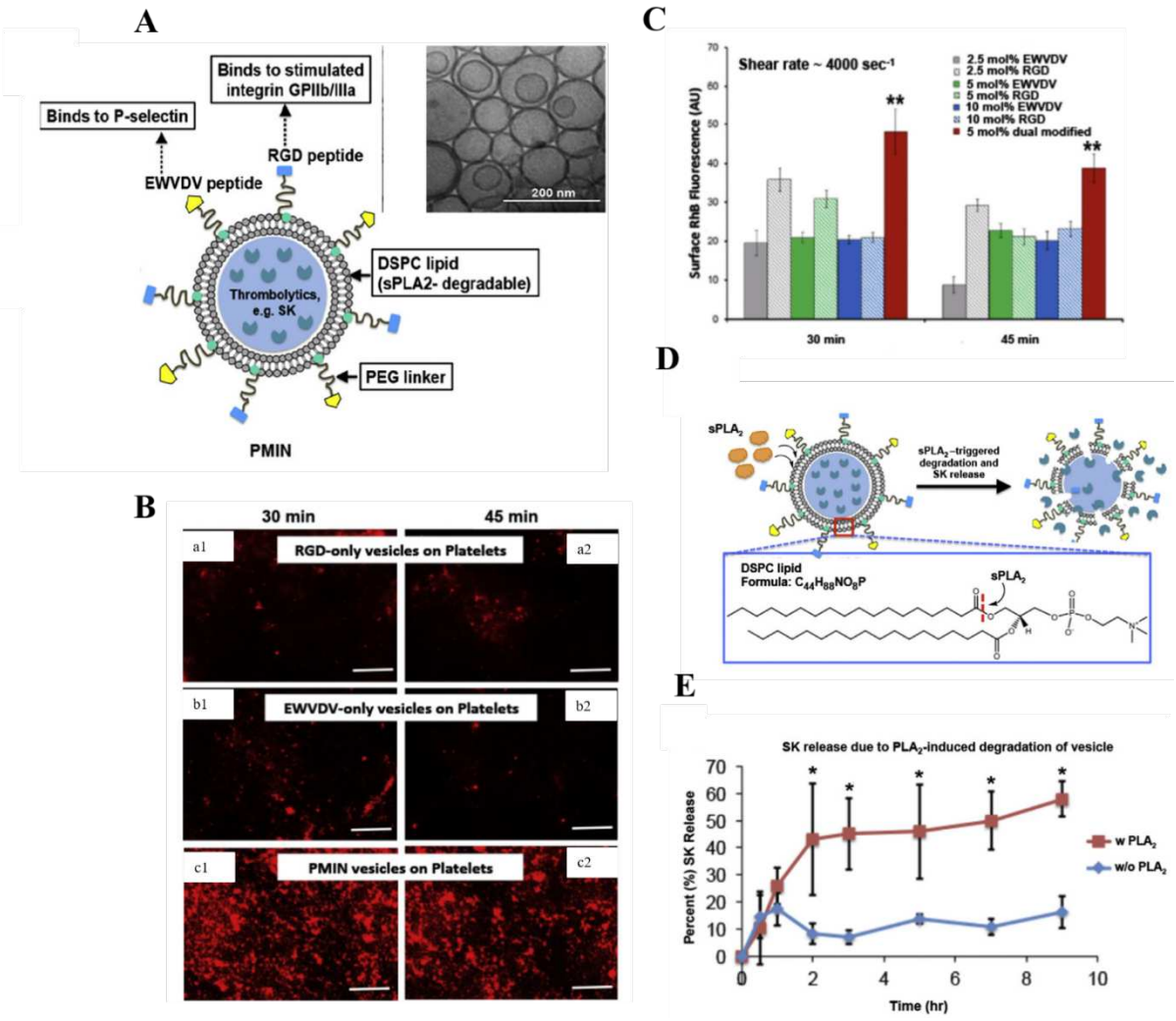


**Figure 5. Platelet-derived liposomal microparticles for thrombosis. A.** Schematic representation of platelet-derived microparticles-inspired nanovesicle (PMIN) with dual-targeting strategy and controlled release of the thrombolytic upon sPLA2 enzyme exposure, with a representative cryo-TEM image of PMINs. **B.** Representative fluorescent images of particle binding show that RGD-decorated vesicles (a1, a2) and EWVDV-decorated vesicles (b1, b2) have a reasonable extent of binding and retention on the platelet-rich thrombus surface. However, the level of binding and retention levels are enhanced for dual modified PMINs (c1, c2). **C**. Quantitative analysis of fluorescence intensity shows that PMINs have significantly higher binding and retention capabilities compared to singly modified vesicles even when the mol% composition of single peptide modification is to twice (10 mol%) that of dual peptide modification (5 mol%) at a high shear rate flow conditions. **D.** Schematic mechanism of sPLA2-induced membrane degradation due to cleavage of sn-2 acyl group of the phosphatidylcholine lipids. **E.** Release kinetics assessment of SK from PMINs shows that upon sPLA2 exposure, the percent (%) release of SK from PMINs is enhanced (~4 fold) compared

to passive release without sPLA2 exposure. Adapted with permission from [57]. Copyright 2017 Elsevier Ltd.

Hsu *et al.* [85] synthesized a hybrid NP-system, PEGylated thermosensitive magnetic liposomes (TMLs), encapsulating $Fe_3O_4$ NPs within liposomes via solvent evaporation/sonication and freeze-thaw cycles method. Thrombolytic activity *in vitro* of rtPA-loaded TMLs at 43 °C was augmented compared to at 37 °C due to enhanced drug release and higher enzyme activity at 43 °C. In addition to magnetic targeting, TMLs demonstrated a first-ever reported dual control mechanism of the drug release in serum: temperature- and magnet-sensitive, increasing at 43 °C and retarding with external magnetic force at 0.5 Tesla in the follow-up work [46]. This technique could allow the liposomes to be magnetically guided toward the thrombus, preventing premature drug release. With appropriate biocompatibility of the nanocarriers, TML@rtPA restored arterial blood flow, iliac blood flow, and hind-limb perfusion, whereas the same dose of rtPA exerted no benefit in the rat embolic model at 0.2 rtPA mg/kg under magnetic force at 43 °C.

### *3.2 SOLID LIPID NANOPARTICLES*

Solid Lipid Nanoparticles (SLNs) is an alternative drug delivery system. Contrary to conventional liposomes, which contain a lipid bilayer with an aqueous core, SLNs consist of lipid monolayer enclosing a solid lipid core stabilized by a surfactant, reaching a higher drug entrapment rate for a hydrophobic drug. Different preparation methods of SLNs include hot or cold homogenization, solvent emulsification/diffusion, or microemulsion [86]. Marsh *et al.* [87] prepared perfluorooctylbromide lipid-encapsulated NPs, which can be assimilated to SLNs with a size 250 nm by emulsification/sonication. Anti-fibrin mAb on the surface of the SLNs specifically targeted fibrin network in a canine model of the electrode-induced arterial

thrombosis. Sulfhydryl functionalized uPA was covalently coupled to these SLNs and retained its fibrinolytic activity *in vitro*.

Overall, cRGD peptide-decorated PEGylated liposomes became a standard engineering approach in thrombolytic research owing to their cyto- and hemocompatibility [56] with a high potential for clinical translation, which might, in contrast, take longer for complex hybrid systems.

## 4 POLYMERIC DRUG DELIVERY

Depending on the preparation method, polymeric NPs can have nanosphere or nanocapsule structures. Both naturally occurring hydrophilic polymers and synthetic biocompatible polymers are used in the NP fabrication and offer simple surface modification and functionalization [88]. Natural polymers such as polysaccharides (hyaluronan, alginate, and chitosan) and proteins (gelatin and albumin) are common [89]. Synthetic polymers come either in prepolymerized forms, such as polyesters like polycaprolactone (PCL), polylactic acid (PLA), or polymerized from the monomers, e.g., poly (methyl methacrylate), poly (alkyl cyanoacrylate) (PACA), poly (acrylic acid) (PAA), poly(lactic-*co*-glycolic acid) (PLGA), poly(2-oxazoline) (POx), and poly(amidoamine) (PAMAM). Synthetic polymers benefit from high purity and reproducibility over natural polymers; the latter, however, represent a significant interest due to their safety, abundance in nature, and low cost. Polymer nanoparticles are conventionally fabricated by two methods: the dispersion of preformed polymers or monomers' polymerization [90]. The plasminogen activators are typically dissolved and entrapped or covalently attached to the surface of the NPs prepared from some of the polymers mentioned above.

*Chitosan* (Cs) and its chemical derivatives have been widely used because of its biocompatibility and biodegradability, low toxicity, and low immunogenicity in thrombolytic

drug delivery. Chitosan is a cationic hydrophilic polysaccharide derived from chitins that forms polyelectrolyte complexes with negatively charged molecules [91].

Self-assembled chitosan NPs were produced via the ionic cross-linking with sodium tripolyphosphate, possessing a size 236 nm, and further loaded with uPA with encapsulation efficiency ~95% [92]. Both intravenous injection and catheter-driven drug delivery were tested in a thrombin-induced rabbit venous thrombosis, pointing out superior thrombolytic efficacy for the latter comparing with free uPA. Another group [93] elaborated a chitosan-based NPs/SK drug complexation via non-covalent interactions. Synthesis conditions such as pH and Cs concentration were optimized using a computational model. The team of Shamsi *et al.* reported the synthesis of uniform and spherical SK-entrapped chitosan NPs with a diameter of 67 ± 13 nm and a narrow polydispersity by microfluidics [94]. A steady and sustained SK release was achieved during 48 h *in vitro* in addition to higher SK amidolytic activity in plasma in rats, compared with free SK. Given that quaternized derivative of chitosan - N,N,N-Trimethyl Chitosan (TMC) has superior solubility and increased charge density, Liao *et al.* covalently grafted TMC with cRGD to target GPIIb/IIIa receptors [95]. The resulted cRGD-LK-NPs were formed with lumbrokinase (LK) via ionic gelation using sodium tripolyphosphate and could effectively accelerate thrombolysis in clot-occluded tubes and $FeCl_3$ rat carotid artery model at 90,000 U/kg of LK.

Jin *et al.* prepared PEG crosslinked glycol chitosan hollow nanogels by an ultrasonic spray technique and loaded uPA with 80% loading efficiency. Such NP design improved uPA half-life in rats from 18 min to 40 min without causing biotoxicity. The diagnostic US application at 2 MHz accelerated uPA release from the nanogels (90% of uPA released within 1 h vs. 80% within 6 h without the US) [53]. While the hollow cavity of the nanogels did not contain gas, they were responsive to the US due to the vibration of the polymer shell. The ultrasonic stimulation enhanced the thrombolysis *in vitro* for both free uPA and the uPA-loaded

nanogels [53]. Notably, the nanogels allowed the delivery of uPA with no signs of a stroke or blood-brain barrier permeability damage after 24 h *in vivo* [96].

*Gelatin*, a protein obtained from the collagen hydrolysis, is an attractive natural macromolecule for a thrombolysis nanocarrier owing to its biocompatibility, biodegradability, and wide availability at low cost [97]. Gelatin-based NPs require crosslinking with glutaraldehyde or another bifunctional cross-linker during preparation, and their surface can be tuned with site-specific ligands, cationized with amine derivatives, or PEGylated.

Polyelectrolyte complex of cationized gelatin and anionic PEGylated gelatin with rtPA mutant (monteplase) fabricated a 200 nm thrombolytic delivery system [98]. While fibrinolytic activity *in vitro* was suppressed to 45% due to nanocomplexation, it was fully recovered under US stimulation (1 MHz, intensity 0.75 W/cm$^2$), demonstrating an ultrasound-responsive rtPA release. US control drug release can be explained by producing a stable cavitation state and shear stress on the surrounding tissues [49]. In a rabbit thrombosis model, a combination of the US with rtPA-NPs allowed full vessel recanalization for all treated animals after 30 min, which was superior to free rtPA (10% recanalization after 60 min) and free rtPA+US (90% recanalization after 30 min).

Uesugi *et al.* further developed a zinc-crosslinked gelatin complex with monteplase [73], which restored its rtPA fibrinolytic activity upon US exposure *in vitro* [73] and *in vivo* to the level of free rtPA [54]. Monteplase-loaded NPs increased thrombus affinity 3-fold as a result of interactions of the gelatin with von Willebrand Factor (vWF), a blood glycoprotein that is a crucial component of platelet-rich thrombi. In a swine model of acute myocardial infarction, treatment with rtPA alone dissolved only 30% of occluded coronary thrombi at a dose of 55,000 IU/kg and no thrombi at 27,500 IU/kg within 60 min, while NPs carrying 55,000 IU/kg rtPA achieved recanalization of 90% thrombi within 30 min comparing to 60% of cases in 60 min at a dose of 27,500 IU/kg, under continuous-wave US field (1 MHz, 1 W/cm$^2$) [54].

*Poly(d,l-lactic-co-glycolic acid)* (PLGA), a synthetic biodegradable polymer that is relatively hydrophobic, has the FDA and the European Medicine Agency (EMA) approval for drug delivery systems. The PLGA micro- or nanoparticles are mostly synthesized by a double emulsion solvent evaporation system with poly(vinyl alcohol) (PVA) as an emulsion stabilizer [99].

In order to establish slow and controlled thrombolysis and prevent abdominal aortic aneurysm rupture, Sivaraman *et al.* produced PLGA NPs with 10 μg rtPA using didodecyldimethylammonium bromide (DMAB) or PVA as a surfactant [100]. DMAB-stabilized NPs demonstrated gradual clot lysis and higher binding to the fibrin clots. The nano-delivery system improved the proliferation of the aneurysmal smooth muscle cells (EaRASMC) exposed to the clot lysis byproducts, attenuated the elastic matrix degradation and proteolytic enzyme activities within EaRASMC cultures.

Surface PEGylation of PLGA NPs plays a favorable role in biocompatibility and improves pharmacokinetics by preventing opsonization. Colasuonno *et al.* formulated discoidal porous nanoconstructs (DPNs) with a mixture of PLGA and PEG and loaded rtPA with efficiency ~100% via EDC/NHS reaction [101]. Despite the absence of active targeting, a high thrombolytic potential of these NPs might be attributed to their erythrocyte-mimicking shape and deformability, leading to efficient circulation profiles and accumulation of rtPA-DPNs at the clot site. A hybrid theranostic system was developed by Zhou *et al.* when rtPA was encapsulated into a shell of PLGA and $Fe_3O_4$, and a chitosan-cRGD peptide was grafted on the surface to target GPIIb/IIIa [69]. Such design addressed a dual function: the early detection of a thrombus and the dynamic monitoring of thrombolytic efficiency using an MRI scanner. The obtained NPs showed a sustainable release profile: a slow-release during the first 15 min and a fast release until 60 min. MRI contrast enhancement was illustrated in the murine thrombus model; effective thrombolysis was performed in the *in vitro* blood clot.

Inspired by pathophysiological mechanisms [72], the microaggregates of multiple PLGA NPs dissociated into rtPA-bearing NPs when exposed to abnormally high hemodynamic shear stress (≥100 dyne/cm$^2$) in the vascular occlusions. The obtained Shear-Activated NanoTherapeutics with rtPA (rtPA-SA-NTs) performed effective thrombolysis in multiple preclinical models, as they delayed the time to full vessel occlusion in a $FeCl_3$ mouse arterial thrombus model, reversed the debilitating hemodynamic changes of acute pulmonary embolism *ex vivo* at a concentration 100-times lower of native rtPA, and increased survival in an otherwise fatal mouse pulmonary embolism model *in vivo*.

*Poly(alkyl cyanoacrylate)* (PACA) is an alternative to PLGA biodegradable polymer that was initially developed and approved as a surgical glue [102]. Juenet *et al.* prepared hydrophilic polysaccharide-decorated poly(isobutyl cyanoacrylate) core-shell NPs with a mean size of 130 nm by redox radical emulsion polymerization and loaded rtPA by adsorption [67] **(Figure 6A)**. Functionalization of the NPs with an algae-derived abundant and cost-effective sulfated polysaccharide fucoidan (Fuco) [103] allowed binding P-selectin on activated platelets under arterial or venous shear stress conditions **(Figure 6B & C)**. As a targeting ligand for P-selectin overexpression in cardiovascular pathologies, fucoidan was prior validated on microscale particles, including polysaccharide microparticles with iron oxide for MRI imaging [104] and polymer microcapsules [105]. Thrombolytic efficacy was 2-fold enhanced for rtPA-loaded Fuco-NPs comparing with rtPA-Control-NPs and free rtPA in $FeCl_3$ murine model of venous thrombosis at the rtPA dose of 2.5 mg/kg [67], which is 4 times lower than a clinical dose in mice [106] **(Figure 6D & E)**.

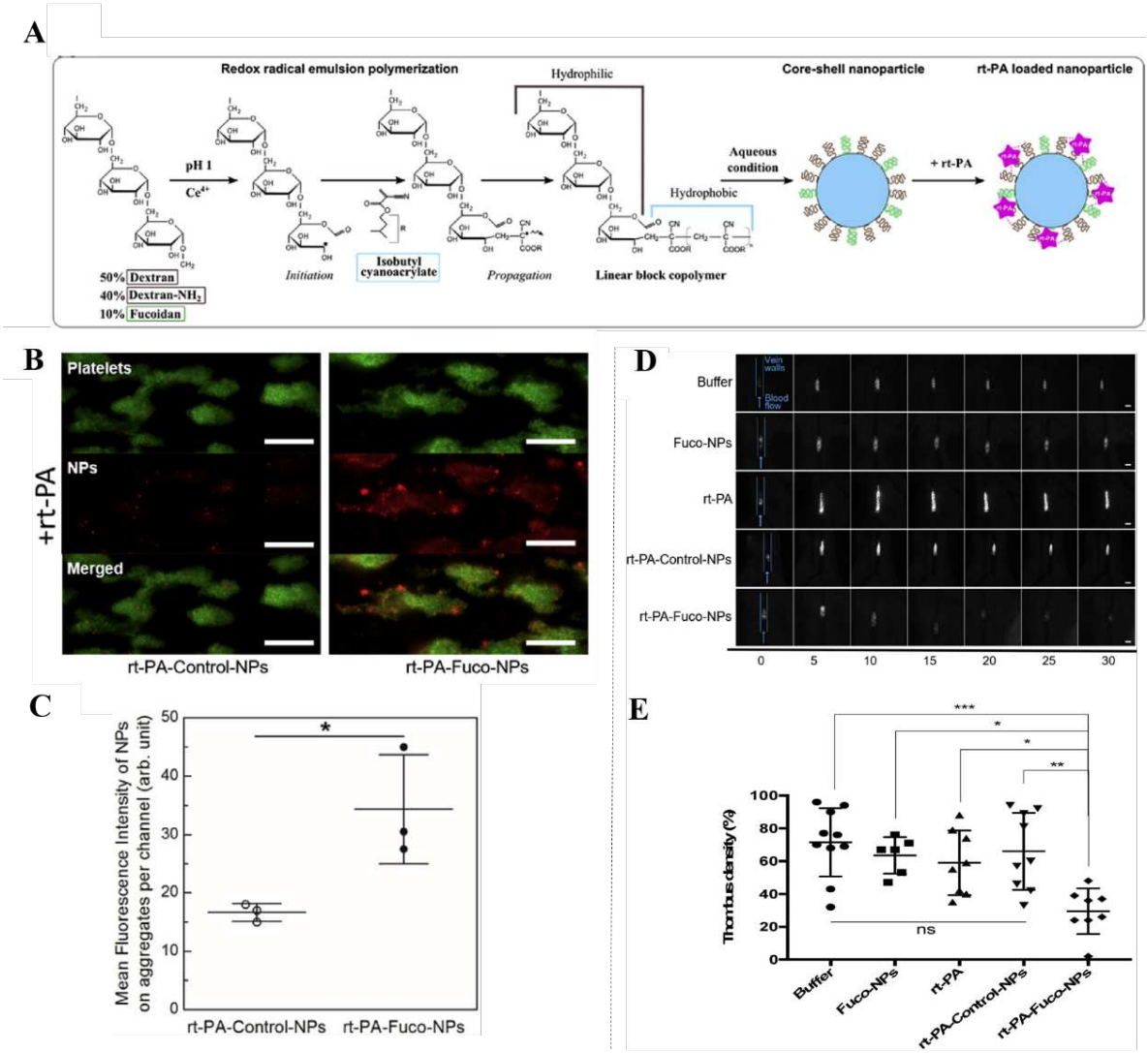


**Figure 6. Polymer NPs with fucoidan for venous thrombosis**. **A.** Formulation of fucoidan-functionalized NPs with rtPA. Cerium (IV) ions oxidize polysaccharide chains. The free radical initiates the radical emulsion polymerization of isobutyl cyanoacrylate monomers and create amphiphilic linear blocks copolymers that assemble into core-shell NPs in water. rt-PA interacts with the NPs by electrostatic interactions. **B.** The fluorescence image shows that rtPA-loaded NPs (in red) with fucoidan adhere notably more onto activated platelet aggregates (in green) than the particles without fucoidan under flow conditions (scale bar = 50 µm). **C.** Corresponding quantitative analysis of rt-PA-loaded NPs on platelet aggregates. **D.** Evaluation of thrombolysis efficiency in a mouse model of venous thrombosis at the rtPA dose of 2.5 mg/kg. Fluorescence images of thrombus evolution after treatment injection as determined by platelet accumulation at different times (scale bar = 200 µm). **E.** Corresponding quantitative analysis of the thrombus density at 30 min after injection. Adapted with permission from [67]. Copyright 2017 Elsevier Ltd.

*Polycaprolactone* (PCL). PCL is a non-toxic, biodegradable hydrophobic polyester approved by the FDA for several medical applications, including targeted drug delivery. Its

slow degradation profile under physiological conditions (from months to years) makes it attractive for long term drug delivery devices or implants [107].

Deng *et al.* synthesized the PEG-PCL NPs by single emulsion and solvent evaporation method and conjugated with rtPA via EDC/NHS [108]. rtPA preserved its amidolytic activity *in vitro* and remained active *in vivo* up to 3h. Despite some reduction in lytic activity in the *in vitro* blood clot test, rtPA-loaded NPs reduced the brain's infarct volume by ~70% compared with free rtPA at 1 mg/kg.

Pan *et al.* produced cationic micelles with a mean size of ~190 nm [109]. Polymeric micelles are a frequently employed class of NPs with a distinct core-shell structure that are self-assembled from amphiphilic components in an aqueous solvent. They were prepared with a mixture of polymers: polycaprolactone-block-poly(2-(dimethylamino)ethylmethacrylate) (PCL-PDMAEMA) – to form NP core, methoxy-PEG-PCL – to enhance the colloidal stability and biocompatibility, and PCL-PEG conjugated with RGDfk peptide – to target GPIIb/IIIa. The micelles adsorbed anionic lumbrokinase (LM) via electrostatic interactions [109]. They could target thrombus and exhibited thrombolytic potential *in vivo* with almost 2-fold reduced bleeding time vs. free LM, thus, mitigating hemorrhagic risks. Two years earlier, the same team published a work similarly dealing with LM-adsorbed micelles from triblock polymer – polycaprolactone-block-poly(2-(dimethylamino) ethyl methacrylate)-block-poly(2-hydroxyethyl methacrylate) (PCL-PDMAEMA-PHEMA) [110]. In a less common targeting strategy, Annexin V, a human phospholipid-binding protein that binds phosphatidylserine on the surface of activated platelets in a calcium-dependent manner and is proposed to play a role in the inhibition of blood coagulation [111], was conjugated to the micelles to target thrombi in a murine $FeCl_3$-induced model and perform the *in vivo* thrombolytic activity.

*Poly(2-oxazoline)* (POx). This hydrophilic biocompatible but non-biodegradable synthetic polymer features a stealth effect similar to PEG [107]. Gunawan *et al.* synthesized

smart multifunctional polymer microcapsules based on a brushlike POx with alkyne functional groups (B-PEtOx$_{Alk}$) polymer via layer-by-layer assembly on removable mesoporous silica templates [74]. uPA was encapsulated onto these microcapsules via electrostatic interactions ($6.4 \times 10^{-15}$ g uPA per capsule) and could be released upon exposure to thrombin owing to the thrombin-sensitive cross-linker peptide (ELTPRGWRLE). The NP surface-functionalization with a single-chain antibody (scFv) enabled a high affinity toward the GPIIb/IIIa on activated platelets in microfluidic flow channels.

*Poly(acrylic acid)* (PAA) is an anionic polyelectrolyte, a synthetic polymer of acrylic acid. PAA is not biodegradable, although it displays excellent biocompatibility and low toxicity [107].

Mei *et al.* successfully combined the thrombolytic and antioxidant strategy, incorporating 4-amino-2,2,6,6-tetramethylpiperidine-1-oxyl (4-amino-TEMPO) antioxidant into polyion complex NPs to eliminate Reactive Oxygen Species (ROS) after ischemia-reperfusion injury [48] **(Figure 7A)**. Self-assembled NPs were composed of anionic PAA, cationic poly(ethylene glycol)-b-poly[4-(2,2,6,6-tetra-methylpiperidine-1-oxyl) aminomethylstyrene] (PEG-b-PMNT) diblock amphiphilic copolymers, and rtPA. The NPs were colloidally stable due to the hydrophobic nature of the core-forming polycationic PMNT segment. Nanocomplexation extended the *in vivo* half-life of rtPA from 8.2 min to 71.2 min. The complex dissociation in the acidic pH, typical for the ischemia, released the drug. At rtPA dose 1 mg/kg, antioxidant-containing NPs improved neurological deficits, reduced cerebral infarct volume, decreased cerebral superoxide ROS and lipid peroxidation levels, as well as subarachnoid hemorrhage, contrary to free rtPA and antioxidant-free nanocomplex **(Figure 7B–G)**.

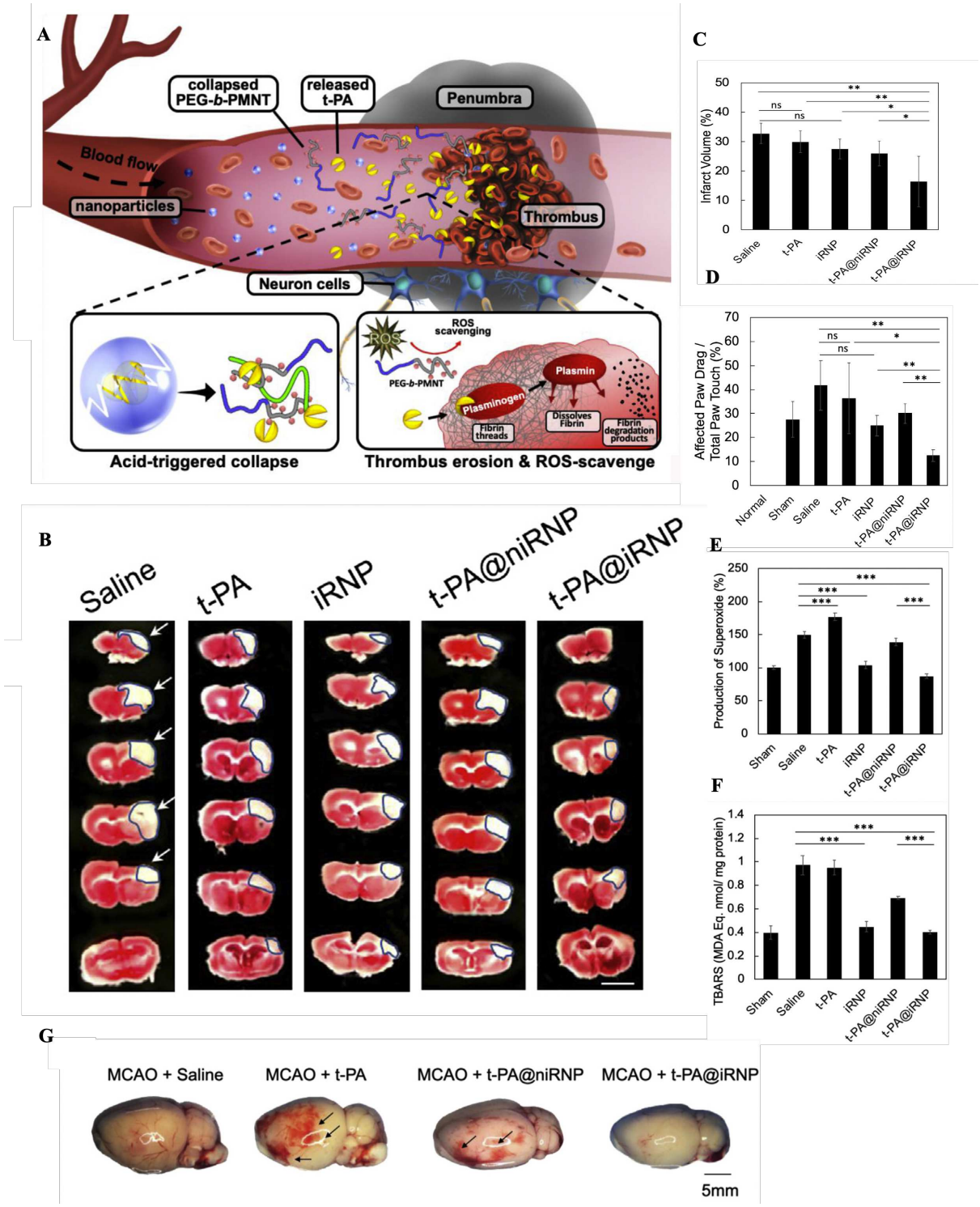


**Figure 7. Polymer micelle NPs with rtPA and antioxidant. A.** Graphical illustration of the mode of action of t-PA-installed polyion complex possessing ROS-scavenging moieties (t-PA@iRNP) in the thrombus: t-PA@iRNP collapse within the acidic ischemic penumbra region, release t-PA, perform thrombosis and antioxidant activity. **(B-G)** The therapeutic effect of t-PA@iRNP *in vivo* after middle cerebral artery occlusion (MCAO). **B.** Representative images of TTC stained cerebral coronal of the mouse brain, white sections indicate the brain infarct zones (scale bar = 0.5 cm). **C.** Corresponding quantification of cerebral infarct volume (%). **D.** Analysis of paw-dragging behavior in the cylinder test reveals a reduction in the neurological

deficit score for the t-PA@iRNP group. **E.** Treatment with t-PA@iRNP decreased cerebral superoxide levels, measured by dihydroethidium, at 24 h after injection. **F.** Treatment with iRNP and t-PA@iRNP reduced thiobarbituric acid-reactive substances (TBARS) level – index of lipid peroxidation in the brain – due to the antioxidant effect. **G.** Treatment with t-PA@iRNP suppressed t-PA induced cerebral subarachnoid hemorrhage (shown with arrows) with representative images at 24 h after treatment. Adapted with permission from [48]. Copyright 2019 Elsevier Ltd.

*Poly(amidoamine)* (PAMAM) is a class of dendrimers – nano-sized, radially symmetric artificial macromolecules with highly branched three-dimensional polymeric structure. Due to the multiple functional surface groups, they are commonly exploited for conjugation with pharmaceutical compounds. Mukhametova *et al.* developed PAMAM dendrimers containing ethylenediamine core with amidoamine internal structure and a primary amine terminal surface [112]. They were covalently grafted with SK by EDC/sulfo-NHS chemistry and preserved up to 85% of thrombolytic activity *in vitro* compared with free SK [112]. Nonetheless, the clinical use of the dendrimers is limited because of high toxicity, unknown biocompatibility, biodistribution, biodegradation, pharmacokinetic profile, and high cost of production [113].

To sum up, multiple excellent papers reported superior thrombolytic potential and favorable therapeutic outcomes with PA-loaded polymeric nanocarriers. These NPs are expected to prevail in thrombolysis research, considering their benefits: simple surface modification & functionalization, "smart" nanoparticulate design with controlled drug release, FDA-approval of some polymers that are both biodegradable and biocompatible.

## 5 INORGANIC NANOPARTICLES

### *5.1 MAGNETIC NANOPARTICLES*

Magnetic nanoparticles (MNP) are of great interest in thrombolytic drug delivery due to their large surface area, small particle size (1-100 nm), strong superparamagnetic properties that

permit their detection by MRI, excellent biocompatibility with low toxicity. Initially, MNP were introduced to the MRI field to overcome the low sensitivity of the standard imaging method. The assumption was to avoid the proton relaxation effect of MRI imaging with direct visualization of NPs containing iron oxide nanocrystals [114]. The system was functionalized with a fibrin-binding peptide that indicated promising results for MRI visualization of *in vitro* blood clots. MNP are usually composed of a metal core of magnetite $Fe_3O_4$ or maghemite γ-$Fe_2O_3$ and a functionalized shell. Co-precipitation and thermal decomposition are among the most widely studied synthesis methods for magnetic NPs. Aside from the typically used iron oxide, other magnetic elements such as Ni, Co, and their oxides can also be applied for NP manufacture. Cheng *et al.* [115] fabricated magnetic Ni nanorods via the oblique angle deposition method (physical vapor deposition technique). Hydrodynamic flows, induced by rotating nanorod suspension with rtPA by a pair of permanent magnets, enhanced rtPA mass transport and accelerated thrombolysis. Nevertheless, due to nickel toxicity, this technology cannot be translated into clinical settings.

Fibrinolytic drug-loaded MNPs can be concentrated at the thrombus under the external high-gradient magnetic field for targeted thrombolysis. Hu *et al.* [55] employed enzymatical (rtPA reaction) and mechanical clot lysis with rtPA-loaded rotating $Fe_3O_4$-C microrods (MRs) under an external magnetic field. These MRs were assembled from smaller particles with nanometric pores and possessed an average length L=1.3 μm and a diameter D=0.5 μm. rtPA-MRs under magnetic field recanalized occluded cerebral artery faster and at a lower dose than free rtPA group (25 min at 0.13 mg/kg vs. 85 min at 10 mg/kg) and diminished the post-stroke infarct volume *in vivo*. Despite the absence of liver and kidney toxicity of the MRs, they aggregated *in vitro* and required sonication to remain homogeneously dispersed in the suspension.

The drawback of uncoated magnetite NPs is that they are prone to oxidation and rapidly aggregate due to strong magnetic dipole-dipole attraction between particles, leading to a loss of magnetization. After the synthesis, a surface coating by $SiO_2$ or biopolymers is required to improve NP environmental stability, stealth effects, and prolong the blood circulation time. It may additionally provide a variety of high-capacity surface functional groups for bioconjugation of the molecules of interest.

Kempe *et al.* produced octahedral silica-coated $Fe_3O_4$ NPs for ferromagnetic implant-assisted magnetic drug targeting of in-stent thrombosis [116]. Silica coating enlarged the hydrodynamic size of the NPs from 10-30 nm to ~300 nm due to the tight aggregation of naked NPs. rtPA was immobilized onto NP surface via EDC/sulfo-NHS chemistry (71 μg rtPA / 1 mg magnetite NPs). In a preliminary experiment on the porcine brachial artery, rtPA-NPs were effective for magnetically guided lysis of in-stent thrombosis at a low rtPA dose of 0.38 mg. In another study [117], silica-coated magnetic nanoparticle ($SiO_2$-MNP), prepared by the sol-gel method, covalently grafted rtPA with a glutaraldehyde (0.5 mg/mL rtPA / 5 mg $SiO_2$-MNP). After nano-conjugation, the rtPA storage stability increased 9.5-fold in the PBS and 2.8-fold in whole blood. Time of thrombolysis of $SiO_2$-MNP-rtPA improved by 65% vs. free rtPA in the *ex vivo* intravascular model under magnetic guidance.

The high porosity of the silica coating promotes the encapsulation of the pharmaceutical drugs inside the pores. Wang *et al.* reported that silica-coated magnetic NPs, prepared by the surfactant templating, with an expanded 6 nm pore size permitted 30-fold more efficient uPA adsorption with sustainable drug release [118]. *In vitro* thrombolytic efficiency was 2-fold superior vs. free uPA and ~1.5-fold faster vs. uPA-loaded supermagnetic non-mesoporous silica NPs under 0.2 Tesla magnet. Yet, silica clinical application needs to be carefully regulated because of the hemolytic effect it might induce as it acts as a hydrogen donor in

interactions with cell membrane phospholipids and generates ROS [119,120]. Additionally, silica is shown to provoke an immune response by releasing pro-inflammatory cytokines [121].

Common in cancer therapy *in vivo*, hyperthermia was used as adjuvant therapy for thrombolysis by Voros *et al.* [75]. Multiple clustered iron oxide nanocubes (NCs), synthesized by a high-temperature thermal decomposition, were surface-coated with a mixture of rtPA and Bovine Serum Albumin (BSA) and produced a local overheating under alternating magnetic fields (295 kHz). rtPA release from NCs doubled at 42 °C from the one at 37 °C within 24 h.

The presence of functional amino and hydroxyl groups makes chitosan and its derivatives a suitable candidate for the magnetic NP surface coating. Chen *et al.* [122] prepared iron oxide MNP by the chemical co-precipitation and coated with chitosan as a dispersing agent. They immobilized rtPA by glutaraldehyde-mediated amide bond formation with loading efficiency 95% (0.5 mg rtPA / 5 mg chitosan-MNP), maintaining its enzymatic and thrombolytic activities *in vitro*. *In vivo* rat arterial embolic model further evidenced tissue perfusion after treatment of 6,000 G magnetically guided Cs-MNP-rtPA at a dosage of 0.2 mg/kg but not of saline. Alternatively, chitosan coating of $Fe_3O_4$ MNPs was achieved by crosslinking with sodium tripolyphosphate via ionic gelation in the presence of rtPA [123]. On top of targeted magnetic delivery, rtPA-encapsulated NPs unveiled a triggered release: in serum at 37 °C, but not in PBS, that was on/off magnet-sensitive that could be retarded in the presence of a magnetic field. According to the *in vivo* study on the rat embolic model, rtPA-NPs restored blood flow at rtPA dose of 2 mg/kg under magnetic guidance in contrast to NP administration alone.

Dextran, complex branched glucose, is largely used in the coating of MNP. Magneto-fluorescent crosslinked dextran-coated iron oxide (CLIO) NPs targeted arterial and venous thrombi *in vivo* via an activated factor XIII (FXIIIa)-sensitive peptide (GNQEQVSPLTLLKC-NH2) [68]. These theranostic NPs generated optical imaging with NIR VivoTag 680

fluorophore and were covalently functionalized with rtPA via PEG. Thrombolytic efficiency was comparable to the one of free rtPA in the humanized mouse model of pulmonary embolism.

Cytocompatibility of dextran-coated superparamagnetic iron oxide NPs (SPIONs) on human umbilical vein endothelial cells (HUVECs) (~85% cell viability) without changes in mitochondrial membrane potential, a DNA degradation or cell cycle alteration was stated by Heid *et al.* [124]. When comparing an adsorptive or covalent (EDC/NHS) method to load an arginine-purified rtPA, >80% loading efficiency was achieved for both approaches. Yet, SPIONs with covalently bound rtPA were more efficient to be targeted by a 0.4 Tesla magnet into fibrin clot and perform a local *in vitro* thrombolysis.

Owing to its natural, biodegradable, and non-toxic character, agarose, a linear polysaccharide extracted from red seaweed, is applied in diverse biotechnological applications. Agarose gel-coated $Fe_3O_4$ NPs were covalently grafted with uPA via EDC/sulfo-NHS [125]. Urokinase-loaded NPs increased the thrombolytic rate by 50% in the *in vitro* blood clot assay vs. free uPA, as well as in a microfluidic test under static magnetic field of 624 A/m.

Prilepskii *et al.* [126] crosslinked MNPs with heparin, FDA-approved polysaccharide with anticoagulant activity, and adsorbed uPA with encapsulation of 99% **(Figure 8A)**. The size of the resulting nanocomposite was around 100 nm **(Figure 8B)**. Without the inhibitory effect of the heparin on uPA, the thrombolysis rate amplified in the presence of a permanent magnet *in vitro* (12 min vs. 7 min for 60% clot reduction) **(Figure 8C)**. In the $FeCl_3$ rat carotid artery and rabbit femoral artery models, the MNPs@uPA group speeded reperfusion time and increased blood flow rate ~4 times compared to that of native uPA **(Figure 8D & E)**.

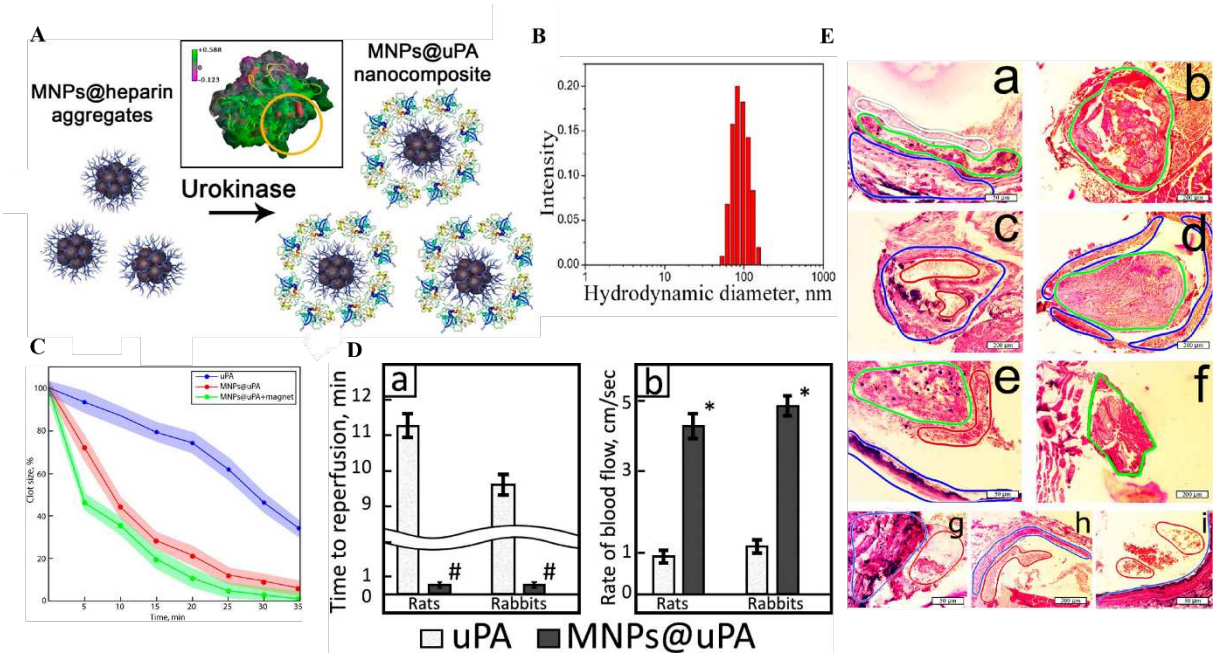


**Figure 8. Example of heparin-coated MNPs in thrombosis. A.** Schematic of the adsorption of uPA to the heparin-coated MNPs to obtain MNPs@uPA. Inset: 3D structure of urokinase with colored electrostatic potentials. Kringle domains responsible for interaction with heparin are in orange. **B.** The hydrodynamic diameter of MNPs@uPA composite. **C.** *In vitro* clot lysis rate upon exposure to uPA and MNPs@uPA with or without a magnetic field. The difference in the thrombolysis for MNPs@uPA with and without magnet within the initial 25 min is statistically significant ($p < 0.05$). **D.** Restoration of blood flow *in vivo* of uPA and MNPs@uPA. (a) Time to vessel reperfusion. (b) Rate of blood flow 24 h post-injection. **E.** Sections of the rat carotid artery and (g–i) rabbit femoral artery 24 h post-clot formation. Colors: blue, vessel walls; red, erythrocyte aggregates; green, red clot; white, white clot. (a, b, g) Saline. The clot tightly adhered to the vessel wall observed in (a) (marked in green). The vessel fully occluded by the clot (encircled in green) presented in (b). (c, d, h) uPA. Note a clear vessel lumen space between the clot (green) and the vessel wall (blue) in (d). (e, f, i) MNPs@uPA. Note a bigger free space in the vessel lumen and reduced size of the clot in (f) and (i). (a, c, e, g–i): H&E staining. (b, d, f): Picro-Mallory staining. Adapted with permission from [126]. Copyright 2018 American Chemical Society.

The synthetic polymer coating is similarly explored for the preparation of magnetic field-responsive and biocompatible NPs. Huang *et al.* [127] stabilized MNPs with PAA by providing electrostatic and steric repulsion and loaded rtPA via EDC/NHS due to PAA abundant carboxyl groups. The clot lysis efficiency of MNP-rtPA was improved under the rotating magnetic field compared to free rtPA *in vitro*. Besides, MNP-rtPA diminished the brain

infarct area in the distal cerebral occlusion *in vivo* model vs. free rtPA (8.65 ± 3.63 $mm^3$ vs. 4.40 ± 2.46 $mm^3$).

Another publication compared covalent vs. non-covalent methods of rtPA loading to polyacrylic acid-co-maleic acid (PAM)-coated SPIONs [128]. Better loading efficiency was reported with a covalent method vs. adsorption (98.6 ± 0.8 % vs. 47.7 ± 5.4 %). Amidolytic and fibrinolytic activities on the PAM-SPIONs with covalent loading were superior and better preserved after 40 days of storage. Hence, the covalent binding of the rtPA was advantageous for the application with SPIONs.

Hung-Wei Yang *et al.* [129] synthesized the magnetic nanocarriers (MNCs) with a water-soluble poly [aniline-co-N-(1-one-butyric acid) aniline] (SPAnH) shell that could load a high amount of rtPA via 1-ethyl-3-(3-dimethylaminopropyl)carbodiimide / N-hydroxysuccinimide (EDC/NHS) chemistry (276 µg rtPA per 1 mg MNC). Magnet-guided MNC-rtPA demonstrated significantly improved thrombolysis in rat iliac embolism model at 0.2 mg/kg rtPA dose.

### *5.2 GOLD NANOPARTICLES*

Gold nanoparticles (AuNPs) benefit from diverse optical and photothermal properties. They are synthesized by the reduction of gold salts to gold metals in the presence of stabilizing agents to prevent aggregation during NP formation, and their tunable size modulates their toxicity and biodistribution. Gold NPs can be applied in photothermal therapy in cancer [130] as well as in drug delivery. Moreover, AuNPs are characterized by their high X-ray absorption coefficient enhancing CT signal. The quantitative imaging method *in vivo* was established to monitor the thrombolysis with rtPA using fibrin-targeted glycol chitosan-coated gold NPs [131]. Direct discrimination of thrombi from the underlying tissue was obtained with gold NPs conjugated with a thrombin-activated fluorescent peptide that discharged a near-infrared signal (NIRF)

when cleaved [132]. This dual NIRF/micro-CT imaging protocol was tested *in vivo* and suggested a high spatial resolution for a rapid and direct thrombi diagnosis. Indeed, gold NPs represent an exciting perspective to overcome the pitfalls of standard imaging protocols and might better triage patients according to their thrombotic conditions.

Gold nanoparticles are similarly capable of delivering large biomolecules, like plasminogen activators. Tang *et al.* conjugated rtPA with AuNPs with a diameter of 37.8 nm via bio-affinity ligation based on the interactions between rtPA and 3-lysine ligand on the AuNPs surface through polyvinyl pyrrolidone (PVP) spacer [51]. Notably, obtained conjugate indicated protection from inhibition by PAI-1 *in vitro* by pre-incubation with the enzyme and prolonged circulation time *in vivo* (6.5 min vs. 20.5 min). Another intelligent nanoplatform for hyperthermia-induced thrombolysis was documented by Wang *et al.* [47]. Gold@mesoporous silica core-shell nanospheres immobilized uPA in the pores by a solid 1-tetradecanol (tet) **(Figure 9A)**. Owing to hyperthermia caused by Au absorption of NIR under NIR laser irradiation, tet transformation to liquid phase stimulated a temperature-sensitive controlled release of uPA, whereas only 10.5% of the drug was released at 37°C vs. 89.5% at 39°C **(Figure 9B & C)**. In the carrageenan-induced murine tail thrombus model, the NIR-irradiated uPA-NPs group enhanced the thrombolytic effect ~2-fold vs. free uPA **(Figure 9D)**.

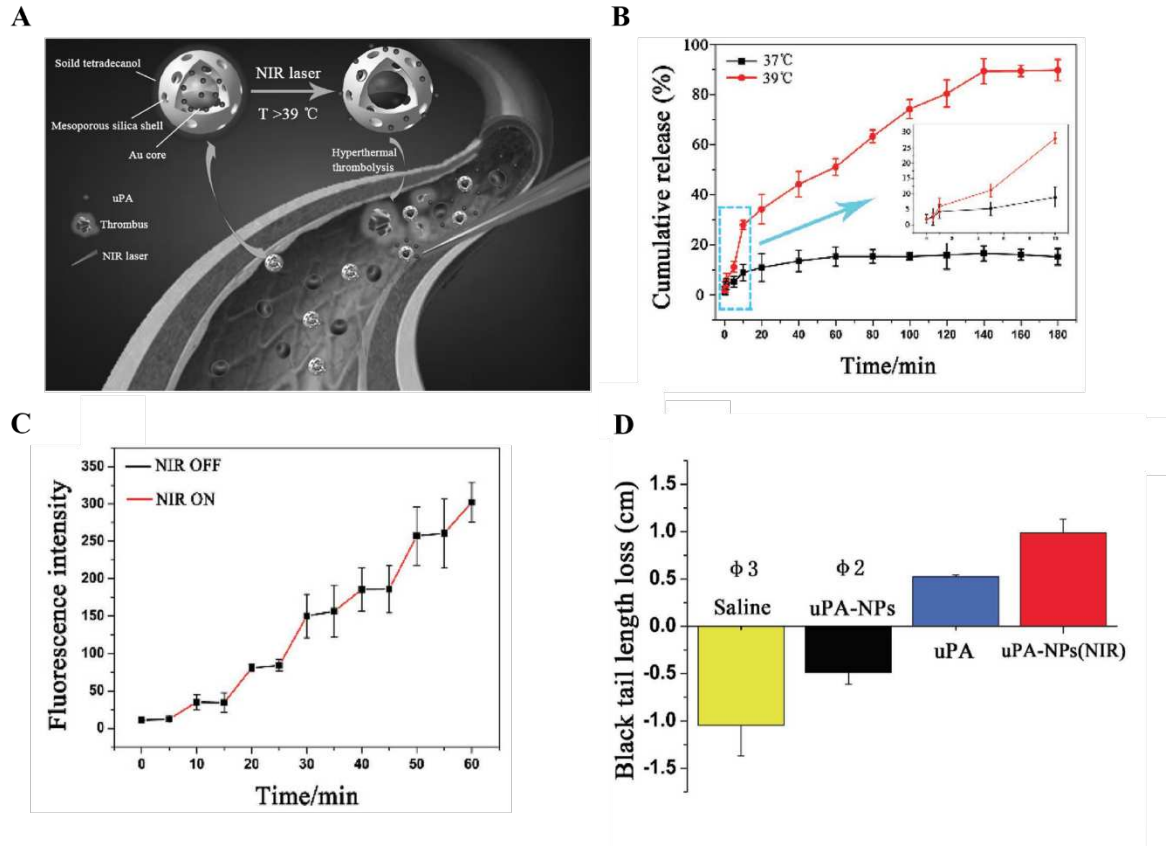


**Figure 9. Enhancement of thrombosis via hyperthermia. A.** Schematic illustration of the hyperthermia-induced enhanced thrombolysis with uPA-immobilized gold@mesoporous silica nanospheres. **B.** *In vitro* release profiles of fluorescent uPA from uPA-NPs at 37 °C and 39 °C, respectively. The enlarged release profile in 10 min is shown in the inset graph. **C.** NIR laser triggers pulsed uPA release profile *in vitro* of fluorescent uPA-NPs. **D.** *In vivo* thrombolysis in murine tail thrombus model via injecting carrageenan. The statistical black tail length loss (thrombolytic effect) of mice after treatment for 9 days, where φ represents the amputated tail, and the number represents the number of mice with the amputated tail. Adapted with permission from [47]. Copyright 2017 WILEY-VCH Verlag GmbH & Co. KGaA, Weinheim.

In conclusion, several remarkable concepts of inorganic PA-bearing NPs for targeted thrombolysis were published in the last 10 years that have the potential to become theranostics. Although most MNP rely on magnet-assisted accumulation on the thrombus, this targeting approach seems to be tricky to accomplish in healthcare settings. An interesting application of inorganic NPs is hyperthermic exposure as adjuvant therapy to fibrinolytic therapy. Nevertheless, it must be remembered that NPs from inorganic materials are difficult to degrade

*in vivo,* and they persist for extended periods (more details on safety and metabolism in Section 7.1).

## 6 BIO-INSPIRED NANOCARRIERS

Nature inspires the development of nanotechnological solutions in drug-delivery systems. Bio-inspiration and biomimicry technologies can not only simulate biological materials by their chemical structure but also by their biological functions [133].

*Camouflage*. An elegant strategy to reduce thrombolytic drug elimination and increase its plasma half-life is camouflaging it as endogenous proteins. This approach was demonstrated by Absar *et al.* [134] when the targeted/triggered release of rtPA was mediated by the presence of thrombin in the thrombus. rtPA was camouflaged by conjugating with human serum albumin (HSA) via a thrombin-cleavable peptide (tcP) and decorated with a homing-peptide targeting GPIIb/IIIa. This construct permitted to temporarily suppress the enzymatic and fibrinolytic activities of camouflaged rtPA, however, to spontaneously restore it upon incubation with thrombin by the cleavage of the peptide linker.

*Red blood cell (RBC)-derived nanocarriers*. Erythrocytes are recognized for their extended blood circulation as they manage to avoid clearance by the macrophages for up to 3 months. A number of factors are believed to contribute to that, including their discoidal shape, deformability, and the expression of self-recognition biomarkers, such as CD47 and CD200 [133,135]. RBC seem to be a particularly promising carrier of thrombolytic drugs that exert their pharmacological activity within blood vessels.

Vankayala *et al.* [136] designed theranostic nanoconstructs for NIR fluorescence imaging and thrombolytic activity. Specifically, after hypotonic treatment of RBCs, obtained erythrocyte ghosts were coupled with indocyanine green, FDA-approved NIR imaging agent, and conjugated with rtPA via amine-aldehyde chemistry. Their thrombolytic efficacy was

comparable to the free rtPA *in vitro*. Erythrocytes have already reached clinical trials as nanocarriers for drug delivery (Clinicaltrials.gov Identifiers: NCT01255358, NCT01171807, NCT00484965) but not in thrombolytic therapy yet [133].

*Platelet-like nanocarriers*. Platelet membrane-camouflaged PLGA-core NPs, conjugated with rtPA, were recently proposed as a biomimetic technique by Xu *et al.* [76]. These so-called "nanoplatelets" behave like platelets in the blood circulation **(Figure 10A & B)** and bind to the thrombus *in vitro* and *ex vivo*. rtPA-NPs treatment was beneficial in multiple *in vivo* models: improved the mouse survival time from 4-7 days to 14.5 days and ~4.5-fold reduced the thrombus area vs. free rtPA in the pulmonary embolism model **(Figure 10C & D)**; stimulated complete thrombus removal contrary to free rtPA in the $FeCl_3$-induced mesenteric arterial model. Notably, post-thrombolytic brain damage was weaker for the rtPA-NPs group as defined by a lower neurological deficit score and smaller ischemic area in the ischemic stroke mouse model, as depicted in **Figure 10E-G**.

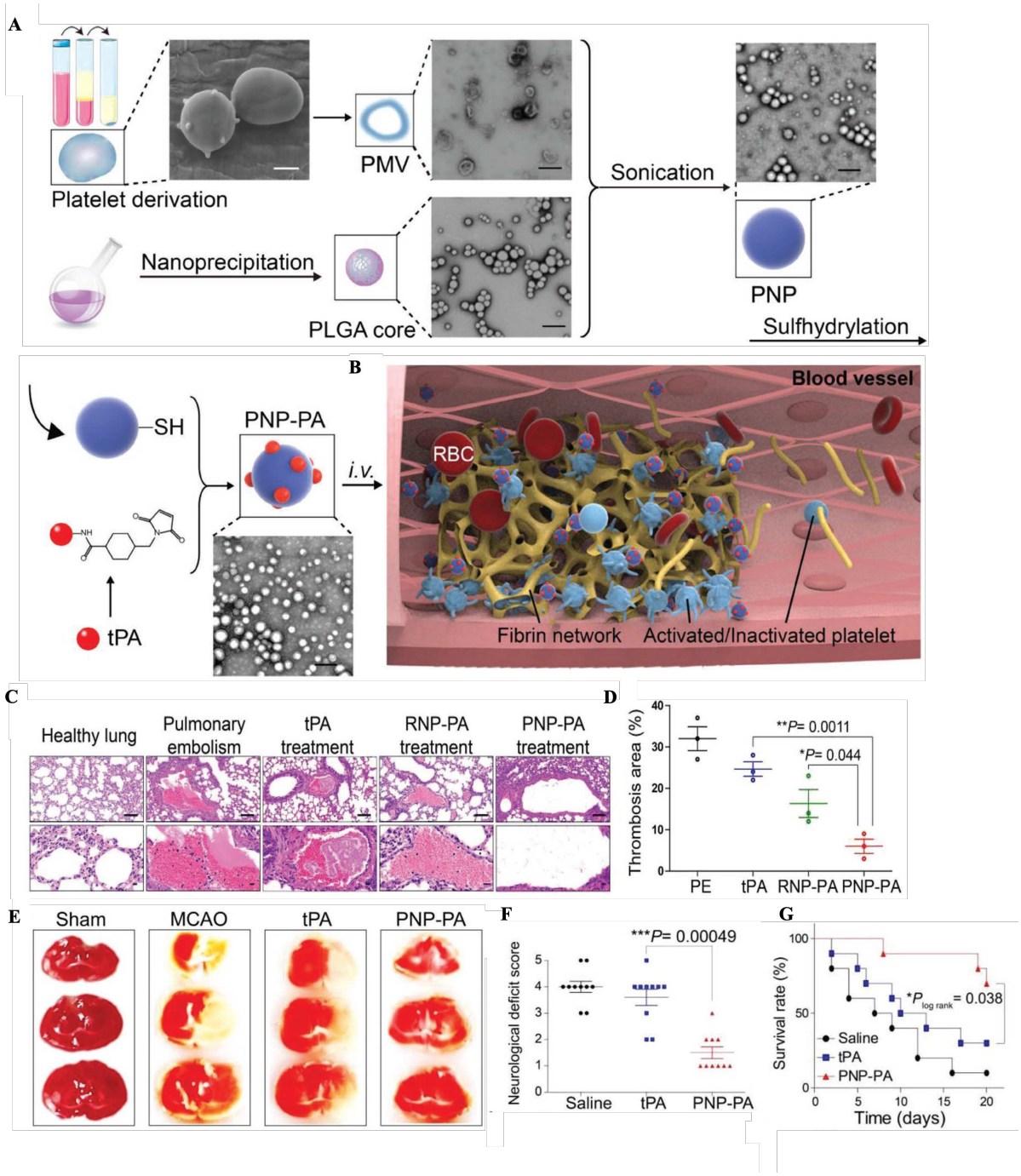


**Figure 10. Nanoplatelets as an efficient carrier of rtPA in multiple thrombosis models. A.** Schematic illustration of the synthesis of PNP-PA NPs. Briefly, the membrane of platelets (scale bar = 1 μm), acquired from the whole blood of mice, were used to coat the PLGA cores (scale bar = 400 nm). t-PA was subsequently conjugated via –SH groups onto the surface of the platelet membrane to form PNP-PA. **B.** The proposed mechanism of action *in vivo*: mimicking platelets, PNP-PA are specifically targeted to the thrombus and dissolve the fibrin clot. **C.** Therapeutic potential of PNP-PA in a pulmonary embolism mouse model. Lung sections with H&E staining administered the indicated treatments (scale bar = 50 μm). **D.** Quantitative analysis of the thrombus area in panel C. **E-G.** Therapeutic effects of PNP-PA in the ischemic stroke mouse model. **E.** Representative TTC staining images of MCAO mouse brains treated with the indicated formulations. **F.** Neurological deficit scores in the treatment

groups of MCAO mice. **G.** The survival rate of MCAO mice treated with the mentioned formulations. Adapted with permission from [76]. Copyright 2019 WILEY-VCH Verlag GmbH & Co. KGaA, Weinheim.

There has been a growing interest in exploring neuroprotective strategies following acute ischemic stroke to reduce brain injury [137]. Another version of the "nanoplatelets" was proposed as a combinational approach for the treatment of acute ischemic stroke based on thrombolysis and neuroprotection [138]. The NPs with a size of ~150 nm contained the core of acetal modified dextran & neuroprotective agent and were covered with a platelet membrane conjugated with thrombin-cleavable Tat-peptide (Tat-LTPRGWRLGGC) that coupled rtPA **(Figure 11A)**. In this nanodesign, rtPA could be released upon thrombin presence while exposing Tat-peptide on the NPs and penetrating the blood-brain barrier (BBB) for neuroprotectant delivery in the brain **(Figure 11B & C)**. In the *in vivo* model of middle cerebral artery (MCA) occlusion, a treatment with this nanocomplex decreased infarct size by 63%, ameliorated neurological deficit, and diminished ROS level of the ischemic region by 52% compared to the free drug combination **(Figure 11D-F).**

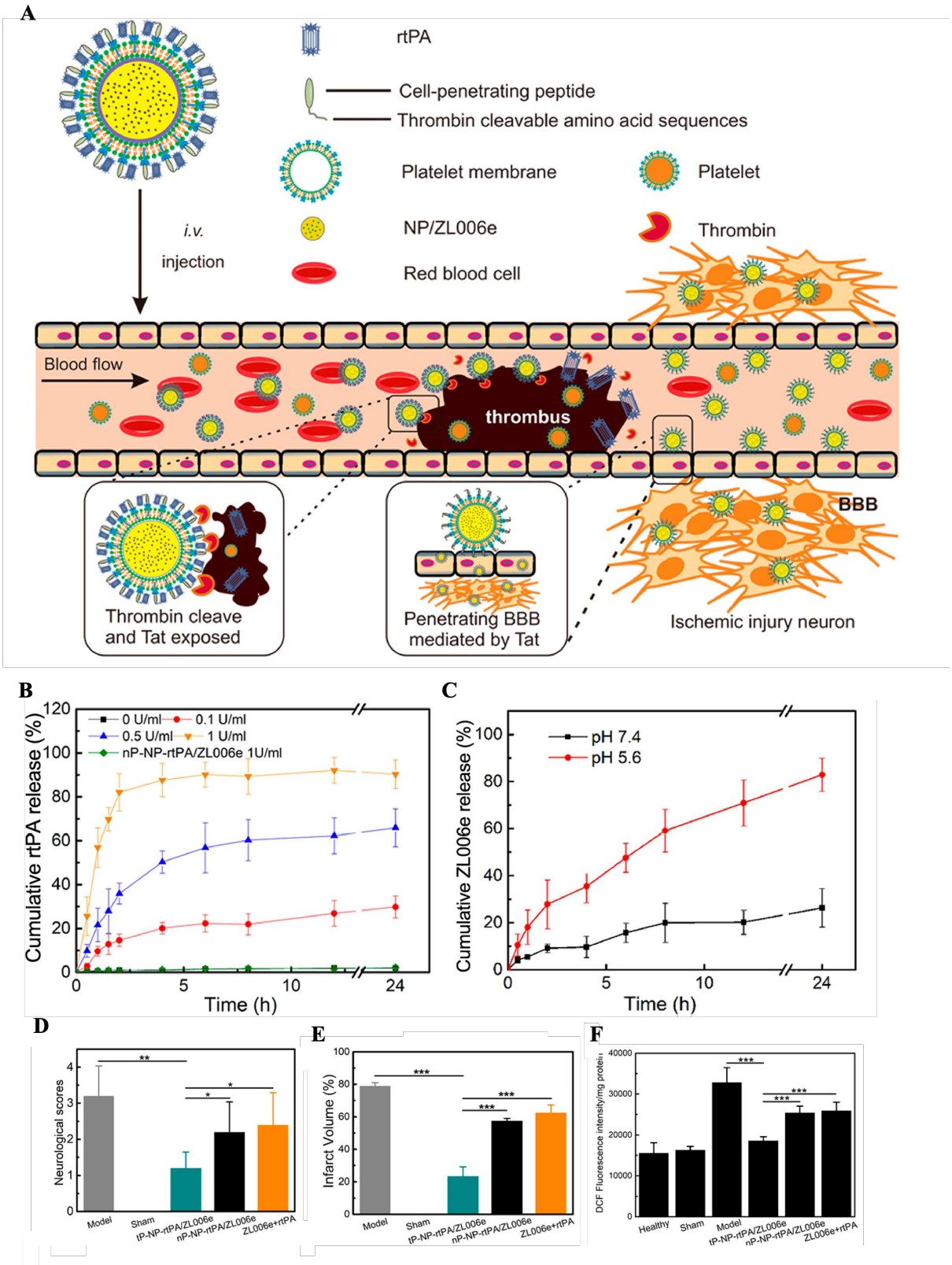


**Figure 11. Synergic effect of neuroprotection and thrombolysis using nanoplatelets. A.** Schematic design of tP-NP-rtPA/ZL006e and its components and mode of action. After intravenous injection, tP-NP-rtPA/ZL006e are targeted to the thrombus for thrombin-triggered release of rtPA and thrombolysis. Nanocarrier transport into the brain via Tat-mediated

transcytosis for neuroprotective activity. **B.** Cumulative release of rtPA from tP-NP-rtPA/ZL006e with different thrombin concentrations. nP-NP-rtPA/ZL006e are the control particles in 1 U/mL thrombin. **C.** *In vitro* neuroprotective effect of tP-NP-rtPA/ZL006e and nP-NP-rtPA/ZL006e with or without thrombin and free ZL006e+rtPA via the coculture model of the BCEC monolayer and glutamate-stimulated PC-12 cells. **D.** Neurological scores of the MCAO rats after the treatment. **E.** Quantification of brain infarct volume/ischemic brain hemisphere at 24 h post-treatment MCAO rats. **F.** ROS level in the ischemic region. Adapted with permission from [138]. Copyright 2019 American Chemical Society.

*Leukocyte-derived microvesicles*. Cell microvesicles that originate from the plasma membrane of most cell types, including blood cells, are essential effectors in intercellular communication and may transport bioactive molecules [139]. Silva *et al.* reported an unconventional method when microvesicles (D = 673 ± 168 nm), secreted from macrophages upon serum depletion cellular stress, were capable of enclosing both iron oxide NPs and rtPA [140]. The work exemplified a biogenic strategy of theranostic application of hybrid microvesicles for MRI imaging and spatially-controlled rtPA delivery via magnetic field gradient targeting.

*Bacterial spores*. In another bio-inspired approach, the spores of bacterium *Bacillus amyloliquefaciens* with peptidoglycans on their surface were prior inactivated with a high-pressure steam sterilizer and used as nanocarriers with uPA and RGDS peptide [141]. The solid monodisperse oval spheres ([0.67 ± 0.20 μm] × [1.27 ± 0.20 μm]) were non-biotoxic following histological evaluation of the heart, kidneys, and liver. With a higher thrombolysis rate *in vitro*, *in vivo* tail bleeding times of the uPA-NPs group were shorter than that of free uPA (601 s vs. 1,145 s), suggesting a lower risk of hemorrhages.

*Viral nanoparticles*. Based on bacteriophages and plant viruses, viral nanoparticles (VNPs) are biocompatible, biodegradable, and nonpathogenic nanocarriers in humans. Because of the remarkable proliferation of viruses, they could be easily manufactured up to an industrial scale. In the NPs based on the tobacco mosaic virus, the nucleic acids are tightly enclosed in a stiff hollow tubular capsid comprising coat proteins [142]. To develop a nanocarrier with

optimal flow properties for thrombolytic therapy, Pitek *et al.* conjugated rtPA to tobacco mosaic virus mutant soft elongated nanorods containing lysine side chain (TMV-Lys) via PEG linkers, obtaining the NPs with dimensions of 300 × 18 nm [143]. TMV-rtPA could passively accumulate at the thrombus at a higher rate than TMV-PEG *in vivo*. Both rtPA and TMV-rtPA resumed the circulation in the mouse thrombosis model, but TMV-rtPA reduced bleeding time ~2-fold vs. free rtPA. Despite an absence of pathogenicity, the potential immunogenicity of nanodelivery systems based on pathogens such as bacteria and viruses should be not be neglected.

To conclude, biomimetic delivery systems have the countless potential for the advancement of drug delivery technologies. The reproduction of the biological complexity on nanocarriers' surface imitates biological features, like biocompatibility, targeting the thrombus tissue, efficient circulation profiles, *etc*. To be suitable for clinical translation, both toxicological (e.g., safety, immunogenicity) and pharmaceutical (e.g., reproducibility, scale-up, standardization of chemical composition) concerns have to be examined [144].

## 7 NANOPARTICLE OPTIMAL DESIGN FOR THROMBOLYTIC THERAPY

### *7.1 PHARMACOKINETICS, BIODISTRIBUTION, AND SAFETY*

After the intravenous administration, nanocarriers for fibrinolytic therapy are subjected to biological barriers and might pose particular safety concerns that would limit a desirable therapeutic outcome. What would be an optimal nanoparticle design to incorporate in order to load plasminogen activator and perform a safe and efficient local thrombolysis?

Primarily, favorable *in vivo* biodistribution and pharmacokinetics of the injectable inorganic, lipid, and polymeric micelle/nanoparticle must be ensured. Particle *in vivo* fate is varied and dictated by the interaction between multiple parameters: nanoparticle size, surface

characteristics, stability, *etc*. For site-specific accumulation of the thrombolytic agent, NPs need to have sufficient circulation time *in vivo*. Ultra-small NPs with diameters < 5.5 nm are rapidly filtered out by renal clearance upon intravenous administration [145]. The elimination of the larger engineered NPs by the MPS represents a substantial obstacle. Plasma proteins, including serum albumin, apolipoproteins, complement components, and immunoglobulins, bind onto the surface of circulating NPs and form the protein corona in a process called particle opsonization [146]. Subsequently, phagocytic cells of MPS – mainly resident macrophages in the spleen, lymph nodes, and liver – sequesters the NPs. There is an evident direct correlation between particle size and serum protein absorption, meaning faster elimination [147]. Typically, rigid spherical NPs with a size of 100–200 nm are long-circulating, being large enough to avoid uptake in the liver but small enough to avoid filtration in the spleen [135]. Particles in the micrometer range (2–5 μm) accumulate within the capillaries of the lungs, as well as in the spleen and liver [33]. The shape of the particles dramatically affects their *in vivo* destiny, as demonstrated in the filamentous polymer micelles that persisted in the circulation for up to one week after the intravenous injection – 10 times longer than the spherical ones [148]. In addition, softer, prone to deformability, NPs have prolonged circulation profiles than solid ones with reduced splenic filtration, as investigated in the nanogels with different crosslinking levels [149]. Irrespective of the size and shape, softer nanoconstructs evaded up to 5 times more efficiently macrophage internalization as compared to rigid nanoconstructs [150].

The biodistribution of nanomaterials is influenced by their surface characteristics. NPs with a neutral and negative surface charge, in contrast to cationic formulations, experience reduced protein adsorption that results in more extended circulation half-lives [33]. Other concerns of the cationic NPs are the stimulation of inflammatory responses of human neutrophils and increased ROS production that was demonstrated on the cationic liposomes

[151] and solid lipid NPs [152]. Cytotoxicity was induced by both cationic polymeric and lipid NPs [153]. In addition, positively charged NPs have a high cellular uptake rate, as revealed that polymeric microparticles with a primary amine at the surface underwent more phagocytosis than those with sulfate, hydroxyl, or carboxyl groups [147]. This makes cationic NPs a suitable vehicle for gene delivery; however, it would probably be preferred to design anionic nanoformulation for thrombolysis.

To avert the opsonization of the naked circulating NPs, their surface can be functionalized with PEG to create a hydrating layer that hinders the formation of a protein corona [33]. In addition to prevalent PEG, which is non-biodegradable and may cause complement activation, alternative hydrophilic polymers, such as poloxamer, polyvinyl alcohol, poly(amino acid)s, and polysaccharides [154] as well as "self" peptide CD47 [155] are researched. As a biomimetic surface, the coating of NPs with cell membranes extracted from autologous leukocytes and red blood cells similarly extends their *in vivo* circulation [133].

These findings collectively demonstrate the importance of tunable particle size and surface composition & functionality to develop long-circulating NPs for thrombolysis.

While the full analysis of the toxicology of NPs is beyond the scope of this Chapter, it is necessary to comment on certain safety issues of the nanomaterials used for a thrombolytic application.

NPs can perturbate vascular hemostasis and blood platelet function. Saikia *et al.* reported that silica NPs induced the overexpression of platelet endothelial cell adhesion molecule-1 on the endothelium that augmented the platelet-endothelial interaction [156]. Moreover, silica NPs triggered inflammation-coagulation response and thrombotic effects *in vivo* via JAK1/TF signaling pathway [157]. Amorphous silica NP penetrated the platelet plasma membrane and stimulated an unfavorably low nitric oxide to peroxynitrite [NO]/[$ONOO^-$] ration that is crucial for cardiovascular homeostasis; they also induced platelet

activation and aggregation via the MMP2 and ADP pathways [158]. Increasing concentrations of gold NPs led to a reduction in mouse body weight, red blood cell count, and hematocrit [159].

Multiple publications reported nanoparticle size-dependent toxicity. For instance, smaller gold, $SiO_2$, or polymer NPs were more hemolytic and provoked higher ROS production levels than larger particles [160]. Cytotoxicity in four different cell lines was observed with the triphenylphosphine-stabilized gold NPs of 1-2 nm diameter, while 15-nm particles were non-toxic even at 100-fold higher concentration [161]. In a size-dependent manner, PEGylated AuNPs affected the normal function of human erythrocytes, such as deformability and oxygen-delivering ability [162]. Alterations of renal, hepatic, and splenic functions were dependent on the particle size and surface chemistry in ultrasmall superparamagnetic iron oxide NPs [163].

Distribution of the NPs in the non-target cells and organs is one of the challenges. The report of Lasagna-Reeves *et al.* suggested that gold NPs were able to cross BBB and accumulated in the neural tissue [164]. Poly(alkyl cyanoacrylate) NPs could enter into the brain both in healthy animals and models of central nervous system diseases [165]. Siddiqi *et al.* concluded that AuNPs generated oxidative stress and an impairment of the antioxidant enzyme glutathione peroxidase in rat brain as well as significantly decreased the levels of dopamine and serotonin neurotransmitters [166]. Given that the BBB integrity is disrupted during ischemic stroke [167], and nanoformulation is assumed to limit the accumulation of nanoparticle-associated rtPA within the brain parenchyma to reduce the risk of cerebral hemorrhages and rtPA-mediated neurotoxicity [168], it would be vital to ensure that the nanotherapeutics are retained within the vascular compartment and do not cross the BBB.

The nanomaterials accumulate substantially in the liver upon intravenous injection. Bartneck *et al.* found that peptide-functionalized gold nanorods induced the prepolarization of hepatic macrophages, which aggravated a liver injury in a model of acute hepatitis [169]. High

doses of silica nanorattle particles could induce liver damages, presumably due to decreased activity of superoxide dismutase [170]. Treatment with silica NPs revealed the hepatic microgranulation and splenic megakaryocyte accumulation by histological analysis [171]. Iron oxide NPs accumulated in liver phagocytes and elicited hepatic lipid peroxidation [172].

Organic biodegradable engineered NPs are likely of lesser concern to toxicity, as they degrade by metabolic pathways. While the *in vitro* tests indicated that amphiphilic polymeric micelles induced an inflammatory response, no pathological changes were observed in the target organs *in vivo* [173]. Both PLGA and Cs NPs at concentrations relevant for drug-delivery application (<10 μg/mL) were platelet-compatible [174].

In contrast, inorganic non-biodegradable NPs, including multifunctional magnetic NPs, may persist for considerable periods, sometimes up to several years [175], resulting in prolonged exposure with still-to-be-determined consequences. Apart from that, the growing presence of non-degradable nanotechnology products and the environmental risks need to be seriously assessed [176]. NPs composed of inorganic materials are difficult to break down by lysosomal enzymes. As an example, AuNPs accumulation in Kupffer cells in the liver and lysosome/endosome-like vesicles was present after six months post-injection in mice [177]. Moreover, Feng *et al.* found that dextran-coated and uncoated SPION administration affected several metabolism pathways, including energy, lipid, glucose, and amino acid metabolism in rodents [178]. PAA-coated iron oxide NPs triggered an inflammatory process *in vivo*, evidenced by abnormal differential blood count of neutrophils and large lymphocytes [172]. $Fe_3O_4$-MNPs significantly augmented ROS production *in vivo*. A sharp decline in RBC counts and hemoglobin concentration indicated an excessive degradation of erythrocytes, suggesting an associated anemia risk [179].

Higher metabolic and functional injuries are generally prompted by uncoated NPs compared to coated ones with potential aggregation in the biological fluids. Surface

modification with polymeric chains ameliorates the nanoparticle stability, masks the existing toxicity of the NPs, and extends their circulation half-life [121,180]. It is worth admitting that the NPs do not exhibit any toxicity until a certain threshold dose [121]. During the preclinical thrombolytic evaluation, it is also essential to verify that the required dose of the NPs is based on estimates of potential future human exposure to avoid unrealistically high nanoparticle doses with no relevance to the clinics. Overall, this is critical to evaluate each newly engineered NPs as an individual case since even slight changes in physicochemical properties to an existing and well-studied particle can result in a completely different toxicological profile.

### *7.2 STRATEGIES FOR THE NANOENCAPSULATION OF PA*

PA are hydrophilic macromolecules (40-70 kDa) that require special nanoparticle design and drug complexation methods. While PA can be incorporated into the aqueous phase during nanoparticle fabrication for lipid or polymeric particles, harsh synthesis conditions – high energy processes (ultrasound, ultraturrax), elevated temperatures, the use of organic solvents – are not suitable for fragile molecules such as proteins [181]. Otherwise, the fibrinolytic agent may be attached to the surface through covalent or non-covalent protocols. The covalent methods provide more stable conjugation (avoiding “burst effect”); however, they sometimes require chemical modification of the drug and might affect changes in the protein structure that might result in its partial denaturation and loss of enzymatic activity [182]. Physical adsorption is a mild drug encapsulation method that results in high loading efficacy for the nanocarriers with hydrophilic surfaces. As PA are predominantly positively charged at physiological pH with an isoelectric point (IP) >7 (except for SK, IP = 5.12), they can form a complexation with anionic NPs due to electrostatic interactions. The existence of a positive charge on the polymer, as, for instance, chitosan, limits the encapsulation of cationic drugs because of repulsive interactions between a drug and polymer [181]. Comparing covalent vs. non-covalent methods,

adsorptive bound PA liberates faster from the particles and diffuses more readily into the clot's fibrin matrix than covalently bound PA [128] and does not impair the biological activity of the drug [183] that may be beneficial in targeted thrombolysis. In addition, effective entrapment of hydrophilic drugs may occur in the crosslinked polymeric network of hydrogel nanoparticles that imbibe large water quantities [184].

To sum up, depending on the type and composition of the nanocarrier, different encapsulation techniques may be applied. Extensive *in vitro* tests demonstrating high loading efficiency, sustainable release, preservation of the amidolytic and fibrinolytic activities of the PA after conjugation must be verified.

## 8 DISCUSSION & PERSPECTIVES

The rapid recanalization of the vascular occlusion is of the utmost importance for patients suffering from acute thrombotic diseases. The innovative nanomedical approaches have been intensively proposed for targeted thrombolytic therapy to address the challenges of systemic drug administration.

The accomplishments of nanomedicine in thrombotic diseases include the protection of thrombolytics from inactivation by PAI-1, improvement in the blood half-life, enhanced thrombolytic effect at a lower dose, reduction in systemic bleeding and post-ischemic infarct zone, *etc*. Recent studies have demonstrated that nanocarriers, such as liposomes, polymeric or inorganic NPs, and bio-inspired nanocarriers provide benefits for thrombolytic therapy either alone or in combination with ultrasound or magnetic force **(Table 2)**. Current nano-approaches in targeted thrombolysis are summarized schematically in **Figure 12**.

**Table 2.** Different nanocarriers for thrombolytic therapy.

| Nanocarriers | Advantages | Disadvantages | Therapeutic effects |
|---|---|---|---|
| Liposomes | Biodegradable, biocompatible, non-toxic<br>Clinically approved | Low PA encapsulation rate<br>Low stability<br>Phospholipids may undergo oxidation and hydrolysis | Improved thrombolysis rate<br>Lower risks of hemorrhages |
| Polymeric | Biocompatible and often biodegradable<br>Easy surface functionalization | High PA encapsulation rate<br>Improved stability | Superior thrombolytic efficacy<br>Accelerated thrombolysis<br>Protection BBB permeability damage<br>Increased survival *in vivo*<br>Improved neurological deficit<br>Reduction in cerebral ROS<br>Reduction in subarachnoid hemorrhage |
| Inorganic<br>$Fe_3O_4$ NPs<br>AuNPs | Biocompatible<br>Superparamagnetic properties<br>Magnet-guided thrombolysis<br>Optical and photothermal properties<br>Multifunctional theranostic systems | May enter BBB and generate ROS<br>Accumulation in the body<br>May induce immunogenic response or inflammation | Faster vessel recanalization<br>Mechanical clot dissolution with an external magnet<br>Hyperthermia as adjuvant therapy<br>Increased blood flow rate<br>Reduction in infarct volume |
| Bio-inspired | Prolonged *in vivo* circulation<br>Natural thrombus targeting | Low reproducibility<br>Lack of standardization<br>Source availability<br>Immunogenicity<br>Scale-up | Improved survival rate<br>Superior thrombolytic efficacy<br>Lower neurological deficit score<br>Smaller ischemic zone<br>Better neurological outcome<br>Diminished ROS level in the brain<br>Lower risk of hemorrhages |

**Abbreviations:** *PA*, plasminogen activator; *BBB*, blood-brain barrier; *NPs*, nanoparticles; *ROS*, reactive oxygen species.

Active drug targeting of the nanocarriers allows drug accumulation at the thrombus site and has the potential to enhance thrombolytic penetration into deeply localized thrombi. This is currently realized by directing NPs mostly towards fibrin and platelets, though identifying the new target molecules and developing inexpensive and specific targeting moieties will be useful. Fucoidan, which is at present under clinical investigation as a diagnostic agent for the imaging of thrombosis [185,186], may become an affordable and high-quality alternative to antibodies and peptides. Another thrombus targeting strategy relies on the use of magnetic NPs under external magnetic force irradiation. Yet, despite an abundance of preclinical works dealing with magnetic field-assisted guiding, there is no clinically approved medical device to impose a high magnetic force on NPs in deep blood vessels. Therefore, it is probably preferable to design NPs capable of targeting thrombosis without external triggers.

A growing number of reports demonstrate a controlled release of the thrombolytics. On top of the ultrasound that can control the drug release from the echogenic liposomes and some polymer (gelatin and chitosan) NPs, other strategies, such as enzyme exposure ($sPLA_2$ or thrombin), pH, temperature, shear stress, magnet, are employed **(Figure 12)**.

Theranostic nanosystems' design with both thrombolytics and imaging agents (e.g., NIR fluorescent probes, gold, iron oxides, or perfluorocarbon) integrates diagnostic and therapeutic modalities. This strategy may not only provide visualization of drug delivery in real-time but also evaluate the effectiveness of treatment by MRI, CT, or US.

It is critical to face the challenges of nanomedicine, particularly in an attempt for clinical translation. To ensure clinical safety, the potential toxicity of NPs needs to be considered with a careful examination of their physical and chemical characteristics and accumulation in the non-target organs and tissues [187]. Indeed, some NPs may cause oxidative stress generation, immunological response, protein misfolding, immune response, and DNA damage [121]. Selecting biocompatible and fully biodegradable materials with FDA-approval,

as well as a scalable production of the nanoformulations according to Good Manufacturing Practice (GMP), is essential [188]. Incorporation of sophisticated nanodesigns (e.g., cell-derived biomimetic surfaces) should accord with a risk analysis of reproducibility, quality control, and toxicity that might complicate regulatory approvals [33].

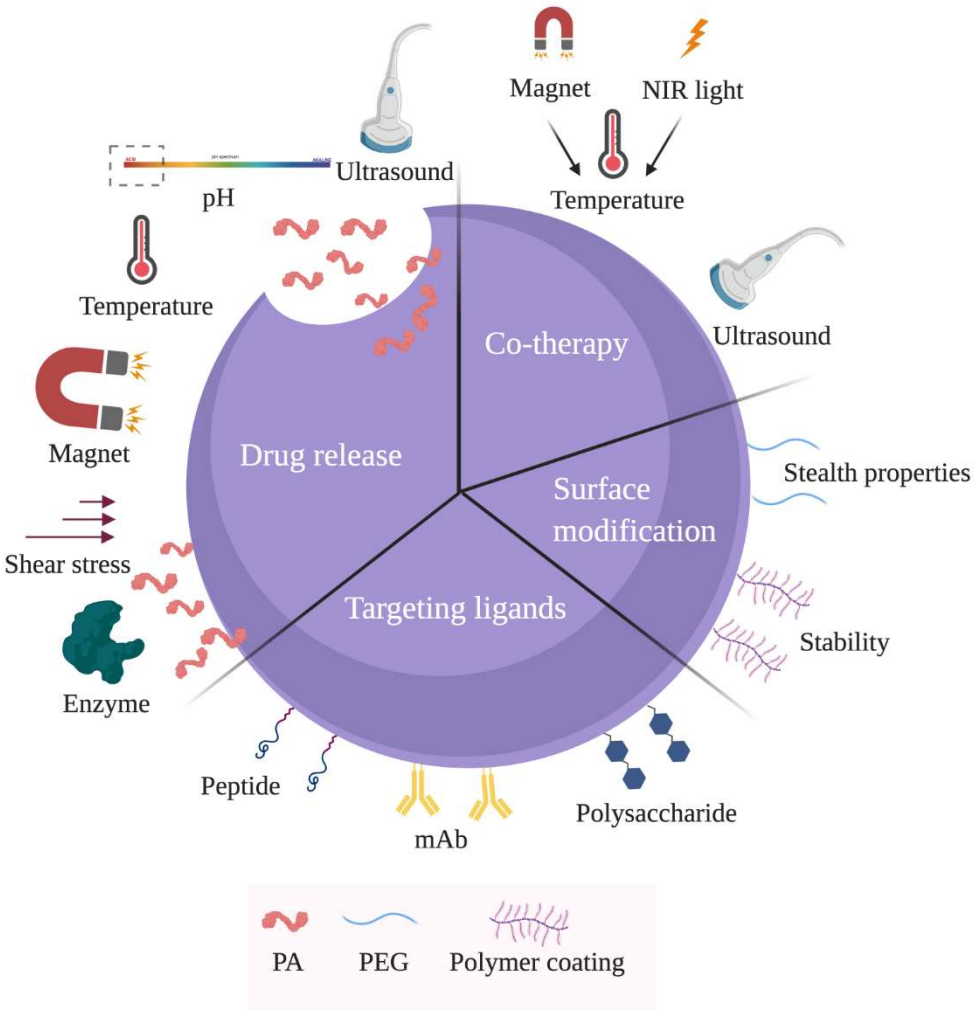


**Figure 12. Schematic illustration of the main strategies in the development of thrombolytic drug delivery nanocarriers.** Surface modification with PEG or other hydrophilic polymeric chains is effectuated to ameliorate the nanoparticle stability, prevent the opsonization, and extend the nanoparticle blood circulation time. Nanoparticles may be decorated with targeting moieties against thrombus biomarkers with monoclonal Ab, peptides, or sulfated polysaccharide fucoidan to attain site-specific thrombolysis. Several endogenous (enzymes in the thrombi, high shear stress in stenotic vessels, or low pH in the ischemic area) and exogenous (magnetic field, elevated temperature, ultrasound) principles are researched for the spatial & temporal control of PA release, prior incorporated either in the core of the nanoparticles or onto their surface. As an adjuvant therapy, elevated temperature by magnet

and NIR light or ultrasound irradiation enhances nanomedicine-assisted thrombolytic efficacy. **Abbreviations**: *PA*, plasminogen activator; *mAb*, monoclonal antibody; *PEG*, Polyethylene glycol; *NIR*, near-infrared.

There is an evident gap between scientific discovery and clinical practice in nanomedicine-guided thrombolytic therapy. An astonishing ~10-fold increase from 2010 to 2020 in the number of publications in the field with beneficial therapeutic effects demonstrates a solid argument towards an imminent clinical translation. At the development stage, the tendency is to design complex targeted biomimetic multifunctional nanocarriers, sometimes bearing several active molecules. By examining nanoparticle delivery systems currently approved or under clinical investigation [35,36], we speculate that the first nanoparticulate candidate for site-specific delivery of PA tested in humans will probably be built on long-established technologies – primarily PEGylated liposomes, but also albumin-coated PA or nanocarriers from FDA-approved polymers. More sophisticated systems with targeting moieties and stimuli-responsive control of drug release will follow.

Meanwhile, public initiatives contribute to nanomedicine development. Recently, the European Union-supported NanoAthero project (http://www.nanoathero.eu/) was completed. It intended to use nanomedicine for molecular imaging and targeted treatment of atherothrombosis with research activities ranging from nanosystems design to clinical validation and industrial production [189]. Several Phase I clinical trials demonstrated its feasibility for patients [186,190–192]. This consortium of 16 partners lasted 5.5 years (February 2013 – July 2018) with the European Commission contribution of 10 million euros.

To conclude, the development of novel nanoparticulate strategies with plasminogen activators for the treatment of thrombotic disease will continue to flourish as they represent a potent evolution to free drug administration. The encouraging results in preclinical research

predict future clinical translation of some formulations and progress in the nanomedicine-based precise therapy of thrombotic pathologies.

## PART 2. POLYSACCHARIDE HYDROGEL NANOCARRIERS FOR CARDIOVASCULAR DISEASES

In Part 2 of the Introduction, we focus more specifically on the polysaccharides as a material of the preference for the synthesis of the hydrogel-based nano- & microsystems, and their advantages, in particular, in the management of cardiovascular diseases.

### 1 HYDROGELS & HYDROGEL-BASED NANO- & MICROPARTICLES

Hydrogels are three-dimensional polymeric rigid networks that are capable of absorbing a large amount of water and swell. They have been researched for various biomedical applications, including wound dressings, transdermal patches, drug-delivery, contact lenses, or reconstructive surgery [184]. The soft and rubbery structure of hydrogels resembles the networks of natural extracellular matrices and prevents tissue irritation or cell adherence [193]. Hydrogels can be produced from hydrophilic natural (e.g., collagen, gelatin, hyaluronate, alginate, starch, chitosan, dextran) or synthetic (PEG, poly(vinyl alcohol), poly(hydroxyethyl methacrylate), *etc*.) polymers, containing hydroxyl, amine, amide, ether, carboxylate, and sulfonate functional groups in their side chains, via various synthesis protocols (outlined below).

To avoid the dissolution of the hydrophilic polymer chains in the aqueous environment and maintain their distinct 3D-structure, hydrogels need to be chemically or physically crosslinked **(Figure 13A & 13B)** [194]. Chemical crosslinking is accomplished by radical polymerization, high-energy irradiation, via enzymes or chemical reactions of complementary groups that normally results in a network with high mechanical strength. However, the use of

the crosslinking agent needs to be carefully evaluated due to the potential toxicity of many of them. Physical crosslinking is based on the formation of nonpermanent bonds – physical interactions between the polymer chains: ionic, hydrophobic, or antigen-antibody interactions, hydrogen bonding, and crystallization. In some cases, stimuli-responsive hydrogels are designed when their formation requires a certain trigger (e.g., temperature, pH, ionic strength, UV irradiation) [195].

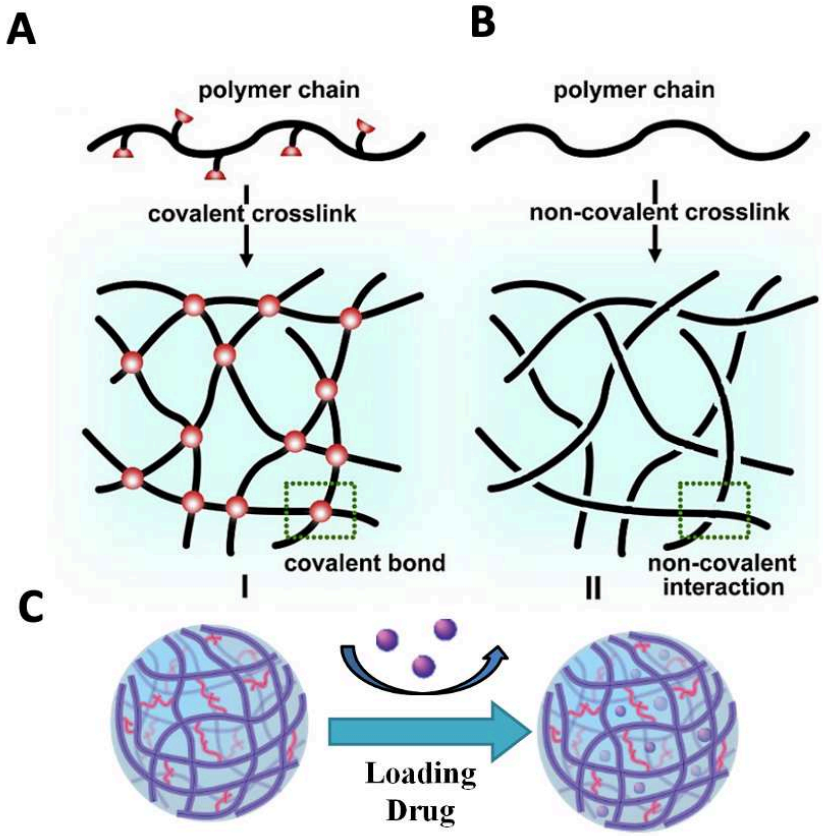


**Figure 13. Schematic image of hydrogels.** Covalent **(A)** and noncovalent **(B)** crosslinking of the hydrogels. Adapted with permission from [196]. Copyright 2017 Elsevier Ltd. **C.** Therapeutic molecule can be loaded onto the hydrogel particles.

Previously, biodegradable hydrogels for bone [197] and vascular [198] tissue regeneration were developed in our laboratory by chemical crosslinking of dextran and pullulan.

Formulation of the hydrogels into nano- or microparticles enables their utilization as an injectable product in the context of macromolecule drug delivery. Highly hydrophilic networks of hydrogels have a lower tendency to adsorb proteins (opsonization) in aqueous body fluids than other types of NPs because of their low interfacial tension, increasing the NP bioavailability and biocompatibility [199]. The hydrogel particles with sizes from 50 nm up to several micrometers can be referred to as nano-/ micro-gels. Their high internal void fraction results in the potential of small molecules or macromolecules to diffuse into their polymeric networks to load high amounts of drugs (**Figure 13C**), the release kinetics of which (i.e., burst or sustained) can be shaped by the microgel design [200].

Microgels benefit from straightforward synthesis procedures that result in monodisperse NPs with long-term stability, biocompatibility, and degradation. Two main strategies for microgel synthesis are typically employed: when bulk hydrogels are broken or milled down into particles or when microgels are constructed from smaller components or building blocks [200]. The latter approach is often preferred that involves the polymerization of monomers or the confined crosslinking of polymer precursors in surfactant-based templates.

Polysaccharides are promising materials for microgel synthesis as these polymers are relatively cheap, nontoxic, biodegradable, and abundant in nature. In Subchapter 2, we are going to further elaborate on their role and utility for this purpose.

## 2 POLYSACCHARIDES AS A STRUCTURAL BIOMATERIAL

Polysaccharides are complex carbohydrate molecules composed of monosaccharide units joined together by glycosidic bonds that may originate from plants, animals, bacteria, and many other microbes, including fungi and algae (**Figure 14**). Despite their various origins, they possess the general properties of natural polymers, such as biocompatibility and biodegradability, low cost, and hydrophilicity. Polysaccharides may derive from multiple

chemical structures that also translate into different molecular weights (MW) and intrinsic characteristics with varied ionic nature [201]. Additionally, polysaccharides also benefit from great structural flexibility, forming either linear or branched structures and easily permitting chemical modifications. Yet, some drawbacks should also be taken into accounts, such as inter-batch variability of the plant-derived polymers related to origin and supplier, difficulty to process, and possible structural differences due to the location and plant collection season.

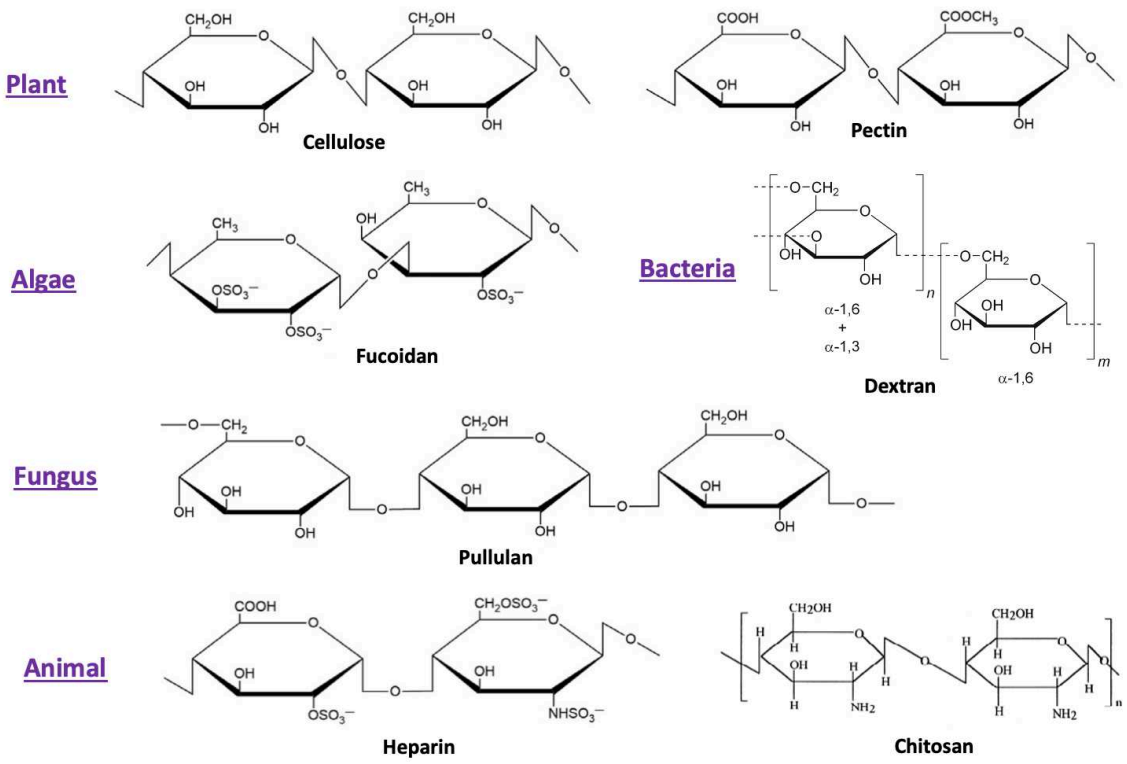


**Figure 14. Chemical structure and origin of different polysaccharides.**

*Dextran*: Dextran is a polysaccharide of microbial origin whose polymer main chain consists of d-glucose monomers connected in α-1,6 glycosidic linkages, with some degree of α-1,3 linkages. The chemical structure of dextran is depicted in **Figure 14**. It is produced by the fermentation of sucrose by certain lactic acid bacteria, such as *Leuconostoc bacteroides* and *Streptococcus mutans* [202]. Dextran is extensively employed in clinics for over 60 years,

particularly in its low molecular weight (40 and 70 kDa), for plasma volume expansion, thrombosis prophylaxis, peripheral blood flow enhancement, and artificial tears [184]. The injectable 6% solution of Dextran 70 is on the World Health Organization (WHO) Model List of Essential Medicines as a blood plasma substitute [203].

Meeting the requirements of biocompatibility, biodegradability, non-immunogenicity, dextran stands out as an attractive biopolymer for nanomedicine purposes. Dextran coating of synthetic polymer or magnetic NPs is applied to ensure environmental stability and to prolong the blood circulation time as well as to provide a framework for further chemical modifications and nanoparticle functionalization [68,124]. The neutral pH of dextran, its high water solubility, and simple repetitive glucose units with a large number of hydroxyl groups make it suitable for chemical crosslinking to design a hydrogel-based nanocarrier for protein deliver-system [184].

*Advantages of polysaccharides in nanomedicine:* Polysaccharide-based nanosystems as drug delivery systems and targeted contrast agents for molecular imaging hold much promise in the management of atherothrombotic diseases [204]. Polysaccharide-based NPs have a number of advantages in nanomedicine. Firstly, natural biomaterials like polysaccharides to prepare NPs limit concerns over nanoparticle toxicity, biodegradability, and physiological stability. Secondly, polysaccharide-based NPs contain a dynamic cloud of hydrophilic and neutral chains on the particle, which prevents opsonization and decreases uptake by MPS over other types of NPs [205]. It results in prolonging the NP *in vivo* circulation time and increases particle accumulation at the disease site. The residence time of polysaccharide-based materials is also extended due to the bio adhesion of polysaccharides, particularly to mucosal surfaces. Natural materials with hydrophilic properties appear suitable for mimicking the aqueous *in vivo* environment. Also, carbohydrates are abundant in nature, making them cost-effective biomaterials to investigate. Finally, most polysaccharide-based NPs hold derivable groups that

can be used to conjugate targeting, therapeutic, or imaging agents, making them diverse multifunctional biomedical tools for theranostic nanomedicine.

## 3 FABRICATION METHODS OF MICROGELS FROM BIOPOLYMERS

The methods to synthesize microgels from natural hydrophilic polymers, including polysaccharides, can be classified into several categories: water-in-oil (W/O) heterogeneous emulsion, inverse nanoprecipitation, electrospray, spray drying method, complex coacervation, self-assembly, *etc*. [206,207].

### 3.1 Water-in-oil (W/O) heterogeneous emulsion

W/O emulsion methods generally combine two steps: emulsification of aqueous droplets of water-soluble biopolymers in continuous oil phase with oil-soluble surfactants and biopolymer crosslinking with water-soluble crosslinkers.

*Inverse (mini)emulsion method (emulsion crosslinking technique):* A W/O emulsion is prepared from a mixture of aqueous biopolymer droplets and a continuous oil phase via a homogenizer or a high-speed mechanical stirrer [16]. Commonly, mineral oil or hexane as hydrophobic organic solvents and Span 80 (sorbitan monooleate), Tween 80 (polysorbate 80*),* or Aerosol OT (sodium bis(2-ethylhexyl) sulfosuccinate) as surfactants are used to achieve colloidal stability of the emulsion. The subsequent aqueous droplets of biopolymers are crosslinked with effective crosslinking agents, soluble in the water phase. The resulting crosslinked microgels, dispersed in organic solvents, need to be purified by precipitation, centrifugation, washing with organic solvents, or lyophilization. The size of the prepared particles can be tuned by the amount of surfactant and crosslinking agents as well as stirring speed during emulsification.

*Membrane emulsification*: This is a relatively novel method for the preparation of spherical particles with a uniform size distribution. The technique involves the use of a membrane, like the Shirasu porous glass (SPG) membrane with a highly uniform pore size ranging from 0.1 to 18 mm, through which a liquid is forced to pass under adequate pressure [208]. The subsequent droplets are formed and detached at the end of the pores in the continuous phase, as simple W/O and O/W emulsions, multiple emulsions such as O/W/O, O/W/O, and solid/O/W dispersions, and the corresponding particles of controlled droplet sizes and narrow droplet size distributions: microspheres, hollow spheres, core-shell microcapsules, and organic-inorganic hybrid materials. Emulsification requires lower consumption of emulsifiers and energy. The membrane emulsification process is generally carried out in cross-flow (continuous or batch) mode or a stirred cell (batch) [209]. Additionally, this synthesis technique can be combined with an ionic or/and chemical crosslinking. A primary limiting factor of the method is the low dispersed phase flux that limits its potential in industrial scale-up.

### 3.2 Inverse nanoprecipitation/solvent displacement

Nanoprecipitation technique is frequently used to fabricate nanospheres from water-insoluble polymers: a polymer solution in an organic, water-miscible solvent, for example, acetone or methanol, is dropwise added to a large volume of an aqueous solution under moderate magnetic stirring. As such, the polymers aggregate into 100 to 1000 nm NPs, with surfactants additionally applied to stabilize the obtained mixture. Next, the organic solvent needs to be removed by dialysis, ultrafiltration, or other techniques. Analogously, hydrophilic polymers can precipitate into nano-sized clusters in an inversed system: when the natural polymer is dissolved in water, which is added to a large volume of a water-miscible organic solvent. A nanogel suspension is obtained after chemical crosslinking and subsequent removal of unreacted polymer, crosslinker, and used surfactants. Inverse nanoprecipitation has been

applied to form NPs with natural polymers such as gelatin, peptidomimetic polymers, and highly hydrophilic polymers, such as dendritic polyglycerol, polyvinyl alcohol, and zwitterions [207]. This method does not require high-shear mixing that might damage the structure of entrapped proteins and DNA; surfactants are needed only at low concentrations.

### 3.3. Electrospray

Electrospraying, a relatively novel technique, is performed as a single step to synthesize the particles without a surfactant. Setup involves a polymer solution with a conductive solvent injected into a syringe connected to an electrode from a high-voltage power source [210]. A collector, an oppositely charged metal foil electrode, is positioned opposite the syringe nozzle. Once the solution enters the electric field from the nozzle of the syringe, the Taylor cone is formed due to the surface tension. The cone breaks into droplets in the high-electric field, giving rise to particles of different sizes and shapes. The parameters that affect the resulting particles are the solution's properties, like concentration, solvent, and viscosity, and the process parameters as flow rate, distance from the tip of the needle to the collector, and voltage [211]. Micro- and nanoparticles obtained by electrospray possess a narrow particle size distribution and a high drug loading efficiency.

### 3.4 Spray drying method

Spray drying is relatively simple, highly efficient, and widely used in the pharmaceutical and materials science technique for the formation of the microgels, which involves using a spray dryer, mainly consisting of the atomizer and drying chamber [206]. Solutions and suspensions of drugs, polymers, and particles are atomized into fine droplets. The particles' sizes range from 0.2 to 500 μm and possess various shapes, porosities, and bulk volumes, depending on the method and preparation material. Polysaccharides are one of the shell materials used during

spray drying. This technique involves preparing a soluble formulation by mixing lipids, surfactants, drug molecules, and solid carriers. The solubilized liquid formulation is then sprayed through an atomizer into droplets, and the droplets are then introduced into a drying chamber with a stream of hot air, where the volatile phase (e.g., the water contained in an emulsion) rapidly evaporates, resulting in dry particles under controlled temperature and airflow conditions [212]. The size of the resulting particles is determined by temperature, nozzle size, spray flow rate, atomization speed, the drying chamber design, and the extent of crosslinking.

### 3.5 Self-assembly

Self-assembly requires the biopolymer to aggregate in an aqueous environment spontaneously. This can be accomplished by incorporating functional groups into a polymer to form physical crosslinks with each other, with other polymer chains, or with crosslinkers. Physical crosslinks rely on Van der Waals' interaction, hydrophobic interactions, or inclusion complex formation [213]. Covalently crosslinked nanogels can be obtained by aggregation and subsequent chemical conjugation. In such a case, an amphiphilic micelle structure is converted to hydrophilic nanogels of small sizes ~10-100 nm [207]. Besides, the process may be followed by photo-crosslinking for stabilization. The self-assembly method is determined by the critical micelle concentration related to the polymer molecular weight and its physical properties. The purification process is simple due to the absence of organic solvents, surfactants, or interphase mixing.

### 3.6 Complex coacervation

Coacervation is a simple solvent-free technique in nano- and micro formulation with a high encapsulation efficiency. When a single biopolymer is utilized, the process is referred to as

simple coacervation, with two or more biopolymers as complex coacervation. Complex coacervation results from the interactions of oppositely-charged polyions in an aqueous medium that undergo an associative phase separation into a dense phase (the coacervate) and a dilute phase (the supernatant) [214]. Complex coacervation typically occurs over a narrow range of pH, between the p$K_a$ (p$K_a$ = -$\log_{10} K_a$, when $K_a$ is an acid dissociation constant of a solution) of the reactive groups along the anionic polysaccharide backbone and the isoelectric point of the loaded protein [210]. The active compound that has to be encapsulated is mixed intensively in one of the solutions. As this method does not require high temperature, entrapped bioactive components (protein or DNA) remain better preserved. Several parameters need to be tuned, like pH, ionic strength, the concentration of polymers (mostly proteins or polysaccharides), molecular weight, and temperature of the solution to fabricate NPs bearing the bioactive compound. Crosslinking may be applied afterward with glutaraldehyde or formaldehyde as a crosslinking agent to create a covalent bond and stabilize the particles. As an example, Sarmento *et al.* reported formulation of the nanoparticle insulin delivery system by dropwise addition of a chitosan solution at pH 5 into a dextran sulfate (DS)/insulin solution at pH 3.2 according to a DS:chitosan mass ratio of 1.5:1 in aqueous solution, followed by 15 min of curing time [215].

## 4 FUNCTIONALISATION OF THE NANOPARTICLES TO TARGET THROMBI

*The rationale for P-selectin as a molecular target of thrombus:* To promote the spatially controlled drug delivery through particle accumulation on the targeted tissue, the NPs need to be labeled with specific targeting moieties for site-specific delivery of their payload and minimize undesirable side effects. In preclinical nanomedicine research on acute thrombotic pathologies, nanoparticles are generally driven towards the main molecular markers of the

thrombus such as fibrin and activated platelets (GPIIb/IIIa and P-selectin). Although P-selectin (CD62P) is tested to a lesser degree than GPIIb/IIIa, this cell adhesion molecule has the advantage to serve as a unique molecular target of the thrombotic and ischemic cardiovascular events to direct nanocarriers [216,217].

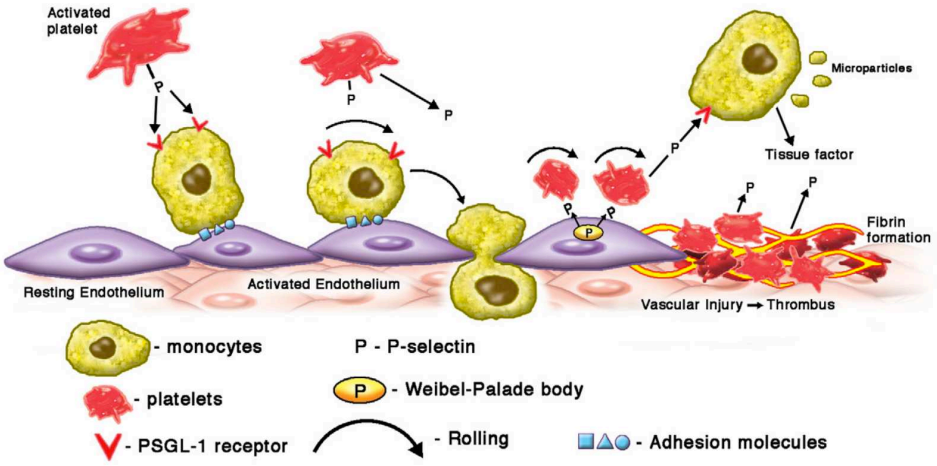


**Figure 15. P-selectin links inflammation and thrombotic pathophysiology pathways at the arterial vessel wall.** Reprinted with permission from [218]. Copyright 2013 Elsevier Inc.

P-selectin is stored in the α-granules of resting platelets, whereas it is found in the Weibel-Palade bodies in endothelial cells (**Figure 15**). It belongs to the family of selectins, calcium-dependent lectins, together with E-, and L-selectins [219]. E-selectin (CD62E) is expressed on activated endothelial cells by cytokines, whereas L-selectin (CD62L) on all granulocytes, monocytes, and most lymphocytes. Upon cell activation, P-selectin rapidly becomes phosphorylated on cytoplasmic tyrosine, threonine, and serine residues [220], and it is translocated to the external plasma cell membrane of activated platelets and on pathological vascular endothelium. As such, P-selectin can serve as a unique key marker of acute thrombotic events to direct nanocarriers and promote the spatially controlled thrombolytic drug delivery. Intriguingly, P-selectin is implicated in the "ischemic memory": when the thrombus is resolved,

the surrounding endothelium still preserves an inflammation reaction [221,222] since activated cells overexpress cell adhesion molecules on their surfaces, including selectins [219]. Hence, P-selectin could also serve as a biological target for the sensitive diagnostic tool to image vascular inflammation for making decisions concerning precise treatments.

P-selectin glycoprotein ligand-1 (PSGL-1) is a cell-surface glycoprotein found on the membrane of various leukocytes and a main physiologically relevant ligand of P-selectin. In the case of inflammation, PSGL-1 binds to P-selectin on the endothelium of blood vessels and/or adherent platelets and plays a vital role in recruiting white blood cells into the thrombi or atherosclerotic lesion [219]. PSGL-1 protein requires tetrasaccharide sialyl Lewis$^X$ (sLe$^X$) and tyrosine sulfation in its structure for selectin recognition activity. Structural features of sialyl Lewis$^X$ essential for the binding P-selectin are the hydroxyl functions of l-fucose and d-galactose and the carboxylic group of sialic acid residues [223].

Generally, P-selectin targeting is established by the functionalization of the NPs with antibodies and/or peptides. Nevertheless, both of them have their limitations concerning clinical translation for molecular imaging and thrombolytic drug delivery. The immunogenicity, purity, sufficient circulation time, and high price are the main concerns of the application of the antibodies [224], while peptides might suffer from weak binding affinity, metabolic instability, and fast renal clearance due to their small sizes, potential immunogenicity, and often a high costs of peptide synthesis [225].

*Fucoidan as a targeting ligand of P-selectin*: Fucoidan is an anionic polysaccharide containing L-fucose and sulfate ester groups that is extracted from the extracellular matrix of brown algae. Structurally, the polysaccharide has a backbone of α-(1–3)-linked fucose units or is composed of repeating disaccharide units of α-(1–3) & α-(1–4) - linked fucose residues with O-2 branches (**Figure 14**). Low MW fractions (below 30 kDa) are preferred as they are considered to be

more biocompatible [226]. Our team previously demonstrated that low molecular weight (LMW) fucoidan inhibited P-selectin binding to $sLe^X$ with a half-maximal inhibitory concentration ($IC_{50}$) of 20 nM and to PSGL-1 with an IC50 of 5 nM, both in a dose-dependent manner. The data also indicated that LMW fucoidan with a dissociation constant ($K_D$) of 1.2 nM is the most effective ligand for the selective binding to P-selectin when compared with other LMW polysaccharides (heparin and dextran sulfate), as well as the synthetic $sLe^X$ mimetic [227,228]. Interestingly, fucoidan exhibits a broad spectrum of pharmacological effects with potential clinical applications, such as anti-coagulant, antitumoral, antiviral, anti-inflammatory activity, and antioxidant properties [229]. Additionally, fucoidan may mediate thrombolysis due to inhibition of the tPA-PAI1 complex [230].

In drug delivery systems, particularly for the imaging and treatment of thrombosis, fucoidan has enormous potential and is approved as a pharmaceutical compound [185]. This affordable and abundant product has been widely studied in preclinical research on various nano- & microsystems in our laboratory [67,104,105,231,232] as it serves as a high-quality targeting ligand to thrombi due to P-selectin interactions [228,233,234].

To ensure the reproducible GMP manufacture of fucoidan, a joint laboratory between LVTS and the Algues & Mer Company was established in 2013 to produce well-defined composition and molecular weight compound (Ascophyscient® from Algues & Mer, Ile d'Ouessant, France: a low molecular weight fucoidan fraction). Next, this compound obtained a label as "raw materials for pharmaceutical uses" in 2015 by the French authorities to become a part of the large scale European Union project NanoAthero for the development of a Single-Photon Emission Computed Tomography (SPECT) imaging of human atherothrombosis [189]. The full physicochemical characterizations were performed on the GMP batch of a low molecular weight fucoidan of 7 kDa. The regulatory toxicology study in rodents proved no adverse effects at the concentrations 500 higher than an estimated human dose as well as

absence of pseudoallergy. In a myocardial ischemia-reperfusion model *in vivo*, the clinical batch of fucoidan labeled with technetium-99m targeted lesion sites [185]. Moreover, the first in the world phase I clinical trial on intravenous delivery of fucoidan radiolabeled with a technetium-99m has already been completed and reported its safety and favorable biodistribution as a potential contrast agent [186], while phase IIa for its thrombosis imaging potential in patients with DVT is ongoing.

# Chapter 2. EXPERIMENTAL PART

# FUCOIDAN-FUNCTIONALIZED POLYSACCHARIDE SUBMICROPARTICLES WITH ALTEPLASE FOR TARGETED THROMBOLYTIC THERAPY

This Chapter features the extended version of the research article submitted for the publication to the scientific journal (**Annex 2**). This work's findings led to patent application #1000497919 to the European Patent Office in June 2020 (**Annex 3**). The poster presentation of this study won the second prize in the category "Translational Nanomedicine" at the international congress on clinical nanomedicine CLINAM 2020 (**Annex 4**).

## ABSTRACT

Thrombolytic therapy is an intravenous administration of clot-busting agents for the treatment of life-threatening acute thromboembolic diseases. However, thrombolytics exhibit limited clinical efficacy because of their short plasma half-lives and risks of hemorrhages. There is a dire need for innovative nanomedicine-based solutions for safe and efficient thrombolysis with a non-toxic, biocompatible, and biodegradable thrombus-targeted nanocarrier.

Herein, polysaccharide hydrogel submicroparticles with remarkable biocompatibility were elaborated by the inverse miniemulsion / crosslinking method. They were functionalized with a fucoidan which has a nanomolar affinity for the P-selectin overexpressed on activated platelets and endothelial cells in the thrombus. Alteplase was loaded onto the submicroparticles by adsorption, and its amidolytic and fibrinolytic activities were maintained *in vitro*. Thrombus targeting potential of these particles was validated in microfluidic assay under arterial and venous blood shear rates on recombinant P-selectin and activated platelet aggregates. The thrombolytic efficacy of the nanomedicine-based product was tested in a murine model of acute ischemic stroke, revealing faster middle cerebral artery recanalization and reduction in the brain infarct volume and blood-brain barrier permeability post-stroke, evidenced by laser

speckle contrast imaging and MRI. Collectively, this proof of concept study demonstrates the potential of biomaterial-based targeted nanomedicine for the personalized treatment of acute thrombotic events.

**KEYWORDS:** Nanomedicine; Drug delivery; Targeted thrombolysis; Polysaccharides; Fucoidan; P-selectin.

## 1 INTRODUCTION

Acute thrombotic pathologies such as myocardial infarction, ischemic stroke, and venous thromboembolism remain a major global healthcare challenge contributing to a significant number of deaths and disabilities [2]. Current thrombolytic therapy, the intravenous injection of Plasminogen Activators (PA), is administrated to lyse a vascular occlusion and restore the blood flow in the vessel. The recombinant tissue plasminogen activator (rtPA) is the most commonly applied clot-busting drug in clinics, and the only one approved for the treatment of acute ischemic stroke [29]. rtPA is a fibrin-specific serine protease that activates the endogenous proenzyme plasminogen and converts it to the active form plasmin, thus, degrading the thrombus fibrin network. However, systemic delivery of rtPA is limited by a narrow therapeutic window (4.5 h of stroke symptom onset), rapid drug elimination (half-life 4-6 min), and physiological deactivation by its antidotes such as Plasminogen Activator Inhibitors (PAI-1 and PAI-2), posing the risks of deleterious side-effects such as intracranial hemorrhages [235]. Moreover, the rate of acute recanalization after intravenous administration of rtPA is low: only ~30% of patients experienced full or partial recanalization [236].

Therapeutic strategies that intend to address the challenges of thrombolytic therapy and to boost survival rates remain of great clinical interest. Certainly, novel thrombolytic molecules are being researched in order to increase reperfusion, improve safety, and protect the brain

neurovascular unit [25,237]. Apart from that, nanomedical approaches for the targeted delivery of thrombolytic agents have been intensively proposed [238]. Korin *et al.* reported the microaggregates of poly (lactic-co-glycolic acid) (PLGA) nanoparticles (NPs) dissociated into rtPA-bearing nanocompounds when exposed to abnormally high hemodynamic shear stress, typical for the vascular occlusions, that performed effective thrombolysis in several preclinical models [72]. Colasuonno *et al.* formulated rtPA-loaded discoidal porous nanoconstructs from a mixture of PLGA and polyethylene glycol (PEG) with high thrombolytic potential presumably attributed to the erythrocyte-mimicking shape of the NPs and their deformability, leading to efficient circulation profiles and accumulation on the clot [101]. While these nanosystems with passive targeting succeeded in a promising thrombolytic efficacy in preclinical studies, more recent and advanced examples are formulated with actively targeted nanocarriers.

Active targeting permits drug accumulation specifically at the thrombus site and has the potential to enhance the enzyme penetration into deeply localized thrombi. Apart from the magnetic nanoparticle targeting under an external magnetic field, active blood clot targeting is currently achieved by directing the functionalized NPs towards fibrin or activated platelets (mostly integrin GPIIb/IIIa and less adhesion receptor P-selectin) with antibodies and/or peptides. Notably, a theranostic system for thrombus molecular imaging and targeted therapy was developed by Zhou *et al.* when rtPA was encapsulated into the $Fe_3O_4$-based PLGA NPs, and a cyclic arginine-glycine-aspartic acid (cRGD) peptide was grafted onto the chitosan surface to target GPIIb/IIIa on activated platelets [69]. Nevertheless, both antibodies and peptides have their limitations for targeted drug delivery. The immunogenicity, purity, and sufficient circulation time are the main concerns of the application of the antibodies [224]. At the same time, peptides might suffer from high costs of synthesis, weak binding affinity,

metabolic instability, potential immunogenicity, and fast renal clearance due to their small sizes [225].

The effective alternative could be the nanoparticle functionalization with fucoidan [103], a naturally-occurring algae-derived sulfated polysaccharide that allows a specific and strong tropism for the P-selectin overexpression in cardiovascular pathologies [228,233]. Fucoidan emerged as an affordable high-quality targeting ligand to P-selectin, which was prior validated by our group on polysaccharide microparticles with iron oxide for MRI imaging [104], Technetium-99m-radiolabeled polysaccharide microparticles for SPECT imaging [231], polymer microcapsules [105], and polymer microbubbles for ultrasound imaging [232].

This is critical to ensure an excellent safety profile of the designed nanocarrier for targeted thrombolysis in future clinical translation. It should be a priority to select biocompatible and fully biodegradable materials with U.S. Food and Drug Administration (FDA)-approval as well as to realize a scalable production of the nanoformulations according to Good Manufacturing Practice (GMP) [188]. Contrary to the popularity of synthetic polymers such as PLGA, the NPs made of polysaccharides are explored to a lesser degree for thrombolytic therapy. Yet, they benefit from the general advantages of natural polymers: biocompatibility, low cost, and hydrophilicity. Polysaccharide hydrogels, which are crosslinked three-dimensional polymer networks, can absorb large quantities of water and can effectively load macromolecules [239], including plasminogen activators, with high encapsulation efficiency. Few publications reported the nanoformulations with chitosan, a cationic chitin-derived polysaccharide that can form polyelectrolyte complexes with negatively charged molecules [91]. For instance, superior thrombolytic potential *in vivo*, both by intravenous injection and catheter-driven, was demonstrated on self-assembled chitosan NPs crosslinked with sodium tripolyphosphate and loaded with urokinase [92]. Liao *et al.* formulated the lumbrokinase-bearing NPs from quaternized derivative of chitosan - N,N,N-

Trimethyl Chitosan covalently grafted with cRGD peptide to target GPIIb/IIIa receptors that could accelerate thrombolysis [95].

Dextran, an exocellular bacterial water-soluble polysaccharide, is extensively employed in clinics, in particular in its low molecular weight (40 and 70 kDa), for plasma volume expansion, thrombosis prophylaxis, peripheral blood flow enhancement, artificial tears, *etc*. [184]. Dextran coating of magnetic NPs is applied to ensure environmental stability and prolong blood circulation time [68,124]. Our group has recently demonstrated that rtPA-immobilized core-shell poly(isobutyl cyanoacrylate) NPs, decorated with dextran and fucoidan, effectively augmented thrombolysis in mice [67]. However, to our knowledge, there are no reported exclusively dextran nanocarriers for thrombolytic therapy. Meeting the requirements of biocompatibility, biodegradability, non-immunogenicity, dextran stands out as an attractive polymer to design a hydrogel-based protein delivery system for the thrombolytic application.

Herein, we designed homogeneous and spherical novel fucoidan-functionalized dextran submicroparticles (SPs) obtained by a green chemistry method using fully biodegradable and biocompatible compounds, all of them approved by the FDA. After extensive physico-chemical characterization of these hydrogel-like SPs that exhibited cyto- and hemocompatibility, rtPA was loaded onto the SPs with a high encapsulation capacity, and its release in saline and *in vitro* characterization of the amidolytic activity and fibrin clot dissolution potency were tested. Through the *in vitro* microfluidic experiments under continuous arterial or venous flow, we provided evidence that Fuco-SPs have a high affinity to P-selectin, but not to E- and L-selectins, and accumulate on activated platelet aggregates. Finally, rtPA-Fuco-SPs proved superior *in vivo* thrombolytic efficacy in a mouse stroke thrombin model with a faster vessel recanalization that minimized cerebral tissue damage: the post-ischemic lesion and blood-brain barrier (BBB) permeability.

## 2 MATERIALS AND METHODS

*Materials:* Dextran 40 kDa and TRITC-dextran 40 kDa were provided by TdB Consultancy (Uppsala, Sweden). Fucoidan (Mn = 18 kDa/Mw = 104 kDa) was a gift from Algues & Mer (Ouessant, France). Sodium trimetaphosphate (STMP), methylene blue hydrate, and Human Serum Albumin (HSA) were purchased from Sigma-Aldrich (Saint-Quentin-Fallavier, France). Polyglycerol polyricinoleate (PGPR) was obtained from Palsgaard France S.A.S. (Lyon, France). Vegetable (sunflower) oil was purchased from a local supermarket. The SPs were encapsulated with commercially available rtPA (Actilyse®, Boehringer Ingelheim) that was reconstituted at 1 mg/mL, aliquoted, and stored at -80 ºC. Chromatography paper was obtained from GE Healthcare (Chicago, Illinois, United States). Fibrillar type I collagen Horm® was obtained from Takeda (Linz, Austria). 96-Well Cell Culture Plates (Costar) were obtained from Corning Incorporated. PPACK (Phe-Pro-Arg-Chloromethylketone) 75 µM tubes were purchased from Cryopep (Montpellier, France). Flow chambers (Vena8 Fluoro+) were provided from Cellix Ltd (Dublin, Ireland).

*Submicroparticle synthesis:* Polysaccharide submicroparticles (SPs) were obtained via a water-in-oil (w/o) emulsification combined with a crosslinking process. Polysaccharide solution was prepared as a mixture of dextran 40 and 5% TRITC-dextran 40 (for fluorescent SPs) at 300 mg/mL, 6 M NaCl. To synthesize functionalized SPs with fucoidan (Fuco-SPs), 10% w/w of fucoidan was added.

First, the organic phase of 15 mL of sunflower oil and 6% w/v PGPR in Falcon® 50 mL was prepared and cooled down for 20 min at -20 ºC. In the meantime, 1,200 mg of the polysaccharide solution was incubated with 120 µL of 10 M NaOH under magnetic stirring for 10 min. 240 µL of STMP solution (30% w/v in water) was added into the aqueous phase under magnetic stirring and mixed for 20 seconds on ice. Next, emulsification was achieved by the

dropwise injection of 600 µL of the aqueous phase into the organic phase and dispersed with a stand-disperser (Polytron PT 3100, dispersing aggregate PT-DA 07/2EC-B101, Kinematica, Luzernerstrasse, Switzerland) at 30,000 rpm for 4 min on ice. The obtained w/o emulsion was transferred into 50 ºC for the crosslinking reaction of polysaccharides with STMP for 20 min. The crosslinked suspension was washed in 30 mL PBS 10x for 40 min under high magnetic stirring at 750 rpm. The mixture was then centrifuged (BR4i, JOUAN SA, Saint Herblain, France) for 10 min at 3,000 g in Falcon tubes. The organic phase was recovered and ultracentrifuged (Optima MAX-XP, Ultracentrifuge, Beckman Coulter, Brea, California, United States) in PBS for 45 min at 15,000 g. The obtained pellet was washed by ultracentrifugation 2 times in 0.04% Sodium Dodecyl Sulfate (SDS) solution and then 3 times in ultrapure water to purify the SPs. The resulting SPs were suspended in water or 0.9% NaCl with 0.02% Tween 20 (Sigma) and stored at 4 ºC.

**Table 3.** The synthesis parameters for the polysaccharide SPs.

| Synthesis method | Polysaccharide [c], mg/mL | STMP, [c], mg/mL | NaOH [c], M | Phase ratio, (Aq/ Org/) | Surfactant | Homogenization | Crosslinking |
|---|---|---|---|---|---|---|---|
| W/O emulsion / crosslinking | 300 | 56.11 | 1.15 | 4% w/v | PGPR, 6% | 30,000 rpm, 4 min, 4 °C | 20 min, 50 ºC |

**Abbreviations:** *W/O*, water-in-oil; *Aq,* aqueous; *Org,* organic.

*Cell culture and cytotoxicity assay:* To evaluate the cytotoxicity of the SPs, Fluorometric Cell Viability Assay (Resazurin) was used on confluent Human Umbilical Vein Endothelial Cells (HUVEC). The cells were cultured in DMEM supplemented with 10% (v/v) fetal bovine serum, 4 mmol of l-glutamine, 100 units/mL of penicillin, and 100 µg/mL of streptomycin and kept in an incubator at 37 °C in a humidified atmosphere of 5% $CO_2$. Cells

were seeded into 96-well plates to adhere, 10,000 cells per well. Following 24 h of incubation to reach ~80% confluency, the medium in the wells was changed to the one containing the SPs at concentrations ranging from 0.1 to 1.5 mg/mL and cultured for another 24h. Culture media were used as a positive control. Next, the medium was replaced with 100 µL 10% Resazurin solution, and the plates were covered in foil and incubated for 2h. The fluorescent signals of the Resazurin were monitored using 540 nm excitation and 590 nm emission wavelengths on Infinite® 200 PRO microplate reader (TECAN Group Ltd., Mannedorf, Switzerland). The obtained fluorescence (Fl) values were blank corrected; and the relative cell viability was expressed as $Fl_{SPs}$ / $Fl_{control}$ × 100%, where $Fl_{control}$ was obtained in the absence of the SPs. The experiment was performed in hexaplicate.

To examine the potential cell cytoskeleton organization mediated by Fuco-SPs, HUVEC cells were cultured in 8-well Lab-Tek II Chamber Slide w/Cover (Lab-Tek®, Thermo Fischer Scientific, Massachusetts, United States) with 10,000 cells per well. The wells' medium was changed 24 h after to the one containing TRITC-Fuco-SPs at 1.5 mg/mL and was incubated for another 24 h. Cells cultured in the medium without the SPs were set as control. Next, cells were fixed with 4% paraformaldehyde for 30 min at room temperature (RT). After rinsing with PBS, cells were labeled and permeabilized with the 200 µL mixture of FITC-Phalloidin (1:200, Sigma-Aldrich, USA) / DAPI (1:100, Thermo Fisher Scientific, Massachusetts, United States) / 0.01% v/v Tween 20 in PBS and incubated under low agitation for 1 h at RT. The cells were afterward washed 3 times with PBS. The support of the chamber slides was removed, and the slides were mounted with a few drops of the aqueous mounting medium and kept at 4 ºC until visualization with the confocal microscope (Zeiss LSM 780, Iena, Germany).

*Hemocompatibility test*: Hemolysis assay was adapted from the publication [231] and performed on washed isolated murine erythrocytes. Murine blood was collected in sodium citrate 3.8% (w/v) and centrifuged at 800 g for 5 min to isolate red blood cells. The supernatant

was removed, and the pellet of erythrocytes was resuspended at 20% (v/v) in distilled water (positive control, 100% hemolysis), normal saline (negative control, no hemolysis), and the Fuco-SPs at concentrations from 0.1 to 1.5 mg/mL in Eppendorf. The tubes were incubated on a rotator at 37 °C for 1.5 h and then centrifuged at 3,000 g for 5 min. The absorbance (A) of the supernatants was measured on Infinite® 200 PRO microplate reader (TECAN Group Ltd., Mannedorf, Switzerland) at 590 nm. Each sample was run in triplicate. The percentage of hemolysis was determined by the formula: Hemolysis degree (%) = 100% x ($A_{sample}$ - $A_{negative\ control}$)/($A_{positive\ control}$ - $A_{negative\ control}$).

*Physico-chemical characterization:* The submicroparticle (SP) formulations were studied for particle morphology, size and zeta potential distributions, mass concentration, and elemental composition.

Particle morphology was visualized by Transmission Electron Microscopy (TEM) (Philips FEI Tecnai 12, Amsterdam, Netherlands), negatively stained with 1% (w/v) uranyl acetate for 5 minutes, and Environmental Scanning Electron Microscopy (ESEM) (Philips XL30 ESEM-FEG, Amsterdam, Netherlands). Hydrodynamic size and Zeta potential (ζ-potential) were measured by Dynamic Light Scattering (DLS) and Electrophoretic Light Scattering (ELS), respectively (Zetasizer Nano ZS, Malvern Instruments SARL, Orsay, France). Samples were diluted in distilled water or saline for size and in 1 mM KCl for ζ-potential determination. All runs were performed at 25 °C in triplicate.

Mass concentration was determined by freeze-drying. An elemental analyzer-mass spectrophotometer was used for the quantification of the sulfur (presence of fucoidan). To prove the crosslinking with STMP, the total reflection X-ray fluorescence spectroscopy (TXRF) technique was applied to quantify the phosphorus content on the SPs (S2 PICOFOX Bruker, Massachusetts, United States).

For Fourier transform infrared (FTIR) spectroscopy measurement, ThermoNicolet AVATAR 370 FTIR spectrometer (Thermo Electron Corporation, Waltham, MA) was used. The samples were blended with KBr and compressed to form a pellet. The transmission spectra were obtained from 400 to 4000 $cm^{-1}$ with a resolution accuracy of 4 $cm^{-1}$.

*Sulfate and fucoidan quantification:* The sulfate content of fucoidan was determined by a semi-quantitative solid-phase colorimetric assay [240]. Briefly, 5 µL of Fuco-SPs in suspension at a concentration of 2 mg/mL were dropped on a piece of Whatman Chromatography paper grade 1. It was repeated 5 times on the same point, allowing the paper to dry at 50 ºC in between. The paper was first soaked into a methanol/acetone (6:4) solution for 3 min and then into a methanol/acetone/water (6:4:15) solution with 50 mM HCl and 0.1% w/w methylene blue for 10 min. Finally, the paper was extensively washed with acetic acid/methanol/acetone/water (5:6:4:75) until no coloration was detected in the washing solution. The paper was then transferred to the Eppendorf, containing 0.5 mL methanol with 2% w/v SDS, and incubated for 15 min at 50 ºC. 0.2 mL of the extracted dye was placed in a 96-well plate, and its concentration was determined by reading absorbance at 663 nm on an Infinite® 200 PRO microplate reader (TECAN Group Ltd., Mannedorf, Switzerland). Standard curves were obtained from fucoidan in solution with known concentrations (**Figure 16)**.

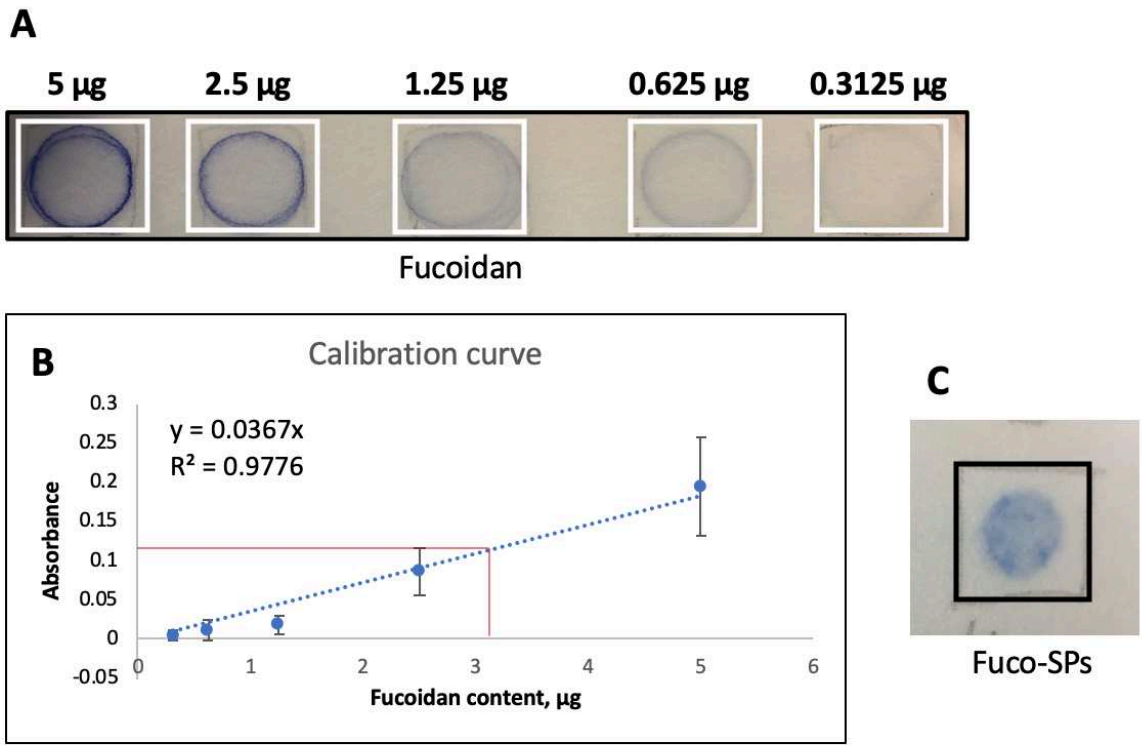


**Figure 16. Quantification of fucoidan content in hydrogel Fuco-SPs by a colorimetric assay. A.** Blue circles from fucoidan of mentioned concentrations were stained with methylene blue. **B.** The calibration curve of fucoidan content by optical density indicated the amount of fucoidan in one sample of Fuco-SPs (red line). **C.** Example of blue spot of hydrolysate solution of Fuco-SPs stained with methylene blue.

*Loading rtPA on the SPs:* rtPA was immobilized onto the SPs by adsorption. 100 µL of SPs (5 mg/mL) was mixed with 100 µL of rtPA (1 mg/mL) in ultrapure water and then incubated for 1 h at RT. Free unabsorbed rtPA was removed by 3 cycles of ultracentrifugation (15 min, 15,000 g). The SPs with adsorbed rtPA (rtPA-SPs) were resuspended in water and used for the drug loading efficiency quantification.

*Drug encapsulation efficiency:* The amount of rtPA loaded on the SPs was measured using the Pierce BCA protein assay kit (Life Technologies SAS, Courtaboeuf, France). Briefly, 200 µL of working reagent was added to 25 µL of each sample in 96 well-plate. The absorbance at 562 nm was read on the Infinite® 200 PRO microplate reader (TECAN Group Ltd., Mannedorf, Switzerland) after 30 min of incubation at 37 °C and cooling to RT for 10 min.

The concentration of the drug was extrapolated by a calibration curve prepared with different concentrations of rtPA.

*In vitro rtPA release:* The release of rtPA from the Fuco-SPs was assessed by flow cytometry [241]. FITC-rtPA (Abcam, Cambridge, United Kingdom) at 1 mg/mL was placed in contact with TRITC Fuco-SPs at 5 mg/mL for 1 h at RT. The suspensions were added to tubes pre-filled with 400 µL of saline and placed under gentle agitation at 37 ºC. At each time point of 0, 15, 30, 45, 60, and 90 min, the tubes were analyzed with a BD FACS Aria™ III flow cytometer (Becton Dickinson, New Jersey, United States). The TRITC-Dextran, excited by a 543 nm laser, was detected at 569 nm, while the FITC-rtPA, excited at 480 nm, was detected on a 530/30 nm PMT. Flow cytometry analyses were performed in triplicates with Diva software (Becton Dickinson). The protein release curve was obtained by normalizing the values of Mean Fluorescence Intensity (MFI) of the FITC-rtPA still associated with TRITC-Fuco-SPs.

*In vitro amidolytic activity of rtPA-loaded SPs:* Amidolytic activity of rtPA loaded SPs was assessed with the fluorogenic substrate PefaFluor® tPA (Cryopep, Montpellier, France). 2.5 µL of samples at 20 µg/mL was put in contact with 97.5 µL of 100 mM HEPES buffer (pH 8.0, 154 mM NaCl, 0.1% HAS) in the 96-well plate. After the addition of 10 µL PefaFluor® at 1 mM, a kinetic profile was obtained by measuring the fluorescence level at 440 nm every 2 min for 90 min at 37 ºC with Infinite® 200 PRO microplate reader (TECAN Group Ltd., Mannedorf, Switzerland). Free rtPA was used at the same concentration based on the Pierce BCA protein assay. Increase of fluorescence corresponded to the fluorogenic peptide substrate hydrolysis by rtPA. Enzymatic activity was determined from the resulting kinetic profile and compared to the one of free rtPA.

*In vitro fibrinolytic activity of rtPA-loaded SPs:* To assess the fibrinolytic activity of rtPA-loaded SPs, a fibrin lysis clot experiment was performed. 5 mL of TRIS Buffer with 3% w/v low melting agarose (Carl Roth GmbH þ Co. KG, Karlsruhe, Germany) were heated to

65 °C. 5 mL of Fibrinogen (from human plasma, Sigma Aldrich) solution in TRIS buffer at 5 mg/mL was slowly heated to 37 °C. Once the agarose solution reached 65 °C, it was cooled to 37 °C, and 2.5 U of thrombin (from human plasma, Sigma Aldrich) was added. Next, a fibrinogen solution was slowly added into the agarose/thrombin mixture under gentle agitation to avoid the formation of bubbles. The reaction mixture was poured into a 9 cm Petri dish and cooled at 4 °C for 30 min until the fibrin clot became visible. On the solidified agarose gel, round wells were formed using a 3 mm punch as sample reservoirs. 5 µl of each sample at 45 µg/mL was dropped into the wells and incubated overnight at 37 °C in a humid environment. The degree of fibrin lysis was quantified with ImageJ by comparing the size of the fibrinolysis circle of the samples and free rtPA at the equivalent concentration based on the Pierce BCA protein assay.

*Flow microchamber experiments:* An *in vitro* flow adhesion assay was performed to evaluate the affinity of the Fuco-SPs with their molecular target. Micro-channels of Vena8 Fluoro$^+$ chambers (width: 0.04 cm, height: 0.01 cm, and length: 2.8 cm; Cellix Ltd, Dublin, Ireland) were coated overnight with recombinant human P-selectin, L-selectin, or E-selectin (R&D systems France, Lille, France) at 100 µg/mL and left overnight at 4 °C. To confirm the concentration-dependent binding of Fuco-SPs to P-selectin, some channels were coated with P-selectin at a range of concentrations (5, 25, 50, and 100 µg/mL). Channels were then washed with NaCl 0.9% and further incubated with HSA at 10 µg/mL for 2h.

A suspension of fluorescently labeled Control-SPs or Fuco-SPs at 1 mg/mL in saline was passed through the channels for 5 min at arterial and venous flow conditions (shear stress 67.5 dyne/cm$^2$ and 6.75 dyne/cm$^2$) using an ExiGo™ pump (Cellix Ltd, Dublin, Ireland). For the competitive binding experiment, fucoidan solution (10 mg/mL) was injected 5 min prior to the Fuco-SPs at the same rate. Then, all the channels were washed with NaCl 0.9% for 1 min. The binding of the adhered SPs was visualized in real-time under fluorescence microscopy

(Axio Observer, Carl Zeiss Microimaging GmbH, Iena, Germany). For the quantitative analysis, the number of fluorescent SP clusters on each channel was measured using the "Analyze particles" tool in the image analysis software ImageJ (NIH, Bethesda, U.S.) with a 4-pixel threshold to eliminate the background noise.

To further investigate the binding efficiency of unloaded and loaded SPs to activated platelets, the microchannels of Vena8 Fluoro$^{+}$ were coated with 50 µg/mL of fibrillar type I collagen Horm® overnight at 4 °C and rinsed with NaCl 0.9% before use. Human whole blood (EFS, Bichat Hospital, Paris, France), collected in the PPACK tubes and labeled with 5 µM DIOC6 (Life Technologies SAS, Saint-Aubin, France), was perfused at arterial shear stress for 5 min to induce platelet activation and aggregation. Platelet aggregation through contact with collagen was visualized in real-time with phase-contrast microscopy (Axio Observer, Carl Zeiss Microscopy, Oberkochen, Germany). After rinsing with NaCl 0.9%, fluorescent Control-SPs or Fuco-SPs (unloaded or loaded with rtPA) at 1 mg/mL were injected into the channels in saline for 5 min. Their accumulation onto activated aggregates was monitored in real-time. Channels were then washed for 1 min with NaCl 0.9%. Finally, the MFI of the fluorescent SPs that are bound to the platelets on each channel was analyzed with ImageJ. Intensity settings were kept the same for both types of SPs.

*Biodistribution of Fuco-SPs in vivo:* Animal studies were performed on C57BL/6 male mice (EJ, Le Genest, St-Berthevin, France) aged 5-8 weeks (~ 25 g weight) in respect of the principles of laboratory about animal experimentation and with the approval of the animal care and use committee of the Claude Bernard Institute (APAFIS #8724, Paris, France). Mice were anesthetized under the application of 2% isoflurane (Aerrane, Baxter). 200 µl of Fuco-SPs at 5 mg/mL were injected through the retro-orbital route (n=3). To histologically analyze the particle accumulation, mice were sacrificed 30 min following their administration. The lungs, liver, kidneys, and spleen were excised, washed in saline, and fixed in paraformaldehyde 4%.

The tissues were then frozen and cryosectioned at 10 µm thickness. The samples were stained with alcian blue staining protocol. Strongly negative structures, including the Fuco-SPs, are stained blue, nuclei are stained pink to red, and cytoplasms appear pale pink. The slides with tissue slices were scanned with the Nanozoomer (Hamamatsu, Hamamatsu City, Japan) and viewed with the NDP.view2 software.

*Animals and thrombin stroke model in vivo:* Animal experiments were carried out on male Swiss wild-type mice (8–9 weeks old; 35-45 g; CURB, Caen, France). All experiments were performed following the French (Decree 87/848) and the European Communities Council (2010/63/EU) guidelines and were approved by the institutional review board (French ministry of Research). All the experiments were validated by Normandy's local ethical committee (CENOMEXA) registered under the reference number APAFIS#13172. Anesthesia was induced by the application of 5% isoflurane (Aerrane, Baxter) and maintained by 2% isoflurane in a mixture of $O_2/N_2O$ (30% / 70%).

Mice were placed in a stereotaxic device, then a small craniotomy was performed, the dura was excised, and the middle cerebral artery (MCA) was exposed. To induce the MCA occlusion, the coagulation cascade was triggered by the pneumatical injection of 1 µL murine α-thrombin (1 IU; Stago BNL) with a glass micropipette, as previously described [242]. Successful MCA occlusion was confirmed by the Laser Doppler flowmeter (Oxford Optronix). For the treatment, the animals were intravenously injected through a tail vein catheter (200 µL, 10% bolus, 90% infusion over 40 minutes) with either saline (n=5) or rtPA-Fuco-SPs (Actilyse® rtPA at 10 mg/kg) (n=6) 20 minutes after thrombus formation. Brain perfusion was monitored by Laser Speckle Contrast Imager (MOOR FLPI-2, Moor Instruments) throughout the treatment. Region of interest (ROI) was selected on the ipsilateral to occlusion and contralateral hemispheres to monitor the relative cerebral blood flow in the affected region ($Fl_t$ = 100% x $Fl_{ipsi}/Fl_{contra}$). The post-stroke reperfusion was expressed as a Growth Rate (GR) of

the blood flow increase in the ipsilateral ROI to contralateral one at a time point, and it was quantified as GR (%) = 100% x ($Fl_{t2}$ - $Fl_{t1}$)/ $Fl_{t1}$.

*Magnetic resonance imaging acquisition and analysis:* Mice were anesthetized with 5% isoflurane and maintained with 1.5-2% isoflurane in a mixture of $O_2$/$N_2O$ (30% / 70%) during the acquisitions. Experiments were carried out on a Pharmascan 7T (Bruker Biospin, Wissembourg, France). Three-dimensional T2-weighted images were acquired using a Multi-Slice Multi-Echo sequence (TE/TR 39.9 ms / 3,500 ms, 2 averages) 24 h after the stroke. Lesion volumes were quantified on these images using ImageJ software (slice thickness 0.5 mm). Magnetic resonance angiography was performed using a 2D-TOF sequence (TE/TR 4.24 ms / 12 ms, 1 average) 24 h after ischemia, and the recanalization status of the MCA was determined blindly from the analysis of the merged MCA angiograms with maximum intensity. The angiographic score is based on the TICI (Thrombolysis in Cerebral Infarction) grade flow scoring (from score 0: no perfusion to score 3: full recanalization). For the *in vivo* detection of the BBB permeability, three dimensional T1 FLASH sequences (TE/TR 4.37 ms / 15.12 ms; 3 averages) were used, 15 min after the intravenous injection of 200 µl of a solution containing 50 µl of gadolinium chelate (DOTAREM) diluted in saline. BBB leakage was measured 4 days after the stroke induction, and its volume was quantified using ImageJ.

*Thrombus targeting by Fuco-SPs in a murine model of venous thrombosis:* Animal studies were done following principles of laboratory about animal care and with the approval of the animal care and use committee of the Claude Bernard Institute (APAFIS #8724, Paris, France). $FeCl_3$-induced *in vivo* thrombosis model on mesenteric vein was carried out on C57BL/6 male mice (EJ, Le Genest, St-Berthevin, France) aged 5-8 weeks. Mice were anesthetized with an intraperitoneal injection of ketamine (100 mg/kg) and xylazine (10 mg/kg). After midline abdominal incision, the mesentery was exposed, and vessels were visualized by an intravital microscope (Leica MacroFluo, Leica Microsystems SAS, Nanterre Cedex, France)

using Orca Flash 4.0 scientific CMOS camera (Hamamatsu Photonics France SARL, Massy, France). For green fluorescent labeling of mitochondria of platelets and leucocytes, DIOC6 (Life Technologies SAS, Saint-Aubin, France) at 25 µM was retro-orbitally injected. The mesentery vein was covered with a 1 mm large Whatman chromatography paper that was prior soaked in a 10% w/v iron chloride (Sigma-Aldrich) solution for 1 min and then washed with saline. The formation of non-occlusive thrombi was monitored in real-time by fluorescence microscopy by the accumulation of fluorescently labeled platelets. TRITC fluorescent-labeled Control-SPs or Fuco-SPs were retro-orbitally injected 10 min after thrombus initiation with the volume of 150 µL (5 mice per group).

For histological evaluation, mice were sacrificed with pentobarbital overdose 5 min after administration of SPs. The affected part of the mesenteric vein was cut, washed in 0.9% NaCl, fixed in paraformaldehyde 4% (w/v), and frozen. The vein samples were cryosectioned at 10 µm thickness. The cell nuclei of a venous vascular wall were labeled with DAPI (Thermo Fisher Scientific, Massachusetts, United States) contained in a mounting medium (Vecto laboratories). The samples were observed by fluorescence microscopy. For the quantitative analysis, normalized MFI of the TRITC signal from SPs was expressed, defined as total TRITC fluorescence intensity divided by the size of the thrombus area on 2 slides from each mouse with the ImageJ (NIH, Bethesda, U.S.).

*Statistical analysis:* Quantitative data were expressed as mean ± standard error of the mean (SEM) ($n \geq 3$). Statistical tests were carried out with GraphPad Prism 8 (GraphPad Software, Inc., La Jolla, U.S.) with a 95% confidence level. Kolmogorov-Smirnov normality test was utilized to examine if variables are normally distributed. Normally distributed data were analyzed then with unpaired t-test or one-way analysis of variance (ANOVA) with post hoc Turkey's test. The Mann-Whitney U test was applied otherwise. The p-values of * $p<0.05$; ** $p<0.01$; *** $p<0.001$ were considered statistically significant.

# 3 RESULTS AND DISCUSSION

## 3.1 Submicroparticle synthesis and characterization

Novel polysaccharide SPs were elaborated by a simple and reproducible two-step synthesis process influenced by [104,231] (**Figure 17A**). First, a stable w/o miniemulsion of the aqueous phase with hydrophilic polysaccharides and vegetable (sunflower) oil was prepared. Chemical crosslinking of polysaccharides with the crosslinking agent STMP under alkaline conditions **(Figure 17B)** produced a suspension of uniform SPs. We refer to the hydrogel particles only from dextran as Control-SPs, and from a mixture of dextran and fucoidan as Fuco-SPs in this manuscript.

To ensure the *in vivo* safety during the preparation of the drug delivery platform, low molecular weight dextran 40 kDa of clinical-grade was utilized without any chemical modification. Having a large number of hydroxyl groups, dextran is a suitable compound for subsequent chemical crosslinking with STMP [184], an FDA-approved non-toxic food additive [243]. Fucoidan, a marine sulfated polysaccharide, is approved as a pharmaceutical compound [185] and exhibits a nanomolar affinity to P-selectin [234]; hence, it served as a targeting ligand to thrombi. A recently completed Phase I clinical trial of fucoidan radiolabeled by Technetium-99m reported its safety and favorable biodistribution as a potential diagnostic agent for thrombosis imaging [186] while a Phase II stage is ongoing. Hence, both natural polysaccharides applied in this study are affordable, biodegradable, biocompatible compounds, non-immunogenic, and approved for clinical applications. Intriguingly, several articles claim that dextran [244] and fucoidan [226,230] themselves exert some antithrombotic action that makes them an excellent starting material for the nanocarrier.

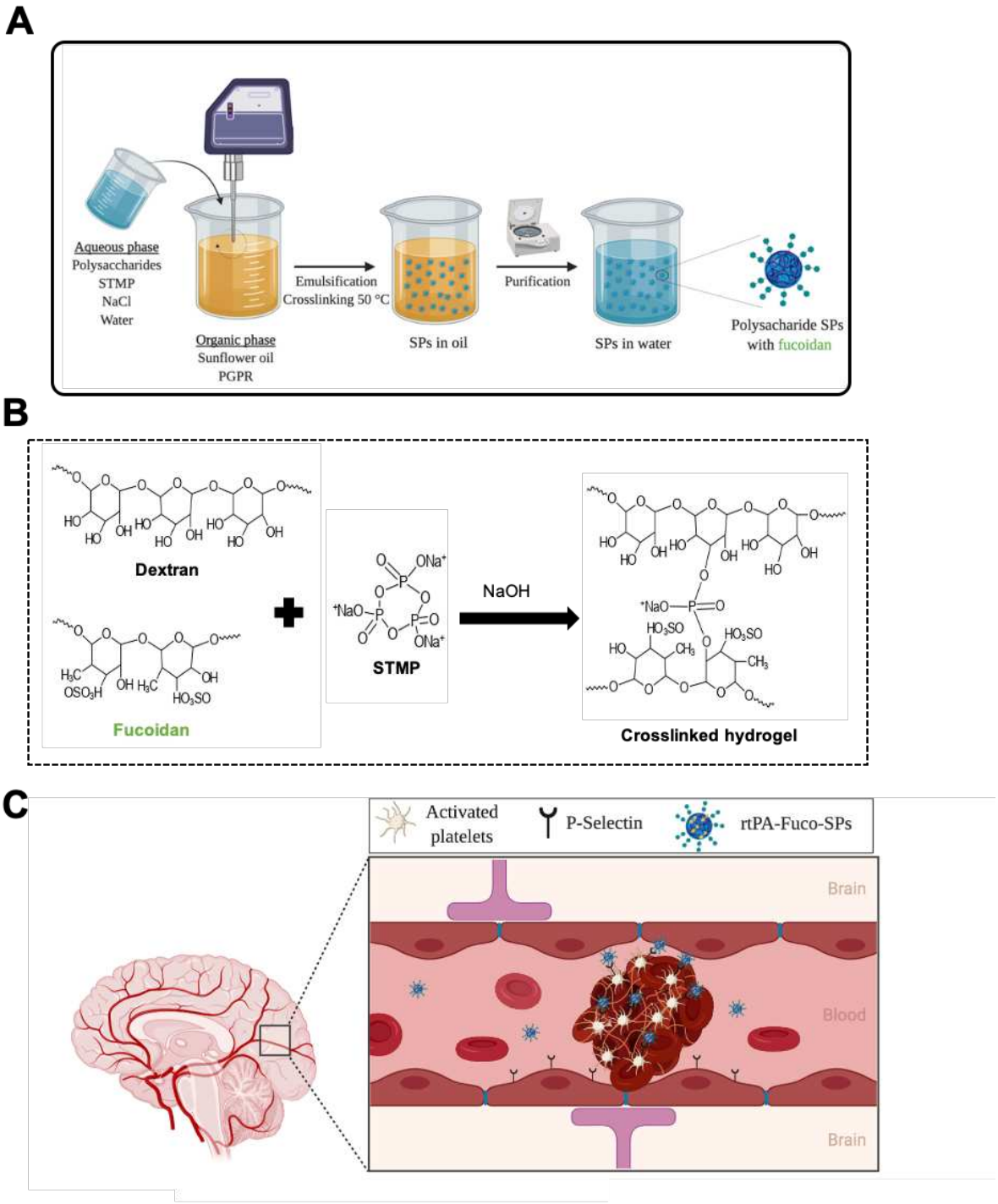


**Figure 17. Synthesis and the *in vivo* proposed mechanism of action of the Fuco-SPs. A.** Overall schematic of the synthesis process of the SPs – miniemulsion / crosslinking. **B.** Crosslinking of the polysaccharides (dextran and fucoidan) with STMP in alkaline conditions. **C.** Proposed therapeutic mode of action of the rtPA-loaded Fuco-SPs after the ischemic stroke: the Fuco-SPs accumulate on the surface of the activated platelets due to P-selectin affinity of fucoidan and perform local thrombolysis with alteplase.

Instead of commonly used organic solvents, sunflower oil was utilized as an emulsion continuous phase. The choice of the stabilizing agent plays an important role in reducing the interfacial tension and Laplace pressure when fabricating a stable emulsion and future nanocarrier. In this work, we selected a potent oil-soluble nonionic surfactant for stabilizing w/o emulsions – PGPR, which is also recognized by the FDA as a safe compound and is frequently used as an emulsifier in the food production industry [245]. In addition, to counteract the Ostwald ripening of water droplets, 6 M NaCl was added to the aqueous phase as an osmotic agent to adjust the osmotic gradient and to stabilize the w/o emulsion further. Overall, multiple parameters were optimized to obtain a stable and homogenous miniemulsion and subsequent nano-delivery system. It was found that the size of the templating droplet and the ultimate hydrogel SPs being directly proportional to the polysaccharide molecular weight and inversely proportional to the amount of surfactant and crosslinking agent as well as homogenization speed (data not shown).

The polysaccharide nature of the particles was proven by comparing their FTIR spectra with the equivalent ones of the polysaccharide themselves with a strong peak, corresponding to the -OH bond **(Figure 18)**.

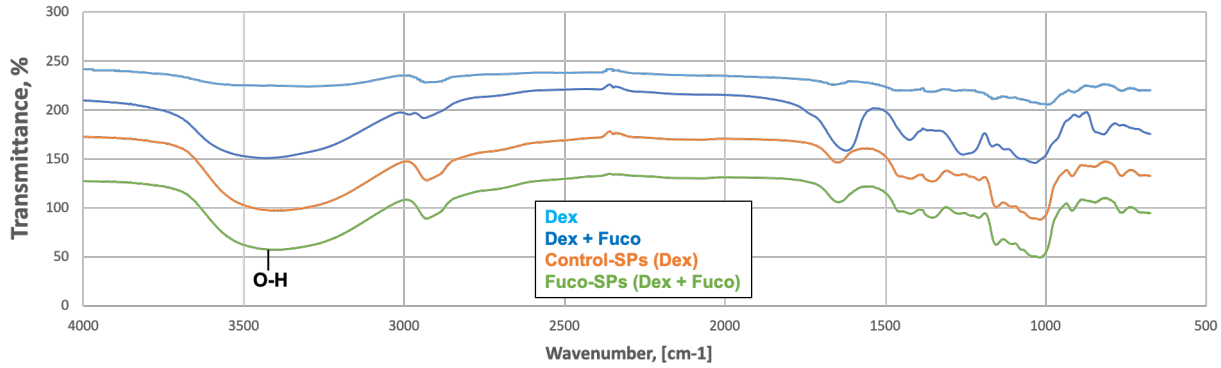


**Figure 18. FTIR spectra of the polysaccharides and SPs.** Control-SPs and Fuco-SPs are composed of dextran and a mixture of dextran and fucoidan, respectively.

ESEM and TEM images revealed a well-defined spherical morphology and uniform size distribution of SPs (**Figure 19A & 19B**). Functionalized Fuco-SPs contained 8.60 ± 0.01% of fucoidan in a mass of the total SPs weight, determined by elemental analysis of sulfur, and 9.30 ± 1.07% of fucoidan by quantification of the sulfate content by a semi-quantitative colorimetric assay. In such a way, two different techniques estimated ~9% fucoidan composition in the SPs. The physico-chemical properties of these nanoformulations are displayed in **Figure 19D**. The SPs exhibited the hydrodynamic size 674.87 ± 59.35 nm (Control-SPs) and 708.48 ± 40.00 nm (Fuco-SPs), determined by DLS. It is essential to highlight that a relatively large size of the SPs might limit the accumulation of associated rtPA within the brain parenchyma and reduce the risk of hemorrhagic events. The negative ζ-potential of the SPs -24.83 ± 0.09 mV for Control-SPs and -27.07 ± 0.39 mV for Fuco-SPs ensured colloidal stability as a result of the anionic nature of the fucoidan and the formation of the anionic phosphate functional groups, produced during the crosslinking reaction with STMP. The phosphorus content of the SPs is indicated in **Figure 19D**.

The obtained SPs preserved their integrity in a physiological solution of 0.9% NaCl. As hydrogel-based particles, they were able to swell in an aqueous medium while maintaining their network structure (**Figure 19C**). These soft particles resemble the networks of natural extracellular matrices that could minimize tissue irritation or cell adherence [193]. The size and zeta potential of both SPs remained relatively stable for at least 30 days at 4 °C storage. In addition, adequate storage of the SPs can be ensured by freeze-drying with 5% (w/v) sucrose as a cryoprotectant and subsequent resuspension in an aqueous medium. The overall yield of the synthesis was 13.4 ± 0.7 mg of SPs.

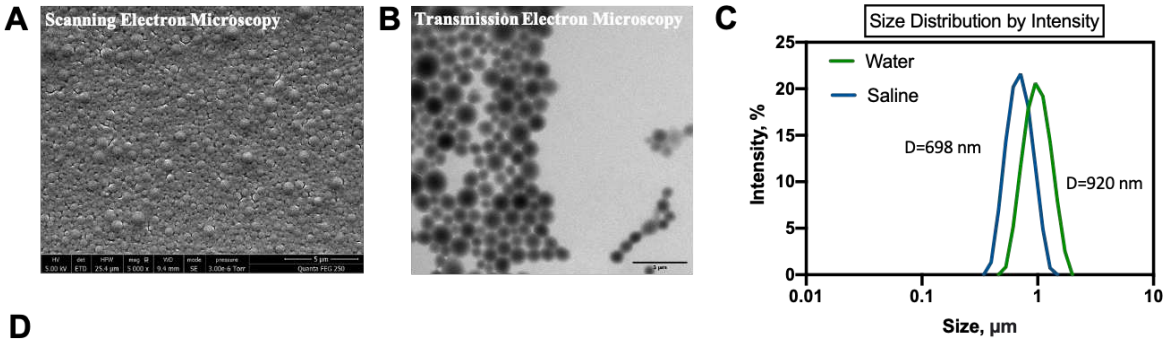


D

| Sample | Size, nm | PDI | Zeta potential, mV | Phosphorus content, mg/l | Fucoidan content (Sulfate), %, w/w | Fucoidan content (Sulfur) %, w/w |
|---|---|---|---|---|---|---|
| Control-SPs | 674.87 ± 59.35 | 0.24 ± 0.05 | -24.83 ± 0.09 | 33.2 ± 0.1 | - | - |
| Fuco-SPs | 708.48 ± 40.00 | 0.21 ± 0.10 | -27.07 ± 0.39 | 30.6 ± 0.1 | 9.30 ± 1.07 | 8.60 ± 0.01 |

**Figure 19. Physico-chemical characterization of the SPs.** SEM **(A)** and TEM **(B)** images of the Fuco-SPs. **C.** Swelling in the water of the Fuco-SPs due to the hydrogel nature of the particles. Size of one sample when resuspended in water (green) and saline (blue). **D**. Size, zeta potential, and chemical composition of the SPs.

It is important to remark that the submicronic particles could also be synthesized from other natural polysaccharides, such as pullulan, a mixture of dextran and pullulan, and a mixture of carboxymethyl dextran with dextran, via the miniemulsion/crosslinking protocol with little modifications. This flexibility permits, for example, to modulate the mechanical properties of the obtained particles and introduce functional such as COOH onto the surface of the SPs that might be relevant for other applications. **Figure 20A** summarizes experimental conditions used for the particle production in a reproducible way, with sizes in the submicronic range. Due to the anionic charges brought by STMP, all the SPs exhibited negative zeta potential.

**A**

| Aqueous Phase | Organic phase | V/N | D(0.1) | D(0.5) | D(0.9) | Span | Zeta potential, mV |
|---|---|---|---|---|---|---|---|
| **Pullulan 20 kDA**<br>**Fucoidan MMW**<br>(450 mg/ml, 6 M NaCl)<br>4.6% w/v STMP, 0.76 M NaOH | 6% PGPR<br>15 mL SO | V | 0.708 | 1.01 | 1.47 | 0.753 | -29.8 |
| | | N | 0.669 | 0.810 | 1.16 | 0.669 | |
| **Pullulan 20/Dextran 40 kDA**<br>65/35<br>**Fucoidan MMW**<br>(450 mg/ml, 6 M NaCl)<br>4.6% w/v STMP, 0.76 M NaOH | 6% PGPR<br>15 mL SO | V | 0.877 | 1.22 | 1.77 | 0.885 | -29.6 |
| | | N | 0.776 | 1.03 | 1.42 | 0.883 | |
| **CM Dextran 40/Dextran 40 kDA**<br>20/80<br>**Fucoidan MMW**<br>(300 mg/ml, 6 M NaCl)<br>4.6% w/v STMP, 0.76 M NaOH | 6% PGPR<br>15 mL SO | V | 0.645 | 0.898 | 1.25 | 0.669 | -29.9 |
| | | N | 0.557 | 0.735 | 1.03 | 0.642 | |

**B**

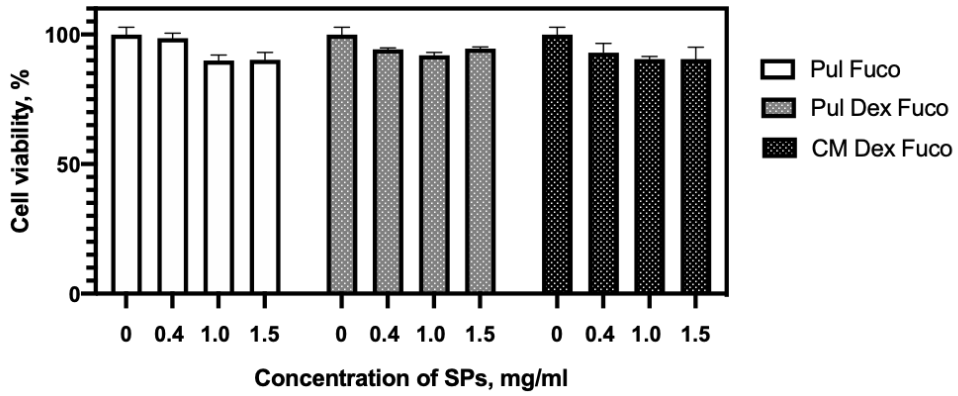


**Figure 20. Formulation and cytocompatibility of polysaccharide submicronic particles from other polymers or their mixtures. A.** Size and zeta potential of the SPs by laser diffraction and ELS, respectively. D(0.1), D(0.5) and D(0.9) are the particle diameters at 10%, 50% and 90% of the particle size distribution by number (N) or volume (V). Span refers to the width of the distribution. **B.** Cytocompatibility of the different types of the SPs on HUVECs by Resazurin assay.

### 3.2 Biocompatibility of the SPs

The injectable hydrogel SPs were produced according to the green chemistry principles through the formulation method without the use of hazardous substances and organic solvents and were expected to be biocompatible.

An initial *in vitro* evaluation of biocompatibility of the developed SPs examined cyto- and hemocompatibility. The cytocompatibility of the SPs was assessed with a resazurin cell viability assay. Following 24 h exposure, Control-SPs and Fuco-SPs did not affect cellular viability and metabolic activity of HUVECs at concentrations ranging from 0.1 to 1.5 mg/mL, exhibiting an excellent cytocompatible profile (cell survival > 90%, up to the highest tested concentrations of SPs) (**Figure 21A**). The upper limit for the tested concentration of 1.5 mg/mL of the SPs was selected to surpass the tested concentrations for the majority of the nanosystems *in vitro* (typically, maximum 400 μg/mL) [246] and the concentration of the SPs employed for further *in vivo* experiments in this work (71 mg SPs per 1 kg body weight or 1.1 mg SPs per 1 mL of blood). There was no significant difference between the Control-SPs and Fuco-SPs, as both did not provoke cytotoxicity. Additionally, high cell viability was similarly observed in the SPs from other polysaccharides (**Figure 20B**).

Since the SPs in this study were designed for intravenous administration and were expected to have direct contact with blood, the Fuco-SPs were examined for their blood-compatible behavior by a hemolysis test on isolated murine red blood cells *in vitro* (**Figure 21B**). Even at the highest concentration of 1.5 mg/mL, the SPs presented a hemolytic index of 1.51 ± 0.02%, below 2%, and considered nonhemolytic according to ISO 10993 - 4 standard [247,248].

Morphology of the cells, co-cultured with Fuco-SPs, was visualized with confocal microscopy. No apparent morphological differences were revealed for HUVECs with Fuco-SPs and negative control, as depicted in **Figure 21C**. FITC-Phalloidin staining was used to visualize a cytoplasm and DAPI for nuclei. Moreover, the SPs were internalized by endocytosis as the merged images of all three probes revealed colocalization of the particles within the dye in the cytoplasm.

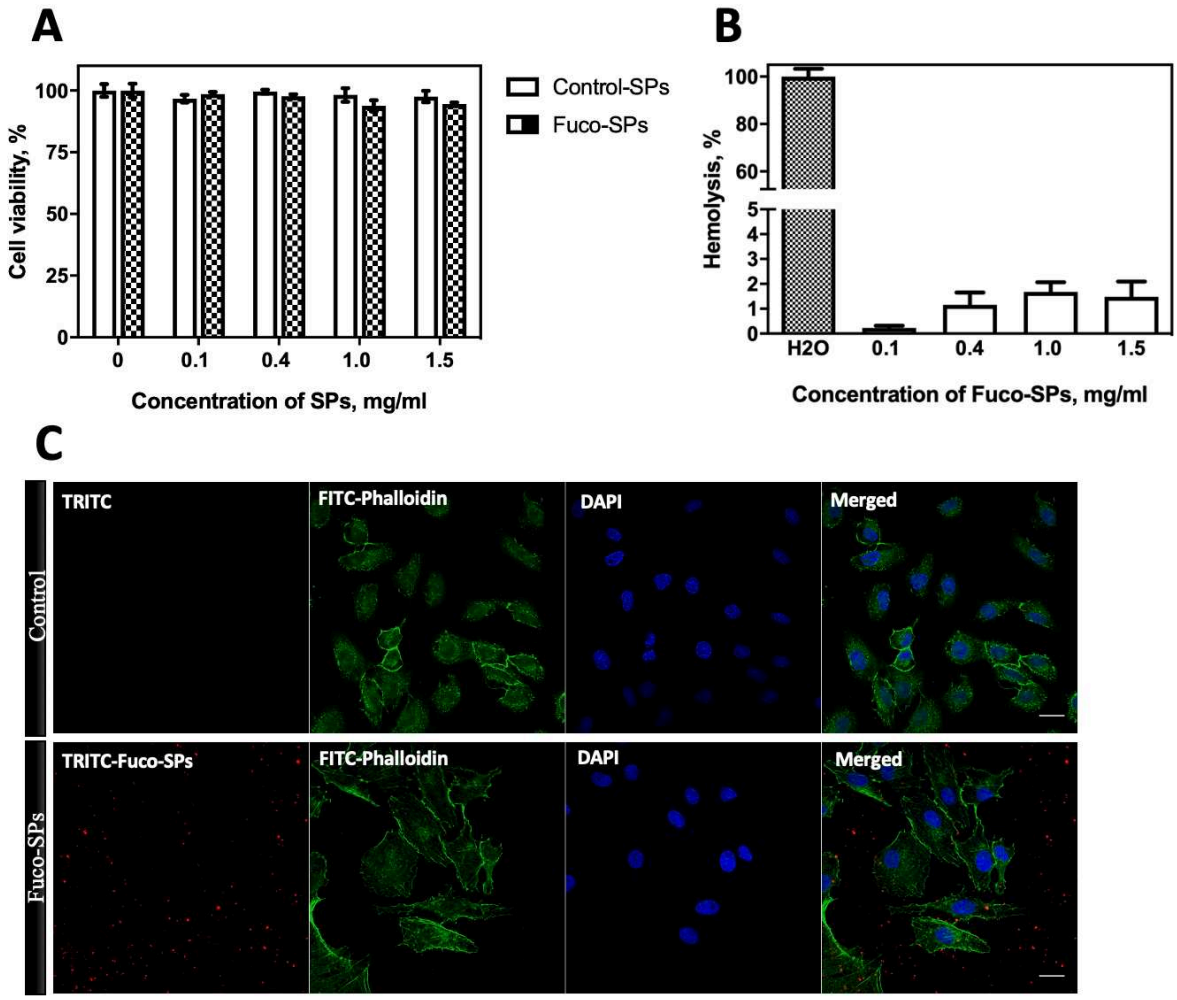


**Figure 21. Biocompatibility of the SPs.** Cytocompatibility **(A)** and hemocompatibility **(B)**. Confocal microscopy of HUVECs cultured without (control) and with Fuco-SPs **(C)** (scale bar = 30 μm).

Collectively, these results suggest that the polysaccharide SPs have favorable biocompatibility for their application *in vivo*.

### 3.3 Binding of SPs to P-selectin *in vitro*

Knowing that fucoidan was homogeneously distributed in the structure of the hydrogel Fuco-SPs and constituted ~ 9% w/w of the composition, we investigated whether its quantity on the surface was sufficient for specific adhesion to its molecular target. While most of the publications assess targeting strategy *in vitro* in static conditions by flow cytometry or confocal

microscopy [82,231,249], our group developed a robust and tunable dynamic microfluidic method, mimicking arterial or venous blood flow conditions, to study the targeting efficacy for recombinant P-selectin or/and human activated platelet aggregates expressing P-selectin and previously validated it with fucoidan-coated nano-/microcarriers [67,105,232] **(Figure 22)**.

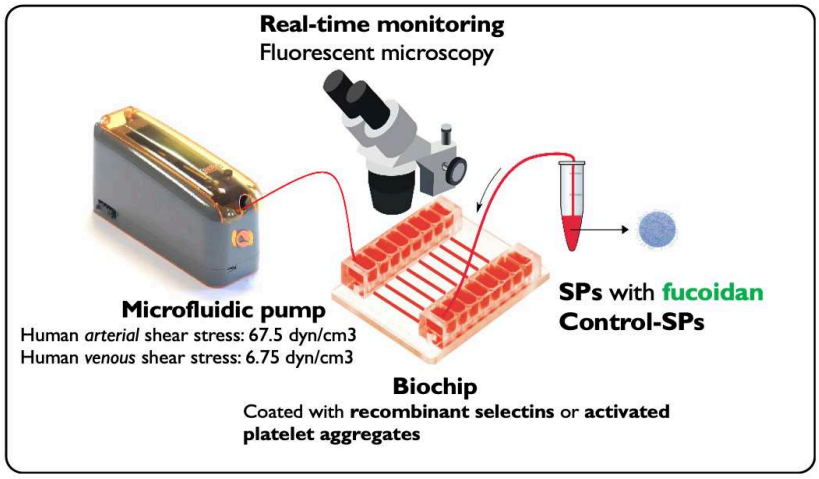


**Figure 22. Schematic illustration of the *in vitro* microfluidic targeting assay.**

First, fluorescent Fuco-SPs and Control-SPs were injected in the microchannels coated with recombinant P-selectin under arterial or venous shear rates (67.5 dyne/cm$^2$ vs. 6.75 dyne/cm$^2$), and their adhesion was visualized and quantified in real-time under fluorescence microscopy. According to obtained results, fluorescent Fuco-SPs depicted a significantly higher adhesion to P-selectin coating than Control-SPs both in arterial (374.25 ± 115.33 adhered Fuco-SPs vs. 30.25 ± 13.84 adhered Control-SPs, * $p < 0.05$) and venous (228.25 ± 36.67 adhered Fuco-SPs vs. 34.50 ± 18.16 adhered Control-SPs, ** $p < 0.01$) flow conditions (**Figure 23A & 23E**). There was no significant difference between the fluorescent signal of Fuco-SPs accumulation for arterial and venous flow conditions ($p=0.2731$). Fuco-SPs accumulation after injection onto P-selectin coating was in a linear dose-dependent manner as regards the P-selectin concentration, $R^2=0.9904$ (**Figure 23B**). An experiment of competitive

interaction illustrates that fucoidan solution pre-injection at 10 mg/mL considerably reduced the attachment of the Fuco-SPs onto the microchannels with P-selectin (374.25 ± 115.33 vs. 19.75 ± 10.06, * p <0.05) (**Figure 23C**).

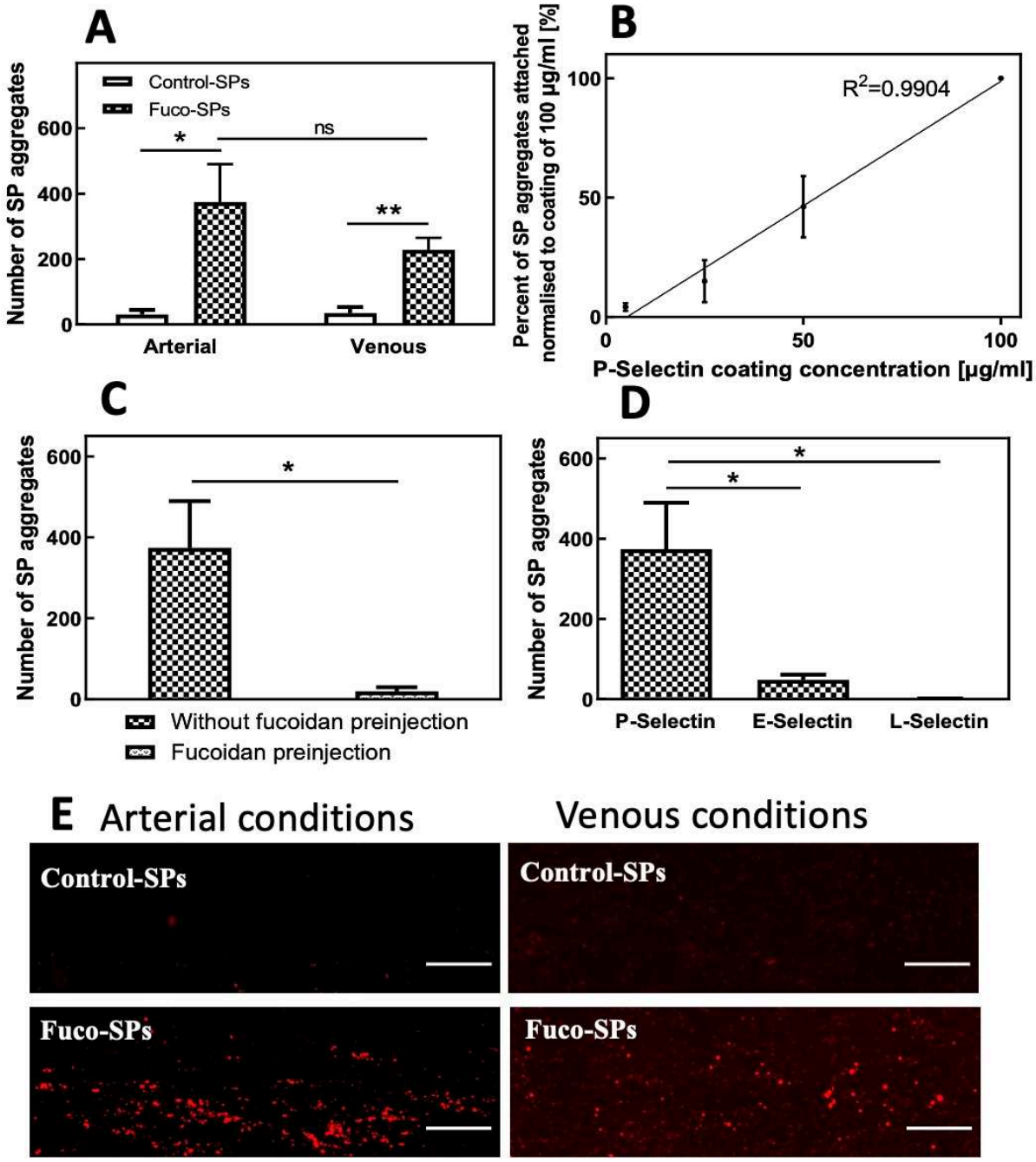


**Figure 23. Evaluation of the SPs interactions with selectins. A.** Adhesion of the Control-SPs or Fuco-SPs on the coating of the recombinant P-selectin in the microfluidic assay under arterial and venous flow conditions (n = 4). **B.** Concentration-dependent binding of the Fuco-

SPs onto the coating of the P-selectin at a range of concentrations. **C.** Fucoidan pre-injection inhibited Fuco-SPs adhesion onto the P-selectin. **D.** Comparison of the Fuco-SPs binding to other selectins: E- and L-selectin. **E.** Fluorescent microscope view of Control-SPs or Fuco-SPs adhesion over a P-selectin coating of 100 µg /mL under arterial and venous shear rates (scale bar = 20 µm).

To establish the specificity of the Fuco-SPs binding to P-selectin, the targeting assay was extended to other members of the selectin family: E- and L-selectin [219]. The percentage of the Fuco-SPs adhered to the E- and L-selectin was normalized over the mean number of the attached Fuco-SPs to a P-selectin coating at the equivalent concentration. Indeed, only 12.73 ± 3.66% of the SPs adhered to E-selectin and 0.26 ± 0.19% to L-selectin coating (**Figure 23D**). Thus, our results indicate that Fuco-SPs bind specifically to P-selectin but not to E- and L-selectins, and these results are in accordance with a previous work of our group published by Bo L. *et al.* of fucoidan-functionalized polymer microcapsules [105].

Overall, these findings are encouraging evidence of the sensitivity and selectivity of the Fuco-SPs, confirming fucoidan potential as a natural ligand of P-selectin.

### 3.4 rtPA loading onto the SPs and its release in saline. *In vitro* thrombolytic activity of rt-PA-loaded SPs

Due to rtPA low bioavailability and high dose administration requirements, coupling this enzyme to the biocompatible nanocarrier could overcome the drawbacks associated with a drug's high dosage. Herein, an efficient rtPA encapsulation was achieved through the physical adsorption method due to electrostatic interaction [250]: the protein, which is an amphoteric molecule, was put in contact with negatively charged polysaccharide SPs in the water at pH below rtPA isoelectric point IP=7.7 [251] when rtPA presented a positive charge. Indeed, BSA as a model protein, having the IP=4.7, could be successfully loaded onto the Fuco-SPs with

90.45 ± 1.35% loading efficiency in the acidic conditions at pH 2.7 (acetic acid 1% + Tween 0.02%) but not in the water when the net charge of BSA is negative.

Since adsorption is a mild drug encapsulation method, it can prevent rtPA from the disadvantages of the covalent bioconjugation, such as changes in the protein structure and function that might result in its partial denaturation and loss of activity [182]. The nanogel nature of the SPs allowed reaching a high encapsulation efficiency of the rtPA of 64.78 ± 2.16% and 81.04 ± 1.86% for Control-SPs and Fuco-SPs, respectively. The confocal microscopy images of FITC-rtPA loaded onto TRITC-labelled Fuco-SPs revealed the uniform distribution of the rtPA within a porous structure of the hydrogel SPs, as evidenced by a green fluorescence from FITC-rtPA colocalized with the red fluorescence from the particles (**Figure 24A**). The amount of rtPA conjugated to Fuco-SPs was growing linearly with the increasing concentration of the input drug to reach the saturation point at 100 µL rtPA per 500 µg SPs. As such, the total rtPA quantity could be tuned by changing the amount of Fuco-SPs.

The release kinetics of rtPA from fucoidan-functionalized SPs was analyzed *in vitro* by flow cytometry [241] in saline at 37 °C under gentle agitation by quantification of the MFI of the FITC-labelled rtPA associated with TRITC-fluorescent Fuco-SPs. **Figure 24B** indicated a gradual and continuous sustained release of the lytic agent from the SPs during the observation period: 46.41 ± 1.34% of the encapsulated protein was released during the first 15 min, and 76.98 ± 1.74% after 90 min. This release profile is classical for the hydrogels [252].

The thrombolytic activity of the rtPA-loaded SPs *in vitro* was analyzed as a combination of amidolytic and fibrinolytic activities and was reported in **Figure 24C – 24G**. Amidolytic or enzymatic activity featured the ability of the proteolytic enzyme to hydrolyze the rtPA substrate. Interestingly, the amidolytic activities of rtPA on Control-SPs and Fuco-SPs were comparable to that of free rtPA (**Figure 24C & 24D**). The fibrinolytic experiment *in vitro* of the rtPA-loaded SPs was performed in a fibrin plate assay (**Figure 24E**). The results

indicated full retention of fibrinolytic activity (**Figure 24F & 24G**). Thus, rtPA loaded onto the SPs appeared to diffuse into the fibrin-agarose matrix and induce fibrinolysis in contact with fibrin. Comparing covalent vs. non-covalent conjugation approaches, Friedrich *et al.* documented that the adsorptive bound rtPA liberated faster from the particles and diffused more readily into the fibrin matrix than covalently bound rtPA [128], which may also be beneficial in targeted thrombolysis. No significant difference was detected between both types of SPs, enabling us to utilize them in the following set of experiments.

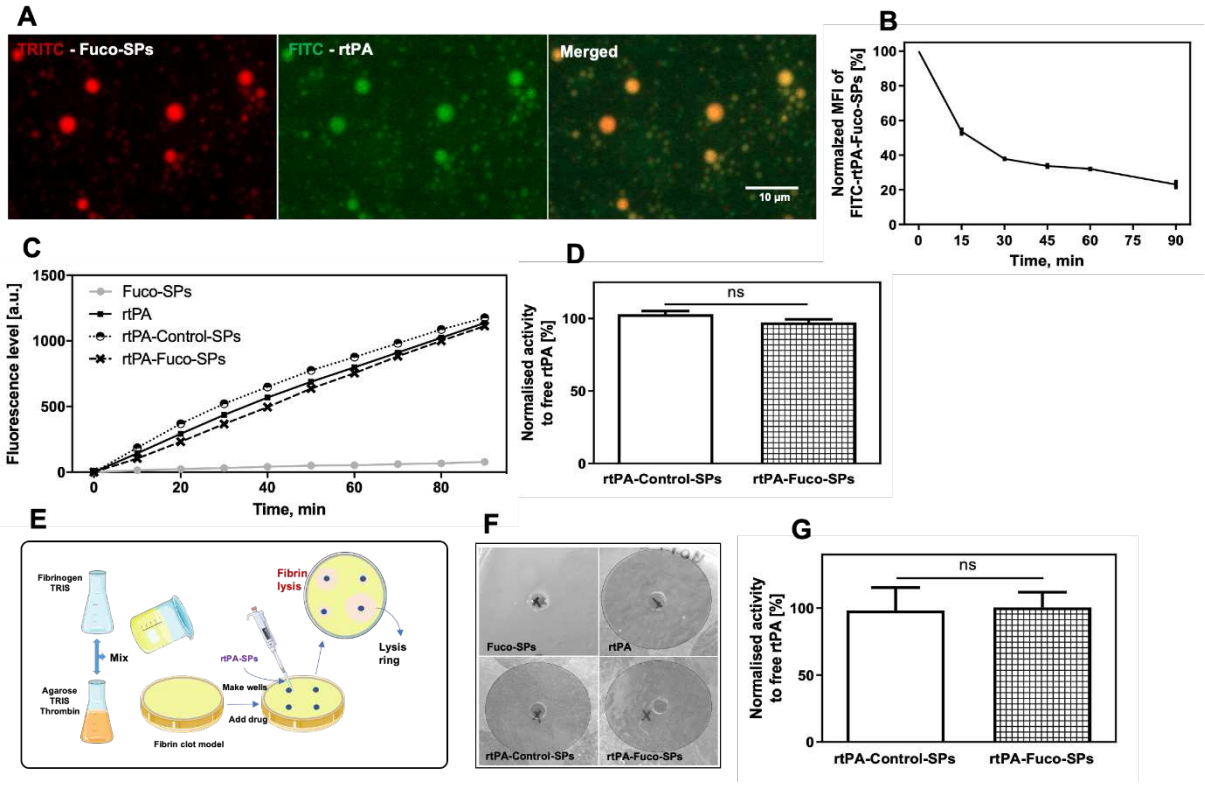


**Figure 24. Loading rtPA & its release from the SPs as well as thrombolytic efficacy *in vitro*. A.** FITC-rtPA loading onto the TRITC-Fuco-SPs visualized by confocal microscopy. **B.** *In vitro* rtPA release from rtPA-encapsulated Fuco-SPs by flow cytometry. **C - D.** Amidolytic activity measured by the PefaFluor® fluorogenic assay **C.** The curves correspond to the fluorescence release and are correlated to the enzymatic velocity over 90 min. **D.** Corresponding quantitative analysis normalized to free rtPA at the same concentration at 90 min. **E - G.** Fibrinolytic activities of the SPs determined by a fibrin-plate agarose assay **E.** Schematic illustration of the *in vitro* fibrinolytic test. **F.** Lysed circles as the fibrinolytic potential of the SPs *in vitro* by a fibrin-plate agarose assay at the equal concentration of the rtPA. **G.** The quantitative analysis normalized to free rtPA at the same concentration.

Overall, the rtPA association with the SPs did not affect the drug amidolytic activity and fibrinolytic potential in our design. This result is in accordance with most studies on nanogels suggesting that drug encapsulation via a passive diffusion into the preformed nanogels does not affect the secondary structure of the adsorbed protein and its biological activity [183].

### 3.5 Unloaded and rtPA-loaded Fuco-SPs adhere to activated platelet aggregates *in vitro* under arterial flow

Because aggregation of activated platelets and platelet-mediated coagulation pathways are hallmark events in thrombosis, activated platelets are a suitable cellular target for nanocarrier binding to thrombi [253]. Before the *in vivo* tests, we complemented the targeting evaluation from Section 3.3 with the second set of microfluidic experiments to validate Fuco-SPs capability to actively anchor onto the surface of activated platelets, expressing P-selectin. Thus, human whole blood was passed into collagen-coated microchannels to induce platelet activation and aggregation. Fuco-SPs or Control-SPs were then perfused at arterial shear stress (67.5 dyne/cm$^2$), and the accumulation of the fluorescence from the adhered SPs was detected on the surface of activated platelet aggregates. A quantitative analysis of the MFI revealed that Fuco-SPs adhered significantly more onto activated platelets than Control-SPs (2,678.34 ± 237.40 for Fuco-SPs vs. 392.44 ± 137.15 for Control-SPs, *** $p < 0.001$, **Figure 25A & 25B Left**). Notably, adsorption of rtPA did not impair the Fuco-SPs clot-binding ability (1,880.80 ± 429.37 for rtPA-Fuco-SPs vs. 77.56 ± 40.25 for rtPA-Control-SPs, ** $p < 0.01$, **Figure 25B Right**). There was no significant difference between unloaded and rtPA-loaded Fuco-SPs adhering to the activated platelets ($p=0.1149$).

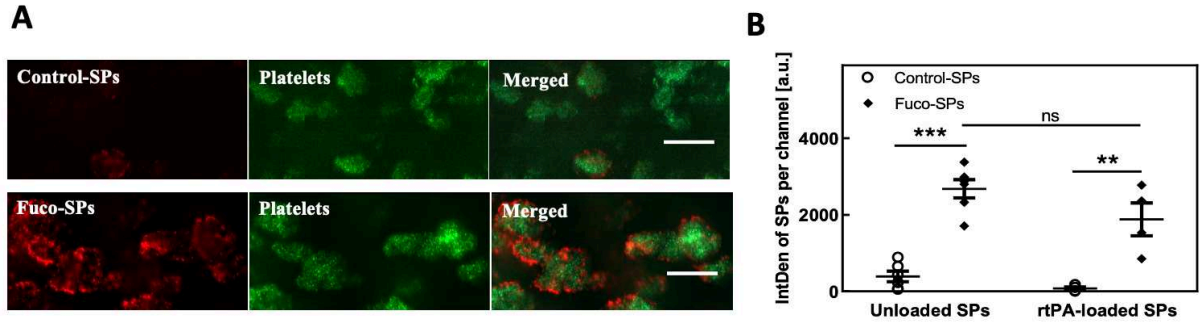


**Figure 25. Adhesion of the Fuco-SPs over activated platelet aggregates. A.** Visualization by fluorescent microscopy of the attached unloaded SPs on the microchannels after the formation of the platelet aggregates (scale bar = 20 µm). **B.** Corresponding quantification of the integral density of the unloaded (n=6) and rtPA-loaded (n=4) Control-SPs and Fuco-SPs in ImageJ.

In conclusion, these *in vitro* experiments provided crucial evidence of molecular interaction and high affinity between the P-selectin on the activated platelets and fucoidan-functionalized SPs, maintained after loading the thrombolytic agent. This finding presumes that the administration of the rtPA-Fuco-SPs could enable a specific delivery of the rtPA-immobilized SPs to the platelet-rich thrombus with higher drug accumulation.

### *3.6* Tissue distribution *in vivo* of fucoidan-functionalized SPs

The distribution *in vivo* of Fuco-SPs after their intravenous injection was examined by histological analysis of the excised tissues after alcian blue staining of negatively charged particles in the healthy mouse. The presence of Fuco-SPs in four main organs of excretion (liver, spleen, lungs, and kidneys) was assessed on several sections for each organ. Our results revealed that the polysaccharide Fuco-SPs distributed primarily into the spleen post-administration, indicating the splenic clearance. The particles accumulated in the liver to a lower extent, while their presence in the kidneys and lungs remained minor. These differences are presented in **Figure 26**. Our data are in agreement with other deformable polymer hydrogel-like particles in their submicron and micron size range [254].

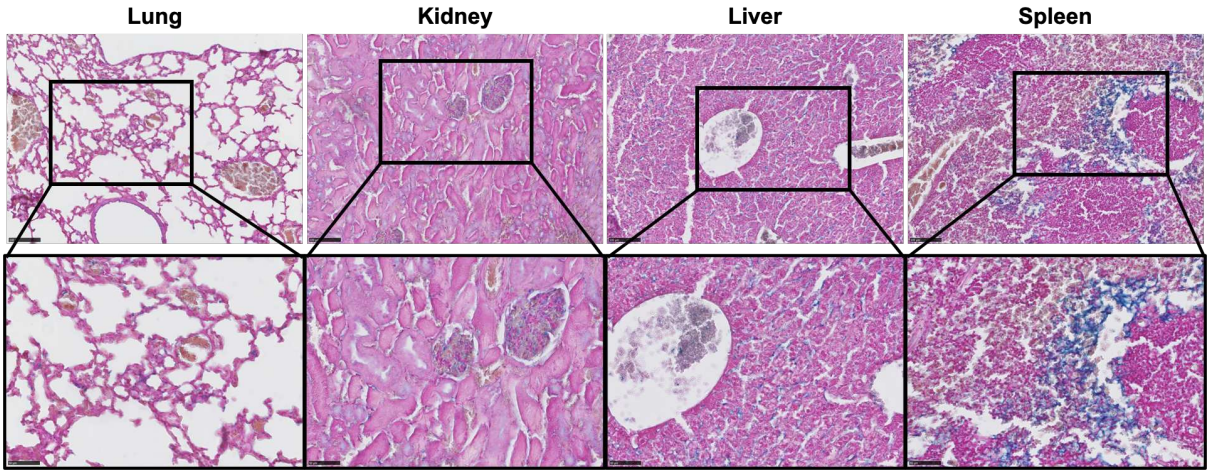


**Figure 26. Histological analysis of Fuco-SPs in four organs of excretion.** The cytoplasm appears pale pink, nuclei are red, and the Fuco-SPs are stained blue. Few particles were detected in the lungs, kidneys, and liver whereas they were mainly accumulated in the spleen. The scale bar in the upper row = 100 μm, in the lower row (magnified image) = 50 μm.

### 3.7 *In vivo* thrombolytic efficacy

Whereas demonstrating the *in vitro* activity of the rtPA immobilized on the drug delivery system is important, the *in vivo* therapeutic effect is paramount. A murine thromboembolic stroke model was established by *in situ* injection of 1 IU of thrombin into the MCA by provoking a coagulation cascade and formation of a fibrin-rich clot in the lumen of the artery [255,256]. **Figure 27A** highlights the *in vivo* experiment design, and **Figure 17C** the potential mode of action of the Fuco-SPs on the thrombus. The treatment options – control saline, rtPA 10 mg/kg, or rtPA-Fuco-SPs at 10 mg/kg – were intravenously injected 20 min after ischemic onset in accordance with rtPA clinical mode of administration: 10% bolus followed by 90% infusion. It is important to note that 10 mg/kg is a relevant dose in mice in place of 0.9 mg/kg in humans because of a lower sensitivity of human rtPA in murine plasma [106]. No morbidity or mortality was observed in the mice during therapeutic experiments, suggesting that rtPA-Fuco-SPs do not provoke acute toxicity under the current conditions.

Cerebral blood flow was monitored throughout the treatment via laser speckle contrast imaging, a high resolution and high-speed technique that instantly visualizes microcirculatory tissue blood perfusion. The blood flow in the ipsilateral cerebral hemisphere was restored by 33.97 ± 5.15% after 40 min treatment with rtPA-Fuco-SPs; by contrast, in the rtPA and saline group, the perfusion was improved only by 10.33 ± 4.62% and 15.16 ± 6.49%, respectively (**Figure 27D**). The representative laser speckle multispectral imaging in the ipsilateral and the contralateral hemispheres at 0 min and 40 min are expressed in **Figure 27C**.

These data were confirmed by the angiographic analysis performed 24 hours later and assessed by a blinded observer based on TICI grade flow scoring measured by magnetic resonance imaging. Indeed, similar to some untreated stroke patients, the blood clots were gradually lysed post-stroke in this murine model: at 24 h after thrombotic occlusion, 40% of mice exhibited a total recanalization (score 3) and 60% partial perfusion (score 1 and score 2) of the MCA when injected with saline (**Figure 27E & 27F**). However, after the treatment with rtPA-Fuco-SPs, most of the cases were entirely recanalized (score 3). For the rtPA treated group, no animal achieved a score 1 of minimal perfusion, and 66.6% of cases showed a partial score 2 level of recanalization.

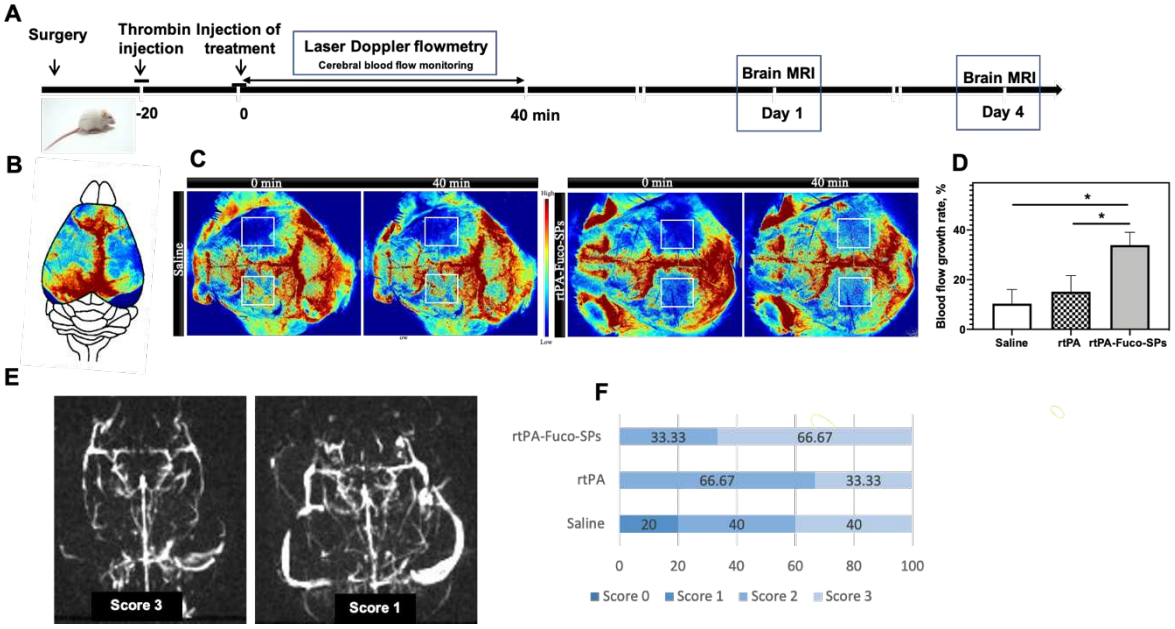


**Figure 27. Thrombolytic efficacy *in vivo* as the analysis of blood reperfusion in the murine ischemic stroke model. A.** Schematic of the design of the *in vivo* experiment. **B – D.** Cerebral blood flow reperfusion monitored by the laser speckle contrast imaging during the 40-min treatment. Schematic image of the perfusion in the microcirculatory brain tissue. **(B)**. The representative multispectral photos in the ROI of ipsilateral (upper) and contralateral (lower) hemispheres at 0 min and 40 min for saline and rtPA-Fuco-SPs groups **(C)**. The growth rate of the cerebral reperfusion in the ipsilateral hemisphere after 40 min treatment injection **(D)**. **E.** Merged image of the MRA scores (Score 3: full recanalization, score 1: low perfusion). **F.** Angiographic scores of the MCA reperfusion at day 1 after stroke induction by MRI.

The prevailing method for assessment of the brain infarct volume is a brain tissue staining with 2% 2,3,5-triphenyltetrazolium chloride (TTC), which labels non-injured tissue and leaves the infarct area white. Several groups previously reported the reduction of the infarct zone in preclinical models by nanomedicine. For example, the magnetic iron oxide ($Fe_3O_4$)-microrods [55] and polyacrylic acid-stabilized magnetic NPs [127] conjugated with rtPA diminished the brain infarct lesion in the $FeCl_3$ murine model of ischemic stroke of MCA. These designs, however, require an external magnet for targeting and to complement chemical lysis with rtPA with mechanical one of the magnetic rotation. Without any clinically approved medical device to impose a high magnetic force on the NPs in deep blood vessels, it would probably be desirable for nanocarrier formulation to avoid external assistance. Mei *et al.* stated

that only the synergistic effect of rtPA-loaded polymer micelles and a reactive oxygen species (ROS)-eliminating antioxidant suppressed an infarct volume and improved neurological deficit after brain ischemia in the mouse model of photo-thrombotic MCA occlusion [48].

In our case, we utilized MRI imaging as a powerful technique to quantify the volume of brain damage. Using T2-weighted MRI sequences, we observed that the size of the ischemic brain lesions for the saline group was 14.80 ± 3.34 $mm^3$ whereas for the rtPA-loaded fucoidan-targeted SPs it was 4.63 ± 1.59 $mm^3$ 24 h post-stroke (**Figure 28A & 28B**). From the recent publication of the same group [256], it is well known that early intravenous administration of free rtPA at the dose of 10 mg/kg diminishes the lesion size by 26.2% in the thrombin model. Our data clearly stated that the rtPA-Fuco-SPs provided superior brain protection than a standard rtPA treatment, which caused the infarct zone of 8.99 ± 2.7 $mm^3$. rtPA-conjugated Fuco-SPs reduced the ischemic zone almost 2-fold of the free rtPA, although these data were non-significant due to the limited number of the animals as to the well-known effect of free rtPA in this murine model. Out of all treated animals with rtPA-Fuco-SPs, 66.6% of the cases had small lesion sizes (<3 $mm^3$), and 33.3% had medium lesions (<11 $mm^3$). In the rtPA group, only 33.3% of the cases resulted in a small infarct zone. In the saline treatment group, we recorded 60% severe (<20 $mm^3$) and critical (>20 $mm^3$) cases and no small lesions (**Figure 28C**). This therapeutic benefit of rtPA-Fuco-SPs could be ascribed to faster MCA reperfusion and, hence, prevention of the major brain injury due to higher rtPA accumulation on the thrombus site as to active targeting and specific P-selectin interactions of the Fuco-SPs.

To monitor the BBB integrity disrupted by ischemic stroke [167], gadolinium hypersignal was detected and quantified on T1-weighted MRI images on day 4 after stroke (**Figure 28D & 28E**). Gadolinium extravasation from the blood into the brain parenchyma was unmistakably located at the ischemia-affected region where the BBB was compromised. rtPA-

Fuco-SPs treatment group demonstrated a significant BBB preservation over control groups of free rtPA and saline with only a subtle BBB breakdown of 3.45 ± 1.40 $mm^3$. It is vital to underline that although in this article we utilized fucoidan on the SPs purely for the P-selectin targeting purpose, new avenues of research are deciphering its neuroprotective role, particularly after cerebral ischemic events as recently reported [257].

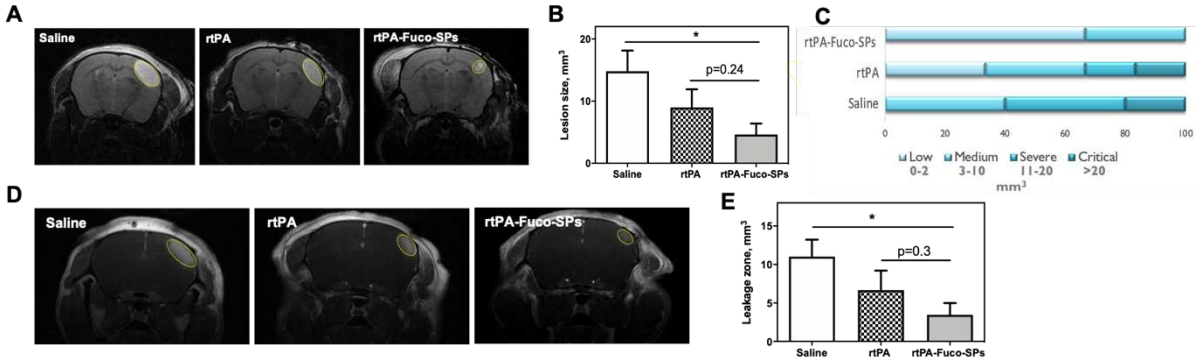


**Figure 28. Thrombolytic efficacy *in vivo* with an assessment of brain injury in the murine ischemic stroke model. A.** MRI images of the infarct lesion 24 h post-stroke with the corresponding quantification of its volume **(B)**. **C.** Distribution of the cases by the infarct zone sizes by MRI 24 h post-stroke. **D.** MRI images of the BBB permeability at day 4 post-stroke with the corresponding quantification of its volume **(E)**.

In order to confirm the accumulation of Fuco-SPs within the thrombus area *in vivo*, we injected fluorescent-labeled SPs at the therapeutic concentration as in the stroke model into the $FeCl_3$ model of venous thrombosis in mice. Upon histological examination of the mesenteric vein's thrombus-affected area, Fuco-SPs were clearly identified on the green-fluorescent labeled thrombus **(Figure 29A)**. By a quantitative analysis of the MFI normalized by the size of the thrombus, it was evidenced a highly increased TRITC signal from fucoidan-functionalized SPs group comparing with Control-SPs (9.48 ± 2.19 for Fuco-SPs vs. 1.48 ± 0.35 for Control-SPs, ** $p < 0.01$, **Figure 29B**).

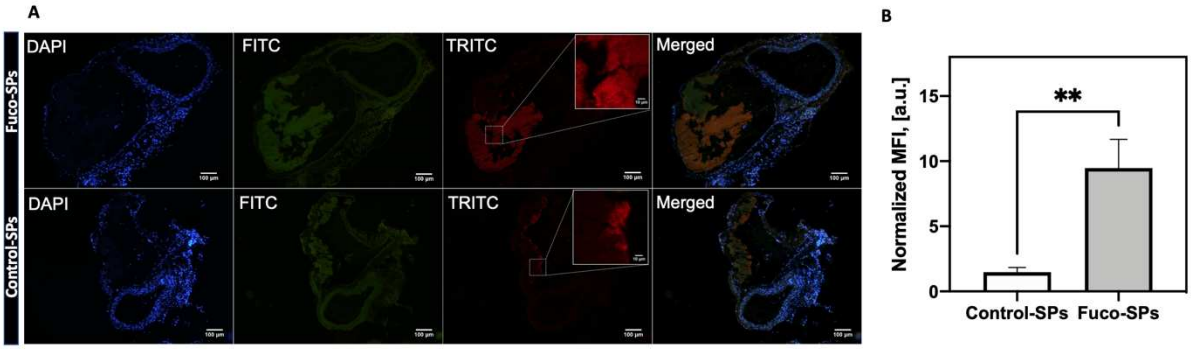


**Figure 29. *In vivo* targeting in the $FeCl_3$ murine model of thrombosis. A.** Histological analysis of thrombi in the mesenteric vein by fluorescent microscopy. The venous vascular wall is visualized with DAPI staining; thrombus is stained in green due to DIOC6 labeling of platelets; Fuco-SPs and Control-SPs are fluorescently labeled with TRITC. Inserts are a magnification of dashed Regions of Interest of the TRITC signal. **B.** Corresponding quantification of MFI from the adhered TRITC-SPs in the thrombi.

Overall, the apparent superiority of rtPA-Fuco-SPs to reduce the brain injury area in comparison with saline and rtPA at the same dose, combined with a favorable safety profile of the SPs, makes them a promising nanomedicine-based approach for the treatment of acute arterial thrombosis. We speculate that the submicron size of the particles as well as their active thrombus-targeting moiety should maintain rtPA-loaded nanocarrier within the intravascular compartment to exert its thrombolytic activity. It should prevent the leakage of rtPA into the brain parenchyma, reducing the risks of NMDA receptors-mediated neurotoxicity and hemorrhages [168]. Further studies could compare a single or a double bolus route of administration of rtPA-Fuco-SPs due to the rtPA preservation by SPs, and, thus, a more comfortable treatment option for patients.

## 4 CONCLUSIONS

In the present study, we designed and fabricated fucoidan-functionalized 100% polysaccharide submicroparticles from biocompatible and FDA approved components as a P-selectin targeting

drug delivery system for thrombolytic therapy. The physico-chemical properties and a biocompatibility analysis of these SPs were thoroughly evaluated, and a clinically used thrombolytic molecule – alteplase or rtPA – was effectively immobilized onto the SPs with full retention of its enzymatic and fibrinolytic potential *in vitro*. We established *in vitro* by dynamic flow microchamber assays that the fucoidan-functionalized nanosystem specifically adhered to the recombinant P-selectin in a dose-dependent manner, but not to E- and L-selectins, and to human activated platelets. Finally, our findings revealed in the murine model of ischemic stroke that rtPA conjugation to the Fuco-SPs could enhance the thrombolytic activity of the clinical agent *in vivo*. The blood flow perfusion was restored more rapidly, which resulted in smaller post-ischemic cerebral infarct lesions and higher BBB protection. In summary, we suggest that a hydrogel-based nano-delivery system with fucoidan holds a significant promise to revolutionize the safety and efficacy of thrombolytic therapy. In future research, our biocompatible Fuco-SPs could also efficiently vehicle other therapeutic or contrast agents in the vascular compartment to target P-selectin overexpressed pathologies, such as cardiovascular diseases [258] or some cancers [259,260].

# Chapter 3. GENERAL DISCUSSION & PERSPECTIVES

In 1987, the first clinical trial of intravenous rtPA for managing acute ischemic stroke was launched with consequent FDA approval in 1996 [261]. rtPA is a recombinant version of the naturally occurring serine protease secreted from the endothelium that, after its binding with fibrin, catalyzes the conversion of plasminogen to plasmin, leading to blood clot breakdown. This revolutionary treatment to dissolve thrombi and restore blood flow is a standard of care in strokes, heart attacks, and pulmonary embolisms, but it is certainly not risk-free. Nanomedicine offers outside-the-box strategies in order to effectively target and dissolve the blood clots in the body with fewer systemic and neurological complications. With dozens of NP formulations for therapeutic purposes of different pathologies (mostly cancers) already approved or in clinical trials [35,36], a forthcoming clinical translation is awaited for nanomedicine-based precise therapy in the context of cardiovascular diseases, and thrombotic events in particular.

From the first-ever nanomedicinal concepts for thrombolysis since the late '80s, as reviewed in **Chapter 1**, a growing number of solutions, such as liposomes, polymeric, inorganic, or bio-inspired nanovectors, for targeted drug delivery have demonstrated that the marriage of fibrinolytics to nanocarriers increases the effectiveness and safety of thrombolytic therapy [262]. These accomplishments include the protection of thrombolytics from inactivation by PAI-1, an increase of the drug circulation half-life, the enhanced fibrinolytic effect at a lower dose, reduction in bleeding complications and post-ischemic infarction zone.

In my PhD project, the thrombolytic drug rtPA was associated with hydrogel-like polysaccharide SPs, synthesized by a simple and reproducible miniemulsion / crosslinking process. This type of nano-delivery system is composed of a chemically crosslinked hydrophilic polymer network that provides a convenient and versatile platform for storage and site-specific release of protein in thrombi, which may diminish deleterious effects of alteplase on brain parenchyma in stroke. The soft structure of hydrogels resembles those of extracellular matrices and may prevent tissue irritation [193]. In general, polymeric nanosystems proved

their utility for biomedical applications due to favorable safety profiles, sufficient stability in biological fluids, effective response to relevant stimuli, and easy synthesis methods, as well as functionalization with cell-targeting ligands. Still, most of the concepts have been produced from synthetic polymers, such as PLGA, PACA, PCL, *etc*.

Regarding natural polymers and polysaccharides, in particular, the literature offers few examples of self-assembled nanoformulations with cationic chitosan or its derivatives [92,95]. Although dextran coating of inorganic and synthetic polymer NPs is common to increase their stability, biocompatibility, and prolong blood circulation time, there is no known entirely dextran nanocarriers for thrombolytic therapy. In 2018, our team published the study in which rtPA-bearing core-shell poly(isobutyl cyanoacrylate) NPs, decorated with dextran and fucoidan, achieved successful thrombolysis at the 4-times lower dose of rtPA than a relevant clinical one in mice **(Figure 6)** [67]. Yet, these NPs were cytocompatible only up to the concentrations of 50 μg/mL in static cell viability assay on HUVECs *in vitro,* whereas under flow conditions, the negative effects of circulating NPs, such as massive endothelial cellular detachment and morphology changes both in the laminar and nonuniform shear stress, were evident at 100 μg/mL after 18 h [246].

The key challenge for my PhD project was to fabricate 100% polysaccharide nanomedicinal product from biocompatible and biodegradable materials, all with FDA-approval. This design would not only allow producing final SPs with a desirably high biosafety **(Figure 21)** but would also enable easier authorization for human trials by regulatory agencies in the future. For instance, STMP was preferred over conventional crosslinker glutaraldehyde that is known for cytotoxicity [194]. Sunflower oil was selected as an emulsion continuous phase in place of commonly used organic solvents. For a stable and homogenous w/o emulsion and consequent nano-delivery system, we applied PGPR as an emulsifier, safe and frequently used in the food industry [245]. As estimated, the obtained SPs were cytocompatible on

HUVECs at concentrations up to 1.5 mg/mL (cell survival > 90%). Such high concentrations of the SPs did not affect HUVECs morphology and metabolic activity. Apart from that, the Fuco-SPs were blood-compatible and nonhemolytic according to a hemolysis test on isolated murine erythrocytes *in vitro.* By histological evaluation, our results revealed that the main pathway of the polysaccharide Fuco-SPs tissue distribution *in vivo* upon intravenous injection was the spleen **(Figure 26)**. For future studies, it would be advisable to expand our basic biocompatibility assessment. We suggest including the *in vivo* data of blood coagulation parameters, such as aPTT (activated partial thromboplastin time), FIB (fibrinogen), PT (prothrombin time), TT (thrombin time), to ensure the absence of thrombogenicity of the designed nanosystem. In addition, histopathology of major organs, including the heart, liver, spleen, lung, and kidney by H&E staining, should be analyzed in healthy rodents. Nanocarrier immunogenicity could be tested too on, for instance, a model of complement system activation CARPA in pigs [263].

The final injectable hydrogel particles were in the submicronic size range of ~700 nm, smaller and more homogeneous than another polysaccharide concept developed previously in our laboratory for molecular imaging with MRI and SPECT [104,231]. The relatively large size of the SPs might prevent them from crossing the BBB and limit the accumulation of loaded rtPA within the brain parenchyma, thus, reducing the risk of hemorrhagic complications.

As a nanocarrier is subjected to biological barriers in the human body after the intravenous injection, this is essential to ensure sufficient bloodstream circulation time to execute an efficient site-specific treatment. Particle *in vivo* fate is affected by the interaction between different parameters: size, surface characteristics, stability, shape, mechanical properties, *etc*. In our case, multiple factors play in favor of the long circulation profile of the SPs to allow them to act as a suitable vehicle for thrombolytic delivery. The negative surface charge of Fuco-SPs, ζ-potential ~30 mV, provides reduced protein adsorption compared to

cationic particles [33]. Moreover, neutral and anionic NPs are shown to induce no effect on BBB disruption and no toxicity on brain microvasculature endothelium, contrary to positively charged particles [264].

Concerning the particle size, although generally 100–200 nm rigid spherical NPs are preferred as they are considered as long-circulating and capable of avoiding rapid opsonization and elimination by MPS [135], hydrogel nanocarriers break this rule. Indeed, studies indicated that soft, elastic and prone to deformability hydrogel carriers, even in their micrometric sizes, had prolonged circulation profiles [149,267] and evaded macrophage internalization compared to rigid nanoconstructs [150]. Interestingly, hydrogel microparticles were capable of passing through pores up to 10 times smaller than the particle diameter, explained by their network flexibility and compressibility [265].

RBC with a diameter of 6 – 8 μm are viewed as a gold standard for drug delivery because of their long *in vivo* circulation due to discoidal shape, deformability, and the expression of self-recognition biomarkers [133,135] that already brought them to clinical trials [133]. Another key parameter to limit the risk of quick MPS uptake is the material of a surface. In our case, the particles were entirely composed of polysaccharides – dextran and fucoidan without any chemical modification. Hydrophilic polysaccharide surfaces avert the formation of a protein corona and early macrophage internalization of the circulating NPs [154].

Despite the overall utility of our constructed SPs for intravascular drug delivery and their potential in loading different molecules of interest, in this project, the goal was to deliver PA and perform local thrombolysis. Intriguingly, the structural materials for the nanocarrier, dextran and fucoidan, may effectuate some antithrombotic action by themselves [226,230,244]. Another paper claims that fucoidan has comparable antithrombotic activity to heparin but does not cause hemorrhagic effects [266]. The Fuco-SPs were associated with a thrombolytic agent by physical adsorption method, which allowed a high encapsulation efficiency of the rtPA of

81.04 ± 1.86%. Classically, alteplase is loaded onto the NPs using the covalent amide bond formation via EDC/NHS reaction between the primary amines on the rtPA molecule and the nanocarriers containing carboxyl groups. Although Juenet *et al.* [67] managed to adsorb rtPA onto the surface of the dextran-coated core-shell polymer NPs with a near-neutral ζ-potential, the presence of the free primary amines was required on chemically modified dextran. Comparing covalent vs. non-covalent methods to conjugate rtPA onto the polymer coating of magnetic NPs [267], better loading capacity (98.6 ± 0.8 % vs. 47.7 ± 5.4 %), as well as superior amidolytic and fibrinolytic activities were described with a covalent one vs. adsorption. In the present project, high encapsulation efficiency of alteplase onto the polysaccharide SPs was attained without any chemical modification of the dextran or fucoidan and despite a distinctively negative surface charge of the SPs, therefore, can be attributed to their hydrogel-based structure. The fibrinolytic drug was associated not only at the surface of the particles but also diffused through the matrix of the porous SPs, fully preserving its thrombolytic potential. As a mild drug encapsulation method, adsorption is preferred to covalent bioconjugation, for example EDC/NHS, to load fragile molecules such as proteins to avoid changes in the protein structure and function that might result in its partial denaturation and loss of biological activity [182]. Alternatively, while streptavidin-biotin chemistry is recognizably versatile, it is known to induce immune responses. In addition, the adsorptive bound rtPA is liberated faster from the particles and diffused more readily into the fibrin matrix than covalently bound rtPA [128], which may also be beneficial in targeted thrombolysis. Although a rising number of recent articles apply a controlled release of the thrombolytics via endogenous and exogenous stimuli **(Figure 13)**, we chose not to incorporate sophisticated nanodesigns and demonstrated a gradual and continuous rtPA release from the SPs without an external trigger in order to facilitate future regulatory approvals **(Figure 24B)**. In addition, the fact that the SPs could be freezedried for long-term storage and they load rtPA by adsorption potentially make this product convenient

for utilization in the clinical settings. Similar to rtPA, which is supplied in a lyophilized powder to be added to the diluent (sterile water) before its administration, both alteplase and Fuco-SPs could be mixed in their powder form in water and injected into the patients once needed.

The clot targeting strategy of the SPs was easily achieved by the introduction of the fucoidan to the polysaccharide solution at 9% w/w. Fucoidan, which is at present under clinical investigation as a diagnostic agent for the imaging of thrombosis [185,186], may become an affordable and high-quality alternative to antibodies and peptides. Functionalization with fucoidan permitted the high-affinity binding of Fuco-SPs to its molecular target P-selectin in a dynamic microfluidic method that mimics arterial or venous blood flow conditions in a dose-dependent manner (**Figure 23A-B, 23E**). Importantly, this type of interaction is selective, as SPs did not adhere to other selectins: E- and L-selectin *in vitro* (**Figure 23D**). When the microchannels were covered with activated platelet aggregates, both unloaded and rtPA-loaded Fuco-SPs were capable of binding these micro-clots (**Figure 25**). Once tested in the *in vivo* model of venous thrombosis, Fuco-SPs were clearly identified on the $FeCl_3$-induced thrombi by histological examination, contrary to Control-SPs **(Figure 29)**. While most of the studies focus on binding fibrin, phosphatidylserine, or GPIIb/IIIa receptors on the platelets, to our knowledge, only one publication was dealing with co-targeting P-selectin using a peptide ligand [57], apart from the previous work from our group on polymer NPs with fucoidan [67]. In conclusion, our data validate an inimitable and efficient thrombus targeting approach of the SPs, using a clinical compound of natural origin.

In spite of the recognition of the unique advantages of fucoidan, a surge in strategies involving dual or even more surface targeting moieties is being witnessed. For instance, the combinatory targeting of GPIIb/IIIa receptors and P-selectin on activated platelets with two peptide ligands on the lipid nanovesicles enhanced thrombus binding capacities in a synergic manner [57]. Another notable example is the biomimetic functionalization of NPs with platelet

membrane coating that enabled thrombus directing via multiple platelet receptors [76]. These combinations of NP modifications represent an encouraging strategy for developing next-generation blood clot-targeting NP platforms for therapy and/or diagnostics.

As our next step, the *in vivo* therapeutic effect of the SPs was validated on the murine thrombin-induced thromboembolic stroke model **(Figure 27 & Figure 28)**. The treatment options were administrated in accordance with rtPA clinical mode of administration: 10% bolus followed by 90% infusion at the rtPA dose of 10 mg/kg (relevant to the clinical dose in mouse). In the rtPA-Fuco-SPs group, we observed a more rapid clot dissolution and MCA reperfusion, which minimized the brain injury and resulted in subsequently smaller infarct area post-stroke by MRI. Moreover, the animals in the rtPA-Fuco-SPs group suffered a lower level of BBB disruption by the ischemic stroke that was quantified on T1-weighted MRI images with gadolinium. These findings of rtPA-loaded fucoidan-functionalized SPs outperformed those of free rtPA at the same amount. This first proof-of-concept *in vivo* results of Fuco-SPs show an astonishing potential of the nanomedicine-based approach for the targeted treatment of acute thrombosis. In the future, we propose to compare a single or double bolus injection of rtPA-Fuco-SPs due to the rtPA preservation by SPs as a more comfortable administration mode for patients.

Nevertheless, it has to be mentioned that none of the available *in vivo* rodent experimental models of acute thrombosis accurately recapitulates all the aspects of human disease progression and heterogeneity. Therefore, it is always recommended to validate any translational effort in multiple models in order to ensure its therapeutic efficacy and safety. Studies conducted in one single model, like the current project, would require further corroboration before initiating large animal tests and first-in-human trials. Notably, in 2019, Xu *et al.* proposed a biomimetic strategy of platelet membrane-camouflaged PLGA NPs with rtPA that was successfully studied in several *in vivo* models: pulmonary embolism, $FeCl_3$-

induced arterial thrombosis, and ischemic stroke model **(Figure 10)** [76]. Additionally, it is well recognized that gender plays a significant role in thrombosis pathogenesis and intervention outcomes. Thus, it is imperative for any novel therapeutic and imaging NP method to be examined in both genders, including female rodents, which are commonly avoided in preclinical stages because of the data variability due to hormone fluctuations.

Apart from the necessity of the rapid restoration of blood flow after thrombotic occlusions, combating the ischemia-reperfusion injury such as inflammation and oxidative damage is vital for a good prognosis. Hence, complementing fibrinolytic therapy with nanodelivery of a potent antioxidant would be a sensible approach. Poly(isobutyl cyanoacrylate)-polysaccharide NPs bearing microRNA-155-5p were proposed as a cardio-protective therapy for MI due to their antioxidant and cytoprotective properties [268]. Besides, rtPA might be accompanied by neuroprotection to prevent brain injury and neuronal damage during or after exposure to ischemia following acute ischemic stroke [269]. Interestingly, a recent publication highlighted a potential neuroprotective role of fucoidan after cerebral ischemic events [257]; therefore, it would be sensible to further study this possibility of Fuco-SPs *in vivo*. The discovery of next-generation thrombolytic drugs is further required to improve the safety and efficacy of nanomedicine-based thrombolysis. For instance, Goulay *et al.* engineered a non-neurotoxic rtPA variant with an equal fibrinolytic potential but without stimulating NMDA-dependent neurotoxicity [270] that could be an alternative molecule to load onto the hydrogel SPs.

Particularly inspiring, owing to NP versatility to adapt to the complexity of thrombotic disease mechanisms and manifestations, combined nanocarrier application in noninvasive, targeted treatment and imaging enhancement could produce innovative theranostic nanomedicines. The polysaccharide SPs in this study could bear fluorescence agents (by introducing 5% TRITC-labelled dextran to the formulation) and be detectable by fluorescent

microscopy. In addition, the possibility to radiolabel fucoidan as in the ongoing clinical trials and consequently rtPA-Fuco-SPs with $^{99m}$Tc opens doors for SPECT or SPECT/CT imaging modality. Other contrast compounds could be incorporated into the hydrophilic particles to design theranostics for additional clinically implanted imaging modalities, such as CT with iodine or MRI with gadolinium [271]. Such design could be of clinical interest when there is a need and technical possibility for real-time monitoring of drug release & distribution and therapeutic response, following the initial diagnosis of the pathology. This is worth noting that the translating process of theranostic NPs is likely to be challenging as they comprise a multifunctional unit and require more precise chemistry, manufacturing, and quality control on a large scale.

Evidently, the clinical translation of drug delivery systems happens slowly, despite the high number of academic achievements and scientific publications. The complexity of the nanopharmaceutical product needs to be reduced to the essential due to potential technical challenges and regulatory requirements. The rtPA-Fuco-SPs representing an actively targeted nanodelivery system reach an exact balance of simplicity and functionality concerning the projected clinical translation. While they were designed and fabricated in the academic laboratory at the range of ~10 mg per batch, the industrial scale-up of the process with high reproducibility under GMP conditions and intended quality standards is essential to establish in order to obtain the necessary amounts for further screening and, ultimately, clinical use. For instance, high-precision microfluidic and micropatterning methods for the fabrication of monodisperse NPs with uniform physicochemical characteristics and low batch-to-batch variability are becoming prevalent and are compatible with GMP standards [272]. Finally, an adequate sterilization method should be validated to prevent nanoparticle damage and alteration in the product's parameters.

# GENERAL CONCLUSION

# GENERAL CONCLUSION

Acute thrombotic events are life-threatening cardiovascular pathologies that represent a clinical emergency. At thrombus sites, the blood vessel occlusion may lead to ischemia and subsequent organ failure. A safe and rapid vessel recanalization is essential to minimize tissue damage and achieve a good prognosis. In spite of encouraging therapeutic outcomes with the interventional endovascular methods, they are limited to large vessel occlusions, and the access to the medical centers providing these treatments is often insufficient. Therefore, standard intravenous delivery of the PA remains a gold treatment in ischemic stroke, heart attacks, and pulmonary embolism, despite its limited efficacy and hemorrhagic complications. Nanomedical solutions for local targeted and/or controlled delivery of "clot-busting" agents exploit a profound understanding of the molecular mechanisms involved in the thrombus formation and are designed to enhance the efficacy and safety of systemic fibrinolysis.

The current research project was focused on the development of the novel biocompatible and biodegradable 100% polysaccharide nanocarrier from FDA-approved compounds to preferentially bind P-selectin, one of the molecular markers of the thrombosis, due to incorporation of the algae-derived compound – fucoidan. Other nano-/microvectors with fucoidan, previously developed in our laboratory, have already shown to be effective for molecular imaging and targeted treatment of cardiovascular pathologies overexpressing P-selectin at preclinical stages. Herein, fucoidan-functionalized hydrogel-like submicroparticles were fabricated, loaded with rtPA, and studied for their drug delivery potential in the context of thrombolytic therapy both *in vitro* and *in vivo*. The experiments on the murine model of ischemic stroke supported this proof-of-concept study by demonstrating that submicroparticle-associated rtPA treatment allowed earlier blood vessel recanalization, which reduced the brain ischemic zone and led to superior neurovascular unit protection. In summary, this PhD project considered the issues imperative for the future clinical translation of nanocarriers by (I) the choice of materials, (II) a relatively simple and efficient production by a mild synthesis method

without the utilization of the hazardous substances and organic solvents, (III) targeting agent of natural origin– fucoidan – that is being validated in clinical trials for thrombosis.

To conclude, an alteplase-associated hydrogel-based nano-delivery system with fucoidan demonstrates a solid argument for improved thrombolytic therapy in terms of safety and efficacy in the preclinical studies. We hope that this technology will keep developing up to the future clinical application. Our biocompatible Fuco-SPs could also vehicle other therapeutic and/or molecular imaging agents to target P-selectin overexpressed pathologies in the following projects. With the clinical translation and regulatory requirements in mind, it is sensible to opt for an efficient and extremely safe nanocarrier for targeted fibrinolysis instead of an excessively complex and innovative nanodelivery system, like multifunctional hybrid nanoparticles with cell-derived biomimetic surfaces and stimuli-responsive drug release. Easy and robust large-scale manufacturing of nanomaterials with a comprehensive assessment of reproducibility, quality control, and toxicity are required to ensure the final product's optimal quality. Overall, we are confident that nanomedicine-assisted approaches will direct towards precision medicine to successfully manage acute thrombotic diseases.

# REFERENCES

[1] World Health Organisation (WHO), [Internet] World Health Organization. Media Centre: Cardiovascular disease, (2020). https://www.who.int/health-topics/cardiovascular-diseases/#tab=tab_1.

[2] E.J. Benjamin, P. Muntner, A. Alonso, M.S. Bittencourt, C.W. Callaway, A.P. Carson, A.M. Chamberlain, A.R. Chang, S. Cheng, S.R. Das, F.N. Delling, L. Djousse, M.S.V. Elkind, J.F. Ferguson, M. Fornage, L.C. Jordan, S.S. Khan, B.M. Kissela, K.L. Knutson, T.W. Kwan, D.T. Lackland, T.T. Lewis, J.H. Lichtman, C.T. Longenecker, M.S. Loop, P.L. Lutsey, S.S. Martin, K. Matsushita, A.E. Moran, M.E. Mussolino, M. O'Flaherty, A. Pandey, A.M. Perak, W.D. Rosamond, G.A. Roth, U.K.A. Sampson, G.M. Satou, E.B. Schroeder, S.H. Shah, N.L. Spartano, A. Stokes, D.L. Tirschwell, C.W. Tsao, M.P. Turakhia, L.B. VanWagner, J.T. Wilkins, S.S. Wong, S.S. Virani, Heart Disease and Stroke Statistics—2019 Update: A Report From the American Heart Association, Circulation. (2019). https://doi.org/10.1161/CIR.0000000000000659.

[3] H. Thomas, J. Diamond, A. Vieco, S. Chaudhuri, E. Shinnar, S. Cromer, P. Perel, G.A. Mensah, J. Narula, C.O. Johnson, G.A. Roth, A.E. Moran, Global Atlas of Cardiovascular Disease 2000-2016: The Path to Prevention and Control, Glob. Heart. 13 (2018) 143–163. https://doi.org/10.1016/j.gheart.2018.09.511.

[4] J. Leal, R. Luengo-Fernández, A. Gray, S. Petersen, M. Rayner, Economic burden of cardiovascular diseases in the enlarged European Union, Eur. Heart J. 27 (2006) 1610–1619. https://doi.org/10.1093/eurheartj/ehi733.

[5] D.N. Granger, P.R. Kvietys, Reperfusion injury and reactive oxygen species: The evolution of a concept, Redox Biol. 6 (2015) 524–551. https://doi.org/10.1016/j.redox.2015.08.020.

[6] C.K. Glass, J.L. Witztum, Atherosclerosis: The Road Ahead, Cell. 104 (2001) 503–516.

https://doi.org/10.5005/jp/books/12883_4.

[7] E. Falk, Pathogenesis of Atherosclerosis, J. Am. Coll. Cardiol. 47 (2006) C7–C12. https://doi.org/10.1016/j.jacc.2005.09.068.

[8] Y.S. Chatzizisis, A.U. Coskun, M. Jonas, E.R. Edelman, C.L. Feldman, P.H. Stone, Role of Endothelial Shear Stress in the Natural History of Coronary Atherosclerosis and Vascular Remodeling. Molecular, Cellular, and Vascular Behavior, J. Am. Coll. Cardiol. 49 (2007) 2379–2393. https://doi.org/10.1016/j.jacc.2007.02.059.

[9] G.G. Caro, Discovery of the role of wall shear in atherosclerosis, Arterioscler. Thromb. Vasc. Biol. 29 (2009) 158–161. https://doi.org/10.1161/ATVBAHA.108.166736.

[10] J. Jongstra-Bilen, M. Haidari, S.N. Zhu, M. Chen, D. Guha, M.I. Cybulsky, Low-grade chronic inflammation in regions of the normal mouse arterial intima predisposed to atherosclerosis, J. Exp. Med. 203 (2006) 2073–2083. https://doi.org/10.1084/jem.20060245.

[11] P. Libby, Inflammation in atherosclerosis, Nature. 420 (2002) 868–874. https://doi.org/10.1038/nature01323.

[12] Z.S. Galis, G.K. Sukhova, R. Kranzhöfer, S. Clark, P. Libby, Macrophage foam cells from experimental atheroma constitutively produce matrix-degrading proteinases, Proc. Natl. Acad. Sci. U. S. A. 92 (1995) 402–406. https://doi.org/10.1073/pnas.92.2.402.

[13] M.R. Dweck, E. Aikawa, D.E. Newby, J.M. Tarkin, J.H.F. Rudd, J. Narula, Z.A. Fayad, Noninvasive Molecular Imaging of Disease Activity in Atherosclerosis, Circ. Res. 119 (2016) 330–340. https://doi.org/10.1161/CIRCRESAHA.116.307971.

[14] A. Shioi, Y. Ikari, Plaque calcification during atherosclerosis progression and regression, J. Atheroscler. Thromb. 25 (2018) 294–303. https://doi.org/10.5551/jat.RV17020.

[15] G. Lippi, M. Franchini, G. Targher, Arterial thrombus formation in cardiovascular disease, Nat. Rev. Cardiol. 8 (2011) 502–512. https://doi.org/10.1038/nrcardio.2011.91.

REFERENCES

[16] N. Mackman, Triggers, targets and treatments for thrombosis, Nature. 451 (2008) 914–918. https://doi.org/10.1038/nature06797.

[17] I. Martinelli, P. Bucciarelli, P.M. Mannucci, Thrombotic risk factors: Basic pathophysiology, Crit. Care Med. 38 (2010). https://doi.org/10.1097/CCM.0b013e3181c9cbd9.

[18] C.T. Esmon, Basic mechanisms and pathogenesis of venous thrombosis, Blood Rev. 23 (2009) 225–229. https://doi.org/10.1016/j.blre.2009.07.002.

[19] J.A. López, J. Chen, Pathophysiology of venous thrombosis, Thromb. Res. 123 (2009) 30–34. https://doi.org/10.1016/S0049-3848(09)70140-9.

[20] A. Bivard, L. Lin, M.W. Parsonsb, Review of Stroke Thrombolytics, J. Stroke. 15 (2013) 90. https://doi.org/10.5853/jos.2013.15.2.90.

[21] C. Kluft, J.J. Sidelmann, J.B. Gram, Assessing Safety of Thrombolytic Therapy, Semin. Thromb. Hemost. 43 (2017) 300–310. https://doi.org/10.1055/s-0036-1584130.

[22] R.S. Marshall, Progress in intravenous thrombolytic therapy for acute stroke, JAMA Neurol. 72 (2015) 928–934. https://doi.org/10.1001/jamaneurol.2015.0835.

[23] V.J. Marder, Thrombolytic Therapy, in: Consult. Hemost. Thromb., Elsevier, 2013: pp. 526–537. https://doi.org/10.1016/B978-1-4557-2296-9.00028-2.

[24] J. Schaller, S.S. Gerber, The plasmin-antiplasmin system: structural and functional aspects, Cell. Mol. Life Sci. 68 (2011) 785–801. https://doi.org/10.1007/s00018-010-0566-5.

[25] A. Pal Khasa, Y. Pal Khasa, The evolution of recombinant thrombolytics: Current status and future directions, Bioengineered. 8 (2017) 331–358. https://doi.org/10.1080/21655979.2016.1229718.

[26] G.N. Levine, E.R. Bates, J.C. Blankenship, S.R. Bailey, J.A. Bittl, B. Cercek, C.E. Chambers, S.G. Ellis, R.A. Guyton, S.M. Hollenberg, U.N. Khot, R.A. Lange, L. Mauri,

R. Mehran, I.D. Moussa, D. Mukherjee, H.H. Ting, P.T. O'Gara, F.G. Kushner, D.D. Ascheim, R.G. Brindis, D.E. Casey, M.K. Chung, J.A. De Lemos, D.B. Diercks, J.C. Fang, B.A. Franklin, C.B. Granger, H.M. Krumholz, J.A. Linderbaum, D.A. Morrow, L.K. Newby, J.P. Ornato, N. Ou, M.J. Radford, J.E. Tamis-Holland, C.L. Tommaso, C.M. Tracy, Y.J. Woo, D.X. Zhao, 2015 ACC/AHA/SCAI Focused Update on Primary Percutaneous Coronary Intervention for Patients with ST-Elevation Myocardial Infarction An Update of the 2011 ACCF/AHA/SCAI Guideline for Percutaneous Coronary Intervention and the 2013 ACCF/AHA Guideline for th, J. Am. Coll. Cardiol. 67 (2016) 1235–1250. https://doi.org/10.1016/j.jacc.2015.10.005.

[27] B. Ibanez, S. James, S. Agewall, M.J. Antunes, C. Bucciarelli-Ducci, H. Bueno, A.L.P. Caforio, F. Crea, J.A. Goudevenos, S. Halvorsen, G. Hindricks, A. Kastrati, M.J. Lenzen, E. Prescott, M. Roffi, M. Valgimigli, C. Varenhorst, P. Vranckx, P. Widimský, A. Baumbach, R. Bugiardini, I.M. Coman, V. Delgado, D. Fitzsimons, O. Gaemperli, A.H. Gershlick, S. Gielen, V.P. Harjola, H.A. Katus, J. Knuuti, P. Kolh, C. Leclercq, G.Y.H. Lip, J. Morais, A.N. Neskovic, F.J. Neumann, A. Niessner, M.F. Piepoli, D.J. Richter, E. Shlyakhto, I.A. Simpson, P.G. Steg, C.J. Terkelsen, K. Thygesen, S. Windecker, J.L. Zamorano, U. Zeymer, M. Chettibi, H.G. Hayrapetyan, B. Metzler, F. Ibrahimov, V. Sujayeva, C. Beauloye, L. Dizdarevic-Hudic, K. Karamfiloff, B. Skoric, L. Antoniades, P. Tousek, C.J. Terkelsen, S.M. Shaheen, T. Marandi, M. Niemel€a, S. Kedev, M. Gilard, A. Aladashvili, A. Elsaesser, I.G. Kanakakis, B. Merkely, T. Gudnason, Z. Iakobishvili, L. Bolognese, S. Berkinbayev, G. Bajraktari, M. Beishenkulov, I. Zake, H. Ben Lamin, O. Gustiene, B. Pereira, R.G. Xuereb, S. Ztot, V. Juliebø, J. Legutko, A.T. Timoteo, G. Tatu-Chit¸oiu, A. Yakovlev, L. Bertelli, M. Nedeljkovic, M. Studencan, M. Bunc, A.M.G. de Castro, P. Petursson, R. Jeger, M.S. Mourali, A. Yildirir, A. Parkhomenko, C.P. Gale, 2017 ESC Guidelines for the management of acute myocardial infarction in

patients presenting with ST-segment elevation, Eur. Heart J. 39 (2018) 119–177. https://doi.org/10.1093/eurheartj/ehx393.

[28] G. Turc, P. Bhogal, U. Fischer, P. Khatri, K. Lobotesis, M. Mazighi, P.D. Schellinger, D. Toni, J. de Vries, P. White, J. Fiehler, European Stroke Organisation (ESO) – European Society for Minimally Invasive Neurological Therapy (ESMINT) Guidelines on Mechanical Thrombectomy in Acute Ischaemic StrokeEndorsed by Stroke Alliance for Europe (SAFE), Eur. Stroke J. 4 (2019) 6–12. https://doi.org/10.1177/2396987319832140.

[29] W.J. Powers, A.A. Rabinstein, T. Ackerson, O.M. Adeoye, N.C. Bambakidis, K. Becker, J. Biller, M. Brown, B.M. Demaerschalk, B. Hoh, E.C. Jauch, C.S. Kidwell, T.M. Leslie-Mazwi, B. Ovbiagele, P.A. Scott, K.N. Sheth, A.M. Southerland, D. V. Summers, D.L. Tirschwell, Guidelines for the Early Management of Patients With Acute Ischemic Stroke: 2019 Update to the 2018 Guidelines for the Early Management of Acute Ischemic Stroke: A Guideline for Healthcare Professionals From the American Heart Association/American Stroke , Stroke. 50 (2019) e344–e418. https://doi.org/10.1161/STR.0000000000000211.

[30] L. Derex, T.H. Cho, Mechanical thrombectomy in acute ischemic stroke, Rev. Neurol. (Paris). 173 (2017) 106–113. https://doi.org/10.1016/j.neurol.2016.06.008.

[31] S.A. Munich, K. Vakharia, E.I. Levy, Overview of Mechanical Thrombectomy Techniques, Clin. Neurosurg. 85 (2019) S60–S67. https://doi.org/10.1093/neuros/nyz071.

[32] G. Forestier, B. Kerleroux, K. Janot, F. Zhu, V. Dumas, J.-F. Hak, E. Shotar, W. BenHassen, R. Bourcier, S. Soize, J. Berge, O. Naggara, H. Desal, G. Boulouis, A. Rouchaud, Mechanical thrombectomy practices in France: exhaustive survey of centers and individual operators, J. Neuroradiol. (2020) 1–14.

https://doi.org/10.1016/j.neurad.2020.05.001.

[33] E. Blanco, H. Shen, M. Ferrari, Principles of nanoparticle design for overcoming biological barriers to drug delivery, Nat. Biotechnol. 33 (2015) 941–951. https://doi.org/10.1038/nbt.3330.

[34] Y. Barenholz, Doxil® - The first FDA-approved nano-drug: Lessons learned, J. Control. Release. 160 (2012) 117–134. https://doi.org/10.1016/j.jconrel.2012.03.020.

[35] A.C. Anselmo, S. Mitragotri, Nanoparticles in the clinic, Bioeng. Transl. Med. 1 (2016) 10–29. https://doi.org/10.1002/btm2.10003.

[36] A.C. Anselmo, S. Mitragotri, Nanoparticles in the clinic: An update, Bioeng. Transl. Med. 4 (2019) 1–16. https://doi.org/10.1002/btm2.10143.

[37] T. Matoba, J.-I. Koga, K. Nakano, K. Egashira, H. Tsutsui, Nanoparticle-mediated drug delivery system for atherosclerotic cardiovascular disease, J. Cardiol. 70 (2017) 206–211. https://doi.org/10.1016/j.jjcc.2017.03.005.

[38] T. Alam, S. Khan, B. Gaba, M.F. Haider, S. Baboota, J. Ali, Nanocarriers as treatment modalities for hypertension, Drug Deliv. 24 (2017) 358–369. https://doi.org/10.1080/10717544.2016.1255999.

[39] C.K.W. Chan, L. Zhang, C.K. Cheng, H. Yang, Y. Huang, X.Y. Tian, C.H.J. Choi, Recent Advances in Managing Atherosclerosis via Nanomedicine, Small. 14 (2018) 1–16. https://doi.org/10.1002/smLl.201702793.

[40] T. Cyrus, S.A. Wickline, G.M. Lanza, Nanotechnology in interventional cardiology, Wiley Interdiscip. Rev. Nanomedicine Nanobiotechnology. 4 (2012) 82–95. https://doi.org/10.1002/wnan.154.

[41] L. Yu, B.J. Scherlag, K. Dormer, K.T. Nguyen, C. Pope, K.M. Fung, S.S. Po, Autonomic denervation with magnetic nanoparticles, Circulation. 122 (2010) 2653–2659. https://doi.org/10.1161/CIRCULATIONAHA.110.940288.

REFERENCES

[42] T. Simon-Yarza, I. Bataille, D. Letourneur, Cardiovascular Bio-Engineering: Current State of the Art, J. Cardiovasc. Transl. Res. 10 (2017) 180–193. https://doi.org/10.1007/s12265-017-9740-6.

[43] D.R. Esfahani, V. Viswanathan, A. Alaraj, Nanoparticles and stem cells–has targeted therapy for aneurysms finally arrived?, Neurol. Res. 37 (2015) 269–277. https://doi.org/10.1179/1743132814Y.0000000435.

[44] C. Psarros, R. Lee, M. Margaritis, C. Antoniades, Nanomedicine for the prevention, treatment and imaging of atherosclerosis, Nanomedicine Nanotechnology, Biol. Med. 8 (2012) S59–S68. https://doi.org/10.1016/j.nano.2012.05.006.

[45] B. Singh, T. Garg, A.K. Goyal, G. Rath, Recent advancements in the cardiovascular drug carriers, Artif. Cells, Nanomedicine Biotechnol. 44 (2016) 216–225. https://doi.org/10.3109/21691401.2014.937868.

[46] C.H. Liu, H.L. Hsu, J.P. Chen, T. Wu, Y.H. Ma, Thrombolysis induced by intravenous administration of plasminogen activator in magnetoliposomes: dual targeting by magnetic and thermal manipulation, Nanomedicine Nanotechnology, Biol. Med. 20 (2019) 1–12. https://doi.org/10.1016/j.nano.2019.03.014.

[47] X. Wang, C. Wei, M. Liu, T. Yang, W. Zhou, Y. Liu, K. Hong, S. Wang, H. Xin, X. Ding, Near-Infrared Triggered Release of uPA from Nanospheres for Localized Hyperthermia-Enhanced Thrombolysis, Adv. Funct. Mater. 27 (2017) 1–8. https://doi.org/10.1002/adfm.201701824.

[48] T. Mei, A. Kim, L.B. Vong, A. Marushima, S. Puentes, Y. Matsumaru, A. Matsumura, Y. Nagasaki, Encapsulation of tissue plasminogen activator in pH-sensitive self-assembled antioxidant nanoparticles for ischemic stroke treatment-Synergistic effect of thrombolysis and antioxidant, Biomaterials. 215 (2019) 1–12. https://doi.org/10.1016/j.biomaterials.2019.05.020.

REFERENCES

[49] Q.L. Zhou, Z.Y. Chen, Y.X. Wang, F. Yang, Y. Lin, Y.Y. Liao, Ultrasound-mediated local drug and gene delivery using nanocarriers, Biomed Res. Int. 2014 (2014). https://doi.org/10.1155/2014/963891.

[50] V. Karagkiozaki, S. Logothetidis, A.M. Pappa, Nanomedicine for atherosclerosis: Molecular imaging and treatment, J. Biomed. Nanotechnol. 11 (2015) 191–210. https://doi.org/10.1166/jbn.2015.1943.

[51] Z. Tang, D. Li, X. Wang, H. Gong, Y. Luan, Z. Liu, J.L. Brash, H. Chen, A t-PA/nanoparticle conjugate with fully retained enzymatic activity and prolonged circulation time, J. Mater. Chem. B. 3 (2015) 977–982. https://doi.org/10.1039/c4tb01625d.

[52] S. Absar, K. Nahar, Y.M. Kwon, F. Ahsan, Thrombus-targeted nanocarrier attenuates bleeding complications associated with conventional thrombolytic therapy, Pharm. Res. 30 (2013) 1663–1676. https://doi.org/10.1007/s11095-013-1011-x.

[53] H. Jin, H. Tan, L. Zhao, W. Sun, L. Zhu, Y. Sun, H. Hao, H. Xing, L. Liu, X. Qu, Y. Huang, Z. Yang, Ultrasound-triggered thrombolysis using urokinase-loaded nanogels, Int. J. Pharm. 434 (2012) 384–390. https://doi.org/10.1016/j.ijpharm.2012.06.001.

[54] H. Kawata, Y. Uesugi, T. Soeda, Y. Takemoto, J.H. Sung, K. Umaki, K. Kato, K. Ogiwara, K. Nogami, K. Ishigami, M. Horii, S. Uemura, M. Shima, Y. Tabata, Y. Saito, A new drug delivery system for intravenous coronary thrombolysis with thrombus targeting and stealth activity recoverable by ultrasound, J. Am. Coll. Cardiol. 60 (2012) 2550–2557. https://doi.org/10.1016/j.jacc.2012.08.1008.

[55] J. Hu, S. Huang, L. Zhu, W. Huang, Y. Zhao, K. Jin, Q. Zhuge, Tissue Plasminogen Activator-Porous Magnetic Microrods for Targeted Thrombolytic Therapy after Ischemic Stroke, ACS Appl. Mater. Interfaces. 10 (2018) 32988–32997. https://doi.org/10.1021/acsami.8b09423.

REFERENCES

[56] N. Zhang, C. Li, D. Zhou, C. Ding, Y. Jin, Q. Tian, X. Meng, K. Pu, Y. Zhu, Cyclic RGD functionalized liposomes encapsulating urokinase for thrombolysis, Acta Biomater. 70 (2018) 227–236. https://doi.org/10.1016/j.actbio.2018.01.038.

[57] C.L. Pawlowski, W. Li, M. Sun, K. Ravichandran, D. Hickman, C. Kos, G. Kaur, A. Sen Gupta, Platelet microparticle-inspired clot-responsive nanomedicine for targeted fibrinolysis, Biomaterials. 128 (2017) 94–108. https://doi.org/10.1016/j.biomaterials.2017.03.012.

[58] V. Torchilin, M. Papisov, N. Orekhova, A. Belyaev, A. Petrov, S. Ragimov, Magnetically driven thrombolytic preparation containing immobilized streptokinase-targeted transport and action, Haemostasis. 18 (1988) 113-116. https://doi.org/10.1159/000215791.

[59] P.D. Nguyen, E.A. O'Rear, A.E. Johnson, E. Patterson, T.L. Whitsett, R. Bhakta, Accelerated thrombolysis and reperfusion in a canine model of myocardial infarction by liposomal encapsulation of streptokinase, Circ. Res. 66 (1990) 875–878. https://doi.org/10.1161/01.RES.66.3.875.

[60] T.R. Porter, R.F. LeVeen, R. Fox, A. Kricsfeld, F. Xie, Thrombolytic enhancement with perfluorocarbon-exposed sonicated dextrose albumin microbubbles, Am. Heart J. 132 (1996) 964–968. https://doi.org/10.1016/S0002-8703(96)90006-X.

[61] J.K. Leach, E. Patterson, E.A. O'Rear, Encapsulation of a plasminogen activator speeds reperfusion, lessens infarct and reduces blood loss in a canine model of coronary artery thrombosis, Thromb. Haemost. 91 (2004) 1213–1218. https://doi.org/10.1160/th03-11-0704.

[62] J.-C. Murciano, S. Medinilla, D. Eslin, E. Atochina, D.B. Cines, V.R. Muzykantov, Prophylactic fibrinolysis through selective dissolution of nascent clots by tPA-carrying erythrocytes, Nat. Biotechnol. 21 (2003) 891–896. https://doi.org/10.1038/nbt846.

REFERENCES

[63] M. Faria, M. Björnmalm, K.J. Thurecht, S.J. Kent, R.G. Parton, M. Kavallaris, A.P.R. Johnston, J.J. Gooding, S.R. Corrie, B.J. Boyd, P. Thordarson, A.K. Whittaker, M.M. Stevens, C.A. Prestidge, C.J.H. Porter, W.J. Parak, T.P. Davis, E.J. Crampin, F. Caruso, Minimum information reporting in bio–nano experimental literature, Nat. Nanotechnol. 13 (2018) 777–785. https://doi.org/10.1038/s41565-018-0246-4.

[64] T.W. Chung, S.S. Wang, W.J. Tsai, Accelerating thrombolysis with chitosan-coated plasminogen activators encapsulated in poly-(lactide-co-glycolide) (PLGA) nanoparticles, Biomaterials. 29 (2008) 228–237. https://doi.org/10.1016/j.biomaterials.2007.09.027.

[65] F. Bi, J. Zhang, Y. Su, Y.C. Tang, J.N. Liu, Chemical conjugation of urokinase to magnetic nanoparticles for targeted thrombolysis, Biomaterials. 30 (2009) 5125–5130. https://doi.org/10.1016/j.biomaterials.2009.06.006.

[66] Y.-H. Ma, S.-Y. Wu, T. Wu, Y.-J. Chang, M.-Y. Hua, J.-P. Chen, Magnetically targeted thrombolysis with recombinant tissue plasminogen activator bound to polyacrylic acid-coated nanoparticles, Biomaterials. 30 (2009) 3343–3351. https://doi.org/10.1016/j.biomaterials.2009.02.034.

[67] M. Juenet, R. Aid-Launais, B. Li, A. Berger, J. Aerts, V. Ollivier, A. Nicoletti, D. Letourneur, C. Chauvierre, Thrombolytic therapy based on fucoidan-functionalized polymer nanoparticles targeting P-selectin, Biomaterials. 156 (2018) 204–216. https://doi.org/10.1016/j.biomaterials.2017.11.047.

[68] J.R. McCarthy, I.Y. Sazonova, S.S. Erdem, T. Hara, B.D. Thompson, P. Patel, I. Botnaru, C.P. Lin, G.L. Reed, R. Weissleder, F.A. Jaffer, Multifunctional nanoagent for thrombus-targeted fibrinolytic therapy, Nanomedicine (Lond). 7 (2012) 1017–1028. https://doi.org/10.2217/nnm.11.179.

[69] J. Zhou, D. Guo, Y. Zhang, W. Wu, H. Ran, Z. Wang, Construction and evaluation of

Fe3O4-based PLGA nanoparticles carrying rtPA used in the detection of thrombosis and in targeted thrombolysis, ACS Appl. Mater. Interfaces. 6 (2014) 5566–5576. https://doi.org/10.1021/am406008k.

[70] S.D. Tiukinhoy-Laing, S. Huang, M. Klegerman, C.K. Holland, D.D. McPherson, Ultrasound-facilitated thrombolysis using tissue-plasminogen activator-loaded echogenic liposomes, Thromb. Res. 119 (2007) 777–784. https://doi.org/10.1016/j.thromres.2006.06.009.

[71] L. Ma, Y. Wang, S. Zhang, X. Qian, N. Xue, Z. Jiang, O. Akakuru, J. Li, Y. Xu, A. Wu, Deep Penetration of Targeted Nanobubbles Enhanced Cavitation Effect on Thrombolytic Capacity, Bioconjug. Chem. 31 (2020) 369–374. https://doi.org/10.1021/acs.bioconjchem.9b00653.

[72] N. Korin, M. Kanapathipillai, B.D. Matthews, M. Crescente, A. Brill, T. Mammoto, K. Ghosh, S. Jurek, S.A. Bencherif, D. Bhatta, A.U. Coskun, C.L. Feldman, D.D. Wagner, D.E. Ingber, Shear-Activated Nanotherapeutics for Drug Targeting to Obstructed Blood Vessels, Science (80-. ). 337 (2012) 738–742. https://doi.org/10.1126/science.1217815.

[73] Y. Uesugi, H. Kawata, Y. Saito, Y. Tabata, Ultrasound-responsive thrombus treatment with zinc-stabilized gelatin nano-complexes of tissue-type plasminogen activator, J. Drug Target. 20 (2012) 224–234. https://doi.org/10.3109/1061186X.2011.633259.

[74] S.T. Gunawan, K. Kempe, T. Bonnard, J. Cui, K. Alt, L.S. Law, X. Wang, E. Westein, G.K. Such, K. Peter, C.E. Hagemeyer, F. Caruso, Multifunctional Thrombin-Activatable Polymer Capsules for Specific Targeting to Activated Platelets, Adv. Mater. 27 (2015) 5153–5157. https://doi.org/10.1002/adma.201502243.

[75] E. Voros, M. Cho, M. Ramirez, A.L. Palange, E. De Rosa, J. Key, Z. Garami, A.B. Lumsden, P. Decuzzi, TPA Immobilization on Iron Oxide Nanocubes and Localized Magnetic Hyperthermia Accelerate Blood Clot Lysis, Adv. Funct. Mater. 25 (2015)

1709–1718. https://doi.org/10.1002/adfm.201404354.

[76] J. Xu, Y. Zhang, J. Xu, G. Liu, C. Di, X. Zhao, X. Li, Y. Li, N. Pang, C. Yang, Y. Li, B. Li, Z. Lu, M. Wang, K. Dai, R. Yan, S. Li, G. Nie, Engineered Nanoplatelets for Targeted Delivery of Plasminogen Activators to Reverse Thrombus in Multiple Mouse Thrombosis Models, Adv. Mater. 1905145 (2019) 1–14. https://doi.org/10.1002/adma.201905145.

[77] U. Bulbake, S. Doppalapudi, N. Kommineni, W. Khan, Liposomal formulations in clinical use: An updated review, Pharmaceutics. 9 (2017) 1–33. https://doi.org/10.3390/pharmaceutics9020012.

[78] S. Mallick, J.S. Choi, Liposomes: Versatile and biocompatible nanovesicles for efficient biomolecules delivery, J. Nanosci. Nanotechnol. 14 (2014) 755–765. https://doi.org/10.1166/jnn.2014.9080.

[79] K. Bowey, J.F. Tanguay, M. Tabrizian, Liposome technology for cardiovascular disease treatment and diagnosis, Expert Opin. Drug Deliv. 9 (2012) 249–265. https://doi.org/10.1517/17425247.2012.647908.

[80] J. Jamasbi, K. Ayabe, S. Goto, B. Nieswandt, K. Peter, W. Siess, Platelet receptors as therapeutic targets: Past, present and future, Thromb. Haemost. 117 (2017) 1249–1257. https://doi.org/10.1160/TH16-12-0911.

[81] S. Koudelka, R. Mikulik, J. Mašek, M. Raška, P. Turánek Knotigová, A.D. Miller, J. Turánek, Liposomal nanocarriers for plasminogen activators, J. Control. Release. 227 (2016) 45–57. https://doi.org/10.1016/j.jconrel.2016.02.019.

[82] B. Vaidya, G.P. Agrawal, S.P. Vyas, Platelets directed liposomes for the delivery of streptokinase: Development and characterization, Eur. J. Pharm. Sci. 44 (2011) 589–594. https://doi.org/10.1016/j.ejps.2011.10.004.

[83] Y. Huang, L. Yu, J. Ren, B. Gu, C. Longstaff, A.D. Hughes, S.A. Thom, X.Y. Xu, R.

Chen, An activated-platelet-sensitive nanocarrier enables targeted delivery of tissue plasminogen activator for effective thrombolytic therapy, J. Control. Release. 300 (2019) 1–12. https://doi.org/10.1016/j.jconrel.2019.02.033.

[84] D. Varon, E. Shai, Platelets and their microparticles as key players in pathophysiological responses, J. Thromb. Haemost. 13 (2015) S40–S46. https://doi.org/10.1111/jth.12976.

[85] H.-L. Hsu, J.-P. Chen, Preparation of thermosensitive magnetic liposome encapsulated recombinant tissue plasminogen activator for targeted thrombolysis, J. Magn. Magn. Mater. 427 (2017) 188–194. https://doi.org/10.1016/j.jmmm.2016.10.122.

[86] P. Ghasemiyeh, S. Mohammadi-Samani, Solid lipid nanoparticles and nanostructured lipid carriers as novel drug delivery systems: Applications, advantages and disadvantages, Res. Pharm. Sci. 13 (2018) 288–303. https://doi.org/10.4103/1735-5362.235156.

[87] J.N. Marsh, G. Hu, M.J. Scott, H. Zhang, M.J. Goette, J. Patrick, S.D. Caruthers, S.A. Wickline, D. Abendschein, M. Gregory, A fibrin-specific thrombolytic nanomedicine approach to acute ischemic stroke, Nanomedicine (Lond). 6 (2011) 605–615. https://doi.org/10.2217/nnm.11.21.A.

[88] A. Bolhassani, S. Javanzad, T. Saleh, M. Hashemi, M.R. Aghasadeghi, Polymeric nanoparticles. Potent vectors for vaccine delivery targeting cancer and infectious diseases, Hum. Vaccin. Immunother. 10 (2014) 321–332. https://doi.org/10.4161/hv.26796.

[89] Y. Zhang, T. Sun, C. Jiang, Biomacromolecules as carriers in drug delivery and tissue engineering, Acta Pharm. Sin. B. 8 (2018) 34–50. https://doi.org/10.1016/j.apsb.2017.11.005.

[90] K.S. Soppimath, T.M. Aminabhavi, A.R. Kulkarni, W.E. Rudzinski, Biodegradable polymeric nanoparticles as drug delivery devices, J. Control. Release. 70 (2001) 1–20.

https://doi.org/10.1016/S0168-3659(00)00339-4.

[91] J. Zhang, W. Xia, P. Liu, Q. Cheng, T. Tahirou, W. Gu, B. Li, Chitosan modification and pharmaceutical/biomedical applications, Mar. Drugs. 8 (2010) 1962–1987. https://doi.org/10.3390/md8071962.

[92] H.J. Jin, H. Zhang, M.L. Sun, B.G. Zhang, J.W. Zhang, Urokinase-coated chitosan nanoparticles for thrombolytic therapy: Preparation and pharmacodynamics in vivo, J. Thromb. Thrombolysis. 36 (2013) 458–468. https://doi.org/10.1007/s11239-013-0951-7.

[93] H. Baharifar, G. Tavoosidana, R. Karimi, S.A. Bidgoli, H. Ghanbari, M.A. Faramarzi, A. Amani, Optimization of Self-Assembled Chitosan/Streptokinase Nanoparticles and Evaluation of Their Cytotoxicity and Thrombolytic Activity, J. Nanosci. Nanotechnol. 15 (2015) 10127–10133. https://doi.org/10.1166/jnn.2015.11696.

[94] M. Shamsi, P. Zahedi, On-Chip Preparation of Streptokinase Entrapped in Chitosan Nanoparticles Used in Thrombolytic Therapy Potentially, J. Pharm. Sci. 106 (2017) 3623–3630. https://doi.org/10.1016/j.xphs.2017.08.001.

[95] J. Liao, X. Ren, B. Yang, H. Li, Y. Zhang, Z. Yin, Targeted thrombolysis by using c-RGD-modified N,N,N-Trimethyl Chitosan nanoparticles loaded with lumbrokinase, Drug Dev. Ind. Pharm. 45 (2019) 88–95. https://doi.org/10.1080/03639045.2018.1522324.

[96] Y. Teng, H. Jin, D. Nan, M. Li, C. Fan, Y. Liu, P. Lv, W. Cui, Y. Sun, H. Hao, X. Qu, Z. Yang, Y. Huang, In vivo evaluation of urokinase-loaded hollow nanogels for sonothrombolysis on suture embolization-induced acute ischemic stroke rat model, Bioact. Mater. 3 (2018) 102–109. https://doi.org/10.1016/j.bioactmat.2017.08.001.

[97] R. Yasmin, M. Shah, S.A. Khan, R. Ali, Gelatin nanoparticles: A potential candidate for medical applications, Nanotechnol. Rev. 6 (2017) 191–207.

https://doi.org/10.1515/ntrev-2016-0009.

[98] Y. Uesugi, H. Kawata, J.I. Jo, Y. Saito, Y. Tabata, An ultrasound-responsive nano delivery system of tissue-type plasminogen activator for thrombolytic therapy, J. Control. Release. 147 (2010) 269–277. https://doi.org/10.1016/j.jconrel.2010.07.127.

[99] C. Englert, J.C. Brendel, T.C. Majdanski, T. Yildirim, S. Schubert, M. Gottschaldt, N. Windhab, U.S. Schubert, Pharmapolymers in the 21st century: Synthetic polymers in drug delivery applications, Prog. Polym. Sci. 87 (2018) 107–164. https://doi.org/10.1016/j.progpolymsci.2018.07.005.

[100] B. Sivaraman, A. Sylvester, A. Ramamurthi, Fibrinolytic PLGA nanoparticles for slow clot lysis within abdominal aortic aneurysms attenuate proteolytic loss of vascular elastic matrix, Mater. Sci. Eng. C-Materials Biol. Appl. 59 (2016) 145–156. https://doi.org/10.1016/j.msec.2015.09.056.

[101] M. Colasuonno, A.L. Palange, R. Aid, M. Ferreira, H. Mollica, R. Palomba, M. Emdin, M. Del Sette, C. Chauvierre, D. Letourneur, P. Decuzzi, Erythrocyte-Inspired Discoidal Polymeric Nanoconstructs Carrying Tissue Plasminogen Activator for the Enhanced Lysis of Blood Clots, ACS Nano. 12 (2018) 12224–12237. https://doi.org/10.1021/acsnano.8b06021.

[102] C. Vauthier, C. Dubernet, E. Fattal, H. Pinto-Alphandary, P. Couvreur, Poly(alkylcyanoacrylates) as biodegradable materials for biomedical applications, Adv. Drug Deliv. Rev. 55 (2003) 519–548. https://doi.org/10.1016/S0169-409X(03)00041-3.

[103] L. Chollet, P. Saboural, C. Chauvierre, J.-N. Villemin, D. Letourneur, F. Chaubet, Fucoidans in Nanomedicine, Mar. Drugs. 14 (2016) 1–24. https://doi.org/10.3390/md14080145.

[104] T. Bonnard, J.-M. Serfaty, C. Journé, B. Ho Tin Noe, D. Arnaud, L. Louedec, M. Derkaoui, D. Letourneur, C. Chauvierre, C. Le Visage, Leukocyte mimetic

polysaccharide microparticles tracked in vivo on activated endothelium and in abdominal aortic aneurysm, Acta Biomater. 10 (2014) 3535–3545. https://doi.org/10.1016/j.actbio.2014.04.015.

[105] B. Li, M. Juenet, R. Aid-Launais, M. Maire, V. Ollivier, D. Letourneur, C. Chauvierre, Development of Polymer Microcapsules Functionalized with Fucoidan to Target P-Selectin Overexpressed in Cardiovascular Diseases, Adv. Healthc. Mater. 6 (2017) 1–11. https://doi.org/10.1002/adhm.201601200.

[106] H.R. Lijnen, B. Van Hoef, V. Beelen, D. Collen, Characterization of the Murine Plasma Fibrinolytic System, Eur. J. Biochem. 224 (1994) 863–871. https://doi.org/10.1111/j.1432-1033.1994.00863.x.

[107] C. Englert, J.C. Brendel, T.C. Majdanski, T. Yildirim, S. Schubert, M. Gottschaldt, N. Windhab, U.S. Schubert, Pharmapolymers in the 21st century: Synthetic polymers in drug delivery applications, Prog. Polym. Sci. 87 (2018) 107–164. https://doi.org/10.1016/j.progpolymsci.2018.07.005.

[108] J. Deng, H. Mei, W. Shi, Z.-Q. Pang, B. Zhang, T. Guo, H.-F. Wang, X.-G. Jiang, Y. Hu, Recombinant Tissue Plasminogen Activator-conjugated Nanoparticles Effectively Targets Thrombolysis in a Rat Model of Middle Cerebral Artery Occlusion, Curr. Med. Sci. 38 (2018) 427–435. https://doi.org/10.1007/s11596-018-1896-z.

[109] Y. Pan, X. Wang, Z. Yin, Synthesis and evaluation of cationic polymeric micelles as carriers of lumbrokinase for targeted thrombolysis, Asian J. Pharm. Sci. 14 (2019) 144–153. https://doi.org/10.1016/j.ajps.2018.03.004.

[110] Y. Pan, X. Ren, S. Wang, X. Li, X. Luo, Z. Yin, Annexin V-Conjugated Mixed Micelles as a Potential Drug Delivery System for Targeted Thrombolysis, Biomacromolecules. 18 (2017) 865–876. https://doi.org/10.1021/acs.biomac.6b01756.

[111] J.F. Tait, M.D. Cerqueira, T.A. Dewhurst, K. Fujikawa, J.L. Ritchie, J.R. Stratton,

Evaluation of annexin V as a platelet-directed thrombus targeting agent., Thromb. Res. 75 (1994) 491–501. https://doi.org/10.1016/0049-3848(94)90224-0.

[112] L.I. Mukhametova, R.B. Aisina, E.M. Zakharyan, E.A. Karakhanov, K.B. Gershkovich, S.D. Varfolomeyev, Thrombolytic and fibrinogenolytic properties of bioconjugate streptokinase-polyamidoamine dendrimers in vitro, Thromb. Res. 154 (2017) 50–52. https://doi.org/10.1016/j.thromres.2017.04.008.

[113] M. Labieniec-Watala, C. Watala, PAMAM dendrimers: Destined for success or doomed to fail? Plain and modified PAMAM dendrimers in the context of biomedical applications, J. Pharm. Sci. 104 (2015) 2–14. https://doi.org/10.1002/jps.24222.

[114] L.W.E. Starmans, D. Burdinski, N.P.M. Haex, R.P.M. Moonen, G.J. Strijkers, K. Nicolay, H. Grüll, Iron Oxide Nanoparticle-Micelles (ION-Micelles) for Sensitive (Molecular) Magnetic Particle Imaging and Magnetic Resonance Imaging, PLoS One. 8 (2013) 1–9. https://doi.org/10.1371/journal.pone.0057335.

[115] R. Cheng, W. Huang, L. Huang, B. Yang, L. Mao, K. Jin, Q. Zhuge, Y. Zhao, Acceleration of tissue plasminogen activator-mediated thrombolysis by magnetically powered nanomotors, ACS Nano. 8 (2014) 7746–7754. https://doi.org/10.1021/nn5029955.

[116] H. Kempe, M. Kempe, The use of magnetite nanoparticles for implant-assisted magnetic drug targeting in thrombolytic therapy, Biomaterials. 31 (2010) 9499–9510. https://doi.org/10.1016/j.biomaterials.2010.07.107.

[117] J.P. Chen, P.C. Yang, Y.H. Ma, S.J. Tu, Y.J. Lu, Targeted delivery of tissue plasminogen activator by binding to silica-coated magnetic nanoparticle, Int. J. Nanomedicine. 7 (2012) 5137–5149. https://doi.org/10.2147/IJN.S36197.

[118] M. Wang, J. Zhang, Z. Yuan, W. Yang, Q. Wu, H. Gu, Targeted thrombolysis by using of magnetic mesoporous silica nanoparticles, J. Biomed. Nanotechnol. 8 (2012) 624–

632. https://doi.org/10.1166/jbn.2012.1416.

[119] B.L. Razzaboni, P. Bolsaitis, Evidence of an oxidative mechanism for the hemolytic activity of silica particles, Environ. Health Perspect. 87 (1990) 337–341. https://doi.org/10.1289/ehp.9087337.

[120] V. Murashov, M. Harper, E. Demchuk, Impact of silanol surface density on the toxicity of silica aerosols measured by erythrocyte haemolysis, J. Occup. Environ. Hyg. 3 (2006) 718–723. https://doi.org/10.1080/15459620601015950.

[121] T. Wu, M. Tang, Review of the effects of manufactured nanoparticles on mammalian target organs, J. Appl. Toxicol. 38 (2018) 25–40. https://doi.org/10.1002/jat.3499.

[122] J.P. Chen, P.C. Yang, Y.H. Ma, Y.J. Lu, Superparamagnetic iron oxide nanoparticles for delivery of tissue plasminogen activator, in: J. Nanosci. Nanotechnol., 2011: pp. 11089–11094. https://doi.org/10.1166/jnn.2011.3953.

[123] J.P. Chen, C.H. Liu, H.L. Hsu, T. Wu, Y.J. Lu, Y.H. Ma, Magnetically controlled release of recombinant tissue plasminogen activator from chitosan nanocomposites for targeted thrombolysis, J. Mater. Chem. B. 4 (2016) 2578–2590. https://doi.org/10.1039/c5tb02579f.

[124] S. Heid, H. Unterweger, R. Tietze, R.P. Friedrich, B. Weigel, I. Cicha, D. Eberbeck, A.R. Boccaccini, C. Alexiou, S. Lyer, Synthesis and Characterization of Tissue Plasminogen Activator-Functionalized Superparamagnetic Iron Oxide Nanoparticles for Targeted Fibrin Clot Dissolution, Int. J. Mol. Sci. 18 (2017). https://doi.org/10.3390/ijms18091837.

[125] M. Chang, Y.H. Lin, J.L. Gabayno, Q. Li, X. Liu, Thrombolysis based on magnetically-controlled surface-functionalized Fe3O4 nanoparticle, Bioengineered. 8 (2017) 29–35. https://doi.org/10.1080/21655979.2016.1227145.

[126] A.Y. Prilepskii, A.F. Fakhardo, A.S. Drozdov, V. V. Vinogradov, I.P. Dudanov, A.A.

Shtil, P.P. Bel'Tyukov, A.M. Shibeko, E.M. Koltsova, D.Y. Nechipurenko, V. V. Vinogradov, Urokinase-Conjugated Magnetite Nanoparticles as a Promising Drug Delivery System for Targeted Thrombolysis: Synthesis and Preclinical Evaluation, ACS Appl. Mater. Interfaces. 10 (2018) 36764–36775. https://doi.org/10.1021/acsami.8b14790.

[127] L. Huang, J. Wang, S. Huang, F. Siaw-Debrah, M. Nyanzu, Q. Zhuge, Polyacrylic acid-coated nanoparticles loaded with recombinant tissue plasminogen activator for the treatment of mice with ischemic stroke, Biochem. Biophys. Res. Commun. 516 (2019) 565–570. https://doi.org/10.1016/j.bbrc.2019.06.079.

[128] R.P. Friedrich, J. Zaloga, E. Schreiber, I.Y. Tóth, E. Tombácz, S. Lyer, C. Alexiou, Tissue Plasminogen Activator Binding to Superparamagnetic Iron Oxide Nanoparticle-Covalent Versus Adsorptive Approach, Nanoscale Res. Lett. 11 (2016) 1–11. https://doi.org/10.1186/s11671-016-1521-7.

[129] H.W. Yang, M.Y. Hua, K.J. Lin, S.P. Wey, R.Y. Tsai, S.Y. Wu, Y.C. Lu, H.L. Liu, T. Wu, Y.H. Ma, Bioconjugation of recombinant tissue plasminogen activator to magnetic nanocarriers for targeted thrombolysis, Int. J. Nanomedicine. 7 (2012) 5159–5173. https://doi.org/10.2147/IJN.S32939.

[130] J.B. Vines, J.H. Yoon, N.E. Ryu, D.J. Lim, H. Park, Gold nanoparticles for photothermal cancer therapy, Front. Chem. 7 (2019) 1–16. https://doi.org/10.3389/fchem.2019.00167.

[131] D.E. Kim, J.Y. Kim, D. Schellingerhout, J.H. Ryu, S.K. Lee, S. Jeon, J.S. Lee, J. Kim, H.J. Jang, J.E. Park, E.J. Kim, I.C. Kwon, C.H. Ahn, M. Nahrendorf, K. Kim, Quantitative Imaging of Cerebral Thromboemboli in Vivo: The Effects of Tissue-Type Plasminogen Activator, Stroke. 48 (2017) 1376–1385. https://doi.org/10.1161/STROKEAHA.117.016511.

[132] S.P. Kwon, S. Jeon, S.H. Lee, H.Y. Yoon, J.H. Ryu, D. Choi, J.Y. Kim, J. Kim, J.H.

Park, D.E. Kim, I.C. Kwon, K. Kim, C.H. Ahn, Thrombin-activatable fluorescent peptide incorporated gold nanoparticles for dual optical/computed tomography thrombus imaging, Biomaterials. 150 (2018) 125–136. https://doi.org/10.1016/j.biomaterials.2017.10.017.

[133] A. Parodi, R. Molinaro, M. Sushnitha, M. Evangelopoulos, J.O. Martinez, N. Arrighetti, C. Corbo, E. Tasciotti, Bio-inspired engineering of cell- and virus-like nanoparticles for drug delivery, Biomaterials. 147 (2017) 155–168. https://doi.org/10.1016/j.biomaterials.2017.09.020.

[134] S. Absar, Y.M. Kwon, F. Ahsan, Bio-responsive delivery of tissue plasminogen activator for localized thrombolysis, J. Control. Release. 177 (2014) 42–50. https://doi.org/10.1016/j.jconrel.2013.12.036.

[135] R.A. Petros, J.M. Desimone, Strategies in the design of nanoparticles for therapeutic applications, Nat. Rev. Drug Discov. 9 (2010) 615–627. https://doi.org/10.1038/nrd2591.

[136] R. Vankayala, S.R. Corber, J.T. Mac, M.P. Rao, M. Shafie, B. Anvari, Erythrocyte-Derived Nanoparticles as a Theranostic Agent for Near-Infrared Fluorescence Imaging and Thrombolysis of Blood Clots, Macromol. Biosci. 18 (2018) 1700379–1700379. https://doi.org/10.1002/mabi.201700379.

[137] S. Nozohouri, A.E. Sifat, B. Vaidya, T.J. Abbruscato, Novel approaches for the delivery of therapeutics in ischemic stroke, Drug Discov. Today. 25 (2020) 535–551. https://doi.org/10.1016/j.drudis.2020.01.007.

[138] J. Xu, X. Wang, H. Yin, X. Cao, Q. Hu, W. Lv, Q. Xu, Z. Gu, H. Xin, Sequentially Site-Specific Delivery of Thrombolytics and Neuroprotectant for Enhanced Treatment of Ischemic Stroke, ACS Nano. 13 (2019) 8577–8588. https://doi.org/10.1021/acsnano.9b01798.

[139] G. Camussi, M.C. Deregibus, S. Bruno, V. Cantaluppi, L. Biancone, Exosomes/microvesicles as a mechanism of cell-to-cell communication, Kidney Int. 78 (2010) 838–848. https://doi.org/10.1038/ki.2010.278.

[140] A.K.A. Silva, N. Luciani, F. Gazeau, K. Aubertin, S. Bonneau, C. Chauvierre, D. Letourneur, C. Wilhelm, Combining magnetic nanoparticles with cell derived microvesicles for drug loading and targeting, Nanomedicine Nanotechnology, Biol. Med. 11 (2015) 645–655. https://doi.org/10.1016/j.nano.2014.11.009.

[141] Y. Zhong, W.J. Gong, X.H. Gao, Y.N. Li, K. Liu, Y.G. Hu, J.S. Qi, Synthesis and Evaluation of a Novel Nanoparticle Carrying Urokinase Used in Targeted Thrombolysis, J. Biomed. Mater. Res. Part A. 108 (2019) 193–200. https://doi.org/10.1002/jbm.a.36803.

[142] K.J. Koudelka, A.S. Pitek, M. Manchester, N.F. Steinmetz, Virus-Based Nanoparticles as Versatile Nanomachines, Annu Rev Virol. 2 (2015) 379–401. https://doi.org/10.1146/annurev-virology-100114-055141.

[143] A.S. Pitek, J. Park, Y. Wang, H. Gao, H. Hu, D.I. Simon, N.F. Steinmetz, Delivery of thrombolytic therapy using rod-shaped plant viral nanoparticles decreases the risk of hemorrhage, Nanoscale. 10 (2018) 16547–16555. https://doi.org/10.1039/c8nr02861c.

[144] J.W. Yoo, D.J. Irvine, D.E. Discher, S. Mitragotri, Bio-inspired, bioengineered and biomimetic drug delivery carriers, Nat. Rev. Drug Discov. 10 (2011) 521–535. https://doi.org/10.1038/nrd3499.

[145] H. Soo Choi, W. Liu, P. Misra, E. Tanaka, J.P. Zimmer, B. Itty Ipe, M.G. Bawendi, J. V Frangioni, Renal clearance of quantum dots, Nat. Biotechnol. 25 (2007) 1165–1170. https://doi.org/10.1038/nbt1340.

[146] A.E. Nel, L. Mädler, D. Velegol, T. Xia, E.M.V. Hoek, P. Somasundaran, F. Klaessig, V. Castranova, M. Thompson, Understanding biophysicochemical interactions at the

nano-bio interface, Nat. Mater. 8 (2009) 543–557. https://doi.org/10.1038/nmat2442.

[147] F. Alexis, E. Pridgen, L.K. Molnar, O.C. Farokhzad, Factors affecting the clearance and biodistribution of polymeric nanoparticles, Mol. Pharm. 5 (2008) 505–515. https://doi.org/10.1021/mp800051m.

[148] Y. Geng, P. Dalhaimer, S. Cai, R. Tsai, M. Tewari, T. Minko, D.E. Discher, Shape effects of filaments versus spherical particles in flow and drug delivery, Nat. Nanotechnol. 2 (2007) 249–255. https://doi.org/10.1038/nnano.2007.70.

[149] L. Zhang, Z. Cao, Y. Li, J.-R. Ella-Menye, T. Bai, S. Jiang, Softer Zwitterionic Nanogels for Longer Circulation and Lower Splenic Accumulation, ACS Nano. 6 (2012) 6681–6686. https://doi.org/10.1021/nn301159a.

[150] R. Palomba, A.L. Palange, I.F. Rizzuti, M. Ferreira, A. Cervadoro, M.G. Barbato, C. Canale, P. Decuzzi, Modulating Phagocytic Cell Sequestration by Tailoring Nanoconstruct Softness, ACS Nano. 12 (2018) 1433–1444. https://doi.org/10.1021/acsnano.7b07797.

[151] N.Y. Lotosh, S.O. Aliaseva, I.K. Malashenkova, G.M. Sorokoumova, R.G. Vasilov, A.A. Selischeva, Cationic Liposomes Cause ROS Generation and Release of Neutrophil Extracellular Traps, Biochem. Suppl. Ser. A Membr. Cell Biol. 13 (2019) 40–49. https://doi.org/10.1134/S1990747818040074.

[152] T.L. Hwang, I.A. Aljuffali, C.F. Hung, C.H. Chen, J.Y. Fang, The impact of cationic solid lipid nanoparticles on human neutrophil activation and formation of neutrophil extracellular traps (NETs), Chem. Biol. Interact. 235 (2015) 106–114. https://doi.org/10.1016/j.cbi.2015.04.011.

[153] T.L. Hwang, I.A. Aljuffali, C.F. Lin, Y.T. Chang, J.Y. Fang, Cationic additives in nanosystems activate cytotoxicity and inflammatory response of human neutrophils: Lipid nanoparticles versus polymeric nanoparticles, Int. J. Nanomedicine. 10 (2015)

371–385. https://doi.org/10.2147/IJN.S73017.

[154] K. Knop, R. Hoogenboom, D. Fischer, U.S. Schubert, Poly(ethylene glycol) in drug delivery: Pros and cons as well as potential alternatives, Angew. Chemie - Int. Ed. 49 (2010) 6288–6308. https://doi.org/10.1002/anie.200902672.

[155] P.L. Rodriguez, T. Harada, D.A. Christian, D.A. Pantano, R.K. Tsai, D.E. Discher, Minimal "Self" Peptides That Inhibit Phagocytic Clearance and Enhance Delivery of Nanoparticles, Science (80-. ). 339 (2013) 971–975. https://doi.org/10.1126/science.1229568.

[156] J. Saikia, R. Mohammadpour, M. Yazdimamaghani, H. Northrup, V. Hlady, H. Ghandehari, Silica Nanoparticle-Endothelial Interaction: Uptake and Effect on Platelet Adhesion under Flow Conditions, ACS Appl. Bio Mater. 1 (2018) 1620–1627. https://doi.org/10.1021/acsabm.8b00466.

[157] J. Duan, S. Liang, Y. Yu, Y. Li, L. Wang, Z. Wu, Y. Chen, M.R. Miller, Z. Sun, Inflammation–coagulation response and thrombotic effects induced by silica nanoparticles in zebrafish embryos, Nanotoxicology. 12 (2018) 470–484. https://doi.org/10.1080/17435390.2018.1461267.

[158] J. Jose Corbalan, C. Medina, A. Jacoby, T. Malinski, M.W. Radomski, Amorphous silica nanoparticles aggregate human platelets: Potential implications for vascular homeostasis, Int. J. Nanomedicine. 7 (2012) 631–639. https://doi.org/10.2147/IJN.S28293.

[159] X.D. Zhang, H.Y. Wu, D. Wu, Y.Y. Wang, J.H. Chang, Z. Bin Zhai, A.M. Meng, P.X. Liu, L.A. Zhang, F.Y. Fan, Toxicologic effects of gold nanoparticles in vivo by different administration routes, Int. J. Nanomedicine. 5 (2010) 771–781. https://doi.org/10.2147/IJN.S8428.

[160] L. Shang, K. Nienhaus, G.U. Nienhaus, Engineered nanoparticles interacting with cells: Size matters, J. Nanobiotechnology. 12 (2014) 1–11. https://doi.org/10.1186/1477-

3155-12-5.

[161] Y. Pan, S. Neuss, A. Leifert, M. Fischler, F. Wen, U. Simon, G. Schmid, W. Brandau, W. Jahnen-Dechent, Size-dependent cytotoxicity of gold nanoparticles, Small. 3 (2007) 1941–1949. https://doi.org/10.1002/smll.200700378.

[162] Z. He, J. Liu, L. Du, The unexpected effect of PEGylated gold nanoparticles on the primary function of erythrocytes, Nanoscale. 6 (2014) 9017–9024. https://doi.org/10.1039/c4nr01857e.

[163] J. Feng, H. Liu, K.K. Bhakoo, L. Lu, Z. Chen, A metabonomic analysis of organ specific response to USPIO administration, Biomaterials. 32 (2011) 6558–6569. https://doi.org/10.1016/j.biomaterials.2011.05.035.

[164] C. Lasagna-Reeves, D. Gonzalez-Romero, M.A. Barria, I. Olmedo, A. Clos, V.M. Sadagopa Ramanujam, A. Urayama, L. Vergara, M.J. Kogan, C. Soto, Bioaccumulation and toxicity of gold nanoparticles after repeated administration in mice, Biochem. Biophys. Res. Commun. 393 (2010) 649–655. https://doi.org/10.1016/j.bbrc.2010.02.046.

[165] K. Andrieux, P. Couvreur, Polyalkylcyanoacrylate nanoparticles for delivery of drugs across the blood-brain barrier, Wiley Interdiscip Rev Nanomed Nanobiotechnol. 1 (2009) 463–474. https://doi.org/10.1002/wnan.5.

[166] N.J. Siddiqi, M.A.K. Abdelhalim, A.K. El-Ansary, A.S. Alhomida, W.Y. Ong, Identification of potential biomarkers of gold nanoparticle toxicity in rat brains, J. Neuroinflammation. 9 (2012) 1–7. https://doi.org/10.1186/1742-2094-9-123.

[167] R. Brouns, P.P. De Deyn, The complexity of neurobiological processes in acute ischemic stroke, Clin. Neurol. Neurosurg. 111 (2009) 483–495. https://doi.org/10.1016/j.clineuro.2009.04.001.

[168] D. Vivien, M. Gauberti, A. Montagne, G. Defer, E. Touzé, Impact of tissue plasminogen

activator on the neurovascular unit: From clinical data to experimental evidence, J. Cereb. Blood Flow Metab. 31 (2011) 2119–2134. https://doi.org/10.1038/jcbfm.2011.127.

[169] M. Bartneck, T. Ritz, H.A. Keul, M. Wambach, J. Bornemann, U. Gbureck, J. Ehling, T. Lammers, F. Heymann, N. Gassler, T. Lüdde, C. Trautwein, J. Groll, F. Tacke, Peptide-functionalized gold nanorods increase liver injury in hepatitis, ACS Nano. 6 (2012) 8767–8777. https://doi.org/10.1021/nn302502u.

[170] C.H. Fu, T.L. Liu, F.Q. Tang, D. Chen, L.L. Li, H.Y. Liu, X.M. Li, Acute toxicity and oxidative damage induced by silica nanorattle in vivo, Chinese Sci. Bull. 57 (2012) 2525–2532. https://doi.org/10.1007/s11434-012-5187-y.

[171] H. Nishimori, M. Kondoh, K. Isoda, S. ichi Tsunoda, Y. Tsutsumi, K. Yagi, Histological analysis of 70-nm silica particles-induced chronic toxicity in mice, Eur. J. Pharm. Biopharm. 72 (2009) 626–629. https://doi.org/10.1016/j.ejpb.2009.03.007.

[172] D. Couto, M. Freitas, V.M. Costa, R.C. Chisté, A. Almeida, M.A. Lopez-Quintela, J. Rivas, P. Freitas, P. Silva, F. Carvalho, E. Fernandes, Biodistribution of polyacrylic acid-coated iron oxide nanoparticles is associated with proinflammatory activation and liver toxicity, J. Appl. Toxicol. 36 (2016) 1321–1331. https://doi.org/10.1002/jat.3323.

[173] B. Zhao, X.Q. Wang, X.Y. Wang, H. Zhang, W.B. Dai, J. Wang, Z.L. Zhong, H.N. Wu, Q. Zhang, Nanotoxicity comparison of four amphiphilic polymeric micelles with similar hydrophilic or hydrophobic structure, Part. Fibre Toxicol. 10 (2013) 1–16. https://doi.org/10.1186/1743-8977-10-47.

[174] X. Li, A. Radomski, O.I. Corrigan, L. Tajber, F. De Sousa Menezes, S. Endter, C. Medina, M.W. Radomski, Platelet compatibility of PLGA, chitosan and PLGA-chitosan nanoparticles, Nanomedicine (Lond). 4 (2009) 735–746. https://doi.org/doi:10.2217/nnm.09.65.

[175] Y. Zhao, D. Sultan, Y. Liu, Biodistribution, excretion, and toxicity of nanoparticles, in: Theranostic Bionanomaterials, Elsevier Inc., 2019: pp. 27–53. https://doi.org/10.1016/B978-0-12-815341-3.00002-X.

[176] K.D. Grieger, I. Linkov, S.F. Hansen, A. Baun, Environmental risk analysis for nanomaterials: Review and evaluation of frameworks, Nanotoxicology. 6 (2012) 196–212. https://doi.org/10.3109/17435390.2011.569095.

[177] E. Sadauskas, G. Danscher, M. Stoltenberg, U. Vogel, A. Larsen, H. Wallin, Protracted elimination of gold nanoparticles from mouse liver, Nanomedicine Nanotechnology, Biol. Med. 5 (2009) 162–169. https://doi.org/10.1016/j.nano.2008.11.002.

[178] J. Feng, H. Liu, L. Zhang, K. Bhakoo, L. Lu, An insight into the metabolic responses of ultra-small superparamagnetic particles of iron oxide using metabonomic analysis of biofluids, Nanotechnology. 21 (2010) 395101. https://doi.org/10.1088/0957-4484/21/39/395101.

[179] Q. Ran, Y. Xiang, Y. Liu, L. Xiang, F. Li, X. Deng, Y. Xiao, L. Chen, L. Chen, Z. Li, Eryptosis Indices as a Novel Predictive Parameter for Biocompatibility of Fe3O4 Magnetic Nanoparticles on Erythrocytes, Sci. Rep. 5 (2015) 16209. https://doi.org/10.1038/srep16209.

[180] K. de la Harpe, P. Kondiah, Y. Choonara, T. Marimuthu, L. du Toit, V. Pillay, The Hemocompatibility of Nanoparticles: A Review of Cell–Nanoparticle Interactions and Hemostasis, Cells. 8 (2019) 1209. https://doi.org/10.3390/cells8101209.

[181] S. Vrignaud, J.P. Benoit, P. Saulnier, Strategies for the nanoencapsulation of hydrophilic molecules in polymer-based nanoparticles, Biomaterials. 32 (2011) 8593–8604. https://doi.org/10.1016/j.biomaterials.2011.07.057.

[182] M. Di Marco, K.A. Razak, A.A. Aziz, C. Devaux, E. Borghi, L. Levy, C. Sadun, Overview of the main methods used to combine proteins with nanosystems : absorption,

bioconjugation, and encapsulation, Int. J. Nanomedicine. 5 (2010) 37–49.

[183] L. Arnfast, C.G. Madsen, L. Jorgensen, S. Baldursdottir, Design and processing of nanogels as delivery systems for peptides and proteins, Ther. Deliv. 5 (2014) 691–708. https://doi.org/10.4155/tde.14.38.

[184] S.R. Van Tomme, W.E. Hennink, Biodegradable dextran hydrogels for protein delivery applications, Expert Rev. Med. Devices. 4 (2007) 147–164. https://doi.org/10.1586/17434440.4.2.147.

[185] C. Chauvierre, R. Aid-Launais, J. Aerts, M. Maire, L. Chollet, L. Rolland, R. Bonaf, S. Rossi, S. Bussi, C. Cabella, D. Laszlo, T. Fülöp, J. Szebeni, Y. Chahid, K.H. Zheng, E.S.G. Stroes, D. Le Guludec, F. Rouzet, D. Letourneur, Pharmaceutical Development and Safety Evaluation of a GMP-Grade Fucoidan for Molecular Diagnosis of Cardiovascular Diseases, Mar. Drugs. 17 (2019) 1–17. https://doi.org/https://doi.org/10.3390/md17120699.

[186] K.H. Zheng, Y. Kaiser, E. Poel, H. Verberne, J. Aerts, F. Rouzet, E. Stroes, D. Letourneur, C. Chauvierre, 99Mtc-Fucoidan As Diagnostic Agent For P-Selectin Imaging: First-In-Human Evaluation (Phase I), Atherosclerosis. 287 (2019) e143. https://doi.org/10.1016/j.atherosclerosis.2019.06.425.

[187] J. Matuszak, P. Dörfler, S. Lyer, H. Unterweger, M. Juenet, C. Chauvierre, A. Alaarg, D. Franke, G. Almer, I. Texier, J.M. Metselaar, R. Prassl, C. Alexiou, H. Mangge, D. Letourneur, I. Cicha, Comparative analysis of nanosystems' effects on human endothelial and monocytic cell functions, Nanotoxicology. 12 (2018) 957–974. https://doi.org/10.1080/17435390.2018.1502375.

[188] I. Cicha, C. Chauvierre, I. Texier, C. Cabella, J.M. Metselaar, J. Szebeni, L. Dézsi, C. Alexiou, F. Rouzet, G. Storm, E. Stroes, D. Bruce, N. MacRitchie, P. Maffia, D. Letourneur, From design to the clinic: Practical guidelines for translating cardiovascular

nanomedicine, Cardiovasc. Res. 114 (2018) 1714–1727. https://doi.org/10.1093/cvr/cvy219.

[189] C. Chauvierre, D. Letourneur, The European project NanoAthero to fight cardiovascular diseases using nanotechnologies, Nanomedicine (Lond). 10 (2015) 3391–3400. https://doi.org/10.2217/nnm.15.170.

[190] K.H. Zheng, J. Schoormans, L.C.A. Stiekema, C. Calcagno, I. Cicha, C. Alexiou, G.J. Strijkers, A.J. Nederveen, E.S.G. Stroes, B.F. Coolen, Plaque Permeability Assessed With DCE-MRI Associates With USPIO Uptake in Patients With Peripheral Artery Disease, JACC Cardiovasc. Imaging. 12 (2019) 2081–2083. https://doi.org/10.1016/j.jcmg.2019.04.014.

[191] F.M. van der Valk, D.F. van Wijk, M.E. Lobatto, H.J. Verberne, G. Storm, M.C.M. Willems, D.A. Legemate, A.J. Nederveen, C. Calcagno, V. Mani, S. Ramachandran, M.P.M. Paridaans, M.J. Otten, G.M. Dallinga-Thie, Z.A. Fayad, M. Nieuwdorp, D.M. Schulte, J.M. Metselaar, W.J.M. Mulder, E.S. Stroes, Prednisolone-containing liposomes accumulate in human atherosclerotic macrophages upon intravenous administration, Nanomedicine Nanotechnology, Biol. Med. 11 (2015) 1039–1046. https://doi.org/10.1016/j.nano.2015.02.021.

[192] K.H. Zheng, F.M. van der Valk, L.P. Smits, M. Sandberg, J.L. Dasseux, R. Baron, R. Barbaras, C. Keyserling, B.F. Coolen, A.J. Nederveen, H.J. Verberne, T.E. Nell, D.J. Vugts, R. Duivenvoorden, Z.A. Fayad, W.J.M. Mulder, G.A.M.S. van Dongen, E.S.G. Stroes, HDL mimetic CER-001 targets atherosclerotic plaques in patients, Atherosclerosis. 251 (2016) 381–388. https://doi.org/10.1016/j.atherosclerosis.2016.05.038.

[193] K.S. Masters, D.N. Shah, L.A. Leinwand, K.S. Anseth, Crosslinked hyaluronan scaffolds as a biologically active carrier for valvular interstitial cells, Biomaterials. 26

(2005) 2517–2525. https://doi.org/10.1016/j.biomaterials.2004.07.018.

[194] W.E. Hennink, C.F. van Nostrum, Novel crosslinking methods to design hydrogels, Adv. Drug Deliv. Rev. 54 (2002) 13–36. https://doi.org/10.1016/S0169-409X(01)00240-X.

[195] P. Gupta, K. Vermani, S. Garg, Hydrogels: From controlled release to pH-responsive drug delivery, Drug Discov. Today. 7 (2002) 569–579. https://doi.org/10.1016/S1359-6446(02)02255-9.

[196] J. Zhou, J. Li, X. Du, B. Xu, Supramolecular biofunctional materials, Biomaterials. 129 (2017) 1–27. https://doi.org/10.1016/j.biomaterials.2017.03.014.

[197] J.C. Fricain, S. Schlaubitz, C. Le Visage, I. Arnault, S.M. Derkaoui, R. Siadous, S. Catros, C. Lalande, R. Bareille, M. Renard, T. Fabre, S. Cornet, M. Durand, A. Léonard, N. Sahraoui, D. Letourneur, J. Amédée, A nano-hydroxyapatite - Pullulan/dextran polysaccharide composite macroporous material for bone tissue engineering, Biomaterials. 34 (2013) 2947–2959. https://doi.org/10.1016/j.biomaterials.2013.01.049.

[198] L. Shi, R. Aid, C. Le Visage, S.Y. Chew, Biomimicking Polysaccharide Nanofibers Promote Vascular Phenotypes: A Potential Application for Vascular Tissue Engineering, Macromol. Biosci. 12 (2012) 395–401. https://doi.org/10.1002/mabi.201100336.

[199] F.J. Holly, Protein and lipid adsorption by acrylic hydrogels and their relation to water wettability, J. Polym. Sci. Polym. Symp. 66 (1979) 409–417. https://doi.org/10.1002/polc.5070660138.

[200] N.M.B. Smeets, T. Hoare, Designing responsive microgels for drug delivery applications, J. Polym. Sci. Part A Polym. Chem. 51 (2013) 3027–3043. https://doi.org/10.1002/pola.26707.

[201] M.A. dos Santos, A. Grenha, Polysaccharide nanoparticles for protein and Peptide delivery: exploring less-known materials, in: Adv. Protein Chem. Struct. Biol., 1st ed., Elsevier Inc., 2015: pp. 223–269. https://doi.org/10.1016/bs.apcsb.2014.11.003.

[202] C. Svensén, P. Rodhe, Intravascular Volume Replacement Therapy, in: Pharmacol. Physiol. Anesth. Found. Clin. Appl., Elsevier, 2013: pp. 574–592. https://doi.org/10.1016/B978-1-4377-1679-5.00033-8.

[203] WHO, World health organization model list of essential medicines, 2019. https://www.who.int/medicines/publications/essentialmedicines/en/.

[204] A.K.A. Silva, D. Letourneur, C. Chauvierre, Polysaccharide nanosystems for future progress in cardiovascular pathologies, Theranostics. 4 (2014) 579–591. https://doi.org/10.7150/thno.7688.

[205] A. Kumari, S.K. Yadav, S.C. Yadav, Biodegradable polymeric nanoparticles based drug delivery systems, Colloids Surfaces B Biointerfaces. 75 (2010) 1–18. https://doi.org/10.1016/j.colsurfb.2009.09.001.

[206] J.K. Oh, R. Drumright, D.J. Siegwart, K. Matyjaszewski, The development of microgels/nanogels for drug delivery applications, Prog. Polym. Sci. 33 (2008) 448–477. https://doi.org/10.1016/j.progpolymsci.2008.01.002.

[207] A.E. Ekkelenkamp, M.R. Elzes, J.F.J. Engbersen, J.M.J. Paulusse, Responsive crosslinked polymer nanogels for imaging and therapeutics delivery, J. Mater. Chem. B. 6 (2018) 210–235. https://doi.org/10.1039/c7tb02239e.

[208] S. Omi, G.-H. Ma, M. Nagai, Membrane emulsification - A versatile tool for the synthesis of polymeric microspheres, Macromol. Symp. 151 (2000) 319–330. https://doi.org/10.1002/1521-3900(200002)151:1<319::AID-MASY319>3.0.CO;2-X.

[209] G. De Luca, F.P. Di Maio, A. Di Renzo, E. Drioli, Droplet detachment in cross-flow membrane emulsification: Comparison among torque- and force-based models, Chem. Eng. Process. Process Intensif. 47 (2008) 1150–1158. https://doi.org/10.1016/j.cep.2007.03.010.

[210] M.Y. Kariduraganavar, G.B. Heggannavar, S. Amado, G.R. Mitchell, Protein

Nanocarriers for Targeted Drug Delivery for Cancer Therapy, in: Nanocarriers Drug Deliv., Elsevier Inc., 2019: pp. 173–204. https://doi.org/10.1016/b978-0-12-814033-8.00006-0.

[211] R.M.D. Soares, N.M. Siqueira, M.P. Prabhakaram, Materials Science & Engineering C Electrospinning and electrospray of bio-based and natural polymers for biomaterials development, Mater. Sci. Eng. C. 92 (2018) 969–982. https://doi.org/10.1016/j.msec.2018.08.004.

[212] D.F. Argenta, T.C. dos Santos, A.M. Campos, T. Caon, Hydrogel Nanocomposite Systems: Physico- Chemical Characterization and Application for Drug-Delivery Systems, in: Nanocarriers Drug Deliv., Elsevier, 2019: pp. 81–131. https://doi.org/https://doi.org/10.1016/B978-0-12-814033-8.00003-5.

[213] A. Sharma, T. Garg, A. Aman, K. Panchal, R. Sharma, S. Kumar, T. Markandeywar, Nanogel - An advanced drug delivery tool: Current and future, Artif. Cells, Nanomedicine Biotechnol. 44 (2016) 165–177. https://doi.org/10.3109/21691401.2014.930745.

[214] C.E. Sing, S.L. Perry, Recent progress in the science of complex coacervation, Soft Matter. 16 (2020) 2885–2914. https://doi.org/10.1039/d0sm00001a.

[215] B. Sarmento, A. Ribeiro, F. Veiga, D. Ferreira, Development and characterization of new insulin containing polysaccharide nanoparticles, Colloids Surfaces B Biointerfaces. 53 (2006) 193–202. https://doi.org/10.1016/j.colsurfb.2006.09.012.

[216] T.J.M. Molenaar, J. Twisk, S.A.M. De Haas, N. Peterse, B.J.C.P. Vogelaar, S.H. Van Leeuwen, I.N. Michon, T.J.C. Van Berkel, J. Kuiper, E.A.L. Biessen, P-selectin as a candidate target in atherosclerosis, Biochem. Pharmacol. 66 (2003) 859–866. https://doi.org/10.1016/S0006-2952(03)00387-3.

[217] J. Kappelmayer, B. Nagy, K. Miszti-Blasius, Z. Hevessy, H. Setiadi, The emerging value

of P-selection as a disease marker, Clin. Chem. Lab. Med. 42 (2004) 475–486. https://doi.org/10.1515/CCLM.2004.082.

[218] F. Alfonso, D.J. Angiolillo, Targeting P-Selectin During Coronary Interventions, J. Am. Coll. Cardiol. 61 (2013) 2056–2059. https://doi.org/10.1016/j.jacc.2013.03.004.

[219] K. Ley, The role of selectins in inflammation and disease, Trends Mol. Med. 9 (2003) 263–268. https://doi.org/10.1016/S1471-4914(03)00071-6.

[220] B.A. Imhof, D. Dunon, Leukocyte migration and adhesion, in: Adv. Immunol., Elsevier, 1995: pp. 345–416. https://doi.org/10.1016/s0065-2776(08)60623-9.

[221] T.R. Porter, Cardiovascular imaging of remote myocardial ischemia: Detecting a molecular trace of evidence left behind, Circulation. 115 (2007) 292–293. https://doi.org/10.1161/CIRCULATIONAHA.106.675413.

[222] R. Thomas, Y. Cheng, J. Yan, T. Bettinger, A. Broillet, G. Rioufol, A.D. Nunn, Upregulation of coronary endothelial P-selectin in a monkey heart ischemia reperfusion model, J. Mol. Histol. 41 (2010) 277–287. https://doi.org/10.1007/s10735-010-9289-z.

[223] Y. Hiramatsu, H. Tsujishita, H. Kondo, Studies on selectin blocker. 3. Investigation of the carbohydrate ligand sialyl Lewis X recognition site of P-selectin, J. Med. Chem. 39 (1996) 4547–4553. https://doi.org/10.1021/jm960134g.

[224] A. Friedman, S. Claypool, R. Liu, The Smart Targeting of Nanoparticles, Curr. Pharm. Des. 19 (2013) 6315–6329. https://doi.org/10.2174/13816128113199990375.

[225] W. jin Jeong, J. Bu, L.J. Kubiatowicz, S.S. Chen, Y.S. Kim, S. Hong, Peptide–nanoparticle conjugates: a next generation of diagnostic and therapeutic platforms?, Nano Converg. 5 (2018) 1–18. https://doi.org/10.1186/s40580-018-0170-1.

[226] E.M. Balboa, E. Conde, A. Moure, E. Falqué, H. Domínguez, In vitro antioxidant properties of crude extracts and compounds from brown algae, Food Chem. 138 (2013) 1764–1785. https://doi.org/10.1016/j.foodchem.2012.11.026.

[227] M.E. Beauharnois, K.C. Lindquist, D. Marathe, P. Vanderslice, J. Xia, K.L. Matta, S. Neelamegham, Affinity and Kinetics of Sialyl Lewis-X and Core-2 Based Oligosaccharides Binding to L- and P-Selectin, Biochemistry. 44 (2005) 9507–9519. https://doi.org/10.1021/bi0507130.

[228] L. Bachelet, I. Bertholon, D. Lavigne, R. Vassy, M. Jandrot-Perrus, F. Chaubet, D. Letourneur, Affinity of low molecular weight fucoidan for P-selectin triggers its binding to activated human platelets, Biochim. Biophys. Acta - Gen. Subj. 1790 (2009) 141–146. https://doi.org/10.1016/j.bbagen.2008.10.008.

[229] J.H. Fitton, D.N. Stringer, A.Y. Park, S.S. Karpiniec, Therapies from fucoidan: New developments, Mar. Drugs. 17 (2019) 1–15. https://doi.org/10.3390/md17100571.

[230] Y. Choi, S.K. Min, R. Usoltseva, A. Silchenko, T. Zvyagintseva, S. Ermakova, J.K. Kim, Thrombolytic fucoidans inhibit the tPA-PAI1 complex, indicating activation of plasma tissue-type plasminogen activator is a mechanism of fucoidan-mediated thrombolysis in a mouse thrombosis model, Thromb. Res. 161 (2018) 22–25. https://doi.org/10.1016/j.thromres.2017.11.015.

[231] T. Bonnard, G. Yang, A. Petiet, V. Ollivier, O. Haddad, D. Arnaud, L. Louedec, L. Bachelet-Violette, S.M. Derkaoui, D. Letourneur, C. Chauvierre, C. Le Visage, Abdominal Aortic Aneurysms Targeted by Functionalized Polysaccharide Microparticles: a new Tool for SPECT Imaging, Theranostics. 4 (2014) 592–603. https://doi.org/10.7150/thno.7757.

[232] B. Li, R. Aid-Launais, M.-N. Labour, A. Zenych, M. Juenet, C. Choqueux, V. Ollivier, O. Couture, D. Letourneur, C. Chauvierre, Functionalized polymer microbubbles as new molecular ultrasound contrast agent to target P-selectin in thrombus, Biomaterials. 194 (2019) 139–150. https://doi.org/10.1016/j.biomaterials.2018.12.023.

[233] P. Saboural, F. Chaubet, F. Rouzet, F. Al-Shoukr, R. Ben Azzouna, N. Bouchemal, L.

Picton, L. Louedec, M. Maire, L. Rolland, G. Potier, D. Le Guludec, D. Letourneur, C. Chauvierre, Purification of a low molecular weight fucoidan for SPECT molecular imaging of myocardial infarction, Mar. Drugs. 12 (2014) 4851–4867. https://doi.org/10.3390/md12094851.

[234] F. Rouzet, L. Bachelet-Violette, J.-M. Alsac, M. Suzuki, A. Meulemans, L. Louedec, A. Petiet, M. Jandrot-Perrus, F. Chaubet, J.-B. Michel, D. Le Guludec, D. Letourneur, Radiolabeled fucoidan as a P-selectin targeting agent for in vivo imaging of platelet-rich thrombus and endothelial activation., J. Nucl. Med. 52 (2011) 1433–1440. https://doi.org/10.2967/jnumed.110.085852.

[235] J. Mican, M. Toul, D. Bednar, J. Damborsky, Structural Biology and Protein Engineering of Thrombolytics, Comput. Struct. Biotechnol. J. 17 (2019) 917–938. https://doi.org/10.1016/j.csbj.2019.06.023.

[236] R. Bhatia, M.D. Hill, N. Shobha, B. Menon, S. Bal, P. Kochar, T. Watson, M. Goyal, A.M. Demchuk, Low rates of acute recanalization with intravenous recombinant tissue plasminogen activator in ischemic stroke: Real-world experience and a call for action, Stroke. 41 (2010) 2254–2258. https://doi.org/10.1161/STROKEAHA.110.592535.

[237] A.M. Thiebaut, M. Gauberti, C. Ali, S. Martinez De Lizarrondo, D. Vivien, M. Yepes, B.D. Roussel, The role of plasminogen activators in stroke treatment: fibrinolysis and beyond, Lancet Neurol. 17 (2018) 1121–1132. https://doi.org/10.1016/S1474-4422(18)30323-5.

[238] S. Liu, X. Feng, R. Jin, G. Li, Tissue plasminogen activator-based nanothrombolysis for ischemic stroke, Expert Opin Drug Deliv. 15 (2018) 173–184. https://doi.org/10.1080/17425247.2018.1384464.

[239] K. Ganguly, K. Chaturvedi, U.A. More, M.N. Nadagouda, T.M. Aminabhavi, Polysaccharide-based micro/nanohydrogels for delivering macromolecular therapeutics,

J. Control. Release. 193 (2014) 162–173. https://doi.org/10.1016/j.jconrel.2014.05.014.

[240] J.M. Lee, Z.-U. Shin, G.T. Mavlonov, I.Y. Abdurakhmonov, T.-H. Yi, Solid-Phase Colorimetric Method for the Quantification of Fucoidan, Appl. Biochem. Biotechnol. 168 (2012) 1019–1024. https://doi.org/10.1007/s12010-012-9837-y.

[241] S. Petersen, A. Fahr, H. Bunjes, Flow cytometry as a new approach to investigate drug transfer between lipid particles, Mol. Pharm. 7 (2010) 350–363. https://doi.org/10.1021/mp900130s.

[242] C. Orset, R. Macrez, A.R. Young, D. Panthou, E. Angles-cano, E. Maubert, V. Agin, D. Vivien, Mouse Model of In Situ Thromboembolic Stroke and Reperfusion, Stroke. 38 (2007) 2771–2778. https://doi.org/10.1161/STROKEAHA.107.487520.

[243] T.E. Furia, CRC Handbook of Food Additives, Second Edi, CRC Press, 1973.

[244] C.I. Jones, D.A. Payne, P.D. Hayes, A.R. Naylor, P.R.F. Bell, M.M. Thompson, A.H. Goodall, The antithrombotic effect of dextran-40 in man is due to enhanced fibrinolysis in vivo, J. Vasc. Surg. 48 (2008) 715–722. https://doi.org/10.1016/j.jvs.2008.04.008.

[245] F. Wolf, K. Koehler, H.P. Schuchmann, Stabilization of water droplets in oil with PGPR for use in oral and dermal applications, J. Food Process Eng. 36 (2013) 276–283. https://doi.org/10.1111/j.1745-4530.2012.00688.x.

[246] J. Matuszak, J. Baumgartner, J. Zaloga, M. Juenet, A.E. da Silva, D. Franke, G. Almer, I. Texier, D. Faivre, J.M. Metselaar, F.P. Navarro, C. Chauvierre, R. Prassl, L. Dézsi, R. Urbanics, C. Alexiou, H. Mangge, J. Szebeni, D. Letourneur, I. Cicha, Nanoparticles for intravascular applications: physicochemical characterization and cytotoxicity testing, Nanomedicine. 11 (2016) 597–616. https://doi.org/10.2217/nnm.15.216.

[247] M. Weber, H. Steinle, S. Golombek, L. Hann, C. Schlensak, H.P. Wendel, M. Avci-Adali, Blood-Contacting Biomaterials: In Vitro Evaluation of the Hemocompatibility, Front. Bioeng. Biotechnol. 6 (2018) 99. https://doi.org/10.3389/fbioe.2018.00099.

[248] ISO 10993-4:2017, Biol. Eval. Med. Devices — Part 4 Sel. Tests Interact. with Blood. (2017). https://www.iso.org/standard/63448.html.

[249] N. Zhang, C. Li, D. Zhou, C. Ding, Y. Jin, Q. Tian, X. Meng, K. Pu, Y. Zhu, Cyclic RGD functionalized liposomes encapsulating urokinase for thrombolysis, Acta Biomater. (2018). https://doi.org/10.1016/j.actbio.2018.01.038.

[250] J.-H. Kim, J.-Y. Yoon, Protein adsorption on polymer particles, in: Encycl. Surf. Colloid Sci., 2002: pp. 4373–4381. https://doi.org/10.1002/jbm.820210202.

[251] I. Politis, L. Wang, J.D. Turner, B.K. Tsang, Changes in Tissue-Type Plasminogen Activator-Like and Plasminogen Activator Inhibitor Activities in Granulosa and Theca Layers during Ovarian Follicle Development in the Domestic Hen1, Biol. Reprod. 42 (1990) 747–754. https://doi.org/10.1095/biolreprod42.5.747.

[252] V. Wintgens, C. Lorthioir, P. Dubot, B. Sébille, C. Amiel, Cyclodextrin/dextran based hydrogels prepared by cross-linking with sodium trimetaphosphate, Carbohydr. Polym. 132 (2015) 80–88. https://doi.org/10.1016/j.carbpol.2015.06.038.

[253] Z.M. Ruggeri, Platelets in atherothrombosis, Nat. Med. 8 (2002) 1227–1234. https://doi.org/10.4065/81.1.59.

[254] T.J. Merkel, K. Chen, S.W. Jones, A.A. Pandya, S. Tian, M.E. Napier, W.E. Zamboni, J.M. Desimone, The effect of particle size on the biodistribution of low-modulus hydrogel PRINT particles, J. Control. Release. 162 (2012) 37–44. https://doi.org/10.1016/j.jconrel.2012.06.009.

[255] C. Orset, B. Haelewyn, S.M. Allan, S. Ansar, F. Campos, T.H. Cho, A. Durand, M. El Amki, M. Fatar, I. Garcia-Yébenes, M. Gauberti, S. Grudzenski, I. Lizasoain, E. Lo, R. Macrez, I. Margaill, S. Maysami, S. Meairs, N. Nighoghossian, J. Orbe, J.A. Paramo, J.J. Parienti, N.J. Rothwell, M. Rubio, C. Waeber, A.R. Young, E. Touzé, D. Vivien, Efficacy of Alteplase in a Mouse Model of Acute Ischemic Stroke: A Retrospective

Pooled Analysis, Stroke. 47 (2016) 1312–1318. https://doi.org/10.1161/STROKEAHA.116.012238.

[256] S.M. De Lizarrondo, C. Gakuba, B.A. Herbig, Y. Repessé, C. Ali, C. V. Denis, P.J. Lenting, E. Touzé, S.L. Diamond, D. Vivien, M. Gauberti, Potent thrombolytic effect of N-acetylcysteine on arterial thrombi, Circulation. 136 (2017) 646–660. https://doi.org/10.1161/CIRCULATIONAHA.117.027290.

[257] H. Kim, J.H. Ahn, M. Song, D.W. Kim, T.K. Lee, J.C. Lee, Y.M. Kim, J.D. Kim, J.H. Cho, I.K. Hwang, B.C. Yan, M.H. Won, J.H. Park, Pretreated fucoidan confers neuroprotection against transient global cerebral ischemic injury in the gerbil hippocampal CA1 area via reducing of glial cell activation and oxidative stress, Biomed. Pharmacother. 109 (2019) 1718–1727. https://doi.org/10.1016/j.biopha.2018.11.015.

[258] S. Yokoyama, H. Ikeda, N. Haramaki, H. Yasukawa, T. Murohara, T. Imaizumi, Platelet P-selectin plays an important role in arterial thrombogenesis by forming large stable platelet-leukocyte aggregates, J. Am. Coll. Cardiol. 45 (2005) 1280–1286. https://doi.org/10.1016/j.jacc.2004.12.071.

[259] S.R. Barthel, J.D. Gavino, L. Descheny, C.J. Dimitroff, Targeting selectins and selectin ligands in inflammation and cancer, Expert Opin. Ther. Targets. 11 (2007) 1473–1491. https://doi.org/10.1517/14728222.11.11.1473.

[260] Y. Shamay, M. Elkabets, H. Li, J. Shah, S. Brook, F. Wang, K. Adler, E. Baut, M. Scaltriti, P. V Jena, E.E. Gardner, J.T. Poirier, C.M. Rudin, J. Baselga, A. Haimovitz-Friedman, D.A. Heller, P-selectin is a nanotherapeutic delivery target in the tumor microenvironment, Sci. Transl. Med. (2016). https://doi.org/10.1126/scitranslmed.aaf7374.

[261] J. Grotta, J. Marler, Intravenous rt-PA: a tenth anniversary reflection, Surg. Neurol. 68 (2007) S1:12–S1:16. https://doi.org/10.1016/j.surneu.2007.07.079.

[262] A. Zenych, L. Fournier, C. Chauvierre, Nanomedicine progress in thrombolytic therapy, Biomaterials. 258 (2020) 120297. https://doi.org/10.1016/j.biomaterials.2020.120297.

[263] J. Szebeni, Complement activation-related pseudoallergy: A stress reaction in blood triggered by nanomedicines and biologicals, Mol. Immunol. 61 (2014) 163–173. https://doi.org/10.1016/j.molimm.2014.06.038.

[264] P.R. Lockman, J.M. Koziara, R.J. Mumper, D. Allen, Nanoparticle surface charges alter blood-brain barrier integrity and permeability, J. Drug Target. 12 (2004) 635–641. https://doi.org/10.1080/10611860400015936.

[265] G.R. Hendrickson, L.A. Lyon, Microgel Translocation Through Pores Under Confinement, Angew. Chemie - Int. Ed. 49 (2010) 2193–2197. https://doi.org/doi:10.1002/anie.200906606.

[266] S.K. Min, O.C. Kwon, S. Lee, K.H. Park, J.K. Kim, An antithrombotic fucoidan, unlike heparin, does not prolong bleeding time in a murine arterial thrombosis model: A comparative study of undaria pinnatifida sporophylls and fucus vesiculosus, Phyther. Res. 26 (2012) 752–757. https://doi.org/10.1002/ptr.3628.

[267] R.P. Friedrich, J. Zaloga, E. Schreiber, I.Y. Tóth, E. Tombácz, S. Lyer, C. Alexiou, Tissue Plasminogen Activator Binding to Superparamagnetic Iron Oxide Nanoparticle—Covalent Versus Adsorptive Approach, Nanoscale Res. Lett. 11 (2016) 1–11. https://doi.org/10.1186/s11671-016-1521-7.

[268] J.C. Antunes, L. Benarroch, F.C. Moraes, M. Juenet, M.S. Gross, M. Aubart, C. Boileau, G. Caligiuri, A. Nicoletti, V. Ollivier, F. Chaubet, D. Letourneur, C. Chauvierre, Core-Shell Polymer-Based Nanoparticles Deliver miR-155-5p to Endothelial Cells, Mol. Ther. - Nucleic Acids. 17 (2019) 210–222. https://doi.org/10.1016/j.omtn.2019.05.016.

[269] B. Ovbiagele, C.S. Kidwell, S. Starkman, J.L. Saver, Potential role of neuroprotective agents in the treatment of patients with acute ischemic stroke, Curr. Treat. Options

Neurol. 5 (2003) 367–375. https://doi.org/10.1007/s11940-003-0027-7.

[270] R. Goulay, M. Naveau, T. Gaberel, D. Vivien, J. Parcq, Optimized tPA: A non-neurotoxic fibrinolytic agent for the drainage of intracerebral hemorrhages, J. Cereb. Blood Flow Metab. 38 (2018) 1180–1189. https://doi.org/10.1177/0271678X17719180.

[271] L.M. Forero Ramirez, E. Gobin, R. Aid-Launais, C. Journe, F.C. Moraes, L. Picton, D. Le Cerf, D. Letourneur, C. Chauvierre, F. Chaubet, Gd(DOTA)-grafted submicronic polysaccharide-based particles functionalized with fucoidan as potential MR contrast agent able to target human activated platelets, Carbohydr. Polym. (2020) 116457. https://doi.org/https://doi.org/10.1016/j.carbpol.2020.116457.

[272] J.P.A. Ioannidis, B.Y.S. Kim, A. Trounson, How to design preclinical studies in nanomedicine and cell therapy to maximize the prospects of clinical translation, Nat. Biomed. Eng. 2 (2018) 797–809. https://doi.org/10.1038/s41551-018-0314-y.

# ANNEXES

ANNEX 1

Biomaterials 258 (2020) 120297

Contents lists available at ScienceDirect

Biomaterials

journal homepage: www.elsevier.com/locate/biomaterials

Review

# Nanomedicine progress in thrombolytic therapy

Alina Zenych, Louise Fournier, Cédric Chauvierre *

*Université de Paris, Université Sorbonne Paris Nord, UMRS1148, INSERM, F-75018, Paris, France*

ARTICLE INFO

*Keywords:*
Thrombolytics
Targeted thrombolysis
Thrombolytic therapy
Nanomedicine
Nanoparticles
Microbubbles

ABSTRACT

Thrombotic occlusions of blood vessels are responsible for life-threatening cardiovascular disorders such as myocardial infarction, ischemic stroke, and venous thromboembolism. Current thrombolytic therapy, the injection of Plasminogen Activators (PA), is yet limited by a narrow therapeutic window, rapid drug elimination, and risks of hemorrhagic complications. Nanomedicine-based vectorization of PA protects the drug from the enzymatic degradation, improves the therapeutic outcomes, and diminishes adverse effects in preclinical models. Herein, we review the pathophysiology of arterial and venous thrombosis and summarize clinically approved PA for the treatment of acute thrombotic diseases. We examine current challenges and perspectives in the recent key research on various (lipid, polymeric, inorganic, biological) targeted nanocarriers intended for the site-specific delivery of PA. Microbubbles and ultrasound-assisted sonothrombolysis that demonstrate thrombolysis enhancement in clinical trials are further discussed. Moreover, this review features strategies for the rational design of nanocarriers for targeted thrombolysis and effective PA encapsulation in view of interactions between nanomaterials and biological systems. Overall, nanomedicine represents a valued approach for the precise treatment of acute thrombotic pathologies.

## 1. Introduction

Cardiovascular diseases (CVD), the major global health threat, are associated with high morbidity and mortality that account for an estimated 17.9 million lives each year (31% of all deaths worldwide) [1], and this figure is expected to rise to >23.6 million annual deaths by 2030 [2]. CVD are a group of disorders of the heart (e.g., heart failure, rheumatic heart disease, abnormal heart rhythms, inflammatory heart diseases, cardiomyopathy) and blood vessels (coronary artery disease, cerebrovascular disease, aortic aneurysms, peripheral artery disease, etc.). CVD affect almost equally men as women, however, the disease develops about seven to ten years later in women as compared to men [3]. Furthermore, CVD are associated with substantial health-care costs, which are estimated at $329.7 billion annually in the United States [2] and nearly €200 billion in the European Union [4].

A large number of CVD may be prevented by addressing major risk factors through lifestyle interventions and pharmaceutical treatment where necessary [1]. Nevertheless, hypertension, the leading cardiovascular risk factor, is attributed to ~13% of global deaths (7.5 million deaths), followed by tobacco use 9%, diabetes 6%, physical inactivity 6%, obesity 5%, and high cholesterol level 4.5% [3].

Three major cardiovascular disorders – myocardial infarction (heart attack), ischemic stroke, and venous thromboembolism defined as deep vein thrombosis and/or pulmonary embolism – are severe complications of thrombosis, the formation of a blood clot in the vessels (Fig. 1). Within all deaths from CVD, 85% are caused by heart attacks and strokes, one-third of them in people under the age of 70 years [1]. To improve human survival and quality of life, early detections and effective treatments are principal.

Thrombolytic drugs are administered to dissolve a thrombus and restore the blood flow in acute thrombotic events, however, they are rapidly inactivated in the blood and trigger hemorrhagic complications, as we explain below. Paradoxically, while rapid reperfusion is the standard of care to minimize the infarct size, the restoration of blood flow itself may provoke irreversible tissue damage in a process called reperfusion injury [5]. Therefore, the pursuit of innovative solutions for the management of thrombotic diseases remains an open field of research, where nanomedicine is emerging to be a promising strategy to improve both the efficacy and safety of thrombolytic therapy.

This review delves into the preclinical research on nano- or microparticles of various composition for delivering fibrinolytic agents, reported during the last 10 years. Ultrasound (US)-responsive microbubbles with thrombolytics are highlighted as a potential theranostic system for both US visualization of the pathologic thrombi and

* Corresponding author.
*E-mail address:* cedric.chauvierre@inserm.fr (C. Chauvierre).

https://doi.org/10.1016/j.biomaterials.2020.120297
Received 22 January 2020; Received in revised form 10 July 2020; Accepted 1 August 2020
Available online 6 August 2020

their destruction by a combination of mechanical stress with increased penetration and drug potency.

The database searched included MEDLINE/PubMed and Science Direct for research articles published in English from 2010 to present, using the combinations of the keywords “nanomedicine”, “nanoparticles”, “microbubbles”, “liposomes”, “streptokinase”, “urokinase”, “tissue plasminogen activator”, “nanothrombolysis”, “thrombolytic therapy”, “drug delivery systems”, “thrombolysis”, “targeted thrombolysis”, etc.

### 1.1. Pathophysiology of arterial and venous thrombosis

Atherosclerosis is the key precursor of cardiovascular pathologies and it starts in adolescence. Atherosclerosis is a complex immune-inflammatory disorder whose progression involves multiple biological pathways that are influenced by genetic and environmental factors. Elevated plasma cholesterol level, hypertension, diabetes, tobacco smoking, male gender, and some inflammatory markers are among the proatherogenic risk factors of atherosclerosis, while physical exercise, a healthy diet, and high High-Density Lipoproteins (HDL) counts have an atheroprotective role [6].

Atherosclerotic lesions are initiated when the endothelium is activated by atherogenic and pro-inflammatory stimuli, such as primarily Vascular Cell Adhesion Molecule-1 (VCAM-1), intercellular adhesion molecule-1, E-selectin, and P-selectin [7]. It has been demonstrated a direct hemodynamic role in atherogenesis, notably by endothelial cells as their numerous signaling pathways are dependent on the hemodynamic patterns [8,9]. Low shear stress and turbulent flow at arterial curvature and branch points are major drivers of plaque development and instability. Plasma molecules and Low-Density Lipoproteins (LDL) penetrate dysfunctional endothelium into the subendothelial space where atherogenic lipoproteins are oxidized, mediated by myeloperoxidase, 15-lipoxygenase, and/or Nitric Oxide Synthase (NOS) [7]. Low-grade inflammation contributes to the disease progression due to the focal recruitment of circulating monocytes and T-lymphocytes [10]. Modulated by chemotactic cytokines, such as oxidized LDL and Monocyte Chemoattractant Protein-1 (MCP-1) [11], monocytes infiltrate arterial intima through transendothelial migration and differentiate into macrophages by internalizing the atherogenic lipoproteins via scavenger receptors. The incidence of the foam cells (lipid-laden macrophages) and their death by apoptosis and necrosis contribute to the formation of destabilizing atheromatous lipid-rich core within the plaque. Moreover, the foam cells express an array of inflammatory factors and produce proteolytic enzymes, such as Matrix MetalloProteinases (MMPs) [11], that are implicated in matrix degradation and plaque disruption [12]. To insulate the thrombogenic lipid-rich core of the atheroma from the bloodstream, the fibrous cap develops at the lesion site as a fibroproliferative response mediated by intimal smooth muscle cells. The recruitment of the smooth muscle cells and the production of the collagen-rich matrix are considered as beneficial since they protect

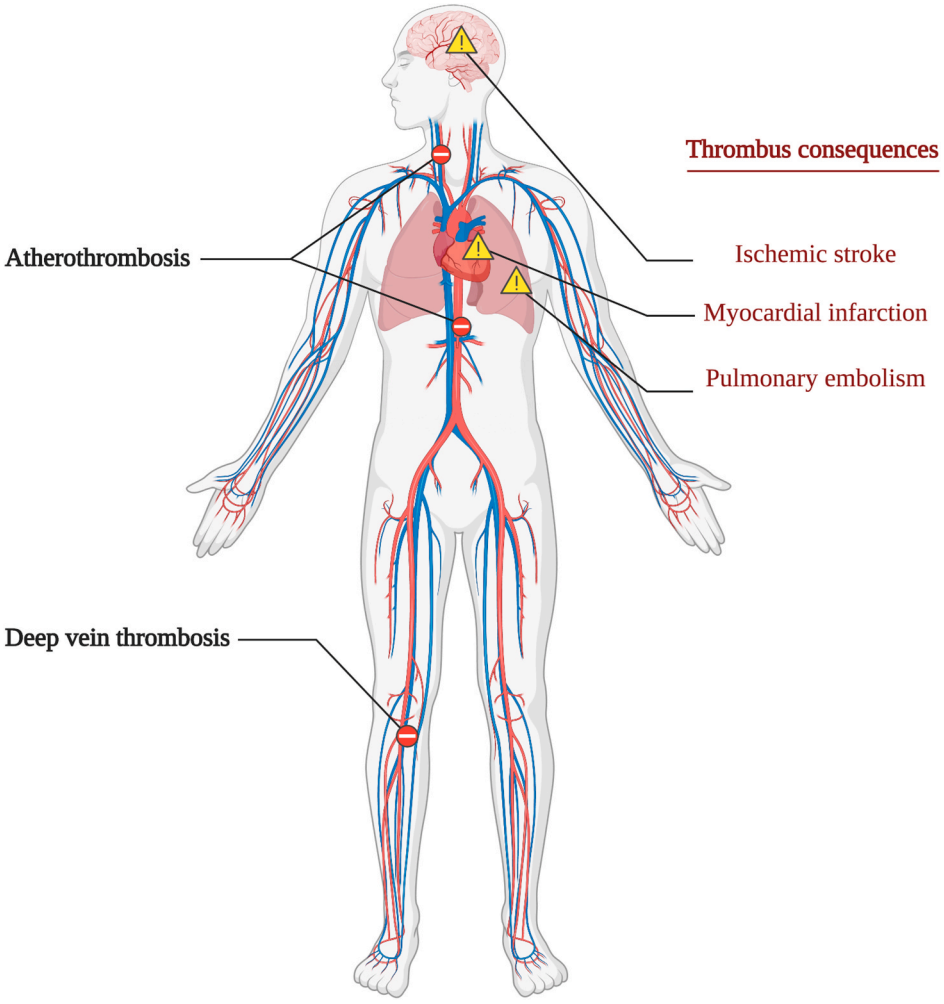


**Fig. 1.** Schematic of thrombotic diseases. Blot clot formation both in arteries (atherothrombosis) and veins (deep vein thrombosis) are influenced by congenital diseases and environmental factors. When the clot obstructs blood vessels in the brain, lungs, or heart, it may induce life-threatening consequences such as ischemic stroke, pulmonary embolism, or myocardial infarction.

the plaques against rupture and subsequent thrombosis. Conversely, the disintegration of foam cells and loss of smooth muscle cells may have detrimental consequences, leading to the formation of a destabilizing lipid-rich core and a fragile and rupture-prone fibrous cap. Atherosclerotic plaque calcification is an inflammation-driven process that manifests in all stages of the disease and should be defined as a two-phase process: microcalcification, the early stage of intimal calcium formation, and the end-stage of macrocalcification. While coronary Computed Tomography (CT)-detected macroscopic calcification in artery plaque acts as a biomarker of the overall disease progression, it is believed to stabilize the plaque and prevent acute events [13]. On the contrary, microcalcification, which can be identified by Positron Emission Tomography (PET)/CT imaging with $^{18}$F-sodium fluoride, is associated with plaque vulnerability and an increased risk of rupture, since it aggravates plaque inflammation and augments mechanical stress in the fibrous cap [14].

Injury of the fibrous cap of atherosclerotic plaque is a primary trigger for arterial thrombosis, promoting hemorrhage and luminal prothrombotic response [15]. For initial flow obstruction, the blood coagulation cascade activates the platelets that are rapidly recruited to the site and aggregate, resulting in rapid thrombus growth [16] (Fig. 2A). Fibrin network then develops for the stabilization of platelet-rich thrombosis. Although most episodes of the ruptured fibrous cap occur silently without clinical symptoms, plague rupture with subsequent thrombosis often culminates in devastating clinical events such as myocardial infarction (MI) or ischemic stroke [15].

Contrary to atherothrombosis, the pathogenesis of Venous Thrombosis (VT) is only partially understood. The main components of the venous thrombi are fibrin and erythrocytes, and less activated platelets [17] (Fig. 2B). VT is initiated at the venous valves where stasis may occur under low shear blood flow [18]. Valvular sinus stasis aggravates hypoxia, promoting activation of the endothelium and leukocytes via mainly Hypoxia-Inducible Factor-1 (HIF-1) and Early Growth Response 1 (EGR-1) pathways. Besides, hypoxia condition modulates hypercoagulability. HIF-1 and EGR-1 pathways up-regulate the expression of P-selectin on endothelium, prompting monocytes to release microvesicles bearing tissue factor, which initiates thrombin production and fibrin deposition around the intact endothelial wall [19]. Both inherited and environmental factors raise the likelihood of the occurrence of venous thrombotic diseases, such as an imbalance of pro-vs. anti--coagulation proteins, as well as cancer, obesity, and major surgery [16].

### 1.2. Clinical treatment of acute thrombotic diseases

For the treatment of acute arterial or venous thrombotic events, fibrinolytic drugs can be administered in order to proteolytically disrupt blood clots and restore blood flow. Fibrinolytic, or thrombolytic, agents are Plasminogen Activators (PA) that activate the proenzyme

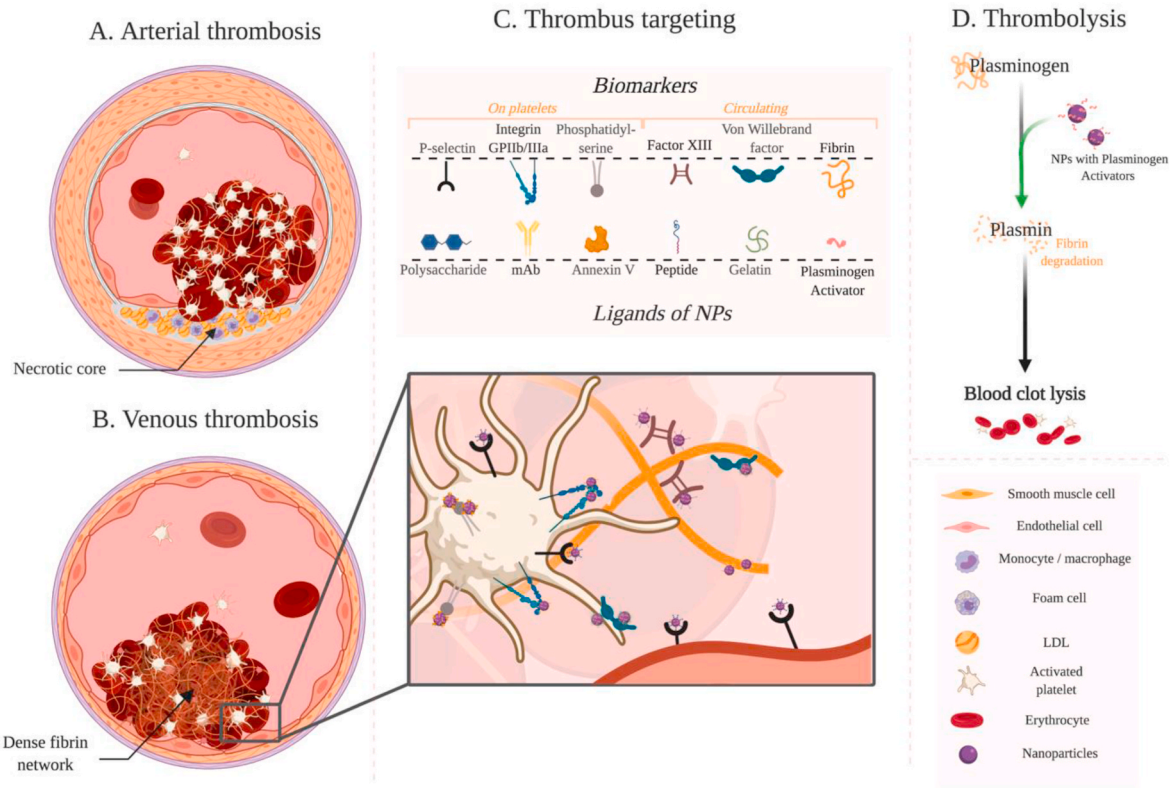


**Fig. 2.** Comparison of the arterial (A) and venous (B) thrombosis. Arterial clots (A) are composed of a high platelet ratio and are so-called "white thrombi". They are mostly the result of atherosclerosis. Multiple cellular pathways that initiate the activation of the endothelial cells are involved in thrombus formation. LDL penetrate the tissue, causing local inflammation and recruitment of circulating inflammatory cells. The disruption of the atherosclerotic plaque triggers the recruitment of smooth muscle cells to prevent wall rupture. Eventually, platelets aggregate on the impaired vessel wall with a consecutive formation of a fibrin network. On the other hand, venous clots (B), "red thrombi", contain erythrocytes and a denser fibrin network with fewer platelets. The thrombus formation is responsive to the following triggers: a vessel wall injury, a stasis of the blood flow, and hypercoagulability of the blood. C. Thrombus targeting with functionalized nano-/microparticles. Thrombi express a variety of cellular and molecular components – the surface of activated platelets (P-selectin, integrin GPIIb/IIIa, phosphatidylserine) or circulating proteins (Factor XIII, vWF, or fibrin) – that can be employed for specific targeting. NPs are designed with different ligands to these biomarkers: polysaccharide fucoidan, peptides, monoclonal antibodies, etc. D. Thrombolysis with PA-bearing and targeted to the thrombi NPs. The PA convert plasminogen into plasmin that breaks down the fibrin network and releases the components of the blood clot. Abbreviations: *LDL*, low-density lipoproteins; *vWF*, von Willebrand factor; *mAb*, monoclonal antibodies; *NPs*, nanoparticles; *PA*, plasminogen activators. (For interpretation of the references to color in this figure legend, the reader is referred to the Web version of this article.)

plasminogen to plasmin that then cleaves fibrin network into soluble degradation products. This activation of the fibrinolytic system destabilizes the structure of a thrombus [20]. Thrombolytic therapy is thereby used in patients with such pathologies as acute MI, acute ischemic stroke, peripheral arterial disease, deep vein thrombosis, and massive pulmonary embolism [21].

U.S. Food and Drug Administration (FDA)-approved "clot busters" drugs for use in thrombotic diseases are recombinant-based PA (e.g., alteplase – rtPA, reteplase – rPA, and tenecteplase – TNK), streptokinase (SK), and urokinase (uPA). The main differences between them relate to their antigenicity, half-life, lytic potential, fibrin specificity, and hemorrhagic risks [22]. First-generation thrombolytic drugs (urokinase, streptokinase) are non-fibrin specific when second and third-generation (alteplase and its variants) overcome this issue. Generally, human protein-derived PA (urokinase, alteplase, reteplase, tenecteplase) are nonantigenic, contrary to those derived from a bacterial species (streptokinase) [23]. The half-life of each PA determines their mode of administration (a bolus injection, short infusion, or continuous intravenous infusion). A comparison of different FDA-approved PA with their clinical indications is summarized in Table 1.

The leading drawbacks of fibrinolytic therapy include treatment failures such as ineffectiveness, re-thrombosis as a result of a persistent vascular lesion and plasma hypercoagulability, and a high risk of bleeding complications, with intracerebral hemorrhages occurring in 1–7% of treated patients [21]. Moreover, PA are physiologically inhibited by Plasminogen Activator Inhibitors (PAI) such as PAI-1 and PAI-2 while alpha 2-antiplasmin and alpha 2-macroglobulin inactivate plasmin, thereby reducing the treatment efficacy [24]. In view of these limitations, the constant development of novel molecules aims to address the problems associated with available thrombolytics. The novel candidates that are mutants of available PA or might be produced from the microbial, plant, and animal origin are discussed in the review [25].

The association of thrombolytic drugs with endovascular methods significantly improved interventional management of acute thrombotic events. The percutaneous coronary intervention has become more common for reperfusion, improving survival rates in patients with MI [26,27]. When available, this catheter-based procedure that is performed by an interventional cardiologist has to be offered promptly after/or in place of initial thrombolytic therapy. Since 2015, mechanical thrombectomy (MT) using a stent retriever is recommended as a complementary treatment to fibrinolytic therapy for ischemic stroke related to large vessel occlusions in the anterior circulation such as in the internal carotid artery and proximal middle cerebral artery [28,29] after multiple positive randomized control trials [30,31]. Yet, since MT needs to be performed by a qualified neurointerventionist at comprehensive stroke centers, access to them often remains difficult. In France, in particular, out of 135 nationwide neurovascular centers, only 40 are capable of performing thrombectomy to date [32]. Therefore, there is still a dire need for a safe and non-invasive solution.

With the advent of the field of nanotechnology, there has been considerable interest in integrating nanomedicine and thrombolytic therapy for the treatment of acute thrombotic events. Nanomedical approaches for targeted fibrinolysis could advance clinical outcomes by improving current pharmaceutical methods when interventional catheter-based strategies are not available or not recommended (as, for example, in ischemic stroke due to occlusions in smaller vessels or posterior circulation). By acting locally at the thrombus site, there is a promise that nanomedicine-delivered "clot-busting" agents deliver superior recanalization rates and attenuate life-threatening bleeding complications associated with their intravenous administration. One may also expect the chance to replace intravenous infusion by bolus injection of the first- and second-generation PA due to the extended drug half-life. In the ideal treatment settings, the synergic combination of endovascular and nanotherapeutic methods would represent a more precise approach to manage thrombotic pathologies.

## 2. Nanomedicine for targeted drug delivery

Nanomedicine, a medical application of nanotechnology, combines a powerful set of nano-engineered devices for diagnostic and/or therapeutic applications. Nanoparticle (NP)-based drug delivery can increase drug circulation time, improve therapeutic efficacy, and reduce unwanted off-target effects by delivering an active molecule to the injury site [33]. The liposomal formulation of doxorubicin – Doxil® – was the first clinically approved nanomedicine therapy by the FDA in 1995 for the Kaposi's sarcoma and other cancers that reduced cardiotoxicity compared with a conventional formulation [34]. Other NP formulations are approved for the treatment of distinct pathologies, such as cancers, fungal infections, iron-deficient anemia, macular degeneration, as well as vaccines for hepatitis A and influenza [35,36].

Different nano- or microcarriers (e.g., liposomes, polymeric, magnetic nano- & microparticles, quantum dots, nanotubes, dendrimers) are similarly researched in the therapeutic area of CVD [37]. Nanotechnology plays a role for wide-ranging cardiovascular applications, such as hypertension [38], atherosclerosis [39], prevention of restenosis following interventional cardiology [40], ablation for atrial fibrillation [41], cardiac tissue engineering [42], but also in the management of aneurysms [43] as well as CVD prevention [44].

**Table 1**
Thrombolytic agents approved by the FDA.

| Agent | Abbreviation | Source | Safety [immunogenicity, fibrin specificity] | Half-life, min | Regimen | Total Dose | Metabolism | Indication |
|---|---|---|---|---|---|---|---|---|
| *First-generation* | | | | | | | | |
| Streptokinase | SK | β-hemolytic streptococcus | Immunogenic<br>Non-fibrin specific | 20 | Infusion | $1.5 \times 10^6$ IU | Renal | PE<br>Acute MI<br>PAO, DVT |
| Urokinase | uPA | Human urine & kidney cell culture | Non-fibrin specific | 15 | Infusion | $2.25–6.25 \times 10^6$ IU | Renal | PE<br>Acute MI<br>PAO, DVT |
| *Second-generation* | | | | | | | | |
| Alteplase | rtPA | Recombinant DNA technology | Fibrin specific (++) | 4–8 | Infusion | MI: 50–100 mg<br>IS: 0.9 mg/kg<br>PE: 100 mg | Hepatic | Acute MI<br>Acute IS<br>PE |
| *Third-generation* | | | | | | | | |
| Reteplase | rPA | Recombinant DNA technology | Fibrin specific (+) | 14–18 | Double bolus | 20 IU | Renal | Acute MI<br>PAO |
| Tenecteplase | TNK | | Fibrin specific (+++) | 11–20 | Bolus | 30–50 mg | Renal | Acute MI |

Abbreviations: *DVT*, Deep Vein Thrombosis; *MI*, Myocardial Infarction, *PAO*, Peripheral Arterial Occlusion; *PE*, Pulmonary Embolism; *IS*, Ischemic Stroke; *IU*, International Units.

### 2.1. Evolution and milestones in the progress of nanomedicine for fibrinolytic therapy

The field of nanomedicine in fibrinolytic therapy is evolving vibrantly, as evidenced by the expanding list of preclinical concepts of nanomaterial complexation with PA. An ideal vehicle for thrombolytic drug delivery should be biocompatible, non-toxic, non-immunogenic, biodegradable, and should avoid rapid clearance by the immune system [45]. The benefits of utilization of the nanoparticles (NPs) are attributed to their high surface-volume ratio, multifunctionality, high bioavailability, and possible control of therapeutic agent release. Control drug release facilitates the release of the payload from the NPs at the thrombus site upon internal or external stimuli such as temperature [46,47], pH [48], US [49], or magnetic field [46], etc. Specific thrombus targeting can be achieved by modifying the surface of nanocarriers with targeting moieties (antibodies, aptamers, polysaccharides, peptides, and small molecules) and/or application of magnetic energy, enhancing the therapeutic effect due to accumulation of thrombolytic drug at the clot surface [50] (Fig. 2C and D). Furthermore, encapsulation of the fibrinolytic drug onto the NPs can protect it from inactivation by PAI-1 in the bloodstream [51] and prolong its blood circulation time [48,52,53], thus achieving safe and effective thrombolysis at a lower dose [54,55]. Nanocarrier protection may further limit drug leakage during circulation, reducing the risk of hemorrhagic complications [56,57] such as cerebral hemorrhages that often accompany the injection of free plasminogen activators.

The timeline shown in Fig. 3 depicts evolution and milestones in the conceptual advances of nanomedicine-facilitated thrombolysis.

The story begins in the late '80s when dextran-coated iron oxide microparticles loaded with SK were utilized for magnetically driven thrombolysis of the carotid arteries in dogs [58]. Around the same time, SK-bearing liposomes entered the field by accelerating reperfusion in acute MI [59]. The first reported microbubbles for sonothrombolysis in 1996 were initially composed of denatured albumin shells, however, this formulation is no longer used due to stability/immunogenicity issues [60]. Polymeric platforms in thrombolytic therapy started to emerge a decade later in order to improve a stability profile of the liposomes in biological fluids. In 2004, first-reported polymer microparticles were designed from Polyethylene Glycol (PEG) and loaded with SK to tackle coronary thrombosis in a canine model [61]. The early success of the rtPA-conjugated erythrocytes in thromboprophylaxis in 2003 led to the further investigation and development of diverse bio-inspired nano solutions [62]. These initial studies evidenced an undoubtable potential of nanomedicine to boost thrombolytic therapy in animal models, however, they often lacked a complete analysis in terms of particle physico-chemistry and safety, drug loading efficiency/release, targeting and thrombolytic efficacy in appropriate *in vitro* and subsequently *in vivo* models, which is currently recognized and adopted [63]. The evolution of nanomedicine-based fibrinolysis continued with the development of surface-coated, mostly nanosized particles that exhibit considerably longer circulation half-life *in vivo* and superior safety profiles than uncoated microparticles. Notable examples from late 00′ are the PA-bearing polymer NPs that were coated with chitosan and cRGD peptide, a prototype of the utilization of a popular targeting ligand of GPIIb/IIIa [64], as well as magnetic NPs coated with dextran [65] and polyacrylic acid [66] for magnetically guided thrombolysis.

The last decade, which we review in this paper, was fruitful for progress in nanomedicine-assisted thrombolysis. During these years, researchers commonly used active targeting strategies. Apart from magnetic targeting of iron oxide NPs, the utilization of monoclonal antibodies (mAb) and peptides that recognize biomarkers associated with thrombotic pathologies have allowed the development of more selective nanosystems that advanced into the multivalent design in 2017 [57]. In 2018, polymeric NPs were functionalized with fucoidan, affordable high-quality P-selectin ligand for site-specific fibrinolytic activity [67] as an alternative to costly mAb and peptides. From 2012, theranostic hybrid approaches emerge: inorganic nanocarriers that serve for thrombolysis and optical imaging [68] or MRI [69]. Echogenic liposomes are widely studied with the *in vitro* clot model for sonothrombolysis due to tunable designs like targeting and/or rtPA loading [70]. Recently, targeting nanobubbles were published that complemented PA with sonothrombolysis, as they penetrate deeper into the clots comparing to microbubbles [71]. The nanoformulations with controlled release start appearing more frequently: via hemodynamic phenomena – increased shear stress in the stenotic arteries [72] and

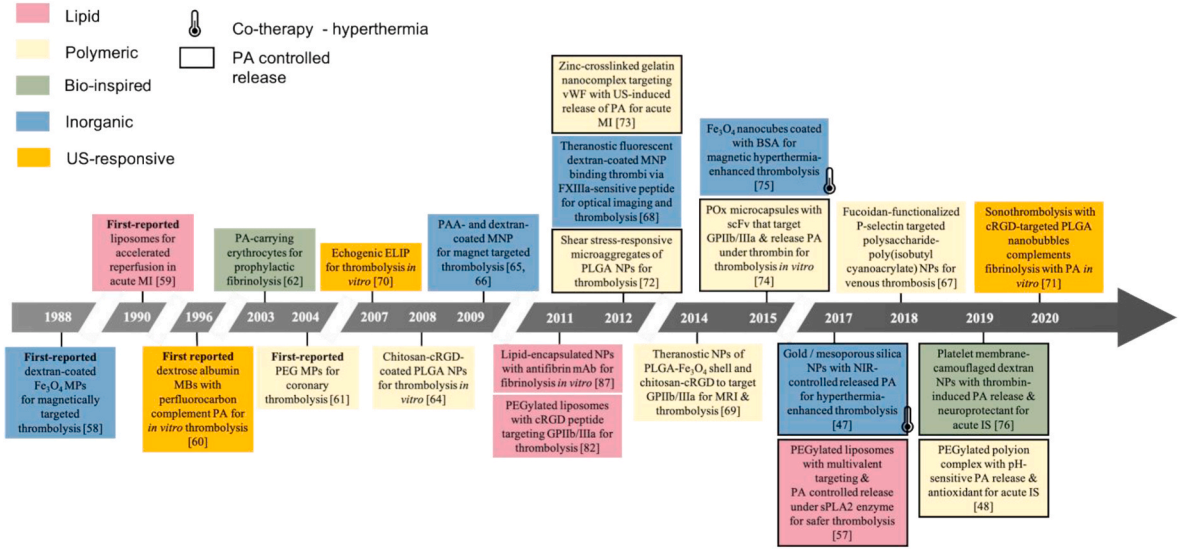


**Fig. 3.** The timeline of evolution and milestones in the progress of nanomedicine for fibrinolytic therapy: history and current trends. This figure mostly comprises the PA-loaded platforms tested with *in vivo* experiments; however, we also included several remarkable *in vitro* concepts. Abbreviations: *PA*, plasminogen activator; *MI*, myocardial infarction; *IS*, ischemic stroke; *PEG*, polyethylene glycol; *PLGA*, poly(lactic-co-glycolic acid); *PAA*, poly (acrylic acid); *BSA*, bovine serum albumin; *POx*, poly(2-oxazoline); *vWF*, von Willebrand Factor; *FXIIIa*, activated factor XIII; *$sPLA_2$*, secreted phospholipase A2 enzyme; *MNP*, magnetic nanoparticles; *MPs*, microparticles; *NPs*, nanoparticles; *MBs*, microbubbles; *ELIP*, echogenic liposomes; *mAb*, monoclonal antibodies; *scFv*, single-chain antibody; *MRI*, magnetic resonance imaging; *US*, ultrasound; *NIR*, near-infrared.

US-induced [73] in 2012, upon enzyme exposure since 2015 [74], elevated temperature since 2017 [47], and low pH in 2019 [48]. To enhance thrombolysis, adjuvant therapy in the form of local hyperthermia by a magnetic field [75] or near-infrared (NIR) light [47] was used in the late 10's.

Nowadays, the trend is to create complex multifunctional but, at the same time, biocompatible and biodegradable nanocarriers. Application of novel biomaterials, hybrid NPs with biomimetic surfaces, incorporating active targeting molecules, and the ability to modulate the release spatially and temporally is being widely researched. The researchers also commenced investigating the solution to complement nanomedicine-based fibrinolysis by counteracting the pathological processes related to ischemia with an antioxidant [48] and neuroprotection [76] approach for ischemic stroke in 2019.

In the next chapters, we are going to describe in detail the complexation of PA with different types of nanocarriers, which are summarized in Fig. 4, and their corresponding therapeutic effects in preclinical studies.

## 3. Lipid drug delivery

### 3.1. Liposomal drug delivery

Liposomes, first described in the mid-'60s, are defined as spherical vehicles made of an aqueous core surrounded by phospholipid bilayers. Since then, because of their excellent biocompatibility, low toxicity, and easy preparation methods, liposomes are considered as one of the most promising tools for drug delivery in medical fields of principally small molecules (e.g., chemotherapeutics) with some being clinically approved [77], but also proteins, DNA, RNA, and imaging probes [78].

Liposomes are generally fabricated by thin-film hydration, which consists of dissolving lipid components in an organic solvent, drying down by rotary evaporation, and rehydrating in water, as well as by freeze-drying, reverse-phase evaporation, or injection of ethanol with phospholipids into an aqueous phase. Membrane extrusion, sonication, and/or freeze-thawing are further employed to modulate the particle size [79]. In terms of the size and number of bilayers, different types of liposomes can be produced, such as small unilamellar vesicles (single phospholipid bilayer sphere), large unilamellar vesicles, and multilamellar vesicles (an onion structure of bilayers) [78]. The amphiphilic properties of liposomes allow them to internalize both hydrophilic and hydrophobic compounds.

Liposomal encapsulation of plasminogen activators for thrombus-specific drug delivery is frequently exploited to improve the drug half-life and reduce hemorrhagic side effects. Given that the conventional liposomes aggregate *in vivo* and undergo rapid systemic clearance via Mononuclear Phagocyte System (MPS) after contact with plasma proteins, decoration with FDA-approved PEG has been adopted to provide steric stabilization and reduce liposomal opsonization, and, therefore, to improve the pharmacokinetics of PA in blood [79].

The liposomal surface modification strategies by site-directed target ligands, such as antibodies, peptides, or stimuli-responsive drug release (thermo- or pH-sensitive liposomes) have been tested in the preclinical development. Most targeting approaches are directed towards Glyco-Protein IIb/IIIa (GPIIb/IIIa). GPIIb/IIIa is an integrin complex on the platelet membrane that mediates platelet adhesion and aggregation during hemostasis. Normally present in its inactive state on resting platelets, it undergoes conformational changes to allow the platelets to bind to fibrin upon platelet stimulation by physiologic ligands such as thrombin or collagen [80]. Thrombolytics are generally incorporated into the inner aqueous core of the liposomes during the synthesis process, however, they can also be adsorbed onto the surface or covalently grafted to the PEGylated liposomes [81].

In the study of Vaidya et al., long circulatory PEGylated liposomes were coupled with a cyclic Arg-Gly-Asp (cRGD) [CNPRGDY(OEt)RC] and targeted GPIIb/IIIa receptor both *in vitro* and *in vivo* [82]. Despite a low level of streptokinase release (12.20 ± 0.94%) over the course of 35 h, the study reported the improved thrombolysis rate of cRGD-targeting liposomal SK compared with free SK after 1 h in rats (34% vs. 22%). When rtPA was loaded onto both non-PEGylated and PEGylated GPIIb/IIIa-targeting liposomes, a favorable rtPA release profile from PEGylated ones was demonstrated in the work [52], with a substantial

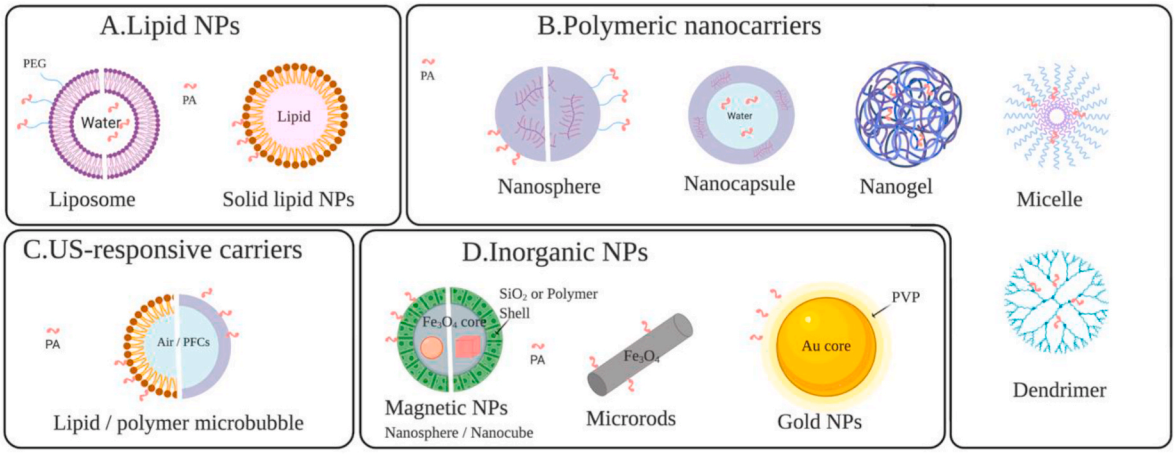


**Fig. 4.** Nanomedicine-based platforms with Plasminogen Activators. A. Lipid nanocarriers. In liposomes, PA may be embodied into the aqueous core or adsorbed/covalently conjugated onto the PEGylated phospholipid shell. In solid lipid NPs, PA is covalently grafted to their surface. B. Polymer-based nanoplatforms. PA are typically entrapped inside amphiphilic micelles and self-assembled gelatin or chitosan nanogels due to electrostatic interactions, incorporated into the aqueous core of nanocapsules, or covalently attached to the surface of the nanospheres and dendrimers via EDC/NHS chemistry. Surface decoration with PEGylation or polysaccharides is common for better stealth effects, particularly significant for the NPs from hydrophobic synthetic polymers. C. Ultrasound-responsive carriers. Microbubbles are microspheres filled with gas (e.g., $C_4F_{10}$, $N_2$, $C_4F_8$) or air, mostly coated with phospholipids or polymers that bind PA onto the outer layer via covalent interactions. Upon exposure to low-frequency ultrasound, microbubbles can burst to realize sonothrombolysis. D. Inorganic nanoparticles. In magnetic NPs, inner core – in the shape of nanospheres or nanocubes – is mostly iron oxide ($Fe_3O_4$), and the surface is decorated with organic (e.g., dextran, chitosan, polyacrylic acid) or inorganic ($SiO_2$) shell. PA is conjugated to the surface via EDC/NHS or simple adsorption. Uncoated iron oxide microrods may load PA via glutaraldehyde. Gold NPs immobilized PA via bio-affinity ligation. Abbreviations: *PEG*, Polyethylene glycol; *PA*, plasminogen activator; *NPs*, nanoparticles; *US*, ultrasound; *PVP*, polyvinyl pyrrolidone; *PFCs*, perfluorocarbons. (For interpretation of the references to color in this figure legend, the reader is referred to the Web version of this article.)

amount of drug released within 30 min after administration followed by a slow continuous release over 24 h. This strategy intends to achieve reperfusion and prevent re-thrombosis. The half-life of rtPA in plasma was prolonged from 7 min for native rtPA to 103 and 141 min for non-PEGylated and PEGylated liposomes. Besides, rtPA-loaded liposomes were 35% more potent than native rtPA for vessel recanalization but produced a 4.3-fold less depletion of circulating fibrinogen, potentially reducing hemorrhagic risks, in $FeCl_3$-rat venous thrombosis model.

Huang et al. exploited the targeted delivery and controlled release of rtPA incorporated into PEGylated liposomes coated with cRGD peptide [83]. Membrane fusion attributed to interactions between cRGD peptides on liposomes and GPIIb/IIIa integrins on activated platelets caused liposomal membrane destabilization and rtPA release. Due to this, over 90% of the entrapped rtPA was released within 1 h in targeted liposomes compared to <10% after 6 h in untargeted ones, and this release profile could be adjusted by altering the concentration of activated platelets. Zhang et al. [56] combined the active thrombus targeting with cRGD and gradual release of the drug from the liposomes without burst effect over 5 h. They improved the *in vivo* thrombolytic efficacy by ~4-fold over free uPA, at the same time shortening bleeding time of the tail bleeding assay of hemostasis, thereby potentially reducing the side effects of uPA.

In the elegant study [57], Pawlowski et al. took inspiration from platelet-derived microparticles that are plasma membrane vehicles shed from platelets that are undergoing activation, stress, or apoptosis (Fig. 5A) [84]. They designed a liposomal system with a multivalent targeting strategy towards both GPIIb/IIIa and P-selectin on activated platelets using the peptides CGSSSG*RGD*SPA and CDA*EWVDV*S, respectively (Fig. 5B and C). As the constructs could be degraded under secreted phospholipase A2 ($sPLA_2$) enzyme, secreted from leukocytes and active platelets in the thrombus, it could so release encapsulated SK (Fig. 5D and E). While thrombolytic efficacy of the targeted liposomes was comparable to free SK in $FeCl_3$-induced carotid artery thrombosis model, hemostatic capability for liposome-encapsulated SK was improved as measured by mouse tail bleeding time.

Hsu et al. [85] synthesized a hybrid NP-system, PEGylated thermosensitive magnetic liposomes (TMLs), encapsulating $Fe_3O_4$ NPs within liposomes, via solvent evaporation/sonication and freeze-thaw method.

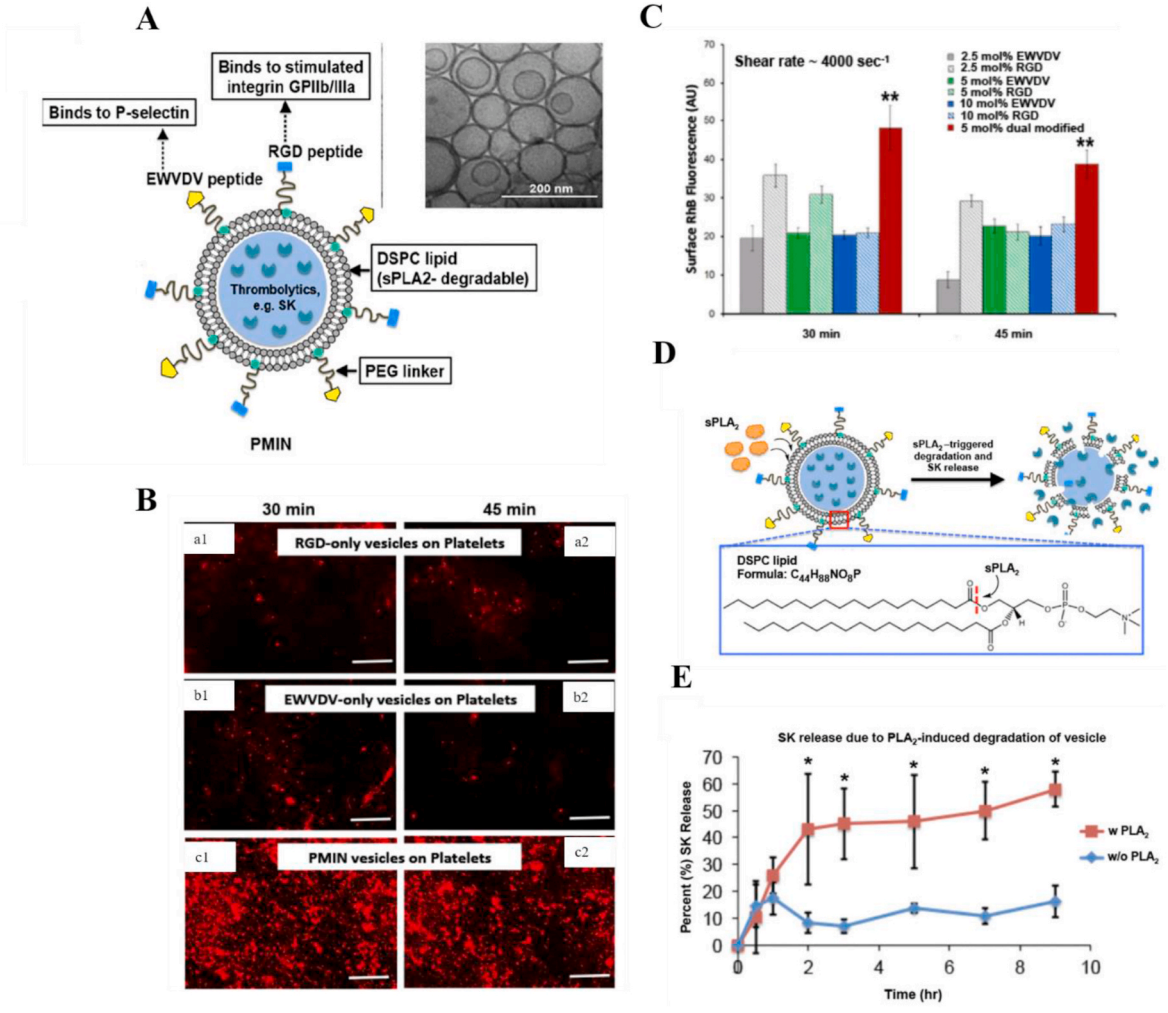


**Fig. 5.** A. Schematic representation of platelet-derived microparticles-inspired nanovesicle (PMIN) with dual-targeting strategy and controlled release of the thrombolytic upon sPLA2 enzyme exposure, with a representative cryo-TEM image of PMINs. B. Representative fluorescent images of particle binding show that RGD-decorated vesicles (a1, a2) and EWVDV-decorated vesicles (b1, b2) have a reasonable extent of binding and retention on the platelet-rich thrombus surface. However, the level of binding and retention levels are enhanced for dual modified PMINs (c1, c2). C. Quantitative analysis of fluorescence intensity shows that PMINs have significantly higher binding and retention capabilities compared to singly modified vesicles even when the mol% composition of single peptide modification is to twice (10 mol%) that of dual peptide modification (5 mol%) at high shear rate flow conditions. D. Schematic mechanism of sPLA2-induced membrane degradation due to cleavage of sn-2 acyl group of the phosphatidylcholine lipids. E. Release kinetics assessment of SK from PMINs shows that upon sPLA2 exposure, the percent (%) release of SK from PMINs is enhanced (~4 fold) compared to passive release without sPLA2 exposure. Adapted with permission from Ref. [57]. Copyright 2017 Elsevier Ltd.

Thrombolytic activity *in vitro* of rtPA-loaded TMLs at 43 °C was augmented as compared to at 37 °C due to enhanced drug release and higher enzyme activity at higher temperature. In addition to magnetic targeting, TMLs demonstrated a first-ever reported dual control mechanism of the drug release in serum: temperature- and magnet-sensitive, increasing at 43 °C and retarding with external magnetic force at 0.5 T in the follow-up work [46]. This technique could allow the liposomes to be magnetically guided toward the thrombus, preventing premature drug release. With appropriate biocompatibility of the nanocarriers, TML@rtPA restored arterial blood flow, iliac blood flow, and hind-limb perfusion, whereas the same dose of rtPA exerted no benefit in rat embolic model at 0.2 rtPA mg/kg under magnetic force at 43 °C.

### 3.2. Solid lipid nanoparticles

Solid Lipid Nanoparticles (SLNs) is an alternative drug delivery system. Contrary to conventional liposomes, which contain a lipid bilayer with an aqueous core, SLNs consist of lipid monolayer enclosing a solid lipid core stabilized by a surfactant, reaching a higher drug entrapment rate for a hydrophobic drug. Different preparation methods of SLNs include hot or cold homogenization, solvent emulsification/diffusion, or microemulsion [86]. Marsh et al. [87] prepared perfluorooctylbromide lipid-encapsulated NPs that can be assimilated to SLNs with a size 250 nm by emulsification/sonication method. Anti-fibrin mAb on the surface of the SLNs specifically targeted fibrin network in a canine model of the electrode-induced arterial thrombosis. Sulfhydryl functionalized uPA was covalently coupled to these SLNs and retained its fibrinolytic activity *in vitro*.

Overall, cRGD peptide-decorated PEGylated liposomes became a standard engineering approach in thrombolytic research owing to their cyto- and hemocompatibility [56] with a high potential for clinical translation, which might, in contrast, take longer for complex hybrid systems.

## 4. Polymeric drug delivery

Depending on the preparation method, polymeric NPs can have nanosphere or nanocapsule structures. Both naturally occurring hydrophilic polymers and synthetic biocompatible polymers are used in the NP fabrication and offer simple surface modification and functionalization [88]. Natural polymers such as polysaccharides (hyaluronan, alginate, and chitosan) and proteins (gelatin and albumin) are common [89]. Synthetic polymers come either in prepolymerized forms, such as polyesters like polycaprolactone (PCL), polylactic acid (PLA), or polymerized from the monomers, e.g., poly (methyl methacrylate), poly (alkyl cyanoacrylate) (PACA), poly (acrylic acid) (PAA), poly(lactic--*co*-glycolic acid) (PLGA), poly(2-oxazoline) (POx), and poly(amidoamine) (PAMAM). Synthetic polymers benefit from high purity and reproducibility over natural polymers; the latter, however, represent a significant interest due to their safety, abundance in nature, and low cost. Polymeric nanoparticles are conventionally fabricated by two methods: the dispersion of preformed polymers or the polymerization of monomers [90]. The plasminogen activators are typically dissolved and entrapped, or covalently attached to the surface of the NPs prepared from some of the above-mentioned polymers.

*Chitosan* (Cs), as well as its chemical derivatives, has been widely used because of its biocompatibility and biodegradability, low toxicity, and low immunogenicity in thrombolytic drug delivery. Chitosan is a cationic hydrophilic polysaccharide, derived from chitins, able to form polyelectrolyte complexes with negatively charged molecules [91].

Self-assembled chitosan NPs were produced via the ionic crosslinking with sodium tripolyphosphate, possessing a size 236 nm, and further loaded with uPA with encapsulation efficiency ~95% [92]. Both intravenous injection and catheter-driven drug delivery were tested in a thrombin-induced rabbit venous thrombosis, pointing out superior thrombolytic efficacy for the latter comparing with free uPA. Another group [93] elaborated a chitosan-based NPs/SK drug complexation via non-covalent interactions. Synthesis conditions such as pH and Cs concentration were optimized using a computational model. The team of Shamsi et al. reported the synthesis of uniform and spherical SK-entrapped chitosan NPs with a diameter 67 ± 13 nm and a narrow polydispersity by microfluidics [94]. A steady and sustained SK release was achieved during 48 h *in vitro* in addition to higher SK amidolytic activity in plasma in rats, comparing with free SK. Given that quaternized derivative of chitosan - N,N,N-Trimethyl Chitosan (TMC) has superior solubility and increased charge density, Liao et al. covalently grafted TMC with cRGD to target GPIIb/IIIa receptors [95]. The resulted cRGD-LK-NPs were formed with lumbrokinase (LK) via ionic gelation using sodium tripolyphosphate and could effectively accelerate thrombolysis in clot-occluded tubes and $FeCl_3$ rat carotid artery model at 90, 000 U/kg of LK.

Jin et al. prepared PEG crosslinked glycol chitosan hollow nanogels by an ultrasonic spray technique and loaded uPA with 80% loading efficiency. Such NP design improved uPA half-life in rats from 18 min to 40 min without causing biotoxicity. The application of diagnostic US at 2 MHz accelerated uPA release from the nanogels (90% of uPA released within 1 h vs. 80% within 6 h without the US) [53]. While the hollow cavity of the nanogels did not contain gas, they were responsive to the US due to the vibration of the polymer shell. The ultrasonic stimulation enhanced the thrombolysis *in vitro* for both free uPA and the uPA-loaded nanogels [53]. Notably, the nanogels allowed the delivery of uPA with no signs of a stroke or blood-brain barrier permeability damage after 24 h *in vivo* [96].

*Gelatin*, a protein obtained from the collagen hydrolysis, is an attractive natural macromolecule for a thrombolytic nanocarrier owing to its biocompatibility and biodegradability, and wide availability at low cost [97]. Gelatin-based NPs require crosslinking with glutaraldehyde or another bifunctional cross-linker during preparation, and their surface can be tuned with site-specific ligands, cationized with amine derivatives, or PEGylated.

Polyelectrolyte complex of cationized gelatin and anionic PEGylated gelatin with rtPA mutant (monteplase) fabricated a 200 nm thrombolytic delivery system [98]. While fibrinolytic activity *in vitro* was suppressed to 45% due to nanocomplexation, it was fully recovered under US stimulation (1 MHz, intensity 0.75 W/cm$^2$), demonstrating an ultrasound-responsive rtPA release. US control drug release can be explained by the production of the stable cavitation state and shear stress on the surrounding tissues [49]. In a rabbit thrombosis model, a combination of the US with rtPA-NPs allowed full vessel recanalization for all treated animals after 30 min, which was superior to free rtPA (10% recanalization after 60 min) and free rtPA + US (90% recanalization after 30 min).

Uesugi et al. further developed a zinc-crosslinked gelatin complex with monteplase [73], which restored its rtPA fibrinolytic activity upon US exposure *in vitro* [73] and *in vivo* to the level of free rtPA [54]. Monteplase-loaded NPs increased thrombus affinity 3-fold as a result of interactions of the gelatin with von Willebrand Factor (vWF), a blood glycoprotein that is a crucial component of platelet-rich thrombi. In a swine model of acute myocardial infarction, treatment with rtPA alone dissolved only 30% of occluded coronary thrombi at a dose of 55,000 IU/kg and no thrombi at 27,500 IU/kg within 60 min, while NPs carrying 55,000 IU/kg rtPA achieved recanalization of 90% thrombi within 30 min comparing to 60% of cases in 60 min at a dose of 27,500 IU/kg, under continuous-wave US field (1 MHz, 1 W/cm$^2$) [54].

*Poly(d,l-lactic-co-glycolic acid)* (PLGA), a synthetic biodegradable polymer that is relatively hydrophobic, has the FDA and the European Medicine Agency (EMA) approval for drug delivery systems. The PLGA micro- or nanoparticles are mostly synthesized by a double emulsion solvent evaporation system with poly(vinyl alcohol) (PVA) as an emulsion stabilizer [99].

In order to establish slow and controlled thrombolysis and prevent abdominal aortic aneurysm rupture, Sivaraman et al. produced PLGA

NPs with 10 μg rtPA using didodecyldimethylammonium bromide (DMAB) or PVA as a surfactant [100]. DMAB-stabilized NPs demonstrated gradual clot lysis and higher binding to the fibrin clots. Nano-delivery system overall improved the proliferation of the aneurysmal smooth muscle cells (EaRASMC) exposed to the clot lysis byproducts, attenuated the elastic matrix degradation and proteolytic enzyme activities within EaRASMC cultures.

Surface PEGylation of PLGA NPs plays a favorable role in biocompatibility and improves pharmacokinetics by preventing opsonization. Colasuonno et al. formulated discoidal porous nanoconstructs (DPNs) with a mixture of PLGA and PEG and loaded rtPA with efficiency ~100% via EDC/NHS reaction [101]. Despite the absence of active targeting, a high thrombolytic potential of these NPs might be attributed to their erythrocyte-mimicking shape and deformability, leading to efficient circulation profiles and accumulation of rtPA-DPNs at the clot site. A hybrid theranostic system was developed by Zhou et al., when rtPA was encapsulated into a shell of PLGA and $Fe_3O_4$, and a chitosan-cRGD peptide was grafted on the surface to target GPIIb/IIIa [69]. Such design addressed a dual function: the early detection of a thrombus and the dynamic monitoring of thrombolytic efficiency using a Magnetic Resonance Imaging (MRI) scanner. The obtained NPs showed a sustainable release profile: a slow-release during the first 15 min and a fast release until 60 min. MRI contrast enhancement was illustrated in the murine thrombus model; effective thrombolysis was performed in the *in vitro* blood clot.

Inspired by pathophysiological mechanisms [72], the microaggregates of multiple PLGA NPs dissociated into rtPA-bearing NPs when exposed to abnormally high hemodynamic shear stress (≥100 dyne/cm$^2$) in the vascular occlusions. The obtained Shear-Activated NanoTherapeutics with rtPA (rtPA-SA-NTs) performed effective thrombolysis in multiple preclinical models, as they delayed the time to full vessel occlusion in a $FeCl_3$ mouse arterial thrombus model, reversed the debilitating hemodynamic changes of acute pulmonary embolism *ex vivo* at a concentration 100-times lower of native rtPA, and increased survival in an otherwise fatal mouse pulmonary embolism model *in vivo*.

*Poly(alkyl cyanoacrylate)* (PACA) is an alternative to PLGA

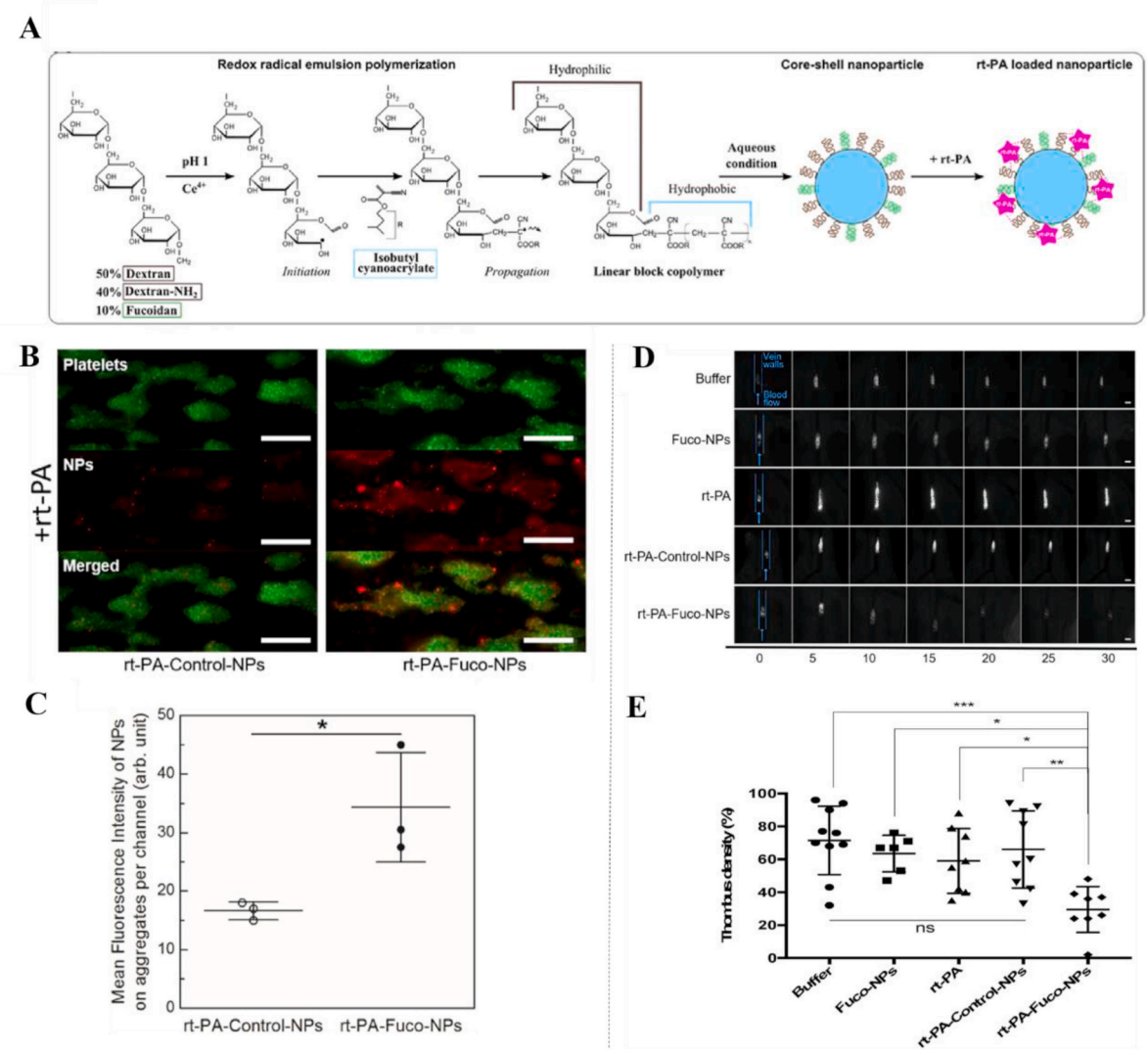


**Fig. 6.** A. Formulation of fucoidan-functionalized NPs with rtPA. Cerium (IV) ions oxidize polysaccharide chains. The free radical initiates the radical emulsion polymerization of isobutyl cyanoacrylate monomers and create amphiphilic linear blocks copolymers that assemble into core-shell NPs in water. rt-PA interacts with the NPs by electrostatic interactions. B. The fluorescence image shows that rtPA-loaded NPs (in red) with fucoidan adhere notably more onto activated platelet aggregates (in green) than the particles without fucoidan under flow conditions (scale bar = 50 μm). C. Corresponding quantitative analysis of rt-PA-loaded NPs on platelet aggregates. D. Evaluation of thrombolysis efficiency in a mouse model of venous thrombosis at the rtPA dose of 2.5 mg/kg. Fluorescence images of thrombus evolution after treatment injection as determined by platelet accumulation at different times (scale bar = 200 μm). E. Corresponding quantitative analysis of the thrombus density at 30 min after injection. Adapted with permission from Ref. [67]. Copyright 2017 Elsevier Ltd. (For interpretation of the references to color in this figure legend, the reader is referred to the Web version of this article.)

biodegradable polymer that was initially developed and approved as a surgical glue [102]. Juenet et al. prepared hydrophilic polysaccharide-decorated poly(isobutyl cyanoacrylate) core-shell NPs with a mean size of 130 nm by redox radical emulsion polymerization and loaded rtPA by adsorption [67] (Fig. 6A). Functionalization of the NPs with an algae-derived abundant and cost-effective sulfated polysaccharide fucoidan (Fuco) [103] allowed binding P-selectin on activated platelets under arterial or venous shear stress conditions (Fig. 6B and C). Fucoidan, as a targeting ligand for P-Selectin overexpression in cardiovascular pathologies, was prior validated on microscale particles, including polysaccharide microparticles with iron oxide for MRI imaging [104] and polymer microcapsules [105]. Thrombolytic efficacy was 2-fold enhanced for rtPA-loaded Fuco-NPs comparing with rtPA-Control-NPs and free rtPA in $FeCl_3$ murine model of venous thrombosis at the rtPA dose of 2.5 mg/kg [67], which is 4 times lower than the appropriate therapeutic dose in mice [106] (Fig. 6D and E).

*Polycaprolactone* (PCL). PCL is a non-toxic biodegradable hydrophobic polyester that is approved by the FDA for several medical applications, including for targeted drug delivery. Its slow degradation profile under physiological conditions (from months to years) makes it attractive for long-term drug delivery devices or implants [107].

Deng et al. synthesized the PEG-PCL NPs by single emulsion and solvent evaporation method and conjugated with rtPA via EDC/NHS [108]. rtPA preserved its amidolytic activity *in vitro* and remained active *in vivo* up to 3 h. Despite some reduction in lytic activity in the *in vitro* blood clot test, rtPA-loaded NPs reduced the infarct volume in the brain by ~70% comparing with free rtPA at 1 mg/kg.

Pan et al. produced cationic micelles with a mean size of ~190 nm [109]. Polymeric micelles are a frequently employed class of NPs with a distinct core-shell structure that are self-assembled from amphiphilic components in an aqueous solvent. They were prepared with a mixture of polymers: polycaprolactone-block-poly(2-(dimethylamino) ethylmethacrylate) (PCL-PDMAEMA) – to form NP core, methoxy-PEG-PCL – to enhance the colloidal stability and biocompatibility, and PCL-PEG conjugated with RGDfk peptide – to target GPIIb/IIIa. The micelles adsorbed anionic LM via electrostatic interactions [109]. They could target thrombus and exhibited thrombolytic potential *in vivo* with almost 2-fold reduced bleeding time vs. free LM, thus, mitigating hemorrhagic risks. Two years earlier, the same team published a work similarly dealing with LM-adsorbed micelles from triblock polymer – polycaprolactone-block-poly(2-(dimethylamino) ethyl methacrylate)-block-poly(2-hydroxyethyl methacrylate) (PCL-PDMAEMA-PHEMA) [110]. In a less common targeting strategy, Annexin V, a human phospholipid-binding protein that binds phosphatidylserine on the surface of activated platelets in a calcium-dependent manner and is proposed to play a role in the inhibition of blood coagulation [111], was conjugated to the micelles to target thrombi in a murine $FeCl_3$-induced model and perform the *in vivo* thrombolytic activity.

*Poly(2-oxazoline)* (POx). This hydrophilic biocompatible but non-biodegradable synthetic polymer features a stealth effect similar to PEG [107]. Gunawan et al. synthesized smart multifunctional polymer microcapsules based on a brushlike POx with alkyne functional groups (B-PEtOx$_{Alk}$) polymer via layer-by-layer assembly on removable mesoporous silica templates [74]. uPA was encapsulated onto these microcapsules via electrostatic interactions ($6.4 \times 10^{-15}$ g uPA per capsule) and could be released upon exposure to thrombin owing to the thrombin-sensitive cross-linker peptide (ELTPRGWRLE). The NP surface-functionalization with a single-chain antibody (scFv) enabled a high affinity toward the GPIIb/IIIa on activated platelets in microfluidic flow channels.

*Poly(acrylic acid)* (PAA) is an anionic polyelectrolyte, which is a synthetic polymer of acrylic acid. PAA is not biodegradable, although it displays excellent biocompatibility and low toxicity [107].

Mei et al. successfully combined the thrombolytic and antioxidant strategy, incorporating 4-amino-2,2,6,6-tetramethylpiperidine-1-oxyl (4-amino-TEMPO) antioxidant into polyion complex NPs as to eliminate Reactive Oxygen Species (ROS) after ischemia-reperfusion injury [48] (Fig. 7A). Self-assembled NPs were composed of anionic PAA, cationic poly(ethylene glycol)-b-poly[4-(2,2,6,6-tetra-methylpiperidine-1-oxyl) aminomethylstyrene] (PEG-b-PMNT) diblock amphiphilic copolymers, and rtPA. The NPs were colloidally stable due to the hydrophobic nature of the core-forming polycationic PMNT segment. Nanocomplexation extended the *in vivo* half-life of rtPA from 8.2 min to 71.2 min. The complex dissociation in the acidic pH, typical for the ischemia, released the drug. At rtPA dose 1 mg/kg, antioxidant-containing NPs improved neurological deficit, reduced cerebral infarct volume, decreased cerebral superoxide ROS and lipid peroxidation levels as well as subarachnoid hemorrhage, contrary to free rtPA and antioxidant-free nanocomplex (Fig. 7B–G).

*Poly(amidoamine)* (PAMAM) is a class of dendrimers – nano-sized, radially symmetric artificial macromolecules with highly branched three-dimensional polymeric structure. Due to the multiple functional surface groups, they are commonly exploited for conjugation with pharmaceutical compounds. Mukhametova et al. developed PAMAM dendrimers, containing ethylenediamine core with amidoamine internal structure and a primary amine terminal surface [112]. They were covalently grafted with SK by EDC/sulfo-NHS chemistry and preserved up to 85% of thrombolytic activity *in vitro* compared with free SK [112]. Nonetheless, the clinical use of the dendrimers is limited because of high toxicity, unknown biocompatibility, biodistribution, biodegradation, and pharmacokinetic profile, and high cost of production [113].

To sum up, multiple excellent papers reported superior thrombolytic potential and favorable therapeutic outcomes with PA-loaded polymeric nanocarriers. These NPs are expected to prevail in thrombolysis research, considering their benefits: simple surface modification & functionalization, "smart" nanoparticulate design with controlled drug release, FDA-approval of some polymers that are both biodegradable and biocompatible.

## 5. Inorganic nanoparticles

### 5.1. Magnetic nanoparticles

Magnetic nanoparticles (MNP) are of great interest in thrombolytic drug delivery due to their large surface area, small particle size (1–100 nm), strong superparamagnetic properties that permit their detection by MRI, excellent biocompatibility with low toxicity. Initially, MNP were introduced to the MRI field to overcome the low sensitivity of the standard imaging method. The assumption was to avoid the proton relaxation effect of MRI imaging with direct visualization of NPs containing iron oxide nanocrystals [114]. The system was functionalized with a fibrin-binding peptide that indicated promising results for MRI visualization of *in vitro* blood clots. MNP are usually composed of a metal core of magnetite $Fe_3O_4$ or maghemite $\gamma$-$Fe_2O_3$ and a functionalized shell. Co-precipitation and thermal decomposition are among the most widely studied synthesis methods for magnetic NPs. Aside from the typically used iron oxide, other magnetic elements such as Ni, Co, and their oxides can also be applied for NP manufacture. Cheng et al. [115] fabricated magnetic Ni nanorods via the oblique angle deposition method (physical vapor deposition technique). Hydrodynamic flows, induced by rotating nanorods suspension with rtPA by a pair of permanent magnets, enhanced rtPA mass transport and accelerated thrombolysis. Nevertheless, due to nickel toxicity, this technology cannot be translated into clinical settings.

Fibrinolytic drug-loaded MNPs can be concentrated at the thrombus under the external high-gradient magnetic field for targeted thrombolysis. Hu et al. [55] employed enzymatical (rtPA reaction) and mechanical clot lysis with rtPA-loaded rotating $Fe_3O_4$–C microrods (MRs) under an external magnetic field. These MRs were assembled from smaller particles with nanometric pores and possessed an average length L = 1.3 μm and a diameter D = 0.5 μm rtPA-MRs under magnetic field recanalized occluded cerebral artery faster and at a lower dose

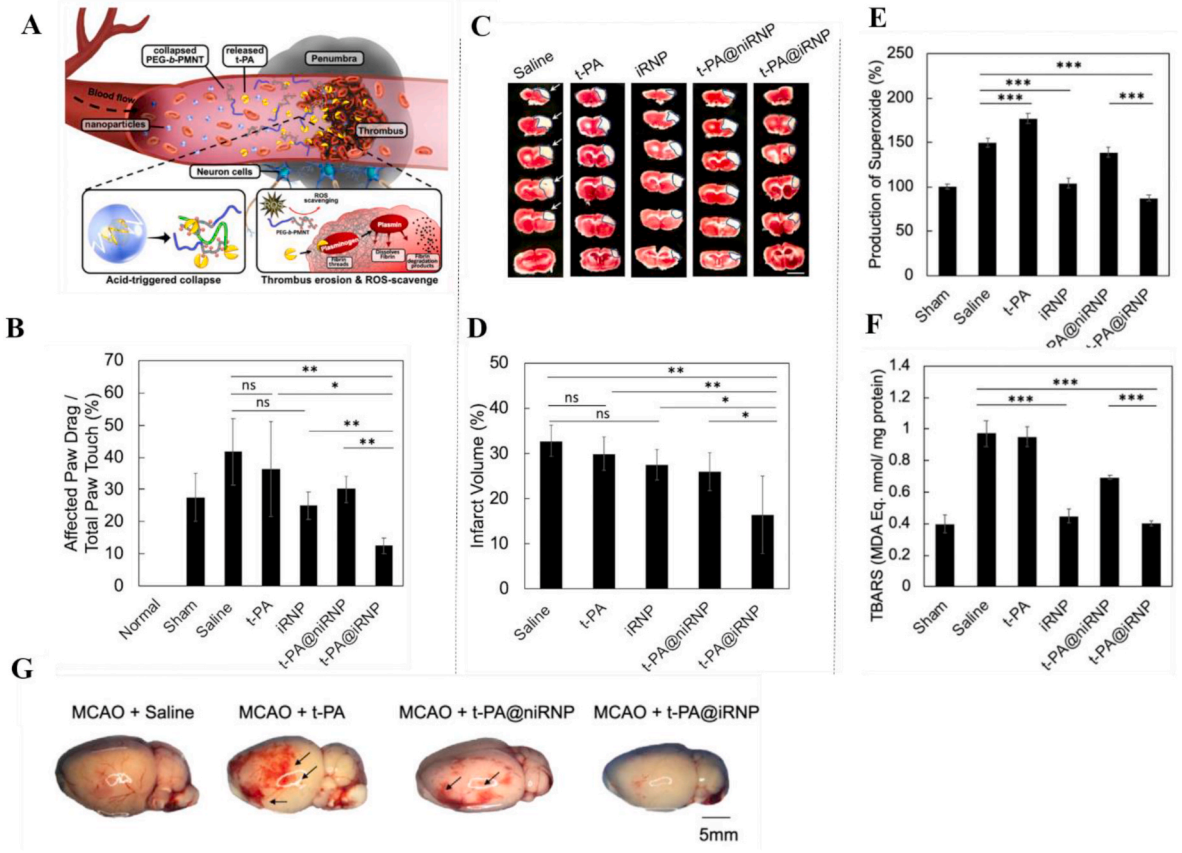


**Fig. 7.** A. Graphical illustration of the mode of action of t-PA-installed polyion complex possessing ROS-scavenging moieties (t-PA@iRNP) in the thrombus: t-PA@iRNP collapse within the acidic ischemic penumbra region, release t-PA, perform thrombosis and antioxidant activity. (B–G) The therapeutic effect of t-PA@iRNP *in vivo* after middle cerebral artery occlusion (MCAO). B. Analysis of paw-dragging behavior in the cylinder test reveals a reduction in the neurological deficit score for the t-PA@iRNP group. C. Representative images of TTC stained cerebral coronal of the mouse brain, white sections indicate the brain infarct zones (scale bar = 0.5 cm). D. Corresponding quantification of cerebral infarct volume (%). E. Treatment with t-PA@iRNP decreased cerebral superoxide levels, measured by dihydroethidium, at 24 h after injection. F. Treatment with iRNP and t-PA@iRNP reduced thiobarbituric acid-reactive substances (TBARS) level – index of lipid peroxidation in the brain – due to the antioxidant effect. G. Treatment with t-PA@iRNP suppressed t-PA induced cerebral subarachnoid hemorrhage (shown with arrows) with representative images at 24 h after treatment. Adapted with permission from Ref. [48]. Copyright 2019 Elsevier Ltd.

compared to free rtPA group (25 min at 0.13 mg/kg vs. 85 min at 10 mg/kg) and diminished the post-stroke infarct volume *in vivo*. Despite the absence of liver and kidney toxicity of the MRs, they aggregated *in vitro* and required sonication to remain homogeneously dispersed in the suspension.

The drawbacks of uncoated magnetite NPs is that they are prone to oxidation and rapidly aggregate due to strong magnetic dipole-dipole attraction between particles, leading to a loss of magnetization. After the synthesis, a surface coating by $SiO_2$ or biopolymers is required to improve NP environmental stability, stealth effects, and prolong the blood circulation time. It may additionally provide a variety of high-capacity surface functional groups for bioconjugation of the molecules of interest.

Kempe et al. produced octahedral silica-coated $Fe_3O_4$ NPs for ferromagnetic implant-assisted magnetic drug targeting of in-stent thrombosis [116]. Silica coating enlarged the hydrodynamic size of the NPs from 10 to 30 nm–~300 nm due to the tight aggregation of naked NPs. rtPA was immobilized onto NP surface via EDC/sulfo-NHS chemistry (71 μg rtPA/1 mg magnetite NPs). In a preliminary experiment on the porcine brachial artery, rtPA-NPs were effective for magnetically guided lysis of in-stent thrombosis at a low rtPA dose of 0.38 mg. In another study [117], silica-coated magnetic nanoparticle ($SiO_2$-MNP), prepared by the sol-gel method, covalently grafted rtPA with a glutaraldehyde (0.5 mg/mL rtPA/5 mg $SiO_2$-MNP). After nano-conjugation, the rtPA storage stability increased 9.5-fold in the PBS and 2.8-fold in whole blood. Time of thrombolysis of $SiO_2$-MNP-rtPA improved by 65% vs. free rtPA in the *ex vivo* intravascular model under magnetic guidance.

The high porosity of the silica coating promotes the encapsulation of the pharmaceutical drugs inside the pores. Wang et al. reported that silica-coated magnetic NPs, prepared by the surfactant templating, with an expanded 6 nm pore size permitted 30-fold more efficient uPA adsorption with sustainable drug release [118]. *In vitro* thrombolytic efficiency was 2-fold superior vs. free uPA and ~1.5-fold faster vs. uPA-loaded supermagnetic non-mesoporous silica NPs under 0.2 T magnet. Yet, silica clinical application needs to be carefully regulated because of the hemolytic effect it might induce as it acts as a hydrogen donor in interactions with cell membrane phospholipids and generates ROS [119,120]. Additionally, silica is shown to provoke an immune response by releasing pro-inflammatory cytokines [121].

Common in cancer therapy *in vivo*, hyperthermia was used as adjuvant therapy for thrombolysis by Voros et al. [75]. Multiple clustered iron oxide nanocubes (NCs), synthesized by a high-temperature thermal decomposition, were surface-coated with a mixture of rtPA and Bovine Serum Albumin (BSA) and produced a local overheating under alternating magnetic fields (295 kHz). rtPA release from NCs doubled at 42 °C from the one at 37 °C within 24 h.

The presence of functional amino and hydroxyl groups makes chitosan and its derivatives a suitable candidate for the magnetic NP surface coating. Chen et al. [122] prepared iron oxide MNP by the chemical co-precipitation and coated with chitosan as a dispersing agent. They immobilized rtPA by glutaraldehyde-mediated amide bond formation

with loading efficiency 95% (0.5 mg rtPA/5 mg chitosan-MNP), maintaining its enzymatic and thrombolytic activities *in vitro*. *In vivo* rat arterial embolic model further evidenced tissue perfusion after treatment of 6,000 G magnetically guided Cs-MNP-rtPA at a dosage of 0.2 mg/kg but not of saline. Alternatively [123], chitosan coating of $Fe_3O_4$ MNPs was achieved by crosslinking with sodium tripolyphosphate via ionic gelation in the presence of rtPA. On top of targeted magnetic delivery, rtPA-encapsulated NPs unveiled a triggered release: in serum at 37 °C, but not in PBS, which was on/off magnet-sensitive and could be retarded in the presence of a magnetic field. According to the *in vivo* study on the rat embolic model, rtPA-NPs restored blood flow at rtPA dose of 2 mg/kg under magnetic guidance in contrast to NP administration alone.

Dextran, complex branched glucose, is largely used in the coating of MNP. Magneto-fluorescent crosslinked dextran-coated iron oxide (CLIO) NPs targeted arterial and venous thrombi *in vivo* via an activated factor XIII (FXIIIa)-sensitive peptide (GNQEQVSPLTLLKC-NH2) [68]. These theranostic NPs generated optical imaging with NIR VivoTag 680 fluorophore and were covalently functionalized with rtPA via PEG. Thrombolytic efficiency was comparable to the one of free rtPA in the humanized mouse model of pulmonary embolism.

Cytocompatibility of dextran-coated superparamagnetic iron oxide NPs (SPIONs) on human umbilical vein endothelial cells (HUVECs) (~85% cell viability) without changes in mitochondrial membrane potential, a DNA degradation or cell cycle alteration was stated by Heid et al. [124]. When comparing an adsorptive or covalent (EDC/NHS) method to load an arginine-purified rtPA, >80% loading efficiency was achieved for both approaches. Yet, SPIONs with covalently bound rtPA were more efficient to be targeted by a 0.4 T magnet into fibrin clot and to perform a local *in vitro* thrombolysis.

Owing to its natural, biodegradable, and non-toxic character, agarose, a linear polysaccharide extracted from red seaweed, is applied in diverse biotechnological applications. Agarose gel-coated $Fe_3O_4$ NPs were covalently grafted with uPA via EDC/sulfo-NHS [125]. Urokinase-loaded NPs increased the thrombolytic rate by 50% in the *in vitro* blood clot assay vs. free uPA, as well as in microfluidics test under a static magnetic field of 624 A/m.

Prilepskii et al. [126] crosslinked MNPs with heparin, FDA-approved polysaccharide with anticoagulant activity, and adsorbed uPA with encapsulation of 99% (Fig. 8A). The size of the resulting nanocomposite was around 100 nm (Fig. 8B). Without the inhibitory effect of the heparin on uPA, the thrombolysis rate amplified in the presence of a permanent magnet *in vitro* (12 min vs. 7 min for 60% clot reduction) (Fig. 8C). In the $FeCl_3$ rat carotid artery and rabbit femoral artery models, the MNPs@uPA group speeded reperfusion time and increased blood flow rate ~4 times compared to that of native uPA (Fig. 8D and E).

The synthetic polymer coating is similarly explored for the preparation of magnetic field-responsive and biocompatible NPs. Huang et al. [127] stabilized MNPs with PAA by providing electrostatic and steric repulsion and loaded rtPA via EDC/NHS due to PAA abundant carboxyl groups. The clot lysis efficiency of MNP-rtPA was improved under the rotating magnetic field compared to free rtPA *in vitro*. Besides, MNP-rtPA diminished the brain infarct area in the distal cerebral occlusion *in vivo* model vs. free rtPA ($8.65 \pm 3.63$ mm$^3$ vs. $4.40 \pm 2.46$ mm$^3$).

Another publication compared covalent vs. non-covalent methods of rtPA loading to polyacrylic acid-co-maleic acid (PAM)-coated SPIONs [128]. Better loading efficiency was reported with a covalent method vs. adsorption ($98.6 \pm 0.8\%$ vs. $47.7 \pm 5.4\%$). Amidolytic and fibrinolytic activities on the PAM-SPIONs with covalent loading were superior and better preserved after 40 days of storage. Hence, the covalent binding of the rtPA was advantageous for the application with SPIONs.

Hung-Wei Yang et al. [129] synthesized the magnetic nanocarriers (MNCs) with a water-soluble poly [aniline-co-N-(1-one-butyric acid) aniline] (SPAnH) shell that could load a high amount of rtPA via

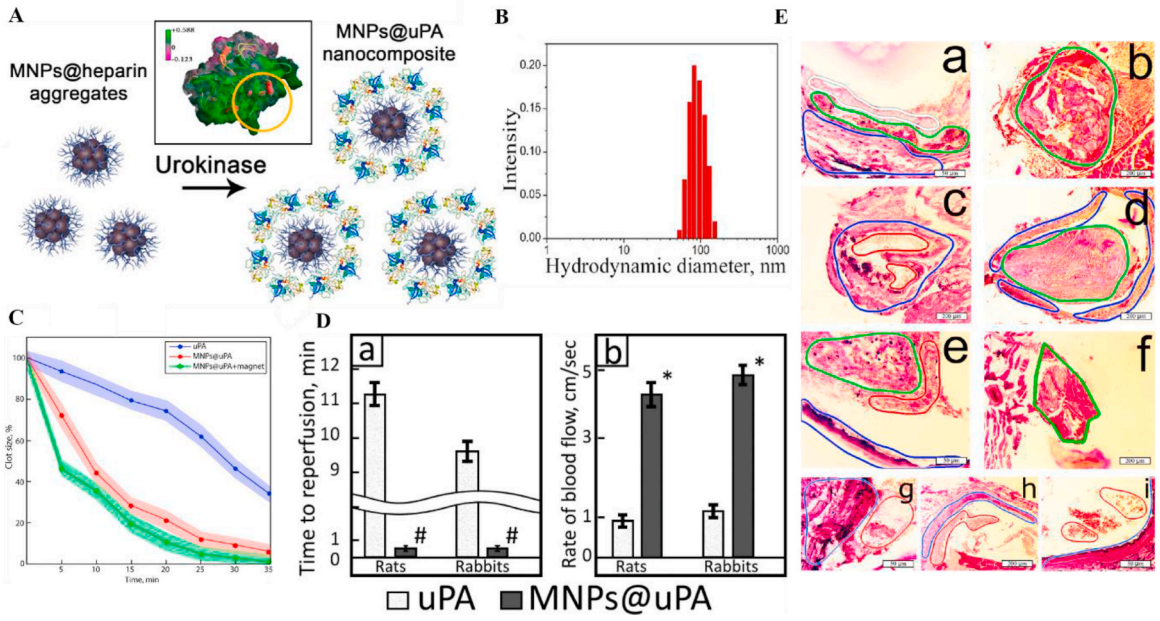


**Fig. 8.** A. Schematic of the adsorption of uPA to the heparin-coated MNPs to obtain MNPs@uPA. Inset: 3D structure of urokinase with colored electrostatic potentials. Kringle domains responsible for interaction with heparin are in orange. B. The hydrodynamic diameter of MNPs@uPA composite. C. *In vitro* clot lysis rate upon exposure to uPA and MNPs@uPA with or without a magnetic field. The difference in the thrombolysis for MNPs@uPA with and without magnet within the initial 25 min is statistically significant ($p < 0.05$). D. Restoration of blood flow *in vivo* of uPA and MNPs@uPA. (a) Time to vessel reperfusion. (b) Rate of blood flow 24 h post-injection. E. Sections of the rat carotid artery and (g–i) rabbit femoral artery 24 h post-clot formation. Colors: blue, vessel walls; red, erythrocyte aggregates; green, red clot; white, white clot. (a, b, g) Saline. The clot tightly adhered to the vessel wall observed in (a) (marked in green). The vessel fully occluded by the clot (encircled in green) presented in (b). (c, d, h) uPA. Note a clear vessel lumen space between the clot (green) and the vessel wall (blue) in (d). (e, f, i) MNPs@uPA. Note a bigger free space in the vessel lumen and reduced size of the clot in (f) and (i). (a, c, e, g–i): H&E staining. (b, d, f): Picro-Mallory staining. Adapted with permission from Ref. [126]. Copyright 2018 American Chemical Society. (For interpretation of the references to color in this figure legend, the reader is referred to the Web version of this article.)

1-ethyl-3-(3-dimethylaminopropyl)carbodiimide/N-hydroxysuccinimide (EDC/NHS) chemistry (276 μg rtPA per 1 mg MNC). Magnet-guided MNC-rtPA demonstrated significantly improved thrombolysis in rat iliac embolism model at 0.2 mg/kg rtPA dose.

### 5.2. Gold nanoparticles

Gold nanoparticles (AuNPs) benefit from diverse optical and photothermal properties. They are synthesized by the reduction of gold salts to gold metals in the presence of stabilizing agents to prevent the aggregation during NP formation, and their tunable size modulates their toxicity and biodistribution. Gold NPs can be applied in photothermal therapy in cancer [130] as well as in drug delivery. Moreover, AuNPs are characterized by their high X-ray absorption coefficient enhancing CT signal. The quantitative imaging method *in vivo* was established to monitor the thrombolysis with rtPA using fibrin-targeted glycol chitosan-coated gold NPs [131]. Direct discrimination of thrombi from the underlying tissue was obtained with gold NPs conjugated with a thrombin activatable fluorescent peptide that discharged a near-infrared signal (NIRF) when cleaved [132]. This dual NIRF/micro-CT imaging protocol was tested *in vivo* and suggested a high spatial resolution for a rapid and direct thrombi diagnosis. Indeed, gold NPs represent an interesting perspective to overcome the pitfalls of standard imaging protocols and might allow a better triaging of patients according to their thrombotic conditions.

Gold nanoparticles are similarly capable of delivering large biomolecules, like plasminogen activators. Tang et al. conjugated rtPA with AuNPs with a diameter of 37.8 nm via bio-affinity ligation that is based on the interactions between rtPA and 3-lysine ligand on the AuNPs surface through polyvinyl pyrrolidone (PVP) spacer [51]. Notably, obtained conjugate indicated protection from inhibition by PAI-1 *in vitro* by pre-incubation with the enzyme and prolonged circulation time *in vivo* (6.5 min vs. 20.5 min). Another intelligent nanoplatform for hyperthermia-induced thrombolysis was documented by Wang et al. [47]. Gold@mesoporous silica core-shell nanospheres immobilized uPA in the pores by a solid 1-tetradecanol (tet) (Fig. 9A). Owing to hyperthermia caused by Au absorption of NIR under NIR laser irradiation, tet transformation to liquid phase stimulated a temperature-sensitive controlled release of uPA, whereas only 10.5% of the drug was released at 37 °C vs. 89.5% at 39 °C (Fig. 9B and C). In the carrageenan-induced murine tail thrombus model, NIR-irradiated uPA-NPs group enhanced thrombolytic effect ~2-fold vs. free uPA (Fig. 9D).

In conclusion, several remarkable concepts of inorganic PA-bearing NPs for targeted thrombolysis were published in the last 10 years that have the potential to become theranostics. Despite most of MNP rely on magnet-assisted accumulation on the thrombus, this targeting approach seems to be tricky to accomplish in healthcare settings. An interesting application of inorganic NPs is hyperthermic exposure as adjuvant therapy to fibrinolytic therapy. Nevertheless, it must be remembered

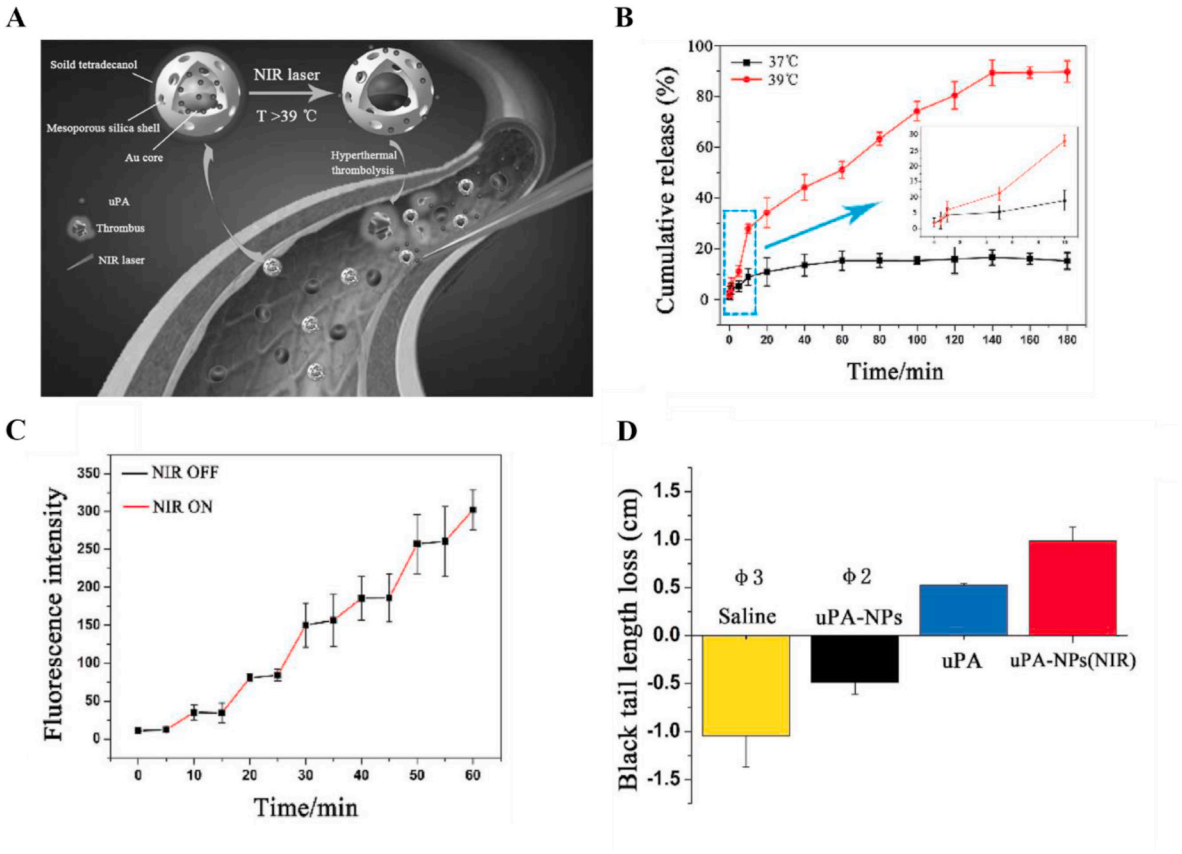


**Fig. 9.** A. Schematic illustration of the hyperthermia-induced enhanced thrombolysis with uPA-immobilized gold@mesoporous silica nanospheres. B. *In vitro* release profiles of fluorescent uPA from uPA-NPs at 37 °C and 39 °C, respectively. The enlarged release profile in 10 min is shown at the inset graph. C. NIR laser triggers pulsed uPA release profile *in vitro* of fluorescent uPA-NPs. D. *In vivo* thrombolysis in murine tail thrombus model via injecting carrageenan. The statistical black tail length loss (thrombolytic effect) of mice after treatment for 9 days, where ϕ represents the amputated tail, and the number represents the number of mice with the amputated tail. Adapted with permission from Ref. [47]. Copyright 2017 WILEY-VCH Verlag GmbH & Co. KGaA, Weinheim. (For interpretation of the references to color in this figure legend, the reader is referred to the Web version of this article.)

that NPs from inorganic materials are difficult to degrade *in vivo* and they persist for long periods (more details on safety and metabolism in Section 8.1).

## 6. Bio-inspired nanocarriers

Nature inspires the development of nanotechnological solutions in drug-delivery systems. Bio-inspiration and biomimicry technologies can not only simulate biological materials by their chemical structure but also by their biological functions [133].

*Camouflage*. An elegant strategy to reduce thrombolytic drug elimination and increase its plasma half-life is to camouflage it as endogenous proteins. This approach was demonstrated by Absar et al. [134] when the targeted/triggered release of rtPA was mediated by the presence of thrombin in the thrombus. rtPA was camouflaged by conjugating with human serum albumin (HSA) via a thrombin-cleavable peptide (tcP) and decorated with a homing-peptide targeting GPIIb/IIIa. This construct permitted to temporarily suppress the enzymatic and fibrinolytic activities of camouflaged rtPA, however, to spontaneously restore it upon incubation with thrombin by the cleavage of the peptide linker.

*Red blood cell (RBC)-derived nanocarriers*. Erythrocytes are recognized for their extended blood circulation as they manage to avoid clearance by the macrophages up to 3 months. A number of factors are believed to contribute to that, including their discoidal shape, deformability, and the expression of self-recognition biomarkers, such as CD47 and CD200 [133,135]. RBC seem to be a particularly promising carrier of thrombolytic drugs that exert their pharmacological activity within blood vessels.

Vankayala et al. [136] designed theranostic nanoconstructs for near-infrared (NIR) fluorescence imaging and thrombolytic activity. Specifically, after hypotonic treatment of RBCs, obtained erythrocyte ghosts were coupled with indocyanine green, FDA-approved NIR imaging agent, and conjugated with rtPA via amine-aldehyde chemistry. Their thrombolytic efficacy was comparable to the free rtPA *in vitro*. Erythrocytes have already reached clinical trials as nanocarriers for drug delivery (Clinicaltrials.gov Identifiers: NCT01255358, NCT01171807, NCT00484965) but not in thrombolytic therapy yet [133].

*Platelet-like nanocarriers*. Platelet membrane-camouflaged PLGA-core NPs, conjugated with rtPA, were recently proposed as a biomimetic technique by Xu et al. [76]. These so-called "nanoplatelets" behave like platelets in the blood circulation (Fig. 10A and B) and bind to the thrombus *in vitro* and *ex vivo*. rtPA-NPs treatment was beneficial in multiple *in vivo* models: improved the mouse survival time from 4-7 days to 14.5 days and ~4.5-fold reduced the thrombus area vs. free rtPA in the pulmonary embolism model (Fig. 10C and D); stimulated complete thrombus removal contrary to free rtPA in the $FeCl_3$-induced mesenteric arterial model. Notably, post-thrombolytic brain damage was weaker for the rtPA-NPs group as defined by a lower neurological deficit score and smaller ischemic area in the ischemic stroke mouse model, as depicted on Fig. 10E–G.

There has been a growing interest in exploring neuroprotective strategies following acute ischemic stroke to reduce brain injury [137]. Another version of the "nanoplatelets" was proposed as a combinational approach for the treatment of acute ischemic stroke based on thrombolysis and neuroprotection [138]. The NPs with a size of ~150 nm contained the core of acetal modified dextran & neuroprotective agent and were covered with a platelet membrane conjugated with thrombin-cleavable Tat-peptide (Tat-LTPRGWRLGGC) that coupled rtPA (Fig. 11A). In this nanodesign, rtPA could be released upon thrombin presence while exposing Tat-peptide on the NPs and

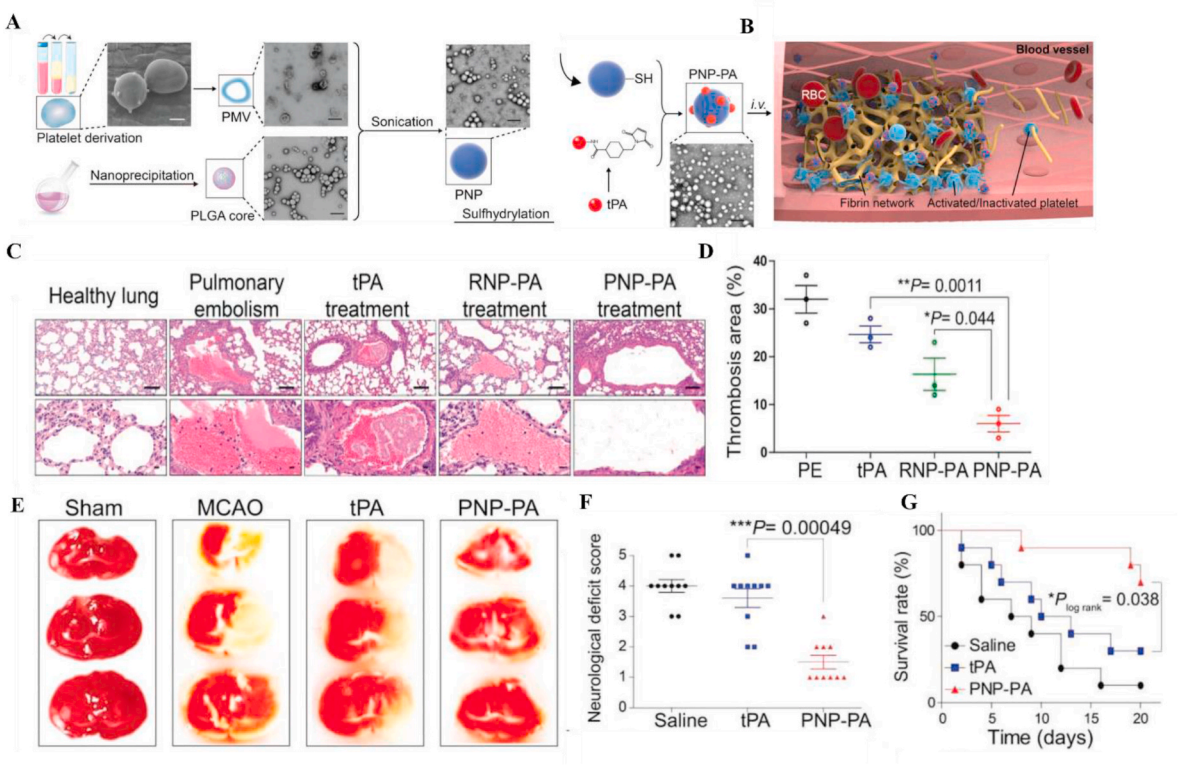


**Fig. 10.** A. Schematic illustration of the synthesis of PNP-PA NPs. Briefly, the membrane of platelets (scale bar = 1 μm), acquired from the whole blood of mice, were used to coat the PLGA cores (scale bar = 400 nm). t-PA was subsequently conjugated via –SH groups onto the surface of the platelet membrane to form PNP-PA. B. The proposed mechanism of action *in vivo*: mimicking platelets, PNP-PA are specifically targeted to the thrombus and dissolve the fibrin clot. C. Therapeutic potential of PNP-PA in a pulmonary embolism mouse model. Lung sections with H&E staining administered the indicated treatments (scale bar = 50 μm). D. Quantitative analysis of the thrombus area in panel C. E-G. Therapeutic effects of PNP-PA in the ischemic stroke mouse model. E. Representative TTC staining images of MCAO mouse brains treated with the indicated formulations. F. Neurological deficit scores in the treatment groups of MCAO mice. G. The survival rate of MCAO mice treated with the mentioned formulations. Adapted with permission from Ref. [76]. Copyright 2019 WILEY-VCH Verlag GmbH & Co. KGaA, Weinheim.

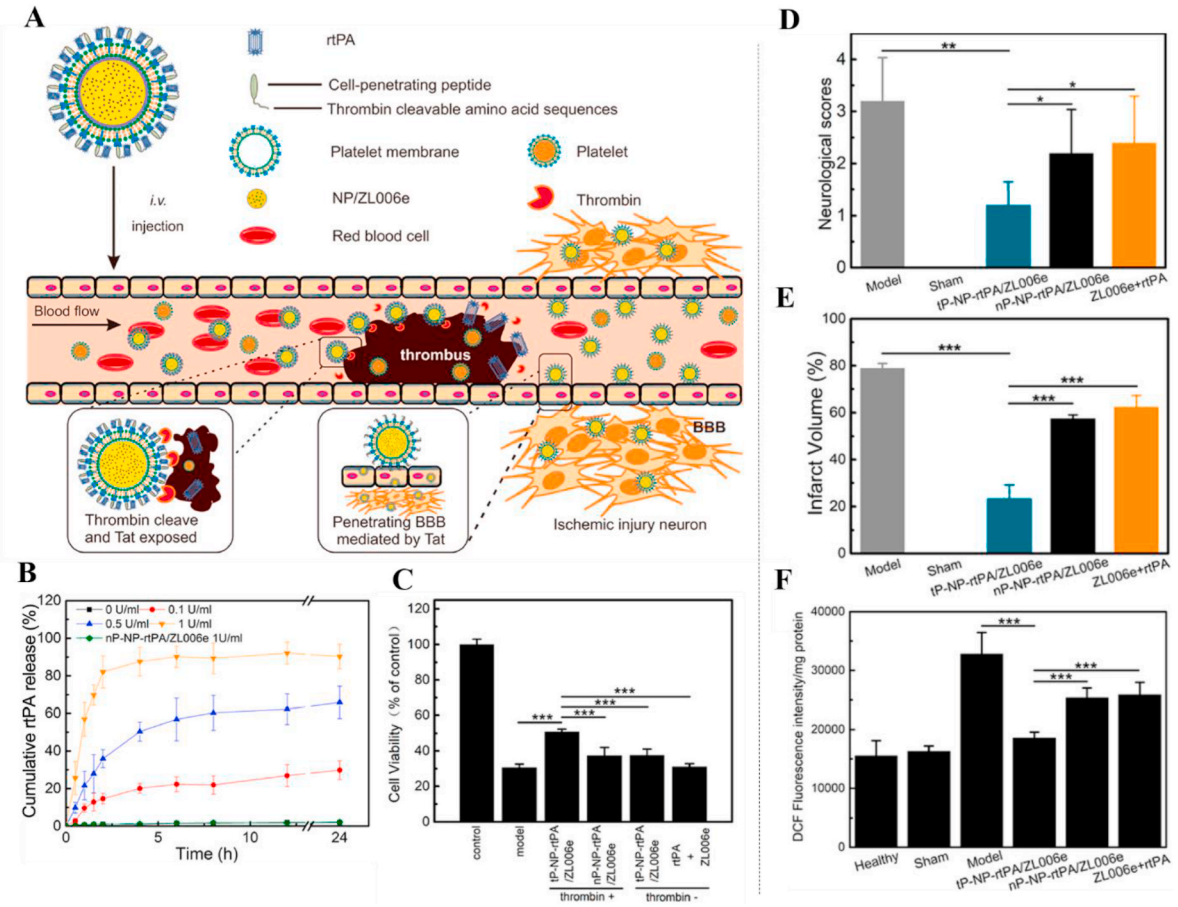


**Fig. 11.** A. Schematic design of tP-NP-rtPA/ZL006e and its components and mode of action. After intravenous injection, tP-NP-rtPA/ZL006e are targeted to the thrombus for thrombin-triggered release of rtPA and thrombolysis. Nanocarrier transport into the brain via Tat-mediated transcytosis for neuroprotective activity. B. Cumulative release of rtPA from tP-NP-rtPA/ZL006e with different thrombin concentrations. nP-NP-rtPA/ZL006e are the control particles in 1 U/mL thrombin. C. *In vitro* neuroprotective effect of tP-NP-rtPA/ZL006e and nP-NP-rtPA/ZL006e with or without thrombin and free ZL006e + rtPA via the coculture model of the BCEC monolayer and glutamate-stimulated PC-12 cells. D. Neurological scores of the MCAO rats after the treatment. E. Quantification of brain infarct volume/ischemic brain hemisphere at 24 h post-treatment MCAO rats. F. ROS level in the ischemic region. Adapted with permission from Ref. [138]. Copyright 2019 American Chemical Society.

penetrating BBB for neuroprotectant delivery in the brain (Fig. 11B and C). In the *in vivo* model of middle cerebral artery (MCA) occlusion, a treatment with this nanocomplex decreased infarct size by 63%, ameliorated neurological deficit, and diminished ROS level of the ischemic region by 52% compared to the free drug combination (Fig. 11D–F).

*Leukocyte-derived microvesicles*. Cell microvesicles that originate from the plasma membrane of most cell types, including blood cells, are essential effectors in the intercellular communication and may transport bioactive molecules [139]. Silva et al. reported an unconventional method when microvesicles (D = 673 ± 168 nm), secreted from macrophages upon serum depletion cellular stress, were capable of enclosing both iron oxide NPs and rtPA [140]. The work exemplified a biogenic strategy of theranostic application of hybrid microvesicles for MRI imaging and spatially-controlled rtPA delivery via magnetic field gradient targeting.

*Bacterial spores*. In another bio-inspired approach, the spores of bacterium *Bacillus amyloliquefaciens* with peptidoglycans on their surface were prior inactivated with a high-pressure steam sterilizer and used as nanocarriers with uPA and RGDS peptide [141]. The solid monodisperse oval spheres ([0.67 ± 0.20 μm] × [1.27 ± 0.20 μm]) were non-biotoxic following histological evaluation of the heart, kidneys, and liver. With a higher thrombolysis rate *in vitro*, *in vivo* tail bleeding times of the uPA-NPs group were shorter than that of free uPA (601 s vs. 1145 s), suggesting a lower risk of hemorrhages.

*Viral nanoparticles*. Based on bacteriophages and plant viruses, viral nanoparticles (VNPs) are biocompatible, biodegradable, and nonpathogenic nanocarriers in humans. Because of the remarkable proliferation of viruses, they could be easily manufactured up to an industrial scale. In the NPs based on the tobacco mosaic virus, the nucleic acids are tightly enclosed in a stiff hollow tubular capsid comprising coat proteins [142]. To develop a nanocarrier with optimal flow properties for thrombolytic therapy, Pitek et al. conjugated rtPA to tobacco mosaic virus mutant soft elongated nanorods containing lysine side chain (TMV-Lys) via PEG linkers, obtaining the NPs with dimensions of 300 × 18 nm [143]. TMV-rtPA could passively accumulate at the thrombus at a higher rate than TMV-PEG *in vivo*. Both rtPA and TMV-rtPA resumed the circulation in the mouse thrombosis model, but TMV-rtPA reduced bleeding time ~2-fold vs. free rtPA. Despite an absence of pathogenicity, the potential immunogenicity of nanodelivery systems based on pathogens such as bacteria and viruses should be not be neglected.

To conclude, biomimetic delivery systems have the countless potential for the advancement of drug delivery technologies. The reproduction of the biological complexity on nanocarriers' surface imitates biological features, like biocompatibility, targeting to the thrombus tissue, efficient circulation profiles, etc. To be suitable for clinical translation, both toxicological (e.g., safety, immunogenicity) and pharmaceutical (e.g., reproducibility, scale-up, standardization of chemical composition) concerns have to be examined [144].

## 7. Ultrasound-responsive carriers & sonothrombolysis

Microbubbles (MBs) are defined as spheroid objects stabilized by a coating material [145], such as lipids, polymers [146], or denatured proteins, and filled with a gas or a combination of gases (air or perfluorocarbons). Their average size should not exceed red blood cell size (6–8 μm) to avoid embolization [147].

The application of these novel therapeutic agents originated from US imaging, since local US insonation induces acoustic steaming of the surrounding tissues [148] that may help drugs to penetrate deeper into the clot by local mechanical stress induction. Sawaguchi et al. illustrated this hypothesis with an *in vitro* blood clot lysis experiment and demonstrated that the US itself can accelerate thrombolysis [149]. Using 500 kHz US insonation, the authors pointed out that the thrombolysis acceleration ratio was about 2.5 times greater with rtPA combined with the US than rtPA treatment alone. Thrombolytic therapy combined with the US could reduce the dose of rtPA by 60% owing to the synergistic effect.

In the cardiovascular field, microbubbles are mostly designed as contrast agents for ultrasound molecular imaging due to their ability of radiation oscillation, upraising the contrast of tissues. Every bubble is subjected to stable cavitation in low range frequencies and can undergo inertial cavitation (burst) under higher frequencies [150]. Cavitation is the process of induced bubble growth and collapse and can be achieved by different mechanisms [151], including ultrasonic waves [152]. Association of ultrasound insonation and microbubble stimulation is called sonothrombolysis (Fig. 12) and is promising to enhance thrombolysis.

The focus on MBs for thrombolytic therapy was initially published by Tachibana et al. [153] and Porter et al. in 1996 [60] with an *in vitro* model of enhanced thrombolysis using dextrose albumin MBs and a low-frequency transducer. Nowadays, most of the lab-made microbubbles are phospholipid-based and obtained from a sonication-lyophilization-rehydration process [154–157], microfluidics [158], or coaxial electrohydrodynamic atomization process [159], and called echogenic liposomes (ELIP) [160]. Laing et al. took benefit from the rehydration step to incorporate rtPA and obtain thrombolytic-loaded ELIP. With natural rtPA affinity to fibrin [156], the authors highlighted the significant contribution of a high mechanical index (0.4) on the recanalization rate of the obstructed artery in the rabbit model. Mechanical Index (MI) is a unitless ratio between the peak of negative pressure and the square root of the frequency in MHz. It is applied to predict the bioeffect of ultrasound; when MI is $> 0.3$, microbubbles are easily destructed [161] but may have harmful bioeffects above 1.9 value [162]. One of the limitations of this study was the lack of stable cavitation of these air-filled MBs. To remediate this issue, other gas fillers were explored, like Shekhar's [155] octafluoropropane targeting ELIP that allowed more robust stable cavitation, significantly enhancing thrombolysis *in vitro*.

Literature accordingly claims that US insonation of microbubbles on the thrombus site triggers sonothrombolysis due to the cavitation process [157]. The average lytic rate obtained with rtPA loaded ELIP and the US was recorded to be over 2-fold higher than free rtPA with an *in vitro* flow model [155]. Zhu et al. [163] published similar results with their uPA loaded targeted microbubbles from Targerson Inc. and the US.

Microbubble targeting agents are similar to other functionalized NPs: mostly RGDS peptide targeting GPIIb/IIIa on activated platelets [163–166], heat denaturated collagen that binds vWF [167], or scFv targeting GPIIb/IIIa grafted on Nonlinear Ultrasound Contrast Agent by Visual Sonics® via biotin/streptavidin coupling [168]. Hua et al. [164] published the *in vivo* study presenting the theranostic potential of their rtPA-loaded MBs with RGD peptide and 2 MHz ultrasound. A high recanalization rate was obtained with a 15 times lower dose of rtPA.

The magnetic field was also observed as a targeting strategy [169] by using ferrofluid in the composition of the MBs. As expected, significant enhancement of the cavitation energy was observed when a magnet was placed on the thrombi location, limiting the prolonged exposure of ultrasonic waves. Potentially, this magnetic element in the MBs may allow MRI imaging [167].

A complete overview of small animal sonothrombolysis stroke models has been published by Auboire et al. [170] in 2018. The overall perspective for further treatment model is suggested to be on the range of sub-Mhz frequencies and intensities that favor stable cavitation of the MBs. It described sonothrombolysis as a potential treatment for small vessel impairment or larger arteries occlusion.

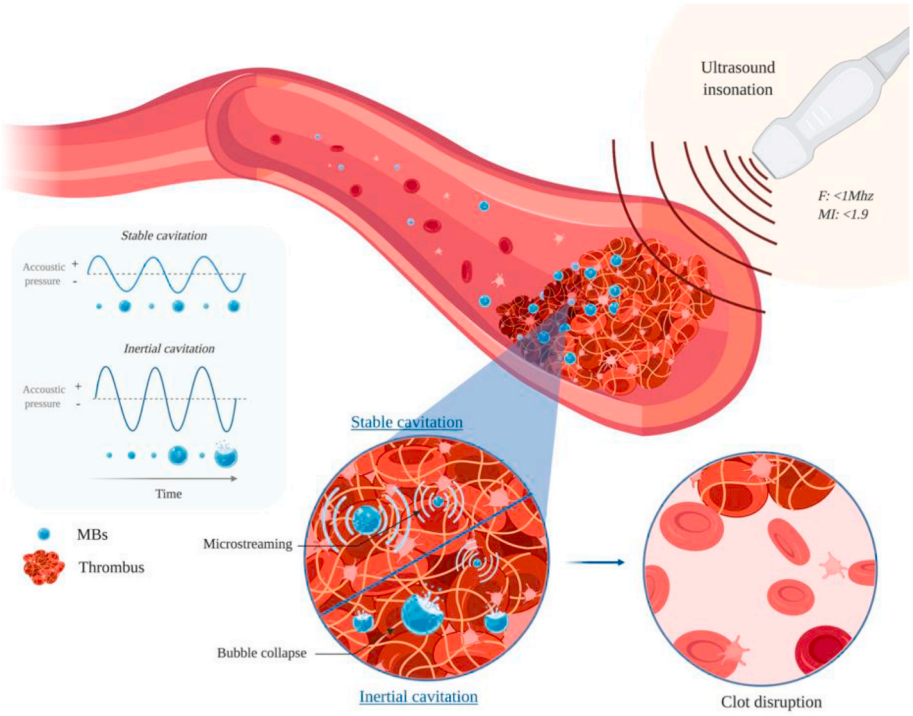


**Fig. 12.** Sonothrombolysis precept for enhanced thrombolysis. Sonothrombolysis is performed by the ultrasound insonation of MBs on the thrombus site. Microbubble radial oscillation properties are sensitive to acoustic pressure. The bubbles can undergo stable cavitation inducing microstreaming of the surrounding environment or inertial cavitation leading to the collapse of the bubble. While MBs alone are proven to destabilize a clot with US insonation, sonothrombolysis efficacy is enhanced with the thrombus specific targeting and loaded thrombolytic agent on the MBs. Abbreviations: *F*, frequency; *MI*, mechanical index; *MBs*, microbubbles.

Preclinical trial on big animals was performed on a porcine model at the VU University Medical center in the Netherlands [166] with RGDS targeted SonoVue® microbubbles loaded with uPA. Pigs received the premedication to prevent the potential allergic reactions to the lipid shells of the MBs. MBs were injected intraluminally to simulate a clinical setting, and 1.1 MI was applied. Three out of 5 pigs of the uPA targeted MBs group showed an increase in the arterial flow and recanalization rate, whereas only 1 out of 4 in the uPA group showed a slight improvement. A major limitation of this study was a lack of information about the exact concentration of the encapsulated drug.

Because of their echogenic properties, some microbubbles are already clinically used as a diagnostic tool [171], such as DEFINITY® (Lantheus Medical Imaging) or SonoVue® (Bracco Diagnostics), in order to enhance ventricular opacification and US imaging of tumor angiogenesis. Those approved microbubbles are composed of a phospholipid shell but not yet loaded with therapeutic agents. Yet, preclinical studies on acute cerebral ischemia on rats demonstrated that focused weak energy US associated with SonoVue® injection was as efficient as fibrinolysis with rtPA [172]. Recanalization in an occluded vein model was efficient with microbubble cavitation only under US insonation directly on the vein within 10 min [173], which may be advantageous to limit hemorrhage risks induced by PA.

Sonothrombolysis treatment has already stepped up to clinical trials with the following ones: MUST (Microbubbles and Ultrasound in Stroke Trial, Clinicaltrials.gov Identifiers: NCT00132691) performed at the University of Toulouse in France and CLOTBUST Hands-Free (Combined Lysis of Thrombus in Brain Ischemia With Transcranial Ultrasound and Systemic T-PA-Hands-Free, ClinicalTrials.gov Identifier: NCT01240356) at The University of Texas Health Science Center, Houston. While MUST trial was aborted after incidences of intracerebral hemorrhages [171], CLOTBUST Hands-Free showed great recanalization rates in combination with systemic rtPA on ischemic stroke patients [174]. Finally, an ongoing clinical trial is evaluating the efficacy of SonoVue® MBs associated with rtPA and US insonation compared to classic rtPA injection on acute ischemic stroke patients in the 4.5 h window treatment. This study takes place in Barcelona, Spain on 24 participants and results have not been reported yet (ClinicalTrials.gov Identifier: NCT01678495).

Recent work focused on nanobubbles (NBs) coupled with cRGD peptide [71], instead of their microscale peers, to facilitate deeper blood clot penetration. Jiang et al. used the high-frequency US to burst these NBs to decrease the risk of clinical bleeding due to the enhancement of permeability of low frequencies. Comparing SonoVue® MBs to the NBs, both in combination with uPA and submitted to the US, it was observed a difference in the clot degradation: a peripheral relaxation in the MBs group vs. a fissure like a collapse in the NBs one. The nanometric scale of these particles seemed to deconstruct the clot from the inside.

Ultrasound is mainly applied in diagnostics in the clinic because it is safe, easy and quick to utilize at an affordable cost. The therapeutic potential of US-responsive carriers and sonothrombolysis is promising in fibrinolytic therapy. The main goal is to improve the efficiency of thrombolytic therapy on highly retracted thrombi where the medications struggle to penetrate [175], but where the mechanical properties of the MBs and NBs could be a significant gain.

## 8. Nanoparticle optimal design for thrombolytic therapy

### 8.1. Pharmacokinetics, biodistribution, and safety

After the intravenous administration, nanocarriers for fibrinolytic therapy are subjected to biological barriers and might pose particular safety concerns that would limit a desirable therapeutic outcome. What would be an optimal nanoparticle design to incorporate in order to load plasminogen activator and perform a safe and efficient local thrombolysis?

Primarily, favorable *in vivo* biodistribution and pharmacokinetics of the injectable inorganic, lipid, and polymeric micelle/nanoparticle must be ensured. Particle *in vivo* fate is varied and dictated by the interaction between multiple parameters: nanoparticle size, surface characteristics, stability, etc. For site-specific accumulation of the thrombolytic agent, NPs need to have sufficient circulation time *in vivo*. Ultra-small NPs with diameters <5.5 nm are rapidly filtered out by renal clearance upon intravenous administration [176]. The elimination of the larger engineered NPs by the MPS represents a substantial obstacle. Plasma proteins, including serum albumin, apolipoproteins, complement components, and immunoglobulins, bind onto the surface of circulating NPs and form the protein corona in a process called particle opsonization [177]. Subsequently, phagocytic cells of MPS – mainly resident macrophages in the spleen, lymph nodes, and liver – sequesters the NPs. There is an evident direct correlation between particle size and serum protein absorption, also meaning faster elimination [178]. Typically, rigid spherical NPs with a size of 100–200 nm are long-circulating, being large enough to avoid uptake in the liver but small enough to avoid filtration in the spleen [135]. Particles in the micrometer range (2–5 μm) accumulate within capillaries of the lungs, as well as in spleen and liver [33]. The shape of the particles has a dramatic effect on their *in vivo* destiny, as demonstrated in the filamentous polymer micelles that persisted in the circulation for up to one week after the intravenous injection – 10 times longer than the spherical ones [179]. In addition, softer, prone to deformability, NPs have prolonged circulation profiles than solid ones with reduced splenic filtration, as investigated in the nanogels with different levels of crosslinking [180]. Irrespective of the size and shape, softer nanoconstructs evaded up to 5 times more efficiently macrophage internalization as compared to rigid nanoconstructs [181].

The biodistribution of nanomaterials is influenced by their surface characteristics. NPs with a neutral and negative surface charge, in contrast to cationic formulations, experience reduced protein adsorption that results in more extended circulation half-lives [33]. Other concerns of the cationic NPs are the stimulation of inflammatory responses of human neutrophils and increased ROS production that was demonstrated on the cationic liposomes [182] and solid lipid NPs [183]. Cytotoxicity was induced by both cationic polymeric and lipid NPs [184]. In addition, positively charged NPs have a high rate of cellular uptake, as revealed that polymeric microparticles with a primary amine at the surface underwent more phagocytosis as compared to the ones having sulfate, hydroxyl, or carboxyl groups [178]. This makes cationic NPs a suitable vehicle for gene delivery; however, it would probably be preferred to design anionic nanoformulation for thrombolysis.

To avert the opsonization of the naked circulating NPs, their surface can be functionalized with PEG to create a hydrating layer that hinders the formation of a protein corona [33]. In addition to prevalent PEG, that is non-biodegradable and may cause complement activation, alternative hydrophilic polymers, such as polaxamer, polyvinyl alcohol, poly(amino acid)s, and polysaccharides [185] as well as "self" peptide CD47 [186] are researched. As a biomimetic surface, the coating of NPs with cell membranes extracted from autologous leukocytes and erythrocytes similarly extends their *in vivo* circulation [133].

Collectively, these findings demonstrate the importance of tunable particle size and surface composition & functionality for the development of long-circulating NPs for thrombolysis.

While the full analysis of the toxicology of NPs is beyond the scope of this paper, it is necessary to comment on certain safety issues of the nanomaterials used for a thrombolytic application.

NPs can perturbate vascular hemostasis and blood platelet function. Saikia et al. reported that silica NPs induced the overexpression of platelet endothelial cell adhesion molecule-1 on the endothelium that augmented the platelet-endothelial interaction [187]. Moreover, silica NPs triggered inflammation-coagulation response and thrombotic effects *in vivo* via JAK1/TF signaling pathway [188]. Amorphous silica NPs penetrated the platelet plasma membrane and stimulated an unfavorably low nitric oxide to peroxynitrite [NO]/[$ONOO^-$] ration that is crucial for cardiovascular homeostasis; they also induced platelet activation and aggregation via the MMP2 and ADP pathways [189].

Increasing concentrations of gold NPs led to a reduction in mouse body weight, red blood cell count, and hematocrit [190].

Multiple publications reported nanoparticle size-dependent toxicity. For instance, smaller gold, $SiO_2$, or polymer NPs were more hemolytic and provoked a higher level of ROS production than larger particles [191]. Cytotoxicity in four different cell lines was observed with the triphenylphosphine-stabilized gold NPs of 1–2 nm diameter, while 15-nm particles were non-toxic even at 100-fold higher concentration [192]. In a size-dependent manner, PEGylated AuNPs affected the normal function of human erythrocytes, such as deformability and oxygen-delivering ability [193]. Alterations of renal, hepatic, and splenic functions were dependent on the particle size and surface chemistry in ultrasmall SPION [194].

Distribution of the NPs in the non-target cells and organs is one of the challenges. The report of Lasagna-Reeves et al. suggested that gold NPs were able to cross the blood-brain barrier (BBB) and accumulated in the neural tissue [195]. Poly(alkyl cyanoacrylate) NPs could enter into the brain both in healthy animals and models of central nervous system diseases [196]. Siddiqi et al. concluded that AuNPs generated oxidative stress and an impairment of the antioxidant enzyme glutathione peroxidase in rat brain as well as significantly decreased the levels of dopamine and serotonin neurotransmitters [197]. Given that the BBB integrity is disrupted during ischemic stroke [198], and nano-formulation is assumed to limit the accumulation of nanoparticle-associated rtPA within the brain parenchyma to reduce the risk of cerebral hemorrhages and rtPA-mediated neurotoxicity [199], it would be vital to ensure that the nanotherapeutics are retained within the vascular compartment and do not cross the BBB.

The nanomaterials accumulate substantially in the liver upon intravenous injection. Bartneck et al. found that peptide-functionalized gold nanorods induced the prepolarization of hepatic macrophages, which aggravated a liver injury in a model of acute hepatitis [200]. High doses of silica nanorattle particles could induce liver damages, presumably due to decreased activity of superoxide dismutase [201]. Treatment with silica NPs revealed the hepatic microgranulation and splenic megakaryocyte accumulation by histological analysis [202]. Iron oxide NPs accumulated in liver phagocytes and elicited hepatic lipid peroxidation [203].

It is likely that organic biodegradable engineered NPs are of lesser concern to toxicity, as they will degrade by metabolic pathways. While the *in vitro* tests indicated that amphiphilic polymeric micelles induced an inflammatory response, no pathological changes were observed in the target organs *in vivo* [204]. Both PLGA and Cs NPs at concentrations relevant for drug-delivery application (<10 μg/mL) were platelet-compatible [205].

In contrast, inorganic non-biodegradable NPs, including multifunctional magnetic NPs, may persist for considerable periods, sometimes up to several years [206], and result in prolonged exposure with still-to-be-determined consequences. Apart from that, the growing presence of non-degradable nanotechnology products and the environmental risks need to be seriously assessed [207]. NPs composed of inorganic materials are difficult to break down by lysosomal enzymes. As an example, AuNPs accumulation in Kupffer cells in the liver and lysosome/endosome-like vesicles was present after six months post-injection in mice [208]. Moreover, Feng et al. found that dextran-coated and uncoated SPION administration affected several metabolism pathways, including energy, lipid, glucose, and amino acid metabolism in rodents [209]. PAA-coated iron oxide NPs triggered an inflammatory process *in vivo*, evidenced by abnormal differential blood count of neutrophils and large lymphocytes [203]. $Fe_3O_4$-MNPs significantly augmented ROS production *in vivo*. A sharp decline in RBC counts and hemoglobin concentration indicated an excessive degradation of erythrocytes, suggesting an associated anemia risk [210].

Generally, higher metabolic and functional injuries are prompted by uncoated NPs compared to coated ones with potential aggregation in the biological fluids. Surface modification with polymeric chains ameliorates the nanoparticle stability, masks the existing toxicity of the NPs, and extends their circulation half-life [121,211]. It is worth admitting that the NPs do not exhibit any toxicity until a certain threshold dose [121]. During the preclinical thrombolytic evaluation, it is also important to verify that the required dose of the NPs is based on estimates of potential future human exposure to avoid unrealistically high nanoparticle doses with no relevance to the clinics. Overall, this is critical to evaluate each newly engineered NPs as an individual case, since even slight changes in physicochemical properties to an existing and well-studied particle can result in a completely different toxicological profile.

### 8.2. Strategies for the nanoencapsulation of PA

PA are hydrophilic macromolecules (40–70 kDa) that require special nanoparticle design and drug complexation methods. While PA can be incorporated into the aqueous phase during nanoparticle fabrication for lipid or polymeric particles, harsh synthesis conditions – high energy processes (ultrasound, ultraturrax), elevated temperatures, the use of organic solvents – are not suitable for fragile molecules such as proteins [212]. Otherwise, the fibrinolytic agent may be attached to the surface through covalent or non-covalent protocols. The covalent methods provide more stable conjugation (avoiding “burst release”), however, they sometimes require chemical modification of the drug and might affect changes in the protein structure that might result in its partial denaturation and loss of enzymatic activity [213]. Physical adsorption is a mild drug encapsulation method that results in high loading efficacy for the nanocarriers with hydrophilic surfaces. As PA are predominantly positively charged at physiological pH with an isoelectric point (IP) $> 7$ (except for SK, IP $= 5.12$), they can form a complexation with anionic NPs due to electrostatic interactions. The existence of a positive charge on the polymer, as, for instance, chitosan, limits the encapsulation of cationic drugs because of repulsive interactions between a drug and polymer [212]. Comparing covalent vs. non-covalent methods, adsorptive bound PA liberates faster from the particles and diffused more readily into the fibrin matrix of the clot than covalently bound PA [128] and does not impair the biological activity of the drug [214] that may be beneficial in targeted thrombolysis. In addition, effective entrapment of hydrophilic drugs may occur in the crosslinked polymeric network of hydrogel nanoparticles that imbibe large quantities of water [215].

To sum up, depending on the type and composition of the nanocarrier, different encapsulation techniques may be applied. Extensive *in vitro* tests demonstrating high loading efficiency, sustainable release, preservation of the amidolytic and fibrinolytic activates of the PA after conjugation must be verified.

## 9. Discussion & conclusion

The rapid recanalization of the vascular occlusion is of the utmost importance for the patients suffering from acute thrombotic diseases. The innovative nanomedical approaches have been intensively proposed for targeted thrombolytic therapy to address the challenges of systemic drug administration.

The accomplishments of nanomedicine in thrombotic diseases include the protection of thrombolytics from inactivation by PAI-1, improvement in the blood half-life, enhanced thrombolytic effect at a lower dose, reduction in systemic bleeding, and post-ischemic infarct zone, etc. Recent studies have demonstrated that nanocarriers, such as liposomes, polymeric or inorganic NPs, bio-inspired nanocarriers, and microbubbles, provide benefits for thrombolytic therapy either alone or in combination with ultrasound or magnetic force (Table 2). Current nano-approaches in targeted thrombolysis are summarized schematically in Fig. 13. Among the numerous thrombolytic-bearing nanocarriers that are tested in preclinical models, sonothrombolysis with lipid-based microbubbles and intravenous rtPA is already being validated in clinical trials with thrombolysis improvement. However, lipid microbubbles

**Table 2**
Different nanocarriers for thrombolytic therapy.

| Nanocarriers | Advantages | Disadvantages | Therapeutic effects |
|---|---|---|---|
| Liposomes | • Biodegradable, biocompatible, non-toxic<br>• Clinically approved | • Low PA encapsulation rate<br>• Low stability<br>• Phospholipids may undergo oxidation and hydrolysis | • Improved thrombolysis rate<br>• Lower risks of hemorrhages |
| Polymeric | • Biocompatible and often biodegradable<br>• Easy surface functionalization | • High PA encapsulation rate<br>• Improved stability | • Superior thrombolytic efficacy<br>• Accelerated thrombolysis<br>• Protection BBB permeability damage<br>• Increased survival *in vivo*<br>• Improved neurological deficit<br>• Reduction in cerebral ROS<br>• Reduction in subarachnoid hemorrhage |
| Inorganic $Fe_3O_4$ NPs AuNPs | • Biocompatible<br>• Superparamagnetic properties<br>• Magnet-guided thrombolysis<br>• Optical and photothermal properties<br>• Multifunctional theranostic systems | • May enter BBB and generate ROS<br>• Accumulation in the body<br>• May induce immunogenic response or inflammation | • Faster vessel recanalization<br>• Mechanical clot dissolution with an external magnet<br>• Hyperthermia as adjuvant therapy<br>• Increased blood flow rate<br>• Reduction in infarct volume |
| Bio-inspired | • Prolonged *in vivo* circulation<br>• Natural thrombus targeting | • Low reproducibility<br>• Lack of standardization<br>• Source availability<br>• Immunogenicity<br>• Scale-up | • Improved survival rate<br>• Superior thrombolytic efficacy<br>• Lower neurological deficit score<br>• Smaller ischemic zone<br>• Better neurological outcome<br>• Diminished ROS level in the brain<br>• Lower risk of hemorrhages |
| US-responsive | • Enhanced thrombolysis with US insonation<br>• Biocompatibility<br>• US imaging | • Low stability<br>• Merging into big MBs<br>• Vessel occlusion | • US stable cavitation - higher penetration of drugs or MBs into the clot<br>• US inertial cavitation: sonothrombolysis |

Abbreviations: *PA*, plasminogen activator; *BBB*, blood-brain barrier; *NPs*, nanoparticles; *ROS*, reactive oxygen species; *US*, ultrasound; *MBs*, microbubbles.

may coalesce and form resonant bubbles with a size of over 20 μm [158], inducing the risk of pulmonary embolism [155]. Alternatively, polymeric microbubbles have enhanced stability *in vivo* over the soft shell ones [216], and the recent work [217] described echogenic polymeric fucoidan-functionalized microbubbles, able to target thrombosis via P-selectin interactions.

Active drug targeting of the nanocarriers allows drug accumulation at the thrombus site and has the potential to enhance thrombolytic penetration into deeply localized thrombi. This is currently realized by directing NPs mostly towards fibrin and platelets, though, identification of the new target molecules and development of the inexpensive and specific targeting moieties will be useful. Fucoidan, which is at present under clinical investigation as a diagnostic agent for the imaging of thrombosis [218,219], may become an affordable and high-quality alternative to antibodies and peptides. Another thrombus targeting strategy relies on the use of magnetic NPs under external magnetic force irradiation. Yet, despite an abundance of preclinical works dealing with magnetic field-assisted guiding, there is no clinically approved medical device to impose a high magnetic force on NPs in deep blood vessels. Therefore, it is probably preferable to design NPs capable of targeting thrombosis without external triggers.

A growing number of reports demonstrate a controlled release of the thrombolytics. On top of the ultrasound that can control the drug release from the echogenic liposomes, microbubbles, and some polymer (gelatin and chitosan) NPs, other strategies, such as enzyme exposure ($sPLA_2$ or thrombin), pH, temperature, shear stress, magnet, are employed (Fig. 13).

Apart from the necessity of the rapid restoration of blood flow after thrombotic occlusions, combating the ischemia-reperfusion injury such as inflammation and oxidative damage is vital for a good prognosis. Hence, complementing fibrinolytic therapy with nanodelivery of a potent antioxidant would be a sensible approach. For instance, poly (isobutyl cyanoacrylate)-polysaccharide NPs bearing microRNA-155–5p were proposed as a cardio-protective therapy for MI due to their antioxidant and cytoprotective properties [220]. Besides, rtPA might be accompanied by neuroprotection to prevent brain injury and neuronal damage during or after exposure to ischemia following acute ischemic stroke [221]. Discovery of next-generation thrombolytic drugs is further required to improve the safety and efficacy of nanomedicine-based thrombolysis. Goulay et al. engineered a non-neurotoxic rtPA variant with an equal fibrinolytic potential but without stimulating NMDA-dependent neurotoxicity [222].

The design of theranostic nanosystems with both thrombolytics and imaging agents (e.g., NIR fluorescent probes, gold, iron oxides, or perfluorocarbon) integrates diagnostic and therapeutic modalities. This strategy may not only provide visualization of drug delivery in real-time but also evaluate the effectiveness of treatment by MRI, CT, or US.

It is critical to face the challenges of nanomedicine, particularly in an attempt for clinical translation. To ensure clinical safety, the potential toxicity of NPs needs to be considered with a careful examination of their physical and chemical characteristics and accumulation in the non-target organs and tissues [223]. Indeed, some NPs may cause oxidative stress generation, immunological response, protein misfolding, immune response, and DNA damage [121]. Selecting biocompatible and fully biodegradable materials with FDA-approval, as well as a scalable production of the nanoformulations according to Good Manufacturing Practice (GMP), is essential [224]. Incorporation of sophisticated nanodesigns (e.g., cell-derived biomimetic surfaces) should accord with a risk analysis of reproducibility, quality control, and toxicity that might complicate regulatory approvals [33].

There is an evident gap between scientific discovery and clinical practice in nanomedicine-guided thrombolytic therapy. An astonishing ~10-fold increase from 2010 to 2020 in the number of publications in the field with beneficial therapeutic effects demonstrates a solid argument towards an imminent clinical translation. At the development stage, the tendency is to design complex targeted biomimetic multifunctional nanocarriers, sometimes bearing several active molecules. By examining nanoparticle delivery systems that are currently approved or under clinical investigation [35,36], we speculate that the first nanoparticulate candidate for site-specific delivery of PA tested in humans will probably be built on long-established technologies – primarily PEGylated liposomes, but also albumin-coated PA or nanocarriers from FDA-approved polymers. More sophisticated systems with targeting moieties, stimuli-responsive control of drug release will follow.

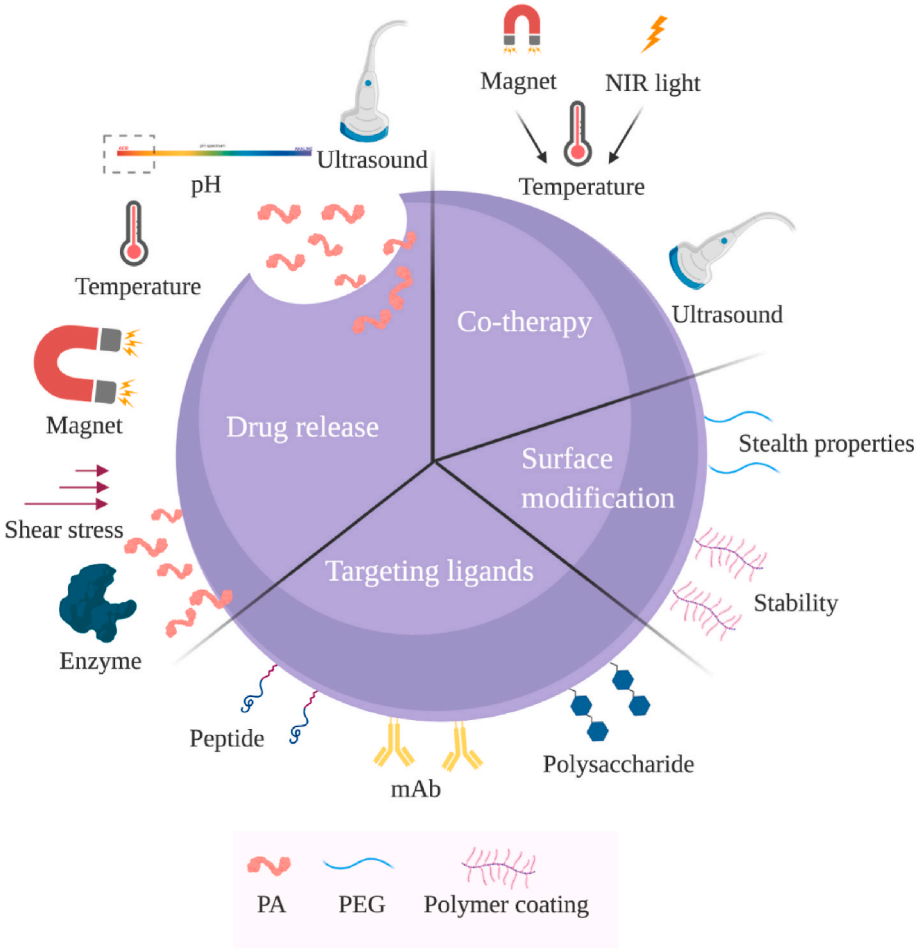


**Fig. 13.** Schematic illustration of the main strategies in the development of thrombolytic drug delivery nanocarriers. Surface modification with PEG or other hydrophilic polymeric chains is effectuated to ameliorate the nanoparticle stability, prevent the opsonization, and extend the nanoparticle blood circulation time. Nanoparticles may be decorated with targeting moieties against thrombus biomarkers with monoclonal antibodies, peptides, or sulfated polysaccharide fucoidan to attain site-specific thrombolysis. Several endogenous (enzymes in the thrombi, high shear stress in stenotic vessels, or low pH in the ischemic area) and exogenous (magnetic field, elevated temperature, ultrasound) principles are researched for the spatial & temporal control of PA release, prior incorporated either in the core of the nanoparticles or onto their surface. As an adjuvant therapy, ultrasound irradiation or elevated temperature by magnet and NIR light enhances nanomedicine-assisted thrombolytic efficacy. Abbreviations: *PA*, plasminogen activator; *mAb*, monoclonal antibody; *PEG*, Polyethylene glycol; *NIR*, near-infrared.

Meanwhile, public initiatives contribute to nanomedicine development. Recently, the European Union project NanoAthero (http://www.nanoathero.eu/) was completed. It intended to use nanomedicine for molecular imaging and targeted treatment of atherothrombosis with research activities ranging from nanosystems design to clinical validation and industrial production [225]. Several Phase I clinical trials demonstrated its feasibility for patients [219,226–228]. This consortium of 16 partners lasted 5.5 years (February 2013–July 2018) with the European Commission contribution of 10 million euros.

To conclude, the development of novel nanoparticulate strategies with plasminogen activators for the treatment of thrombotic disease will continue to flourish as they represent a potent evolution to free drug administration. The encouraging results in preclinical research predict future clinical translation of some of the formulations and progress in the nanomedicine-based precise therapy of thrombotic pathologies.

## Author contributions

Alina Zenych: Conceptualization, Writing - original draft, Visualization; Louise Fournier: Writing - original draft (Section: 7 Ultrasound-Responsive Carriers & Sonothrombolysis), Visualization; Cédric Chauvierre: Writing - review & editing, Supervision, Funding acquisition.

## Declaration of competing interest

The authors declare that they have no known competing financial interests or personal relationships that could have appeared to influence the work reported in this paper.

## Acknowledgment

Authors thank INSERM, Université de Paris, and Université Sorbonne Paris Nord for the financial support. This work also received funding from the EU project FP7-NMP-2012-LARGE-6-309820 “NanoAthero”. Alina Zenych is grateful for the Ph.D. fellowship from the INSPIRE program of the European Union’s Horizon 2020 research and innovation program (Marie Sklodowska-Curie grant # 665850). The illustrations were designed with BioRender software (biorender.com).

## References

[1] World Health Organisation (WHO), [Internet] World Health Organization, Media Centre: Cardiovascular disease, 2020. https://www.who.int/health-topics/cardiovascular-diseases/#tab=tab_1.

[2] E.J. Benjamin, P. Muntner, A. Alonso, M.S. Bittencourt, C.W. Callaway, A. P. Carson, A.M. Chamberlain, A.R. Chang, S. Cheng, S.R. Das, F.N. Delling, L. Djousse, M.S.V. Elkind, J.F. Ferguson, M. Fornage, L.C. Jordan, S.S. Khan, B. M. Kissela, K.L. Knutson, T.W. Kwan, D.T. Lackland, T.T. Lewis, J.H. Lichtman, C. T. Longenecker, M.S. Loop, P.L. Lutsey, S.S. Martin, K. Matsushita, A.E. Moran, M.E. Mussolino, M. O'Flaherty, A. Pandey, A.M. Perak, W.D. Rosamond, G. A. Roth, U.K.A. Sampson, G.M. Satou, E.B. Schroeder, S.H. Shah, N.L. Spartano, A. Stokes, D.L. Tirschwell, C.W. Tsao, M.P. Turakhia, L.B. VanWagner, J. T. Wilkins, S.S. Wong, S.S. Virani, Heart disease and stroke statistics—2019 update: a report from the American heart association, Circulation (2019), https://doi.org/10.1161/CIR.0000000000000659.

[3] H. Thomas, J. Diamond, A. Vieco, S. Chaudhuri, E. Shinnar, S. Cromer, P. Perel, G.A. Mensah, J. Narula, C.O. Johnson, G.A. Roth, A.E. Moran, Global atlas of cardiovascular disease 2000-2016: the path to prevention and control, Glob. Heart. 13 (2018) 143–163, https://doi.org/10.1016/j.gheart.2018.09.511.

[4] J. Leal, R. Luengo-Fernández, A. Gray, S. Petersen, M. Rayner, Economic burden of cardiovascular diseases in the enlarged European Union, Eur. Heart J. 27 (2006) 1610–1619, https://doi.org/10.1093/eurheartj/ehi733.

[5] D.N. Granger, P.R. Kvietys, Reperfusion injury and reactive oxygen species: the evolution of a concept, Redox Biol 6 (2015) 524–551, https://doi.org/10.1016/j.redox.2015.08.020.

[6] C.K. Glass, J.L. Witztum, Atherosclerosis: the road ahead, Cell 104 (2001) 503–516, https://doi.org/10.5005/jp/books/12883_4.

[7] E. Falk, Pathogenesis of atherosclerosis, J. Am. Coll. Cardiol. 47 (2006) C7–C12, https://doi.org/10.1016/j.jacc.2005.09.068.

[8] Y.S. Chatzizisis, A.U. Coskun, M. Jonas, E.R. Edelman, C.L. Feldman, P.H. Stone, Role of endothelial shear stress in the natural history of coronary atherosclerosis and vascular remodeling. Molecular, cellular, and vascular behavior, J. Am. Coll. Cardiol. 49 (2007) 2379–2393, https://doi.org/10.1016/j.jacc.2007.02.059.

[9] G.G. Caro, Discovery of the role of wall shear in atherosclerosis, Arterioscler. Thromb. Vasc. Biol. 29 (2009) 158–161, https://doi.org/10.1161/ATVBAHA.108.166736.

[10] J. Jongstra-Bilen, M. Haidari, S.N. Zhu, M. Chen, D. Guha, M.I. Cybulsky, Low-grade chronic inflammation in regions of the normal mouse arterial intima predisposed to atherosclerosis, J. Exp. Med. 203 (2006) 2073–2083, https://doi.org/10.1084/jem.20060245.

[11] P. Libby, Inflammation in atherosclerosis, Nature 420 (2002) 868–874, https://doi.org/10.1038/nature01323.

[12] Z.S. Galis, G.K. Sukhova, R. Kranzhöfer, S. Clark, P. Libby, Macrophage foam cells from experimental atheroma constitutively produce matrix-degrading proteinases, Proc. Natl. Acad. Sci. U.S.A. 92 (1995) 402–406, https://doi.org/10.1073/pnas.92.2.402.

[13] M.R. Dweck, E. Aikawa, D.E. Newby, J.M. Tarkin, J.H.F. Rudd, J. Narula, Z. A. Fayad, Noninvasive molecular imaging of disease activity in atherosclerosis, Circ. Res. 119 (2016) 330–340, https://doi.org/10.1161/CIRCRESAHA.116.307971.

[14] A. Shioi, Y. Ikari, Plaque calcification during atherosclerosis progression and regression, J. Atherosclerosis Thromb. 25 (2018) 294–303, https://doi.org/10.5551/jat.RV17020.

[15] G. Lippi, M. Franchini, G. Targher, Arterial thrombus formation in cardiovascular disease, Nat. Rev. Cardiol. 8 (2011) 502–512, https://doi.org/10.1038/nrcardio.2011.91.

[16] N. Mackman, Triggers, targets and treatments for thrombosis, Nature 451 (2008) 914–918, https://doi.org/10.1038/nature06797.

[17] I. Martinelli, P. Bucciarelli, P.M. Mannucci, Thrombotic risk factors: basic pathophysiology, Crit. Care Med. 38 (2010), https://doi.org/10.1097/CCM.0b013e3181c9cbd9.

[18] C.T. Esmon, Basic mechanisms and pathogenesis of venous thrombosis, Blood Rev. 23 (2009) 225–229, https://doi.org/10.1016/j.blre.2009.07.002.

[19] J.A. López, J. Chen, Pathophysiology of venous thrombosis, Thromb. Res. 123 (2009) 30–34, https://doi.org/10.1016/S0049-3848(09)70140-9.

[20] A. Bivard, L. Lin, M.W. Parsonsb, Review of stroke thrombolytics, J. Stroke. 15 (2013) 90, https://doi.org/10.5853/jos.2013.15.2.90.

[21] C. Kluft, J.J. Sidelmann, J.B. Gram, Assessing safety of thrombolytic therapy, Semin. Thromb. Hemost. 43 (2017) 300–310, https://doi.org/10.1055/s-0036-1584130.

[22] R.S. Marshall, Progress in intravenous thrombolytic therapy for acute stroke, JAMA Neurol 72 (2015) 928–934, https://doi.org/10.1001/jamaneurol.2015.0835.

[23] V.J. Marder, Thrombolytic therapy. Consult. Hemost. Thromb., Elsevier, 2013, pp. 526–537, https://doi.org/10.1016/B978-1-4557-2296-9.00028-2.

[24] J. Schaller, S.S. Gerber, The plasmin-antiplasmin system: structural and functional aspects, Cell, Mol. Life Sci. 68 (2011) 785–801, https://doi.org/10.1007/s00018-010-0566-5.

[25] A. Pal Khasa, Y. Pal Khasa, The evolution of recombinant thrombolytics: current status and future directions, Bioengineered 8 (2017) 331–358, https://doi.org/10.1080/21655979.2016.1229718.

[26] G.N. Levine, E.R. Bates, J.C. Blankenship, S.R. Bailey, J.A. Bittl, B. Cercek, C. E. Chambers, S.G. Ellis, R.A. Guyton, S.M. Hollenberg, U.N. Khot, R.A. Lange, L. Mauri, R. Mehran, I.D. Moussa, D. Mukherjee, H.H. Ting, P.T. O'Gara, F. G. Kushner, D.D. Ascheim, R.G. Brindis, D.E. Casey, M.K. Chung, J.A. De Lemos, D.B. Diercks, J.C. Fang, B.A. Franklin, C.B. Granger, H.M. Krumholz, J. A. Linderbaum, D.A. Morrow, L.K. Newby, J.P. Ornato, N. Ou, M.J. Radford, J. E. Tamis-Holland, C.L. Tommaso, C.M. Tracy, Y.J. Woo, D.X. Zhao, 2015 ACC/AHA/SCAI focused update on primary percutaneous coronary intervention for patients with ST-elevation myocardial infarction an update of the 2011 ACCF/AHA/SCAI guideline for percutaneous coronary intervention and the 2013 ACCF/AHA guideline for th, J. Am. Coll. Cardiol. 67 (2016) 1235–1250, https://doi.org/10.1016/j.jacc.2015.10.005.

[27] B. Ibanez, S. James, S. Agewall, M.J. Antunes, C. Bucciarelli-Ducci, H. Bueno, A.L. P. Caforio, F. Crea, J.A. Goudevenos, S. Halvorsen, G. Hindricks, A. Kastrati, M. J. Lenzen, E. Prescott, M. Roffi, M. Valgimigli, C. Varenhorst, P. Vranckx, P. Widimský, A. Baumbach, R. Bugiardini, I.M. Coman, V. Delgado, D. Fitzsimons, O. Gaemperli, A.H. Gershlick, S. Gielen, V.P. Harjola, H.A. Katus, J. Knuuti, P. Kolh, C. Leclercq, G.Y.H. Lip, J. Morais, A.N. Neskovic, F.J. Neumann, A. Niessner, M.F. Piepoli, D.J. Richter, E. Shlyakhto, I.A. Simpson, P.G. Steg, C. J. Terkelsen, K. Thygesen, S. Windecker, J.L. Zamorano, U. Zeymer, M. Chettibi, H.G. Hayrapetyan, B. Metzler, F. Ibrahimov, V. Sujayeva, C. Beauloye, L. Dizdarevic-Hudic, K. Karamfiloff, B. Skoric, L. Antoniades, P. Tousek, C. J. Terkelsen, S.M. Shaheen, T. Marandi, M. Niemelᵭa, S. Kedev, M. Gilard, A. Aladashvili, A. Elsaesser, I.G. Kanakakis, B. Merkely, T. Gudnason, Z. Iakobishvili, L. Bolognese, S. Berkinbayev, G. Bajraktari, M. Beishenkulov, I. Zake, H. Ben Lamin, O. Gustiene, B. Pereira, R.G. Xuereb, S. Ztot, V. Juliebø, J. Legutko, A.T. Timoteo, G. Tatu-Chitoiu, A. Yakovlev, L. Bertelli, M. Nedeljkovic, M. Studencan, M. Bunc, A.M.G. de Castro, P. Petursson, R. Jeger, M.S. Mourali, A. Yildirir, A. Parkhomenko, C.P. Gale, 2017 ESC Guidelines for the management of acute myocardial infarction in patients presenting with ST-segment elevation, Eur. Heart J. 39 (2018) 119–177, https://doi.org/10.1093/eurheartj/ehx393.

[28] G. Turc, P. Bhogal, U. Fischer, P. Khatri, K. Lobotesis, M. Mazighi, P. D. Schellinger, D. Toni, J. de Vries, P. White, J. Fiehler, European stroke organisation (ESO) – European society for minimally invasive neurological therapy (ESMINT) guidelines on mechanical thrombectomy in acute ischaemic StrokeEndorsed by stroke alliance for europe (SAFE), Eur. Stroke J. 4 (2019) 6–12, https://doi.org/10.1177/2396987319832140.

[29] W.J. Powers, A.A. Rabinstein, T. Ackerson, O.M. Adeoye, N.C. Bambakidis, K. Becker, J. Biller, M. Brown, B.M. Demaerschalk, B. Hoh, E.C. Jauch, C. S. Kidwell, T.M. Leslie-Mazwi, B. Ovbiagele, P.A. Scott, K.N. Sheth, A. M. Southerland, D.V. Summers, D.L. Tirschwell, Guidelines for the early management of patients with acute ischemic stroke: 2019 update to the 2018 guidelines for the early management of acute ischemic stroke: a guideline for healthcare professionals from the American heart association/American stroke, Stroke 50 (2019) e344–e418, https://doi.org/10.1161/STR.0000000000000211.

[30] L. Derex, T.H. Cho, Mechanical thrombectomy in acute ischemic stroke, Rev. Neurol. (Paris) 173 (2017) 106–113, https://doi.org/10.1016/j.neurol.2016.06.008.

[31] S.A. Munich, K. Vakharia, E.I. Levy, Overview of mechanical thrombectomy techniques, Clin. Neurosurg. 85 (2019) S60–S67, https://doi.org/10.1093/neuros/nyz071.

[32] G. Forestier, B. Kerleroux, K. Janot, F. Zhu, V. Dumas, J.-F. Hak, E. Shotar, W. BenHassen, R. Bourcier, S. Soize, J. Berge, O. Naggara, H. Desal, G. Boulouis, A. Rouchaud, Mechanical thrombectomy practices in France: exhaustive survey of centers and individual operators, J. Neuroradiol. (2020) 1–14, https://doi.org/10.1016/j.neurad.2020.05.001.

[33] E. Blanco, H. Shen, M. Ferrari, Principles of nanoparticle design for overcoming biological barriers to drug delivery, Nat. Biotechnol. 33 (2015) 941–951, https://doi.org/10.1038/nbt.3330.

[34] Y. Barenholz, Doxil® - the first FDA-approved nano-drug: lessons learned, J. Contr. Release 160 (2012) 117–134, https://doi.org/10.1016/j.jconrel.2012.03.020.

[35] A.C. Anselmo, S. Mitragotri, Nanoparticles in the clinic, Bioeng. Transl. Med. 1 (2016) 10–29, https://doi.org/10.1002/btm2.10003.

[36] A.C. Anselmo, S. Mitragotri, Nanoparticles in the clinic: an update, Bioeng. Transl. Med. 4 (2019) 1–16, https://doi.org/10.1002/btm2.10143.

[37] T. Matoba, J.-I. Koga, K. Nakano, K. Egashira, H. Tsutsui, Nanoparticle-mediated drug delivery system for atherosclerotic cardiovascular disease, J. Cardiol. 70 (2017) 206–211, https://doi.org/10.1016/j.jjcc.2017.03.005.

[38] T. Alam, S. Khan, B. Gaba, M.F. Haider, S. Baboota, J. Ali, Nanocarriers as treatment modalities for hypertension, Drug Deliv. 24 (2017) 358–369, https://doi.org/10.1080/10717544.2016.1255999.

[39] C.K.W. Chan, L. Zhang, C.K. Cheng, H. Yang, Y. Huang, X.Y. Tian, C.H.J. Choi, Recent advances in managing atherosclerosis via nanomedicine, Small 14 (2018) 1–16, https://doi.org/10.1002/smll.201702793.

[40] T. Cyrus, S.A. Wickline, G.M. Lanza, Nanotechnology in interventional cardiology, Wiley Interdiscip. Rev. Nanomedicine Nanobiotechnology. 4 (2012) 82–95, https://doi.org/10.1002/wnan.154.

[41] L. Yu, B.J. Scherlag, K. Dormer, K.T. Nguyen, C. Pope, K.M. Fung, S.S. Po, Autonomic denervation with magnetic nanoparticles, Circulation 122 (2010) 2653–2659, https://doi.org/10.1161/CIRCULATIONAHA.110.940288.

[42] T. Simon-Yarza, I. Bataille, D. Letourneur, Cardiovascular bio-engineering: current state of the art, J. Cardiovasc. Transl. Res. 10 (2017) 180–193, https://doi.org/10.1007/s12265-017-9740-6.

[43] D.R. Esfahani, V. Viswanathan, A. Alaraj, Nanoparticles and stem cells–has targeted therapy for aneurysms finally arrived? Neurol. Res. 37 (2015) 269–277, https://doi.org/10.1179/1743132814Y.0000000435.

[44] C. Psarros, R. Lee, M. Margaritis, C. Antoniades, Nanomedicine for the prevention, treatment and imaging of atherosclerosis, Nanomed. Nanotechnol. Biol. Med. 8 (2012) S59–S68, https://doi.org/10.1016/j.nano.2012.05.006.

[45] B. Singh, T. Garg, A.K. Goyal, G. Rath, Recent advancements in the cardiovascular drug carriers, Artif. Cells, Nanomedicine Biotechnol 44 (2016) 216–225, https://doi.org/10.3109/21691401.2014.937868.

[46] C.H. Liu, H.L. Hsu, J.P. Chen, T. Wu, Y.H. Ma, Thrombolysis induced by intravenous administration of plasminogen activator in magnetoliposomes: dual targeting by magnetic and thermal manipulation, Nanomed. Nanotechnol. Biol. Med. 20 (2019) 1–12, https://doi.org/10.1016/j.nano.2019.03.014.

[47] X. Wang, C. Wei, M. Liu, T. Yang, W. Zhou, Y. Liu, K. Hong, S. Wang, H. Xin, X. Ding, Near-infrared triggered release of uPA from nanospheres for localized hyperthermia-enhanced thrombolysis, Adv. Funct. Mater. 27 (2017) 1–8, https://doi.org/10.1002/adfm.201701824.

[48] T. Mei, A. Kim, L.B. Vong, A. Marushima, S. Puentes, Y. Matsumaru, A. Matsumura, Y. Nagasaki, Encapsulation of tissue plasminogen activator in pH-sensitive self-assembled antioxidant nanoparticles for ischemic stroke treatment-Synergistic effect of thrombolysis and antioxidant, Biomaterials 215 (2019) 1–12, https://doi.org/10.1016/j.biomaterials.2019.05.020.

[49] Q.L. Zhou, Z.Y. Chen, Y.X. Wang, F. Yang, Y. Lin, Y.Y. Liao, Ultrasound-mediated local drug and gene delivery using nanocarriers, BioMed Res. Int. 2014 (2014), https://doi.org/10.1155/2014/963891.

[50] V. Karagkiozaki, S. Logothetidis, A.M. Pappa, Nanomedicine for atherosclerosis: molecular imaging and treatment, J. Biomed. Nanotechnol. 11 (2015) 191–210, https://doi.org/10.1166/jbn.2015.1943.

[51] Z. Tang, D. Li, X. Wang, H. Gong, Y. Luan, Z. Liu, J.L. Brash, H. Chen, A t-PA/nanoparticle conjugate with fully retained enzymatic activity and prolonged circulation time, J. Mater. Chem. B. 3 (2015) 977–982, https://doi.org/10.1039/c4tb01625d.
[52] S. Absar, K. Nahar, Y.M. Kwon, F. Ahsan, Thrombus-targeted nanocarrier attenuates bleeding complications associated with conventional thrombolytic therapy, Pharm. Res. (N. Y.) 30 (2013) 1663–1676, https://doi.org/10.1007/s11095-013-1011-x.
[53] H. Jin, H. Tan, L. Zhao, W. Sun, L. Zhu, Y. Sun, H. Hao, H. Xing, L. Liu, X. Qu, Y. Huang, Z. Yang, Ultrasound-triggered thrombolysis using urokinase-loaded nanogels, Int. J. Pharm. 434 (2012) 384–390, https://doi.org/10.1016/j.ijpharm.2012.06.001.
[54] H. Kawata, Y. Uesugi, T. Soeda, Y. Takemoto, J.H. Sung, K. Umaki, K. Kato, K. Ogiwara, K. Nogami, K. Ishigami, M. Horii, S. Uemura, M. Shima, Y. Tabata, Y. Saito, A new drug delivery system for intravenous coronary thrombolysis with thrombus targeting and stealth activity recoverable by ultrasound, J. Am. Coll. Cardiol. 60 (2012) 2550–2557, https://doi.org/10.1016/j.jacc.2012.08.1008.
[55] J. Hu, S. Huang, L. Zhu, W. Huang, Y. Zhao, K. Jin, Q. Zhuge, Tissue plasminogen activator-porous magnetic microrods for targeted thrombolytic therapy after ischemic stroke, ACS Appl. Mater. Interfaces 10 (2018) 32988–32997, https://doi.org/10.1021/acsami.8b09423.
[56] N. Zhang, C. Li, D. Zhou, C. Ding, Y. Jin, Q. Tian, X. Meng, K. Pu, Y. Zhu, Cyclic RGD functionalized liposomes encapsulating urokinase for thrombolysis, Acta Biomater. 70 (2018) 227–236, https://doi.org/10.1016/j.actbio.2018.01.038.
[57] C.L. Pawlowski, W. Li, M. Sun, K. Ravichandran, D. Hickman, C. Kos, G. Kaur, A. Sen Gupta, Platelet microparticle-inspired clot-responsive nanomedicine for targeted fibrinolysis, Biomaterials 128 (2017) 94–108, https://doi.org/10.1016/j.biomaterials.2017.03.012.
[58] V. Torchilin, M. Papisov, N. Orekhova, A. Belyaev, A. Petrov, S. Ragimov, Magnetically driven thrombolytic preparation containing immobilized streptokinase-targeted transport and action, Haemostasis 18 (1988) 113-116, https://doi.org/10.1159/000215791.
[59] P.D. Nguyen, E.A. O'Rear, A.E. Johnson, E. Patterson, T.L. Whitsett, R. Bhakta, Accelerated thrombolysis and reperfusion in a canine model of myocardial infarction by liposomal encapsulation of streptokinase, Circ. Res. 66 (1990) 875–878, https://doi.org/10.1161/01.RES.66.3.875.
[60] T.R. Porter, R.F. LeVeen, R. Fox, A. Kricsfeld, F. Xie, Thrombolytic enhancement with perfluorocarbon-exposed sonicated dextrose albumin microbubbles, Am. Heart J. 132 (1996) 964–968, https://doi.org/10.1016/S0002-8703(96)90006-X.
[61] J.K. Leach, E. Patterson, E.A. O'Rear, Encapsulation of a plasminogen activator speeds reperfusion, lessens infarct and reduces blood loss in a canine model of coronary artery thrombosis, Thromb, Haemostasis 91 (2004) 1213–1218, https://doi.org/10.1160/th03-11-0704.
[62] J.-C. Murciano, S. Medinilla, D. Eslin, E. Atochina, D.B. Cines, V.R. Muzykantov, Prophylactic fibrinolysis through selective dissolution of nascent clots by tPA-carrying erythrocytes, Nat. Biotechnol. 21 (2003) 891–896, https://doi.org/10.1038/nbt846.
[63] M. Faria, M. Björnmalm, K.J. Thurecht, S.J. Kent, R.G. Parton, M. Kavallaris, A.P. R. Johnston, J.J. Gooding, S.R. Corrie, B.J. Boyd, P. Thordarson, A.K. Whittaker, M.M. Stevens, C.A. Prestidge, C.J.H. Porter, W.J. Parak, T.P. Davis, E.J. Crampin, F. Caruso, Minimum information reporting in bio–nano experimental literature, Nat. Nanotechnol. 13 (2018) 777–785, https://doi.org/10.1038/s41565-018-0246-4.
[64] T.W. Chung, S.S. Wang, W.J. Tsai, Accelerating thrombolysis with chitosan-coated plasminogen activators encapsulated in poly-(lactide-co-glycolide) (PLGA) nanoparticles, Biomaterials 29 (2008) 228–237, https://doi.org/10.1016/j.biomaterials.2007.09.027.
[65] F. Bi, J. Zhang, Y. Su, Y.C. Tang, J.N. Liu, Chemical conjugation of urokinase to magnetic nanoparticles for targeted thrombolysis, Biomaterials 30 (2009) 5125–5130, https://doi.org/10.1016/j.biomaterials.2009.06.006.
[66] Y.-H. Ma, S.-Y. Wu, T. Wu, Y.-J. Chang, M.-Y. Hua, J.-P. Chen, Magnetically targeted thrombolysis with recombinant tissue plasminogen activator bound to polyacrylic acid-coated nanoparticles, Biomaterials 30 (2009) 3343–3351, https://doi.org/10.1016/j.biomaterials.2009.02.034.
[67] M. Juenet, R. Aid-Launais, B. Li, A. Berger, J. Aerts, V. Ollivier, A. Nicoletti, D. Letourneur, C. Chauvierre, Thrombolytic therapy based on fucoidan-functionalized polymer nanoparticles targeting P-selectin, Biomaterials 156 (2018) 204–216, https://doi.org/10.1016/j.biomaterials.2017.11.047.
[68] J.R. McCarthy, I.Y. Sazonova, S.S. Erdem, T. Hara, B.D. Thompson, P. Patel, I. Botnaru, C.P. Lin, G.L. Reed, R. Weissleder, F.A. Jaffer, Multifunctional nanoagent for thrombus-targeted fibrinolytic therapy, Nanomedicine 7 (2012) 1017–1028, https://doi.org/10.2217/nnm.11.179.
[69] J. Zhou, D. Guo, Y. Zhang, W. Wu, H. Ran, Z. Wang, Construction and evaluation of Fe3O4-based PLGA nanoparticles carrying rtPA used in the detection of thrombosis and in targeted thrombolysis, ACS Appl. Mater. Interfaces 6 (2014) 5566–5576, https://doi.org/10.1021/am406008k.
[70] S.D. Tiukinhoy-Laing, S. Huang, M. Klegerman, C.K. Holland, D.D. McPherson, Ultrasound-facilitated thrombolysis using tissue-plasminogen activator-loaded echogenic liposomes, Thromb. Res. 119 (2007) 777–784, https://doi.org/10.1016/j.thromres.2006.06.009.
[71] L. Ma, Y. Wang, S. Zhang, X. Qian, N. Xue, Z. Jiang, O. Akakuru, J. Li, Y. Xu, A. Wu, Deep penetration of targeted nanobubbles enhanced cavitation effect on thrombolytic capacity, Bioconjugate Chem. 31 (2020) 369–374, https://doi.org/10.1021/acs.bioconjchem.9b00653.
[72] N. Korin, M. Kanapathipillai, B.D. Matthews, M. Crescente, A. Brill, T. Mammoto, K. Ghosh, S. Jurek, S.A. Bencherif, D. Bhatta, A.U. Coskun, C.L. Feldman, D. D. Wagner, D.E. Ingber, Shear-activated nanotherapeutics for drug targeting to obstructed blood vessels, Science 337 (2012) 738–742, https://doi.org/10.1126/science.1217815.
[73] Y. Uesugi, H. Kawata, Y. Saito, Y. Tabata, Ultrasound-responsive thrombus treatment with zinc-stabilized gelatin nano-complexes of tissue-type plasminogen activator, J. Drug Target. 20 (2012) 224–234, https://doi.org/10.3109/1061186X.2011.633259.
[74] S.T. Gunawan, K. Kempe, T. Bonnard, J. Cui, K. Alt, L.S. Law, X. Wang, E. Westein, G.K. Such, K. Peter, C.E. Hagemeyer, F. Caruso, Multifunctional thrombin-activatable polymer capsules for specific targeting to activated platelets, Adv. Mater. 27 (2015) 5153–5157, https://doi.org/10.1002/adma.201502243.
[75] E. Voros, M. Cho, M. Ramirez, A.L. Palange, E. De Rosa, J. Key, Z. Garami, A. B. Lumsden, P. Decuzzi, TPA immobilization on iron oxide nanocubes and localized magnetic hyperthermia accelerate blood clot lysis, Adv. Funct. Mater. 25 (2015) 1709–1718, https://doi.org/10.1002/adfm.201404354.
[76] J. Xu, Y. Zhang, J. Xu, G. Liu, C. Di, X. Zhao, X. Li, Y. Li, N. Pang, C. Yang, Y. Li, B. Li, Z. Lu, M. Wang, K. Dai, R. Yan, S. Li, G. Nie, Engineered nanoplatelets for targeted delivery of plasminogen activators to reverse thrombus in multiple mouse thrombosis models, Adv. Mater. 1905145 (2019) 1–14, https://doi.org/10.1002/adma.201905145.
[77] U. Bulbake, S. Doppalapudi, N. Kommineni, W. Khan, Liposomal formulations in clinical use: an updated review, Pharmaceutics 9 (2017) 1–33, https://doi.org/10.3390/pharmaceutics9020012.
[78] S. Mallick, J.S. Choi, Liposomes: versatile and biocompatible nanovesicles for efficient biomolecules delivery, J. Nanosci. Nanotechnol. 14 (2014) 755–765, https://doi.org/10.1166/jnn.2014.9080.
[79] K. Bowey, J.F. Tanguay, M. Tabrizian, Liposome technology for cardiovascular disease treatment and diagnosis, Expet Opin. Drug Deliv. 9 (2012) 249–265, https://doi.org/10.1517/17425247.2012.647908.
[80] J. Jamasbi, K. Ayabe, S. Goto, B. Nieswandt, K. Peter, W. Siess, Platelet receptors as therapeutic targets: past, present and future, Thromb. Haemostasis 117 (2017) 1249–1257, https://doi.org/10.1160/TH16-12-0911.
[81] S. Koudelka, R. Mikulik, J. Mašek, M. Raška, P. Turánek Knotigová, A.D. Miller, J. Turánek, Liposomal nanocarriers for plasminogen activators, J. Contr. Release 227 (2016) 45–57, https://doi.org/10.1016/j.jconrel.2016.02.019.
[82] B. Vaidya, G.P. Agrawal, S.P. Vyas, Platelets directed liposomes for the delivery of streptokinase: development and characterization, Eur. J. Pharmaceut. Sci. 44 (2011) 589–594, https://doi.org/10.1016/j.ejps.2011.10.004.
[83] Y. Huang, L. Yu, J. Ren, B. Gu, C. Longstaff, A.D. Hughes, S.A. Thom, X.Y. Xu, R. Chen, An activated-platelet-sensitive nanocarrier enables targeted delivery of tissue plasminogen activator for effective thrombolytic therapy, J. Contr. Release 300 (2019) 1–12, https://doi.org/10.1016/j.jconrel.2019.02.033.
[84] D. Varon, E. Shai, Platelets and their microparticles as key players in pathophysiological responses, J. Thromb. Haemostasis 13 (2015) S40–S46, https://doi.org/10.1111/jth.12976.
[85] H.-L. Hsu, J.-P. Chen, Preparation of thermosensitive magnetic liposome encapsulated recombinant tissue plasminogen activator for targeted thrombolysis, J. Magn. Magn Mater. 427 (2017) 188–194, https://doi.org/10.1016/j.jmmm.2016.10.122.
[86] P. Ghasemiyeh, S. Mohammadi-Samani, Solid lipid nanoparticles and nanostructured lipid carriers as novel drug delivery systems: applications, advantages and disadvantages, Res. Pharm. Sci. 13 (2018) 288–303, https://doi.org/10.4103/1735-5362.235156.
[87] J.N. Marsh, G. Hu, M.J. Scott, H. Zhang, M.J. Goette, J. Patrick, S.D. Caruthers, S. A. Wickline, D. Abendschein, M. Gregory, A fibrin-specific thrombolytic nanomedicine approach to acute ischemic stroke, Nanomedicine 6 (2011) 605–615, https://doi.org/10.2217/nnm.11.21.A.
[88] A. Bolhassani, S. Javanzad, T. Saleh, M. Hashemi, M.R. Aghasadeghi, Polymeric nanoparticles. Potent vectors for vaccine delivery targeting cancer and infectious diseases, Hum. Vaccines Immunother. 10 (2014) 321–332, https://doi.org/10.4161/hv.26796.
[89] Y. Zhang, T. Sun, C. Jiang, Biomacromolecules as carriers in drug delivery and tissue engineering, Acta Pharm. Sin. B. 8 (2018) 34–50, https://doi.org/10.1016/j.apsb.2017.11.005.
[90] K.S. Soppimath, T.M. Aminabhavi, A.R. Kulkarni, W.E. Rudzinski, Biodegradable polymeric nanoparticles as drug delivery devices, J. Contr. Release 70 (2001) 1–20, https://doi.org/10.1016/S0168-3659(00)00339-4.
[91] J. Zhang, W. Xia, P. Liu, Q. Cheng, T. Tahirou, W. Gu, B. Li, Chitosan modification and pharmaceutical/biomedical applications, Mar. Drugs 8 (2010) 1962–1987, https://doi.org/10.3390/md8071962.
[92] H.J. Jin, H. Zhang, M.L. Sun, B.G. Zhang, J.W. Zhang, Urokinase-coated chitosan nanoparticles for thrombolytic therapy: preparation and pharmacodynamics in vivo, J. Thromb. Thrombolysis 36 (2013) 458–468, https://doi.org/10.1007/s11239-013-0951-7.
[93] H. Baharifar, G. Tavoosidana, R. Karimi, S.A. Bidgoli, H. Ghanbari, M. A. Faramarzi, A. Amani, Optimization of self-assembled chitosan/streptokinase nanoparticles and evaluation of their cytotoxicity and thrombolytic activity, J. Nanosci. Nanotechnol. 15 (2015) 10127–10133, https://doi.org/10.1166/jnn.2015.11696.
[94] M. Shamsi, P. Zahedi, On-chip preparation of streptokinase entrapped in chitosan nanoparticles used in thrombolytic therapy potentially, J. Pharmacol. Sci. 106 (2017) 3623–3630, https://doi.org/10.1016/j.xphs.2017.08.001.
[95] J. Liao, X. Ren, B. Yang, H. Li, Y. Zhang, Z. Yin, Targeted thrombolysis by using c-RGD-modified N,N,N-Trimethyl Chitosan nanoparticles loaded with

lumbrokinase, Drug Dev. Ind. Pharm. 45 (2019) 88–95, https://doi.org/10.1080/03639045.2018.1522324.
[96] Y. Teng, H. Jin, D. Nan, M. Li, C. Fan, Y. Liu, P. Lv, W. Cui, Y. Sun, H. Hao, X. Qu, Z. Yang, Y. Huang, In vivo evaluation of urokinase-loaded hollow nanogels for sonothrombolysis on suture embolization-induced acute ischemic stroke rat model, Bioact. Mater. 3 (2018) 102–109, https://doi.org/10.1016/j.bioactmat.2017.08.001.
[97] R. Yasmin, M. Shah, S.A. Khan, R. Ali, Gelatin nanoparticles: a potential candidate for medical applications, Nanotechnol. Rev. 6 (2017) 191–207, https://doi.org/10.1515/ntrev-2016-0009.
[98] Y. Uesugi, H. Kawata, J.I. Jo, Y. Saito, Y. Tabata, An ultrasound-responsive nano delivery system of tissue-type plasminogen activator for thrombolytic therapy, J. Contr. Release 147 (2010) 269–277, https://doi.org/10.1016/j.jconrel.2010.07.127.
[99] C. Englert, J.C. Brendel, T.C. Majdanski, T. Yildirim, S. Schubert, M. Gottschaldt, N. Windhab, U.S. Schubert, Pharmapolymers in the 21st century: synthetic polymers in drug delivery applications, Prog. Polym. Sci. 87 (2018) 107–164, https://doi.org/10.1016/j.progpolymsci.2018.07.005.
[100] B. Sivaraman, A. Sylvester, A. Ramamurthi, Fibrinolytic PLGA nanoparticles for slow clot lysis within abdominal aortic aneurysms attenuate proteolytic loss of vascular elastic matrix, Mater. Sci. Eng. C-Materials Biol. Appl. 59 (2016) 145–156, https://doi.org/10.1016/j.msec.2015.09.056.
[101] M. Colasuonno, A.L. Palange, R. Aid, M. Ferreira, H. Mollica, R. Palomba, M. Emdin, M. Del Sette, C. Chauvierre, D. Letourneur, P. Decuzzi, Erythrocyte-inspired discoidal polymeric nanoconstructs carrying tissue plasminogen activator for the enhanced lysis of blood clots, ACS Nano 12 (2018) 12224–12237, https://doi.org/10.1021/acsnano.8b06021.
[102] C. Vauthier, C. Dubernet, E. Fattal, H. Pinto-Alphandary, P. Couvreur, Poly (alkylcyanoacrylates) as biodegradable materials for biomedical applications, Adv. Drug Deliv. Rev. 55 (2003) 519–548, https://doi.org/10.1016/S0169-409X(03)00041-3.
[103] L. Chollet, P. Saboural, C. Chauvierre, J.-N. Villemin, D. Letourneur, F. Chaubet, Fucoidans in Nanomedicine, Mar. Drugs. 14 (2016) 1–24, https://doi.org/10.3390/md14080145.
[104] T. Bonnard, J.-M. Serfaty, C. Journé, B. Ho Tin Noe, D. Arnaud, L. Louedec, M. Derkaoui, D. Letourneur, C. Chauvierre, C. Le Visage, Leukocyte mimetic polysaccharide microparticles tracked in vivo on activated endothelium and in abdominal aortic aneurysm, Acta Biomater. 10 (2014) 3535–3545, https://doi.org/10.1016/j.actbio.2014.04.015.
[105] B. Li, M. Juenet, R. Aid-Launais, M. Maire, V. Ollivier, D. Letourneur, C. Chauvierre, Development of polymer microcapsules functionalized with fucoidan to target P-selectin overexpressed in cardiovascular diseases, Adv. Healthc. Mater. 6 (2017) 1–11, https://doi.org/10.1002/adhm.201601200.
[106] H.R. Lijnen, B. Van Hoef, V. Beelen, D. Collen, Characterization of the murine plasma fibrinolytic system, Eur. J. Biochem. 224 (1994) 863–871, https://doi.org/10.1111/j.1432-1033.1994.00863.x.
[107] C. Englert, J.C. Brendel, T.C. Majdanski, T. Yildirim, S. Schubert, M. Gottschaldt, N. Windhab, U.S. Schubert, Pharmapolymers in the 21st century: synthetic polymers in drug delivery applications, Prog. Polym. Sci. 87 (2018) 107–164, https://doi.org/10.1016/j.progpolymsci.2018.07.005.
[108] J. Deng, H. Mei, W. Shi, Z.-Q. Pang, B. Zhang, T. Guo, H.-F. Wang, X.-G. Jiang, Y. Hu, Recombinant tissue plasminogen activator-conjugated nanoparticles effectively targets thrombolysis in a rat model of middle cerebral artery occlusion, Curr. Med. Sci. 38 (2018) 427–435, https://doi.org/10.1007/s11596-018-1896-z.
[109] Y. Pan, X. Wang, Z. Yin, Synthesis and evaluation of cationic polymeric micelles as carriers of lumbrokinase for targeted thrombolysis, Asian J. Pharm. Sci. 14 (2019) 144–153, https://doi.org/10.1016/j.ajps.2018.03.004.
[110] Y. Pan, X. Ren, S. Wang, X. Li, X. Luo, Z. Yin, Annexin V-conjugated mixed micelles as a potential drug delivery system for targeted thrombolysis, Biomacromolecules 18 (2017) 865–876, https://doi.org/10.1021/acs.biomac.6b01756.
[111] J.F. Tait, M.D. Cerqueira, T.A. Dewhurst, K. Fujikawa, J.L. Ritchie, J.R. Stratton, Evaluation of annexin V as a platelet-directed thrombus targeting agent, Thromb. Res. 75 (1994) 491–501, https://doi.org/10.1016/0049-3848(94)90224-0.
[112] L.I. Mukhametova, R.B. Aisina, E.M. Zakharyan, E.A. Karakhanov, K. B. Gershkovich, S.D. Varfolomeyev, Thrombolytic and fibrinogenolytic properties of bioconjugate streptokinase-polyamidoamine dendrimers in vitro, Thromb. Res. 154 (2017) 50–52, https://doi.org/10.1016/j.thromres.2017.04.008.
[113] M. Labieniec-Watala, C. Watala, PAMAM dendrimers: destined for success or doomed to fail? Plain and modified PAMAM dendrimers in the context of biomedical applications, J. Pharmacol. Sci. 104 (2015) 2–14, https://doi.org/10.1002/jps.24222.
[114] L.W.E. Starmans, D. Burdinski, N.P.M. Haex, R.P.M. Moonen, G.J. Strijkers, K. Nicolay, H. Grüll, Iron oxide nanoparticle-micelles (ION-micelles) for sensitive (molecular) magnetic particle imaging and magnetic resonance imaging, PloS One 8 (2013) 1–9, https://doi.org/10.1371/journal.pone.0057335.
[115] R. Cheng, W. Huang, L. Huang, B. Yang, L. Mao, K. Jin, Q. Zhuge, Y. Zhao, Acceleration of tissue plasminogen activator-mediated thrombolysis by magnetically powered nanomotors, ACS Nano 8 (2014) 7746–7754, https://doi.org/10.1021/nn5029955.
[116] H. Kempe, M. Kempe, The use of magnetite nanoparticles for implant-assisted magnetic drug targeting in thrombolytic therapy, Biomaterials 31 (2010) 9499–9510, https://doi.org/10.1016/j.biomaterials.2010.07.107.
[117] J.P. Chen, P.C. Yang, Y.H. Ma, S.J. Tu, Y.J. Lu, Targeted delivery of tissue plasminogen activator by binding to silica-coated magnetic nanoparticle, Int. J. Nanomed. 7 (2012) 5137–5149, https://doi.org/10.2147/IJN.S36197.
[118] M. Wang, J. Zhang, Z. Yuan, W. Yang, Q. Wu, H. Gu, Targeted thrombolysis by using of magnetic mesoporous silica nanoparticles, J. Biomed. Nanotechnol. 8 (2012) 624–632, https://doi.org/10.1166/jbn.2012.1416.
[119] B.L. Razzaboni, P. Bolsaitis, Evidence of an oxidative mechanism for the hemolytic activity of silica particles, Environ. Health Perspect. 87 (1990) 337–341, https://doi.org/10.1289/ehp.9087337.
[120] V. Murashov, M. Harper, E. Demchuk, Impact of silanol surface density on the toxicity of silica aerosols measured by erythrocyte haemolysis, J. Occup. Environ. Hyg. 3 (2006) 718–723, https://doi.org/10.1080/15459620601015950.
[121] T. Wu, M. Tang, Review of the effects of manufactured nanoparticles on mammalian target organs, J. Appl. Toxicol. 38 (2018) 25–40, https://doi.org/10.1002/jat.3499.
[122] J.P. Chen, P.C. Yang, Y.H. Ma, Y.J. Lu, Superparamagnetic iron oxide nanoparticles for delivery of tissue plasminogen activator, J. Nanosci. Nanotechnol. (2011) 11089–11094, https://doi.org/10.1166/jnn.2011.3953.
[123] J.P. Chen, C.H. Liu, H.L. Hsu, T. Wu, Y.J. Lu, Y.H. Ma, Magnetically controlled release of recombinant tissue plasminogen activator from chitosan nanocomposites for targeted thrombolysis, J. Mater. Chem. B. 4 (2016) 2578–2590, https://doi.org/10.1039/c5tb02579f.
[124] S. Heid, H. Unterweger, R. Tietze, R.P. Friedrich, B. Weigel, I. Cicha, D. Eberbeck, A.R. Boccaccini, C. Alexiou, S. Lyer, Synthesis and characterization of tissue plasminogen activator-functionalized superparamagnetic iron oxide nanoparticles for targeted fibrin clot dissolution, Int. J. Mol. Sci. 18 (2017), https://doi.org/10.3390/ijms18091837.
[125] M. Chang, Y.H. Lin, J.L. Gabayno, Q. Li, X. Liu, Thrombolysis based on magnetically-controlled surface-functionalized Fe3O4 nanoparticle, Bioengineered 8 (2017) 29–35, https://doi.org/10.1080/21655979.2016.1227145.
[126] A.Y. Prilepskii, A.F. Fakhardo, A.S. Drozdov, V.V. Vinogradov, I.P. Dudanov, A. A. Shtil, P.P. Bel'Tyukov, A.M. Shibeko, E.M. Koltsova, D.Y. Nechipurenko, V. V. Vinogradov, Urokinase-conjugated magnetite nanoparticles as a promising drug delivery system for targeted thrombolysis: synthesis and preclinical evaluation, ACS Appl. Mater. Interfaces 10 (2018) 36764–36775, https://doi.org/10.1021/acsami.8b14790.
[127] L. Huang, J. Wang, S. Huang, F. Siaw-Debrah, M. Nyanzu, Q. Zhuge, Polyacrylic acid-coated nanoparticles loaded with recombinant tissue plasminogen activator for the treatment of mice with ischemic stroke, Biochem. Biophys. Res. Commun. 516 (2019) 565–570, https://doi.org/10.1016/j.bbrc.2019.06.079.
[128] R.P. Friedrich, J. Zaloga, E. Schreiber, I.Y. Tóth, E. Tombácz, S. Lyer, C. Alexiou, Tissue plasminogen activator binding to superparamagnetic iron oxide nanoparticle-covalent versus adsorptive approach, Nanoscale Res. Lett. 11 (2016) 1, https://doi.org/10.1186/s11671-016-1521-7.
[129] H.W. Yang, M.Y. Hua, K.J. Lin, S.P. Wey, R.Y. Tsai, S.Y. Wu, Y.C. Lu, H.L. Liu, T. Wu, Y.H. Ma, Bioconjugation of recombinant tissue plasminogen activator to magnetic nanocarriers for targeted thrombolysis, Int. J. Nanomed. 7 (2012) 5159–5173, https://doi.org/10.2147/IJN.S32939.
[130] J.B. Vines, J.H. Yoon, N.E. Ryu, D.J. Lim, H. Park, Gold nanoparticles for photothermal cancer therapy, Front. Chem. 7 (2019) 1–16, https://doi.org/10.3389/fchem.2019.00167.
[131] D.E. Kim, J.Y. Kim, D. Schellingerhout, J.H. Ryu, S.K. Lee, S. Jeon, J.S. Lee, J. Kim, H.J. Jang, J.E. Park, E.J. Kim, I.C. Kwon, C.H. Ahn, M. Nahrendorf, K. Kim, Quantitative imaging of cerebral thromboemboli in vivo: the effects of tissue-type plasminogen activator, Stroke 48 (2017) 1376–1385, https://doi.org/10.1161/STROKEAHA.117.016511.
[132] S.P. Kwon, S. Jeon, S.H. Lee, H.Y. Yoon, J.H. Ryu, D. Choi, J.Y. Kim, J. Kim, J. H. Park, D.E. Kim, I.C. Kwon, K. Kim, C.H. Ahn, Thrombin-activatable fluorescent peptide incorporated gold nanoparticles for dual optical/computed tomography thrombus imaging, Biomaterials 150 (2018) 125–136, https://doi.org/10.1016/j.biomaterials.2017.10.017.
[133] A. Parodi, R. Molinaro, M. Sushnitha, M. Evangelopoulos, J.O. Martinez, N. Arrighetti, C. Corbo, E. Tasciotti, Bio-inspired engineering of cell- and virus-like nanoparticles for drug delivery, Biomaterials 147 (2017) 155–168, https://doi.org/10.1016/j.biomaterials.2017.09.020.
[134] S. Absar, Y.M. Kwon, F. Ahsan, Bio-responsive delivery of tissue plasminogen activator for localized thrombolysis, J. Contr. Release 177 (2014) 42–50, https://doi.org/10.1016/j.jconrel.2013.12.036.
[135] R.A. Petros, J.M. Desimone, Strategies in the design of nanoparticles for therapeutic applications, Nat. Rev. Drug Discov. 9 (2010) 615–627, https://doi.org/10.1038/nrd2591.
[136] R. Vankayala, S.R. Corber, J.T. Mac, M.P. Rao, M. Shafie, B. Anvari, Erythrocyte-derived nanoparticles as a theranostic agent for near-infrared fluorescence imaging and thrombolysis of blood clots, Macromol. Biosci. 18 (2018), https://doi.org/10.1002/mabi.201700379, 1700379–1700379.
[137] S. Nozohouri, A.E. Sifat, B. Vaidya, T.J. Abbruscato, Novel approaches for the delivery of therapeutics in ischemic stroke, Drug Discov. Today 25 (2020) 535–551, https://doi.org/10.1016/j.drudis.2020.01.007.
[138] J. Xu, X. Wang, H. Yin, X. Cao, Q. Hu, W. Lv, Q. Xu, Z. Gu, H. Xin, Sequentially site-specific delivery of thrombolytics and neuroprotectant for enhanced treatment of ischemic stroke, ACS Nano 13 (2019) 8577–8588, https://doi.org/10.1021/acsnano.9b01798.
[139] G. Camussi, M.C. Deregibus, S. Bruno, V. Cantaluppi, L. Biancone, Exosomes/microvesicles as a mechanism of cell-to-cell communication, Kidney Int. 78 (2010) 838–848, https://doi.org/10.1038/ki.2010.278.
[140] A.K.A. Silva, N. Luciani, F. Gazeau, K. Aubertin, S. Bonneau, C. Chauvierre, D. Letourneur, C. Wilhelm, Combining magnetic nanoparticles with cell derived

microvesicles for drug loading and targeting, Nanomed. Nanotechnol. Biol. Med. 11 (2015) 645–655, https://doi.org/10.1016/j.nano.2014.11.009.
[141] Y. Zhong, W.J. Gong, X.H. Gao, Y.N. Li, K. Liu, Y.G. Hu, J.S. Qi, Synthesis and evaluation of a novel nanoparticle carrying urokinase used in targeted thrombolysis, J. Biomed. Mater. Res. 108 (2019) 193–200, https://doi.org/10.1002/jbm.a.36803.
[142] K.J. Koudelka, A.S. Pitek, M. Manchester, N.F. Steinmetz, Virus-based nanoparticles as versatile nanomachines, Annu Rev Virol 2 (2015) 379–401, https://doi.org/10.1146/annurev-virology-100114-055141.
[143] A.S. Pitek, J. Park, Y. Wang, H. Gao, H. Hu, D.I. Simon, N.F. Steinmetz, Delivery of thrombolytic therapy using rod-shaped plant viral nanoparticles decreases the risk of hemorrhage, Nanoscale 10 (2018) 16547–16555, https://doi.org/10.1039/c8nr02861c.
[144] J.W. Yoo, D.J. Irvine, D.E. Discher, S. Mitragotri, Bio-inspired, bioengineered and biomimetic drug delivery carriers, Nat. Rev. Drug Discov. 10 (2011) 521–535, https://doi.org/10.1038/nrd3499.
[145] E.C. Unger, T. Porter, W. Culp, R. Labell, T. Matsunaga, R. Zutshi, Therapeutic applications of lipid-coated microbubbles, Adv. Drug Deliv. Rev. 56 (2004) 1291–1314, https://doi.org/10.1016/j.addr.2003.12.006.
[146] B. Li, R. Aid-Launais, M.N. Labour, A. Zenych, M. Juenet, C. Choqueux, V. Ollivier, O. Couture, D. Letourneur, C. Chauvierre, Functionalized polymer microbubbles as new molecular ultrasound contrast agent to target P-selectin in thrombus, Biomaterials 194 (2019) 139–150, https://doi.org/10.1016/j.biomaterials.2018.12.023.
[147] C.M. Moran, Ultrasonic contrast agents, Clin. Ultrasound. 1 (2011) 77–89, https://doi.org/10.1016/B978-0-7020-3131-1.00006-7.
[148] K.B. Bader, G. Bouchoux, C.K. Holland, Sonothrombolysis (2016), https://doi.org/10.1007/978-3-319-22536-4_19.
[149] Y. Sawaguchi, Z. Wang, Ultrasound acceleration of rt-PA thrombolysis depends on acoustic intensity, Biol. Pharm. Bull. 40 (2017) 97–103, https://doi.org/10.1248/bpb.b16-00702.
[150] A. Goyal, F.T.H. Yu, M.G. Tenwalde, X. Chen, A. Althouse, F.S. Villanueva, J. J. Pacella, Inertial cavitation ultrasound with microbubbles improves reperfusion efficacy when combined with tissue plasminogen activator in an in vitro model of microvascular obstruction, Ultrasound Med. Biol. 43 (2017) 1391–1400, https://doi.org/10.1016/j.ultrasmedbio.2017.02.013.
[151] T.R. Porter, The utilization of ultrasound and microbubbles for therapy in acute coronary syndromes, Cardiovasc, Res. 83 (2009) 636–642, https://doi.org/10.1093/cvr/cvp206.
[152] A. Agarwal, W.J. Ng, Y. Liu, Principle and applications of microbubble and nanobubble technology for water treatment, Chemosphere 84 (2011) 1175–1180, https://doi.org/10.1016/j.chemosphere.2011.05.054.
[153] K. Tachibana, S. Tachibana, Albumin microbubble echo-contrast material as an enhancer for ultrasound accelerated thrombolysis, Circulation 92 (1995) 1148–1150, https://doi.org/10.1161/01.CIR.92.5.1148.
[154] K.B. Bader, G. Bouchoux, T. Peng, M.E. Klegerman, D.D. McPherson, C. K. Holland, Thrombolytic efficacy and enzymatic activity of rt-PA-loaded echogenic liposomes, J. Thromb. Thrombolysis 40 (2015) 144–155, https://doi.org/10.1007/s11239-015-1204-8.
[155] H. Shekhar, K.B. Bader, S. Huang, T. Peng, S. Huang, D.D. McPherson, C. K. Holland, In vitro thrombolytic efficacy of echogenic liposomes loaded with tissue plasminogen activator and octafluoropropane gas, Phys. Med. Biol. 62 (2017) 517–538, https://doi.org/10.1088/1361-6560/62/2/517.
[156] S.T. Laing, M.R. Moody, H. Kim, B. Smulevitz, S.L. Huang, C.K. Holland, D. D. McPherson, M.E. Klegerman, Thrombolytic efficacy of tissue plasminogen activator-loaded echogenic liposomes in a rabbit thrombus model, Thromb. Res. 130 (2012) 629–635, https://doi.org/10.1016/j.thromres.2011.11.010.
[157] S.T. Laing, M. Moody, B. Smulevitz, H. Kim, P. Kee, S. Huang, C.K. Holland, D. D. McPherson, Ultrasound-enhanced thrombolytic effect of tissue plasminogen activator-loaded echogenic liposomes in an in vivo rabbit aorta thrombus model-brief report, Arterioscler. Thromb. Vasc. Biol. 31 (2011) 1357–1359, https://doi.org/10.1161/ATVBAHA.111.225938.
[158] M.A. Kandadai, P. Mukherjee, H. Shekhar, G.J. Shaw, I. Papautsky, C.K. Holland, Microfluidic manufacture of rt-PA -loaded echogenic liposomes, Biomed, Microdevices 18 (2016) 1–21, https://doi.org/10.1007/s10544-016-0072-0.
[159] W.C. Yan, Q.W. Chua, X.J. Ong, V.K. Sharma, Y.W. Tong, C.H. Wang, Fabrication of ultrasound-responsive microbubbles via coaxial electrohydrodynamic atomization for triggered release of tPA, J. Colloid Interface Sci. 501 (2017) 282–293, https://doi.org/10.1016/j.jcis.2017.04.073.
[160] D. Susan, Tiukinhoy-Laing, Ultrasound-facilitated thrombolysis using tissue-plasminogen activator-loaded echogenic liposomes, Bone 23 (2011) 1–7, https://doi.org/10.1161/CIRCULATIONAHA.110.956839.
[161] J.M. Correas, L. Bridal, A. Lesavre, A. Méjean, M. Claudon, O. Hélénon, Ultrasound contrast agents: properties, principles of action, tolerance, and artifacts, Eur. Radiol. 11 (2001) 1316–1328, https://doi.org/10.1007/s003300100940.
[162] T. Şen, O. Tüfekçioğlu, Y. Koza, Mechanical index, Anadolu Kardiyol. Derg. 15 (2015) 334–336, https://doi.org/10.5152/akd.2015.6061.
[163] Y. Zhu, L. Guan, Y. Mu, Combined low-frequency ultrasound and urokinase-containing microbubbles in treatment of femoral artery thrombosis in a rabbit model, PloS One 11 (2016) 1–13, https://doi.org/10.1371/journal.pone.0168909.
[164] X. Hua, L. Zhou, P. Liu, Y. He, K. Tan, Q. Chen, Y. Gao, Y. Gao, In vivo thrombolysis with targeted microbubbles loading tissue plasminogen activator in a rabbit femoral artery thrombus model, J. Thromb. Thrombolysis 38 (2014) 57–64, https://doi.org/10.1007/s11239-014-1071-8.
[165] X. Hua, P. Liu, Y.H. Gao, K. Bin Tan, L.N. Zhou, Z. Liu, X. Li, S.W. Zhou, Y.J. Gao, Construction of thrombus-targeted microbubbles carrying tissue plasminogen activator and their in vitro thrombolysis efficacy: a primary research, J. Thromb. Thrombolysis 30 (2010) 29–35, https://doi.org/10.1007/s11239-010-0450-z.
[166] J.H. Nederhoed, H.P. Ebben, J. Slikkerveer, A.W.J. Hoksbergen, O. Kamp, G. J. Tangelder, W. Wisselink, R.J.P. Musters, K.K. Yeung, Intravenous targeted microbubbles carrying urokinase versus urokinase alone in acute peripheral arterial thrombosis in a porcine model, Ann. Vasc. Surg. 44 (2017) 400–407, https://doi.org/10.1016/j.avsg.2017.05.011.
[167] C. Correa-Paz, M.F. Navarro Poupard, E. Polo, M. Rodríguez-Pérez, P. Taboada, R. Iglesias-Rey, P. Hervella, T. Sobrino, D. Vivien, J. Castillo, P. del Pino, F. Campos, B. Pelaz, In vivo ultrasound-activated delivery of recombinant tissue plasminogen activator from the cavity of sub-micrometric capsules, J. Contr. Release 308 (2019) 162–171, https://doi.org/10.1016/j.jconrel.2019.07.017.
[168] X. Wang, Y. Gkanatsas, J. Palasubramaniam, J.D. Hohmann, Y.C. Chen, B. Lim, C. E. Hagemeyer, K. Peter, Thrombus-targeted theranostic microbubbles: a new technology towards concurrent rapid ultrasound diagnosis and bleeding-free fibrinolytic treatment of thrombosis, Theranostics 6 (2016) 726–738, https://doi.org/10.7150/thno.14514.
[169] M. de Saint Victor, L.C. Barnsley, D. Carugo, J. Owen, C.C. Coussios, E. Stride, Sonothrombolysis with magnetically targeted microbubbles, Ultrasound Med. Biol. 45 (2019) 1151–1163, https://doi.org/10.1016/j.ultrasmedbio.2018.12.014.
[170] L. Auboire, C.A. Sennoga, J.M. Hyvelin, F. Ossant, J.M. Escoffre, F. Tranquart, A. Bouakaz, Microbubbles combined with ultrasound therapy in ischemic stroke: a systematic review of in-vivo preclinical studies, PloS One 13 (2018) 1–19, https://doi.org/10.1371/journal.pone.0191788.
[171] C.A. Sennoga, E. Kanbar, L. Auboire, P.A. Dujardin, D. Fouan, J.M. Escoffre, A. Bouakaz, Microbubble-mediated ultrasound drug-delivery and therapeutic monitoring, Expet Opin. Drug Deliv. 14 (2017) 1031–1043, https://doi.org/10.1080/17425247.2017.1266328.
[172] A. Moumouh, L. Barentin, F. Tranquart, S. Serrierre, I. Bonnaud, J.P. Tasu, Fibrinolytic effects of transparietal ultrasound associated with intravenous infusion of an ultrasound contrast agent: study of a rat model of acute cerebral stroke, Ultrasound Med. Biol. 36 (2010) 51–57, https://doi.org/10.1016/j.ultrasmedbio.2009.06.1103.
[173] R. Chen, D.G. Paeng, K.H. Lam, Q. Zhou, K.K. Shung, N. Matsuoka, M. S. Humayun, In vivo sonothrombolysis of ear marginal vein of rabbits monitored with high-frequency ultrasound needle transducer, J. Med. Biol. Eng. 33 (2013) 103–110, https://doi.org/10.5405/jmbe.1219.
[174] A.D. Barreto, A.V. Alexandrov, L. Shen, A. Sisson, A.W. Bursaw, P. Sahota, H. Peng, M. Ardjomand-Hessabi, R. Pandurengan, M.H. Rahbar, K. Barlinn, H. Indupuru, N.R. Gonzales, S.I. Savitz, J.C. Grotta, Clotbust-hands free: pilot safety study of a novel operator-independent ultrasound device in patients with acute ischemic stroke, Stroke 44 (2013) 3376–3381, https://doi.org/10.1161/STROKEAHA.113.002713.
[175] Jonathan T. Sutton, et al., Clot retraction affects the extent of ultrasound-enhanced thrombolysis in an ex vivo porcine thrombosis model Jonathan, Ultrasound Med. Biol. 23 (2013) 1–7, https://doi.org/10.1038/jid.2014.371.
[176] H. Soo Choi, W. Liu, P. Misra, E. Tanaka, J.P. Zimmer, B. Itty Ipe, M.G. Bawendi, J. V Frangioni, Renal clearance of quantum dots, Nat. Biotechnol. 25 (2007) 1165–1170, https://doi.org/10.1038/nbt1340.
[177] A.E. Nel, L. Mädler, D. Velegol, T. Xia, E.M.V. Hoek, P. Somasundaran, F. Klaessig, V. Castranova, M. Thompson, Understanding biophysicochemical interactions at the nano-bio interface, Nat. Mater. 8 (2009) 543–557, https://doi.org/10.1038/nmat2442.
[178] F. Alexis, E. Pridgen, L.K. Molnar, O.C. Farokhzad, Factors affecting the clearance and biodistribution of polymeric nanoparticles, Mol. Pharm. 5 (2008) 505–515, https://doi.org/10.1021/mp800051m.
[179] Y. Geng, P. Dalhaimer, S. Cai, R. Tsai, M. Tewari, T. Minko, D.E. Discher, Shape effects of filaments versus spherical particles in flow and drug delivery, Nat. Nanotechnol. 2 (2007) 249–255, https://doi.org/10.1038/nnano.2007.70.
[180] L. Zhang, Z. Cao, Y. Li, J.-R. Ella-Menye, T. Bai, S. Jiang, Softer zwitterionic nanogels for longer circulation and lower splenic accumulation, ACS Nano 6 (2012) 6681–6686, https://doi.org/10.1021/nn301159a.
[181] R. Palomba, A.L. Palange, I.F. Rizzuti, M. Ferreira, A. Cervadoro, M.G. Barbato, C. Canale, P. Decuzzi, Modulating phagocytic cell sequestration by tailoring nanoconstruct softness, ACS Nano 12 (2018) 1433–1444, https://doi.org/10.1021/acsnano.7b07797.
[182] N.Y. Lotosh, S.O. Aliaseva, I.K. Malashenkova, G.M. Sorokoumova, R.G. Vasilov, A.A. Selischeva, Cationic liposomes cause ROS generation and release of neutrophil extracellular traps, Biochem. Suppl. Ser. A Membr. Cell Biol. 13 (2019) 40–49, https://doi.org/10.1134/S1990747818040074.
[183] T.L. Hwang, I.A. Aljuffali, C.F. Hung, C.H. Chen, J.Y. Fang, The impact of cationic solid lipid nanoparticles on human neutrophil activation and formation of neutrophil extracellular traps (NETs), Chem. Biol. Interact. 235 (2015) 106–114, https://doi.org/10.1016/j.cbi.2015.04.011.
[184] T.L. Hwang, I.A. Aljuffali, C.F. Lin, Y.T. Chang, J.Y. Fang, Cationic additives in nanosystems activate cytotoxicity and inflammatory response of human neutrophils: lipid nanoparticles versus polymeric nanoparticles, Int. J. Nanomed. 10 (2015) 371–385, https://doi.org/10.2147/IJN.S73017.
[185] K. Knop, R. Hoogenboom, D. Fischer, U.S. Schubert, Poly(ethylene glycol) in drug delivery: pros and cons as well as potential alternatives, Angew. Chem. Int. Ed. 49 (2010) 6288–6308, https://doi.org/10.1002/anie.200902672.
[186] P.L. Rodriguez, T. Harada, D.A. Christian, D.A. Pantano, R.K. Tsai, D.E. Discher, Minimal "self" peptides that inhibit phagocytic clearance and enhance delivery of

nanoparticles, Science 339 (2013) 971–975, https://doi.org/10.1126/science.1229568.
[187] J. Saikia, R. Mohammadpour, M. Yazdimamaghani, H. Northrup, V. Hlady, H. Ghandehari, Silica nanoparticle-endothelial interaction: uptake and effect on platelet adhesion under flow conditions, ACS Appl. Bio Mater. 1 (2018) 1620–1627, https://doi.org/10.1021/acsabm.8b00466.
[188] J. Duan, S. Liang, Y. Yu, Y. Li, L. Wang, Z. Wu, Y. Chen, M.R. Miller, Z. Sun, Inflammation–coagulation response and thrombotic effects induced by silica nanoparticles in zebrafish embryos, Nanotoxicology 12 (2018) 470–484, https://doi.org/10.1080/17435390.2018.1461267.
[189] J. Jose Corbalan, C. Medina, A. Jacoby, T. Malinski, M.W. Radomski, Amorphous silica nanoparticles aggregate human platelets: potential implications for vascular homeostasis, Int. J. Nanomed. 7 (2012) 631–639, https://doi.org/10.2147/IJN.S28293.
[190] X.D. Zhang, H.Y. Wu, D. Wu, Y.Y. Wang, J.H. Chang, Z. Bin Zhai, A.M. Meng, P. X. Liu, L.A. Zhang, F.Y. Fan, Toxicologic effects of gold nanoparticles in vivo by different administration routes, Int. J. Nanomed. 5 (2010) 771–781, https://doi.org/10.2147/IJN.S8428.
[191] L. Shang, K. Nienhaus, G.U. Nienhaus, Engineered nanoparticles interacting with cells: size matters, J. Nanobiotechnol. 12 (2014) 1, https://doi.org/10.1186/1477-3155-12-5.
[192] Y. Pan, S. Neuss, A. Leifert, M. Fischler, F. Wen, U. Simon, G. Schmid, W. Brandau, W. Jahnen-Dechent, Size-dependent cytotoxicity of gold nanoparticles, Small 3 (2007) 1941–1949, https://doi.org/10.1002/smll.200700378.
[193] Z. He, J. Liu, L. Du, The unexpected effect of PEGylated gold nanoparticles on the primary function of erythrocytes, Nanoscale 6 (2014) 9017–9024, https://doi.org/10.1039/c4nr01857e.
[194] J. Feng, H. Liu, K.K. Bhakoo, L. Lu, Z. Chen, A metabonomic analysis of organ specific response to USPIO administration, Biomaterials 32 (2011) 6558–6569, https://doi.org/10.1016/j.biomaterials.2011.05.035.
[195] C. Lasagna-Reeves, D. Gonzalez-Romero, M.A. Barria, I. Olmedo, A. Clos, V. M. Sadagopa Ramanujam, A. Urayama, L. Vergara, M.J. Kogan, C. Soto, Bioaccumulation and toxicity of gold nanoparticles after repeated administration in mice, Biochem. Biophys. Res. Commun. 393 (2010) 649–655, https://doi.org/10.1016/j.bbrc.2010.02.046.
[196] K. Andrieux, P. Couvreur, Polyalkylcyanoacrylate nanoparticles for delivery of drugs across the blood-brain barrier 1, Wiley Interdiscip Rev Nanomed Nanobiotechnol, 2009, pp. 463–474, https://doi.org/10.1002/wnan.5.
[197] N.J. Siddiqi, M.A.K. Abdelhalim, A.K. El-Ansary, A.S. Alhomida, W.Y. Ong, Identification of potential biomarkers of gold nanoparticle toxicity in rat brains, J. Neuroinflammation 9 (2012) 1–7, https://doi.org/10.1186/1742-2094-9-123.
[198] R. Brouns, P.P. De Deyn, The complexity of neurobiological processes in acute ischemic stroke, Clin. Neurol. Neurosurg. 111 (2009) 483–495, https://doi.org/10.1016/j.clineuro.2009.04.001.
[199] D. Vivien, M. Gauberti, A. Montagne, G. Defer, E. Touzé, Impact of tissue plasminogen activator on the neurovascular unit: from clinical data to experimental evidence, J. Cerebr. Blood Flow Metabol. 31 (2011) 2119–2134, https://doi.org/10.1038/jcbfm.2011.127.
[200] M. Bartneck, T. Ritz, H.A. Keul, M. Wambach, J. Bornemann, U. Gbureck, J. Ehling, T. Lammers, F. Heymann, N. Gassler, T. Lüdde, C. Trautwein, J. Groll, F. Tacke, Peptide-functionalized gold nanorods increase liver injury in hepatitis, ACS Nano 6 (2012) 8767–8777, https://doi.org/10.1021/nn302502u.
[201] C.H. Fu, T.L. Liu, F.Q. Tang, D. Chen, L.L. Li, H.Y. Liu, X.M. Li, Acute toxicity and oxidative damage induced by silica nanorattle in vivo, Chin. Sci. Bull. 57 (2012) 2525–2532, https://doi.org/10.1007/s11434-012-5187-y.
[202] H. Nishimori, M. Kondoh, K. Isoda, S. ichi Tsunoda, Y. Tsutsumi, K. Yagi, Histological analysis of 70-nm silica particles-induced chronic toxicity in mice, Eur. J. Pharm. Biopharm. 72 (2009) 626–629, https://doi.org/10.1016/j.ejpb.2009.03.007.
[203] D. Couto, M. Freitas, V.M. Costa, R.C. Chisté, A. Almeida, M.A. Lopez-Quintela, J. Rivas, P. Freitas, P. Silva, F. Carvalho, E. Fernandes, Biodistribution of polyacrylic acid-coated iron oxide nanoparticles is associated with proinflammatory activation and liver toxicity, J. Appl. Toxicol. 36 (2016) 1321–1331, https://doi.org/10.1002/jat.3323.
[204] B. Zhao, X.Q. Wang, X.Y. Wang, H. Zhang, W.B. Dai, J. Wang, Z.L. Zhong, H. N. Wu, Q. Zhang, Nanotoxicity comparison of four amphiphilic polymeric micelles with similar hydrophilic or hydrophobic structure, Part, Fibre Toxicol 10 (2013) 1–16, https://doi.org/10.1186/1743-8977-10-47.
[205] X. Li, A. Radomski, O.I. Corrigan, L. Tajber, F. De Sousa Menezes, S. Endter, C. Medina, M.W. Radomski, Platelet compatibility of PLGA, chitosan and PLGA-chitosan nanoparticles, Nanomedicine 4 (2009) 735–746, https://doi.org/10.2217/nnm.09.65.
[206] Y. Zhao, D. Sultan, Y. Liu, Biodistribution, excretion, and toxicity of nanoparticles. Theranostic Bionanomaterials, Elsevier Inc., 2019, pp. 27–53, https://doi.org/10.1016/B978-0-12-815341-3.00002-X.
[207] K.D. Grieger, I. Linkov, S.F. Hansen, A. Baun, Environmental risk analysis for nanomaterials: review and evaluation of frameworks, Nanotoxicology 6 (2012) 196–212, https://doi.org/10.3109/17435390.2011.569095.
[208] E. Sadauskas, G. Danscher, M. Stoltenberg, U. Vogel, A. Larsen, H. Wallin, Protracted elimination of gold nanoparticles from mouse liver, Nanomed. Nanotechnol. Biol. Med. 5 (2009) 162–169, https://doi.org/10.1016/j.nano.2008.11.002.
[209] J. Feng, H. Liu, L. Zhang, K. Bhakoo, L. Lu, An insight into the metabolic responses of ultra-small superparamagnetic particles of iron oxide using metabonomic analysis of biofluids, Nanotechnology 21 (2010) 395101, https://doi.org/10.1088/0957-4484/21/39/395101.
[210] Q. Ran, Y. Xiang, Y. Liu, L. Xiang, F. Li, X. Deng, Y. Xiao, L. Chen, L. Chen, Z. Li, Eryptosis indices as a novel predictive parameter for biocompatibility of Fe3O4 magnetic nanoparticles on erythrocytes, Sci. Rep. 5 (2015) 16209, https://doi.org/10.1038/srep16209.
[211] K. de la Harpe, P. Kondiah, Y. Choonara, T. Marimuthu, L. du Toit, V. Pillay, The hemocompatibility of nanoparticles: a review of cell–nanoparticle interactions and hemostasis, Cells 8 (2019) 1209, https://doi.org/10.3390/cells8101209.
[212] S. Vrignaud, J.P. Benoit, P. Saulnier, Strategies for the nanoencapsulation of hydrophilic molecules in polymer-based nanoparticles, Biomaterials 32 (2011) 8593–8604, https://doi.org/10.1016/j.biomaterials.2011.07.057.
[213] M. Di Marco, K.A. Razak, A.A. Aziz, C. Devaux, E. Borghi, L. Levy, C. Sadun, Overview of the main methods used to combine proteins with nanosystems : absorption, bioconjugation, and encapsulation, Int. J. Nanomed. 5 (2010) 37–49.
[214] L. Arnfast, C.G. Madsen, L. Jorgensen, S. Baldursdottir, Design and processing of nanogels as delivery systems for peptides and proteins, Ther. Deliv. 5 (2014) 691–708, https://doi.org/10.4155/tde.14.38.
[215] S.R. Van Tomme, W.E. Hennink, Biodegradable dextran hydrogels for protein delivery applications, Expet Rev. Med. Dev. 4 (2007) 147–164, https://doi.org/10.1586/17434440.4.2.147.
[216] X. Xiong, F. Zhao, M. Shi, H. Yang, Y. Liu, Polymeric microbubbles for ultrasonic molecular imaging and targeted therapeutics, J. Biomater. Sci. Polym. Ed. 22 (2011) 417–428, https://doi.org/10.1163/092050610X540440.
[217] B. Li, R. Aid-Launais, M.-N. Labour, A. Zenych, M. Juenet, C. Choqueux, V. Ollivier, O. Couture, D. Letourneur, C. Chauvierre, Functionalized polymer microbubbles as new molecular ultrasound contrast agent to target P-selectin in thrombus, Biomaterials 194 (2019) 139–150, https://doi.org/10.1016/j.biomaterials.2018.12.023.
[218] C. Chauvierre, R. Aid-Launais, J. Aerts, M. Maire, L. Chollet, L. Rolland, R. Bonaf, S. Rossi, S. Bussi, C. Cabella, D. Laszlo, T. Fülöp, J. Szebeni, Y. Chahid, K. H. Zheng, E.S.G. Stroes, D. Le Guludec, F. Rouzet, D. Letourneur, Pharmaceutical development and safety evaluation of a GMP-grade fucoidan for molecular diagnosis of cardiovascular diseases, Mar. Drugs 17 (2019) 1–17, https://doi.org/10.3390/md17120699.
[219] K.H. Zheng, Y. Kaiser, E. Poel, H. Verberne, J. Aerts, F. Rouzet, E. Stroes, D. Letourneur, C. Chauvierre, 99Mtc-Fucoidan as diagnostic agent for P-selectin imaging: first-in-human evaluation (phase I), Atherosclerosis 287 (2019) e143, https://doi.org/10.1016/j.atherosclerosis.2019.06.425.
[220] J.C. Antunes, L. Benarroch, F.C. Moraes, M. Juenet, M.S. Gross, M. Aubart, C. Boileau, G. Caligiuri, A. Nicoletti, V. Ollivier, F. Chaubet, D. Letourneur, C. Chauvierre, Core-shell polymer-based nanoparticles deliver miR-155-5p to endothelial cells, Mol. Ther. Nucleic Acids 17 (2019) 210–222, https://doi.org/10.1016/j.omtn.2019.05.016.
[221] B. Ovbiagele, C.S. Kidwell, S. Starkman, J.L. Saver, Potential role of neuroprotective agents in the treatment of patients with acute ischemic stroke, Curr. Treat. Options Neurol. 5 (2003) 367–375, https://doi.org/10.1007/s11940-003-0027-7.
[222] R. Goulay, M. Naveau, T. Gaberel, D. Vivien, J. Parcq, Optimized tPA: a non-neurotoxic fibrinolytic agent for the drainage of intracerebral hemorrhages, J. Cerebr. Blood Flow Metabol. 38 (2018) 1180–1189, https://doi.org/10.1177/0271678X17719180.
[223] J. Matuszak, P. Dörfler, S. Lyer, H. Unterweger, M. Juenet, C. Chauvierre, A. Alaarg, D. Franke, G. Almer, I. Texier, J.M. Metselaar, R. Prassl, C. Alexiou, H. Mangge, D. Letourneur, I. Cicha, Comparative analysis of nanosystems' effects on human endothelial and monocytic cell functions, Nanotoxicology 12 (2018) 957–974, https://doi.org/10.1080/17435390.2018.1502375.
[224] I. Cicha, C. Chauvierre, I. Texier, C. Cabella, J.M. Metselaar, J. Szebeni, L. Dézsi, C. Alexiou, F. Rouzet, G. Storm, E. Stroes, D. Bruce, N. MacRitchie, P. Maffia, D. Letourneur, From design to the clinic: practical guidelines for translating cardiovascular nanomedicine, Cardiovasc. Res. 114 (2018) 1714–1727, https://doi.org/10.1093/cvr/cvy219.
[225] C. Chauvierre, D. Letourneur, The European project NanoAthero to fight cardiovascular diseases using nanotechnologies, Nanomedicine 10 (2015) 3391–3400, https://doi.org/10.2217/nnm.15.170.
[226] K.H. Zheng, J. Schoormans, L.C.A. Stiekema, C. Calcagno, I. Cicha, C. Alexiou, G. J. Strijkers, A.J. Nederveen, E.S.G. Stroes, B.F. Coolen, Plaque permeability assessed with DCE-MRI associates with USPIO uptake in patients with peripheral artery disease, JACC Cardiovasc. Imaging 12 (2019) 2081–2083, https://doi.org/10.1016/j.jcmg.2019.04.014.
[227] F.M. van der Valk, D.F. van Wijk, M.E. Lobatto, H.J. Verberne, G. Storm, M.C. M. Willems, D.A. Legemate, A.J. Nederveen, C. Calcagno, V. Mani, S. Ramachandran, M.P.M. Paridaans, M.J. Otten, G.M. Dallinga-Thie, Z.A. Fayad, M. Nieuwdorp, D.M. Schulte, J.M. Metselaar, W.J.M. Mulder, E.S. Stroes, Prednisolone-containing liposomes accumulate in human atherosclerotic macrophages upon intravenous administration, Nanomed. Nanotechnol. Biol. Med. 11 (2015) 1039–1046, https://doi.org/10.1016/j.nano.2015.02.021.
[228] K.H. Zheng, F.M. van der Valk, L.P. Smits, M. Sandberg, J.L. Dasseux, R. Baron, R. Barbaras, C. Keyserling, B.F. Coolen, A.J. Nederveen, H.J. Verberne, T.E. Nell, D.J. Vugts, R. Duivenvoorden, Z.A. Fayad, W.J.M. Mulder, G.A.M.S. van Dongen, E.S.G. Stroes, HDL mimetic CER-001 targets atherosclerotic plaques in patients, Atherosclerosis 251 (2016) 381–388, https://doi.org/10.1016/j.atherosclerosis.2016.05.038.

ANNEX 2

**Fucoidan-Functionalized Polysaccharide Submicroparticles Loaded with Alteplase for Efficient Targeted Thrombolytic Therapy**

*Alina Zenych, Charlène Jacqmarcq, Rachida Aid, Louise Fournier, Laura M. Forero Ramirez, Thomas Bonnard, Denis Vivien, Didier Letourneur, Cédric Chauvierre**

A. Zenych, C. Jacqmarcq, R. Aid, L. Fournier, Dr. L. M. Forero Ramirez, Dr. T. Bonnard, Prof. D. Vivien, Dr. D. Letourneur, Dr. C. Chauvierre

Université de Paris, Université Sorbonne Paris Nord, UMR S1148, INSERM
F-75018 Paris, France
E-mail: cedric.chauvierre@inserm.fr

R. Aid

Université de Paris, FRIM, UMS 034, INSERM
F-75018 Paris, France

C. Jacqmarcq, Dr. T. Bonnard, Prof. D. Vivien

INSERM U1237 Physiopathology and Imaging of Neurological Disorders (PhIND)
Institut Blood and Brain @ Caen Normandie (BB@C), GIP Cyceron
14074 Caen, France

Prof. D. Vivien

Department of Clinical Research, Caen Normandie University Hospital (CHU)
14074 Caen, France

**Keywords**: nanomedicine, drug delivery, targeted thrombolysis, polysaccharides, fucoidan, P-selectin

**ABSTRACT**

Intravenous administration of fibrinolytic drugs is the standard treatment of acute thrombotic diseases. However, current fibrinolytics exhibit limited clinical efficacy because of their short plasma half-lives and might trigger hemorrhagic transformations. Therefore, it is mandatory to develop innovative nanomedicine-based solutions for more efficient and safer thrombolysis with biocompatible and biodegradable thrombus-targeted nanocarrier. Herein, fucoidan-functionalized hydrogel polysaccharide submicroparticles with high biocompatibility are elaborated by the inverse miniemulsion / crosslinking method. They are loaded with the gold standard fibrinolytic – alteplase – to direct site-specific fibrinolysis due to nanomolar interactions between fucoidan and P-selectin overexpressed on activated platelets and endothelial cells in the thrombus area. The thrombus targeting properties of these particles are validated in a microfluidic assay containing recombinant P-selectin and activated platelets under arterial and venous blood shear rates as well as *in vivo*. The experiments on the murine model of acute thromboembolic ischemic stroke support this product's therapeutic efficacy, revealing a faster recanalization rate in the middle cerebral artery than with free alteplase, which reduces post-ischemic cerebral infarct lesions and blood-brain barrier permeability. Altogether, this proof-of-concept study demonstrates the potential of a biomaterial-based targeted nanomedicine for the precise treatment of acute thrombotic events, such as ischemic stroke.

## 1. INTRODUCTION

Acute thrombotic pathologies such as myocardial infarction, ischemic stroke, and venous thromboembolism remain a major global healthcare challenge contributing to a significant number of deaths and disabilities.[1] Current thrombolytic therapy, the intravenous injection of Plasminogen Activators (PA), is administrated to lyse a clot-induced vascular occlusion and restore the blood flow in the vessel. The recombinant tissue plasminogen activator (rtPA) is the most commonly applied clot-busting drug in clinics and the only one approved to treat acute ischemic stroke.[2] rtPA is a fibrin-specific serine protease that activates the endogenous proenzyme plasminogen and converts it to the active form plasmin, thus, degrading the thrombus fibrin network. However, systemic delivery of rtPA is limited by the rapid drug elimination (half-life 4-6 min), physiological deactivation by its antidotes such as Plasminogen Activator Inhibitors (PAI-1 and PAI-2), and deleterious side-effects such as intracranial hemorrhages.[3] This restricts its use to a narrow therapeutic window (4.5 h of stroke symptom onset when injected alone and 6 h when combined with mechanical thrombectomy) beyond which the deleterious effects of rtPA overcome its benefits. Moreover, the rate of acute recanalization after intravenous administration of rtPA is low: only ~30% of patients experienced full or partial recanalization.[4]

Therapeutic strategies that intend to address the challenges of thrombolytic therapy and boost survival rates remain of great clinical interest. Certainly, novel thrombolytic molecules are being researched to increase reperfusion, improve safety, and protect the brain

neurovascular unit.[5,6] Apart from that, nanomedical approaches for the targeted delivery of thrombolytic agents have been intensively proposed.[7] Korin *et al.* reported the microaggregates of poly (lactic-co-glycolic acid) (PLGA) nanoparticles (NPs) dissociated into rtPA-bearing nanocompounds when exposed to abnormally high hemodynamic shear stress, typical for the vascular occlusions, that performed effective thrombolysis in several preclinical models.[8] Colasuonno *et al.* formulated rtPA-loaded discoidal porous nanoconstructs from a mixture of PLGA and polyethylene glycol (PEG) with high thrombolytic potential presumably attributed to the erythrocyte-mimicking shape of the NPs and their deformability, leading to efficient circulation profiles and accumulation on the clot.[9] While these nanosystems with passive targeting succeeded in a promising thrombolytic efficacy in preclinical studies, more recent and advanced examples are formulated with actively targeted nanocarriers.

Active targeting permits drug accumulation specifically at the thrombus site and has the potential to enhance the enzyme penetration into deeply localized thrombi. Apart from the magnetic nanoparticle targeting under an external magnetic field, active blood clot targeting is currently achieved by directing the functionalized NPs towards fibrin or activated platelets (mostly integrin GPIIb/IIIa and less adhesion receptor P-selectin) with antibodies and/or peptides. Notably, a theranostic system for thrombus molecular imaging and targeted therapy was developed by Zhou *et al.* when rtPA was encapsulated into the $Fe_3O_4$-based PLGA NPs, and a cyclic arginine-glycine-aspartic acid (cRGD) peptide was grafted onto the chitosan surface to target GPIIb/IIIa on activated platelets.[10] Nevertheless, both antibodies and peptides have their limitations for targeted drug delivery. The immunogenicity, purity, and sufficient circulation time are the main concerns of the application of the antibodies[11], while peptides might suffer from weak binding affinity, immunogenicity, a high costs of peptide synthesis, and metabolic instability with fast renal clearance due to their small sizes.[12]

An effective alternative could be the nanoparticle functionalization with fucoidan,[13] a naturally-occurring algae-derived sulfated polysaccharide that exhibits a strong and specific tropism for the P-selectin overexpression in cardiovascular pathologies.[14,15] Fucoidan emerged as an affordable, high-quality targeting ligand to P-selectin that was prior validated by our group on various polysaccharide-based nano- & microsystems for molecular diagnostics and targeted therapy.[16–20] Following the obtention of the label “raw materials for pharmaceutical uses” in 2015 in France, it became a part of the large-scale European Union project NanoAthero as a contrast agent for Single-Photon Emission Computed Tomography (SPECT) imaging in human atherothrombosis, coordinated by our laboratory.[21] The first in the world Phase I clinical trial on intravenous delivery of fucoidan radiolabeled by Technetium-99m reported its safety and

favorable biodistribution,[22] while Phase IIa for the imaging of deep vein thrombosis is ongoing.

It is critical to ensure an excellent safety profile of the designed nanocarrier for targeted thrombolysis in future clinical translation by selecting biocompatible and fully biodegradable materials with the U.S. Food and Drug Administration (FDA)-approval.[23] Contrary to the attractiveness of synthetic polymers such as PLGA, the NPs made of polysaccharides are explored to a lesser degree for thrombolytic therapy. Yet, they benefit from the general advantages of natural polymers: biocompatibility, low cost, and hydrophilicity. Polysaccharide hydrogels, which are crosslinked three-dimensional polymer networks, absorb large quantities of water and can effectively load macromolecules with high encapsulation efficiency,[24] including plasminogen activators. Few publications reported the nanoformulations with chitosan, a cationic chitin-derived polysaccharide that can form polyelectrolyte complexes with negatively charged molecules.[25] For instance, superior thrombolytic potential *in vivo* was demonstrated on self-assembled chitosan NPs crosslinked with sodium tripolyphosphate and loaded with urokinase.[26] Liao *et al.* formulated the lumbrokinase-bearing NPs from quaternized derivative of chitosan - N,N,N-Trimethyl Chitosan covalently grafted with cRGD peptide to target GPIIb/IIIa receptors that could accelerate thrombolysis.[27]

Dextran, an exocellular bacterial water-soluble polysaccharide, is extensively employed in clinics, particularly in its low molecular weight (40 and 70 kDa), for plasma volume expansion, thrombosis prophylaxis, peripheral blood flow enhancement, artificial tears, *etc*. [28] Dextran coating of magnetic NPs is applied to ensure their environmental stability and prolong the blood circulation time.[29,30] However, there is no reported exclusively dextran nanocarrier with hydrogel structure for thrombolytic application to our knowledge. Meeting the requirements of biocompatibility, biodegradability, non-immunogenicity, dextran stands out as an attractive polymer to design an alteplase delivery system.

Herein, we fabricated novel fucoidan-functionalized dextran submicroparticles (SPs) by a green chemistry method using fully biodegradable and biocompatible compounds, all of them approved by the FDA. After physico-chemical and biosafety characterization of these hydrogel-like SPs, rtPA was loaded onto the SPs with a high encapsulation capacity, and its release in saline and *in vitro* amidolytic and fibrinolytic activities were tested. Through the *in vitro* microfluidic experiments under continuous arterial or venous flow, we provided evidence that fucoidan-functionalized SPs (Fuco-SPs) have a high and specific affinity to P-selectin and accumulate on activated platelet aggregates. Also, these particles bind to the thrombi *in vivo*. Finally, rtPA-associated Fuco-SPs proved superior *in vivo* thrombolytic efficacy in a mouse

stroke thrombin model with a faster vessel recanalization that minimized cerebral tissue damage: the post-ischemic lesion and blood-brain barrier (BBB) permeability.

## 2. RESULTS

### 2.1. Submicroparticle synthesis and characterization

Novel polysaccharide SPs were elaborated by a simple and reproducible two-step synthesis process (**Figure 1**A). First, a stable w/o miniemulsion of the aqueous phase with hydrophilic polysaccharides and vegetable (sunflower) oil was prepared. Chemical crosslinking of polysaccharides with the crosslinking agent STMP under alkaline conditions (Figure 1B) produced a suspension of uniform SPs. We refer to the hydrogel particles only from dextran as Control-SPs, and from a mixture of dextran and fucoidan as Fuco-SPs in this manuscript.

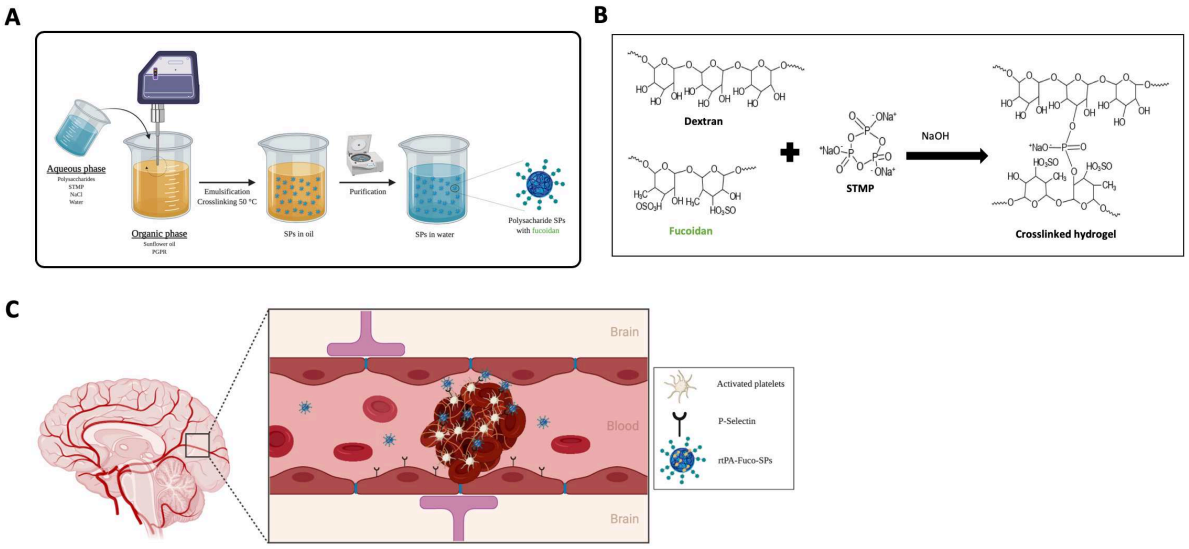


**Figure 1. Synthesis and the proposed mechanism of action *in vivo* of the Fuco-SPs. A.** Overall schematic of the synthesis process of the SPs – miniemulsion / crosslinking. **B.** Crosslinking of the polysaccharides (dextran and fucoidan) with STMP in alkaline conditions. **C.** Proposed therapeutic mode of action of the rtPA-loaded Fuco-SPs after the ischemic stroke: the Fuco-SPs accumulate on the surface of the activated platelets due to P-selectin affinity of fucoidan and perform local thrombolysis with alteplase.

To ensure desirable safety of the future drug delivery platform, a thoughtful approach to material selection was effectuated. Low molecular weight dextran 40 kDa of clinical-grade was utilized without any chemical modification. Having a large number of hydroxyl groups, dextran is a suitable compound for subsequent chemical crosslinking with STMP,[28] an FDA-approved food additive[31] that is preferred over conventional crosslinker glutaraldehyde known

for cytotoxicity.[32] Fucoidan, a marine polysaccharide approved as a pharmaceutical compound[33] that exhibits a nanomolar affinity to P-selectin,[34] served as a targeting ligand to thrombi. Hence, both natural polysaccharides applied in this study are affordable, biodegradable, biocompatible compounds, non-immunogenic, and approved for clinical applications.

Instead of commonly used organic solvents, sunflower oil was applied as an emulsion continuous phase. The choice of the stabilizing agent plays an important role in reducing the interfacial tension and Laplace pressure when fabricating a stable emulsion and future nanocarrier. In this work, we selected a potent oil-soluble nonionic surfactant for stabilizing w/o emulsions – PGPR, which is also recognized by the FDA as a safe compound and is frequently used as an emulsifier in the food production industry.[35] In addition, to counteract the Ostwald ripening of water droplets, 6 M NaCl was added to the aqueous phase as an osmotic agent to adjust the osmotic gradient and to stabilize the w/o emulsion further. Overall, multiple parameters were optimized to obtain a stable and homogenous miniemulsion and subsequent nano-delivery system. It was found that the size of the templating droplet and the ultimate hydrogel SPs being directly proportional to the polysaccharide molecular weight and inversely proportional to the amount of surfactant and crosslinking agent as well as homogenization speed (data not shown).

ESEM and TEM images revealed a well-defined spherical morphology and uniform size distribution of SPs (**Figure 2**A, B). As hydrogel-based particles, they could swell in an aqueous medium while maintaining their network structure (Figure 2C).

Functionalized Fuco-SPs contained 8.60 ± 0.01% of fucoidan in a mass of the total SPs weight, determined by elemental analysis of sulfur, and 9.30 ± 1.07% of fucoidan by quantification of the sulfate content by a semi-quantitative colorimetric assay. In such a way, two different techniques estimated ~9% fucoidan composition in the SPs. The physico-chemical properties of these nanoformulations are displayed in Figure 2D. The SPs exhibited the hydrodynamic size 674.87 ± 59.35 nm (Control-SPs) and 708.48 ± 40.00 nm (Fuco-SPs), determined by DLS. It is important to highlight that a relatively large size of the SPs might limit the accumulation of associated rtPA within the brain parenchyma and reduce the risk of hemorrhagic events. The negative ζ-potential of the SPs -24.83 ± 0.09 mV for Control-SPs and -27.07 ± 0.39 mV for Fuco-SPs ensured colloidal stability as a result of the anionic nature of the fucoidan and the formation of the anionic phosphate functional groups, produced during the crosslinking reaction with STMP. The phosphorus content of the SPs is indicated in Figure 2D.

The size and zeta potential of both SPs remained relatively stable for at least 30 days at 4 °C. Besides, effective storage of the SPs can be ensured by freeze-drying with 5% (w/v) sucrose as a cryoprotectant and subsequent resuspension in an aqueous medium. The overall yield of the synthesis was 13.4 ± 0.7 mg of SPs.

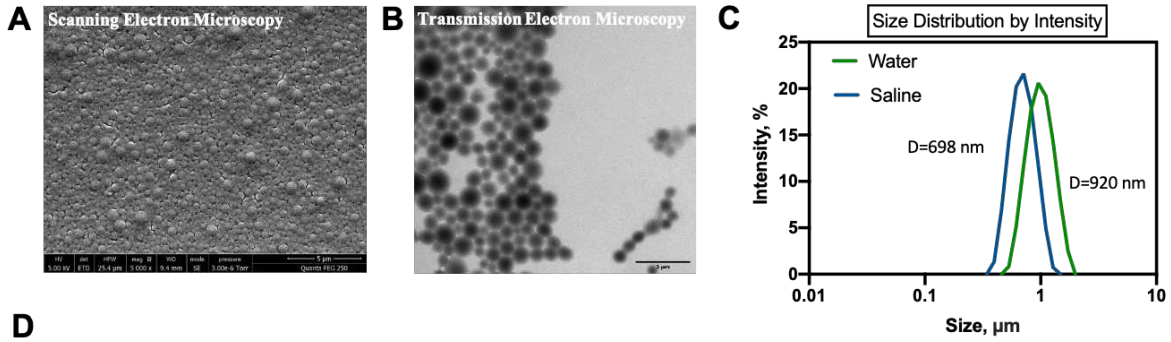


D

| Sample | Size, nm | PDI | Zeta potential, mV | Phosphorus content, mg/l | Fucoidan content (Sulfate), %, w/w | Fucoidan content (Sulfur) %, w/w |
|---|---|---|---|---|---|---|
| Control-SPs | 674.87 ± 59.35 | 0.24 ± 0.05 | -24.83 ± 0.09 | 33.2 ± 0.1 | - | - |
| Fuco-SPs | 708.48 ± 40.00 | 0.21 ± 0.10 | -27.07 ± 0.39 | 30.6 ± 0.1 | 9.30 ± 1.07 | 8.60 ± 0.01 |

**Figure 2. Physico-chemical characterization of the SPs.** SEM **(A)** and TEM **(B)** images of the Fuco-SPs. **C.** Swelling in the water of the Fuco-SPs due to the hydrogel nature of the particles. The size of one sample when resuspended in water (green) and in saline (blue). **D.** Size, zeta potential, and chemical composition of the SPs.

### 2.2.Biocompatibility of the SPs

The injectable hydrogel SPs were produced according to the green chemistry principles through the formulation method without using hazardous substances and organic solvents and were expected to be biocompatible.

An initial *in vitro* evaluation of biocompatibility of the developed SPs examined cyto- and hemocompatibility. The cytocompatibility of the SPs was assessed with a resazurin cell viability assay on endothelial cells. Following 24 h exposure, Control-SPs and Fuco-SPs did not affect cellular viability and metabolic activity of HUVECs at concentrations ranging from 0.1 to 1.5 mg $mL^{-1}$, exhibiting an excellent cytocompatible profile (cell survival > 90%, up to the highest tested concentrations of SPs) (**Figure 3**A). The upper limit for the tested concentration 1.5 mg $mL^{-1}$ of the SPs was selected to surpass the tested concentrations for the majority of the nanosystems *in vitro* (typically, maximum 400 µg $mL^{-1}$)[36] and the concentration of the SPs employed for further *in vivo* experiments in this work (71 mg SPs per 1 kg body weight or 1.1 mg SPs per 1 mL of blood). There was no significant difference between the Control-SPs and Fuco-SPs, as both did not provoke cytotoxicity.

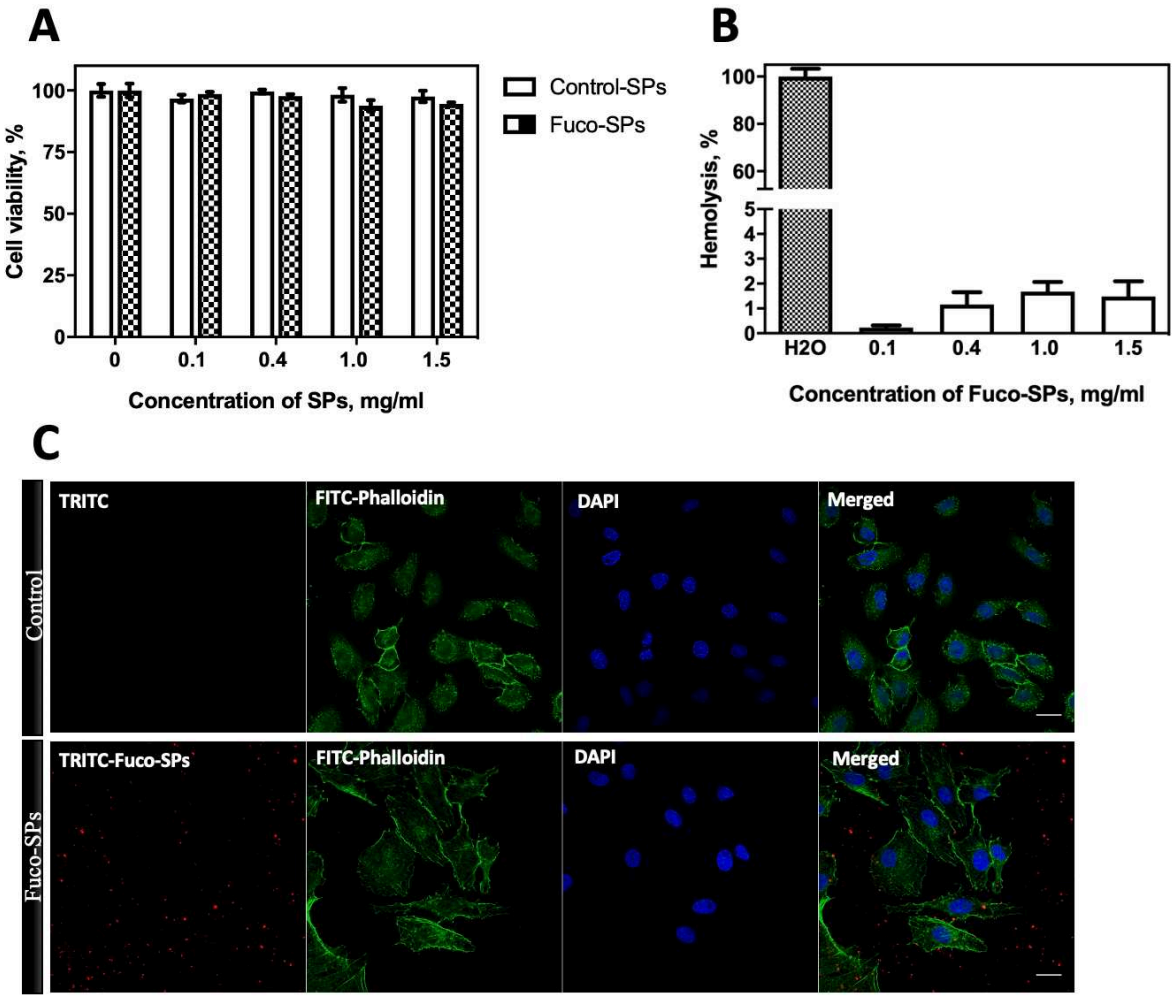


**Figure 3. Biocompatibility of the SPs.** Cytocompatibility **(A)** and hemocompatibility **(B)**. Confocal microscopy of HUVECs cultured without (control) and with Fuco-SPs **(C)** (scale bar = 30 μm).

Since the SPs in this study were designed for intravenous administration and were expected to have direct contact with blood, the Fuco-SPs were examined for their blood-compatible behavior by a hemolysis test on isolated murine red blood cells *in vitro* (Figure 3B). Even at the highest concentration of 1.5 mg $mL^{-1}$, the SPs presented a hemolytic index 1.51 ± 0.02%, below 2%, and considered nonhemolytic according to ISO 10993 - 4 standard.[37,38]

Morphology of the cells, co-cultured with Fuco-SPs, was visualized with confocal microscopy. No obvious morphological differences were revealed for HUVECs with Fuco-SPs and negative control, as depicted in Figure 3C. FITC-Phalloidin staining was used to visualize a cytoplasm and DAPI for nuclei. Moreover, the SPs were internalized by endocytosis as the merged images of all three probes revealed colocalization of the particles within the dye in the cytoplasm.

Collectively, these results suggest that the polysaccharide SPs have favorable biocompatibility for their application *in vivo*.

### 2.3.Binding of SPs to P-selectin *in vitro*

Knowing that fucoidan was homogeneously distributed in the structure of the hydrogel Fuco-SPs and constituted ~ 9% w/w of the composition, we investigated whether its quantity on the surface was sufficient for specific adhesion to its molecular target. While most of the publications assess targeting strategy *in vitro* in static conditions by flow cytometry or confocal microscopy,[17,39,40] our group developed a robust and tunable dynamic microfluidic method that mimics arterial or venous blood flow conditions to study the targeting efficacy for recombinant P-selectin or/and human activated platelet aggregates expressing P-selectin. It was previously validated on fucoidan-coated nano-/microcarriers (Figure S1, Supporting Information).[18–20]

First, fluorescent Fuco-SPs and Control-SPs were injected in the microchannels coated with recombinant P-selectin under arterial or venous shear rates (67.5 dyne $cm^{-2}$ vs. 6.75 dyne $cm^{-2}$), and their adhesion was visualized and quantified in real-time under fluorescence microscopy. According to obtained results, fluorescent Fuco-SPs depicted a significantly higher adhesion to P-selectin coating than Control-SPs both in arterial (374.25 ± 115.33 adhered Fuco-SPs vs. 30.25 ± 13.84 adhered Control-SPs, * $p < 0.05$) and venous (228.25 ± 36.67 adhered Fuco-SPs vs. 34.50 ± 18.16 adhered Control-SPs, ** $p < 0.01$) flow conditions (**Figure 4**A, E). There was no significant difference between the fluorescent signal of Fuco-SPs accumulation for arterial and venous flow conditions ($p=0.2731$). Fuco-SPs accumulation after injection onto P-selectin coating was in a linear dose-dependent manner as regards to the P-selectin concentration, $R^2=0.9904$ (Figure 4B). An experiment of competitive interaction illustrates that fucoidan solution pre-injection at 10 mg $mL^{-1}$ considerably reduced the attachment of the Fuco-SPs onto the microchannels with P-selectin (374.25 ± 115.33 vs. 19.75 ± 10.06, * $p < 0.05$) (Figure 4C).

To establish the specificity of the Fuco-SPs binding to P-selectin, the targeting assay was extended to other members of the selectin family: E- and L-selectin.[41] The percentage of the Fuco-SPs adhered to the E- and L-selectin was normalized over the mean number of the attached Fuco-SPs to a P-selectin coating at the equivalent concentration. Indeed, only 12.73 ± 3.66% of the SPs adhered to E-selectin and 0.26 ± 0.19% to L-selectin coating (Figure 4D). Thus, our results indicate that Fuco-SPs bind specifically to P-selectin but not to E- and L-

selectins, and these results are in accordance with a previous work of our group published by Bo L. *et al.* of fucoidan-functionalized polymer microcapsules.[18]

Overall, these findings are encouraging evidence of the sensitivity and selectivity of the Fuco-SPs, confirming fucoidan potential as a natural ligand of P-selectin.

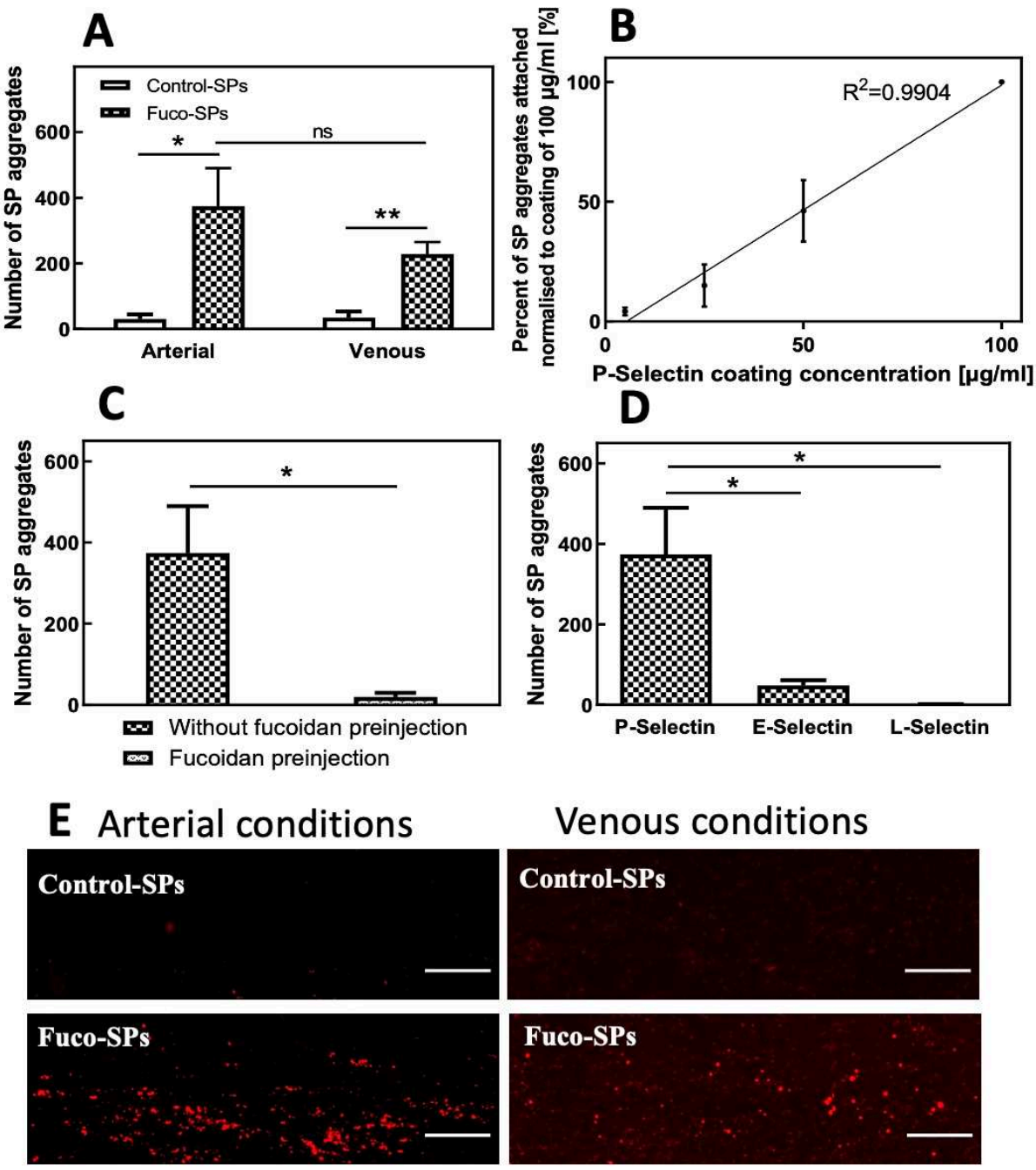


**Figure 4. Evaluation of the SPs interactions with selectins**. **A.** Adhesion of the Control-SPs or Fuco-SPs on the coating of the recombinant P-selectin in the microfluidic assay under arterial and venous flow conditions (n = 4). **B.** Concentration-dependent binding of the Fuco-SPs onto the coating of the P-selectin at a range of concentrations. **C.** Fucoidan pre-injection inhibited Fuco-SPs adhesion onto the P-selectin. **D.** Comparison of the Fuco-SPs binding to other selectins: E- and L-Selectin. **E.** Fluorescent microscope view of Control-SPs or Fuco-SPs

adhesion over a P-selectin coating of 100 µg $mL^{-1}$ under arterial and venous shear rates (scale bar = 20 µm).

## 2.4.rtPA loading onto the SPs and its release in saline. *In vitro* thrombolytic activity o rtPA-loaded SPs

Due to rtPA low bioavailability and requirement of high dose administration, coupling this enzyme to the biocompatible nanocarrier could overcome the drawbacks associated with a drug high dosage. Herein, an efficient rtPA encapsulation was achieved through the physical adsorption method due to electrostatic interaction: the protein, which is an amphoteric molecule, was put in contact with negatively charged polysaccharide SPs in the water at pH below rtPA isoelectric point IP=7.7[42,43] when rtPA presented a positive charge. The hydrogel nature of the SPs allowed reaching a high encapsulation efficiency of the rtPA of 64.78 ± 2.16% and 81.04 ± 1.86% for Control-SPs and Fuco-SPs, respectively. The confocal microscopy images of FITC-rtPA loaded onto TRITC-labelled Fuco-SPs revealed the uniform distribution of the rtPA within a porous structure of the hydrogel SPs, as evidenced by a green fluorescence from FITC-rtPA colocalized with the red fluorescence from the particles (Figure S2A, Supporting Information).

The release kinetics of rtPA from fucoidan-functionalized SPs was analyzed *in vitro* by flow cytometry[44] in saline at 37 °C under gentle agitation by quantifying the MFI of the FITC-labelled rtPA associated with TRITC-fluorescent Fuco-SPs. Figure S2B, Supporting Information indicated a gradual and continuous sustained release of the lytic agent from the SPs during the observation period: 46.41 ± 1.34% of the encapsulated protein was released during the first 15 min, and 76.98 ± 1.74% after 90 min. This release profile is classical for the hydrogels.[45]

The thrombolytic activity of the rtPA-loaded SPs *in vitro* was analyzed as a combination of amidolytic and fibrinolytic activities (**Figure 5**A, B, C). Amidolytic or enzymatic activity featured the ability of the proteolytic enzyme to hydrolyze the rtPA substrate. Interestingly, the amidolytic activities of rtPA on Control-SPs and Fuco-SPs were comparable to that of free rtPA (Figure 5A & 5B). The fibrinolytic experiment *in vitro* of the rtPA-loaded SPs was performed in a fibrin plate assay (Figure S3A, Supporting Information). The results indicated full retention of fibrinolytic activity (Figure 5C; Figure S3B, Supporting Information). rtPA loaded onto the SPs appeared to diffuse into the fibrin-agarose matrix and induce fibrinolysis in contact with fibrin. No significant difference was detected between both types of SPs, enabling us to utilize them in the following experiments.

Overall, the rtPA association with the SPs did not affect the drug amidolytic activity and fibrinolytic potential in our design. This result is in accordance with most studies on nanogels suggesting that drug encapsulation via a passive diffusion into the preformed nanogels does not affect the secondary structure of the adsorbed protein and its biological activity.[46]

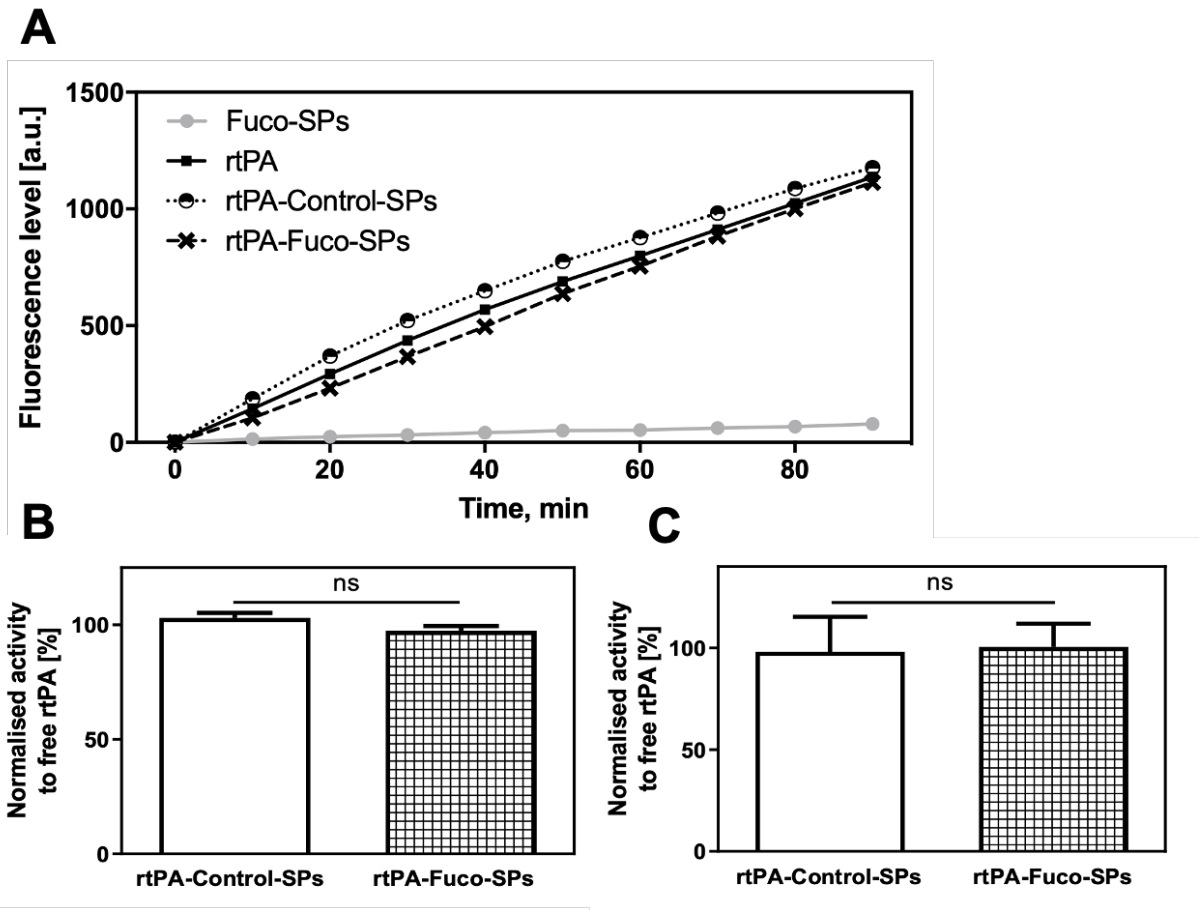


**Figure 5**. **Thrombolytic efficacy *in vitro* of the rtPA-loaded SPs. A - B.** Amidolytic activity measured by the PefaFluor® fluorogenic assay. **A.** The curves correspond to the fluorescence release and are correlated to the enzymatic velocity over 90 min. **B.** Corresponding quantitative analysis normalized to free rtPA at the same concentration at 90 min (n=3). **C.** Fibrinolytic activities of the SPs determined by a fibrin-plate agarose assay. The quantitative analysis normalized to free rtPA at the same concentration (n=3).

## 2.5. Unloaded and rtPA-loaded Fuco-SPs adhere to activated platelet aggregates *in vitro* under arterial flow

Since aggregation of activated platelets and platelet-mediated coagulation pathways are hallmark events in thrombosis, activated platelets are a suitable cellular target for nanocarrier binding to thrombi.[47] Before the *in vivo* tests, we complemented the targeting evaluation on selectins with the second set of microfluidic experiments to validate Fuco-SPs capability to

actively anchor onto the surface of activated platelets, expressing P-selectin. Thus, human whole blood was passed into collagen-coated microchannels to induce platelet activation and aggregation. Fuco-SPs or Control-SPs were then perfused at arterial shear stress and the accumulation of the fluorescence from the adhered SPs was detected on the surface of activated platelet aggregates. A quantitative analysis of the MFI revealed that Fuco-SPs adhered significantly more onto activated platelets than Control-SPs (2,678.34 ± 237.40 for Fuco-SPs vs. 392.44 ± 137.15 for Control-SPs, *** p <0.001, **Figure 6**A & 6B Left). Notably, adsorption of rtPA did not impair the Fuco-SPs clot-binding ability (1,880.80 ± 429.37 for rtPA-Fuco-SPs vs. 77.56 ± 40.25 for rtPA-Control-SPs, ** p <0.01, Figure 6B Right). There was no significant difference between unloaded and rtPA-loaded Fuco-SPs adhering to the activated platelets (p=0.1149).

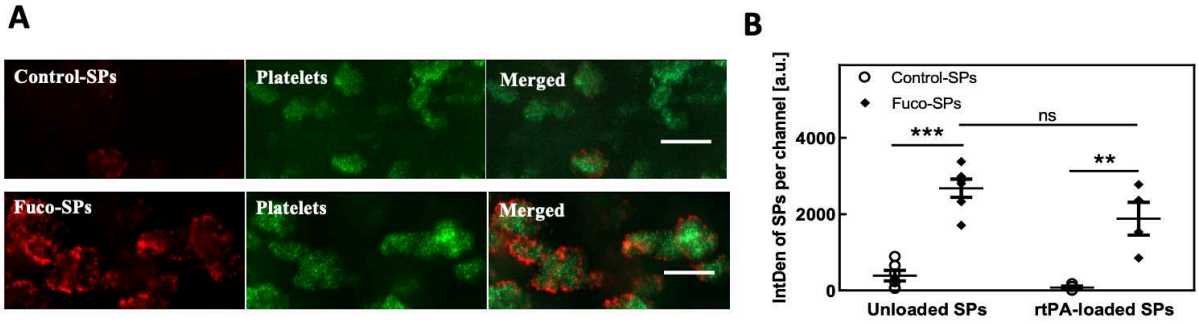


**Figure 6. Adhesion of the SPs over activated platelet aggregates. A.** Visualization by fluorescent microscopy of the attached unloaded SPs on the microchannels after the formation of the platelet aggregates (scale bar = 20 µm). **B.** Corresponding quantification of the integral density of the unloaded (n=6) and rtPA-loaded (n=4) Control-SPs and Fuco-SPs in ImageJ.

In conclusion, these *in vitro* experiments provided crucial evidence of molecular interaction and high affinity between the P-selectin on the activated platelets and fucoidan-functionalized SPs, which was maintained after loading the thrombolytic agent. This finding presumes that the administration of the rtPA-Fuco-SPs could enable a specific delivery of the rtPA-immobilized SPs to the platelet-rich thrombus with higher drug accumulation.

### 2.6.Tissue distribution in vivo of fucoidan-functionalized SPs

After their intravenous injection, the distribution *in vivo* of Fuco-SPs was examined by histological analysis of the excised tissues with alcian blue staining of negatively charged particles in the healthy mouse. The presence of Fuco-SPs in four main organs of excretion (liver, spleen, lungs, and kidneys) was assessed on several sections for each organ. Our results revealed that the polysaccharide Fuco-SPs distributed primarily into the spleen post-

administration, indicating the splenic clearance. The particles accumulated in the liver to a lower extent, while their presence in the kidneys and lungs remained minor. These differences are presented in Figure S4, Supporting Information. Our data are in agreement with other deformable polymer hydrogel-like particles in their submicron and micron size range.[48]

### 2.7.*In vivo* thrombolytic efficacy

Whereas demonstrating the *in vitro* activity of the rtPA immobilized on the drug delivery system is important, the *in vivo* therapeutic effect is paramount. A murine thromboembolic stroke model was established by *in situ* injection of 1 IU of thrombin into the MCA by provoking a coagulation cascade and formation of both fibrin- and platelet-rich clots in the lumen of the artery.[49,50] **Figure 7**A highlights the *in vivo* experiments design, and Figure 1C the potential mode of action of the Fuco-SPs on the thrombus. The treatment options – control saline, rtPA 10 mg $kg^{-1}$, or rtPA-Fuco-SPs at 10 mg $kg^{-1}$ – were intravenously injected 20 min after ischemic onset under rtPA clinical mode of administration: 10% bolus followed by 90% infusion. It is important to note that 10 mg $kg^{-1}$ is a relevant dose in mice in place of 0.9 mg $kg^{-1}$ in humans because of a lower sensitivity of human rtPA in murine plasma.[51] No morbidity or mortality was observed in the mice during therapeutic experiments, suggesting that rtPA-Fuco-SPs do not provoke acute toxicity under the current conditions.

Cerebral blood flow was monitored throughout the treatment via laser Doppler speckle contrast imaging, a high resolution and high-speed technique that instantly visualizes microcirculatory tissue blood perfusion. The reduction of the blood flow in the ipsilateral cerebral hemisphere due to the stroke was restored by 33.97 ± 5.15% after 40 min treatment with rtPA-Fuco-SPs; by contrast, in the rtPA and saline group for which the perfusion was improved only by 15.16 ± 6.49% and 10.33 ± 4.62%, respectively, in this experiment (Figure 7D). The representative laser Doppler speckle multispectral imaging in the ipsilateral and the contralateral hemispheres at 0 min and 40 min are expressed in Figure 7C. Accelerated Video S1A, B, C recorded the perfusion in real-time for all conditions. These data were confirmed by the angiographic analysis performed 24 hours later and assessed by a blinded observer based on TICI grade flow scoring measured by magnetic resonance angiography (MRA). Indeed, similar to some untreated stroke patients, the blood clots were gradually lysed post-stroke in this murine model: at 24 h after thrombotic occlusion, 40% of mice exhibited a total recanalization (score 3) and 60% partial perfusion (score 1 and score 2) of the MCA when injected with saline (Figure 7G; Figure S5A, Supporting Information). However, after the treatment with rtPA-Fuco-SPs, most of the cases were entirely recanalized (score 3). For the

rtPA treated group, no animal achieved a score 1 of minimal perfusion, and 66.6% of cases showed a partial score 2 level of recanalization.

We then utilized magnetic resonance imaging as a powerful technique to quantify the volume of brain damage at 24 hours after stroke onset. Using T2-weighted MRI sequences, we observed that the size of the ischemic brain lesions for the control saline group was 14.80 ± 3.34 $mm^3$ whereas for the rtPA-loaded fucoidan-targeted SPs it was 4.63 ± 1.59 $mm^3$ (Figure 7E & 7F). rtPA-conjugated Fuco-SPs reduced the ischemic zone almost 2-fold of the free rtPA, despite the fact that these data were non-significant due to the limited number of the animals as to the well-known effect of free rtPA in this murine model.[50] Out of all treated animals with rtPA-Fuco-SPs, 66.6% of the animals displayed small lesion sizes (<3 $mm^3$), and 33.3% had medium lesion sizes (<11 $mm^3$). In the rtPA group, only 33.3% of the animals displayed a small infarct zone. In the saline treatment group, we recorded 60% of the animals with severe (<20 $mm^3$) and critical (>20 $mm^3$) lesions and no animals with small lesions (Figure S5B, Supporting Information).

To monitor the BBB integrity disrupted by ischemic stroke,[52] extravasation of gadolinium injected intravenously was detected and quantified on T1-weighted MRI images at day 4 after stroke (Figure 7H & 7I). Gadolinium extravasation from the blood into the brain parenchyma was unmistakably located at the ischemia-affected region where the BBB is compromised. rtPA-Fuco-SPs treatment group demonstrated a significant BBB preservation over control groups of free rtPA and saline with only a subtle BBB breakdown of 3.45 ± 1.40 $mm^3$.

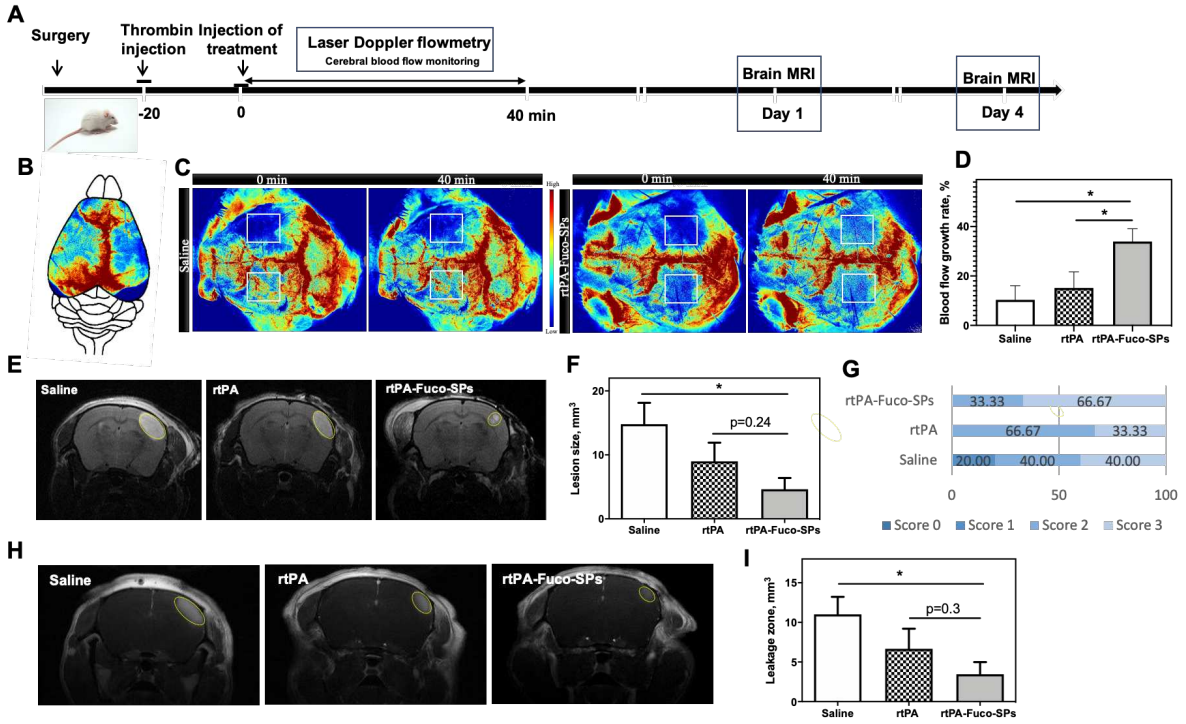


**Figure 7. Thrombolytic efficacy *in vivo* in the murine ischemic stroke model**. **A.** Schematic of the design of the *in vivo* experiment. **B – D.** Cerebral blood flow reperfusion monitored by the laser speckle contrast imaging during the 40-min treatment (n≥5). Schematic image of the perfusion in the microcirculatory brain tissue. **(B)**. The representative multispectral photos in the ROI of ipsilateral (upper) and contralateral (lower) hemispheres at 0 min and 40 min for saline and rtPA-Fuco-SPs groups **(C)**. The growth rate of the cerebral reperfusion in the ipsilateral hemisphere after 40 min treatment injection **(D)**. **E.** MRI images of the infarct lesion 24 h post-stroke with the corresponding quantification of its volume **(F)**, (n≥5). **G.** Angiographic scores of the MCA reperfusion at day 1 after stroke induction by MRI. **H.** MRI images of the BBB permeability at day 4 post-stroke with the corresponding quantification of its volume **(I)**, (n≥5).

In order to confirm the accumulation of Fuco-SPs within the thrombus area *in vivo*, we injected fluorescent-labeled SPs at the therapeutic concentration as in the stroke model into the $FeCl_3$ model of venous thrombosis in mice. Upon histological examination of the thrombus-affected area of the mesenteric vein, Fuco-SPs were clearly identified on the green-fluorescent labeled thrombus **(Figure 8**A**)**. By a quantitative analysis of the MFI normalized by the size of the thrombus, it was evidenced a highly increased TRITC signal from fucoidan-functionalized SPs group comparing with Control-SPs (9.48 ± 2.19 for Fuco-SPs vs. 1.48 ± 0.35 for Control-SPs, ** $p < 0.01$, Figure 8B).

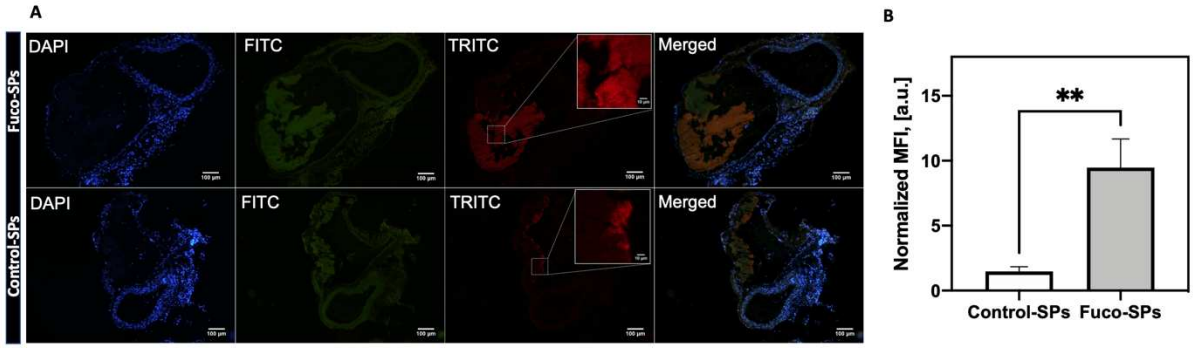


**Figure 8. *In vivo* targeting in the $FeCl_3$ murine model of thrombosis. A.** Histological analysis of thrombi in the mesenteric vein by fluorescent microscopy. The venous vascular wall is visualized with DAPI staining; thrombus is stained in green due to DIOC6 labeling of platelets; Fuco-SPs and Control-SPs are fluorescently labeled with TRITC. Inserts are a magnification of dashed Regions of Interest of the TRITC signal. **B.** Corresponding quantification of MFI from the adhered TRITC-SPs in the thrombi (n=5).

Overall, the apparent superiority of rtPA-Fuco-SPs to reduce the brain tissue injury area in comparison with saline and rtPA at the same dose, combined with a favorable safety profile of the SPs, makes them a promising nanomedicine-based approach for the treatment of acute arterial thrombosis.

## 3. DISCUSSION

The revolutionary treatment with alteplase to dissolve thrombi and restore blood flow is a standard of care in acute thrombotic events, but it is certainly not risk-free. Nanomedicine exploits a profound understanding of the molecular mechanisms involved in thrombus formation and offers outside-the-box strategies to effectively target and dissolve the blood clots in the body with fewer systemic and neurological complications.[53]

In this study, rtPA was associated with hydrogel-like polysaccharide SPs, synthesized by a simple and reproducible miniemulsion / crosslinking process. The soft structure of chemically crosslinked hydrogels resembles those of extracellular matrices and may prevent tissue irritation, providing a convenient and versatile platform for storage and site-specific delivery of a drug to the thrombi.[54] Our approach's novelty is exclusively polysaccharide nature of the particles – from dextran and fucoidan without any chemical modification, as well as green chemistry synthesis technique. Intriguingly, several articles claim that dextran[55] and fucoidan[56,57] themselves exert some antithrombotic action that makes them an excellent starting material for the nanocarrier. Hydrophilic polysaccharide surfaces lead to longer circulating NPs since they avert the formation of a protein corona and early macrophage internalization.[58] Moreover, natural polysaccharides are advantageous to synthetic polymers

in terms of safety, abundance in nature, and low cost. Overall, we considered the issues imperative for high biosafety and potential future clinical translation of Fuco-SPs by (I) the choice of biocompatible and biodegradable materials, all with FDA-approval; (II) a relatively simple and efficient production by a mild synthesis method without the utilization of the hazardous substances and organic solvents; (III) targeting agent of natural origin– fucoidan – that is being validated in clinical trials for thrombosis.

After fabrication and extensive physico-chemical characterization of the SPs, we confirmed their cyto- and hemocompatibility at concentrations up to 1.5 mg $mL^{-1}$ (Figure 3A & 3B). The main pathway of the polysaccharide Fuco-SPs tissue distribution *in vivo* upon intravenous injection was the spleen (Figure S4, Supporting Information). Future studies should include the tests of thrombogenicity and immunogenicity *in vivo*.

The Fuco-SPs were associated with a thrombolytic agent by physical adsorption, allowing a high encapsulation efficiency of the rtPA of 81.04 ± 1.86% due to their hydrogel-based structure. Classically, alteplase is loaded onto the NPs using the covalent amide bond formation via EDC/NHS reaction between the primary amines on the rtPA molecule and the nanocarriers containing carboxyl groups. As a mild drug encapsulation method, adsorption is preferred to covalent bioconjugation to load fragile molecules such as proteins to avoid changes in the protein structure and function that might result in its partial denaturation and loss of biological activity.[59] The fibrinolytic diffused through the matrix of the porous SPs (Figure S2A, Supporting Information), fully preserving its enzymatic and fibrinolytic potential *in vitro* (Figure 5). Friedrich *et al*. demonstrated that the adsorptive bound rtPA liberated faster from the particles and spread more readily into the fibrin matrix than covalently bound rtPA,[60] which may be beneficial in targeted thrombolysis. Although a rising number of recent articles apply a controlled release of the thrombolytics via endogenous and exogenous stimuli, we chose not to incorporate sophisticated nanodesigns and demonstrated a gradual and continuous rtPA release from the SPs without an external trigger (Figure S2B, Supporting Information) so as to facilitate future regulatory approvals.

The clot targeting strategy of the SPs was achieved by the introduction of the fucoidan to the polysaccharide solution at 9% w/w. Functionalization with fucoidan permitted the high-affinity binding of Fuco-SPs to its molecular target P-selectin in a dynamic microfluidic method that mimics arterial or venous blood flow conditions in a dose-dependent manner (Figure 4A-B, AE). Importantly, this type of interaction is selective, as SPs did not adhere to other selectins: E- and L-selectin *in vitro* (Figure 4D). When the microchannels were covered with activated platelet aggregates, both unloaded and rtPA-loaded Fuco-SPs were capable of binding these

micro-clots (Figure 6). Once tested in the *in vivo* model of venous thrombosis, Fuco-SPs were identified on the $FeCl_3$-induced thrombi by histological examination, contrary to Control-SPs (Figure 8). Our data validate an inimitable and efficient thrombus targeting approach of the Fuco-SPs, using a clinical algae-derived compound. Yet, a surge in strategies involving dual or even more surface targeting moieties is being witnessed in academic works. For instance, the combinatory targeting of GPIIb/IIIa receptors and P-selectin on activated platelets with two peptide ligands on the lipid nanovesicles enhanced thrombus binding capacities in a synergic manner.[61] Another notable example is the biomimetic functionalization of NPs with platelet membrane coating that enabled thrombus directing via multiple platelet receptors.[62] These combinations of NP modifications represent a promising strategy for developing next-generation blood clot-targeting NP platforms for therapy and/or diagnostics.

The experiments on the murine thrombin-induced thromboembolic stroke model supported the therapeutic effect of the rtPA-Fuco-SPs *in vivo* (Figure 7). The findings of the submicroparticle-associated rtPA treatment group outperformed those of free rtPA at the same concentration, as we observed a more rapid clot dissolution and MCA reperfusion, which minimized the brain injury and resulted in subsequently smaller infarct area post-stroke by MRI. The prevailing method for assessing the brain infarct volume is a brain tissue staining with 2% 2,3,5-triphenyltetrazolium chloride (TTC), which labels non-injured tissue and leaves the infarct area white. Several groups previously reported the reduction of the infarct zone in preclinical models by nanomedicinal product. For example, the magnetic iron oxide ($Fe_3O_4$)-microrods[63] and polyacrylic acid-stabilized magnetic NPs[64] conjugated with rtPA diminished the brain infarct lesion in the $FeCl_3$ murine model of ischemic stroke of MCA. These designs, however, require an external magnet for targeting and to complement chemical lysis with rtPA with mechanical one of the magnetic rotations. Without any clinically approved medical device to impose a high magnetic force on the NPs in deep blood vessels, it would probably be desirable for nanocarrier formulation to avoid external assistance. Mei *et al.* stated that only the synergistic effect of rtPA-loaded polymer micelles and a reactive oxygen species (ROS)-eliminating antioxidant suppressed an infarct volume and improved neurological deficit after brain ischemia in the mouse model of photo-thrombotic MCA occlusion.[65] In our case, the therapeutic benefit of rtPA-Fuco-SPs could be ascribed to faster MCA reperfusion and, hence, prevention of the major brain injury due to higher rtPA accumulation on the thrombus site as to active targeting and specific P-selectin interactions of the Fuco-SPs.

Moreover, the animals in the rtPA-Fuco-SPs group suffered a lower level of BBB disruption by the ischemic stroke that was quantified on T1-weighted MRI images with

gadolinium. It is vital to underline that although in this article we utilized fucoidan on the SPs purely for the P-selectin targeting purpose, new avenues of research are deciphering its neuroprotective role, particularly after cerebral ischemic events.[66] Altogether, this first proof-of-concept *in vivo* results of Fuco-SPs show an astonishing potential of the nanomedicine-based approach for the targeted treatment of acute thrombosis. We speculate that the submicron size of the particles, along with their active thrombus-targeting moiety, should maintain rtPA-loaded nanocarrier within the intravascular compartment to exert its thrombolytic activity. It should prevent the leakage of rtPA into the brain parenchyma, reducing the risks of NMDA receptors-mediated neurotoxicity and hemorrhages.[67] Further studies could compare a single or a double bolus route of administration of rtPA-Fuco-SPs due to the rtPA preservation by SPs, and, thus, a more comfortable treatment option for patients.

Nevertheless, as none of the available *in vivo* rodent experimental models of acute thrombosis accurately recapitulates all the aspects of human disease progression and heterogeneity, it is recommended to validate any translational concept in multiple models to ensure its therapeutic efficacy and safety. Notably, in 2019, Xu *et al.* proposed a biomimetic strategy of platelet membrane-camouflaged PLGA NPs with rtPA that was studied in several *in vivo* models: pulmonary embolism, $FeCl_3$-induced arterial thrombosis, and ischemic stroke model.[62]

Due to technical challenges and strict regulatory requirements, the clinical translation of the nanopharmaceutical products happens slowly. The rtPA-Fuco-SPs representing an actively targeted nanodelivery system reach a balance of safety, simplicity, and functionality concerning the projected clinical application. While they were designed and fabricated in the academic laboratory at the range of ~10 mg per batch, the industrial scale-up of the process with high reproducibility under GMP conditions and intended quality standards is essential to establish in order to obtain the necessary amounts for further screening and, ultimately, clinical use. For instance, high-precision microfluidic and micropatterning methods for the fabrication of monodisperse NPs with uniform physicochemical characteristics and low batch-to-batch variability are becoming prevalent and are compatible with GMP standards.[68] Finally, an adequate sterilization method should be validated to prevent nanoparticle damage and alteration in the product's parameters.

## 4. CONCLUSION

In the present study, we designed and fabricated fucoidan-functionalized 100% polysaccharide submicroparticles from biocompatible and FDA approved components as a P-selectin targeting

drug delivery system for thrombolytic therapy. The physico-chemical properties and a biocompatibility analysis of these SPs were thoroughly evaluated, and alteplase was effectively immobilized onto the SPs with full retention of its enzymatic and fibrinolytic potential *in vitro* and sustained drug-release kinetics. We established *in vitro* by dynamic flow microchamber assays that the fucoidan-functionalized nanosystem specifically adhered to the recombinant P-selectin in a dose-dependent manner, but not to E- and L-Selectins, and to human activated platelets. In $FeCl_3$ model of thrombosis, Fuco-SPs accumulated in the thrombus. Finally, our findings revealed in the murine model of ischemic stroke that rtPA conjugation to the Fuco-SPs could enhance the thrombolytic activity of the clinical agent *in vivo*. The blood flow perfusion was restored more rapidly, which resulted in smaller post-ischemic cerebral infarct lesions and higher BBB protection. In summary, an alteplase-associated hydrogel-based nano-delivery system with fucoidan demonstrates a solid argument for improved thrombolytic therapy in terms of safety and efficacy in the preclinical studies. In future research, our biocompatible Fuco-SPs could also vehicle other therapeutic and/or molecular imaging agents in the vascular compartment to target P-selectin overexpressed pathologies, such as cardiovascular diseases[69] or some cancers.[70,71]

## 5. EXPERIMENTAL SECTION

*Materials:* Dextran 40 kDa and TRITC-dextran 40 kDa were provided by TdB Consultancy (Uppsala, Sweden). Fucoidan (Mn = 18 kDa/Mw = 104 kDa) was a gift from Algues & Mer (Ouessant, France). Sodium trimetaphosphate (STMP), methylene blue hydrate, and Human Serum Albumin (HSA) were purchased from Sigma-Aldrich (Saint-Quentin-Fallavier, France). Polyglycerol polyricinoleate (PGPR) was obtained from Palsgaard France S.A.S. (Lyon, France). Vegetable (sunflower) oil was purchased from a local supermarket. The SPs were encapsulated with commercially available rtPA (Actilyse®, Boehringer Ingelheim) that was reconstituted at 1 mg $mL^{-1}$, aliquoted, and stored at -80 ºC. Chromatography paper was obtained from GE Healthcare (Chicago, Illinois, United States). Fibrillar type I collagen Horm® was obtained from Takeda (Linz, Austria). 96-Well Cell Culture Plates (Costar) were obtained from Corning Incorporated. PPACK (Phe-Pro-Arg-Chloromethylketone) 75 µM tubes were purchased from Cryopep (Montpellier, France). Flow chambers (Vena8 Fluoro+) were provided from Cellix Ltd (Dublin, Ireland).

*Submicroparticle synthesis:* Polysaccharide submicroparticles (SPs) were obtained via a water-in-oil (w/o) emulsification combined with a crosslinking process.[16,17] Polysaccharide solution (300 mg $mL^{-1}$, 6 M NaCl) was prepared as a mixture of dextran 40 and 5% TRITC-dextran 40 (for fluorescent SPs). To synthesize functionalized SPs with fucoidan (Fuco-SPs), 10% w/w of fucoidan was added. Table S1, Supporting Information describes the synthesis parameters of SPs.

First, the organic phase of 15 mL of sunflower oil and 6% w/v PGPR in Falcon® 50 mL was prepared and cooled down for 20 min at -20 ºC. In the meantime, 1,200 mg of the polysaccharide solution was incubated with 120 µL of 10 M NaOH under magnetic stirring for 10 min. 240 µL of STMP solution (30% w/v in water) was added into the aqueous phase under magnetic stirring and mixed for 20 seconds on ice. Next, emulsification was achieved by the dropwise injection of 600 µL of the aqueous phase into the organic phase and dispersed with a stand-disperser (Polytron PT 3100, dispersing aggregate PT-DA 07/2EC-B101, Kinematica, Luzernerstrasse, Switzerland) at 30,000 rpm for 4 min on ice. The obtained w/o emulsion was transferred into 50 ºC for the crosslinking reaction of polysaccharides with STMP for 20 min. The crosslinked suspension was washed in 30 mL PBS 10x for 40 min under high magnetic stirring at 750 rpm. The mixture was then centrifuged (BR4i, JOUAN SA, Saint Herblain, France) for 10 min at 3,000 g in Falcon tubes. The organic phase was recovered and

ultracentrifuged (Optima MAX-XP, Ultracentrifuge, Beckman Coulter, Brea, California, United States) in PBS for 45 min at 15,000 g. The obtained pellet was washed by ultracentrifugation 2 times in 0.04% Sodium Dodecyl Sulfate (SDS) solution and then 3 times in ultrapure water to purify the SPs. The resulting SPs were suspended in water or 0.9% NaCl with 0.02% Tween 20 (Sigma) and stored at 4 ºC.

*Cell culture and cytotoxicity assay:* To evaluate the cytotoxicity of the SPs, Fluorometric Cell Viability Assay (Resazurin) was used on confluent Human Umbilical Vein Endothelial Cells (HUVECs). The cells were cultured in DMEM supplemented with 10% (v/v) fetal bovine serum, 4 mmol of l-glutamine, 100 units $mL^{-1}$ of penicillin, and 100 µg $mL^{-1}$ of streptomycin and kept in an incubator at 37 °C in a humidified atmosphere of 5% $CO_2$. Cells were seeded into 96-well plates to adhere, 10,000 cells per well. Following 24 h of incubation to reach ~80% confluency, the medium in the wells was changed to the one containing the SPs at concentrations ranging from 0.1 to 1.5 mg $mL^{-1}$ and cultured for another 24h. The SPs were prior sterilized under the UV light for 15 min. Next, the medium was replaced with 100 µL 10% Resazurin solution, and the plates were covered in foil and incubated for 2h. Culture media were used as a positive control. The Resazurin's fluorescent signals were monitored using 540 nm excitation and 590 nm emission wavelengths on Infinite® 200 PRO microplate reader (TECAN Group Ltd., Mannedorf, Switzerland). The obtained fluorescence (Fl) values were blank corrected, and the relative cell viability was expressed as $Fl_{SPs}$ / $Fl_{control}$ × 100%, where $Fl_{control}$ was obtained in the absence of the SPs. The experiment was performed in hexaplicate.

To examine the potential cell cytoskeleton organization mediated by Fuco-SPs, HUVECs cells were cultured in 8-well Lab-Tek II Chamber Slide w/Cover (Lab-Tek®, Thermo Fischer Scientific, Massachusetts, United States) with 10,000 cells per well. The wells' medium was changed 24 h after to the one containing TRITC-Fuco-SPs at 1.5 mg $mL^{-1}$ and was incubated for another 24 h. Cells cultured in the medium without the SPs were set as control. Next, cells were fixed with 4% paraformaldehyde for 30 min at room temperature (RT). After rinsing with PBS, cells were labeled and permeabilized with the 200 µl mixture of FITC-Phalloidin (1:200, Sigma-Aldrich, USA) / DAPI (1:100, Thermo Fisher Scientific, Massachusetts, United States) / 0.01% v/v Tween 20 in PBS and incubated under low agitation for 1 h at RT. The cells were afterward washed 3 times with PBS. The support of the chamber slides was removed, and the slides were mounted with a few drops of the aqueous mounting medium and kept at 4 ºC until visualization with the confocal microscope (Zeiss LSM 780, Iena, Germany).

*Hemocompatibility test*: Hemolysis assay was adapted from the publication[17] and performed on washed isolated murine erythrocytes. Murine blood was collected in sodium citrate 3.8% (w/v) and centrifuged at 800 g for 5 min to isolate red blood cells. The supernatant was removed, and the pellet of erythrocytes was resuspended at 20% (v/v) in distilled water (positive control, 100% hemolysis), normal saline (negative control, no hemolysis), and the Fuco-SPs at concentrations from 0.1 to 1.5 mg $mL^{-1}$ in Eppendorf. The tubes were incubated on a rotator at 37 °C for 1.5 h and then centrifuged at 3,000 g for 5 min. The absorbance (A) of the supernatants was measured on Infinite® 200 PRO microplate reader (TECAN Group Ltd., Mannedorf, Switzerland) at 590 nm. Each sample was run in triplicate. The percentage of hemolysis was determined by the formula: Hemolysis degree (%) = 100% x $(A_{sample} - A_{negative\ control})/(A_{positive\ control} - A_{negative\ control})$.

*Physico-chemical characterization:* The submicroparticle (SP) formulations were studied for particle morphology, size and zeta potential distributions, mass concentration, and elemental composition.

Particle morphology was visualized by Transmission Electron Microscopy (TEM) (Philips FEI Tecnai 12, Amsterdam, Netherlands), negatively stained with 1% (w/v) uranyl acetate for 5 minutes, and Environmental Scanning Electron Microscopy (ESEM) (Philips XL30 ESEM-FEG, Amsterdam, Netherlands). Hydrodynamic size and Zeta potential (ζ-potential) were measured by Dynamic Light Scattering (DLS) and Electrophoretic Light Scattering (ELS), respectively (Zetasizer Nano ZS, Malvern Instruments SARL, Orsay, France). Samples were diluted in distilled water or saline for size and in 1 mM KCl for ζ-potential determination. All runs were performed at 25 °C in triplicate.

Mass concentration was determined by freeze-drying. An elemental analyzer-mass spectrophotometer was used for the quantification of the sulfur (presence of fucoidan). To prove the crosslinking with STMP, the total reflection X-ray fluorescence spectroscopy (TXRF) technique was applied to quantify the phosphorus content on the SPs (S2 PICOFOX Bruker, Massachusetts, United States).

*Sulfate and fucoidan quantification:* The sulfate content of fucoidan was determined by a semi-quantitative solid-phase colorimetric assay.[72] Briefly, 5 µL of Fuco-SPs in suspension at a concentration of 2 mg $mL^{-1}$ were dropped on a piece of Whatman Chromatography paper grade 1. This was repeated 5 times on the same point, allowing the paper to dry at 50 ºC in between. The paper was first soaked into a methanol/acetone (6:4) solution for 3 min and then into a methanol/acetone/water (6:4:15) solution with 50 mM HCl and 0.1% w/w methylene blue for 10 min. Finally, the paper was extensively washed with acetic

acid/methanol/acetone/water (5:6:4:75) until no coloration was detected in the washing solution. The paper was then transferred to the Eppendorf, containing 0.5 mL methanol with 2% w/v SDS, and incubated for 15 min at 50 ºC. 0.2 mL of the extracted dye was placed in a 96-well plate, and its concentration was determined by reading absorbance at 663 nm on an Infinite® 200 PRO microplate reader (TECAN Group Ltd., Mannedorf, Switzerland). Standard curves were obtained from fucoidan in solution with known concentrations.

*Loading rtPA on the SPs:* rtPA was immobilized onto the SPs by adsorption. 100 µl of SPs (5 mg $mL^{-1}$) was mixed with 100 µl of rtPA (1 mg $mL^{-1}$) in ultrapure water and then incubated for 1 h at RT. Free unabsorbed rtPA was removed by 3 cycles of ultracentrifugation (15 min, 15,000 g). The SPs with adsorbed rtPA (rtPA-SPs) were resuspended in water and used for the drug loading efficiency quantification.

*Drug encapsulation efficiency:* The amount of rtPA loaded on the SPs was measured using the Pierce BCA protein assay kit (Life Technologies SAS, Courtaboeuf, France). Briefly, 200 µl of working reagent was added to 25 µL of each sample in 96 well-plate. The absorbance at 562 nm was read on the Infinite® 200 PRO microplate reader (TECAN Group Ltd., Mannedorf, Switzerland) after 30 min of incubation at 37 °C and cooling to RT for 10 min. The concentration of the drug was extrapolated by a calibration curve prepared with different concentrations of rtPA.

The encapsulation efficacy (EE) was calculated as EE (%) = 100% x B/A, whereas B is the amount of rtPA loaded onto the SPs and A is the total quantity of rtPA put in contact with the SPs.

*In vitro rtPA release:* The release of rtPA from the Fuco-SPs was assessed by flow cytometry.[44] FITC-rtPA (Abcam, Cambridge, United Kingdom) at 1 mg $mL^{-1}$ was placed in contact with TRITC Fuco-SPs at 5 mg $mL^{-1}$ for 1 h at RT. The suspensions were added to tubes pre-filled with 400 µL of saline and placed under gentle agitation at 37 ºC. At each time point of 0, 15, 30, 45, 60, and 90 min, the tubes were analyzed with a BD FACS Aria™ III flow cytometer (Becton Dickinson, New Jersey, United States). The TRITC-Dextran, excited by a 543 nm laser, was detected at 569 nm, while the FITC-rtPA, excited at 480 nm, was detected on a 530/30 nm PMT. Flow cytometry analyses were performed in triplicates with Diva software (Becton Dickinson). The protein release curve was obtained by normalizing the values of Mean Fluorescence Intensity (MFI) of the FITC-rtPA still associated with TRITC-Fuco-SPs.

*In vitro amidolytic activity of rtPA-loaded SPs:* Amidolytic activity of rtPA loaded SPs was assessed with the fluorogenic substrate PefaFluor® tPA (Cryopep, Montpellier, France). 2.5 µL of samples (20 µg $mL^{-1}$) was put in contact with 97.5 µL of 100 mM HEPES buffer (pH

8.0, 154 mM NaCl, 0.1% HAS) in the 96-well plate. After the addition of 10 µL PefaFluor® at 1 mM, a kinetic profile was obtained by measuring the fluorescence level at 440 nm every 2 min for 90 min at 37 ºC with Infinite® 200 PRO microplate reader (TECAN Group Ltd., Mannedorf, Switzerland). Free rtPA was used at the same concentration based on the Pierce BCA protein assay. Increase of fluorescence corresponded to the fluorogenic peptide substrate hydrolysis by rtPA. Enzymatic activity was determined from the resulting kinetic profile and compared to the one of free rtPA.

*In vitro fibrinolytic activity of rtPA-loaded SPs:* To assess the fibrinolytic activity of rtPA-loaded SPs, a fibrin lysis clot experiment was performed. 5 mL of TRIS Buffer with 3% w/v low melting agarose (Carl Roth GmbH þ Co. KG, Karlsruhe, Germany) were heated to 65 °C. 5 mL of fibrinogen (from human plasma, Sigma Aldrich) solution in TRIS buffer (5 mg $mL^{-1}$) was slowly heated to 37 °C. Once the agarose solution reached 65 °C, it was cooled to 37 °C, and 2.5 U of thrombin (from human plasma, Sigma Aldrich) was added. Next, a fibrinogen solution was slowly added into the agarose/thrombin mixture under gentle agitation to avoid the formation of bubbles. The reaction mixture was poured into a 9 cm Petri dish and cooled at 4 °C for 30 min until the fibrin clot became visible. On the solidified agarose gel, round wells were formed using a 3 mm punch as sample reservoirs. 5 µL of each SPs sample (45 µg $mL^{-1}$) was dropped into the wells and incubated overnight at 37 °C in a humid environment. The degree of fibrin lysis was quantified with ImageJ by comparing the size of the fibrinolysis circle of the samples and free rtPA at the equivalent concentration based on the Pierce BCA protein assay.

*Flow microchamber experiments:* An *in vitro* flow adhesion assay was performed to evaluate the affinity of the Fuco-SPs with their molecular target. Micro-channels of Vena8 $Fluoro^{+}$ chambers (width: 0.04 cm, height: 0.01 cm, and length: 2.8 cm; Cellix Ltd, Dublin, Ireland) were coated overnight with recombinant human P-selectin, L-selectin or E-selectin (R&D systems France, Lille, France) at 100 µg $mL^{-1}$ and left overnight at 4 °C. To confirm the concentration-dependent binding of Fuco-SPs to P-selectin, some channels were coated with P-selectin at a range of concentrations (5, 25, 50, and 100 µg $mL^{-1}$). Channels were then washed with NaCl 0.9% and further incubated with HSA at 10 µg $mL^{-1}$ for 2 h.

A suspension of fluorescently labeled Control-SPs or Fuco-SPs (1 mg $mL^{-1}$) in saline was passed through the channels for 5 min at arterial and venous flow conditions (shear stress 67.5 dyne $cm^{-2}$ and 6.75 dyne $cm^{-2}$) using an ExiGo™ pump (Cellix Ltd, Dublin, Ireland). For the competitive binding experiment, fucoidan solution (10 mg $mL^{-1}$) was injected 5 min prior to the Fuco-SPs at the same rate. Then, all the channels were washed with NaCl 0.9% for 1 min.

The binding of the adhered SPs was visualized in real-time under fluorescence microscopy (Axio Observer, Carl Zeiss Microimaging GmbH, Iena, Germany). For the quantitative analysis, the number of fluorescent SP clusters on each channel was measured using the "Analyze particles" tool in the image analysis software ImageJ (NIH, Bethesda, U.S.) with a 4-pixel threshold to eliminate the background noise.

To further investigate the binding efficiency of unloaded and loaded SPs to activated platelets, the microchannels of Vena8 Fluoro$^{+}$ were coated with fibrillar type I collagen Horm® (50 µg mL$^{-1}$) overnight at 4 °C and rinsed with NaCl 0.9% before use. Human whole blood (EFS, Bichat Hospital, Paris, France), collected in the PPACK tubes and labeled with 5 µM DIOC6 (Life Technologies SAS, Saint-Aubin, France), was perfused at arterial shear stress for 5 min to induce platelet activation and aggregation. Platelet aggregation through contact with collagen was visualized in real-time with phase-contrast microscopy (Axio Observer, Carl Zeiss Microscopy, Oberkochen, Germany). After rinsing with NaCl 0.9%, fluorescent Control-SPs or Fuco-SPs (unloaded or loaded with rtPA) at 1 mg mL$^{-1}$ were injected into the channels in saline for 5 min. Their accumulation onto activated aggregates was monitored in real-time. Channels were then washed for 1 min with NaCl 0.9%. Finally, the MFI of the fluorescent SPs bound to the platelets on each channel was analyzed with ImageJ. Intensity settings were kept the same for both types of SPs.

*Tissue distribution of Fuco-SPs in vivo:* Animal studies were performed on C57BL/6 male mice (EJ, Le Genest, St-Berthevin, France) aged 5-8 weeks (~ 25 g weight) in respect of the principles of laboratory about animal experimentation and with the approval of the animal care and use committee of the Claude Bernard Institute (APAFIS #8724, Paris, France). Mice were anesthetized under the application of 2% isoflurane (Aerrane, Baxter). 200 µL of Fuco-SPs (5 mg mL$^{-1}$) were injected through the retro-orbital route (n=3). To histologically analyze the particle accumulation, mice were sacrificed 30 min following their administration. The liver, spleen, lungs, and kidneys were excised, washed in saline, and fixed in paraformaldehyde 4%. The tissues were then frozen and cryosectioned at 10 µm thickness. The samples were stained with alcian blue & nuclear fast red staining protocol. Strongly negative structures, including the Fuco-SPs, are stained blue, nuclei are stained pink to red, and cytoplasms appear pale pink. The slides with tissue slices were scanned with the Nanozoomer (Hamamatsu, Hamamatsu City, Japan) and viewed with the NDP.view2 software.

*Animals and thromboembolic stroke model in vivo:* Animal experiments were carried out on male Swiss wild-type mice (8–9 weeks old; 35-45 g; CURB, Caen, France). All experiments were performed following the French (Decree 87/848) and the European

Communities Council (2010/63/EU) guidelines and were approved by the institutional review board (French ministry of Research). All the experiments were validated by the local ethical committee of Normandy (CENOMEXA) registered under the reference number APAFIS#13172. Anesthesia was induced by the application of 5% isoflurane (Aerrane, Baxter) and maintained by 2% isoflurane in a mixture of $O_2/N_2O$ (30% / 70%).

Mice were placed in a stereotaxic device, then a small craniotomy was performed, the dura was excised, and the middle cerebral artery (MCA) was exposed. To induce the occlusion of the MCA, the coagulation cascade was triggered by the pneumatical injection of 1 µL murine α-thrombin (1 IU; Stago BNL) with a glass micropipette, as previously described.[73] Successful MCA occlusion was confirmed by the Laser Doppler flowmeter (Oxford Optronix). For the treatment, the animals were intravenously injected through a tail vein catheter (200 µL, 10% bolus, 90% infusion over 40 minutes) with either saline, Actilyse® rtPA 10 mg $kg^{-1}$, or rtPA-Fuco-SPs (rtPA at 10 mg $kg^{-1}$, SPs at 71 mg $kg^{-1}$) 20 minutes after thrombus formation ($n \geq 5$). Brain perfusion was monitored by Laser Speckle Contrast Imager (MOOR FLPI-2, Moor Instruments) throughout the treatment. Region of interest (ROI) was selected on the ipsilateral to occlusion and contralateral hemispheres to monitor the relative cerebral blood flow in the affected region $Fl_t$ (%) = 100% x $Fl_{ipsi}/Fl_{contra}$. The post-stroke reperfusion was expressed as a Growth Rate (GR) of the blood flow increase in the ipsilateral ROI to contralateral one at a time point, and it was quantified as GR (%) = 100% x $(Fl_{t2} - Fl_{t1})/ Fl_{t1}$.

*Magnetic resonance imaging acquisition and analysis:* Mice were anesthetized with 5% isoflurane and maintained with 1.5-2% isoflurane in a mixture of $O_2/N_2O$ (30% / 70%) during the acquisitions. Experiments were carried out on a Pharmascan 7T (Bruker Biospin, Wissembourg, France). Three-dimensional T2-weighted images were acquired using a Multi-Slice Multi-Echo sequence (TE/TR 39.9 ms / 3,500 ms, 2 averages) 24 h after the stroke. Lesion volumes were quantified on these images using ImageJ software (slice thickness 0.5 mm). Magnetic resonance angiography was performed using a 2D-TOF sequence (TE/TR 4.24 ms / 12 ms, 1 average) 24 h after ischemia, and the recanalization status of the MCA was determined blindly from the analysis of the merged MCA angiograms with maximum intensity. The angiographic score is based on the TICI (Thrombolysis in Cerebral Infarction) grade flow scoring (from Score 0: no perfusion to Score 3: full recanalization). For the *in vivo* detection of the BBB permeability, three dimensional T1 FLASH sequences (TE/TR 4.37 ms / 15.12 ms; 3 averages) were used, 15 min after the intravenous injection of 200 µL gadolinium chelate (DOTAREM) in saline (0.25 mg $mL^{-1}$). BBB leakage was measured 4 days after the stroke induction, and its volume was quantified using ImageJ.

*Thrombus targeting by Fuco-SPs in a murine model of venous thrombosis:* Animal studies were done following principles of laboratory animal care and with the approval of the animal care and use committee of the Claude Bernard Institute (APAFIS #8724, Paris, France). $FeCl_3$-induced *in vivo* thrombosis model on mesenteric vein was carried out on C57BL/6 male mice (EJ, Le Genest, St-Berthevin, France) aged 5-8 weeks. Mice were anesthetized with an intraperitoneal injection of ketamine (100 mg $kg^{-1}$) and xylazine (10 mg $kg^{-1}$). After midline abdominal incision, the mesentery was exposed, and vessels were visualized by an intravital microscope (Leica MacroFluo, Leica Microsystems SAS, Nanterre Cedex, France) using Orca Flash 4.0 scientific CMOS camera (Hamamatsu Photonics France SARL, Massy, France). For green fluorescent labeling of mitochondria of platelets and leucocytes, DIOC6 (Life Technologies SAS, Saint-Aubin, France) at 25 µM was retro-orbitally injected. The mesentery vein was covered with a 1 mm Whatman chromatography paper that was prior soaked in a 10% w/v iron chloride (Sigma-Aldrich) solution for 1 min, and then washed with saline. The formation of non-occlusive thrombi was monitored in real-time by fluorescence microscopy by an accumulation of fluorescently labeled platelets. TRITC-fluorescent labeled Control-SPs or Fuco-SPs were retro-orbitally injected 10 min after thrombus initiation with the volume of 150 µL (5 mice per group).

For histological evaluation, mice were sacrificed with pentobarbital overdose 5 min after administration of SPs. The affected part of the mesenteric vein was cut, washed in 0.9% NaCl, fixed in paraformaldehyde 4% (w/v), and frozen. The vein samples were cryosectioned at 10 µm thickness. The cell nuclei of a venous vascular wall were labeled with DAPI (Thermo Fisher Scientific, Massachusetts, United States) contained in a mounting medium (Vecto laboratories). The samples were observed by fluorescence microscopy. For the quantitative analysis, normalized MFI of the TRITC signal from SPs was expressed, defined as total TRITC fluorescence intensity divided by the size of the thrombus area on 2 slides from each mouse with the ImageJ (NIH, Bethesda, U.S.).

*Statistical analysis:* Quantitative data were expressed as mean ± standard error of the mean (SEM) ($n \geq 3$). Statistical tests were carried out with GraphPad Prism 9 (GraphPad Software, Inc., La Jolla, U.S.) with a 95% confidence level. Kolmogorov-Smirnov normality test was utilized to examine if variables are normally distributed. Normally distributed data were analyzed then with unpaired t-test or one-way analysis of variance (ANOVA) with post hoc Turkey's test. The Mann-Whitney U test was applied otherwise. The p-values of * $p<0.05$; ** $p<0.01$; *** $p<0.001$ were considered statistically significant.

**Supporting Information**
Supporting Information is available from the Wiley Online Library or from the author.

**Acknowledgments**

The authors would like to acknowledge Marie-Françoise Bricot from the Institut de Chimie des Substances Naturelles of the Université Paris-Saclay for performing a microanalysis of the fucoidan and the Fuco-SPs. We also thank the ImagoSeine core facility of the Institut Jacques Monod, a member of IBiSA and France-Bio-Imaging (ANR-10-INBS-04) infrastructures for the TEM. The authors are grateful for Christine Choqueux, who performed the Environmental SEM at Université de Technologie de Compiègne, Compiègne, France. We kindly thank Pr. Antonino Nicoletti for his advice on designing an *in vitro* release study and Dr. Kevin Guedj for assistance with flow cytometry. We also thank Dr. Yoann Lalatonne for the technical support with the TXRF technique and Dr. Samira Benadda with confocal microscopy. The illustrations were designed with BioRender software (biorender.com). **Author contributions:** A.Z.: Conceptualization; Investigation; Data Curation; Formal analysis; Writing - Original Draft; Visualization. C.J.: Investigation (Thrombolytic efficacy *in vivo*). R.A.: Investigation (Tissue distribution *in vivo* & thrombus targeting *in vivo*); Validation. L.F.: Investigation (Quantification of the fucoidan & fibrinolytic activity *in vitro*). L.M.F.R.: Methodology. T.B.: Methodology; Investigation (Thrombolytic efficacy *in vivo* - MRI); Validation; Writing - Review & Editing. D.V.: Resources; Project administration; Writing - Review & Editing. D.L.: Resources; Project administration. C.C.: Conceptualization; Validation; Resources; Writing - Review & Editing; Supervision; Project administration; Funding acquisition. C.J. and R.A. as well as D.L and D.V. contributed equally to this work. All the authors approved the final version of the manuscript. **Funding**: The authors thank INSERM, Université de Paris, and Université Sorbonne Paris Nord for financial support. This work also received funding from the EU project FP7-NMP-2012-LARGE-6-309820 "NanoAthero" and ANR-13-LAB1-0005-01 "FucoChem". Alina Zenych is grateful for the Ph.D. fellowship from the INSPIRE program of the European Union's Horizon 2020 research and innovation program (Marie Sklodowska-Curie grant # 665850).

**Conflict of interests**
The authors declare no competing interests.

Received:
Revised:
Published online:

## REFERENCES


[1] E. J. Benjamin, P. Muntner, A. Alonso, M. S. Bittencourt, C. W. Callaway, A. P. Carson, A. M. Chamberlain, A. R. Chang, S. Cheng, S. R. Das, F. N. Delling, L. Djousse, M. S. V. Elkind, J. F. Ferguson, M. Fornage, L. C. Jordan, S. S. Khan, B. M. Kissela, K. L. Knutson, T. W. Kwan, D. T. Lackland, T. T. Lewis, J. H. Lichtman, C. T. Longenecker, M. S. Loop, P. L. Lutsey, S. S. Martin, K. Matsushita, A. E. Moran, M. E. Mussolino, M. O'Flaherty, A. Pandey, A. M. Perak, W. D. Rosamond, G. A. Roth, U. K. A. Sampson, G. M. Satou, E. B. Schroeder, S. H. Shah, N. L. Spartano, A. Stokes, D. L. Tirschwell, C. W. Tsao, M. P. Turakhia, L. B. VanWagner, J. T. Wilkins, S. S. Wong, S. S. Virani, *Circulation* **2019**, DOI 10.1161/CIR.0000000000000659.

[2] W. J. Powers, A. A. Rabinstein, T. Ackerson, O. M. Adeoye, N. C. Bambakidis, K. Becker, J. Biller, M. Brown, B. M. Demaerschalk, B. Hoh, E. C. Jauch, C. S. Kidwell, T. M. Leslie-Mazwi, B. Ovbiagele, P. A. Scott, K. N. Sheth, A. M. Southerland, D. V. Summers, D. L. Tirschwell, *Stroke* **2019**, *50*, e344.

[3] J. Mican, M. Toul, D. Bednar, J. Damborsky, *Comput. Struct. Biotechnol. J.* **2019**, *17*, 917.

[4] R. Bhatia, M. D. Hill, N. Shobha, B. Menon, S. Bal, P. Kochar, T. Watson, M. Goyal, A. M. Demchuk, *Stroke* **2010**, *41*, 2254.

[5] A. M. Thiebaut, M. Gauberti, C. Ali, S. Martinez De Lizarrondo, D. Vivien, M. Yepes, B. D. Roussel, *Lancet Neurol.* **2018**, *17*, 1121.

[6] A. Pal Khasa, Y. Pal Khasa, *Bioengineered* **2017**, *8*, 331.

[7] S. Liu, X. Feng, R. Jin, G. Li, *Expert Opin Drug Deliv* **2018**, *15*, 173.

[8] N. Korin, M. Kanapathipillai, B. D. Matthews, M. Crescente, A. Brill, T. Mammoto, K. Ghosh, S. Jurek, S. A. Bencherif, D. Bhatta, A. U. Coskun, C. L. Feldman, D. D. Wagner, D. E. Ingber, *Science* **2012**, *337*, 738-42.

[9] M. Colasuonno, A. L. Palange, R. Aid, M. Ferreira, H. Mollica, R. Palomba, M. Emdin, M. Del Sette, C. Chauvierre, D. Letourneur, P. Decuzzi, *ACS Nano* **2018**, *12*, 12224.

[10] J. Zhou, D. Guo, Y. Zhang, W. Wu, H. Ran, Z. Wang, *ACS Appl. Mater. Interfaces* **2014**, *6*, 5566.

[11] A. Friedman, S. Claypool, R. Liu, *Curr. Pharm. Des.* **2013**, *19*, 6315.

[12] W. jin Jeong, J. Bu, L. J. Kubiatowicz, S. S. Chen, Y. S. Kim, S. Hong, *Nano Converg.* **2018**, *5*, 1.

[13] L. Chollet, P. Saboural, C. Chauvierre, J.-N. Villemin, D. Letourneur, F. Chaubet, *Mar. Drugs* **2016**, *14*, 1.

[14] L. Bachelet, I. Bertholon, D. Lavigne, R. Vassy, M. Jandrot-Perrus, F. Chaubet, D. Letourneur, *Biochim. Biophys. Acta - Gen. Subj.* **2009**, *1790*, 141.

[15] P. Saboural, F. Chaubet, F. Rouzet, F. Al-Shoukr, R. Ben Azzouna, N. Bouchemal, L. Picton, L. Louedec, M. Maire, L. Rolland, G. Potier, D. Le Guludec, D. Letourneur, C. Chauvierre, *Mar. Drugs* **2014**, *12*, 4851.

[16] T. Bonnard, J.-M. Serfaty, C. Journé, B. Ho Tin Noe, D. Arnaud, L. Louedec, M. Derkaoui, D. Letourneur, C. Chauvierre, C. Le Visage, *Acta Biomater.* **2014**, *10*, 3535.

[17] T. Bonnard, G. Yang, A. Petiet, V. Ollivier, O. Haddad, D. Arnaud, L. Louedec, L. Bachelet-Violette, S. M. Derkaoui, D. Letourneur, C. Chauvierre, C. Le Visage, *Theranostics* **2014**, *4*, 592.

[18] B. Li, M. Juenet, R. Aid-Launais, M. Maire, V. Ollivier, D. Letourneur, C. Chauvierre, *Adv. Healthc. Mater.* **2017**, *6*, 1.

[19] B. Li, R. Aid-Launais, M.-N. Labour, A. Zenych, M. Juenet, C. Choqueux, V. Ollivier, O. Couture, D. Letourneur, C. Chauvierre, *Biomaterials* **2019**, *194*, 139.

[20] M. Juenet, R. Aid-Launais, B. Li, A. Berger, J. Aerts, V. Ollivier, A. Nicoletti, D.

Letourneur, C. Chauvierre, *Biomaterials* **2018**, *156*, 204.
[21] C. Chauvierre, D. Letourneur, *Nanomedicine (Lond)* **2015**, *10*, 3391.
[22] K. H. Zheng, Y. Kaiser, E. Poel, H. Verberne, J. Aerts, F. Rouzet, E. Stroes, D. Letourneur, C. Chauvierre, *Atherosclerosis* **2019**, *287*, e143.
[23] I. Cicha, C. Chauvierre, I. Texier, C. Cabella, J. M. Metselaar, J. Szebeni, L. Dézsi, C. Alexiou, F. Rouzet, G. Storm, E. Stroes, D. Bruce, N. MacRitchie, P. Maffia, D. Letourneur, *Cardiovasc. Res.* **2018**, *114*, 1714.
[24] K. Ganguly, K. Chaturvedi, U. A. More, M. N. Nadagouda, T. M. Aminabhavi, *J. Control. Release* **2014**, *193*, 162.
[25] J. Zhang, W. Xia, P. Liu, Q. Cheng, T. Tahirou, W. Gu, B. Li, *Mar. Drugs* **2010**, *8*, 1962.
[26] H. J. Jin, H. Zhang, M. L. Sun, B. G. Zhang, J. W. Zhang, *J. Thromb. Thrombolysis* **2013**, *36*, 458.
[27] J. Liao, X. Ren, B. Yang, H. Li, Y. Zhang, Z. Yin, *Drug Dev. Ind. Pharm.* **2019**, *45*, 88.
[28] S. R. Van Tomme, W. E. Hennink, *Expert Rev. Med. Devices* **2007**, *4*, 147.
[29] J. R. McCarthy, I. Y. Sazonova, S. S. Erdem, T. Hara, B. D. Thompson, P. Patel, I. Botnaru, C. P. Lin, G. L. Reed, R. Weissleder, F. A. Jaffer, *Nanomedicine (Lond)* **2012**, *7*, 1017.
[30] S. Heid, H. Unterweger, R. Tietze, R. P. Friedrich, B. Weigel, I. Cicha, D. Eberbeck, A. R. Boccaccini, C. Alexiou, S. Lyer, *Int. J. Mol. Sci.* **2017**, *18*, 1837.
[31] T. E. Furia, *CRC Handbook of Food Additives*, CRC Press, **1973**.
[32] W. E. Hennink, C. F. van Nostrum, *Adv. Drug Deliv. Rev.* **2002**, *54*, 13.
[33] C. Chauvierre, R. Aid-Launais, J. Aerts, M. Maire, L. Chollet, L. Rolland, R. Bonaf, S. Rossi, S. Bussi, C. Cabella, D. Laszlo, T. Fülöp, J. Szebeni, Y. Chahid, K. H. Zheng, E. S. G. Stroes, D. Le Guludec, F. Rouzet, D. Letourneur, *Mar. Drugs* **2019**, *17*, 1.
[34] F. Rouzet, L. Bachelet-Violette, J.-M. Alsac, M. Suzuki, A. Meulemans, L. Louedec, A. Petiet, M. Jandrot-Perrus, F. Chaubet, J.-B. Michel, D. Le Guludec, D. Letourneur, *J. Nucl. Med.* **2011**, *52*, 1433.
[35] F. Wolf, K. Koehler, H. P. Schuchmann, *J. Food Process Eng.* **2013**, *36*, 276.
[36] J. Matuszak, J. Baumgartner, J. Zaloga, M. Juenet, A. E. da Silva, D. Franke, G. Almer, I. Texier, D. Faivre, J. M. Metselaar, F. P. Navarro, C. Chauvierre, R. Prassl, L. Dézsi, R. Urbanics, C. Alexiou, H. Mangge, J. Szebeni, D. Letourneur, I. Cicha, *Nanomedicine* **2016**, *11*, 597.
[37] M. Weber, H. Steinle, S. Golombek, L. Hann, C. Schlensak, H. P. Wendel, M. Avci-Adali, *Front. Bioeng. Biotechnol.* **2018**, *6*, 99.
[38] "ISO 10993-4:2017," https://www.iso.org/standard/63448.html, **2017**.
[39] B. Vaidya, G. P. Agrawal, S. P. Vyas, *Eur. J. Pharm. Sci.* **2011**, *44*, 589.
[40] N. Zhang, C. Li, D. Zhou, C. Ding, Y. Jin, Q. Tian, X. Meng, K. Pu, Y. Zhu, *Acta Biomater.* **2018**, *70*, 227-236.
[41] K. Ley, *Trends Mol. Med.* **2003**, *9*, 263.
[42] J.-H. Kim, J.-Y. Yoon, in *Encycl. Surf. Colloid Sci.*, **2002**, pp. 4373–4381.
[43] I. Politis, L. Wang, J. D. Turner, B. K. Tsang, *Biol. Reprod.* **1990**, *42*, 747.
[44] S. Petersen, A. Fahr, H. Bunjes, *Mol. Pharm.* **2010**, *7*, 350.
[45] V. Wintgens, C. Lorthioir, P. Dubot, B. Sébille, C. Amiel, *Carbohydr. Polym.* **2015**, *132*, 80.
[46] L. Arnfast, C. G. Madsen, L. Jorgensen, S. Baldursdottir, *Ther. Deliv.* **2014**, *5*, 691.
[47] Z. M. Ruggeri, *Nat. Med.* **2002**, *8*, 1227.
[48] T. J. Merkel, K. Chen, S. W. Jones, A. A. Pandya, S. Tian, M. E. Napier, W. E. Zamboni, J. M. Desimone, *J. Control. Release* **2012**, *162*, 37.
[49] C. Orset, B. Haelewyn, S. M. Allan, S. Ansar, F. Campos, T. H. Cho, A. Durand, M. El Amki, M. Fatar, I. Garcia-Yébenes, M. Gauberti, S. Grudzenski, I. Lizasoain, E. Lo, R.

Macrez, I. Margaill, S. Maysami, S. Meairs, N. Nighoghossian, J. Orbe, J. A. Paramo, J. J. Parienti, N. J. Rothwell, M. Rubio, C. Waeber, A. R. Young, E. Touzé, D. Vivien, *Stroke* **2016**, *47*, 1312.
[50] S. M. De Lizarrondo, C. Gakuba, B. A. Herbig, Y. Repessé, C. Ali, C. V. Denis, P. J. Lenting, E. Touzé, S. L. Diamond, D. Vivien, M. Gauberti, *Circulation* **2017**, *136*, 646.
[51] H. R. Lijnen, B. Van Hoef, V. Beelen, D. Collen, *Eur. J. Biochem.* **1994**, *224*, 863.
[52] R. Brouns, P. P. De Deyn, *Clin. Neurol. Neurosurg.* **2009**, *111*, 483.
[53] A. Zenych, L. Fournier, C. Chauvierre, *Biomaterials* **2020**, *258*, 120297.
[54] K. S. Masters, D. N. Shah, L. A. Leinwand, K. S. Anseth, *Biomaterials* **2005**, *26*, 2517.
[55] C. I. Jones, D. A. Payne, P. D. Hayes, A. R. Naylor, P. R. F. Bell, M. M. Thompson, A. H. Goodall, *J. Vasc. Surg.* **2008**, *48*, 715.
[56] E. M. Balboa, E. Conde, A. Moure, E. Falqué, H. Domínguez, *Food Chem.* **2013**, *138*, 1764.
[57] Y. Choi, S. K. Min, R. Usoltseva, A. Silchenko, T. Zvyagintseva, S. Ermakova, J. K. Kim, *Thromb. Res.* **2018**, *161*, 22.
[58] K. Knop, R. Hoogenboom, D. Fischer, U. S. Schubert, *Angew. Chemie - Int. Ed.* **2010**, *49*, 6288.
[59] M. Di Marco, K. A. Razak, A. A. Aziz, C. Devaux, E. Borghi, L. Levy, C. Sadun, *Int. J. Nanomedicine* **2010**, *5*, 37.
[60] R. P. Friedrich, J. Zaloga, E. Schreiber, I. Y. Tóth, E. Tombácz, S. Lyer, C. Alexiou, *Nanoscale Res. Lett.* **2016**, *11*, 1.
[61] C. L. Pawlowski, W. Li, M. Sun, K. Ravichandran, D. Hickman, C. Kos, G. Kaur, A. Sen Gupta, *Biomaterials* **2017**, *128*, 94.
[62] J. Xu, Y. Zhang, J. Xu, G. Liu, C. Di, X. Zhao, X. Li, Y. Li, N. Pang, C. Yang, Y. Li, B. Li, Z. Lu, M. Wang, K. Dai, R. Yan, S. Li, G. Nie, *Adv. Mater.* **2019**, *32*, 1905145.
[63] J. Hu, S. Huang, L. Zhu, W. Huang, Y. Zhao, K. Jin, Q. Zhuge, *ACS Appl. Mater. Interfaces* **2018**, *10*, 32988.
[64] L. Huang, J. Wang, S. Huang, F. Siaw-Debrah, M. Nyanzu, Q. Zhuge, *Biochem. Biophys. Res. Commun.* **2019**, *516*, 565.
[65] T. Mei, A. Kim, L. B. Vong, A. Marushima, S. Puentes, Y. Matsumaru, A. Matsumura, Y. Nagasaki, *Biomaterials* **2019**, *215*, 1.
[66] H. Kim, J. H. Ahn, M. Song, D. W. Kim, T. K. Lee, J. C. Lee, Y. M. Kim, J. D. Kim, J. H. Cho, I. K. Hwang, B. C. Yan, M. H. Won, J. H. Park, *Biomed. Pharmacother.* **2019**, *109*, 1718.
[67] D. Vivien, M. Gauberti, A. Montagne, G. Defer, E. Touzé, *J. Cereb. Blood Flow Metab.* **2011**, *31*, 2119.
[68] J. P. A. Ioannidis, B. Y. S. Kim, A. Trounson, *Nat. Biomed. Eng.* **2018**, *2*, 797.
[69] S. Yokoyama, H. Ikeda, N. Haramaki, H. Yasukawa, T. Murohara, T. Imaizumi, *J. Am. Coll. Cardiol.* **2005**, *45*, 1280.
[70] S. R. Barthel, J. D. Gavino, L. Descheny, C. J. Dimitroff, *Expert Opin. Ther. Targets* **2007**, *11*, 1473.
[71] Y. Shamay, M. Elkabets, H. Li, J. Shah, S. Brook, F. Wang, K. Adler, E. Baut, M. Scaltriti, P. V Jena, E. E. Gardner, J. T. Poirier, C. M. Rudin, J. Baselga, A. Haimovitz-Friedman, D. A. Heller, *Sci. Transl. Med.* **2016**, *8*, 345ra87.
[72] J. M. Lee, Z.-U. Shin, G. T. Mavlonov, I. Y. Abdurakhmonov, T.-H. Yi, *Appl. Biochem. Biotechnol.* **2012**, *168*, 1019.
[73] C. Orset, R. Macrez, A. R. Young, D. Panthou, E. Angles-cano, E. Maubert, V. Agin, D. Vivien, *Stroke* **2007**, *38*, 2771.

**Table of Contents**

*Alina Zenych, Charlène Jacqmarcq, Rachida Aid, Louise Fournier, Laura M. Forero Ramirez, Thomas Bonnard, Denis Vivien, Didier Letourneur, Cédric Chauvierre**

**Fucoidan-Functionalized Polysaccharide Submicroparticles Loaded with Alteplase for Efficient Targeted Thrombolytic Therapy**

Owing to limited effectiveness and deleterious complications of current thrombolytic therapy, the challenge remains to improve its safety and efficacy for acute thrombotic events. This study intends to develop biocompatible fucoidan-functionalized polysaccharide nanocarrier from FDA-approved compounds that delivers a fibrinolytic – alteplase – by binding to P-selectin in the thrombi and evaluate the therapeutic efficacy of this product in preclinical models.

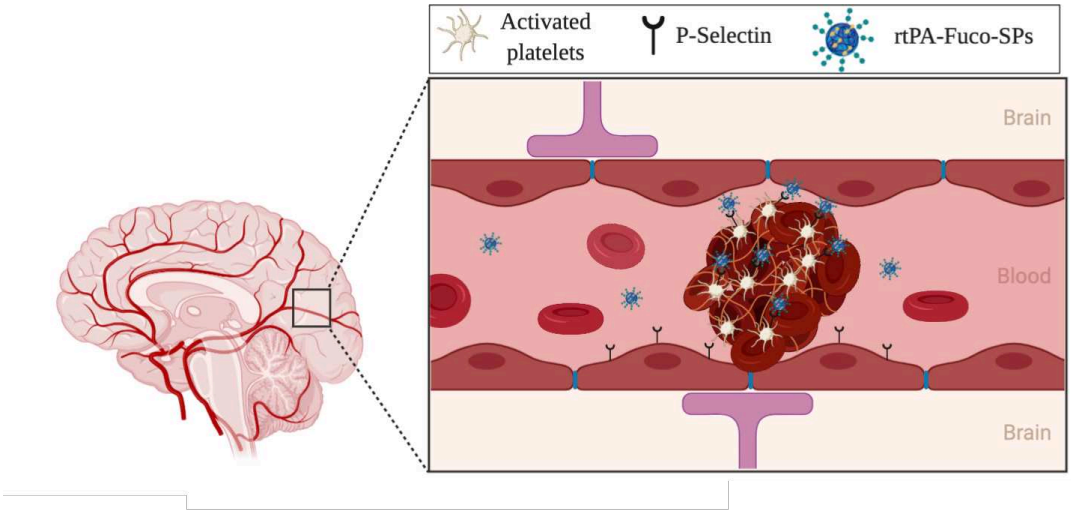


Scheme 1. Mode of action of the rtPA-Fuco-SPs in the treatment of ischemic stroke.

Supporting Information

**Fucoidan-Functionalized Polysaccharide Submicroparticles Loaded with Alteplase for Efficient Targeted Thrombolytic Therapy**

*Alina Zenych, Charlène Jacqmarcq, Rachida Aid, Louise Fournier, Laura M. Forero Ramirez, Thomas Bonnard, Denis Vivien, Didier Letourneur, Cédric Chauvierre**

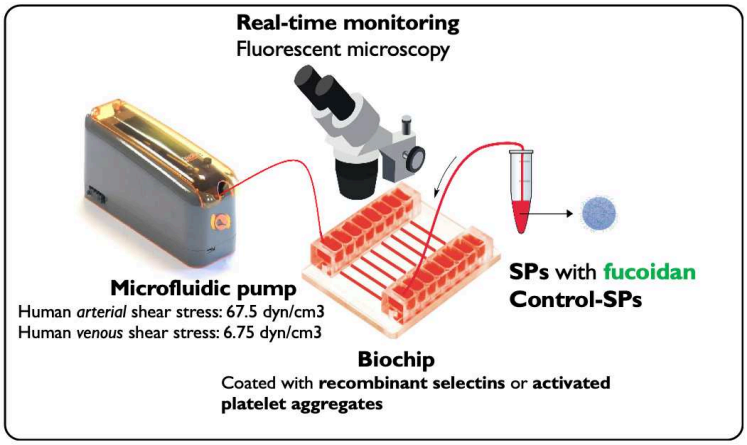


**Figure S1. Schematic illustration of the *in vitro* targeting assay.**

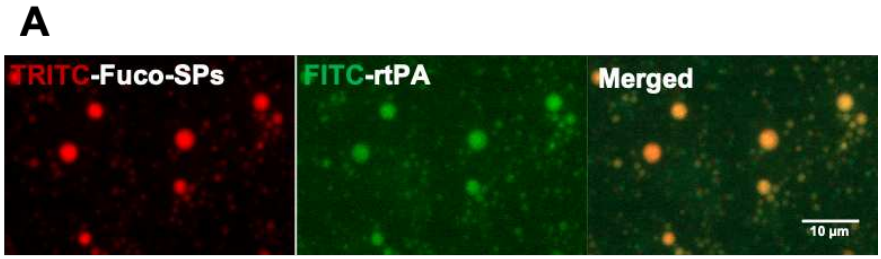


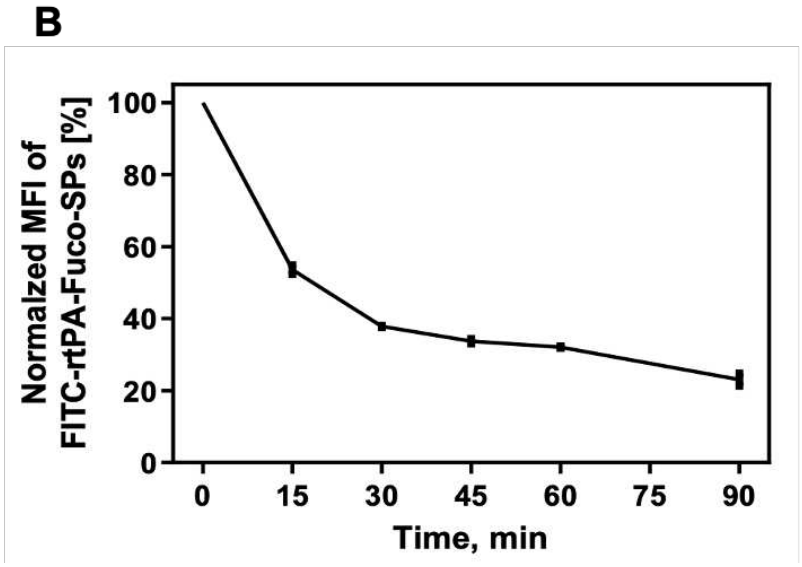

**Figure S2. Loading and release of rtPA from Fuco-SPs. A.** FITC-rtPA loading onto the TRITC-Fuco-SPs visualized by confocal microscopy. **B.** *In vitro* rtPA release from rtPA-encapsulated Fuco-SPs by flow cytometry.

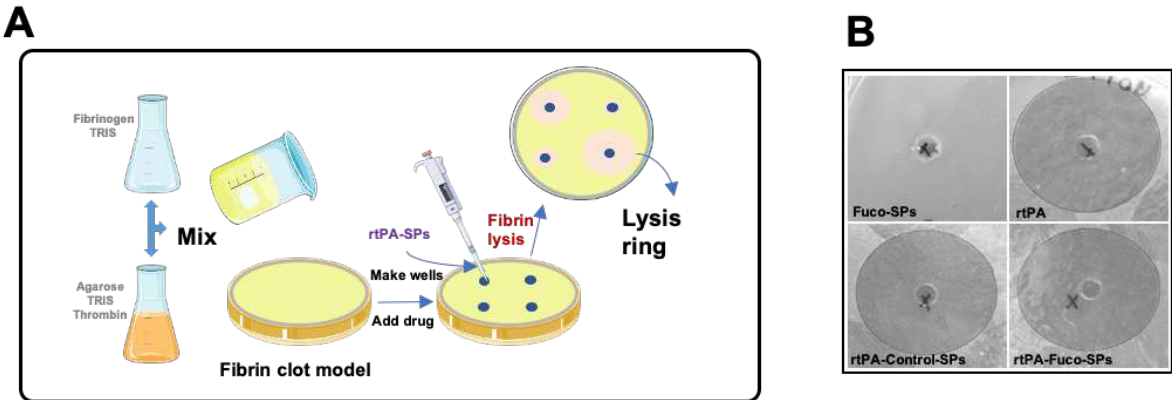


**Figure S3. Fibrinolytic activity of the rtPA-loaded SPs *in vitro*. A.** Schematic illustration of the *in vitro* fibrinolytic test. **B.** Lysed circles as the fibrinolytic potential of the SPs *in vitro* by a fibrin-plate agarose assay at the equal concentration of the rtPA.

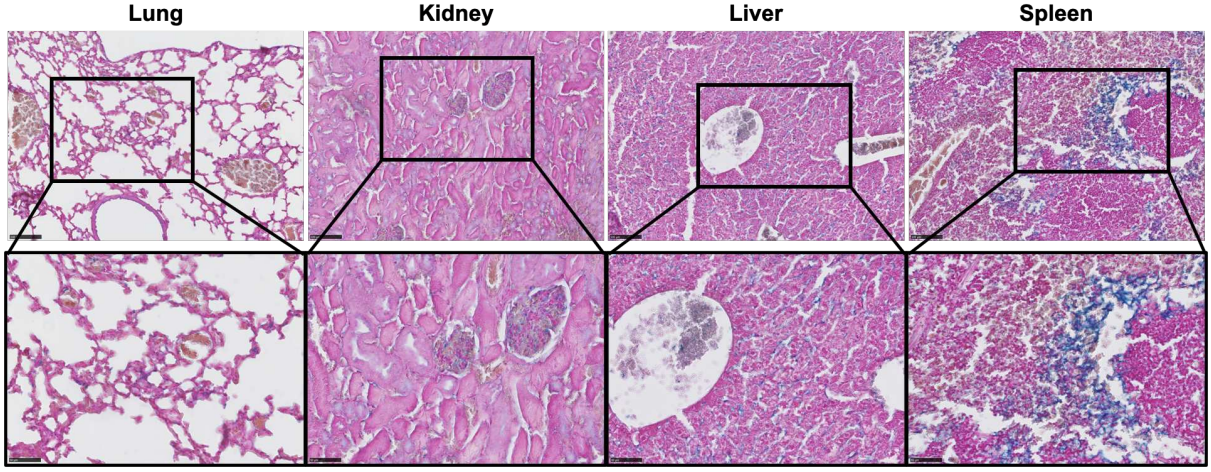


**Figure S4. Histological analysis of Fuco-SPs in four organs of excretion.** The cytoplasm appears pale pink, nuclei are red, and the Fuco-SPs are stained blue. Few particles were detected in the lungs, kidneys, and liver, whereas they were mainly accumulated in the spleen. The scale bar in the upper row = 100 μm, in the lower row (magnified image) = 50 μm.

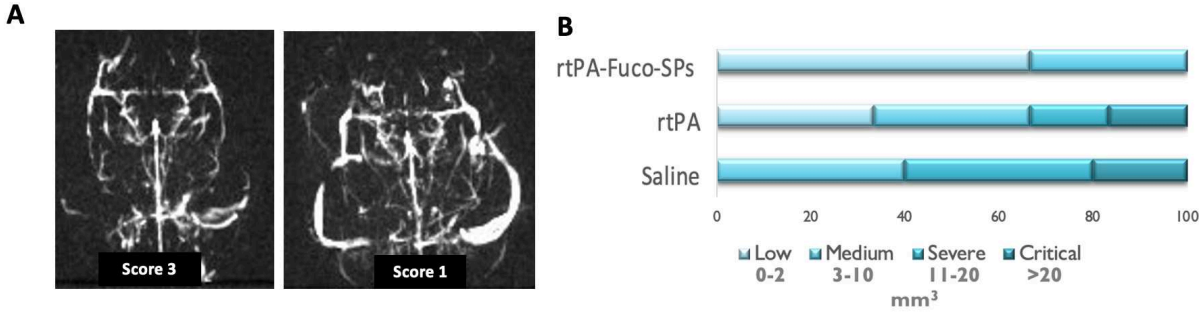

**Figure S5. Therapeutic efficacy of the rtPA-Fuco-SPs *in vivo*. A.** Merged image of the MRA scores (Score 3: full recanalization, score 1: low perfusion). **B.** Distribution of the cases by the infarct zone sizes by MRI 24 h post-stroke.

**Video S1.** Cerebral blood flow reperfusion monitored by the laser speckle contrast imaging during the 40-min treatment regimen with saline (**A**), rtPA (**B**), and rtPA-Fuco-SPs (**C**) in the ROI of ipsilateral (2) and contralateral (1) hemispheres.

**Table S1**. The synthesis parameters for the polysaccharide SPs.

| Synthesis method | Polysaccharide [c], mg $mL^{-1}$ | STMP, [c], mg $mL^{-1}$ | NaOH [c], M | Phase ratio, (Aq/ Org/) | Surfactant | Homogenization | Crosslinking |
|---|---|---|---|---|---|---|---|
| W/O emulsion / crosslinking | 300 | 56.11 | 1.15 | 4% w/v | PGPR, 6% | 30,000 rpm, 4 min, 4 °C | 20 min, 50 ºC |

Abbreviation: W/O, water-in-oil; Aq, aqueous; Org organic.

# ANNEX 3

Europäisches Patentamt | European Patent Office | Office européen des brevets

## Acknowledgement of receipt

We hereby acknowledge receipt of your request for grant of a European patent as follows:

| | | |
|---|---|---|
| Submission number | 1000497919 | |
| Application number | EP20305615.5 | |
| File No. to be used for priority declarations | EP20305615 | |
| Date of receipt | 09 June 2020 | |
| Your reference | CHAUVIERE20221MC | |
| Applicant | INSERM (Institut National de la Santé et de la Recherche Médicale) | |
| Country | FR | |
| Title | FUCOIDAN-FUNCTIONALIZED POLYSACCHARIDE PARTICLES WITH T-PA FOR TARGETED THROMBOLYTIC THERAPY | |
| Documents submitted | package-data.xml | ep-request.xml |
| | application-body.xml | ep-request.pdf (5 p.) |
| | SPECEPO-1.pdf\Text_20221EP.pdf (44 p.) | SPECEPO-2.pdf\Drawings_20221EP.pdf (4 p.) |
| Submitted by | EMAIL=nicolas.crouvezier@inserm-transfert.fr,CN=Nicolas CROUVEZIER,O=SOCIETE INSERM TRANSFERT,C=FR | |
| Method of submission | Online | |
| Date and time receipt generated | 09 June 2020, 13:52:20 (CEST) | |
| Official Digest of Submission | ED:56:D3:85:90:CA:DA:44:C5:39:EC:52:56:7F:17:7B:BB:56:EE:B1 | |

/INPI, section dépôt/

# FUCOIDAN-FUNCTIONALIZED POLYSACCHARIDE PARTICLES WITH T-PA FOR TARGETED THROMBOLYTIC THERAPY

---

## FIELD OF THE INVENTION:

The present invention is in the field of medicine and in particular nanomedicine, hematology, and cardiology.

## BACKGROUND OF THE INVENTION:

Acute thrombotic pathologies such as myocardial infarction, ischemic stroke, and venous thromboembolism remain a major global healthcare challenge contributing to a significant number of deaths and disabilities [1]. Current thrombolytic therapy, the intravenous injection of Plasminogen Activators (PA), is administrated to lyse a vascular occlusion and restore the blood flow in the vessel. The recombinant tissue plasminogen activator (rtPA) is the most commonly applied clot-busting drug in clinics and the only one approved for the treatment of acute ischemic stroke [2]. rtPA is a fibrin-specific serine protease that activates the endogenous proenzyme plasminogen and converts it to the active form plasmin, thus, degrading the thrombus fibrin network. However, systemic delivery of rtPA is limited by a narrow therapeutic window (4.5 h of stroke symptom onset), rapid drug elimination (half-life 4-6 min), and physiological deactivation by its antidotes such as Plasminogen Activator Inhibitors (PAI-1 and PAI-2), posing the risks of deleterious side-effects such as intracranial hemorrhages [3]. Moreover, the rate of acute recanalization after intravenous administration of rtPA is low: only ~30% of patients experienced full or partial recanalization identified by CT angiography according to the study [4].

Therapeutic strategies that intend to address the challenges of thrombolytic therapy and to boost survival rates remain of great clinical interest. Certainly, novel thrombolytic molecules are being researched in order to increase reperfusion, improve safety, and protect the brain neurovascular unit [5,6]. Apart from that, nanomedical approaches for targeted delivery of thrombolytic agents have been intensively proposed [7]. Korin *et al.* reported the microaggregates of poly (lactic-co-glycolic acid) (PLGA) nanoparticles (NPs) dissociated into rtPA-bearing nanocompounds when exposed to abnormally high hemodynamic shear stress, typical for the vascular occlusions, that performed effective thrombolysis in several preclinical models [8]. Colasuonno *et al.* formulated rtPA-loaded discoidal porous nanoconstructs from a

mixture of PLGA and polyethylene glycol (PEG) with high thrombolytic potential that was presumably attributed to the erythrocyte-mimicking shape of the NPs and their deformability, leading to efficient circulation profiles and accumulation on the clot [9]. While these systems with a passive targeting succeeded in a promising thrombolytic efficacy in preclinical studies, more recent and advanced examples are formulated with actively targeted nanocarriers.

Active targeting permits drug accumulation specifically at the thrombus site and has the potential to enhance the enzyme penetration into deeply localized thrombi. Apart from the magnetic nanoparticle targeting under an external magnetic field, active blood clot targeting is currently achieved by directing the functionalized NPs towards fibrin or activated platelets (mostly integrin GPIIb/IIIa and less adhesion receptor P-selectin) with antibodies and/or peptides. Notably, a theranostic system for thrombus molecular imaging and targeted therapy was developed by Zhou *et al.* when rtPA was encapsulated into the $Fe_3O_4$-based PLGA NPs, and a cyclic arginine-glycine-aspartic acid (cRGD) peptide was grafted onto the chitosan surface to target GPIIb/IIIa on activated platelets [10]. Nevertheless, both antibodies and peptides have their limitations for targeted drug delivery. The immunogenicity, purity, and sufficient circulation time are the main concerns of the application of the antibodies [11] while peptides might suffer from weak binding affinity, metabolic instability and fast renal clearance due to their small sizes, potential immunogenicity, and often a high costs of peptide synthesis [12].

The effective alternative could be the nanoparticle functionalization with fucoidan [13], a naturally-occurring algae-derived sulfated polysaccharide, that allows a strong tropism for the P-selectin overexpression in cardiovascular pathologies [14,15]. Fucoidan emerged as an affordable high-quality targeting ligand to P-selectin, that was prior validated by our group on polysaccharide microparticles with iron oxide for MRI imaging [16], Technetium-99m-radiolabeled polysaccharide microparticles for SPECT imaging [17], polymer microcapsules [18], and polymer microbubbles for ultrasound imaging [19].

This is critical to ensure an excellent safety profile of the designed carrier for targeted thrombolysis in an attempt for future clinical translation. It should be a priority to select biocompatible and fully biodegradable materials with U.S. Food and Drug Administration (FDA)-approval as well as to realize a scalable production of the nanoformulations according to Good Manufacturing Practice (GMP) [20]. Contrary to the popularity of synthetic polymers

such as PLGA, the NPs made of the polysaccharides are explored to a lesser degree for thrombolytic therapy. Yet, they benefit from the general advantages of natural polymers: biocompatibility, low cost, and hydrophilicity. Polysaccharide hydrogels, that are crosslinked three-dimensional polymer networks, are capable of absorbing large quantities of water and can effectively load macromolecules [21], including plasminogen activators, with high encapsulation efficiency. Only a few publications reported the nanoformulations with chitosan, a cationic chitin-derived polysaccharide that can form polyelectrolyte complexes with negatively charged molecules [22]. For instance, superior thrombolytic potential *in vivo*, both by intravenous injection and catheter-driven, was demonstrated on self-assembled chitosan NPs crosslinked with sodium tripolyphosphate and loaded with urokinase [23]. Liao *et al.* formulated the lumbrokinase-bearing NPs from quaternized derivative of chitosan - N,N,N-Trimethyl Chitosan covalently grafted with cRGD peptide to target GPIIb/IIIa receptors that could accelerate thrombolysis [24].

Dextran, an exocellular bacterial water-soluble polysaccharide, is extensively employed in clinics, in particular in its low molecular weight (40 and 70 kDa), for plasma volume expansion, thrombosis prophylaxis, peripheral blood flow enhancement, artificial tears, etc. [25]. Dextran coating of magnetic NPs is applied to ensure environmental stability and to prolong the blood circulation time [26,27]. Our group has recently demonstrated that rtPA-immobilized core-shell poly(isobutyl cyanoacrylate) NPs, decorated with dextran and fucoidan, effectively augmented thrombolysis in mice [28]. However, to our knowledge, there are no reported exclusively dextran carriers for thrombolytic therapy. Meeting the requirements of biocompatibility, biodegradability, non-immunogenicity, dextran stands out as an attractive polymer to design a hydrogel-based protein delivery system for the thrombolytic application.

**SUMMARY OF THE INVENTION:**

As defined by the claims, the present invention relates to fucoidan-functionalized polysaccharide particles with t-PA for targeted thrombolytic therapy.

**DETAILED DESCRIPTION OF THE INVENTION:**

Thrombolytic therapy is an intravenous administration of clot-busting agents for the treatment of life-threatening acute thromboembolic diseases. However, thrombolytics exhibit limited clinical efficacy because of their short plasma half-lives and risks of hemorrhages. There is a

dire need for innovative nanomedicine-based solutions for safe and efficient thrombolysis with a non-toxic, biocompatible, and biodegradable thrombus-targeted carrier.

In the present invention, polysaccharide hydrogel submicroparticles with remarkable biocompatibility were elaborated by the inverse miniemulsion / crosslinking method. They were functionalized with a fucoidan which has a nanomolar affinity for the P-selectin overexpressed on activated platelets and endothelial cells in vascular diseases. Surprisingly, the inventors show that rtPA (i.e. Alteplase) can be loaded onto the submicroparticles by adsorption, and its amidolytic and fibrinolytic activities were maintained *in vitro* and *in vivo*. Thrombus targeting potential of these particles was validated in microfluidic assay under arterial and venous blood shear rates on recombinant P-selectin and activated platelet aggregates. The thrombolytic efficacy of the nanomedicine-based product was tested in a murine model of acute ischemic stroke, revealing faster middle cerebral artery recanalization and reduction in the brain infarct volume and blood-brain barrier permeability post-stroke, evidenced by laser speckle contrast imaging and MRI. Collectively, this proof of concept study demonstrates the potential of these particles for the precise treatment of acute thrombotic events.

Accordingly, the first object of the invention relates to a cross-linked polysaccharide particle comprising an amount of fucoidan and loaded with an amount of t-PA.

As used herein, the term "**particle**" refers to polysaccharide composition of the invention having a substantially spherical or ovoid shape. Typically, the particles of the invention have a size from 1 nm to 1,000 nm, preferably from 250 to 900 nm and even more preferably from 500 to 850 nm in size. In some embodiments, the size of the particle is about 708.48 ± 40.00 nm. For most nanoparticles, the size of the nanoparticles is the distance between the two most distant points in the nanoparticle. Nanoparticle size can be determined by different methods such as Dynamic Light Scattering (DLS), Small Angle X-ray Scattering (SAXS), Scanning Mobility Particle Sizer (SMPS), Scanning Electron Microscopy (SEM), Transmission Electron Microscopy (TEM) (*Orts-Gil, G., K. Natte, et al. (2011), Journal of Nanoparticle Research 13(4): 1593-1604; Alexandridis, P. and B. Lindman (2000), Amphiphilic Block Copolymers: Self-Assembly and Applications, Elsevier Science; Hunter, R. J. and L. R. White (1987). Foundations of colloid science, Clarendon Press.*).

As used herein, the term **"polysaccharide"** refers to a molecule comprising two or more monosaccharide units. The term "**saccharide unit**" as used herein means one saccharide molecule. A saccharide unit is a monomeric unit of a polysaccharide. The term "**saccharid**e" is inclusive of carbohydrates, such as glucose, fructose or galactose, and derivatives thereof, such as mannuronic acid or guluronic acid.

Typically, the polysaccharide is selected from the group consisting of dextran, pullulan, agar, alginic acid, hyaluronic acid, inulin, heparin, chitosan and mixtures thereof. More preferably, the polysaccharide is dextran.

As used herein, the term "**dextran**" has its general meaning in the art and is understood to refer to an a-D-1 ,6 glucose-linked glucan with side chains 1 -3 linked to the backbone units of the polysaccharide.

One important feature of the invention is that the polysaccharide is not chemically modified. In particular, the polysaccharide (e.g. dextran) is not aminated by a covalent linkage between the reducing end of the said polysaccharide and a chemical group comprising one or more amino groups. An "**amino group**" (-$NH_2$) refers to any chemical group with a free (-$NH_2$) radical, in particular primary amine groups and guanidine groups, and more particularly primary amine groups. In a non-limitative way, an amino group may be selected in the group consisting in lysine, arginine, ornithine, or γ-aminobutyric acid. Therefore, the particles as described in *Juenet M, Aid-Launais R, Li B, et al. Thrombolytic therapy based on fucoidan-functionalized polymer nanoparticles targeting P-selectin. Biomaterials. 2018;156:204□216. doi:10.1016/j.biomaterials.2017.11.047* are excluded from the scope of the invention.

As used herein, the "**cross-linked**" is intended to refer to two or more polymer chains of the polysaccharide which have been covalently bonded via a cross-linking agent.

As used herein, the term **"cross-linking"** refers to the linking of one polysaccharide chain to another one with covalent bonds.

As used herein, the term **"cross-linking agent"** encompasses any agent able to introduce cross-links between the chains of the polysaccharides of the invention.

As used herein, the term "**fucoidan**" has its general meaning in the art and refers a type of polysaccharide, which contains substantial percentages of L-fucose and sulfate ester groups, mainly derived from brown seaweed and some other marine invertebrates. Fucoidans are indeed generally made of a linear backbone built up of α- 1,3-L Fuc or alternating α- 1,3-L Fuc, α- 1,4-L Fuc, or α- 1,2-L Fuc which can be present in the backbone branching. Sulfate groups occupy the C-2 and/or C-3 or C-4 of fucose. In some embodiments, fucoidans are α- 1,2- or α-1,3-linked L-fucose polymers that are mainly sulfated on position 4 and position 2 or 3 following the glycosidic linkage. However, besides fucose and sulfate residues, fucoidans also contain other monosaccharides (e.g., mannose, galactose, glucose, xylose, etc.) and uronic acid groups. It is known in the art that the structure of fucoidans from different brown algae varies from species to species. When fucoidans contain uronic acid (UA) and other hexoses, the structure of said fucoidans may be built around a polysulfated poly-L fucose linear backbone bearing substituents selected in a group consisting of: uronic acid, an hexose (1 unit), a sulfate group, and an acetyl group. As an example, the schematic widely admitted structure of fucoidan extracted from the brown seaweed *Ascophyllum nodosum* is given in *Berteau & Mulloy or Pomin & Mourao (O. Berteau and B. Mulloy, 2003, Glycobiology, 13(6) 29-40, DOI: 10.1093/glycob/cwg058; V. Pomin and PAS Mourao, 2008, Glycobiology 18(12) 1016-1027, review, DOI:10.1093/glycob/cwn085*). In some embodiments, a fucoidan can be composed of a repeating unit of formula (I):

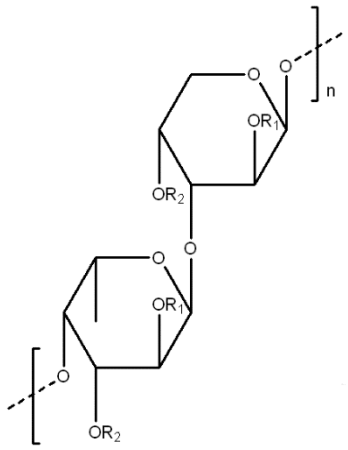


(I)

wherein

- $R_1$ and $R_2$ mean, one independently from the other: H, a sulfate group, an acetyl group, an hexose and/or uronic acid,
- n is equal or superior to 1.

In some embodiments, the fucoidan suitable for the invention is obtained from seaweed, and in particular brown seaweed (B. Li et al, Molecules, 2008, 13: 1671-1695; M. Kusaykin et al, Biotechnol. J., 2008, 3: 904-915).

Variant forms of fucoidans have also been found in marine animal species, including the sea cucumber. Thus, compared to other sulfated polysaccharides, fucoidans are widely available from various kinds of cheap sources, and easily obtained using methods of extraction known in the art (*C. Colliec et al, Phytochemistry, 1994, 35(3):697-700*). These methods of extraction generally yield fucoidans with molecular weights in the 70-800 kDa range. Processes have also been developed to depolymerize high molecular weight fucoidans in low molecular weight fucoidans, e.g., lower than about 20 kDa (EP 0403 377B, US Pat. No. 5,321,133), or lower than about 10 kDa (EP 0 846 129 B; U.S. Pat. No. 6,028,191; *A. Nardella et al, Carbohydr. Res., 1996, 289: 201-208*).

In some embodiments, fucoidans can be obtained commercially from the following companies: Fucoidan from Sigma-Aldrich company (USA): Crude fucoidan (from *Fucus vesiculosus*) ref F5631, CAS Number 9072-19-9. MM=20,000-200,000 g/mol; Fucoidan from Algues-et-Mer company (France): Asphyscient® (from *Ascophyllum nodosum*), on request, MM=5,000-10,000 g/mol; Fucoidan from Kraeber GmbH (Germany): on request, LMWF, 8,500 g/mol, HMWF, 600,000 g/mol, from different brown algae.

In some embodiments, the structure of fucoidans can also be chemically modified. For example, methods have been developed to increase the percentage of sulfate groups of fucoidans in order to obtain oversulfated fucoidans or oversulfated fucoidan fragments (*T. Nishino et al, Carbohydr. Res., 1992, 229: 355-362; S. Soeda et al, Thromb. Res., 1993, 72: 247- 256*). According to a particular embodiment, the fucoidan is polysulfated. According to a more particular embodiment, said polysulfated fucoidan has a sulfate-to-sugar ratio superior to 1, in particular superior to 1.2, preferably superior or equal to 1.9.

In some embodiments, the fucoidans can be of high molecular weight or low molecular weight.

As used herein, the term "**molecular weight"** relates to the average molecular weight, or Mw. A "**low molecular weight fucoidan**" relates to any fucoidan with an average molecular weight equal or lower than 20,000 Da, in particular within a range between 2,000 and 20,000 Da. A

"**high molecular weight fucoidan**" relates to any fucoidan with an average molecular weight superior to 20,000 Da, in particular within a range between 20,000 and 600,000 Da.

In some embodiments, the fucoidan has an average molecular weight of about 2,000 to about 100,000 Da. In some embodiments, the fucoidan has an average molecular weight of about 20,000 to about 70,000 Da. In some embodiments, the fucoidan has an average molecular weight of about 100,000 to about 500,000 Da. In some embodiments, the fucoidan has an average molecular weight which is lower than 100,000 Da, and preferably lower than 20,000 Da, for instance between 2,000 and 20,000 Da. In some embodiments, the fucoidan has an average molecular weight ranging from 2,000 Da to 1,5000 Da. In some embodiments, the fucoidan is chosen among low molecular weight fucoidans, such as the ones described in WO2010116209.

As used herein, the term "**t-PA**" has its general meaning in the art and refers to tissue-type plasminogen activator. The term includes native t-PA and recombinant t-PA, as well as modified forms of t-PA that retain the enzymatic or fibrinolytic activities of native t-PA. The enzymatic activity of t-PA can be measured by assessing the ability of the molecule to convert plasminogen to plasmin. The fibrinolytic activity of t-PA may be determined by any in vitro clot lysis activity known in the art. Recombinant t-PA has been described extensively in the prior art and is known to the person of skill. t-PA is commercially available as alteplase (Activase® or Actilyse®). Modified forms of t-PA ("**modified t-PA**") have been characterized and are known to those skilled in the art. Modified t-PAs include, but are not limited to, variants having deleted or substituted amino acids or domains, variants conjugated to or fused with other molecules, and variants having chemical modifications, such as modified glycosylation. Several modified t-PAs have been described in PCT Publication No. WO93/24635; EP 352,119; EP382174.

In some embodiments, the cross-linked polysaccharide particle of the invention is obtainable by the method that comprises the following steps:

a) preparing an alkaline aqueous solution comprising an amount of at least one polysaccharide, the amount of fucoidan and an amount of a cross linking agent;

b) dispersing said alkaline aqueous solution into a hydrophobic phase in order to obtain w/o emulsion; and

c) transforming the w/o emulsion into particle by placing said w/o emulsion at a temperature from about 4°C to about 80°C for a sufficient time to allow the cross-linking of said amount of polysaccharide and fucoidan,

d) loading the amount of t-PA into the particles obtained at step c).

As used herein, the term **"alkaline solution"** refers to a solution having a pH strictly superior to 7.

As used herein, the term **"aqueous solution"** refers to a solution in which the solvent is water.

In some embodiments, the cross-linking agent is selected from the group consisting of trisodium trimetaphosphate (STMP), phosphorus oxychloride ($POCl_3$), epichlorohydrin, formaldehydes, carbodiimides, and glutaraldehydes. Preferably, said cross-linking agent is STMP. Typically, the weight ratio of the polysaccharide to the cross-linking agent is in the range from 15:1 to 1:1, preferably 6:1.

As used herein, **"w/o emulsion"** or **'water-in-oil emulsion"**, refers to the dispersion of an aqueous phase into a lipophilic phase. The term encompasses stable and non-stable emulsion.

As used herein, the terms **"non-aqueous phase"**, **"lipophilic phase"**, **"hydrophobic phase"**, and **"oily phase"** may be used in an interchangeable manner.

The skilled artisan is aware of the hydrophobic phases suitable for the purpose of the invention. Non-limiting examples of hydrophobic phases are vegetal oils, such as canola oil, corn oil, cottonseed oil, safflower oil, soybean oil, extra virgin olive oil, sunflower oil, palm oil, MCT oil, and trioleic oil. Preferably, said hydrophobic phase is sunflower oil. Alternatively, said hydrophobic phase is a silicon fluid. Typically, the quantity of hydrophobic phase in the w/o emulsion (volume of lipophilic phase/volume of the water-in-oil emulsion; v/v) represents from about 10% to about 90% v/v, preferably from about 20% to about 80% v/v, preferably from about 50% to about 80% v/v and most preferably about 70% v/v of the w/o emulsion.

Typically, the step b) of dispersing the alkaline aqueous solution into the hydrophobic phase is performed under mechanical stirring. Typically, such a dispersing step is performed during 10

min. Alternatively, the emulsification process can be performed using a high-performance disperser, such as Polytron® Homogenizer.

In some embodiments, step b) of the method of the invention is carried out in presence of a surfactant.

As used herein, "**surfactant**" or "**emulsifier**" refers to a compound that lowers the surface tension of a liquid, the interfacial tension between two liquids, or that between a liquid and a solid. In particular a surfactant has an amphiphilic structure which confers thereon a particular affinity for interfaces of water/oil type, thereby giving it the ability to lower the free energy of these interfaces and to stabilize dispersed systems.

In some embodiments, the surfactant is selected from the group consisting of polyglycerol polyricinoleate and PEG-30 dipolyhydroxystearate. Polyglycerol polyricinoleate or PGPR (Palsgaard®4125, Palsgaard®4150, Palsgaard®4110, Palsgaard®4120 or Palsgaard®4175) is a surfactant which has, as hydrophilic group, polyglycerol (preferably consisting of at least 75% of di- and triglycerol and of at most 10% of heptaglycerol) and, as hydrophobic group, interesterified ricinoleiques fatty acids. PEG-30 dipolyhydroxystearate includes Cithrol® DPHS and formerly Arlacel® P135 sold by the company Croda.

In some embodiments, step b) is carried out in presence of an osmotic agent.

As used herein, the term "**osmotic agent**" refers to a material which creates an osmotic pressure within the oral dosage form which adopted the osmotic system. Upon penetration of fluid into the oral dosage form through semipermeable membrane, osmotic agents are dissolved in the fluid, which creates an osmotic gradient and generates a driving force for the uptake of fluid. Osmotic agents usually are ionic compounds which include but not limited to water-soluble salts, hydrophilic polymers, carbohydrates and water-soluble amino acids. Several osmotic agents are known in the field, which include salts (e.g. NaCl, MgCl2, or KN03), sugars (e.g. sucrose, glucose or fructose), or volatile solutes (e.g. SO2) or certain mixtures thereof.

According to the invention, the particles obtained at step c) have a negative zeta potential.

As used herein, the term "**zeta-potential**" or "**ζ-potential**" has its general meaning in the art and refers to the electrical potential that exists across the interface of all solids and liquids, e.g., the potential across the diffuse layer of ions surrounding the particle. Zeta potential can be calculated from electrophoretic mobilities, i.e., the rates at which the particles travel between charged electrodes placed in contact with the substance to be measured, using techniques well known in the art. Typically, said methods include Electrophoretic Light Scattering as described in EXAMPLE.

In particular, the loading of t-PA into the particles obtained at step d) is carried out by mixing the particles with a solution comprising an amount of t-PA. Typically, the loading is carried out by adsorption.

As used herein, the term "**adsorption**" has its general meaning in the art and refer to adherence of atoms, ions, or molecules of a first substance (e.g. t-PA) the surface of another substance (e.g. cross-linked polysaccharide particle) referred to herein as "**the sorbent**". According to the invention the adsorption of t-PA to the surface of the particle does not involve covalent bonds.

Typically, the adsorption is carried out as described in the EXAMPLE. More particularly, the solution comprising the t-PA has a pH below t-PA isoelectric point IP=7.7.

In some embodiments, the method of the invention further comprises a step of calibrating the polysaccharide particles according to their size. After performing said step of calibrating, the person skilled in the art may obtain particles of the desired size.

The size of the polysaccharide particles would be chosen with precaution by the skilled man in regard with the desired use. The size of the polysaccharide particles of the invention is dependent on the characteristics and parameters of the method of preparing such polysaccharide particles. Typically, the size of the polysaccharide particle of the invention may depend on the nature of the polysaccharide, the agitation provided during the process and the distribution of the polysaccharide within the polysaccharide particles. The person skilled in the art may easily adapt and calibrate the particles in order to obtain a desired size. Typically, said adaptation and/or calibration may be performed by the following techniques: sieving or filtration though nylon filter.

In the context of the invention, particles of the invention are "**functionalized**" by fucoidan meaning that fucoidan is used as a vectorizing agent to confer its specificity/selectivity/affinity property to the selectin. The fucoidan has some degree of affinity for selectins, in particular P-selectin, and that can play a targeting role when they are part of a vectorizing agent. Suitable fucoidan moieties thus include fucoidans that exhibit affinity and specificity for only one of the selectins (i.e., for L-selectin, E-selectin or P-selectin) as well as fucoidans that exhibit affinity and specificity for more than one selectin, including those moieties which can efficiently interact with, bind to or associate with all three selectins. Preferably, the interaction between a selectin and a fucoidan as part of a vectorizing agent is strong enough for at least the time necessary to vectorize t-PA to a thrombus.

As used herein, the terms "**binding affinity**" and "**affinity**" are used herein interchangeably and refer to the level of attraction between molecular entities. Affinities can be expressed quantitatively as dissociation constant ($K_D$), or its inverse, the association constant ($K_A$). In some embodiments, a suitable fucoidan interacts with a selectin with a dissociation constant ($K_D$) between about 0.1 nM and about 500 nM, preferably between about 0.5 nM and about 10 nM, more preferably between about 1 nM and about 5 nM.

As used herein, the term "**selectin**" has its art understood meaning and refers to any member of the family of carbohydrate-binding, calcium-dependent cell adhesion molecules that are constitutively or inductively present on the surface of leukocytes, endothelial cells or platelets. The term "**E-selectin**", as used herein, has its art understood meaning and refers to the cell adhesion molecule also known as SELE; CD62E; ELAM; ELAM1; ESEL; or LECAM2 (Genbank Accession Numbers for human E-selectin: NM_000450 (mRNA) and NP_000441 (protein)). As used herein, the term "**L-selectin**" has its art understood meaning and refers to the cell adhesion molecule also known as SELL; CD62L; LAM-1; LAM1; LECAM1; LNHR; LSEL; LYAM1; Leu-8; Lyam-1; PLNHR; TQ1; or hLHRc (Genbank Accession Numbers for human L-selectin: NM_000655 (mRNA) and NP_000646 (protein)). The term "**P-selectin**", as used herein, has its art understood meaning and refers to the cell adhesion molecule also known as a SELP; CD62; CD62P; FLJ45155; GMP140; GRMP; PADGEM; or PSEL (Genbank Accession Numbers for human P-selectin: NM_003005 (mRNA) and NP_002996 (protein)).

A further object of the invention relates to the use of the particles of the invention for therapy (i.e. as a drug).

As used herein, the term "**treating**", "**treatment**" and **"therapy"** refers to reversing, alleviating, inhibiting the progress of, or preventing the disorder or condition to which such term applies, or one or more symptoms of such disorder or condition. In particular, the term "**treatment**" or "*treat*" refer to both prophylactic or preventive treatment as well as curative or disease modifying treatment, including treatment of patient at risk of contracting the disease or suspected to have contracted the disease as well as patients who are ill or have been diagnosed as suffering from a disease or medical condition, and includes suppression of clinical relapse. The treatment may be administered to a patient having a medical disorder or who ultimately may acquire the disorder, in order to prevent, cure, delay the onset of, reduce the severity of, or ameliorate one or more symptoms of a disorder or recurring disorder, or in order to prolong the survival of a patient beyond that expected in the absence of such treatment. By "**therapeutic regimen**" is meant the pattern of treatment of an illness, e.g., the pattern of dosing used during therapy. A therapeutic regimen may include an induction regimen and a maintenance regimen. The phrase "**induction regimen**" or "**induction period**" refers to a therapeutic regimen (or the portion of a therapeutic regimen) that is used for the initial treatment of a disease. The general goal of an induction regimen is to provide a high level of drug to a patient during the initial period of a treatment regimen. An induction regimen may employ (in part or in whole) a "**loading regimen**", which may include administering a greater dose of the drug than a physician would employ during a maintenance regimen, administering a drug more frequently than a physician would administer the drug during a maintenance regimen, or both. The phrase "**maintenance regimen**" or "**maintenance period**" refers to a therapeutic regimen (or the portion of a therapeutic regimen) that is used for the maintenance of a patient during treatment of an illness, e.g., to keep the patient in remission for long periods of time (months or years). A maintenance regimen may employ continuous therapy (e.g., administering a drug at a regular interval, e.g., weekly, monthly, yearly, etc.) or intermittent therapy (e.g., interrupted treatment, intermittent treatment, treatment at relapse, or treatment upon achievement of a particular predetermined criteria [e.g., pain, disease manifestation, etc.]).

In particular, the particles of the invention are particularly suitable for the treatment of thrombotic diseases.

A used herein, the term “**thrombotic diseases**” and “**thrombotic disorders**” are diseases and/or disorders which are associated with the appearance, or persistence, of undesirable

intravascular thrombus. The term "**thrombus**" or "**blood clot**" as used herein refers to a solid or semi-solid mass formed from the constituents of blood within the vascular system that is the product of blood coagulation. There are two components to a thrombus, aggregated platelets that form a platelet plug, and a mesh of cross-linked fibrin protein.

Thrombotic diseases are well-known in the art and can have various causes. They can be primary or acquired diseases. In particular, they can be hereditary, and/or linked to genetic predispositions. Examples of such diseases comprise, for instance, haemophilias, Von Willebrand disease, and other coagulopathies linked to hyper- and hypo-coagulability.

Thrombotic disorders and diseases disclosed herein may, for instance, result in the formation of venous thrombosis such as deep vein thrombosis, portal vein thrombosis, renal vein thrombosis, jugular vein thrombosis, or cerebral venous sinus thrombosis. In some cases, said thrombosis may lead to phlebitis, also referred herein as thrombophlebitis, and sometimes to pulmonary embolisms. It may also involve atrial and ventricular thrombi related to heart arrythmias. They may also result in arterial thrombosis, which is often a consequence of the rupture of an atherosclerotic plaque, in which case it can be also referred as atherothrombosis. An arterial thrombosis may, for instance, lead to a stroke, a myocardial infarction and/or an arterial embolus.

Thus, a further object of the invention relates to a method of treating a thrombotic disease or disorder in a patient in need thereof comprising administering to the patient a therapeutically effective amount a particle of the invention.

As used herein, the expression "**therapeutically effective amount**" as above described is meant a sufficient amount of the particle for the treatment of the thrombotic disease or disorder. It will be understood, however, that the total daily usage of the compounds and compositions of the invention will be decided by the attending physician within the scope of sound medical judgment. The specific therapeutically effective dose level for any particular patient will depend upon a variety of factors including the disorder being treated and the severity of the disorder; activity of the specific compound employed; the specific composition employed, the age, body weight, general health, sex and diet of the patient; the time of administration, route of administration, and rate of excretion of the specific compound employed; the duration of the treatment; drugs used in combination with the specific agonist employed; and like factors well

known in the medical arts. For example, it is well known within the skill of the art to start doses of the compound at levels lower than those required to achieve the desired therapeutic effect and to gradually increase the dosage until the desired effect is achieved. However, the daily dosage of the products may be varied over a wide range from 0.01 to 1,000 mg per adult per day. Preferably, the compositions contain 0.01, 0.05, 0.1, 0.5, 1.0, 2.5, 5.0, 10.0, 15.0, 25.0, 50.0, 100, 250 and 500 mg of the active ingredient for the symptomatic adjustment of the dosage to the patient to be treated. A medicament typically contains from about 0.01 mg to about 500 mg of the active ingredient, preferably from 1 mg to about 100 mg of the active ingredient. An effective amount of the drug is ordinarily supplied at a dosage level from 0.0002 mg/kg to about 20 mg/kg of body weight per day, especially from about 0.001 mg/kg to 7 mg/kg of body weight per day.

A further object of the invention relates to a pharmaceutical composition comprising an amount of the particles of the invention.

Often, pharmaceutical compositions will be administered by injection. For administration by injection, pharmaceutical compositions of thrombolytic agents may be formulated as sterile aqueous or non-aqueous solutions or alternatively as sterile powders for the extemporaneous preparation of sterile injectable solutions. Such pharmaceutical compositions should be stable under the conditions of manufacture and storage, and must be preserved against the contaminating action of microorganisms such as bacteria and fungi. Pharmaceutically acceptable carriers for administration by injection are solvents or dispersion media such as aqueous solutions (e.g., Hank's solution, alcoholic/aqueous solutions, or saline solutions), and non-aqueous carriers (e.g., propylene glycol, polyethylene glycol, vegetable oil and injectable organic esters such as ethyl oleate). Injectable pharmaceutical compositions may also contain parenteral vehicles (such as sodium chloride and Ringer's dextrose), and/or intravenous vehicles (such as fluid and nutrient replenishers); as well as other conventional, pharmaceutically acceptable, non-toxic excipients and additives including salts, buffers, and preservatives such as antibacterial and antifungal agents (e.g., parabens, chlorobutanol, phenol, sorbic acid, thirmerosal, and the like). Prolonged absorption of the injectable compositions can be brought about by adding agents that can delay absorption (e.g., aluminum monostearate and gelatin). The pH and concentration of the compositions can readily be determined by those skilled in the art. Sterile injectable solutions are prepared by incorporating the active compound(s) and other ingredients in the required amount of an appropriate solvent, and then by sterilizing the resulting

mixture, for example, by filtration or irradiation. The methods of manufacture of sterile powders for the preparation of sterile injectable solutions are well known in the art and include vacuum drying and freeze-drying techniques. In general, the dosage of the particle will vary depending on considerations such as age, sex and weight of the patient, as well as the particular pathological condition suspected to affect the patient, the extent of the disease, or the area(s) of the body to be examined. Factors such as contra-indications, therapies, and other variables are also to be taken into account to adjust the dosage of the agent to be administered.

The invention will be further illustrated by the following figures and examples. However, these examples and figures should not be interpreted in any way as limiting the scope of the invention.

**FIGURES:**

**Figure 1.** Crosslinking of the polysaccharides (dextran and fucoidan) with STMP in alkaline conditions.

**Figure 2.** Evaluation of the SPs interactions with P-Selectin. **A.** Adhesion of the Control-SPs or Fuco-SPs on the coating of the recombinant P-Selectin in the microfluidic assay under arterial and venous flow conditions (n = 4). **B.** Concentration dependent binding of the Fuco-SPs onto the coating of the P-Selectin at a range of concentrations. **C.** Fucoidan pre-injection inhibited Fuco-SPs adhesion onto the P-Selectin. **D.** Comparison of the Fuco-SPs binding to other selectins: E- and L-Selectin.

**Figure 3**. **A**. *In vitro* rtPA release from rtPA-encapsulated Fuco-SPs by flow cytometry. **B - C.** Amidolytic activity measured by the PefaFluor® fluorogenic assay. **B.** The curves correspond to the fluorescence release and are correlated to the enzymatic velocity over 90 min. **C.** Corresponding quantitative analysis normalized to free rtPA at the same concentration at 90 min. **D.** Fibrinolytic activities of the SPs determined by a fibrin-plate agarose assay. The quantitative analysis normalized to free rtPA at the same concentration.

**Figure 4.** Adhesion of the SPs over activated platelet aggregates. Visualization by fluorescent microscopy of the attached unloaded SPs was carried out on the microchannels after formation of the platelet aggregates. The figure displays corresponding quantification of integral density of the unloaded (n=6) and rtPA-loaded (n=4) Control-SPs and Fuco-SPs in ImageJ.

**Figure 5.** Thrombolytic efficacy *in vivo* in the murine ischemic stroke model. **A.** Cerebral blood flow reperfusion monitored by the laser speckle contrast imaging during the 40-min treatment. **B.** Quantification of the volume of the infarct lesion 24 h post-stroke detected by MRI. **C.** Quantification of the BBB permeability at day 4 post-stroke detected by MRI.

**EXAMPLE:**

**Methods:**

***Materials:*** Dextran 40 kDa and TRITC-dextran 40 kDa were provided by TdB Consultancy (Uppsala, Sweden). Fucoidan (Mn = 18 kDa/Mw = 104 kDa) was a gift from Algues & Mer (Ouessant, France). *Sodium* trimetaphosphate (STMP), methylene blue hydrate, and Human Serum Albumin (HSA) were purchased from Sigma-Aldrich (Saint-Quentin-Fallavier, France). Polyglycerol polyricinoleate (PGPR) was obtained from Palsgaard France S.A.S. (Lyon, France). Vegetable (sunflower) oil was purchased from a local supermarket. The SPs were encapsulated with commercially available rtPA (Actilyse®, Boehringer Ingelheim) that was reconstituted at 1 mg/ml, aliquoted, and stored at -80 □C. Chromatography paper was obtained from GE Healthcare (Chicago, Illinois, United States). Fibrillar type I collagen Horm® was obtained from Takeda (Linz, Austria). 96-Well Cell Culture Plates (Costar) were obtained from Corning Incorporated. PPACK (Phe-Pro-Arg-Chloromethylketone) 75 μM tubes were purchased from Cryopep (Montpellier, France). Flow chambers (Vena8 Fluoro+) were provided from Cellix Ltd (Dublin, Ireland).

***Submicroparticle synthesis:*** Polysaccharide submicroparticles (SPs) were obtained via a water-in-oil (w/o) emulsification combined with a crosslinking process. Polysaccharide solution was prepared as a mixture of dextran 40 and 5% TRITC-dextran 40 (for fluorescent SPs) at 300 mg/ml, 6 M NaCl. To synthesize functionalized SPs with fucoidan (Fuco-SPs), 10% w/w of fucoidan was added.

First, the organic phase of 15 ml of sunflower oil and 6% w/v PGPR in Falcon® 50 ml was prepared and cooled down for 20 min at -20 □C. In the meantime, 1,200 mg of the polysaccharide solution was incubated with 120 ml of 10 M NaOH under magnetic stirring for 10 min. 240 ml of STMP solution (30% w/v in water) was added into the aqueous phase under

magnetic stirring and mixed for 20 seconds on ice. Next, emulsification was achieved by the dropwise injection of 600 ml of the aqueous phase into the organic phase and dispersed with a stand-disperser (Polytron PT 3100, dispersing aggregate PT-DA 07/2EC-B101, Kinematica, Luzernerstrasse, Switzerland) at 30,000 rpm for 4 min on ice. The obtained w/o emulsion was transferred into 50 □C for the crosslinking reaction of polysaccharide with STMP for 20 min. The crosslinked suspension was washed in 30 ml PBS 10x during 40 min under high magnetic stirring at 750 rpm. The mixture was then centrifuged (BR4i, JOUAN SA, Saint Herblain, France) for 10 min at 3,000 g in Falcon tubes. The organic phase was recovered and ultracentrifuged (Optima MAX-XP, Ultracentrifuge, Beckman Coulter, Brea, California, United States) for 45 min at 15,000 g. Obtained pellet was washed by ultracentrifugation 2 times in 0.04% Sodium Dodecyl Sulfate (SDS) solution and then 2 times in ultrapure water to purify the SPs. The resulting SPs were suspended in water or 0.9% NaCl with 0.02% Tween 20 (Sigma) and stored at 4 □C.

**Table 1**. The synthesis parameters for the polysaccharide SPs.

| Synthesis method | Polysaccharide [c], mg/ml | STMP, [c], mg/ml | NaOH [c], M | Phase ratio, (Aq/ Org/) | Surfactant | Homogenization | Crosslinking |
|---|---|---|---|---|---|---|---|
| W/O emulsion / crosslinking | 300 | 56.11 | 1.15 | 4% w/v | PGPR, 6% | 30,000 rpm, 4 min, 4 °C | 20 min, 50 □C |

Aq: aqueous; Org: organic.

***Cell culture and cytotoxicity assay:*** To evaluate the cytotoxicity of the SPs, Fluorometric Cell Viability Assay (Resazurin) was used on confluent Human Umbilical Vein Endothelial Cells (HUVEC). The cells were cultured in DMEM supplemented with 10% (v/v) fetal bovine serum, 4 mmol of l-glutamine, 100 units/mL of penicillin, and 100 µg/mL of streptomycin and kept in an incubator at 37 °C in a humidified atmosphere of 5% $CO_2$. Cells were seeded into 96-well plates to adhere, 10,000 cells per well. Following 24 h of incubation, the medium in the wells was changed to the one containing the SPs at concentrations ranging from 0.1 to 1.5 mg/ml and cultured for another 24h. Culture media were used as a positive control. Next, the medium was replaced with 100 µL 10% Resazurin solution, and the plates were covered in foil and incubated for 2h. The fluorescent signals of the Resazurin were monitored using 540 nm excitation and 590 nm emission wavelengths on Infinite® 200 PRO microplate reader (TECAN Group Ltd., *Mannedorf*, Switzerland). The obtained fluorescence (Fl) values were blank corrected; and the

relative cell viability was expressed as $Fl_{SPs}$ / $Fl_{control}$ × 100%, where $Fl_{control}$ was obtained in the absence of the SPs. The experiment was performed in hexaplicate.

To examine the potential cell cytoskeleton organization mediated by Fuco-SPs, HUVEC cells were cultured in 8-well Lab-Tek II Chamber Slide w/Cover (Lab-Tek®, Thermo Fischer Scientific, Massachusetts, United States) with 10,000 cells per well. The medium in the wells was changed 24 h after to the one containing TRITC-Fuco-SPs at 1.5 mg/ml and was incubated for another 24 h. Cells cultured in the medium without the SPs were set as control. Next, cells were fixed with 4% paraformaldehyde for 30 min at RT. After rinsing with PBS, cells were labeled and permeabilized with the 200 µl mixture of FITC-Phalloidin (1:200, Sigma-Aldrich, USA) / DAPI (1:100, Thermo Fisher Scientific, Massachusetts, United States) / 0.01% v/v Tween 20 in PBS and incubated under low agitation for 1h at RT. The cells were afterward washed 3 times with PBS. The support of the chamber slides was removed, and the slides were mounted with a few drops of the aqueous mounting medium and kept at 4 □C until visualization with the confocal microscope (Zeiss LSM 780, Iena, Germany).

***Hemocompatibility test*:** Hemolysis assay was adapted from the publication [17] and performed on washed isolated murine erythrocytes. Murine blood was collected in sodium citrate 3.8% (w/v) and centrifuged at 800 g for 5 min to isolate red blood cells. The supernatant was removed, and the pellet of erythrocytes was resuspended at 20% (v/v) in distilled water (positive control, 100% hemolysis), normal saline (negative control, no hemolysis), and the Fuco-SPs at the concentrations from 0.1 to 1.5 mg/ml in Eppendorf. The tubes were incubated on a rotator at 37 °C for 1.5 h and then centrifuged at 3,000 g for 5 min. The absorbance (A) of the supernatants was measured on Infinite® 200 PRO microplate reader (TECAN Group Ltd., *Mannedorf*, Switzerland) at 590 nm. Each sample was run in triplicate. The percentage of hemolysis was determined by the formula: Hemolysis degree (%) = 100% x $(A_{sample} - A_{negative\ control})/(A_{positive\ control} - A_{negative\ control})$.

***Physico-chemical characterization:*** The submicroparticle (SP) formulations were studied for particle morphology, size and zeta potential distributions, mass concentration, and elemental composition.

Particle morphology was visualized by Transmission Electron Microscopy (TEM) (Philips FEI Tecnai 12, Amsterdam, Netherlands), negatively stained with 1% (w/v) uranyl acetate for 5

minutes, and Environmental Scanning Electron Microscopy (ESEM) (Philips XL30 ESEM-FEG, Amsterdam, Netherlands). Hydrodynamic size and Zeta potential (ζ-potential) were measured by Dynamic Light Scattering (DLS) and Electrophoretic Light Scattering (ELS), respectively (Zetasizer Nano ZS, Malvern Instruments SARL, Orsay, France). Samples were dissolved in distilled water or saline for size and in 1 mM KCl for ζ-potential determination. All runs were performed at 25 °C in triplicate.

Mass concentration was determined by freeze-drying. An elemental analyzer-mass spectrophotometer was used for the quantification of the sulfur (presence of fucoidan). To prove the crosslinking with STMP, total reflection X-ray fluorescence spectroscopy (TXRF) technique was applied to quantify the phosphorus content on the SPs (S2 PICOFOX Bruker, Massachusetts, United States).

***Sulfate and fucoidan quantification:*** The sulfate content of fucoidan was determined by a semi-quantitative solid-phase colorimetric assay [29]. Briefly, 5 µL of Fuco-SPs in suspension at a concentration of 2 mg/mL were dropped on a piece of Whatman Chromatography paper grade 1. This was repeated 5 times on the same point, allowing the paper to dry at 50 □C in between. The paper was first soaked into a methanol/acetone (6:4) solution for 3 min and then into a methanol/acetone/water (6:4:15) solution with 50 mM HCl and 0.1% w/w methylene blue for 10 min. Finally, the paper was extensively washed with acetic acid/methanol/acetone/water (5:6:4:75) until no coloration was detected in the washing solution. The paper was then transferred to the Eppendorf, containing 0.5 mL methanol with 2% w/v SDS, and incubated for 15 min at 50 □C. 0.2 mL of the extracted dye was placed in a 96-well plate, and its concentration was determined by reading absorbance at 663 nm on an Infinite® 200 PRO microplate reader (TECAN Group Ltd., *Mannedorf*, Switzerland). Standard curves were obtained from fucoidan in solution with known concentrations.

***Loading rtPA on the SPs:*** rtPA was immobilized onto the SPs by adsorption. 100 µl of SPs (5 mg/ml) was mixed with 100 µl of rtPA (1 mg/ml) in ultrapure water and then incubated for 1h at RT. Free unabsorbed rtPA was removed by 3 cycles of ultracentrifugation (15 min, 15,000 g). The SPs with adsorbed rtPA (rtPA-SPs) were resuspended in water and used for the drug loading efficiency quantification.

***Drug encapsulation efficiency:*** The amount of rtPA loaded on the SPs was measured using the Pierce BCA protein assay kit (Life Technologies SAS, Courtaboeuf, France). Briefly, 200 µl of working reagent was added to 25 µl of each sample in 96 well-plate. The absorbance at 562 nm was read on the Infinite® 200 PRO microplate reader (TECAN Group Ltd., *Mannedorf*, Switzerland) after 30 min of incubation at 37 °C and cooling to RT for 10 min. The concentration of the drug was extrapolated by a calibration curve prepared with different concentrations of rtPA.

***In vitro rtPA release:*** The release of rtPA from the Fuco-SPs was assessed by flow cytometry [30]. FITC-rtPA (Abcam, Cambridge, United Kingdom) at 1 mg/mL was placed in contact with TRITC Fuco-SPs at 5 mg/mL for 1h at RT. The suspensions were added to tubes pre-filled with 400 mL of saline and placed under gentle agitation at 37 □C. At each time point of 0, 15, 30, 45, 60, and 90 min, the tubes were analyzed with a BD FACS Aria™ III flow cytometer (Becton Dickinson, New Jersey, United States). The TRITC-Dextran, excited by a 543 nm laser, was detected at 569 nm while the FITC-rtPA, excited at 480 nm, was detected on a 530/30 nm PMT. Flow cytometry analyses were performed in triplicates with Diva software (Becton Dickinson). The protein release curve was obtained by normalizing the values of Mean Fluorescence Intensity (MFI) of the FITC-rtPA still associated with TRITC-Fuco-SPs.

***In vitro amidolytic activity of rtPA-loaded SPs:*** Amidolytic activity of rtPA loaded SPs was assessed with the fluorogenic substrate PefaFluor® tPA (Cryopep, Montpellier, France). 2.5 µL of samples at 20 µg/ml was put in contact with 97.5 µL of 100 mM HEPES buffer (pH 8.0, 154 mM NaCl, 0.1% HAS) in the 96-well plate. After the addition of 10 µL PefaFluor® at 1 mM, a kinetic profile was obtained by measuring the fluorescence level at 440 nm every 2 min during 90 min at 37 □C with Infinite® 200 PRO microplate reader (TECAN Group Ltd., *Mannedorf*, Switzerland). Free rtPA was used at the same concentration based on the Pierce BCA protein assay. Increase of fluorescence corresponded to the fluorogenic peptide substrate hydrolysis by rtPA. Enzymatic activity was determined from the resulting kinetic profile and compared to the one of free rtPA.

***In vitro fibrinolytic activity of rtPA-loaded SPs:*** To assess the fibrinolytic activity of rtPA-loaded SPs, a fibrin lysis clot experiment was performed. 5 ml of TRIS Buffer with 3% w/v low melting agarose (Carl Roth GmbH þ Co. KG, Karlsruhe, Germany) were heated to 65 °C. 5 ml of Fibrinogen (from human plasma, Sigma Aldrich) solution in TRIS buffer at 5 mg/ml

was slowly heated to 37 °C. Once the agarose solution reached 65 °C, it was cooled to 37 °C, and 2.5 U of thrombin (from human plasma, Sigma Aldrich) was added. Next, a fibrinogen solution was slowly added into the agarose/thrombin mixture under gentle agitation to avoid the formation of bubbles. The reaction mixture was poured into a 9 cm Petri dish and cooled at 4 °C for 30 min until the fibrin clot became visible. On the solidified agarose gel, round wells were formed using a 3 mm punch as sample reservoirs. 5 µl of each sample at 45 µg/ml was dropped into the wells and incubated overnight at 37 °C in a humid environment. The degree of fibrin lysis was quantified with ImageJ by comparing the size of the fibrinolysis circle of the samples and free rtPA at the equivalent concentration based on the Pierce BCA protein assay.

***Flow microchamber experiments:*** An *in vitro* flow adhesion assay was performed to evaluate the affinity of the Fuco-SPs with their molecular target. Micro-channels of Vena8 Fluoro$^+$ chambers (width: 0.04 cm, height: 0.01 cm, and length: 2.8 cm; Cellix Ltd, Dublin, Ireland) were coated overnight with recombinant human P-selectin, L-selectin or E-selectin (R&D systems France, Lille, France) at 100 µg/mL and left overnight at 4 °C. To confirm the concentration-dependent binding of Fuco-SPs to P-selectin, some channels were coated with P-selectin at a range of concentrations (5, 25, 50, and 100 µg/mL). Channels were then washed with NaCl 0.9% and further incubated with HSA at 10 µg/mL for 2h.

A suspension of fluorescently labeled Control-SPs or Fuco-SPs at 1 mg/ml in saline was passed through the channels during 5 min at arterial and venous flow conditions (shear stress 67.5 dyne/cm$^2$ and 6.75 dyne/cm$^2$) using an ExiGo™ pump (Cellix Ltd, Dublin, Ireland). For the competitive binding experiment, fucoidan solution (10 mg/ml) was injected 5 min prior to the Fuco-SPs at the same rate. Then, all the channels were washed with NaCl 0.9% for 1 min. The binding of the adhered SPs was visualized in real-time under fluorescence microscopy (Axio Observer, Carl Zeiss Microimaging GmbH, Iena, Germany). For the quantitative analysis, the number of fluorescent SP clusters on each channel was measured using the "Analyze particles" tool in the image analysis software ImageJ (NIH, Bethesda, U.S.) with a 4-pixel threshold to eliminate the background noise.

To further investigate the binding efficiency of unloaded and loaded SPs to activated platelets, the microchannels of Vena8 Fluoro$^+$ were coated with 50 µg/mL of fibrillar type I collagen Horm® overnight at 4 °C and rinsed with NaCl 0.9% before use. Human whole blood (EFS, Bichat Hospital, Paris, France), collected in the PPACK tubes and labeled with 5 mM DIOC6

(Life Technologies SAS, Saint-Aubin, France), was perfused at arterial shear stress for 5 min to induce platelet activation and aggregation. Platelet aggregation through contact with collagen was visualized in real-time with phase-contrast microscopy (Axio Observer, Carl Zeiss Microscopy, Oberkochen, Germany). After rinsing with NaCl 0.9%, fluorescent Control-SPs or Fuco-SPs (unloaded or loaded with rtPA) at 1 mg/ml were injected into the channels in saline for 5 min. Their accumulation onto activated aggregates was monitored in real-time. Channels were then washed for 1 min with NaCl 0.9%. Finally, the MFI of the fluorescent SPs that are bound to the platelets on each channel was analyzed with ImageJ. Intensity settings were kept the same for both types of SPs.

***Animals and thrombin stroke model in vivo:*** Animal experiments were carried out on male Swiss wild-type mice (15–18 weeks old; 35-45 g; CURB, Caen, France). All experiments were performed following the French (Decree 87/848) and the European Communities Council (2010/63/EU) guidelines and were approved by the institutional review board (French ministry of Research). All the experiments were validated by the local ethical committee of Normandy (CENOMEXA) registered under the reference CENOMEXA-0113-03 and received the agreement number N/03-01-13/03/01 to 18. Anesthesia was induced by application of 5% isoflurane (Aerrane, Baxter) and maintained by 2% isoflurane in a mixture of $O_2/N_2O$ (30% / 70%).

Mice were placed in a stereotaxic device, then a small craniotomy was performed, the dura was excised, and the middle cerebral artery (MCA) was exposed. To induce the occlusion of the MCA, the coagulation cascade was triggered by the pneumatical injection of 1 µL murine α-thrombin (1 IU; Enzyme Research Labs) with a glass micropipette, as previously described [31]. Successful MCA occlusion was confirmed by the Laser Doppler flowmeter (Oxford Optronix). For the treatment, the animals were intravenously injected through a tail vein catheter (200 µL, 10% bolus, 90% infusion over 40 minutes) with either saline (n=5) or rtPA-Fuco-SPs (Actilyse® rtPA at 10 mg/kg) (n=6) 20 minutes after thrombus formation. Brain perfusion was monitored by Laser Speckle Contrast Imager (MOOR FLPI-2, Moor Instruments) throughout the treatment. Region of interest (ROI) was selected on the ipsilateral to occlusion and contralateral hemispheres to monitor the relative cerebral blood flow in the effected region ($Fl_t$ = 100% x $Fl_{ipsi}/Fl_{contra}$). The post-stroke reperfusion was expressed as a Growth Rate (GR) of the blood flow increase in the ipsilateral ROI to contralateral one at a time point, and it was quantified as GR (%) = 100% x ($Fl_{t2}$ - $Fl_{t1}$)/ $Fl_{t1}$.

***Magnetic resonance imaging acquisition and analysis:*** Mice were anesthetized with 5% isoflurane and maintained with 1.5-2% isoflurane in a mixture of $O_2/N_2O$ (30% / 70%) during the acquisitions. Experiments were carried out on a Pharmascan 7T (Bruker Biospin, Wissembourg, France). Three-dimensional T2-weighted images were acquired using a Multi-Slice Multi-Echo sequence (TE/TR 33 ms / 2,500 ms) 24 h after the stroke. Lesion volumes were quantified on these images using ImageJ software (slice thickness 0.5 mm). Magnetic resonance angiography was performed using a 2D-TOF sequence (TE/TR 12 ms / 7 ms) 24 h after ischemia, and the recanalization status of the MCA was determined blindly from the analysis of the merged MCA angiograms with maximum intensity. The angiographic score is based on the TICI (Thrombolysis in Cerebral Infarction) grade flow scoring (from Score 0: no perfusion to Score 3: full recanalization). For the *in vivo* detection of the BBB permeability, three dimensional T1 FLASH sequences (spatial resolution 70 mm× 70 mm; TE/TR 4.46 / 15; 3 averages; 4 min 2 s) were used, 15 min after the intravenous injection of 200 µl of a solution containing 50 µl of gadolinium chelate (DOTAREM) diluted in saline. BBB leakage was measured 4 days after the stroke induction, and its volume was quantified using ImageJ.

***Statistical analysis:*** Quantitative data were expressed as mean ± SEM ($n \geq 3$). Statistical tests were carried out with GraphPad Prism 8 (GraphPad Software, Inc., La Jolla, U.S.) with a 95% confidence level. Kolmogorov-Smirnov normality test was utilized to examine if variables are normally distributed. Normally distributed data were analyzed then with unpaired t-test or one-way analysis of variance (ANOVA) with post hoc Turkey's test. The Mann-Whitney U test was applied otherwise. The p-values of * $p<0.05$; ** $p<0.01$; *** $p<0.001$ were considered statistically significant.

**Results and discussion:**

***Submicroparticle synthesis and characterization***

Novel polysaccharide SPs were elaborated by a simple and reproducible two-step synthesis process influenced by [16,17]. First, a stable w/o miniemulsion of the aqueous phase with hydrophilic polysaccharides and vegetable (sunflower) oil was prepared. Chemical crosslinking of polysaccharides with the crosslinking agent STMP under alkaline conditions **(Figure 1)**

produced a suspension of uniform SPs. We refer to the hydrogel particles only from dextran as Control-SPs, and from a mixture of dextran and fucoidan as Fuco-SPs in this EXAMPLE.

To ensure the *in vivo* safety during the preparation of the drug delivery platform, low molecular weight dextran 40 kDa of clinical-grade was utilized without any chemical modification. Having a large number of hydroxyl groups, dextran is a suitable compound for subsequent chemical crosslinking with STMP [25], an FDA-approved non-toxic food additive [32]. Fucoidan, a murine sulfated polysaccharide, is approved as a pharmaceutical compound [33] and exhibits a nanomolar affinity to P-selectin [34], thus, it served as a targeting ligand to thrombi. A recently completed phase 1 clinical trial of fucoidan radiolabeled by Technetium-99m reported its safety and favorable biodistribution as a potential diagnostic agent for the imaging of thrombosis [35]. Hence, both natural polysaccharides applied in this study are affordable, biodegradable, biocompatible compounds, non-immunogenic, and approved for clinical applications. Intriguingly, several articles claim that dextran [36] and fucoidan [37,38] themselves exert some antithrombotic action that makes them an excellent starting material for the carrier.

The choice of the stabilizing agent plays an important role in reducing the interfacial tension and Laplace pressure when fabricating a stable emulsion and future carrier. In this work, we selected a potent oil-soluble nonionic surfactant for stabilizing w/o emulsions – PGPR, which is also recognized by the FDA as a safe compound and is frequently used as an emulsifier in the food production industry [39]. Additionally, to counteract the Ostwald ripening of water droplets, 6 M NaCl was added to the aqueous phase as an osmotic agent to adjust the osmotic gradient and to further stabilize the w/o emulsion. Overall, multiple parameters were optimized to obtain a stable and homogenous miniemulsion and subsequent nano-delivery system. It was found that the size of the generated hydrogel SPs being directly proportional to the polysaccharide molecular weight and inversely proportional to the amount of surfactant and crosslinking agent as well as homogenization speed (data not shown).

ESEM and TEM images revealed a well-defined spherical morphology and uniform size distribution of SPs (**data not shown**). Functionalized Fuco-SPs contained 8.60 ± 0.01% of fucoidan in a mass of the total SPs weight, determined by elemental analysis of sulfur, and 9.30 ± 1.07% of fucoidan by quantification of the sulfate content by a semi-quantitative colorimetric assay. In such a way, two different techniques estimated ~9% fucoidan composition in the SPs.

The SPs exhibited the hydrodynamic size of 674.87 ± 59.35 nm (Control-SPs) and 708.48 ± 40.00 nm (Fuco-SPs) determined by DLS. It is important to highlight that a relatively large size of the SPs might limit the accumulation of associated rtPA within the brain parenchyma and reduce the risk of hemorrhagic events. The negative ζ-potential of the SPs was -24.83 ± 0.09 mV for Control-SPs and -27.07 ± 0.39 mV for Fuco-SPs ensured colloidal stability as a result of the anionic nature of the fucoidan and the formation of the anionic phosphate functional groups, produced during the crosslinking reaction with STMP.

The obtained SPs preserved their integrity in a physiological solution of 0.9% NaCl. As hydrogel-based particles, they were able to swell in an aqueous medium while maintaining their network structure (**data not shown**). These soft particles resemble the networks of natural extracellular matrices that could minimize tissue irritation or cell adherence [40]. Size and zeta potential of both SPs remained to be stable at least 30 days at 4 °C storage (**data not shown**).

***Biocompatibility of the SPs***

The injectable hydrogel SPs were produced according to the green chemistry principles through the formulation method without the use of hazardous substances and organic solvents and were expected to be biocompatible.

An initial *in vitro* evaluation of biocompatibility of the developed SPs examined cyto- and hemocompatibility. The cytocompatibility of the SPs was assessed with a resazurin cell viability assay. Following 24 h exposure, Control-SPs and Fuco-SPs did not affect cellular viability and metabolic activity of HUVECs at concentrations ranging from 0.1 to 1.5 mg/ml, exhibiting an excellent cytocompatible profile (cell survival > 90%, up to the highest tested concentrations of SPs) (**data not shown**). The upper limit for the tested concentration 1.5 mg/ml of the SPs was selected to surpass the tested concentrations for the majority of the systems *in vitro* (typically, maximum 400 μg/ml) [41] and the concentration of the SPs employed for further *in vivo* experiments in this work (71 mg SPs per 1 kg body weight or 1.1 mg SPs per 1 ml of blood). There was no significant difference between the Control-SPs and Fuco-SPs, as both of them did not provoke cytotoxicity.

Since the SPs in this study were designed for intravenous administration and were expected to have direct contact with blood, the Fuco-SPs were examined for their blood-compatible

behavior by a hemolysis test on isolated murine red blood cells *in vitro* (**data not shown**). Even at the highest concentration of 1.5 mg/ml, the SPs presented a hemolytic index 1.51 ± 0.02%, which is below 2% and considered to be nonhemolytic according to ISO 10993 - 4 standard [42,43].

Morphology of the cells, co-cultured with Fuco-SPs, was visualized with confocal microscopy. No obvious morphological differences were revealed for HUVECs with Fuco-SPs and negative control (**data not shown**). FITC-Phalloidin staining was used to visualize a cytoplasm and DAPI for nuclei. Moreover, the SPs were internalized by endocytosis as the merged images of all three probes revealed colocalization of the particles within the dye in the cytoplasm.

Collectively, these results suggest that the polysaccharide SPs have favorable biocompatibility for their application *in vivo*.

***Binding of SPs to P-selectin in vitro***

Knowing that fucoidan was homogeneously distributed in the structure of the hydrogel Fuco-SPs and constituted ~9% w/w of the composition, we investigated whether its quantity on the surface was sufficient for specific adhesion to its molecular target. While most of the publications assess targeting strategy *in vitro* in static conditions by flow cytometry or confocal microscopy [17,44,45], our group developed a robust and tunable dynamic microfluidic method to study the targeting efficacy for recombinant P-selectin or/and human activated platelet aggregates expressing P-selectin and previously validated it with fucoidan-coated nano- / microcarriers [18,19,28] (**data not shown**).

First, fluorescent Fuco-SPs and Control-SPs were injected in the microchannels coated with recombinant P-selectin under arterial or venous shear rates (67.5 dyne/cm$^2$ vs. 6.75 dyne/cm$^2$), and their adhesion was visualized and quantified in real-time under fluorescence microscopy. According to obtained results, fluorescent Fuco-SPs depicted a significantly higher adhesion to P-selectin coating than Control-SPs both in arterial (374.25 ± 115.33 adhered Fuco-SPs vs. 30.25 ± 13.84 adhered Control-SPs, * $p < 0.05$) and venous (228.25 ± 36.67 adhered Fuco-SPs vs. 34.50 ± 18.16 adhered Control-SPs, ** $p < 0.01$) flow conditions (**Figure 2A**). There was no significant difference between the fluorescent signal of Fuco-SPs accumulation for arterial and venous flow conditions. Fuco-SPs accumulation after injection onto P-selectin coating was

in a linear dose-dependent manner as regards to the P-selectin concentration, $R^2$=0.9904 (**Figure 2B**). An experiment of competitive interaction illustrates that fucoidan solution pre-injection at 10 mg/ml considerably reduced the attachment of the Fuco-SPs onto the microchannels with P-selectin (374.25 ± 115.33 vs. 19.75 ± 10.06, * p <0.05) (**Figure 2C**).

To establish the specificity of the Fuco-SPs binding to P-selectin, the targeting assay was extended to other members of the selectin family: E- and L-selectin [46]. The percentage of the Fuco-SPs adhered to the E- and L-selectin was normalized over the mean number of the attached Fuco-SPs to a P-selectin coating at the equivalent concentration. Indeed, only 12.73 ± 3.66% of the SPs adhered to E-selectin and 0.26 ± 0.19% to L-selectin coating (**Figure 2D**). Thus, our results indicate that Fuco-SPs bind specifically to P-selectin but not to E- and L-selectins, and these results are in accordance with a previous work of our group published by Bo L. *et al.* of fucoidan-functionalized polymer microcapsules [18].

Overall, these findings are encouraging evidence of the sensitivity and selectivity of the Fuco-SPs, confirming fucoidan potential as a natural ligand of P-selectin.

***rtPA loading onto the SPs and its release in saline. In vitro thrombolytic activity of rt-PA-loaded SPs***

Due to rtPA low bioavailability and requirement of high dose administration, coupling this enzyme to the biocompatible carrier could overcome the drawbacks associated with a drug high dosage. Herein, an efficient rtPA encapsulation was achieved through the physical adsorption method due to electrostatic interaction [47]: the protein was put in contact with negatively charged polysaccharide SPs in the water at pH below rtPA isoelectric point IP=7.7 [48] when rtPA presented a positive charge. Since adsorption is a mild drug encapsulation method, it can prevent rtPA from the disadvantages of the covalent bioconjugation such as changes in the protein structure and function that might result in its partial denaturation and loss of activity [49]. The nanogel nature of the SPs allowed reaching a high encapsulation efficiency of the rtPA of 64.78 ± 2.16 % and 81.04 ± 1.86 % for Control-SPs and Fuco-SPs, respectively. The confocal microscopy images of FITC-rtPA loaded onto TRITC-labelled Fuco-SPs revealed the uniform distribution of the rtPA within a porous structure of the hydrogel SPs, as evidenced by a green fluorescence from FITC-rtPA colocalized with the red fluorescence from the particles (**data not shown**).

The release kinetics of rtPA from fucoidan-functionalized SPs was analyzed *in vitro* by flow cytometry [30] in saline at 37 °C under gentle agitation by quantification of the MFI of the FITC-labelled rtPA associated with TRITC-fluorescent Fuco-SPs. **Figure 3A** indicated a gradual and continuous sustained release of the lytic agent from the SPs during the observation period: 46.41 ± 1.34% of the encapsulated protein was released during the first 15 min and 76.98 ± 1.74% after 90 min. This release profile is classical for the hydrogels [50].

The thrombolytic activity of the rtPA-loaded SPs *in vitro* was analyzed as a combination of amidolytic and fibrinolytic activities and was reported in **Figure 3 (B, C, D)**. Amidolytic or enzymatic activity featured the ability of the proteolytic enzyme to hydrolyze the rtPA substrate. Interestingly, the amidolytic activities of rtPA on Control-SPs and Fuco-SPs were comparable to that of free rtPA (**Figure 3B & 3C**). The fibrinolytic experiment *in vitro* of the rtPA-loaded SPs was performed in a fibrin plate assay. The results indicated full retention of fibrinolytic activity (**Figure 3D**). Thus, rtPA loaded onto the SPs appeared to be able to diffuse into the fibrin-agarose matrix and to induce fibrinolysis in contact with fibrin. Comparing covalent vs. non-covalent conjugation approaches, Friedrich *et al.* documented that the adsorptive bound rtPA liberated faster from the particles and diffused more readily into the fibrin matrix than covalently bound rtPA [51] which may also be beneficial in targeted thrombolysis. No significant difference was detected between both types of SPs enabling to utilize them in the following set of experiments.

Overall, the rtPA association with the SPs did not affect the drug amidolytic activity and fibrinolytic potential in our design. This result is in accordance with the most studies on nanogels suggesting that drug encapsulation via a passive diffusion into the preformed nanogels does not affect the secondary structure of the adsorbed protein and its biological activity [52].

***Unloaded and rtPA-loaded Fuco-SPs adhere to activated platelet aggregates in vitro under arterial flow***

Because aggregation of activated platelets and platelet-mediated coagulation pathways are hallmark events in thrombosis, activated platelets are a suitable cellular target for carrier binding to thrombi [53]. Before the *in vivo* tests, we complemented the targeting evaluation with the second set of microfluidic experiments to validate Fuco-SPs capability to actively

anchor onto the surface of activated platelets, expressing P-selectin. Thus, human whole blood was passed into collagen-coated microchannels to induce platelet activation and aggregation. Fuco-SPs or Control-SPs were then perfused at arterial shear stress (67.5 dyne/cm$^2$), and the accumulation of the fluorescence from the adhered SPs was detected on the surface of activated platelet aggregates. By a quantitative analysis of the MFI (**Figure 4)**, it was revealed that Fuco-SPs adhered significantly more onto activated platelets than Control-SPs (2678.34 ± 237.40 for Fuco-SPs vs. 392.44 ± 137.15 for Control-SPs, *** $p < 0.001$). Notably, adsorption of rtPA did not impair the Fuco-SPs clot-binding ability (1880.80 ± 429.37 for rtPA-Fuco-SPs vs. 77.56 ± 40.25 for rtPA-Control-SPs, ** $p < 0.01$). There was also no significant difference between unloaded and rtPA-loaded Fuco-SPs adhering to the activated platelets.

To conclude, these *in vitro* experiments provided crucial evidence of molecular interaction and high affinity between the P-selectin on the activated platelets and fucoidan-functionalized SPs, which is maintained after loading of the thrombolytic agent. This finding presumes that the administration of the rtPA-Fuco-SPs could enable a specific delivery of the rtPA-immobilized SPs to the platelet-rich thrombus with higher drug accumulation.

***In vivo thrombolytic efficacy***

Whereas demonstrating the *in vitro* activity of the rtPA immobilized on the drug delivery system is important, the *in vivo* therapeutic effect is paramount. A murine thromboembolic stroke model was established by *in situ* injection of 1 IU of thrombin into the MCA by provoking a coagulation cascade and formation of a fibrin-rich clot in the lumen of the artery [54,55]. The treatment options – control saline or 10 mg/kg rtPA-Fuco-SPs – were intravenously injected 20 min after ischemic onset in accordance with rtPA clinical mode of administration: 10% bolus followed by 90% infusion. It is important to note that 10 mg/kg is a relevant dose in mice in place of 0.9 mg/kg in humans because of a lower sensitivity of human rtPA in murine plasma [56].

Cerebral blood flow was monitored throughout the treatment via laser speckle contrast imaging, a high resolution and high-speed technique that instantly visualizes microcirculatory tissue blood perfusion. The blood flow in the ipsilateral cerebral hemisphere was restored by 24.78 ± 3.00% after 40 min treatment with rtPA-Fuco-SPs; by contrast, in the saline group the perfusion was improved only by 7.01 ± 3.13% (**Figure 5A**). The representative laser speckle multispectral

imaging in the ipsilateral and the contralateral hemispheres are expressed at 0 min and 40 min (**data not shown**).

The prevailing method for assessment of the brain infarct volume is a brain tissue staining with 2% 2,3,5-triphenyltetrazolium chloride (TTC) which labels non-injured tissue and leaves the infarct area white. Several groups previously reported the reduction of the infarct zone in preclinical models by nanomedicine. For example, the magnetic iron oxide ($Fe_3O_4$)-microrods [57] and polyacrylic acid-stabilized magnetic NPs [58] conjugated with rtPA diminished the brain infarct lesion in $FeCl_3$ murine model of ischemic stroke of MCA. These designs, however, require an external magnet for targeting and to complement chemical lysis with rtPA with mechanical one of the magnetic rotation. Without any clinically approved medical device to impose a high magnetic force on the NPs in deep blood vessels, it would probably be desirable for nanocarrier formulation to avoid external assistance. Mei *et al.* stated that only the synergistic effect of rtPA-loaded polymer micelles and a reactive oxygen species (ROS)-eliminating antioxidant suppressed an infarct volume and improved neurological deficit after brain ischemia in the mouse model of photo-thrombotic MCA occlusion [59].

In our case, we utilized MRI imaging as a powerful technique to quantify the volume of brain damage. Using T2-weighted MRI sequences, we observed that the size of the ischemic brain lesions for the saline group was 14.80 ± 3.34 $mm^3$ whereas for the rtPA-loaded fucoidan-targeted SPs it was 4.63 ± 1.59 $mm^3$ 24 h post-stroke (**Figure 5B**). From the recent publication of the same group [55], it is well known that early intravenous administration of free rtPA at the dose of 10 mg/kg diminishes the lesion size by 26.2% in the thrombin model. Our data clearly stated that the rtPA-Fuco-SPs provided superior brain protection than a standard rtPA treatment by reducing the ischemic zone by 69%, almost 3-fold higher of free rtPA. Out of all treated animals with rtPA-Fuco-SPs, 66.6% of the cases had small lesion sizes (<3 $mm^3$) and 33.3% had medium lesions (<11 $mm^3$). In the saline treatment group, we recorded 60% severe (<20 $mm^3$) and critical (>20 $mm^3$) cases and no small lesions (**data not shown**). This therapeutic benefit could be ascribed to faster MCA reperfusion and, hence, prevention of the major brain injury due to higher rtPA accumulation on the thrombus site as to active targeting and specific P-selectin interactions of the Fuco-SPs.

To monitor the BBB integrity disrupted by ischemic stroke [60], gadolinium hypersignal was detected and quantified on T1-weighted MRI images at day 4 after stroke. Gadolinium

extravasation from the blood into the brain parenchyma was unmistakably located at the ischemia-affected region where the BBB was compromised. rtPA-Fuco-SPs treatment group demonstrated a significant BBB preservation over saline with only a subtle BBB breakdown of $3.45 \pm 1.40$ mm$^3$ vs. $11.02 \pm 1.71$ mm$^3$ in a saline group (**Figure 5C**). It is vital to underline that although in this article we utilized fucoidan on the SPs purely for the P-selectin targeting purpose, new avenues of research are deciphering its neuroprotective role, particularly after cerebral ischemic events as recently reported [61].

Similar to some untreated stroke patients, the blood clots were gradually lysed post-stroke in this murine model: at 24 h after thrombotic occlusion, 40% of mice exhibited a total (Score 3) recanalization and 60% partial perfusion (Score 1 and Score 2) of the MCA when injected with saline (**data not shown**). However, after the treatment with rtPA-Fuco-SPs, most of the cases were entirely recanalized (Score 3) with an absence of Score 1. These angiographic analyses were assessed by a blinded observer based on TICI grade flow scoring.

Overall, the apparent superiority of rtPA-Fuco-SPs to reduce the brain injury area in comparison with saline and rtPA at the same dose, combined with a favorable safety profile of the SPs, makes them a promising nanomedicine-based approach for the treatment of acute arterial thrombosis. We speculate that the submicron size of the particles as well as their active thrombus-targeting moiety should maintain rtPA-loaded carrier within the intravascular compartment to exert its thrombolytic activity. This should prevent the leakage of rtPA into the brain parenchyma, reducing the risks of NMDA receptors-mediated neurotoxicity and hemorrhages [62]. Further studies could compare a single or a double bolus route of administration of rtPA-Fuco-SPs due to the rtPA preservation by SPs, and, thus, a more comfortable treatment option for patients.

***Conclusions:***

In the present study, we designed and fabricated fucoidan-functionalized 100% polysaccharide submicroparticles from biocompatible and FDA approved components as a P-selectin targeting drug delivery system for thrombolytic therapy. The physico-chemical properties and a biocompatibility analysis of these SPs were thoroughly evaluated, and a clinically used thrombolytic molecule – alteplase or rtPA – was effectively immobilized onto the SPs with full retention of its enzymatic and fibrinolytic potential *in vitro* and *in vivo*. The commercially

available alteplase requires an excess of L-arginine (3.5 mg amino acid per 100 mg rtPA) to stabilize the formulation by enhancing its solubility and preventing aggregation. L-arginine, whose pK value (negative of the logarithm of the dissociation constant for the -COOH group) equals 2.17, bears at least two free primary amine groups and carries a positive charge at physiological pH. Classically, rtPA is loaded onto the carriers using the covalent bond formation via EDC/NHS reaction. Although Juenet *et al.* [28] managed to adsorb rtPA onto the surface of the dextran-coated core-shell polymer NPs with a near-neutral ζ-potential, the presence of the free primary amines was required on chemically modified dextran. Comparing covalent vs. non-covalent methods to conjugate rtPA onto the polymer coating of magnetic NPs [63], better loading efficiency was described with a covalent one vs. adsorption (98.6 ± 0.8 % vs. 47.7 ± 5.4 %), as well as superior amidolytic and fibrinolytic activities. In the present report, high encapsulation efficiency of alteplase (~80%) onto the polysaccharide SPs was attained without any chemical modification of the dextran or fucoidan and despite a distinctively negative surface charge of the SPs, therefore, can be attributed to their hydrogel-based structure. The fibrinolytic drug was associated not only at the surface of the particles but it also diffused through the matrix of the porous SPs, fully preserving its thrombolytic potential.

We established *in vitro* by dynamic flow microchamber assays that the fucoidan-functionalized particles specifically adhered to the recombinant P-selectin in a dose-dependent manner, but not to E- and L-Selectins, and to human activated platelets. Finally, our findings revealed in the murine model of ischemic stroke that rtPA conjugation to the Fuco-SPs could enhance the thrombolytic activity of the clinical agent *in vivo*. The blood flow perfusion was restored more rapidly which resulted in smaller post-ischemic cerebral infarct lesions and higher BBB protection. In summary, we suggest that a hydrogel-based delivery system with fucoidan holds a significant promise to revolutionize the safety and efficacy of thrombolytic therapy. In the future research, our biocompatible Fuco-SPs could also efficiently vehicle other therapeutic or contrast agents in the vascular compartment to target P-selectin overexpressed pathologies, such as cardiovascular diseases [64] or some cancers [65,66].

**REFERENCES:**

Throughout this application, various references describe the state of the art to which this invention pertains. The disclosures of these references are hereby incorporated by reference into the present disclosure.

[1] E.J. Benjamin, P. Muntner, A. Alonso, M.S. Bittencourt, C.W. Callaway, A.P. Carson, A.M. Chamberlain, A.R. Chang, S. Cheng, S.R. Das, F.N. Delling, L. Djousse, M.S.V. Elkind, J.F. Ferguson, M. Fornage, L.C. Jordan, S.S. Khan, B.M. Kissela, K.L. Knutson, T.W. Kwan, D.T. Lackland, T.T. Lewis, J.H. Lichtman, C.T. Longenecker, M.S. Loop, P.L. Lutsey, S.S. Martin, K. Matsushita, A.E. Moran, M.E. Mussolino, M. O'Flaherty, A. Pandey, A.M. Perak, W.D. Rosamond, G.A. Roth, U.K.A. Sampson, G.M. Satou, E.B. Schroeder, S.H. Shah, N.L. Spartano, A. Stokes, D.L. Tirschwell, C.W. Tsao, M.P. Turakhia, L.B. VanWagner, J.T. Wilkins, S.S. Wong, S.S. Virani, Heart Disease and Stroke Statistics—2019 Update: A Report From the American Heart Association, Circulation. (2019). https://doi.org/10.1161/CIR.0000000000000659.

[2] W.J. Powers, A.A. Rabinstein, T. Ackerson, O.M. Adeoye, N.C. Bambakidis, K. Becker, J. Biller, M. Brown, B.M. Demaerschalk, B. Hoh, E.C. Jauch, C.S. Kidwell, T.M. Leslie-Mazwi, B. Ovbiagele, P.A. Scott, K.N. Sheth, A.M. Southerland, D. V. Summers, D.L. Tirschwell, Guidelines for the Early Management of Patients With Acute Ischemic Stroke: 2019 Update to the 2018 Guidelines for the Early Management of Acute Ischemic Stroke: A Guideline for Healthcare Professionals From the American Heart Association/American Stroke , Stroke. 50 (2019) e344–e418. https://doi.org/10.1161/STR.0000000000000211.

[3] J. Mican, M. Toul, D. Bednar, J. Damborsky, Structural Biology and Protein Engineering of Thrombolytics, Comput. Struct. Biotechnol. J. 17 (2019) 917–938. https://doi.org/10.1016/j.csbj.2019.06.023.

[4] R. Bhatia, M.D. Hill, N. Shobha, B. Menon, S. Bal, P. Kochar, T. Watson, M. Goyal, A.M. Demchuk, Low rates of acute recanalization with intravenous recombinant tissue plasminogen activator in ischemic stroke: Real-world experience and a call for action, Stroke. 41 (2010) 2254–2258. https://doi.org/10.1161/STROKEAHA.110.592535.

[5] A.M. Thiebaut, M. Gauberti, C. Ali, S. Martinez De Lizarrondo, D. Vivien, M. Yepes, B.D. Roussel, The role of plasminogen activators in stroke treatment: fibrinolysis and beyond, Lancet Neurol. 17 (2018) 1121–1132. https://doi.org/10.1016/S1474-4422(18)30323-5.

[6] A. Pal Khasa, Y. Pal Khasa, The evolution of recombinant thrombolytics: Current status and future directions, Bioengineered. 8 (2017) 331–358. https://doi.org/10.1080/21655979.2016.1229718.

[7] S. Liu, X. Feng, R. Jin, G. Li, Tissue plasminogen activator-based nanothrombolysis for

ischemic stroke, Expert Opin Drug Deliv. 15 (2018) 173–184. https://doi.org/10.1080/17425247.2018.1384464.

[8] N. Korin, M. Kanapathipillai, B.D. Matthews, M. Crescente, A. Brill, T. Mammoto, K. Ghosh, S. Jurek, S.A. Bencherif, D. Bhatta, A.U. Coskun, C.L. Feldman, D.D. Wagner, D.E. Ingber, Shear-Activated Nanotherapeutics for Drug Targeting to Obstructed Blood Vessels, Science (80-. ). 337 (2012) 738–742. https://doi.org/10.1126/science.1217815.

[9] M. Colasuonno, A.L. Palange, R. Aid, M. Ferreira, H. Mollica, R. Palomba, M. Emdin, M. Del Sette, C. Chauvierre, D. Letourneur, P. Decuzzi, Erythrocyte-Inspired Discoidal Polymeric Nanoconstructs Carrying Tissue Plasminogen Activator for the Enhanced Lysis of Blood Clots, ACS Nano. 12 (2018) 12224–12237. https://doi.org/10.1021/acsnano.8b06021.

[10] J. Zhou, D. Guo, Y. Zhang, W. Wu, H. Ran, Z. Wang, Construction and evaluation of Fe3O4-based PLGA nanoparticles carrying rtPA used in the detection of thrombosis and in targeted thrombolysis, ACS Appl. Mater. Interfaces. 6 (2014) 5566–5576. https://doi.org/10.1021/am406008k.

[11] A. Friedman, S. Claypool, R. Liu, The Smart Targeting of Nanoparticles, Curr. Pharm. Des. 19 (2013) 6315–6329. https://doi.org/10.2174/13816128113199990375.

[12] W. jin Jeong, J. Bu, L.J. Kubiatowicz, S.S. Chen, Y.S. Kim, S. Hong, Peptide–nanoparticle conjugates: a next generation of diagnostic and therapeutic platforms?, Nano Converg. 5 (2018) 1–18. https://doi.org/10.1186/s40580-018-0170-1.

[13] L. Chollet, P. Saboural, C. Chauvierre, J.-N. Villemin, D. Letourneur, F. Chaubet, Fucoidans in Nanomedicine, Mar. Drugs. 14 (2016) 1–24. https://doi.org/10.3390/md14080145.

[14] L. Bachelet, I. Bertholon, D. Lavigne, R. Vassy, M. Jandrot-Perrus, F. Chaubet, D. Letourneur, Affinity of low molecular weight fucoidan for P-selectin triggers its binding to activated human platelets, Biochim. Biophys. Acta - Gen. Subj. 1790 (2009) 141–146. https://doi.org/10.1016/j.bbagen.2008.10.008.

[15] P. Saboural, F. Chaubet, F. Rouzet, F. Al-Shoukr, R. Ben Azzouna, N. Bouchemal, L. Picton, L. Louedec, M. Maire, L. Rolland, G. Potier, D. Le Guludec, D. Letourneur, C. Chauvierre, Purification of a low molecular weight fucoidan for SPECT molecular imaging of myocardial infarction, Mar. Drugs. 12 (2014) 4851–4867. https://doi.org/10.3390/md12094851.

[16] T. Bonnard, J.-M. Serfaty, C. Journé, B. Ho Tin Noe, D. Arnaud, L. Louedec, M. Derkaoui, D. Letourneur, C. Chauvierre, C. Le Visage, Leukocyte mimetic

polysaccharide microparticles tracked in vivo on activated endothelium and in abdominal aortic aneurysm, Acta Biomater. 10 (2014) 3535–3545. https://doi.org/10.1016/j.actbio.2014.04.015.

[17] T. Bonnard, G. Yang, A. Petiet, V. Ollivier, O. Haddad, D. Arnaud, L. Louedec, L. Bachelet-Violette, S.M. Derkaoui, D. Letourneur, C. Chauvierre, C. Le Visage, Abdominal Aortic Aneurysms Targeted by Functionalized Polysaccharide Microparticles: a new Tool for SPECT Imaging, Theranostics. 4 (2014) 592–603. https://doi.org/10.7150/thno.7757.

[18] B. Li, M. Juenet, R. Aid-Launais, M. Maire, V. Ollivier, D. Letourneur, C. Chauvierre, Development of Polymer Microcapsules Functionalized with Fucoidan to Target P-Selectin Overexpressed in Cardiovascular Diseases, Adv. Healthc. Mater. 6 (2017) 1–11. https://doi.org/10.1002/adhm.201601200.

[19] B. Li, R. Aid-Launais, M.-N. Labour, A. Zenych, M. Juenet, C. Choqueux, V. Ollivier, O. Couture, D. Letourneur, C. Chauvierre, Functionalized polymer microbubbles as new molecular ultrasound contrast agent to target P-selectin in thrombus, Biomaterials. 194 (2019) 139–150. https://doi.org/10.1016/j.biomaterials.2018.12.023.

[20] I. Cicha, C. Chauvierre, I. Texier, C. Cabella, J.M. Metselaar, J. Szebeni, L. Dézsi, C. Alexiou, F. Rouzet, G. Storm, E. Stroes, D. Bruce, N. MacRitchie, P. Maffia, D. Letourneur, From design to the clinic: Practical guidelines for translating cardiovascular nanomedicine, Cardiovasc. Res. 114 (2018) 1714–1727. https://doi.org/10.1093/cvr/cvy219.

[21] K. Ganguly, K. Chaturvedi, U.A. More, M.N. Nadagouda, T.M. Aminabhavi, Polysaccharide-based micro/nanohydrogels for delivering macromolecular therapeutics, J. Control. Release. 193 (2014) 162–173. https://doi.org/10.1016/j.jconrel.2014.05.014.

[22] J. Zhang, W. Xia, P. Liu, Q. Cheng, T. Tahirou, W. Gu, B. Li, Chitosan modification and pharmaceutical/biomedical applications, Mar. Drugs. 8 (2010) 1962–1987. https://doi.org/10.3390/md8071962.

[23] H.J. Jin, H. Zhang, M.L. Sun, B.G. Zhang, J.W. Zhang, Urokinase-coated chitosan nanoparticles for thrombolytic therapy: Preparation and pharmacodynamics in vivo, J. Thromb. Thrombolysis. 36 (2013) 458–468. https://doi.org/10.1007/s11239-013-0951-7.

[24] J. Liao, X. Ren, B. Yang, H. Li, Y. Zhang, Z. Yin, Targeted thrombolysis by using c-RGD-modified N,N,N-Trimethyl Chitosan nanoparticles loaded with lumbrokinase, Drug Dev. Ind. Pharm. 45 (2019) 88–95.

https://doi.org/10.1080/03639045.2018.1522324.

[25] S.R. Van Tomme, W.E. Hennink, Biodegradable dextran hydrogels for protein delivery applications, Expert Rev. Med. Devices. 4 (2007) 147–164. https://doi.org/10.1586/17434440.4.2.147.

[26] J.R. McCarthy, I.Y. Sazonova, S.S. Erdem, T. Hara, B.D. Thompson, P. Patel, I. Botnaru, C.P. Lin, G.L. Reed, R. Weissleder, F.A. Jaffer, Multifunctional nanoagent for thrombus-targeted fibrinolytic therapy, Nanomedicine (Lond). 7 (2012) 1017–1028. https://doi.org/10.2217/nnm.11.179.

[27] S. Heid, H. Unterweger, R. Tietze, R.P. Friedrich, B. Weigel, I. Cicha, D. Eberbeck, A.R. Boccaccini, C. Alexiou, S. Lyer, Synthesis and Characterization of Tissue Plasminogen Activator-Functionalized Superparamagnetic Iron Oxide Nanoparticles for Targeted Fibrin Clot Dissolution, Int. J. Mol. Sci. 18 (2017). https://doi.org/10.3390/ijms18091837.

[28] M. Juenet, R. Aid-Launais, B. Li, A. Berger, J. Aerts, V. Ollivier, A. Nicoletti, D. Letourneur, C. Chauvierre, Thrombolytic therapy based on fucoidan-functionalized polymer nanoparticles targeting P-selectin, Biomaterials. 156 (2018) 204–216. https://doi.org/10.1016/j.biomaterials.2017.11.047.

[29] J.M. Lee, Z.-U. Shin, G.T. Mavlonov, I.Y. Abdurakhmonov, T.-H. Yi, Solid-Phase Colorimetric Method for the Quantification of Fucoidan, Appl. Biochem. Biotechnol. 168 (2012) 1019–1024. https://doi.org/10.1007/s12010-012-9837-y.

[30] S. Petersen, A. Fahr, H. Bunjes, Flow cytometry as a new approach to investigate drug transfer between lipid particles, Mol. Pharm. 7 (2010) 350–363. https://doi.org/10.1021/mp900130s.

[31] C. Orset, R. Macrez, A.R. Young, D. Panthou, E. Angles-cano, E. Maubert, V. Agin, D. Vivien, Mouse Model of In Situ Thromboembolic Stroke and Reperfusion, Stroke. 38 (2007) 2771–2778. https://doi.org/10.1161/STROKEAHA.107.487520.

[32] T.E. Furia, CRC Handbook of Food Additives, Second Edi, CRC Press, 1973.

[33] C. Chauvierre, R. Aid-Launais, J. Aerts, M. Maire, L. Chollet, L. Rolland, R. Bonaf, S. Rossi, S. Bussi, C. Cabella, D. Laszlo, T. Fülöp, J. Szebeni, Y. Chahid, K.H. Zheng, E.S.G. Stroes, D. Le Guludec, F. Rouzet, D. Letourneur, Pharmaceutical Development and Safety Evaluation of a GMP-Grade Fucoidan for Molecular Diagnosis of Cardiovascular Diseases, Mar. Drugs. 17 (2019) 1–17. https://doi.org/https://doi.org/10.3390/md17120699.

[34] F. Rouzet, L. Bachelet-Violette, J.-M. Alsac, M. Suzuki, A. Meulemans, L. Louedec, A.

Petiet, M. Jandrot-Perrus, F. Chaubet, J.-B. Michel, D. Le Guludec, D. Letourneur, Radiolabeled fucoidan as a P-selectin targeting agent for in vivo imaging of platelet-rich thrombus and endothelial activation., J. Nucl. Med. 52 (2011) 1433–1440. https://doi.org/10.2967/jnumed.110.085852.

[35] K.H. Zheng, Y. Kaiser, E. Poel, H. Verberne, J. Aerts, F. Rouzet, E. Stroes, D. Letourneur, C. Chauvierre, 99Mtc-Fucoidan As Diagnostic Agent For P-Selectin Imaging: First-In-Human Evaluation (Phase I), Atherosclerosis. 287 (2019) e143. https://doi.org/10.1016/j.atherosclerosis.2019.06.425.

[36] C.I. Jones, D.A. Payne, P.D. Hayes, A.R. Naylor, P.R.F. Bell, M.M. Thompson, A.H. Goodall, The antithrombotic effect of dextran-40 in man is due to enhanced fibrinolysis in vivo, J. Vasc. Surg. 48 (2008) 715–722. https://doi.org/10.1016/j.jvs.2008.04.008.

[37] E.M. Balboa, E. Conde, A. Moure, E. Falqué, H. Domínguez, In vitro antioxidant properties of crude extracts and compounds from brown algae, Food Chem. 138 (2013) 1764–1785. https://doi.org/10.1016/j.foodchem.2012.11.026.

[38] Y. Choi, S.K. Min, R. Usoltseva, A. Silchenko, T. Zvyagintseva, S. Ermakova, J.K. Kim, Thrombolytic fucoidans inhibit the tPA-PAI1 complex, indicating activation of plasma tissue-type plasminogen activator is a mechanism of fucoidan-mediated thrombolysis in a mouse thrombosis model, Thromb. Res. 161 (2018) 22–25. https://doi.org/10.1016/j.thromres.2017.11.015.

[39] F. Wolf, K. Koehler, H.P. Schuchmann, Stabilization of water droplets in oil with PGPR for use in oral and dermal applications, J. Food Process Eng. 36 (2013) 276–283. https://doi.org/10.1111/j.1745-4530.2012.00688.x.

[40] K.S. Masters, D.N. Shah, L.A. Leinwand, K.S. Anseth, Crosslinked hyaluronan scaffolds as a biologically active carrier for valvular interstitial cells, Biomaterials. 26 (2005) 2517–2525. https://doi.org/10.1016/j.biomaterials.2004.07.018.

[41] J. Matuszak, J. Baumgartner, J. Zaloga, M. Juenet, A.E. da Silva, D. Franke, G. Almer, I. Texier, D. Faivre, J.M. Metselaar, F.P. Navarro, C. Chauvierre, R. Prassl, L. Dézsi, R. Urbanics, C. Alexiou, H. Mangge, J. Szebeni, D. Letourneur, I. Cicha, Nanoparticles for intravascular applications: physicochemical characterization and cytotoxicity testing, Nanomedicine. 11 (2016) 597–616. https://doi.org/10.2217/nnm.15.216.

[42] M. Weber, H. Steinle, S. Golombek, L. Hann, C. Schlensak, H.P. Wendel, M. Avci-Adali, Blood-Contacting Biomaterials: In Vitro Evaluation of the Hemocompatibility, Front. Bioeng. Biotechnol. 6 (2018). https://doi.org/10.3389/fbioe.2018.00099.

[43] ISO 10993-4:2017, Biol. Eval. Med. Devices — Part 4 Sel. Tests Interact. with Blood.

(2017). https://www.iso.org/standard/63448.html.

[44] B. Vaidya, G.P. Agrawal, S.P. Vyas, Platelets directed liposomes for the delivery of streptokinase: Development and characterization, Eur. J. Pharm. Sci. 44 (2011) 589–594. https://doi.org/10.1016/j.ejps.2011.10.004.

[45] N. Zhang, C. Li, D. Zhou, C. Ding, Y. Jin, Q. Tian, X. Meng, K. Pu, Y. Zhu, Cyclic RGD functionalized liposomes encapsulating urokinase for thrombolysis, Acta Biomater. (2018). https://doi.org/10.1016/j.actbio.2018.01.038.

[46] K. Ley, The role of selectins in inflammation and disease, Trends Mol. Med. 9 (2003) 263–268. https://doi.org/10.1016/S1471-4914(03)00071-6.

[47] J.-H. Kim, J.-Y. Yoon, Protein adsorption on polymer particles, in: Encycl. Surf. Colloid Sci., 2002: pp. 4373–4381. https://doi.org/10.1002/jbm.820210202.

[48] I. Politis, L. Wang, J.D. Turner, B.K. Tsang, Changes in Tissue-Type Plasminogen Activator-Like and Plasminogen Activator Inhibitor Activities in Granulosa and Theca Layers during Ovarian Follicle Development in the Domestic Hen1, Biol. Reprod. 42 (1990) 747–754. https://doi.org/10.1095/biolreprod42.5.747.

[49] M. Di Marco, K.A. Razak, A.A. Aziz, C. Devaux, E. Borghi, L. Levy, C. Sadun, Overview of the main methods used to combine proteins with systems : absorption , bioconjugation , and encapsulation, Int. J. Nanomedicine. 5 (2010) 37–49.

[50] V. Wintgens, C. Lorthioir, P. Dubot, B. Sébille, C. Amiel, Cyclodextrin/dextran based hydrogels prepared by cross-linking with sodium trimetaphosphate, Carbohydr. Polym. 132 (2015) 80–88. https://doi.org/10.1016/j.carbpol.2015.06.038.

[51] R.P. Friedrich, J. Zaloga, E. Schreiber, I.Y. Tóth, E. Tombácz, S. Lyer, C. Alexiou, Tissue Plasminogen Activator Binding to Superparamagnetic Iron Oxide Nanoparticle-Covalent Versus Adsorptive Approach, Nanoscale Res. Lett. 11 (2016) 1–11. https://doi.org/10.1186/s11671-016-1521-7.

[52] L. Arnfast, C.G. Madsen, L. Jorgensen, S. Baldursdottir, Design and processing of nanogels as delivery nanosystems for peptides and proteins, Ther. Deliv. 5 (2014) 691–708. https://doi.org/10.4155/tde.14.38.

[53] Z.M. Ruggeri, Platelets in atherothrombosis, Nat. Med. 8 (2002) 1227–1234. https://doi.org/10.4065/81.1.59.

[54] C. Orset, B. Haelewyn, S.M. Allan, S. Ansar, F. Campos, T.H. Cho, A. Durand, M. El Amki, M. Fatar, I. Garcia-Yébenes, M. Gauberti, S. Grudzenski, I. Lizasoain, E. Lo, R. Macrez, I. Margaill, S. Maysami, S. Meairs, N. Nighoghossian, J. Orbe, J.A. Paramo, J.J. Parienti, N.J. Rothwell, M. Rubio, C. Waeber, A.R. Young, E. Touzé, D. Vivien,

Efficacy of Alteplase in a Mouse Model of Acute Ischemic Stroke: A Retrospective Pooled Analysis, Stroke. 47 (2016) 1312–1318. https://doi.org/10.1161/STROKEAHA.116.012238.

[55] S.M. De Lizarrondo, C. Gakuba, B.A. Herbig, Y. Repessé, C. Ali, C. V. Denis, P.J. Lenting, E. Touzé, S.L. Diamond, D. Vivien, M. Gauberti, Potent thrombolytic effect of N-acetylcysteine on arterial thrombi, Circulation. 136 (2017) 646–660. https://doi.org/10.1161/CIRCULATIONAHA.117.027290.

[56] H.R. Lijnen, B. Van Hoef, V. Beelen, D. Collen, Characterization of the Murine Plasma Fibrinolytic System, Eur. J. Biochem. 224 (1994) 863–871. https://doi.org/10.1111/j.1432-1033.1994.00863.x.

[57] J. Hu, S. Huang, L. Zhu, W. Huang, Y. Zhao, K. Jin, Q. Zhuge, Tissue Plasminogen Activator-Porous Magnetic Microrods for Targeted Thrombolytic Therapy after Ischemic Stroke, ACS Appl. Mater. Interfaces. 10 (2018) 32988–32997. https://doi.org/10.1021/acsami.8b09423.

[58] L. Huang, J. Wang, S. Huang, F. Siaw-Debrah, M. Nyanzu, Q. Zhuge, Polyacrylic acid-coated nanoparticles loaded with recombinant tissue plasminogen activator for the treatment of mice with ischemic stroke, Biochem. Biophys. Res. Commun. 516 (2019) 565–570. https://doi.org/10.1016/j.bbrc.2019.06.079.

[59] T. Mei, A. Kim, L.B. Vong, A. Marushima, S. Puentes, Y. Matsumaru, A. Matsumura, Y. Nagasaki, Encapsulation of tissue plasminogen activator in pH-sensitive self-assembled antioxidant nanoparticles for ischemic stroke treatment-Synergistic effect of thrombolysis and antioxidant, Biomaterials. 215 (2019) 1–12. https://doi.org/10.1016/j.biomaterials.2019.05.020.

[60] R. Brouns, P.P. De Deyn, The complexity of neurobiological processes in acute ischemic stroke, Clin. Neurol. Neurosurg. 111 (2009) 483–495. https://doi.org/10.1016/j.clineuro.2009.04.001.

[61] H. Kim, J.H. Ahn, M. Song, D.W. Kim, T.K. Lee, J.C. Lee, Y.M. Kim, J.D. Kim, J.H. Cho, I.K. Hwang, B.C. Yan, M.H. Won, J.H. Park, Pretreated fucoidan confers neuroprotection against transient global cerebral ischemic injury in the gerbil hippocampal CA1 area via reducing of glial cell activation and oxidative stress, Biomed. Pharmacother. 109 (2019) 1718–1727. https://doi.org/10.1016/j.biopha.2018.11.015.

[62] D. Vivien, M. Gauberti, A. Montagne, G. Defer, E. Touzé, Impact of tissue plasminogen activator on the neurovascular unit: From clinical data to experimental evidence, J. Cereb. Blood Flow Metab. 31 (2011) 2119–2134.

https://doi.org/10.1038/jcbfm.2011.127.

[63] R.P. Friedrich, J. Zaloga, E. Schreiber, I.Y. Tóth, E. Tombácz, S. Lyer, C. Alexiou, Tissue Plasminogen Activator Binding to Superparamagnetic Iron Oxide Nanoparticle—Covalent Versus Adsorptive Approach, Nanoscale Res. Lett. 11 (2016) 1–11. https://doi.org/10.1186/s11671-016-1521-7.

[64] S. Yokoyama, H. Ikeda, N. Haramaki, H. Yasukawa, T. Murohara, T. Imaizumi, Platelet P-selectin plays an important role in arterial thrombogenesis by forming large stable platelet-leukocyte aggregates, J. Am. Coll. Cardiol. 45 (2005) 1280–1286. https://doi.org/10.1016/j.jacc.2004.12.071.

[65] S.R. Barthel, J.D. Gavino, L. Descheny, C.J. Dimitroff, Targeting selectins and selectin ligands in inflammation and cancer, Expert Opin. Ther. Targets. 11 (2007) 1473–1491. https://doi.org/10.1517/14728222.11.11.1473.

[66] Y. Shamay, M. Elkabets, H. Li, J. Shah, S. Brook, F. Wang, K. Adler, E. Baut, M. Scaltriti, P. V Jena, E.E. Gardner, J.T. Poirier, C.M. Rudin, J. Baselga, A. Haimovitz-Friedman, D.A. Heller, P-selectin is a nanotherapeutic delivery target in the tumor microenvironment, Sci. Transl. Med. (2016). https://doi.org/10.1126/scitranslmed.aaf7374.

## CLAIMS:

1. A cross-linked polysaccharide particle comprising an amount of fucoidan and loaded by adsorption with an amount of t-PA.

2. The cross-linked polysaccharide particle of claim 1 wherein the polysaccharide is selected from the group consisting of dextran, pullulan, agar, alginic acid, hyaluronic acid, inulin, heparin, chitosan and mixtures thereof.

3. The cross-linked polysaccharide particle of claim 1 wherein the polysaccharide is dextran.

4. The cross-linked polysaccharide particle of claim 1 wherein the fucoidan has an average molecular weight ranging from 2 kDa to 100 kDa.

5. A method of obtaining the cross-linked polysaccharide particle of claim 1 comprising the steps of

   a) preparing an alkaline aqueous solution comprising an amount of at least one polysaccharide, the amount of fucoidan and an amount of a cross linking agent;

   b) dispersing said alkaline aqueous solution into a hydrophobic phase in order to obtain w/o emulsion; and

   c) transforming the w/o emulsion into particle by placing said w/o emulsion at a temperature from about 4°C to about 80°C for a sufficient time to allow the cross-linking of said amount of polysaccharide and fucoidan,

   d) loading the amount of t-PA into the particles obtained at step c).

6. The method of claim 5 wherein the cross-linking agent is selected from the group consisting of trisodium trimetaphosphate (STMP), phosphorus oxychloride (POCl3), epichlorohydrin, formaldehydes, carbodiimides, and glutaraldehydes.

7. The method of claim 5 wherein the cross-linking agent is trisodium trimetaphosphate (STMP).

8. The method of claim 5 wherein hydrophobic phase of step b) is sunflower oil.

9. The method of claim 5 wherein step b) is carried out in presence of a surfactant.

10. The method of claim 9 wherein the surfactant is selected from the group consisting of polyglycerol polyricinoleate and PEG-30 dipolyhydroxystearate.

11. The method of claim 5 wherein step b) is carried out in presence of an osmotic agent.

12. The method of claim 11 wherein the osmotic agent is selected from the group consisting of salts (e.g. NaCl, MgCl2, or KN03), sugars (e.g. sucrose, glucose or fructose), volatile solutes (e.g. SO2) and mixtures thereof.

13. The method of claim 5 wherein the loading of t-PA into the particles obtained at step c) is carried out by adsorption by mixing the particles with a solution comprising an amount of t-PA.

14. A method of treating a thrombotic disease or disorder in a patient in need thereof comprising administering to the patient a therapeutically effective amount the cross-linked polysaccharide particle of claim 1.

15. A pharmaceutical composition comprising an amount of the cross-linked polysaccharide particle of claim 1.

## ABSTRACT OF THE INVENTION

# FUCOIDAN-FUNCTIONALIZED POLYSACCHARIDE PARTICLES WITH T-PA FOR TARGETED THROMBOLYTIC THERAPY

There is a dire need for innovative nanomedicine-based solutions for safe and efficient thrombolysis with a non-toxic, biocompatible, and biodegradable thrombus-targeted carrier. In the present invention, polysaccharide hydrogel submicroparticles with remarkable biocompatibility were elaborated by the inverse miniemulsion / crosslinking method. They were functionalized with a fucoidan which has a nanomolar affinity for the P-selectin overexpressed on activated platelets and endothelial cells in vascular diseases. Surprisingly, the inventors show that rtPA (i.e. Alteplase) can be loaded onto the submicroparticles by adsorption, and its amidolytic and fibrinolytic activities were maintained *in vitro* and *in vivo*. Thrombus targeting potential of these particles was validated in microfluidic assay under arterial and venous blood shear rates on recombinant P-selectin and activated platelet aggregates. The thrombolytic efficacy of the nanomedicine-based product was tested in a murine model of acute ischemic stroke, revealing faster middle cerebral artery recanalization and reduction in the brain infarct volume and blood-brain barrier permeability post-stroke, evidenced by laser speckle contrast imaging and MRI. Collectively, this proof of concept study demonstrates the potential of these particles for the precise treatment of acute thrombotic events.

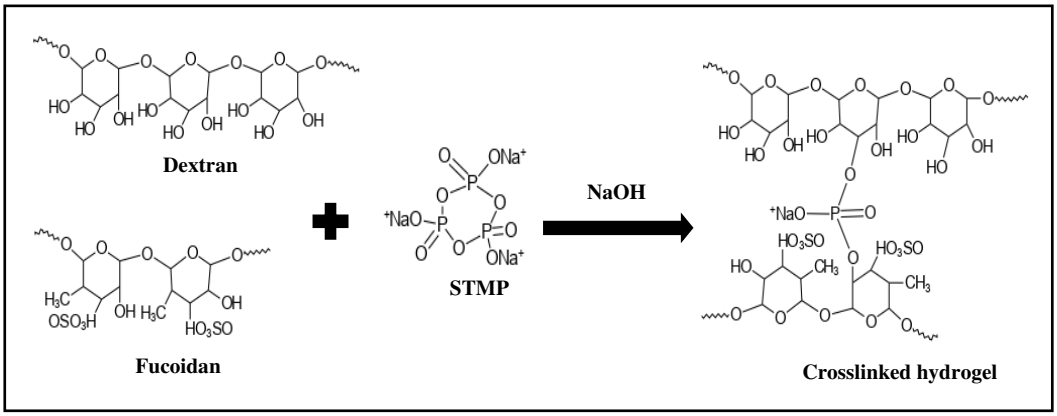


**Figure 1**

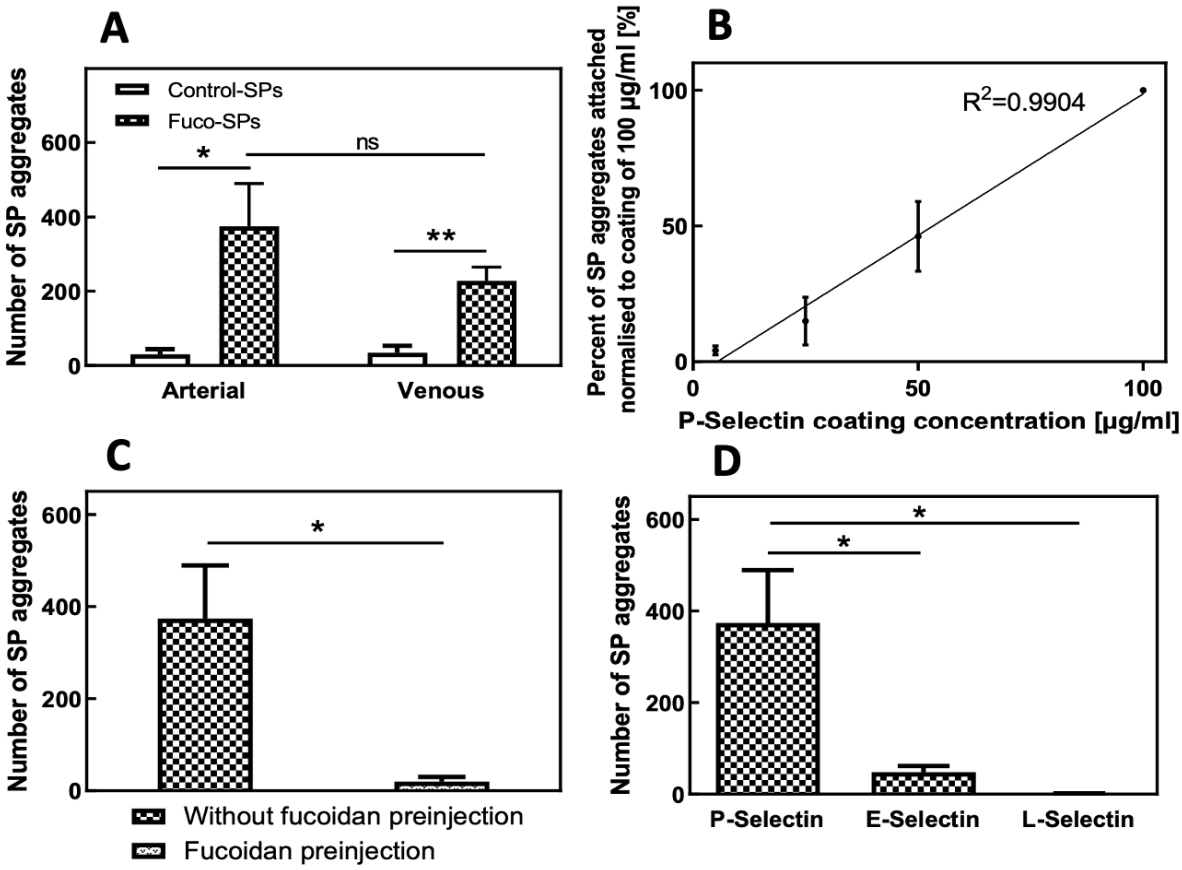


**Figure 2**

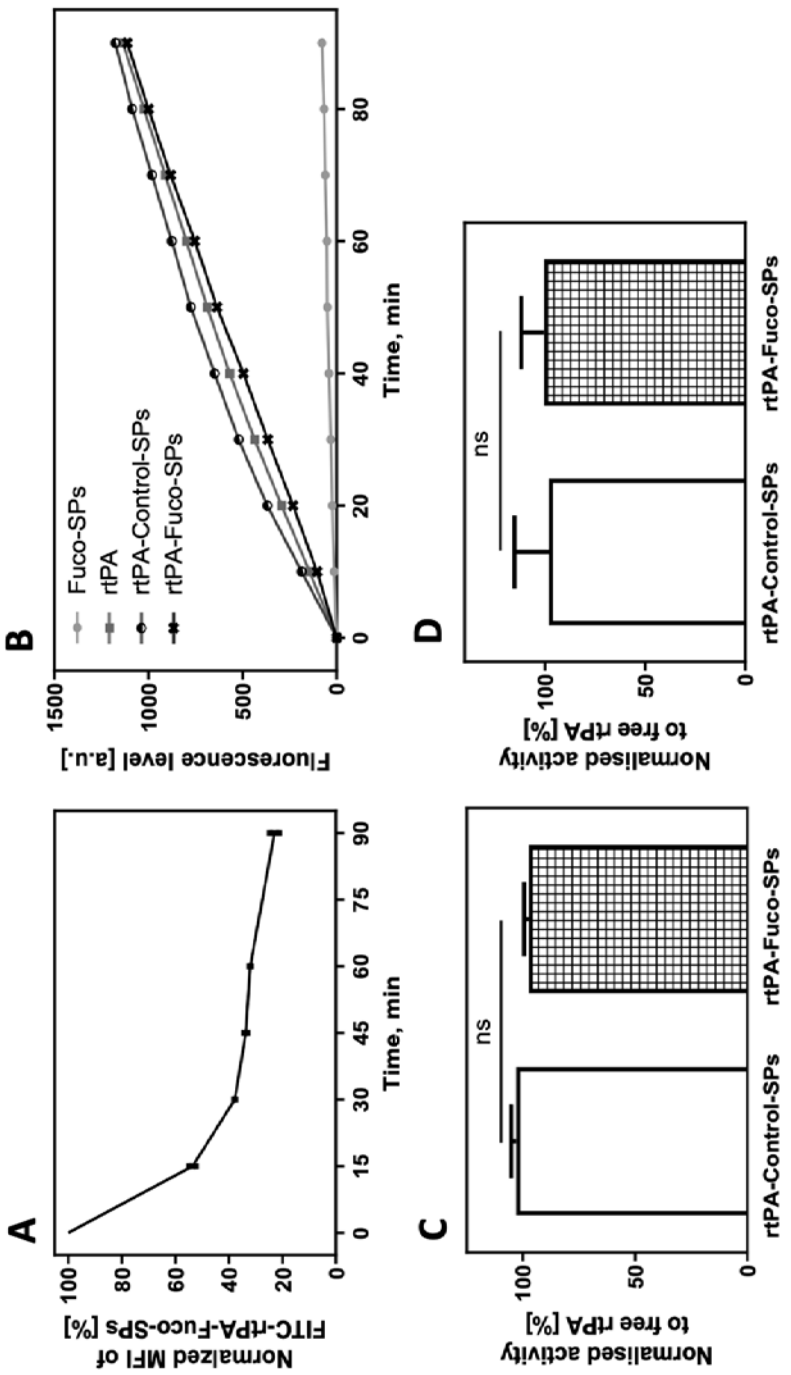
A
Normalized MFI of
FITC-rtPA-Fuco-SPs [%]
Time, min
B
Fluorescence level [a.u.]
Time, min
Fuco-SPs
rtPA
rtPA-Control-SPs
rtPA-Fuco-SPs
C
Normalised activity
to free rtPA [%]
ns
rtPA-Control-SPs
rtPA-Fuco-SPs
D
Normalised activity
to free rtPA [%]
ns
rtPA-Control-SPs
rtPA-Fuco-SPs

**Figure 3**

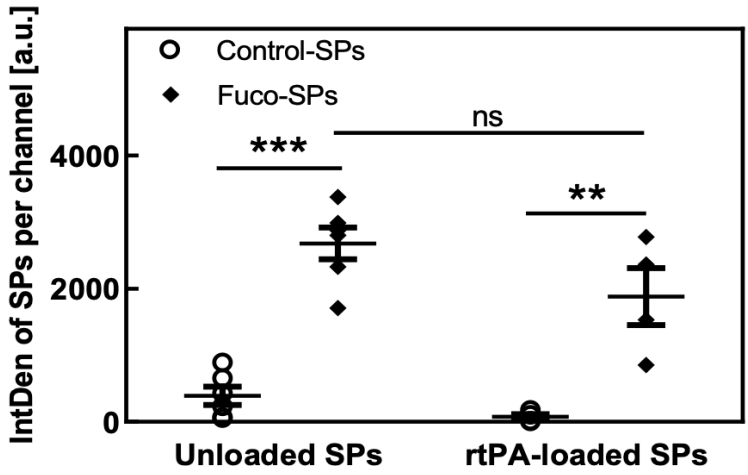


Figure 4

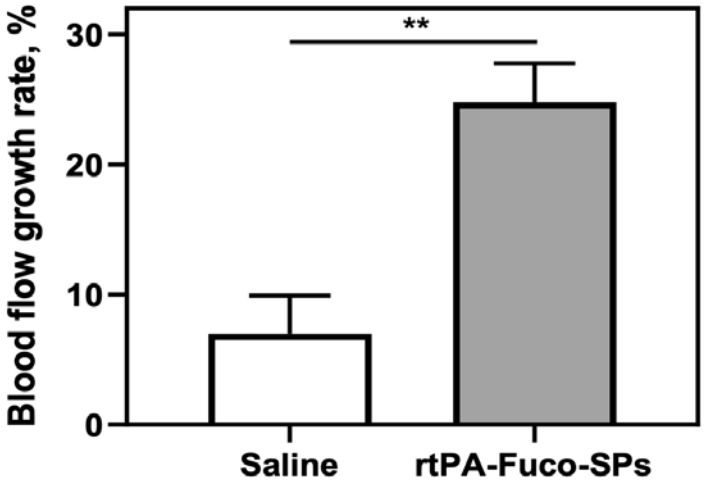


Figure 5A

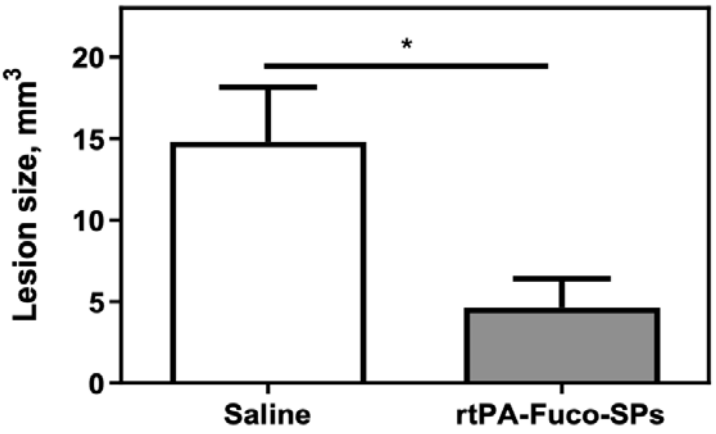


Figure 5B

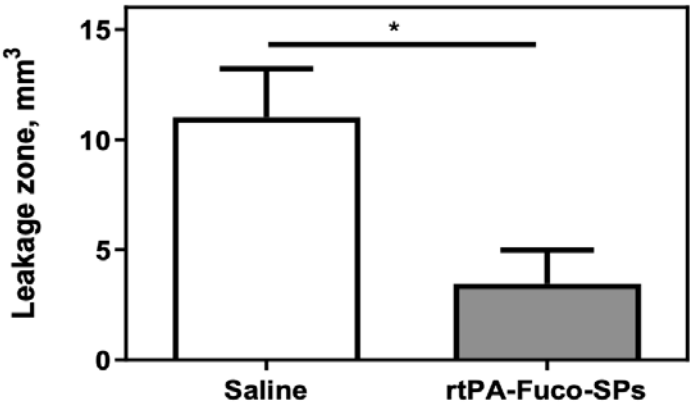


**Figure 5C**

ANNEX 4

EUROPEAN & GLOBAL SUMMIT FOR
CLINICAL NANOMEDICINE & PRECISION MEDICINE

# POSTER SESSIONS SECOND PRICE

*awarded to:*

*Alina Zenych*

FOR THE POSTER IN CATEGORY
**TRANSLATIONAL NANOMEDICINE**

12/2020

Basel, October 26–28

*Dr. Ruth Schmid and Prof. Dr. Yechezkel (Chezy) Barenholz*
*Chairs of the Poster Committee CLINAM 12 /2020*

CLINAM
European Foundation for Clinical Nanomedicine
BASEL, SITZERLAND

12/2020
Basel, October 25–28

# P-Selectin Targeted Polysaccharide Submicroparticles for Thrombolytic Therapy

**Alina Zenych[1], R. Aid-Launais[1], C. Jacqmarcq[2], L. M. Forero Ramirez[1], L. Fournier[1], T. Bonnard[2] , D. Letourneur[1], C. Chauvierre[1]**

1. Inserm U1148 - LVTS, Université de Paris,[1] Université Paris 13, Paris France
2. INSERM U1237 Physiopathology and Imaging of Neurological Disorders, GIP Cyceron, Caen France

## Nanomedicine in atherothrombosis

**Atherosclerosis** is an **asymptomatic disease** which may lead to acute and severe cardiovascular events due to the atherosclerotic plaque rupture [1].

The intravenous injection of **recombinant tissue plasminogen activator** (rtPA), the **gold standard** for thrombolytic therapy, possesses high risks of **intracranial hemorrhages and neurotoxicity** [2]. Hence, there is an unmet medical need for **safe nanomedicine-based** thrombus targeting **solutions**. The objective is to create a **non-toxic, biocompatible, and biodegradable nanocarrier** which is functionalized with a targeting agent and suitable for thrombotic diseases. **Fucoidan**, a natural anionic polysaccharide, holds thrombus targeting properties due to its strong **affinity for P-selectin**, an inflammatory adhesion molecule [3], [4].

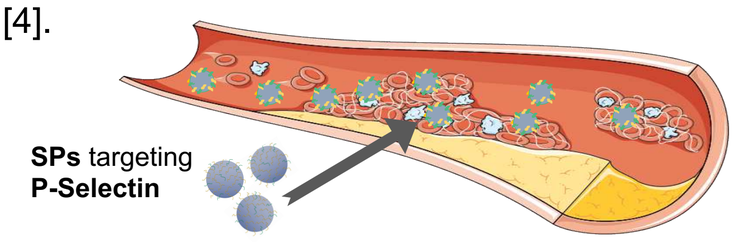


## Synthesis of the particles

### 100% Polysaccharide Submicroparticles (SPs)

**Organic phase**
- Vegetable oil
- Surfactant

**Aqueous phase**
- Polysaccharides
- Crosslinking agent
- Water

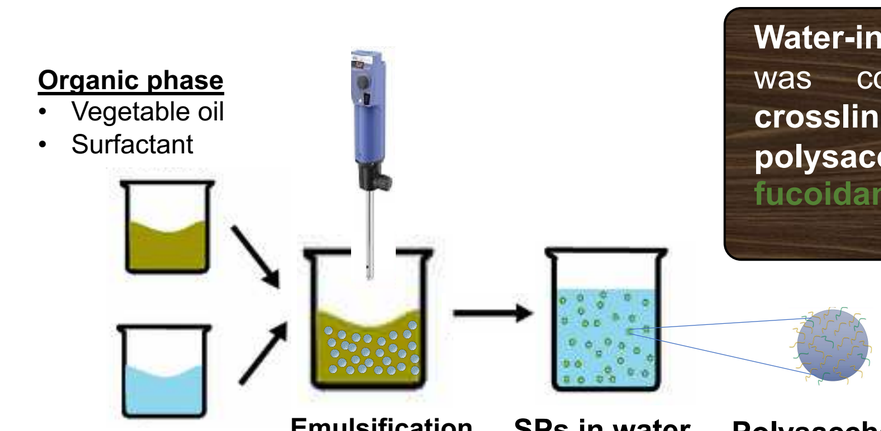


**Water-in-oil emulsification** was combined with a **crosslinking process** of **polysaccharides**: dextran, **fucoidan** with STMP

A simple and reproducible **emulsification** based **crosslinking protocol** allows to obtain **100% polysaccharide SPs**

## Physico-chemical characterization

### Morphology

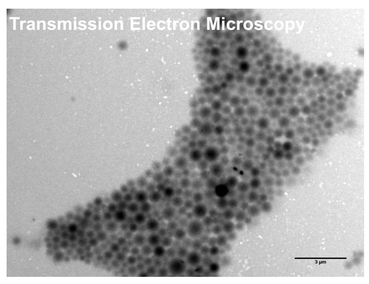


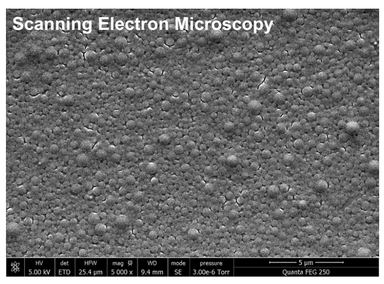


| Size (nm) | Zeta Potential (mV) | Fucoidan,% w/w |
|---|---|---|
| 662.2 ± 26.7 | -30.30 ± 0.14 | 8.60 ± 0.01 |

**Spherical polysaccharide SPs** carry a negative surface charge and possess a **hydrogel** behavior as they swell in water

## Biocompatibility

### Cytocompatibility
Resazurin assay at 24h

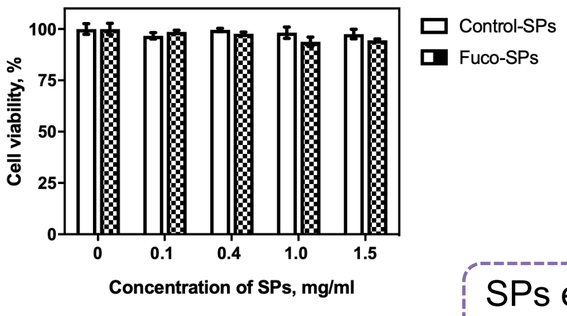


### Hemocompatibility

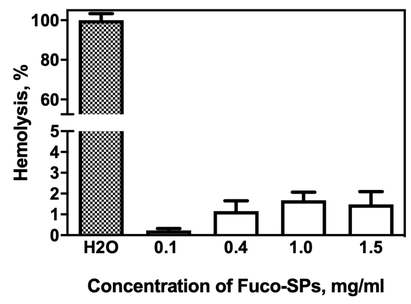


SPs exhibit a **favorable biocompatibility** profile *in vitro*

## Targeting P-Selectin *in vitro*

**Method:** *In vitro* flow assay

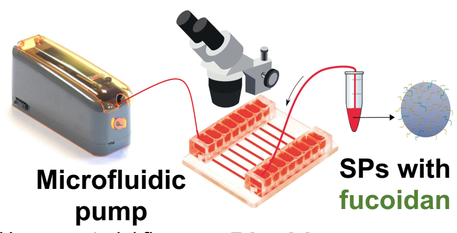


Human *arterial flow*: 60 µl/min

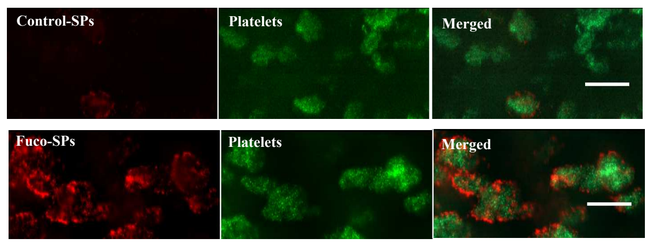


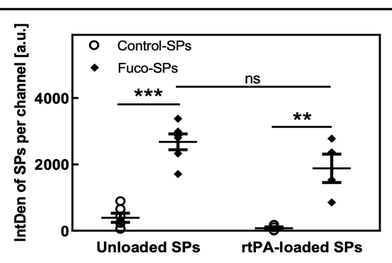


**Fucoidan increases binding** of unloaded or rtPA-loaded SPs to **platelet aggregates** at arterial shear stress conditions *in vitro*

## Thrombolytic activity

**rtPA (**Actilyse®) loaded onto Fuco-SPs via **adsorption**

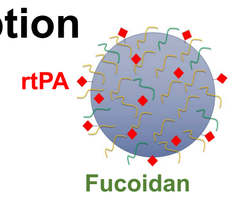


### Amidolytic activity
PefaFluor® assay

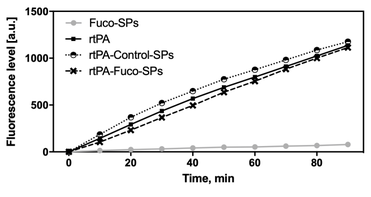


### Fibrinolytic activity
Fibrin-plate agarose test

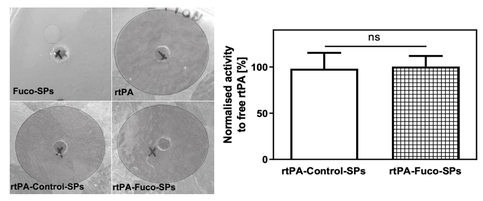


**rtPA-loaded SPs** maintain their **amidolytic** and **fibrinolytic** activity ***in vitro*** in contact with fibrin

### Thrombolytic efficacity *in vivo*
Stroke thrombin model

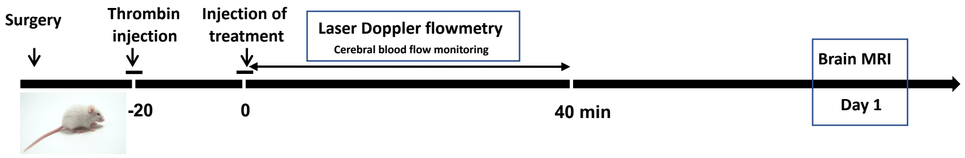


Reperfusion *by Laser Doppler*

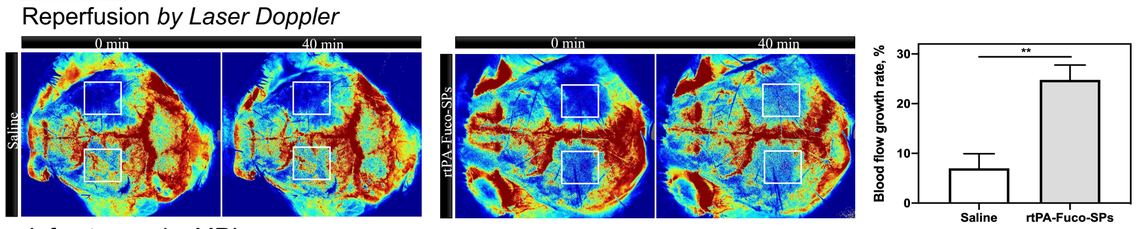


Infarct zone *by MRI*

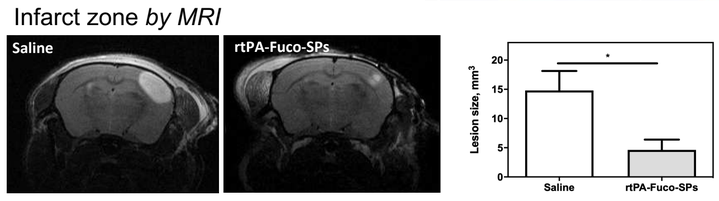


rtPA-loaded Fuco-SPs perform **effective thrombolysis** in the murine **model of stroke**

## Conclusion

- ✓ **Biocompatible & biodegradable 100% polysaccharides SPs**
- ✓ Functionalized with **fucoidan** to target **P-selectin** in thrombus area
- ✓ **rtPA** loaded onto SPs via **adsorption**
- ✓ **rtPA-loaded SPs** maintain **amidolytic** and **fibrinolytic activity** *in vitro* and perform **effective thrombolysis** ***in vivo*** stroke model

➢ **Proof of the concept** study for **safe** preclinical **thrombolytic therapy**

**Acknowledgment**: This study is funded by an INSPIRE programme of the European Union's Horizon 2020 research and innovation programme (Marie Skodowska-Curie grant # 665850). Authors also thank INSERM, Université de Paris, and Université Paris Nord for the financial support.

**References:** [1] P. Libby, Intern. Med. 263 (2008) 517–527. [2] J. Álvarez-Sabín, Lancet Neurol. 12 (2013) 689–705. [3] K.J. Woollard, Inflamm. Allergy Drug Targets. 6 (2007) 69–74. [4] L. Bachelet, Biochim. Biophys. Acta - Gen. Subj. 1790 (2009) 141–146.

ANNEX 5

Biomaterials 194 (2019) 139–150

Contents lists available at ScienceDirect

Biomaterials

journal homepage: www.elsevier.com/locate/biomaterials

# Functionalized polymer microbubbles as new molecular ultrasound contrast agent to target P-selectin in thrombus

Bo Li[a,b,c], Rachida Aid-Launais[a,b], Marie-Noëlle Labour[a,b], Alina Zenych[a,b], Maya Juenet[a,b], Christine Choqueux[a,b], Véronique Ollivier[a,b], Olivier Couture[d], Didier Letourneur[a,b], Cédric Chauvierre[a,b,*]

[a] INSERM, U1148, Laboratory for Vascular Translational Science, CHU X. Bichat, Paris Diderot University, 46 Rue H. Huchard, 75018 Paris, France
[b] Institut Galilée, Paris 13 University, 99 Avenue JB Clément, 93430 Villetaneuse, France
[c] Key Laboratory of Biomaterials of Guangdong Higher Education Institute, Department of Biomedical Engineering, Jinan University, Guangzhou 510632, China
[d] Institut Langevin - Ondes et Images, ESPCI ParisTech, PSL Research University, CNRS UMR7587, INSERM U979, 1, Rue Jussieu, 75238 Paris, Cedex 05, France

ARTICLE INFO

*Keywords:*
Polymer microbubbles
Fucoidan
P-selectin
Molecular ultrasound imaging
Thrombosis

ABSTRACT

Thrombotic diseases rarely cause symptoms until advanced stage and sudden death. Thus, early detection of thrombus by a widely spread imaging modality can improve the prognosis and reduce mortality. Here, polymer microbubbles (MBs) made of degradable poly(IsoButylCyanoAcrylate) and functionalized with fucoidan (Fucoidan-MBs) were designed as a new targeted ultrasound contrast agent to image venous thrombus. The physicochemical characterizations demonstrate that the MBs with fucoidan surface exhibit a size of 2–6 μm and stability in suspension at 4 °C up to 2 months. MBs exhibit high echogenicity and could be completely burst under high destructive pulse. Flow chamber experiments on activated human platelets show a higher affinity of Fucoidan-MBs than control anionic MBs (CM-Dextran-MBs) under shear stress conditions. *In vivo* analysis by ultrasound and histological results demonstrate that Fucoidan-MBs are localized in rat venous thrombotic wall, whereas few CM-Dextran-MBs are present. In addition, the binding of Fucoidan-MBs in healthy vein is not observed. Collectively, Fucoidan-MBs appear as a promising functionalized carrier for ultrasound molecular imaging in thrombotic diseases.

## 1. Introduction

Thrombotic diseases, such as deep vein thrombosis, are often called “the silent killer” because they rarely cause symptoms until an advanced stage [1–3]. Early detection and treatment can improve the prognosis and reduce mortality. P-selectin, an adhesion molecule, mainly expressed on the surface of activated platelets and injured vascular endothelium, is involved in the pathophysiology of intraluminal thrombus formation and other cardiovascular diseases [4,5]. These features suggest that P-selectin can be an important target for molecular imaging of thrombosis or in acute and chronic cardiovascular diseases [6–8].

We have previously demonstrated that fucoidan, an abundant and cost-effective marine polysaccharide with sulfated chains, exhibits a high affinity for immobilized P-selectin *in vitro* [9,10]. $^{99m}$Tc-fucoidan as a radiotracer has already proved *in vivo* to be able to detect thrombus and heart ischemia associated with the P-selectin overexpression in our previous studies [11,12]. Recently, we have developed fucoidan functionalized core-shell polymer microcapsules and proved that they have high specific binding efficiency to P-selectin under flow conditions [13]. Moreover, fucoidan functionalized nano-/microparticles have also been developed as a molecular contrast agent to monitor thrombi by Magnetic Resonance Imaging (MRI) or Single-Photon Emission Computed Tomography (SPECT) imaging [14–16].

Compared to other imaging modalities, ultrasound imaging has numerous advantages, including comfortable, noninvasive, portable, low cost real-time imaging, lack of ionizing radiation and excellent safety profile [17,18]. Ultrasound imaging equipment is already present in most hospitals all around the world and even in private health centers. However, ultrasound image quality is limited by its poor contrast due to the low differences in acoustic characteristics of organs *in vivo*. The development and use of microbubbles (MBs) have redeemed this shortage tremendously [19–22]. Traditional MBs are mainly made up of albumin/lipid/surfactant shells and have not only been applied as

* Corresponding author. INSERM, U1148, Laboratory for Vascular Translational Science, CHU X. Bichat, Paris Diderot University, 46 rue H. Huchard, 75018 Paris, France.
*E-mail address:* cedric.chauvierre@inserm.fr (C. Chauvierre).

https://doi.org/10.1016/j.biomaterials.2018.12.023
Received 3 September 2018; Received in revised form 28 November 2018; Accepted 20 December 2018
Available online 23 December 2018
0142-9612/ 

ultrasound agents, but also have been used in versatile biomedical applications including drugs, genes and drug-loaded nanoparticles targeted delivery [23,24]. Recently, polymeric shells MBs have received increasing attention due to their improved stability and some polymersomes have also been applied in drug controlled release at the target site under a specific stimulus such as ultrasound [25,26]. Poly (AlkylCyanoAcrylate) with long alkylcyanoacrylate monomers (for example, *n*-butyl, isobutyl, isohexyl and octyl) has been extensively investigated to design micro-/nanocarriers since the 80s [27,28]. The first Poly(ButylCyanoAcrylate) microbubbles called Sonavist® were manufactured by one-step process through adding the *n*-butyl-2-cyanoacrylate monomers into gas-water emulsion [29,30]. Palmowski et al. further synthesized streptavidin-coated PBCA microbubbles and investigated their physicochemical properties [31–33]. Subsequent studies proved that these microbubbles could be functionalized by conjugating with monoclonal antibodies that recognize receptor proteins involved in various diseases [34–36]. However, employing, for instance, biotin/streptavidin and antibodies limited their use in humans because of the costs and potential immunogenicity of streptavidin and antibodies. Recently, various bubbles using small peptides instead of antibodies for binding without using the biotin-streptavidin coupling strategy have already been developed to address these problems [37,38]. Among them, BR55, as the most potential targeted-MBs contrast agent, shows that it could be used to detect the prostate cancer or monitor breast and ovarian lesions in human clinical trials [39,40]. In the view of future clinical applications, MBs assembled by clinically approved polymers and suitable targeting ligands are interesting for clinical use and market requirements.

In this work, we report a new one-step process to obtain polysaccharide-coated poly(IsoButylCyanoAcrylate) (PIBCA) microbubbles. Among them, fucoidan functionalized microbubbles (Fucoidan-MBs) were considered as a targeted ultrasound molecular imaging probe for P-selectin. Targeting of Fucoidan-MBs was evaluated *in vitro* using flow chambers with activated human platelets. *In vivo* experiments performed in a $FeCl_3$-induced thrombus rat model showed that Fucoidan-MBs were located in the thrombotic area but not in healthy rats, which confirms the ability of Fucoidan-MBs to specifically target P-selectin. These functionalized echogenic microbubbles appear as new tools for imaging at molecular level cardiovascular events in which P-selectin is overexpressed.

## 2. Materials and methods

*Materials:* Dextran 70, anionic CarboxyMethyl-Dextran 40 (CM-Dextran), FITC-CarboxyMethyl-Dextran 40 (FITC-CM-Dextran) and cationic 2-DiEthylAminoethyl-Dextran 70 (DEAE-Dextran) were provided from TdB Consultancy (Uppsala, Sweden). Fucoidan (Mn = 18 kDa/ Mw = 104 kDa) was obtained from Algues & Mer (Ouessant, France). Isobutylcyanoacrylate (IBCA) monomers were purchased by ORAPI (Saint Vulbas, France). Methylene blue hydrate was purchased from Sigma-Aldrich. Chromatography was obtained from GE Healthcare. Mouse anti-human CD62P-FITC and mouse IgG1-FITC Isotype Control were provided from Beckman Coulter (Villepinte, France). Fibrillar type I collagen Horm® was obtained from Takeda (Linz, Austria). 24-, 96-Well Cell Culture Plates (Costar) were obtained from Corning Incorporated. PPACK tubes were purchased from Cryopep (Montpellier, France). Flow chambers (Vena8 Fluoro+) were provided from Cellix Ltd (Dublin, Ireland).

*Synthesis of Microbubbles:* Poly(IsoButylCyanoAcrylate) (PIBCA) shelled air-containing microbubbles (MBs) were prepared by modification of established emulsion polymerization process as described by Palmowski et al. [33]. Briefly, 700 μL of IBCA monomer was loaded in a 1 mL plastic syringe, injected into 50 mL of an aqueous solution of 1% Tween 20 at pH 2.5 via a catheter at a constant flow rate of 5 mL $h^{-1}$, and dispersed at 20,000 rpm for 60 min with a homogenizer (ULTRA-TURRAX®, IKA, Germany). The syringe pump (AL-300, World Precision Instruments, Florida, USA) was used to control flow rate. The resulting microbubble suspension was then washed three times by centrifugation (500 rpm, 20 min, 5702RH centrifuge Beckman Coulter, Villepinte, France) to obtain the monodispersed bubble populations and to remove the polymeric scrap. Subsequently, the resulted emulsion was placed into a separatory funnel overnight, and the aqueous layer was removed. The microbubbles layer was redispersed in 30 mL of 0.02% Tween 20 for storage at 4 °C. To prepare polysaccharide functionalized microbubbles (Dextran-MBs, DEAE-Dextran-MBs, CM-Dextran-MBs and Fucoidan-MBs), 500 mg of corresponding polysaccharides were dissolved in an aqueous solution before IBCA introduction. For Rhodamine B loaded CM-Dextran-MBs and Fucoidan-MBs (CM-Dextran-RhoB-MBs and Fucoidan-RhoB-MBs, respectively), 1 mg of Rhodamine B was added into an aqueous solution before synthesis. FITC-CM-Dextran-MBs and FITC-Fucoidan-MBs were obtained by using 10 mg of FITC-CM-Dextran mixed with 490 mg of CM-Dextran and 10 mg of FITC-Fucoidan mixed with 490 mg of Fucoidan, respectively. Rhodamine B loaded FITC-CM-Dextran-MBs and FITC-Fucoidan-MBs were prepared by combining two protocols.

*Microbubbles Size and Zeta Potential Analysis:* The size range of microbubbles was determined using a Mastersizer 3000 (Malvern Instruments, UK) equipped with a Hydro SM sample dispersion unit. A suspension of microbubbles was dispersed into 0.02% Tween 20 solution and stirred at 1500 rpm for 1 min before an examination. Zeta potential (ζ) of the microbubbles was measured with samples diluted into electrolyte solution ($1 \times 10^{-3}$ M KCl & 0.02% Tween 20) using electrophoretic light scattering apparatus (Nano ZS, Malvern Instruments, UK) at 25 °C. All the measurements were performed at least three times.

*Environmental Scanning Electron Microscopy (ESEM) and Scanning Electron Microscopy* (*SEM*): The surface morphology of microbubbles was imaged using an ESEM apparatus (Philips XL30 ESEM-FEG, Amsterdam, Netherlands) and SEM apparatus (JSM-IT100, Jeol, Japan). The interaction of Fucoidan-MBs with activated platelets on an *ex vivo* platelets-rich thrombus was also visualized using ESEM. Briefly, to obtain the *ex vivo* platelets-rich thrombus, the blood was collected in citrate tubes and then centrifuged at 120 G for 15min. Plasma rich in platelets (PRP) was collected and distributed in small glass tubes (370 μL). To activate platelets, calcium chloride was added (7 μL at 1 M) and the tubes were incubated at 37 °C for 1 h. The platelet-rich thrombus was detached from the walls of the glass tubes and then transferred to a 96-well plate where it was be put in contact with Fucoidan-MBs for 5 min. After several rinses with 0.9% NaCl, the thrombus was fixed at 4% paraformaldehyde for 24 h and then rinsed for visualization by ESEM.

The binding of Fucoidan-MBs on the luminal thrombus of inferior vena cava was observed using ESEM. Briefly, we performed an inferior vena cava thrombus rat model induced by ferric chloride ($FeCl_3$), and injected Fucoidan-MBs. The rat was then euthanatized and the inferior vena cava with thrombus was picked up and fixed in 4% paraformaldehyde for 24 h and rinsed in saline. The inferior vena cava was opened longitudinally on the top to observe the thrombus by ESEM.

*Confocal imaging:* Microbubbles were imaged using Zeiss LSM 780 confocal microscope fitted with 63× objective. Microbubbles were detected using rhodamine B and polysaccharides with FITC-Fucoidan and FITC-CM-Dextran.

*Quantification of Fucoidan content:* The amount of fucoidan in microbubbles was determined by methylene blue staining of sulfated polysaccharides [41]. Several 1 × 1 cm square chromatography paper were placed in 24-well plate. The solution was cautiously added dropwise at the center of these squares, 2 μL for each drop; the next portions were dropped on the same point after drying off the last drop in the oven (Jouan, France) for 10 min at 50 °C. The filter papers with loaded sample drops were kept in the oven overnight at 50 °C, dried thoroughly and then treated with a mixture of methanol and acetone (6:4) for 3 min. Fucoidan spots on filter paper were visualized after

10 min at room temperature in staining solution containing 50 mM HCl and 0.1% (w/w) methylene blue in a mixture of methanol/acetone/water (6:4:15). The filter paper was washed several times with a mixture of acetic acid/methanol/acetone/water (5:6:4:75) to remove the excess of methylene blue. Images were taken, and filter paper squares were put into 1.5 mL Eppendorf centrifuge tubes with 0.5 mL of methanol containing 2% SDS during 15 min at 50 °C. A volume of 0.1 mL of this extract was transferred into 96-well plate, and absorbance was determined at 663 nm by infinite® 200 PRO (TECAN, Switzerland). The series of filter paper squares containing stained standard solution spots was obtained by adding 5 drops (10 μL) of different concentration of fucoidan or CM-Dextran solutions (0.5, 0.25, 0.125, 0.0625 and 0.3125 mg $mL^{-1}$) to each filter paper. The relative absorbance (△abs) of fucoidan - methylene blue complex at $A_{663}$ nm was expressed as [abs (fucoidan) - abs (CM-Dextran)]. Fucoidan content was plotted against the △abs for the regression line. For MBs samples, $3 \times 10^8$ Fucoidan or CM-Dextran microbubble suspension was placed into a separatory funnel overnight, and the aqueous layer was removed to eliminate free fucoidan. The clot of microbubbles was totally hydrolysed by mixing with alkaline solution (0.1 N NaOH and 0.02% Tween 20) overnight, and the resulted solution was added dropwise on filter paper square.

*Flow Chamber Experiments:* Platelet dynamic binding experiments were performed according to our previous methods [13]. Briefly, Vena8 Fluoro + channels were coated with 50 μg $mL^{-1}$ of collagen overnight in a wet chamber at 4 °C and washed with 0.9% NaCl before use. Collagen fibers covering the channels were visualized by phase contrast microscopy. Human whole blood samples (EFS, Hôpital Bichat, Paris, France) were collected in 75 μM PPACK tubes and perfused through the channels for 5–10 min at arterial shear stress (67.5 dyn $cm^{-2}$). Platelet activation and aggregation through contact with collagen in the channels were visualized in real time with phase contrast microscopy (Carl Zeiss Microscopy, Oberkochen, Germany). Channels were washed for 1 min with 0.9% NaCl. To confirm P-selectin expression on platelets, 20 μg $mL^{-1}$ of FITC anti-CD62P antibody was infused into one channel after platelet aggregation at arterial shear stress for 5 min, and the same concentration of isotype-matched FITC-IgG was injected through the other channel as a control. For binding assay, platelets were labeled with DIOC6 ($0.15 \times 10^{-3}$ M) before their injection. After platelet aggregation, fluorescent microbubbles (CM-Dextran-RhoB-MBs or Fucoidan-RhoB-MBs) were injected through the channels at $1 \times 10^8$ $mL^{-1}$ for 5 min under venous shear stress (6.75 dyn $cm^{-2}$). Channels were finally washed for 15 min with 0.9% NaCl at the same shear stress. Fluorescence microscopy videos and images were taken along each channel using the same parameters. Quantitative analysis was performed on 7 channels per type of microbubbles. The mean fluorescent intensity of the red fluorescence channel of twenty aggregates was measured using Zen 2012 Software (Carl Zeiss, Oberkochen, Germany).

*In Vitro Ultrasound Imaging:* Ultrasound imaging performances were evaluated with a VisualSonics Vevo® 2100 imaging system (FUJIFILM VisualSonics Inc., Canada) connected to a high-frequency transducer (MS550D, VisualSonics). The set-up parameters were: frequency (40 MHz), the acquisition contrast gain (20 dB), the transmit power (4%), the frame rate (33) and the dynamic range (35 dB). All the parameters were constant throughout all image acquisition. A suspension of MBs ($10^5$ $mL^{-1}$) dispersed into thin-wall PCR tubes was placed on the top of the probe, and the images were obtained by B-mode and linear contrast mode. The burst of microbubbles was performed by using high mechanical index destructive pulse (duration: 1 s). The values of B-mode mean power of 100 frames before and after the destructive pulse were calculated by VevoCQ™ advanced contrast quantification software and shown within the scatter plot. To analyze quantitatively the contrast enhancement effect, the mean values of B-mode power of 100 frames before and after burst were calculated.

*In Vitro Cytotoxicity:* Mouse fibroblast 3T3 cells were cultured in Dulbecco's Modified Eagle Medium (DMEM) supplemented with 10% (v/v) fetal bovine serum, 4 mmol of L-glutamine, 1% (v/v) of penicillin and 1% (v/v) of streptomycin. The cells were kept in an incubator at 37 °C in a humidified atmosphere of 5% $CO_2$, 95% air. Cells were seeded (at the density of $10^4$ cells per well) in 96-well plates and incubated for 24 h. The cell culture medium was removed, and 200 μL of series of dilution ($10^7$, $10^6$, $10^5$ and $10^4$ $mL^{-1}$) of microbubbles were added in the medium. Culture media were used as a control. After 24 h of incubation, the supernatant was removed, 10 μL (5 mg $mL^{-1}$) of MTT solution was added to the medium in each well, and the plates were incubated for 4 h at 37 °C and 5% $CO_2$. The medium with MTT was removed, and 100 μL per well of isopropanol solution was added to each well to dissolve the formazan crystals. Absorbance was measured immediately using a TECAN (Infinite M200 PRO) at 490 nm. The relative cell viability was expressed as (absorbance of microbubbles/absorbance of the control) × 100%.

*In Vivo Model of Thrombosis on Rat Deep Vein:* Animal studies were done in accordance with principles of laboratory animal care and with the approval of the animal care and use committee of the Claude Bernard Institute (N°2012-15/698-0100, Paris, France). $FeCl_3$-induced thrombosis model on rat deep vein was induced based on the previous work [42]. Briefly, Wistar male rats (Janvier Labs, Le Genest-Saint-Isle, France) aged around 7 weeks were anesthetized with an intraperitoneal injection of pentobarbital (1 μL $g^{-1}$ body weight, Ceva Santé Animale SA, La Ballastiere, France). A midline abdominal incision was performed to expose the inferior vena cava (IVC). Venous thrombus was generated by applying a 2 mm Whatman chromatography paper saturated with 10% $FeCl_3$ on top of the IVC in contact with the adventitial surface of the vessel for 5 min. After the paper was removed, the vein was washed several times with a saline solution. Typically, thrombus development was completed 30 min post $FeCl_3$ injury. Ten thrombosis-bearing rats were randomly divided into two groups, one group of rats received Fucoidan-MBs intracavernous injection (200 μL, $1 \times 10^8$/mL), the other group was injected with CM-Dextran-MBs (200 μL, $1 \times 10^8$/mL). As the control, three healthy rats were also injected with Fucoidan-MBs (200 μL, $1 \times 10^8$/mL). All rats were kept anesthetized during the entire imaging process.

*In Vivo Ultrasound Molecular Imaging:* Ultrasound imaging of venous thrombosis (in rat thrombus model) or venous wall (in healthy rats) was performed using a VisualSonics Vevo® 2100 imaging system with the same parameters used *in vitro*. Briefly, the ultrasound transducer was placed perpendicular and parallel to the IVC, 10 min after injection of MBs. A cine loop was acquired in the B-mode and linear contrast mode which made series of imaging frames before and after a high mechanical index destructive pulse (duration: 1 s). Using the Advanced Contrast Quantification Software Analysis Tool (VevoCQ, VisualSonics, Canada), a region of interest (ROI) was defined around the bound MBs area (1 $cm^2$). The mean contrast intensity within the ROI before and after the destructive pulse was evaluated, and each data point corresponded to the mean of the contrast intensity in the ROI in each frame. To highlight the contrast effect of targeted MBs, 50 frames after the destructive pulse were selected to create a reference baseline, and the frames before destructive pulse were overlaid to the reference baseline. The system isolated the targeted MBs echo from the tissue ultrasound signal data and identified them in green color. The process persistence filter was set to Smooth (to remove transient bubble data from the image), the contrast overlay dynamic range and threshold were used as default (50%). To analyze quantitatively the contrast enhancement effect, the mean values of contrast power of 200 frames before and after the destructive pulse were calculated by VevoCQ™ advanced contrast quantification software. The signal from the targeted MB was determined by subtracting the mean value after the destructive pulse from the one before. The obtained signal from the targeted MB was normalized to the value before the destructive pulse.

*Histological Evaluations:* Rats were sacrificed with pentobarbital overdose 1 h after injection of Fucoidan-RhoB-MBs. Inferior vena cave with thrombus was removed, washed in 0.9% NaCl, fixed in paraformaldehyde 4% (w/v), and then frozen. The vena samples were

cryosectioned at 10 μm thickness and then stained with hematoxylin and eosin. The cell nuclei of a venous vascular wall were labeled with 4'6-DiAmidino-2-PhenylIndole (DAPI) contained in mounting medium (Vecto laboratories), and Fucoidan-RhoB-MBs were visualized in red thanks to rhodamine B. Stained sections were observed by light/fluorescence microscopy using the NDPview software (Hamamatsu, Japan). The magnified images of the region of interest were used to show the position of microbubbles.

Biodistribution of Fucoidan-RhoB-MBs was studied in a similar way. Briefly, liver, spleen, lungs, and kidneys were excised and washed at 1 h after injection of Fucoidan-RhoB-MBs. The samples were cryosectioned, cell nuclei were labeled with DAPI, and observed by fluorescence microscopy.

*Statistical Analysis:* All results are presented as the mean ± standard deviation (SD). Statistical differences for multiple groups were determined using a one-way ANOVA, and each experiment was performed using Student's t-test. Probabilities of $p < 0.05$ were considered significant. Statistical analyses were performed using GraphPad Prism 5.0.

## 3. Results and discussion

### 3.1. Preparation and characterization of microbubbles

Limitations of the first generation of MBs were addressed either by incorporating the echogenic reflective air component into less permeable coatings, such as organic polymers and cross-linked proteins, or by employing less soluble gaseous compounds [43]. Since the first PBCA MBs developed by Harris et al., several antibodies and peptides were employed to produce targeted PBCA MBs with a multi-step synthesis for molecular ultrasound imaging [44]. However, immunogenicity and cost of antibodies limited their use in humans. Moreover, the production of these targeted bubbles is also time-consuming due to their multi-step synthesis (carboxyl groups introduced on the surface through partial hydrolysis of the shell of PBCA MBs [45]). Furthermore, the degree of hydrolysis is difficult to control, and the excess of hydroxyl or redundant reaction time may induce rapid depolymerization reaction destroying the structure of MBs and producing short chains of PBCA [46].

In this work, we reported air-filled PIBCA MBs coated with various polysaccharides in a novel simple one-pot procedure (Fig. 1). The size distribution of MBs before and after polysaccharide functionalization was not altered (Table 1), all MBs showing a single peak with a narrow size distribution (Fig. S1 **Left**). The surface charge of MBs was similar to the charge of polysaccharides (Table 1 and Fig. S1 **Right**), indicating that polysaccharides were present at the surface of the MBs [47,48]. Among the polysaccharides, DEAE-Dextran and CM-Dextran could respectively provide amino groups and carboxyl groups on the surface of PIBCA MBs for further functionalization.

**Table 1**
Characteristics of non-functionalized and polysaccharide functionalized microbubbles.

| | Size distributions | | | ζ (mV) |
|---|---|---|---|---|
| | $D_{10}$ (μm) | $D_{50}$ (μm) | $D_{90}$ (μm) | |
| MBs | 2.34 ± 0.01 | 3.69 ± 0.01 | 5.85 ± 0.01 | −15.33 ± 0.40 |
| Dextran-MBs | 2.46 ± 0.01 | 3.90 ± 0.02 | 6.18 ± 0.06 | −8.56 ± 0.50 |
| DEAE-Dextran-MBs | 2.63 ± 0.05 | 4.03 ± 0.10 | 6.06 ± 0.21 | 44.20 ± 2.38 |
| CM-Dextran-MBs | 2.53 ± 0.02 | 4.03 ± 0.05 | 6.44 ± 0.14 | −34.33 ± 0.47 |
| Fucoidan-MBs | 2.40 ± 0.02 | 3.83 ± 0.03 | 6.23 ± 0.12 | −42.80 ± 1.47 |

Since CM-dextran had a similar negative surface charge but without the sulfate groups of fucoidan that are involved in its interaction with P-selectin, CM-Dextran-MBs were chosen as a control to assess the benefit of using targeted MBs (Fucoidan-MBs). Morphology images of CM-Dextran-MBs and Fucoidan-MBs obtained by electron microscopy showed that all MBs were spherical with an empty core loaded with air (Fig. 2 **Left**). Under Environmental Scanning Electron Microscopy (ESEM), low vacuum protected the integrity of MBs structure, and both MBs presented similar size by DLS measurement. Fluorophore-labeled MBs in combination with fluorescence microscopy were very powerful tools for clearly visualizing and validating *in vitro* and *in vivo* binding studies. However, the loading strategy should be carefully designed to avoid an alteration of the surface functional groups of MBs. Here, rhodamine-loaded Fucoidan-MBs (Fucoidan-RhoB-MBs) and CM-Dextran-MBs (CM-Dextran-RhoB-MBs) were prepared by modification of the synthesis methods of Liu [49]. The loading of rhodamine into the MBs polymer membrane did not affect the size distribution and zeta potential of MBs. To demonstrate the presence of CM-Dextran or fucoidan on MBs, FITC-CM-Dextran or FITC-fucoidan was added, respectively (Fig. S2). Size distribution and zeta potential of all the

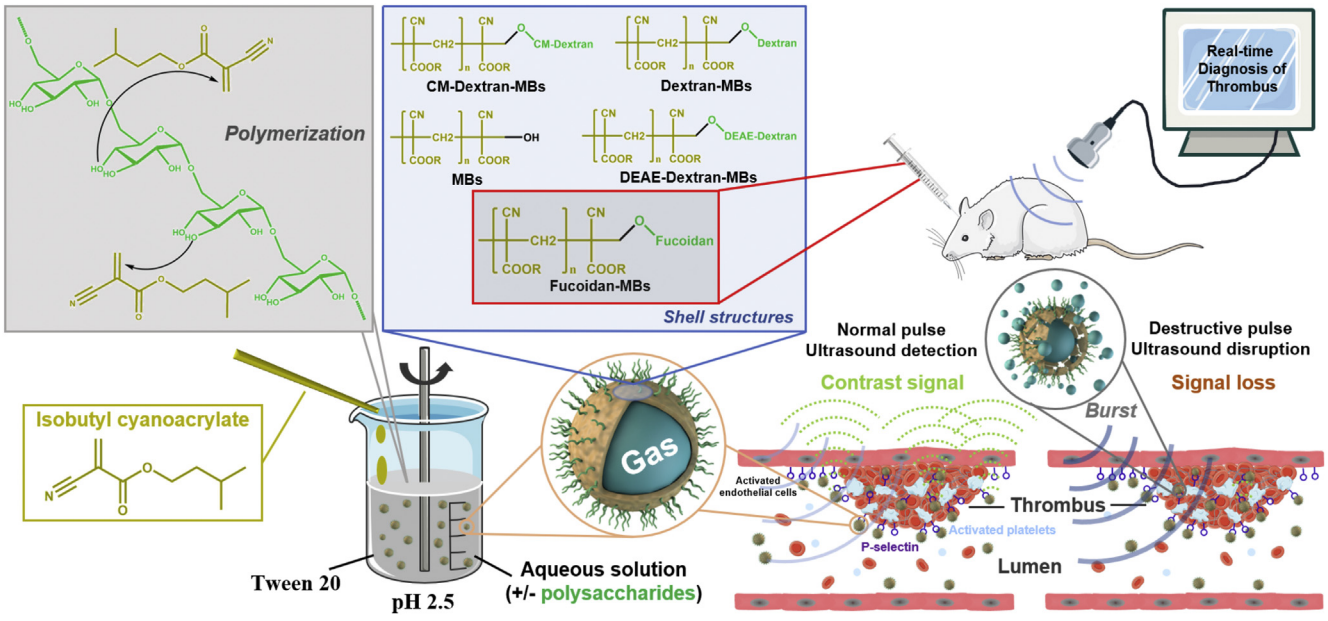


**Fig. 1.** Overall schematic diagram of one-step protocol for microbubbles and their use as molecular ultrasound contrast agent.

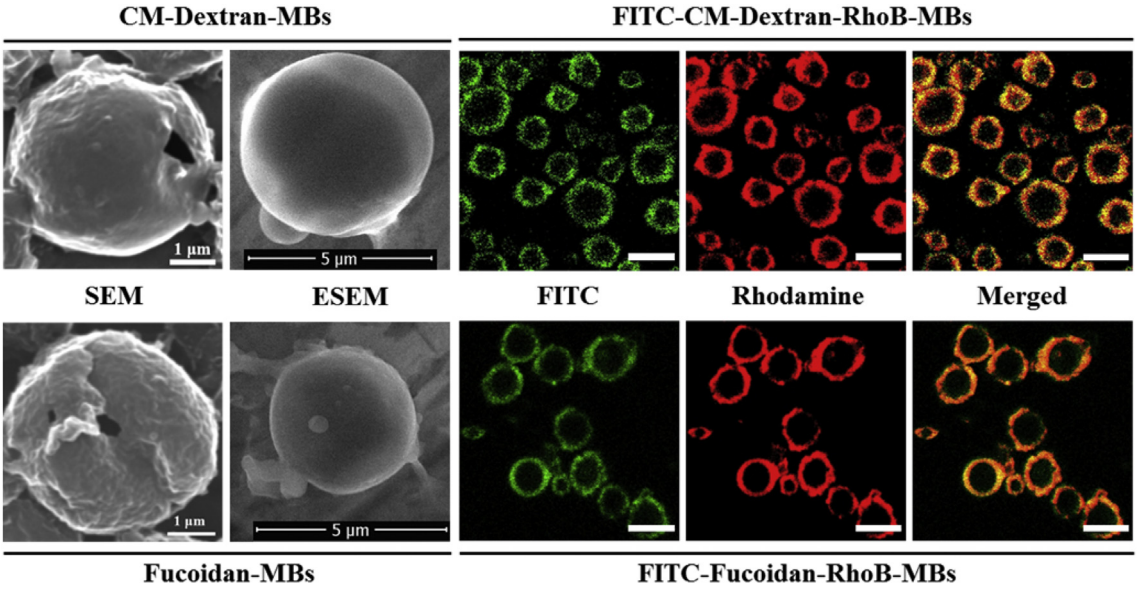


**Fig. 2.** Morphology characterizations of CM-Dextran-MBs and Fucoidan-MBs (**Left**) and fluorescently labeled microbubbles (**Right**). The green fluorescence signal is from FITC-CM-Dextran or FITC-Fucoidan, and the red fluorescence signal is from rhodamine (Scale bar for confocal images: 5 μm).

labeled MBs were presented in Table S1. The double-labeled MBs observed by confocal microscopy imaging confirmed the core-shell structure of MBs and the presence of polysaccharides on the shell (Fig. 2 **Right**).

The amount of fucoidan coupled to the MBs was quantified by a solid-phase colorimetric assay described by Lee [41]. Based on the standard curves, we calculated the fucoidan content of Fucoidan-MBs to be of $8.6 \times 10^{-15}$ g per Fucoidan-MB (Fig. S3).

As a potential contrast agent, the storage of MBs is very important. Long-term storage stability of the MBs in aqueous suspensions at 4 °C was evaluated. Results showed that size and zeta potential remained stable for at least 2 months for both MBs (Fig. 3).

### 3.2. In vitro flow experiments

Flow chamber experiments are used to mimic the interactions of MBs with purified P-Selectin or activated human platelets under physiological conditions *in vitro* [36,50]. After perfusion of human whole blood at high shear stress, activated DIOC6 stained human platelets aggregated on collagen-coated chambers. Human platelet aggregates were visualized in real time under the fluorescent microscope (Video S1). P-selectin expression on activated platelets was evidenced by the green fluorescence uptake observed after injection of FITC-*anti*-CD62P antibody through the channel; no signal was detected after injection of FITC-IgG control (Fig. S4). After perfusion at venous shear stress (6.75 dyn $cm^{-2}$) to mimic venous flow conditions of Fucoidan-RhoB-MBs (Video 1) or CM-Dextran-RhoB-MBs (Video S2) on preformed platelet aggregates, an uptake of red fluorescence was observed over time at the surface of the aggregates. After washing, bound Fucoidan-RhoB-MBs remained attached to the aggregates, whereas almost no remaining binding was observed with control CM-Dextran-RhoB-MBs (Fig. 4A). Quantitative analysis confirmed that the mean fluorescent intensity (MFI) of fluorescent MBs was significantly higher for Fucoidan-RhoB-MBs than for CM-Dextran-RhoB-MBs (4387 ± 178.9 versus 1640 ± 10.53, respectively, $p < 0.0001$) (Fig. 4B). To further confirm these results, CM-Dextran-RhoB-MBs and Fucoidan-RhoB-MBs were successively perfused into the same channel at constant shear stress, and the results showed clearly different targeting responses (Video S3).

Supplementary video related to this article can be found at https://doi.org/10.1016/j.biomaterials.2018.12.023.

To confirm the binding of Fucoidan-MBs to activated platelets, we performed an *ex vivo* platelets-rich thrombus and added a suspension of Fucoidan-MBs for 5 min. After rinsing with saline, we observed the

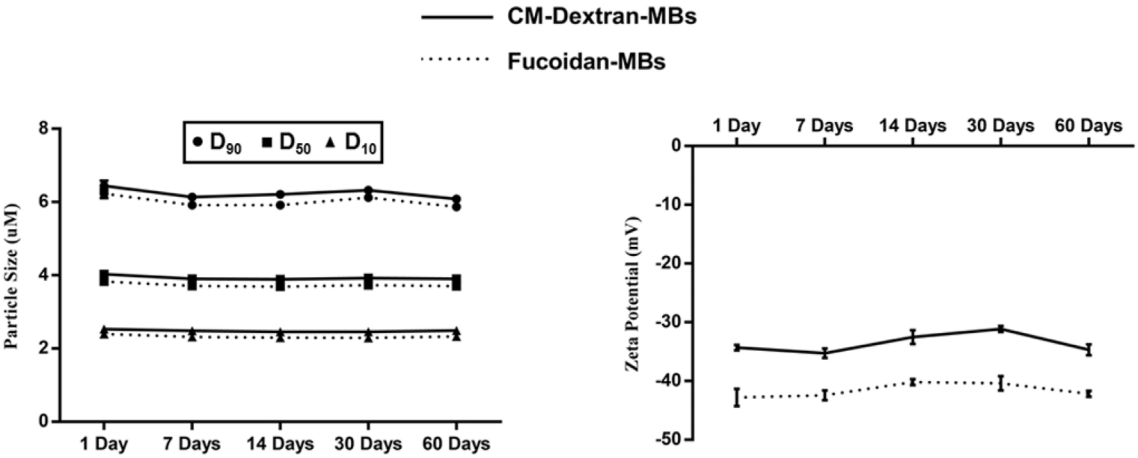


**Fig. 3.** Stability of size and zeta potential of CM-Dextran-MBs and Fucoidan-MBs kept at 4 °C for 60 days (n = 3).

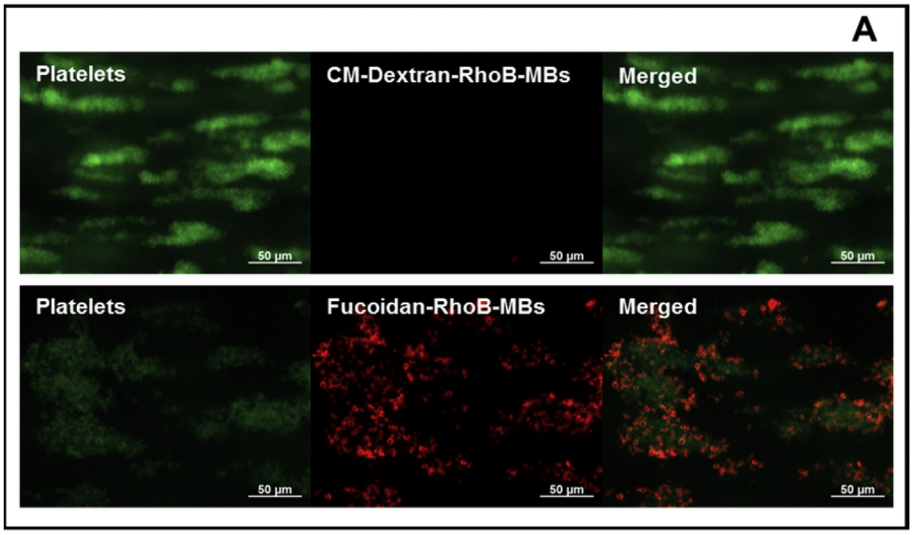


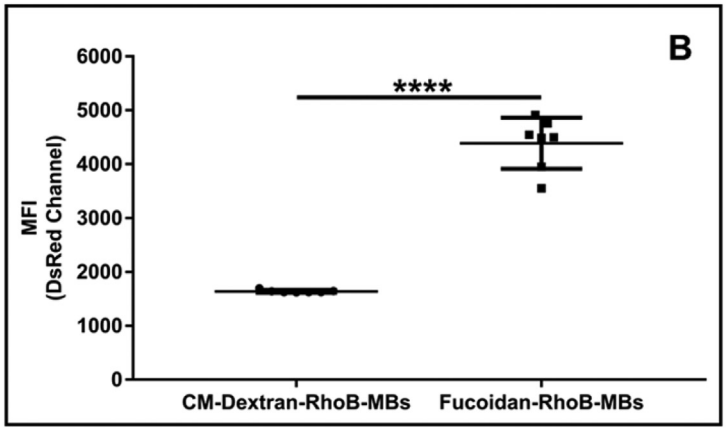


**Fig. 4.** Binding of microbubbles on activated platelet aggregates under flow conditions *in vitro*. **A)** Human whole blood labeled with 5 µM of DIOC6 (green) was first injected into channels coated with collagen to induce platelet aggregation (Left panels). Rhodamine labeled CM-Dextran-MBs or Fucoidan-MBs (red) were infused for 5 min onto activated platelet aggregates under venous flow conditions (6.75 dyn $cm^{-2}$). Channels were washed and observed by fluorescent microscopy (middle and right panels). **B)** Quantitative analysis of the mean fluorescent intensity (MFI) on platelet aggregates. One MFI value was obtained per channel on 20 platelet aggregates from 7 independent experiments (**** indicated $p < 0.0001$).

thrombus by Environmental Scanning Electron Microscopy. The ESEM images of the platelets-rich thrombus without MBs exhibited activated platelets and fibrin (Fig. S5 **Left**). In contrast, the ESEM images of the platelets-rich thrombus in contact with Fucoidan-MBs showed many spherical micrometer particles (as Fig. 2 **Left)** associated with the activated platelets confirming that Fucoidan-MBs bind to activated platelets overexpressing P-selectin.

### 3.3. In vitro ultrasound imaging

The potential of CM-Dextran-MBs and Fucoidan-MBs as contrast agents for ultrasound imaging was first assessed *in vitro*. A suspension of MBs ($10^5$ $mL^{-1}$) was put into the thin-wall tube and placed on the top of the probe (Fig. 5A **Left**), and the echogenicity of MBs was evaluated by Vevo 2100. A Control suspension was used to check the background signal (Fig. 5A **Middle**) which remained at low level (Fig. 5A **Right**). For MBs suspensions, the imaging showed a high and stable enhancement of monodisperse contrast signal, which could be eliminated by destructive pulse (Fig. 5B). Quantitative analysis proved that CM-Dextran-MBs and Fucoidan-MBs have similar contrast signals and both of them could be reduced to background level after burst (Fig. 5C). These results indicated that the variation in echo after the burst could be used *in vivo* to ensure that the enhanced contrast signal was coming from MBs and not from motion artifact caused by respiratory and cardiac activities.

### 3.4. Cell viability

The cytotoxicity of Fucoidan-MBs was evaluated by MTT assay [51] with mouse fibroblast 3T3 cells exposed to various concentrations of Fucoidan-MBs or CM-Dextran-MBs. As shown in Fig. S6, the results demonstrated that none of these MBs affected the cell viability (cell viability > 80% even at the highest concentrations of $10^7$ $mL^{-1}$), suggesting an excellent *in vitro* safety of these MBs. Moreover, no significant difference was observed between CM-Dextran-MBs and Fucoidan-MBs.

### 3.5. In vivo ultrasound imaging and Environmental Scanning Electron Microscopy

To evaluate the *in vivo* targeting of Fucoidan-MBs to P-selectin overexpressed on thrombus, the ferric chloride ($FeCl_3$) induced inferior vena cava (IVC) non-occlusive thrombus rat model was performed. The presence of non-occlusive thrombus was inspected by B-mode, and the venous blood flow around thrombi was confirmed by Color Doppler Flow Imaging (Fig. S7). Ten minutes after the injection of Fucoidan-MBs, the presence of bound Fucoidan-MBs in the thrombus region was accurately validated (green color) (Video 2). The signal intensity of binding area in the thrombus was remarkably decreased after MBs burst by destructive pulse (Fig. 6B). In contrast, the rats injected with control CM-Dextran-MBs showed few MBs in the thrombus region (Video S4), and the signal intensity declined only slightly after the destructive pulse (Fig. 6A). Subsequent quantifications of the decreased signal intensity in the thrombus area before and after destructive pulse evidenced a

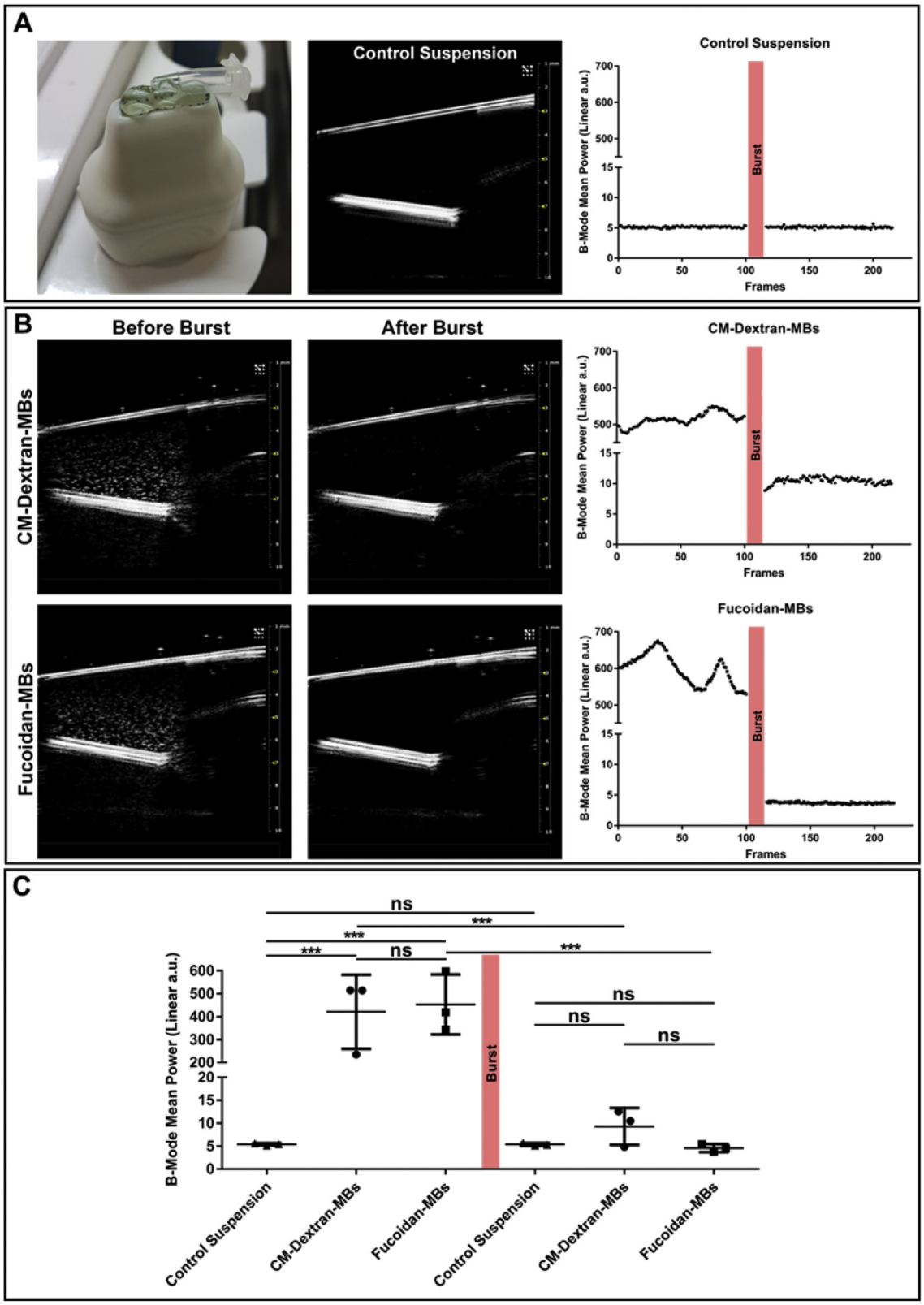


**Fig. 5.** *In vitro* ultrasound signals of CM-Dextran-MBs and Fucoidan-MBs under B-mode. **A)** Image of the experimental set-up (**Left**); The control suspension of MBs shows the baseline signal (**Middle**); The B-mode mean power of 100 frames before and after high mechanical destructive pulse were calculated by VevoCQ™ and displayed by scatter plot (**Right**). **B)** Visualization of the contrast intensities before and after the burst to destroy CM-Dextran-MBs (**Up**) and Fucoidan-MBs (**Down**). **C)** Quantitative analysis of the B-mode mean power signals before and after the burst. (n = 3; ns: non-significant; ***p < 0.001).

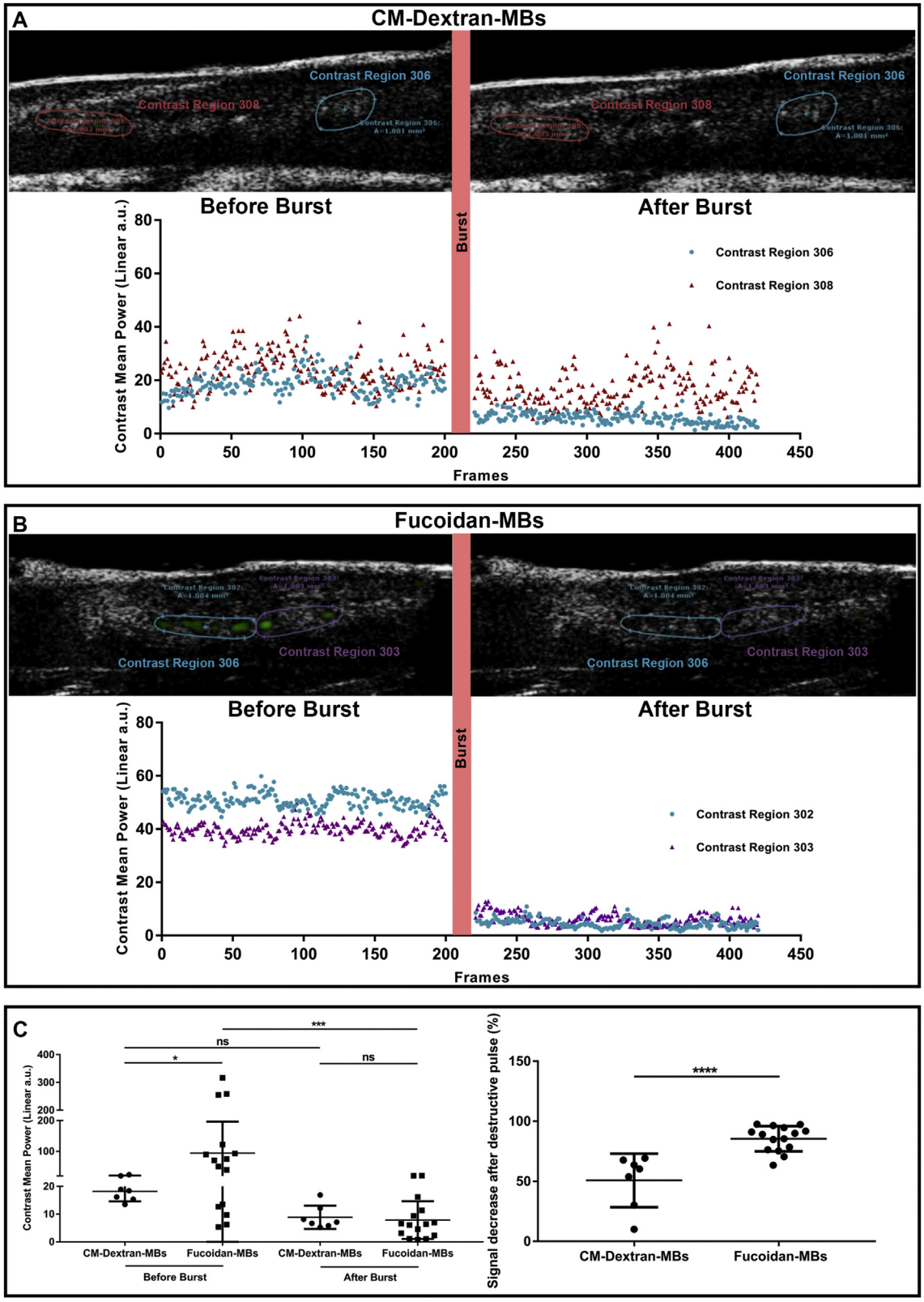


**Fig. 6.** The thrombus area ultrasound imaging of ferric-chloride-induced inferior vena cava thrombosis rat model was acquired and analyzed for 10 min after injection of MBs. 50 frames after the destructive pulse were selected as a reference, and the contrast signals that only exist in the frame before burst were highlighted by green color. The contrast mean power of 200 frames before and after high mechanical destructive pulse was calculated by VevoCQ™ and represented in scatter plot. The mean value of contrast mean power before and after the burst was used for the following quantitative analyses. **A)** After injection of CM-Dextran-MBs, few bound MBs were found in thrombus region. **B)** A significant microbubble-induced signal (green) was present in the thrombus area after injection of Fucoidan-MBs. **C)** Quantitative analysis of the signals before and after the burst. On the right panel, the contrast mean power after the burst was normalized to the one before the burst (5 rats for CM-Dextran-MBs and 5 rats for Fucoidan-MBs, ****$p < 0.0001$).

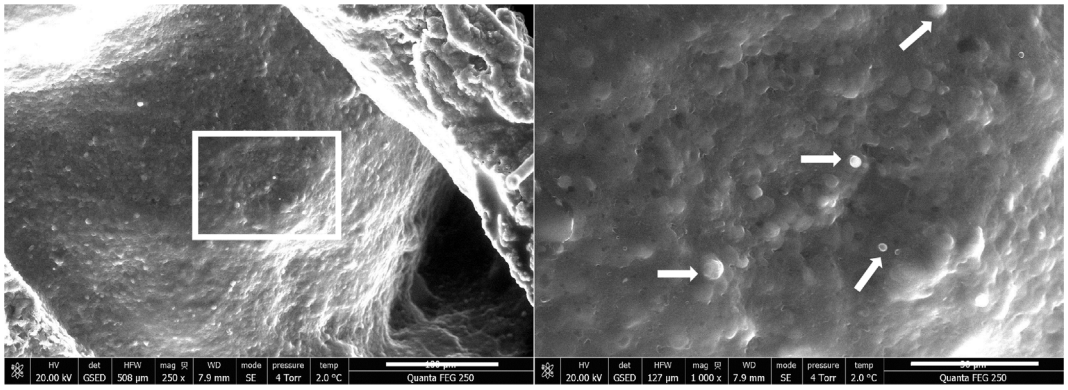


**Fig. 7.** Environmental Scanning Electron Microscopy (ESEM) images of a non-occlusive inferior vena cava thrombus rat model with Fucoidan-MBs bound at the luminal surface of the thrombus (**Left**). Magnification of a region of interest and white arrows highlight the Fucoidan-MBs (**Right**). Scale bars are 100 µm and 30 µm for the magnified area.

significantly higher accumulation of Fucoidan-MBs in comparison to CM-Dextran-MBs (85.5 ± 2.7% versus 50.8 ± 8.4%, respectively, $p < 0.0001$) (Fig. 6C). Furthermore, no Fucoidan-MBs were detected in the inferior vein wall of healthy rats (Fig. S8). In addition, the healthy rats used in these experiments were still alive a few months after injection of MBs and without any side effects.

Supplementary video related to this article can be found at https://doi.org/10.1016/j.biomaterials.2018.12.023.

To confirm the presence of Fucoidan-MBs bound onto the thrombus, we visualized the opened inferior cava vena with thrombus by Environmental Scanning Electron Microscopy (ESEM). ESEM images proved that the thrombus rat model induced by ferric chloride ($FeCl_3$) was non-occlusive (Fig. 7 **Left**) and that there were many Fucoidan-MBs at the luminal surface of the thrombus targeting the P-selectin over-expressed (Fig. 7 **Right**).

Owing to the poor contrast, quantitative analysis of ultrasound signal modification has been a difficult issue in the field of ultrasound molecular imaging [42,52,53]. Unlike non-motile solid tumor, blood vessel walls are always dilated or contracted due to the heartbeat, adding to the difficulty of thrombi imaging analysis. Currently, the main ultrasound imaging methods of thrombus analysis are based on the contrast overlay data that is created by comparing the imaging before and after the injection of MBs [42,52,53]. This approach could potentially overcome the interference of motion artifacts, but it failed to distinguish the false increased contrast signal caused by the growth of thrombi. Herein, we exploited a differential imaging method to evaluate the targeting efficiency of MBs. Thanks to this method, we were able to distinctly see the binding site of MBs, quantify the number of targeted MBs, and also monitor the elimination of MBs. Previous studies have shown that the combination of MBs and ultrasound can help temporarily to open the blood-brain-barrier via sonoporation mechanisms, these phenomena can contribute to the delivery of pharmaceutical treatments [54–57]. Herein, we observed for the first time that Fucoidan-MBs which were localized in the thrombus could be destroyed by a destructive pulse. These results indicated that Fucoidan-MBs carrying thrombolytic drugs could be a promising delivery system to improve thrombolytic efficiency while reducing hemorrhagic complications via the local release of the drug-loaded Fucoidan-MBs at the pathological site.

### 3.6. Tissue distribution in healthy and thrombus-induced rats

To evaluate the biodistribution in healthy rats, the presence of Fucoidan-RhoB-MBs in four main organs of excretion (liver, spleen, lungs and kidneys) was assessed by histological analysis of several sections for each organ (Fig. S9). Results revealed that few Fucoidan-RhoB-MBs were found in liver, lungs and kidneys (indicated by the arrows). Conversely, red fluorescence was detected in the spleen with irregular shapes probably due to the degradation of the microbubbles. Indeed, various degradation processes of PACA nanoparticles were described [58,59]. One leading view was that the main products of biodegradation of PACA nanoparticles were polymer chains and the corresponding alcohol, which were formed after cleavage of ester bond by esterases [60–62]. This also confirmed that the red fluorescent fragments we observed possibly arise from enzymatic hydrolysis in the spleen. Considering the results of the absence of cell toxicity and the low injection doses of Fucoidan-MBs or CM-Dextran-MBs *in vivo,* these MBs seem to be safe.

To assess whether Fucoidan-MBs accumulated *in vivo* within an inferior venous thrombus, histology was performed under bright field and fluorescent microscopes. Results confirmed that thrombus existed in the inferior deep vein (Fig. 8A), smooth muscle cells from venous vascular wall labeled with DAPI showed blue color (Fig. 8B), and many scattered Fucoidan-RhoB-MBs (indicated by the arrows) were localized in the thrombus area (Fig. 8C and D). Few MBs showed microbubble-like shapes, most of them were altered and fractured (Fig. 8C and D **Right**), likely due to high destructive pulse that destroyed their structure.

## 4. Conclusion

In this work, various polysaccharide-coated PIBCA MBs were developed according to a new easy one-step polymerization reaction. This method allowed convenient modulation of the different surface functional groups of MBs, which were prone to further functionalization. Among the polysaccharides, fucoidan was especially considered to functionalize the MBs due to its high affinity for P-selectin. Compared to anionic carboxymethylated dextran MBs, Fucoidan-MBs specifically bind to P-selectin expressed by human activated platelets at venous shear stress. An *in vivo* rat model showed that Fucoidan-MBs were able to target thrombus. We evidenced their presence in the thrombus by ultrasound imaging and histology analysis. This approach offers a sensitive and specific method to detect microthrombi before complete occlusion of the vessel using an inexpensive and widely used ultrasound equipment in hospitals and medical centers worldwide. Fucoidan-MBs application could also be extended to molecular monitoring of P-selectin expression in severe diseases. More in-depth studies of the *in vivo* performance of Fucoidan-MBs should be performed before moving towards clinical implementation. In addition, antithrombotic or fibrinolytic drugs could be incorporated into the Fucoidan-MBs, and these targeted MBs burst by ultrasound could locally deliver the drugs at the thrombus site, which represents a new promising theranostic system.

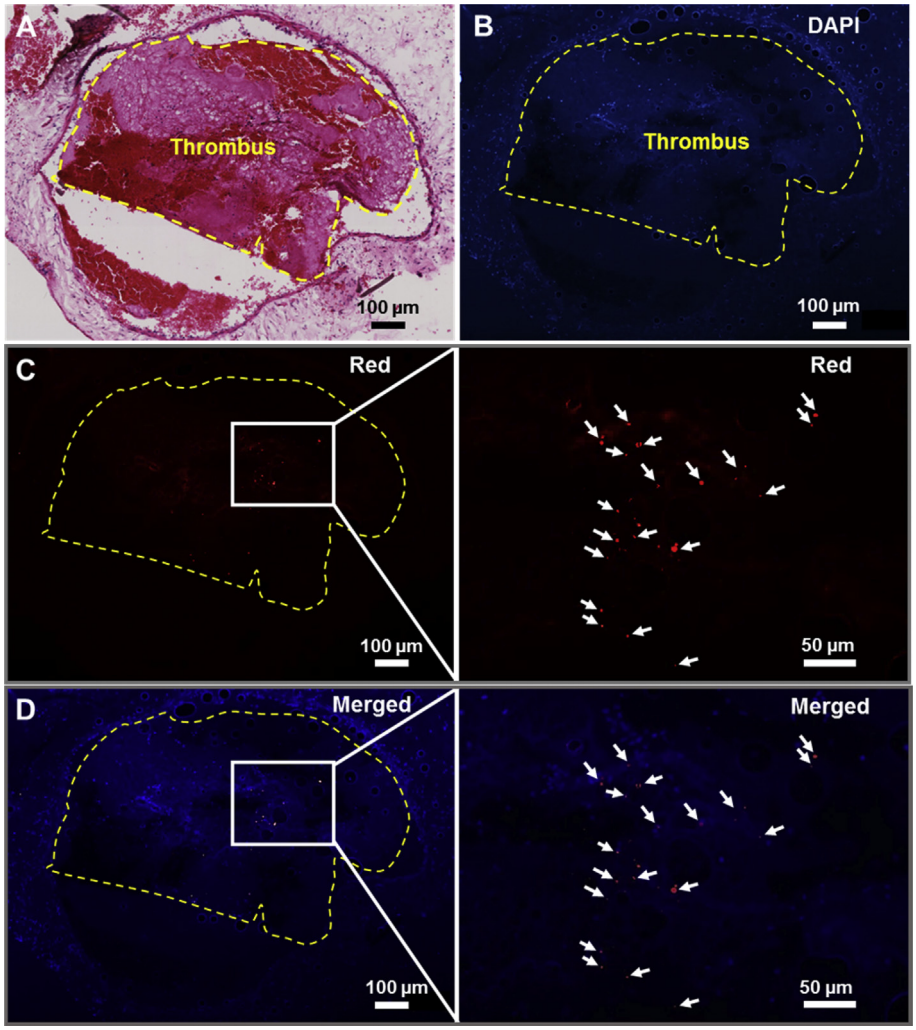


**Fig. 8.** Histological analysis of thrombi in the IVC sections. Hematoxylin and Eosin staining (**A**) and DAPI staining (**B**). Red Fucoidan-RhoB-MBs were only observed in the thrombus area (**C**). Merge section of DAPI and Fucoidan-RhoB-MBs (**D**). Inserts are magnification of Regions of Interest (**C & D Right**). The region of thrombus is denoted with the yellow dotted line.

## Data availability statement

Authors confirm that the raw/processed data required to reproduce these findings can be shared upon demand.

## Acknowledgements

This study was supported by Inserm, Paris Diderot University, and Paris 13 University. Dr. B. Li is a recipient of the China Scholarship Council (CSC, No. 201206180031), he designed the study, collected and interpreted the data, and wrote the draft version of the manuscript. R. Aid-Launais (Engineer) carried out the rat experiment, histology and cytotoxicity analysis. Dr. M-N. Labour (Post-Doc) performed the confocal imaging. A. Zenych (PhD student), a recipient of the European Union's Horizon 2020 research and innovation programme (Marie Skodowska-Curie grant # 665850), realized the physico-chemical characterizations of the MBs and M. Juenet (PhD student) the characterization of fucoidan content. C. Choqueux (Engineer) designed and performed the Environmental Scanning Electron Microscopy experiments. V. Ollivier (Engineer) designed the flow experiments. D. Letourneur (Head of the Unit) provided the funding, discussed the results and corrected the manuscript. O. Couture (Researcher) analyzed the *in vitro* and *in vivo* ultrasound imaging. C. Chauvierre (Researcher) supervised the thesis of Bo Li, discussed the results and corrected the manuscript. The authors are most grateful to E. Teston (INSERM U979) for *in vitro* ultrasound imaging experiment on agarose, F. Nadaud (UTC Compiègne, France) for ESEM images and to CRI U1149 imaging facilities for confocal imaging. This work received the financial support of the ANR (ANR-12-EMMA-0020-01 "MicroSound" and ANR-13-LAB1-0005-01 "FucoChem"), and the EU project FP7-NMP-2012-LARGE-6-309820 "NanoAthero". The authors have declared that no competing interest exists.

## Appendix A. Supplementary data

Supplementary data to this article can be found online at https://doi.org/10.1016/j.biomaterials.2018.12.023.

## References

[1] N. Mackman, Triggers, targets and treatments for thrombosis, Nature 451 (7181) (2008) 914–918.
[2] G. Lippi, M. Franchini, G. Targher, Arterial thrombus formation in cardiovascular disease, Nat. Rev. Cardiol. 8 (9) (2011) 502–512.
[3] S.P. Jackson, Arterial thrombosis–insidious, unpredictable and deadly, Nat. Med. 17 (11) (2011) 1423–1436.
[4] R.P. Choudhury, V. Fuster, Z.A. Fayad, Molecular, cellular and functional imaging of atherothrombosis, Nat. Rev. Drug Discov. 3 (11) (2004) 913–925.
[5] S. Yokoyama, H. Ikeda, N. Haramaki, H. Yasukawa, T. Murohara, T. Imaizumi, Platelet P-selectin plays an important role in arterial thrombogenesis by forming large stable platelet-leukocyte aggregates, J. Am. Coll. Cardiol. 45 (8) (2005)

1280–1286.
[6] H.H. Boersma, H.J. de Haas, C.P. Reutelingsperger, R.H. Slart, P-selectin imaging in cardiovascular disease: what you see is what you get? J. Nucl. Med. 52 (9) (2011) 1337–1338.
[7] J.K. Schaefer, B. Jacobs, T.W. Wakefield, S.L. Sood, New biomarkers and imaging approaches for the diagnosis of deep venous thrombosis, Curr. Opin. Hematol. 24 (3) (2017) 274–281.
[8] J. Brangsch, C. Reimann, F. Collettini, R. Buchert, R.M. Botnar, M.R. Makowski, Molecular imaging of abdominal aortic aneurysms, Trends Mol. Med. 23 (2) (2017) 150–164.
[9] L. Bachelet, I. Bertholon, D. Lavigne, R. Vassy, M. Jandrot-Perrus, F. Chaubet, D. Letourneur, Affinity of low molecular weight fucoidan for P-selectin triggers its binding to activated human platelets, Biochim. Biophys. Acta 1790 (2) (2009) 141–146.
[10] A.K. Silva, D. Letourneur, C. Chauvierre, Polysaccharide nanosystems for future progress in cardiovascular pathologies, Theranostics 4 (6) (2014) 579–591.
[11] F. Rouzet, L. Bachelet-Violette, J.M. Alsac, M. Suzuki, A. Meulemans, L. Louedec, A. Petiet, M. Jandrot-Perrus, F. Chaubet, J.B. Michel, D. Le Guludec, D. Letourneur, Radiolabeled fucoidan as a p-selectin targeting agent for in vivo imaging of platelet-rich thrombus and endothelial activation, J. Nucl. Med. 52 (9) (2011) 1433–1440.
[12] P. Sabboural, F. Chaubet, F. Rouzet, F. Al-Shoukr, R.B. Azzouna, N. Bouchemal, L. Picton, L. Louedec, M. Maire, L. Rolland, G. Potier, D.L. Guludec, D. Letourneur, C. Chauvierre, Purification of a low molecular weight fucoidan for SPECT molecular imaging of myocardial infarction, Mar. Drugs 12 (9) (2014) 4851–4867.
[13] B. Li, M. Juenet, R. Aid-Launais, M. Maire, V. Ollivier, D. Letourneur, C. Chauvierre, Development of polymer microcapsules functionalized with fucoidan to target P-selectin overexpressed in cardiovascular diseases, Adv. Healthc. Mater. 6 (4) (2017) 1601200.
[14] M. Suzuki, L. Bachelet-Violette, F. Rouzet, A. Beilvert, G. Autret, M. Maire, C. Menager, L. Louedec, C. Choqueux, P. Sabboural, O. Haddad, C. Chauvierre, F. Chaubet, J.B. Michel, J.M. Serfaty, D. Letourneur, Ultrasmall superparamagnetic iron oxide nanoparticles coated with fucoidan for molecular MRI of intraluminal thrombus, Nanomedicine 10 (1) (2015) 73–87.
[15] T. Bonnard, G. Yang, A. Petiet, V. Ollivier, O. Haddad, D. Arnaud, L. Louedec, L. Bachelet-Violette, S.M. Derkaoui, D. Letourneur, C. Chauvierre, C. Le Visage, Abdominal aortic aneurysms targeted by functionalized polysaccharide micro-particles: a new tool for SPECT imaging, Theranostics 4 (6) (2014) 592–603.
[16] T. Bonnard, J.M. Serfaty, C. Journe, B. Ho Tin Noe, D. Arnaud, L. Louedec, S.M. Derkaoui, D. Letourneur, C. Chauvierre, C. Le Visage, Leukocyte mimetic polysaccharide microparticles tracked in vivo on activated endothelium and in abdominal aortic aneurysm, Acta Biomater. 10 (8) (2014) 3535–3545.
[17] P. Emilia, T. Nicolas, G. Belfor, S. Mathieu, B. Romain, T. Nicolas, K. Erol, L. Olivier, O. Michèle, D.B. Thuy, B.J. Claude, G. Brigitte, U. Wladimir, B.S. Lori, F. Elias, Perfluorooctyl bromide polymeric capsules as dual contrast agents for ultra-sonography and magnetic resonance imaging, Adv. Funct. Mater. 18 (19) (2008) 2963–2971.
[18] R.H. Perera, C. Hernandez, H. Zhou, P. Kota, A. Burke, A.A. Exner, Ultrasound imaging beyond the vasculature with new generation contrast agents, Rev. Nanomed. Nanobiotechnol. 7 (4) (2015) 593–608.
[19] E. Stride, N. Saffari, Microbubble ultrasound contrast agents: a review, Proc. Inst. Mech. Eng. H. 217 (6) (2003) 429–447.
[20] D. Cosgrove, Ultrasound contrast agents: an overview, Eur. J. Radiol. 60 (3) (2006) 324–330.
[21] R. Gessner, P.A. Dayton, Advances in molecular imaging with ultrasound, Mol. Imag. 9 (3) (2010) 117–127.
[22] F. Kiessling, S. Fokong, P. Koczera, W. Lederle, T. Lammers, Ultrasound micro-bubbles for molecular diagnosis, therapy, and theranostics, J. Nucl. Med. 53 (3) (2012) 345–348.
[23] J. Wang, P. Li, R. Tian, W. Hu, Y. Zhang, P. Yuan, Y. Tang, Y. Jia, L. Zhang, A novel microbubble capable of ultrasound-triggered release of drug-loaded nanoparticles, J. Biomed. Nanotechnol. 12 (3) (2016) 516–524.
[24] C. Huang, H. Zhang, R. Bai, Advances in ultrasound-targeted microbubble-mediated gene therapy for liver fibrosis, Acta Pharm. Sin. B 7 (4) (2017) 447–452.
[25] X. Xiong, F. Zhao, M. Shi, H. Yang, Y. Liu, Polymeric microbubbles for ultrasonic molecular imaging and targeted therapeutics, Journal of biomaterials science, Polymer Ed. 22 (4–6) (2011) 417–428.
[26] J. Liao, C. Wang, Y. Wang, F. Luo, Z. Qian, Recent advances in formation, properties, and applications of polymersomes, Curr. Pharmaceut. Des. 18 (23) (2012) 3432–3441.
[27] C. Vauthier, C. Dubernet, E. Fattal, H. Pinto-Alphandary, P. Couvreur, Poly(alkylcyanoacrylates) as biodegradable materials for biomedical applications, Adv. Drug Deliv. Rev. 55 (4) (2003) 519–548.
[28] V. Delplace, J. Nicolas, Degradable vinyl polymers for biomedical applications, Nat. Chem. 7 (2015) 771.
[29] M.D. Stein, D. Heldmann, T.D. Fritzsch, J.D. Siegert, G.D. Rössling, U.P. Speck, Ultrasonic Imaging Agents, Process for Their Preparation and Their Diagnostic and Therapeutical Use, Google Patents, 1989.
[30] J.R. Harris, F. Depoix, K. Urich, The structure of gas-filled n-butyl-2-cyanoacrylate (BCA) polymer particles, Micron 26 (2) (1995) 103–111.
[31] M. Palmowski, J. Huppert, P. Hauff, M. Reinhardt, K. Schreiner, M.A. Socher, P. Hallscheidt, G.W. Kauffmann, W. Semmler, F. Kiessling, Vessel fractions in tumor xenografts depicted by flow- or contrast-sensitive three-dimensional high-frequency Doppler ultrasound respond differently to antiangiogenic treatment, Canc. Res. 68 (17) (2008) 7042–7049.
[32] M. Palmowski, J. Huppert, G. Ladewig, P. Hauff, M. Reinhardt, M.M. Mueller, E.C. Woenne, J.W. Jenne, M. Maurer, G.W. Kauffmann, W. Semmler, F. Kiessling, Molecular profiling of angiogenesis with targeted ultrasound imaging: early assessment of antiangiogenic therapy effects, Mol. Canc. Therapeut. 7 (1) (2008) 101–109.
[33] M. Palmowski, B. Morgenstern, P. Hauff, M. Reinhardt, J. Huppert, M. Maurer, E.C. Woenne, S. Doerk, G. Ladewig, J.W. Jenne, S. Delorme, L. Grenacher, P. Hallscheidt, G.W. Kauffmann, W. Semmler, F. Kiessling, Pharmacodynamics of streptavidin-coated cyanoacrylate microbubbles designed for molecular ultrasound imaging, Invest. Radiol. 43 (3) (2008) 162–169.
[34] P. Koczera, Z. Wu, S. Fokong, B. Theek, L. Appold, S. Jorge, D. Mockel, Z. Liu, A. Curaj, G. Storm, M. van Zandvoort, F. Kiessling, T. Lammers, Fluorescently labeled microbubbles for facilitating translational molecular ultrasound studies, Drug Deliv. Transl. Res. 2 (1) (2012) 56–64.
[35] S. Fokong, B. Theek, Z. Wu, P. Koczera, L. Appold, S. Jorge, U. Resch-Genger, M. van Zandvoort, G. Storm, F. Kiessling, T. Lammers, Image-guided, targeted and triggered drug delivery to tumors using polymer-based microbubbles, J. Contr. Release 163 (1) (2012) 75–81.
[36] Z. Wu, A. Curaj, S. Fokong, E.A. Liehn, C. Weber, T. Lammers, F. Kiessling, M. Zandvoort van, Rhodamine-loaded intercellular adhesion molecule-1-targeted microbubbles for dual-modality imaging under controlled shear stresses, Circ. Cardiovasc. Imag. 6 (6) (2013) 974–981.
[37] S. Fokong, A. Fragoso, A. Rix, A. Curaj, Z. Wu, W. Lederle, O. Iranzo, J. Gatjens, F. Kiessling, M. Palmowski, Ultrasound molecular imaging of E-selectin in tumor vessels using poly n-butyl cyanoacrylate microbubbles covalently coupled to a short targeting peptide, Invest. Radiol. 48 (12) (2013) 843–850.
[38] I. Spivak, A. Rix, G. Schmitz, S. Fokong, O. Iranzo, W. Lederle, F. Kiessling, Low-dose molecular ultrasound imaging with E-selectin-targeted PBCA microbubbles, Mol. Imag. Biol. 18 (2) (2016) 180–190.
[39] M. Smeenge, F. Tranquart, C.K. Mannaerts, T.M. de Reijke, M.J. van de Vijver, M.P. Laguna, S. Pochon, J. de la Rosette, H. Wijkstra, First-in-human ultrasound molecular imaging with a VEGFR2-specific ultrasound molecular contrast agent (BR55) in prostate cancer: a safety and feasibility pilot study, Invest. Radiol. 52 (7) (2017) 419–427.
[40] J.K. Willmann, L. Bonomo, A. Carla Testa, P. Rinaldi, G. Rindi, K.S. Valluru, G. Petrone, M. Martini, A.M. Lutz, S.S. Gambhir, Ultrasound molecular imaging with BR55 in patients with breast and ovarian lesions: first-in-human results, J. Clin. Oncol. 35 (19) (2017) 2133–2140.
[41] J.M. Lee, Z.-U. Shin, G.T. Mavlonov, I.Y. Abdurakhmonov, T.H. Yi, Solid-phase colorimetric method for the quantification of fucoidan, Appl. Biochem. Biotechnol. 168 (5) (2012) 1019–1024.
[42] T. Wang, C. Yuan, B. Dai, Y. Liu, M. Li, Z. Feng, Q. Jiang, Z. Xu, N. Zhao, N. Gu, F. Yang, Click-chemistry-Mediated rapid microbubble capture for acute thrombus ultrasound molecular imaging, Chembiochem 18 (14) (2017) 1364–1368.
[43] N. Guvener, L. Appold, F. de Lorenzi, S.K. Golombek, L.Y. Rizzo, T. Lammers, F. Kiessling, Recent advances in ultrasound-based diagnosis and therapy with micro- and nanometer-sized formulations, Methods 130 (2017) 4–13.
[44] A. Curaj, Z. Wu, A. Rix, O. Gresch, M. Sternkopf, S. Alampour-Rajabi, T. Lammers, M. van Zandvoort, C. Weber, R.R. Koenen, E.A. Liehn, F. Kiessling, Molecular ultrasound imaging of junctional adhesion molecule a depicts acute alterations in blood flow and early endothelial dysregulation, Arterioscler. Thromb. Vasc. Biol. 38 (1) (2018) 40–48.
[45] P. Koczera, L. Appold, Y. Shi, M. Liu, A. Dasgupta, V. Pathak, T. Ojha, S. Fokong, Z. Wu, M. van Zandvoort, O. Iranzo, A.J.C. Kuehne, A. Pich, F. Kiessling, T. Lammers, PBCA-based polymeric microbubbles for molecular imaging and drug delivery, J. Contr. Release 259 (2017) 128–135.
[46] B. Ryan, G. McCann, Novel sub-ceiling temperature rapid depolymerization-re-polymerization reactions of cyanoacrylate polymers, Macromol. Rapid Commun. 17 (4) (1996) 217–227.
[47] C. Chauvierre, D. Labarre, P. Couvreur, C. Vauthier, Novel polysaccharide-decorated poly(isobutyl cyanoacrylate) nanoparticles, Pharm. Res. 20 (11) (2003) 1786–1793.
[48] C. Chauvierre, C. Vauthier, D. Labarre, P. Couvreur, M.C. Marden, L. Leclerc, A new generation of polymer nanoparticles for drug delivery, Cell. Mol. Biol. 50 (3) (2004) 233–239.
[49] Z. Liu, P. Koczera, D. Doleschel, F. Kiessling, J. Gatjens, Versatile synthetic strategies for PBCA-based hybrid fluorescent microbubbles and their potential theranostic applications to cell labelling and imaging, Chem. Commun. 48 (42) (2012) 5142–5144.
[50] W. Wu, Y. Wang, S. Shen, J. Wu, S. Guo, L. Su, F. Hou, Z. Wang, Y. Liao, J. Bin, In vivo ultrasound molecular imaging of inflammatory thrombosis in arteries with cyclic Arg-Gly-asp–modified microbubbles targeted to glycoprotein IIb/IIIa, Invest. Radiol. 48 (11) (2013) 803–812.
[51] J. Matuszak, J. Baumgartner, J. Zaloga, M. Juenet, A.E. da Silva, D. Franke, G. Almer, I. Texier, D. Faivre, J.M. Metselaar, F.P. Navarro, C. Chauvierre, R. Prassl, L. Dezsi, R. Urbanics, C. Alexiou, H. Mangge, J. Szebeni, D. Letourneur, I. Cicha, Nanoparticles for intravascular applications: physicochemical characterization and cytotoxicity testing, Nanomedicine 11 (6) (2016) 597–616.
[52] X. Wang, C.E. Hagemeyer, J.D. Hohmann, E. Leitner, P.C. Armstrong, F. Jia, M. Olschewski, A. Needles, K. Peter, I. Ahrens, Novel single-chain antibody-targeted microbubbles for molecular ultrasound imaging of thrombosis: validation of a unique noninvasive method for rapid and sensitive detection of thrombi and monitoring of success or failure of thrombolysis in mice, Circulation 125 (25) (2012) 3117–3126.
[53] X. Wang, Y. Gkanatsas, J. Palasubramaniam, J.D. Hohmann, Y.C. Chen, B. Lim, C.E. Hagemeyer, K. Peter, Thrombus-targeted theranostic microbubbles: a new technology towards concurrent rapid ultrasound diagnosis and bleeding-free fibrinolytic treatment of thrombosis, Theranostics 6 (5) (2016) 726–738.

[54] M.A. Nakatsuka, R.F. Mattrey, S.C. Esener, J.N. Cha, A.P. Goodwin, Aptamer-crosslinked microbubbles: smart contrast agents for thrombin-activated ultrasound imaging, Adv. Mater. 24 (45) (2012) 6010–6016.
[55] E. Unger, T. Porter, J. Lindner, P. Grayburn, Cardiovascular drug delivery with ultrasound and microbubbles, Adv. Drug Deliv. Rev. 72 (2014) 110–126.
[56] T. Lammers, P. Koczera, S. Fokong, F. Gremse, J. Ehling, M. Vogt, A. Pich, G. Storm, M. van Zandvoort, F. Kiessling, Theranostic USPIO-loaded microbubbles for mediating and monitoring blood-brain barrier permeation, Adv. Funct. Mater. 25 (1) (2015) 36–43.
[57] C.H. Fan, C.Y. Lin, H.L. Liu, C.K. Yeh, Ultrasound targeted CNS gene delivery for Parkinson's disease treatment, J. Contr. Release 261 (2017) 246–262.
[58] V. Lenaerts, P. Couvreur, D. Christiaens-Leyh, E. Joiris, M. Roland, B. Rollman, P. Speiser, Degradation of poly (isobutyl cyanoacrylate) nanoparticles, Biomaterials 5 (2) (1984) 65–68.
[59] R.H. Muller, C. Lherm, J. Herbort, P. Couvreur, In vitro model for the degradation of alkylcyanoacrylate nanoparticles, Biomaterials 11 (8) (1990) 590–595.
[60] M. Stein, E. Hamacher, Degradation of polybutyl 2-cyanoacrylate microparticles, Int. J. Pharm. 80 (1) (1992) R11–R13.
[61] D. Scherer, J.R. Robinson, J. Kreuter, Influence of enzymes on the stability of polybutylcyanoacrylate nanoparticles, Int. J. Pharm. 101 (1) (1994) 165–168.
[62] C. O'Sullivan, C. Birkinshaw, Hydrolysis of poly (n-butylcyanoacrylate) nanoparticles using esterase, Polym. Degrad. Stabil. 78 (1) (2002) 7–15.

# ABSTRACT
# RÉSUMÉ
# CV

# ABSTRACT

Atherosclerosis is a chronic disease which may lead to acute thromboembolic events. Current thrombolytic therapy, the intravenous injection of recombinant tissue plasminogen activator (rtPA), is administrated to lyse a vascular occlusion and restore the blood flow in the vessel. However, systemic delivery of rtPA exhibits limited clinical efficacy because of its short plasma half-live and risks of hemorrhages. Herein, we explore the utilization of 100% polysaccharide submicronic particles as the biocompatible and biodegradable thrombus-targeting nanovector for safe and efficient thrombolysis.

The inflammatory adhesion molecule P-selectin was selected to be a molecular target, as it is overexpressed by the platelets and vascular endothelium upon activation. Fucoidan, a sulfated polysaccharide from brown algae, was used as a targeting ligand due to its affinity to P-selectin and biocompatibility. The submicronic polysaccharide particles demonstrated their thrombus targeting *in vitro* and *in vivo*. In the murine model of ischemic stroke, rtPA conjugated to the submicronic particles enhanced the thrombolytic activity of clinical agent *in vivo*.

To conclude, novel biocompatible fucoidan-functionalized polysaccharide particles were designed and tested for thrombolytic therapy in preclinical models. This proof-of-concept study demonstrates the promise of biomaterial-based targeted nanomedicine to improve the safety and efficacy of systemic thrombolysis for future clinical application.



**Keywords**: Nanomedicine; Drug delivery; Targeted thrombolysis; Polysaccharides; Fucoidan; P-selectin.

# RÉSUMÉ

L'athérosclérose est une maladie chronique qui peut entraîner des événements thromboemboliques aigus. La thérapie thrombolytique actuelle, l'injection intraveineuse d'activateur tissulaire du plasminogène recombinant (rtPA), est utilisée pour lyser une occlusion vasculaire. Cependant, l'administration systémique de rtPA présente une efficacité clinique limitée en raison de sa courte demi-vie plasmatique et des risques d'hémorragie. Ce projet de Doctorat explore l'utilisation de particules submicroniques 100% polysaccharidiques en tant que nanovecteur ciblant le thrombus, biocompatible et biodégradable pour une thrombolyse plus sûre et plus efficace.

La molécule d'adhésion inflammatoire P-sélectine a été une cible moléculaire, car elle est surexprimée par les plaquettes et l'endothélium vasculaire lors de leur activation. Le fucoïdane, un polysaccharide sulfaté issu d'algues brunes, a été utilisé comme agent de ciblage en raison de sa forte affinité pour la P-sélectine et de sa biocompatibilité. Les particules de polysaccharide ont démontré leur potentiel de ciblage du thrombus *in vitro* et *in vivo*. La conjugaison du rtPA aux particules pourrait améliorer l'activité thrombolytique de l'agent clinique *in vivo* dans un modèle murin d'Accident Vasculaire Cérébral ischémique.

Pour conclure, de nouvelles particules submicroniques polysaccharidiques biocompatibles fonctionnalisées avec du fucoïdane ont été conçues pour effectuer une thérapie thrombolytique dans des modèles précliniques. Cette étude de preuve de concept démontre la promesse de la nanomédecine ciblée à base de biomatériaux pour améliorer la sécurité et l'efficacité de la thrombolyse systémique en clinique.



**Mots clés** : Nanomédecine ; Délivrance de médicaments ; Thrombolyse ciblée ; Polysaccharides ; Fucoïdane ; P-sélectine.

CURRICULUM VITAE

# Alina ZENYCH

*Paris, FRANCE*

## Academic Background

**Ph.D. in Nanomedicine** — **2017 – 2021**
Sorbonne Paris Nord University — Paris, France

**Laboratory for Vascular Translational Science - INSERM U1148**
**Project**: *"Targeted treatment of thrombotic diseases using functionalized polysaccharide submicroparticles"*

**M.Sc.** with "mention Bien" **in Biomedical Engineering (Molecular and Cellular Biotherapies)** — **2015 - 2016**
Paris Descartes University — Paris, France

**M.Sc.** with honours **in Medical Instruments and Systems** — **2012 - 2015**
National Technical University of Ukraine "Kyiv Polytechnic Institute" — Kyiv, Ukraine

- One-year exchange **Master's Programme in Biomedical Engineering** — **2013 - 2014**
  University of Groningen, EMERGE Erasmus Mundus Action 2 Scholarship — Groningen, Netherlands

**B.Sc.** with honours **in Instrument Making / Medical Instruments and Systems** — **2008 - 2012**
National Technical University of Ukraine "Kyiv Polytechnic Institute" — Kyiv, Ukraine

## Professional Experience

***Junior Project Manager*** — **10/2016 - 06/2017**
**Adsy** — Kyiv, Ukraine

- Creating a detailed work plan, road mapping, setting tasks, review of the progress, problem assessment, monitoring of the IT project delivery;
- Project evaluation and documentation creation.

***Product Manager of Cardiovascular Medical Devices*** — **10/2014 - 01/2015**
**Medicor** — Kyiv, Ukraine

- Developing marketing plans and activities for Abbott Vascular product lines;
- Certification and registration of medical devices in Ukraine.

***Medical Devices Sales Representative*** — **03/2013 - 07/2013**
**Medigran** — Kyiv, Ukraine

- Education of customers through conversations, presentations, and literature;
- Building relationships with key decision makers in the hospital environment.

***Internship in Clinical Physics*** — **10/2012 - 12/2012**
**National Children's Specialized Hospital "OHMATDYT"** — Kyiv, Ukraine

- Consultation of medical staff on technical issues;
- Translation of equipment regulations.

## Skills

| | |
|---|---|
| **Languages** | **Ukrainian, Russian** – Native; **English** – C1; **French** – B2 |
| **Digital competences** | GraphPad Prism, Image J, Illustrator, AutoCAD, SolidWorks, Matlab, Microsoft Office. |
| **Professional skills & techniques** | Nanomaterial characterization. Biocompatibility assays. Biochemistry and Cell Molecular Biology skills. Microfluidics. High-resolution imaging. Scientific writing. Presentation skills. Problem-solving skills & analytical thinking. |
| **Communication & management** | Time & project management. Multitasking and prioritization. Interpersonal skills. Ability to adapt to multicultural environment. |

## Publications


1. B. Li, R. Aid-Launais, M.-N. Labour, A. Zenych, M. Juenet, C. Choqueux, V. Ollivier, O. Couture, D. Letourneur, C. Chauvierre, Functionalized polymer microbubbles as new molecular ultrasound contrast agent to target P-selectin in thrombus, *Biomaterials*. 194 (2019) 139–150. https://doi.org/10.1016/j.biomaterials.2018.12.023.
2. A. Zenych, L. Fournier, C. Chauvierre, Nanomedicine progress in thrombolytic therapy, *Biomaterials*. 258 (2020) 120297. https://doi.org/10.1016/j.biomaterials.2020.120297.



+33651636338 | alina.zenych@gmail.com